Sequence-Controlled Polymers: Synthesis, Self-Assembly, and Properties

ACS SYMPOSIUM SERIES **1170**

Sequence-Controlled Polymers: Synthesis, Self-Assembly, and Properties

Jean-François Lutz, Editor
Institut Charles Sadron

Tara Y. Meyer, Editor
University of Pittsburgh

Makoto Ouchi, Editor
Kyoto University

Mitsuo Sawamoto, Editor
Kyoto University

American Chemical Society, Washington, DC

Distributed in print by Oxford University Press

The paper used in this publication meets the minimum requirements of American National Standard for Information Sciences—Permanence of Paper for Printed Library Materials, ANSI Z39.48n1984.

PRINTED IN THE UNITED STATES OF AMERICA

Foreword

The ACS Symposium Series was first published in 1974 to provide a mechanism for publishing symposia quickly in book form. The purpose of the series is to publish timely, comprehensive books developed from the ACS sponsored symposia based on current scientific research. Occasionally, books are developed from symposia sponsored by other organizations when the topic is of keen interest to the chemistry audience.

Before agreeing to publish a book, the proposed table of contents is reviewed for appropriate and comprehensive coverage and for interest to the audience. Some papers may be excluded to better focus the book; others may be added to provide comprehensiveness. When appropriate, overview or introductory chapters are added. Drafts of chapters are peer-reviewed prior to final acceptance or rejection, and manuscripts are prepared in camera-ready format.

As a rule, only original research papers and original review papers are included in the volumes. Verbatim reproductions of previous published papers are not accepted.

ACS Books Department

Preface

The present volume of the ACS Symposium series is dedicated to the emerging field of sequence-controlled polymers. The objectives of that new research discipline include the synthesis, characterization, and exploitation of synthetic macromolecules containing ordered sequences of comonomers. This topic has gained significant importance in academic polymer research during the last several years. The community, which was initially composed of a few isolated researchers, has rapidly grown in a dynamic international network. As a consequence, the first international symposium on sequence-controlled polymers was organized at the 246th American Chemical Society national meeting in Indianapolis. All the chapters in this volume are related to the invited oral presentations that were given during the symposium. This selection of papers gives an overview of the field and highlights its interdisciplinarity. Indeed, the symposium participants and the authors of this book are not only polymer chemists, but also organic chemists, supramolecular chemists, and physico-chemists. As a matter of fact, the design of tailor-made sequence-controlled polymers is a topic that goes beyond the traditional barriers of synthetic polymer science. Thus, we sincerely hope that this volume of ACS Symposium Series will be of interest to a broad readership. It should be stated that this book is the first one to explore the important topic of sequence-controlled polymers but probably not the last. Based on its recent academic impact, it is reasonable to expect that this field of research will grow further in the next decades.

Jean-François Lutz
Precision Macromolecular Chemistry
Institut Charles Sadron – UPR22-CNRS
23 rue du Loess,
67034 Strasbourg, France

Tara Y. Meyer
Department of Chemistry
University of Pittsburgh
Chevron Science Center
219 Parkman Avenue
Pittsburgh, PA 15260

Makoto Ouchi
Department of Polymer Chemistry
Graduate School of Engineering
Kyoto University, Katsura, Nishikyo-ku
Kyoto 615-8510, Japan

Mitsuo Sawamoto
Department of Polymer Chemistry
Graduate School of Engineering
Kyoto University, Katsura, Nishikyo-ku
Kyoto 615-8510, Japan

Editors' Biographies

Jean-François Lutz

Jean-François Lutz is a CNRS research director, deputy director of the Institut Charles Sadron in Strasbourg, and head of the Precision Macromolecular Chemistry group. He received his doctoral degree from the University of Montpellier II (France) in 2000 and his habilitation degree from the University of Potsdam (Germany) in 2009. Before joining the CNRS, he was a post-doctoral fellow in the group of Krzysztof Matyjaszewski at Carnegie Mellon University (2001-2003) and afterwards, leader of the research group Nanotechnology for Life Science at the Fraunhofer Institute for Applied Polymer Research (2003-2010). His current research interests include the synthesis of sequence-controlled and sequence-defined polymers, the structuration of polymer chains by intramolecular chemistry, and the design of information-containing macromolecules. He is author of over 150 publications, book chapters, and patents and serves as an executive advisory board member for all Macromolecular journals as well as an editorial board member for Progress in Polymer Science, Polymer Chemistry, European Polymer Journal, and Design Monomers and Polymers. Among various distinctions, he received the joint prize of the polymer division of the French Chemical Society (SFC) and of the French Polymer Group (GFP) in 2008. Since 2010, he is also a laureate of the European Research Council (ERC).

Tara Y. Meyer

Tara Y. Meyer received her B.A. from Grinnell College in 1991 and her Ph.D. from the University of Iowa in 1991. Her doctoral thesis, under the supervision of Prof. Louis Messerle, focused on the reactivity of early transition metal acyl complexes. She carried out postdoctoral work at both the University of Iowa (1991-1992) under the supervision of Prof. Richard F. Jordan and the University of California, Berkeley (1992-1994) under the joint supervision of Prof. Robert G. Bergman and Bruce M. Novak. Dr. Meyer joined the faculty at the University of Pittsburgh department of Chemistry in 1994 and is a member of the McGowan Institute for Regenerative Medicine. Her work has been recognized by both CAREER and Sloan Foundation Awards, and a sabbatical stay at MIT (2003) was supported by an NIH Ruth L. Kirschstein National Research Service Award. Dr. Meyer's research focuses on synthesis and structure/function studies on repeating sequence copolymers and on the design of stimuli responsive materials.

Makoto Ouchi

Makoto Ouchi is an associate professor at Kyoto University and concurrently a PRESTO researcher with Japan Science and Technology Agency (JST). He received his doctoral degree from Kyoto University in 2001 and then joined Toyota Central R&D Labs., Inc. as a researcher before moving to Graduate School of Engineering of Kyoto University as an assistant professor. He received the Young Scientist Prize of the Annual Kobe Polymer Research Symposium (2011) and the Polymer Journal Zeon Award (2012).

Mitsuo Sawamoto

Mitsuo Sawamoto (b. 1951, Japan) received his B.S. (1974), M.S. (1976), and Ph.D. degrees (1979) in polymer chemistry from Kyoto University. After postdoctoral research at the University of Akron (1980–81), he joined the Department of Polymer Chemistry, Kyoto University in 1981 and has been a professor of Polymer Chemistry since 1994. He is an executive member of the Science Council of Japan (2005–), a titular member of IUPAC Polymer Division (2008–), the immediate past president of the Society of Polymer Science, Japan (SPSJ) (2008–2010), and one of the editors for the Journal of Polymer Science, Part A, Polymer Chemistry (1995–). He was also the leader of the Kyoto University Global Center of Excellence (GCOE) Project, "Integrated Materials Science" (2007–2011). His research interest includes development of precision polymerizations and catalysis, the synthesis of designed functional polymers, and most recently, the sequence regulation in chain-growth polymerization. The first paper on his living radical polymerization has been cited over 2250 times (Macromolecules #2 most cited) and served a review over 2360 times [Chemical Reviews top <1% ACS Highly Cited Papers (1998–2007)]. With >370 original papers, >35 reviews, and >15,000 total citations, he has received the Award of The Society of Polymer Science, Japan (1992); the Divisional Research Award of the Chemical Society of Japan (1999); the Arthur K. Doolittle Award of PMSE Division, the American Chemical Society (2002); the Macro Group UK Medal for Outstanding Achievement in Polymer Science, the Royal Society of Chemistry (2012); and the SPSJ Award for Outstanding Achievement in Polymer Science and Technology (2013).

Chapter 1

An Introduction to Sequence-Controlled Polymers

Jean-François Lutz[*]

Precision Macromolecular Chemistry, Institut Charles Sadron, BP 84047, 23 rue du Loess, 67034 Strasbourg Cedex 2, France
[*]E-mail: jflutz@unistra.fr

Monomer sequence regulation in macromolecules is one of the most important aspects of natural sciences. Indeed, ordered comonomer sequences constitute the basis for genetics and, more generally speaking, for the development of all of Earth's known life-forms. However, even though monomer sequence regulation is a keystone of the central dogma of molecular biology for more than 50 years, it was for a rather long time not perceived as a priority topic in synthetic polymer science. The aim of the present volume of the ACS Symposium Series is to show that this situation has drastically changed over the past few years. Indeed, it is now widely recognized that monomer sequence control is a crucial parameter for tuning the structure, properties, and functions of manmade materials. Thus, sequence-controlled polymer synthesis has recently become a distinct discipline involving a fast-growing community of scientists. In this context, the objective of this first introduction chapter is to describe the rise and the development of this field of research. Recent progress, current limitations, and future challenges are discussed in this chapter.

Introduction

"Sequences, sequences and sequences"… this is the title of a classic overview article published by Frederick Sanger a bit more than 25 years ago (*1*).

It evidences the importance of controlled monomer sequences in the science of the 20th century. Indeed, Frederick Sanger has marked his time with the discovery of chemical methods for proteins and nucleic acids sequencing (*2*, *3*). His remarkable findings were complemented by those of Max Perutz (*4*), Har Gobind Khorana (*5*), Bruce Merrifield (*6*), James Watson and Francis Crick (*7*), as well as many other heroes of last century's science. However, all these discoveries have been essentially made by molecular biologists who studied the macromolecules of life. As a matter of fact, monomer sequence regulation is the key strategy used by nature for developing molecularly-encoded self-replicators, which are the essence of all known living matter.

The basic topic of monomer sequence regulation, however, is not a matter of biology but more a problem of chemistry, and more specifically, a problem of polymer chemistry. Fundamentally speaking, there are two core questions that still need to be solved by polymer scientists: *(i)* how to assemble comonomer units in a controlled linear arrangement and *(ii)* how ordered primary structures correlate with the structure and properties of matter. However, these crucial questions were scarcely addressed by polymer chemists during the 20th century (*8*). Some tools for sequence regulation (e.g., solid-phase chemistry, dendrimer synthesis, living polymerizations) and many types of copolymers have been developed and studied during the last decades, but monomer sequence control was not addressed as a research topic of its own (*9*).

In fact, it was only a few years ago that the broad polymer community fully realized the importance of monomer sequences in materials design (*10*). During the last five years, the number of academic publication on that topic has been rapidly increasing. New approaches for monomer sequence-control in polymerizations are now reported almost every week. Thus, the sequence-control polymers community, which was initially composed of isolated research groups, has recently grown into a broad international scientific network. As a consequence, the first ACS symposium on that topic was organized in Indianapolis in September 2013. This event was the nucleation point of the present volume of the ACS Symposium Series. Indeed, this book regroups a selection of the most active researchers in the field. Still, the research topics presented herein are extremely diverse. Some methods for monomer sequence-regulation are based on biological concepts, whereas others use only synthetic chemistry protocols. In this context, the aim of this first chapter is to clearly define this emerging discipline. The history and the main milestones in the field will be presented in a first paragraph. Afterwards, the main approaches for monomer-sequence regulation will be briefly presented and classified. Such an analysis of the field is probably needed because this domain is too recent to be already described and classified in general textbooks.

Of course, the present volume of the ACS Symposium Series is only the cornerstone of a probably much longer scientific development. The field of sequence-controlled polymers is just starting and many challenges and drawbacks remain to be solved in the future. Hence, some prospects and future research directions are listed and discussed in the last paragraph of this chapter.

A Bit of History

As mentioned in the introduction, significant discoveries have been made on macromolecular sequences during the 20th century. However, many of them occurred in the context of molecular biology. The top of Figure 1 shows the historical milestones for the synthesis and sequencing of sequence-defined proteins and nucleic acids. It appears clearly that a somewhat linear progress – punctuated by regular breakthroughs – was made in that area.
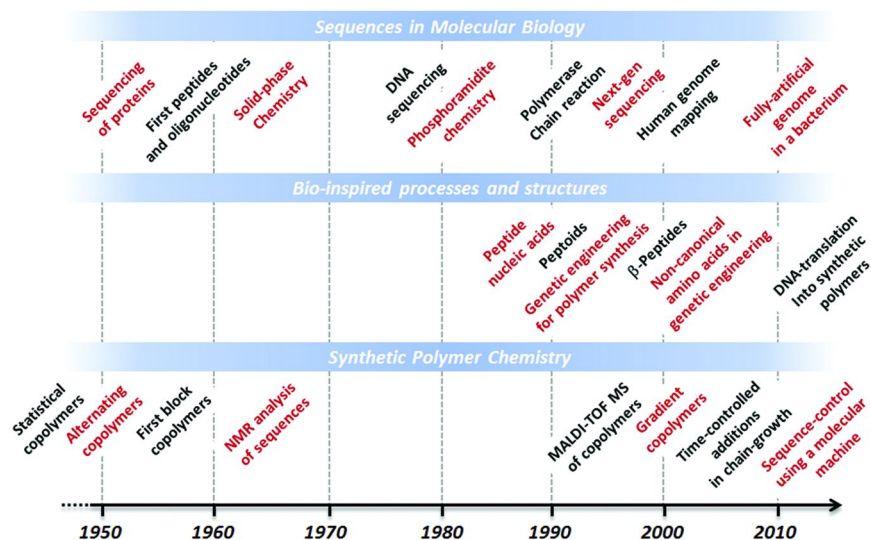

Figure 1. Chronological summary of important discoveries related to the synthesis and characterization of ordered comonomer sequences in synthetic and biological macromolecules.

The first notion of an ordered comonomer sequence appeared in the late-1930s in the context of protein research (*11*). Historical textbooks and websites often mention that the scientific community believed until the late 1940s/early 1950s that proteins were ill-defined amorphous polymers and that Frederick Sanger demonstrated alone that they are composed of ordered amino-acids sequences. In fact, in his 1988 essay, Sanger clarified that the idea was in the air for some years (*1*). Still, his description of the primary structure of insulin was the first convincing experimental demonstration that proteins are made of ordered comonomer sequences (*2*). Afterwards, significant advances were made for the chemical synthesis of sequence-defined oligopeptides. Although the roots of peptide chemistry go back to the early 1930s (*12*), one of the earliest examples of functional oligopeptide sequence is the synthesis of oxytocin reported by Du Vigneaud in 1954 (*13*). Later, sequence-defined oligopeptide synthesis was greatly facilitated by the introduction of solid-phase chemistry by Merrifield (*6*) and its subsequent automatization.

The history of sequence-defined nucleic acids has followed a slightly different discovery pattern. Shortly after the identification of the double-helix of DNA by Watson and Crick (*7*), the groups of Khorana (*5*) and Letsinger (*14*) have reported seminal articles on oligonucleotide chemical synthesis. However, although the synthesis of sequence-defined nucleic acids was chemically possible, protocols for DNA sequencing were discovered two decades later by Sanger (*3*) and Gilbert (*15*). Afterwards, nucleic acids research was greatly accelerated by the discoveries of fast phosphoramidite protocols by Caruthers (*16*), polymerase chain reaction (PCR) amplification by Mullis (*17*) and a plethora of next-generation sequencing methods (*18*). All these breakthroughs have led to genomics as we know it today. The most impressive consequences of these developments were the full mapping of the human genome in 2001 (*19*) and the recent description of a living bacterium controlled by a fully synthetic genome (*20*).

Progress in developing non-biological sequence-controlled polymers has been much more modest during the last 70 years. Some interesting advances have been made with polymers that are not natural but possess molecular structures that closely resemble those of biopolymers (Figure 1, middle). For instance, peptidomimetics are unnatural peptide-like structures that share some features with natural biomacromolecules. For instance, peptide nucleic acids (PNA) introduced by Nielsen (*21*), peptoids introduced by Zuckermann (*22*), and oligocarbamates described by Schultz (*23*) are early examples of sequence-defined unnatural polymers. Other interesting structures, such as β-peptides, have been also developed with the aim of making foldamers (i.e. oligomers that fold into ordered 3D structures) (*24*). Steps forward were also made using enzyme-free, DNA-templated reactions. This field of research is probably too broad and complex to be covered precisely in this short chapter but accurate details can be found in an excellent recent review of the Liu group (*25*). Another interesting development in the late 20th century was the application by Tirrell of genetic engineering for polymer and materials synthesis (*26*). In this process, recombinant plasmids are used to control the production of specific proteins in bacteria. While this technique was at first limited to natural protein structures, methods for incorporating non-canonical amino acids were later developed (*27*).

The study of comonomer sequences in synthetic polymerizations such as chain-growth and step-growth polymerizations has followed a more irregular discovery path (Figure 1, bottom) as compared to the developments described above. Very significant progress in this area was made in the very early days of polymer science. Shortly after the pioneer works of Staudinger, various types of copolymers have been described in the scientific literature. Nylon-type polyamides discovered by Carothers are early examples of alternating copolymers prepared by step-growth copolymerization of two building-blocks (*28*), even though these macromolecules are commonly regarded as homopolymers. In chain-growth polymerizations, various examples of vinyl copolymers have been reported in the 1930-40s. However, the most important contributions in that area were probably made by Mayo and Lewis who described the fundamental rules of copolymerization and reported early examples of statistical and alternating copolymers (*29*, *30*). Methods for preparing block copolymers appeared later in the literature with the pioneer works of Melville (*31*) and Szwarc (*32*). In

addition, starting in the 1960s, substantial work was done on the characterization of synthetic polymer sequences. For instance, Bovey and coworkers reported several methods for NMR sequence analysis (*33*). During the 1970s and 1980s, many original procedures for the synthesis and characterization of block, alternating, and periodic copolymers have been reported (*8*). These decades have brought interesting progress but no paradigm shift in copolymer synthesis. The next interesting developments in the field appeared shortly after the discovery of controlled/living radical polymerization (CRP) methods in the mid 1990s (*34–36*). Due to the living mechanism of CRP, these polymerization techniques allow to "imprint" monomers composition drifts in the chain-microstructures of the formed copolymers. For instance, gradient copolymers reported by Matyjaszewski (*37*) and one-pot block copolymers described by Hawker (*38*) were synthesized using simple CRP protocols. Using time-controlled of ultra-reactive comonomers in a CRP process, our group reported in 2007 the first example of complex aperiodic copolymer (*39*). This method was later optimized to prepare complex encoded microstructures (*40, 41*). In very recent years, the field of sequence-controlled copolymers has progressed significantly, and many interesting findings have been reported (*42–44*). For instance, interesting methods have been published for preparing monodisperse synthetic sequence-defined polymers using solid-supports or templates (*45–50*). The recent reports of Leigh on the use of molecular machines for controlling sequences clearly shows that the field is moving fast (*51, 52*).

Main Approaches for Synthesis

Many different approaches have been reported for the synthesis of sequence-controlled copolymers. These methods are comprehensively described in recent reviews (*8–10, 25*) and will therefore not be discussed in detail here. However, in order to guide the readers through the present volume of the ACS Symposium Series, some general information has to be reminded. In a few words, two main trends exist in the field of sequence-controlled polymers: *(i)* synthesis using biological processes such as replication or translation and *(ii)* synthesis by purely chemical means. The first strategy is somehow a "sure bet," because it relies on biopolymerization mechanisms that have been optimized through long aeons of chemical evolution. As described in the previous section, the 20th century has brought major progress in understanding and mimicking the role of sequences in molecular biology. As a consequence, methods such as PCR and genetic engineering have been developed and later used for the preparation of original sequence-controlled polymers (*53–55*). In PCR, polymerases from extremophile bacteria are used to control the replication and amplification of DNA strands *in vitro*. In genetic engineering, recombinant plasmids are used to encode and produce specific proteins in bacterial hosts. These biological methods are very efficient and allow preparation of advanced functional materials. However, they are, by essence, restricted to the synthesis of sequence-controlled copolymers with natural backbones.

Besides biological concepts, diverse synthetic chemistry procedures have been explored for preparing sequence-defined macromolecules. Manmade approaches are currently less efficient for monomer sequence-regulation than natural processes. However, they may offer other interesting advantages such as: *(i)* a broader chemical diversity, *(ii)* easier and cheaper protocols, and *(iii)* high-scale synthesis. The most common approach for preparing sequence-defined oligomers is the stepwise iterative attachment of monomers on a solid-support. Initially developed by Merrifield (vide supra) for peptide synthesis (*6*), this method has been extended to the synthesis of a wide variety of unnatural sequence-defined copolymers (*8*). Thus, several chapters of the present volume describe the iterative synthesis of sequence-defined oligomers on solid supports. For instance, the preparation of peptoids, glycooligomers and peptide-polymer bio-hybrids is described in this book. In addition to iterative methods, interesting protocols have been recently reported for controlling comonomer sequences in chain-growth and step-growth polymerizations (*39*, *42–44*, *56–62*). Although not perfect, these novel approaches are particularly interesting because they allow synthesis of sequence-controlled copolymers using facile polymerization protocols. A large part of the present volume is dedicated to these recent developments.

Classification and Nomenclature

As discussed in the introduction of this chapter, the field of sequence-controlled polymers is too recent (and too diverse) to already have its own rules, terminology, and nomenclature. For instance, only classical copolymer types such as statistical, alternating, periodic, and block copolymers have an official IUPAC definition (*63*). The current state-of-the-art cannot be fully depicted using these historical terms. In this context, Figure 2 is an attempt to organize the field.
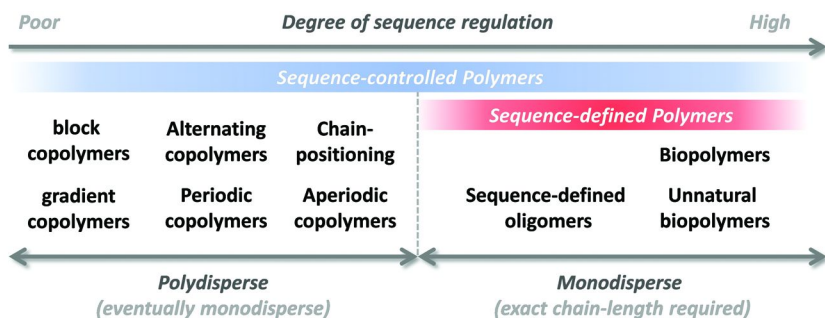

Figure 2. Classification of different types of sequence-controlled polymers.

First of all, it is important to make a distinction between different terms that can be found in recent literature such as sequence-controlled, sequence-regulated, sequence-defined, and sequence-ordered. Although they appear interchangeable,

these terms do not have exactly the same meaning. For instance, the terms sequence-defined and sequence-ordered usually refer to polymers that have perfectly-defined primary structures (*64*), whereas other terminologies may be more general.

As proposed in a recent review (*10*), the term sequence-controlled polymers is a generic name that describes all types of copolymers, in which comonomer sequences are not statistical or random (i.e., sequence distribution follows more or less the same pattern in all chains). However, sequence-controlled polymers can be of very different types. For instance, this term does not necessarily imply that a given monomer is placed at the same exact position in all polymer chains (*64*). Many sequence-controlled copolymers exhibit a polydisperse chain-length distribution and therefore chain-to-chain sequence inhomogeneity. For example, block copolymers exhibit a sequence-controlled microstructure (i.e., segregation of the comonomers in distinct parts of the chains), even though the exact length of each block varies from chain to chain. Likewise, gradient copolymers contain comparable gradual comonomer distributions in all chains but do not have homogeneous primary structures (*65*). Alternating and periodic copolymers, in which a given sequence pattern is repeated periodically along the chains, usually have a more defined primary structure than block and gradient copolymers. When they are synthesized by chain-growth or step-growth copolymerization, these polymers are polydisperse (i.e. $1.05 < M_w/M_n < 2$). However, they exhibit relatively regular - albeit very simple - microstructures.

As discussed in the previous sections of this chapter, no other major types of sequence-controlled copolymers were reported in the literature until a few years ago. However, recent kinetic methods that allow precise monomer-positioning in chain-growth copolymerizations have opened new avenues for copolymer design (*39*). For instance, it allows preparation of controlled microstructures containing precisely located functional sites (e.g., reactive groups) (*66–69*). Beyond that, it also enables synthesis of complex copolymers that contain aperiodic sequence patterns (*40, 70, 71*). Such aperiodic copolymers open up new avenues for the design of complex encrypted polymeric microstructures.

As specified above, sequence-defined copolymers exhibit perfectly controlled primary structures and are therefore a very important class of macromolecules in the broad family of sequence-controlled polymers (Figure 2). In such macromolecules, the comonomer sequences are fully controlled and each monomer is located at a precise position in the chain. Such absolute monomer control has one obvious implication, which is that all chains of a sequence-defined polymer have equal length (i.e., they are monodisperse). Consequently, a polydisperse polymer is never fully sequence-defined. Monodisperse polymers can eventually be sequence-uncontrolled (Figure 2) but sequence-defined polymers have to be monodisperse. Biopolymers obtained by replication or translation and oligomers prepared using controlled iterative processes are prime examples of sequence-defined polymers. It should be noted that these types of microstructures, which were principally studied in molecular biology and biochemistry until a few years ago, have not yet be fully included in the vocabulary of synthetic polymer chemists. Moreover, the picture shown in Figure 2 is probably far from being a final representation of the field of sequence-controlled

polymers. Given the recent progress in the field, it is highly expectable that new words and definitions will be needed very soon.

Challenges and Future Prospects

The information that the readers will find in this introduction and in this whole volume of the ACS Symposium Series suggests that the field of sequence-controlled polymers is just starting. Even though the last few years have seen the emergence of an international scientific community on the topic, the ultimate objective of developing industry-relevant sequence-controlled polymers is not yet fully fulfilled. Many scientific aspects need to be adjusted prior to reach that goal. For instance, in terms of polymer synthesis, further efforts have to be pursued in order to simplify and optimize the synthesis of perfectly sequence-defined copolymers. Currently most of the known iterative pathways are restricted to the synthesis of low-molecular weight oligomers. In addition, the time and efforts required for preparing such polymers are currently way too demanding for practical applications. It should be also mentioned that the role of tacticity is often neglected is sequence-controlled polymerizations. Therefore, methods allowing simultaneous control of tacticity and comonomer sequences need to be developed (*72*). Apart from synthesis, tools for the characterization of sequence-controlled macromolecules are still missing. NMR tools that are conventionally used in polymer analytics are not sufficient to fully describe comonomer sequences (*73*, *74*). Some sequencing methods that have been developed in protein and nucleic acids research can be certainly adapted to synthetic polymer science (*75*, *76*). Ultimately, the correlation between primary structure and properties have to be addressed. Several research groups have already reported that monomer sequence-regulation significantly influence microscopic and macroscopic properties (*44*, *77–81*), some examples of which are shown in the present book. However, this is probably just a sample of what can be done. Hence, the present volume of the ACS Symposium Series is the first - but certainly not the last – published book on the thrilling topic of sequence-controlled polymers.

References

1. Sanger, F. *Annu. Rev. Biochem.* **1988**, *57*, 1–29.
2. Sanger, F.; Tuppy, H. *Biochem J.* **1951**, *49*, 481–490.
3. Sanger, F.; Nicklen, S.; Coulson, A. R. *Proc. Natl. Acad. Sci. U.S.A.* **1977**, *74*, 5463–5467.
4. Perutz, M. F. *Nature* **1962**, *194*, 914–917.
5. Gilham, P. T.; Khorana, H. G. *J. Am. Chem. Soc.* **1958**, *80*, 6212–6222.
6. Merrifield, R. B. *J. Am. Chem. Soc.* **1963**, *85*, 2149–2154.
7. Watson, J. D.; Crick, F. H. C. *Nature* **1953**, *171*, 737–738.
8. Badi, N.; Lutz, J.-F. *Chem. Soc. Rev.* **2009**, *38*, 3383–3390.
9. Lutz, J.-F. *Polym. Chem.* **2010**, *1*, 55–62.

10. Lutz, J.-F.; Ouchi, M.; Liu, D. R.; Sawamoto, M. *Science* **2013**, *341*, 1238149.
11. Bergmann, M.; Niemann, C. *J. Biol. Chem.* **1938**, *122*, 577–596.
12. Bergmann, M.; Zervas, L. *Ber. Dtsch. Chem. Ges.* **1932**, *65*, 1192–1201.
13. du Vigneaud, V.; Ressler, C.; Swan, J. M.; Roberts, C. W.; Katsoyannis, P. G. *J. Am. Chem. Soc.* **1954**, *76*, 3115–3121.
14. Letsinger, R. L.; Ogilvie, K. K. *J. Am. Chem. Soc.* **1969**, *91*, 3350–3355.
15. Maxam, A. M.; Gilbert, W. *Proc. Natl. Acad. Sci. U.S.A.* **1977**, *74*, 560–564.
16. Beaucage, S. L.; Caruthers, M. H. *Tetrahedron Lett.* **1981**, *22*, 1859–1862.
17. Saiki, R. K.; Gelfand, D. H.; Stoffel, S.; Scharf, S. J.; Higuchi, R.; Horn, G. T.; Mullis, K. B.; Erlich, H. A. *Science* **1988**, *239*, 487–491.
18. Metzker, M. L. *Nat. Rev. Genet.* **2010**, *11*, 31–46.
19. Venter, J. C.; et al. *Science* **2001**, *291*, 1304–1351.
20. Gibson, D. G.; Glass, J. I.; Lartique, C.; Noskov, V. N.; Chuang, R. Y.; Algire, M. A.; Benders, G. A.; Montague, M. G.; Ma, L.; Moodie, M. M.; Merryman, C.; Vashee, S.; Krishnakumar, R.; Assad-Garcia, N.; Andrews-Pfannkoch, C.; Denisova, E. A.; Young, L.; Qi, Z. Q.; Segall-Shapiro, T. H.; Calvey, C. H.; Parmar, P. P.; Hutchison, C. A., III; Smith, H. O.; Venter, J. C. *Science* **2010**, *329*, 52–56.
21. Nielsen, P. E.; Egholm, M.; Berg, R. H.; Buchardt, O. *Science* **1991**, *254*, 1497–1500.
22. Zuckermann, R. N.; Kerr, J. M.; Kent, S. B. H.; Moos, W. H. *J. Am. Chem. Soc.* **1992**, *114*, 10646–10647.
23. Cho, C. Y.; Moran, E. J.; Cherry; Stephans, J. C.; Fodor, S. P.; Adams, C. L.; Sundaram, A.; Jacobs, J. W.; Schultz, P. G. *Science* **1993**, *261*, 1303–1305.
24. Gellman, S. H. *Acc. Chem. Res.* **1998**, *31*, 173–180.
25. Brudno, Y.; Liu, D. R. *Chem. Biol.* **2009**, *16*, 265–276.
26. McGrath, K. P.; Fournier, M. J.; Mason, T. L.; Tirrell, D. A. *J. Am. Chem. Soc.* **1992**, *114*, 727–733.
27. Wang, L.; Brock, A.; Herberich, B.; Schultz, P. G. *Science* **2001**, *292*, 498–500.
28. Carothers, W. H. Linear polyamides and their production. US 2130523 A, 1938.
29. Mayo, F. R.; Lewis, F. M. *J. Am. Chem. Soc.* **1944**, *66*, 1594–1601.
30. Mayo, F. R.; Lewis, F. M.; Walling, C. *J. Am. Chem. Soc.* **1948**, *70*, 1529–1533.
31. Dunn, A. S.; Melville, H. W. *Nature* **1952**, *169*, 699–700.
32. Szwarc, M.; Levy, M.; Milkovich, R. *J. Am. Chem. Soc.* **1956**, *78*, 2656–2657.
33. Bovey, F. A. *J. Polym. Sci.* **1962**, *62*, 197–209.
34. Georges, M. K.; Veregin, R. P. N.; Kazmaier, P. M.; Hamer, G. K. *Macromolecules* **1993**, *26*, 2987–2988.
35. Kato, M.; Kamigaito, M.; Sawamoto, M.; Higashimura, T. *Macromolecules* **1995**, *28*, 1721–1723.
36. Wang, J. S.; Matyjaszewski, K. *J. Am. Chem. Soc.* **1995**, *117*, 5614–5615.
37. Matyjaszewski, K.; Ziegler, M. J.; Arehart, S. V.; Greszta, D.; Pakula, T. *J. Phys. Org. Chem.* **2000**, *13*, 775–786.

38. Benoit, D.; Hawker, C. J.; Huang, E. E.; Lin, Z.; Russell, T. P. *Macromolecules* **2000**, *33*, 1505–1507.
39. Pfeifer, S.; Lutz, J.-F. *J. Am. Chem. Soc.* **2007**, *129*, 9542–9543.
40. Chan-Seng, D.; Zamfir, M.; Lutz, J.-F. *Angew. Chem., Int. Ed.* **2012**, *51*, 12254–12257.
41. Zamfir, M.; Lutz, J.-F. *Nat. Commun.* **2012**, *3*, 1138.
42. Ida, S.; Terashima, T.; Ouchi, M.; Sawamoto, M. *J. Am. Chem. Soc.* **2009**, *131*, 10808–10809.
43. Satoh, K.; Matsuda, M.; Nagai, K.; Kamigaito, M. *J. Am. Chem. Soc.* **2010**, *132*, 10003–10005.
44. Stayshich, R. M.; Meyer, T. Y. *J. Am. Chem. Soc.* **2010**, *132*, 10920–10934.
45. Pfeifer, S.; Zarafshani, Z.; Badi, N.; Lutz, J.-F. *J. Am. Chem. Soc.* **2009**, *131*, 9195–9196.
46. McKee, M. L.; Milnes, P. J.; Bath, J.; Stulz, E.; Turberfield, A. J.; O'Reilly, R. K. *Angew. Chem., Int. Ed.* **2010**, *49*, 7948–7951.
47. Espeel, P.; Carrette, L. L. G.; Bury, K.; Capenberghs, S.; Martins, J. C.; Du Prez, F. E.; Madder, A. *Angew. Chem., Int. Ed.* **2013**, *52*, 13261–13264.
48. Niu, J.; Hili, R.; Liu, D. R. *Nat. Chem.* **2013**, *5*, 282–292.
49. Edwardson, T. G. W.; Carneiro, K. M. M.; Serpell, C. J.; Sleiman, H. F. *Angew. Chem., Int. Ed.* **2014**, *53*, 4567–4571.
50. Solleder, S. C.; Meier, M. A. R. *Angew. Chem., Int. Ed.* **2014**, *53*, 711–714.
51. Lewandowski, B.; De Bo, G.; Ward, J. W.; Papmeyer, M.; Kuschel, S.; Aldegunde, M. J.; Gramlich, P. M. E.; Heckmann, D.; Goldup, S. M.; D'Souza, D. M.; Fernandes, A. E.; Leigh, D. A. *Science* **2013**, *339*, 189–193.
52. De Bo, G.; Kuschel, S.; Leigh, D. A.; Lewandowski, B.; Papmeyer, M.; Ward, J. W. *J. Am. Chem. Soc.* **2014**, *136*, 5811–5814.
53. Petka, W. A.; Harden, J. L.; McGrath, K. P.; Wirtz, D.; Tirrell, D. A. *Science* **1998**, *281*, 389–392.
54. van Hest, J. C. M.; Tirrell, D. A. *Chem. Commun.* **2001**, *0*, 1897–1904.
55. Alemdaroglu, F. E.; Safak, M.; Wang, J.; Berger, R.; Herrmann, A. *Chem. Commun.* **2007**, *13*, 1358–1359.
56. Satoh, K.; Ozawa, S.; Mizutani, M.; Nagai, K.; Kamigaito, M. *Nat. Commun.* **2010**, *1*, 6.
57. Hibi, Y.; Ouchi, M.; Sawamoto, M. *Angew. Chem., Int. Ed.* **2011**, *50*, 7434–7437.
58. Lutz, J.-F.; Schmidt, B. V. K. J.; Pfeifer, S. *Macromol. Rapid Commun.* **2011**, *32*, 127–135.
59. Thomas, C. M.; Lutz, J.-F. *Angew. Chem., Int. Ed.* **2011**, *50*, 9244–9246.
60. Tong, X.; Guo, B.-h.; Huang, Y. *Chem. Commun.* **2011**, *47*, 1455–1457.
61. Hisano, M.; Takeda, K.; Takashima, T.; Jin, Z.; Shiibashi, A.; Matsumoto, A. *Macromolecules* **2013**, *46*, 7733–7744.
62. Vandenbergh, J.; Reekmans, G.; Adriaensens, P.; Junkers, T. *Chem. Commun.* **2013**, *49*, 10358–10360.
63. Ring, W.; Mita, I.; Jenkins, A. D.; Bikales, N. M. *Pure Appl. Chem.* **1985**, *57*, 1427–1440.
64. Zamfir, M.; Lutz, J.-F. In *Progress in Controlled Radical Polymerization: Materials and Applications*; ACS Symposium Series; Matyjaszewski,

K., Sumerlin, B. S., Tsarevsky, N. V., Eds.; American Chemical Society: Washington, DC, 2012; Vol. 1101, pp 1−12.

65. Van Steenberge, P. H. M.; D'hooge, D. R.; Wang, Y.; Zhong, M.; Reyniers, M.-F.; Konkolewicz, D.; Matyjaszewski, K.; Marin, G. B. *Macromolecules* **2012**, *45*, 8519–8531.

66. Schmidt, B. V. K. J.; Fechler, N.; Falkenhagen, J.; Lutz, J.-F. *Nat. Chem.* **2011**, *3*, 234–238.

67. Kakuchi, R.; Zamfir, M.; Lutz, J.-F.; Theato, P. *Macromol. Rapid Commun.* **2012**, *33*, 54–60.

68. Baradel, N.; Fort, S.; Halila, S.; Badi, N.; Lutz, J.-F. *Angew. Chem., Int. Ed.* **2013**, *52*, 2335–2339.

69. Baradel, N.; Gok, O.; Zamfir, M.; Sanyal, A.; Lutz, J.-F. *Chem. Commun.* **2013**, *49*, 7280–7282.

70. Lutz, J.-F. *Acc. Chem. Res.* **2013**, *46*, 2696–2705.

71. Moatsou, D.; Hansell, C. F.; O'Reilly, R. K. *Chem. Sci.* **2014**, *5*, 2246–2250.

72. Satoh, K.; Kamigaito, M. *Chem. Rev.* **2009**, *109*, 5120–5156.

73. Randall, J. C. *Polymer sequence determination: carbon-13 NMR method*; Academic Press: New York, 1977; p 155.

74. Bovey, F. A.; Mirau, P. A. *NMR of Polymers*; Academic Press: San Diego, 1996; p 459.

75. Zhu, Z.; Cardin, C. J.; Gan, Y.; Colquhoun, H. M. *Nat. Chem.* **2010**, *2*, 653–660.

76. Colquhoun, H. M.; Lutz, J.-F. *Nat. Chem.* **2014**, *5*, 455–456.

77. Rosales, A. M.; McCulloch, B. L.; Zuckermann, R. N.; Segalman, R. A. *Macromolecules* **2012**, *45*, 6027–6035.

78. van Zoelen, W.; Zuckermann, R. N.; Segalman, R. A. *Macromolecules* **2012**, *45*, 7072–7082.

79. Norris, B. N.; Zhang, S.; Campbell, C. M.; Auletta, J. T.; Calvo-Marzal, P.; Hutchison, G. R.; Meyer, T. Y. *Macromolecules* **2013**, *46*, 1384–1392.

80. Srichan, S.; Kayunkid, N.; Oswald, L.; Lotz, B.; Lutz, J.-F. *Macromolecules* **2014**, *47*, 1570–1577.

81. Trinh, T. T.; Oswald, L.; Chan-Seng, D.; Lutz, J.-F. *Macromol. Rapid Commun.* **2014**, *35*, 141–145.

The Language of Protein Polymers

Felipe García Quiroz and Ashutosh Chilkoti[*]

Department of Biomedical Engineering, Duke University, Durham, North Carolina 27708, USA
Center for Biologically Inspired Materials and Material Systems, Duke University, Box 90300, North Carolina 27708, USA
[*]E-mail: chilkoti@duke.edu

Proteins are heteropolymers of one or more amino acid residues arranged in a molecularly defined fashion. The precise control of amino acid sequence in protein biosynthesis programs the folding of these heteropolymers into diverse three-dimensional structures. The language of proteins, however, as seen in nature, encompasses limitless amino acid "phrases" (heteropolymers) written in peptide "words" (amino acid motifs) that span the entire structural spectrum from tightly folded to unstructured. Because protein sequences do not always have an obvious syntactic unit (word), herein we focus on protein polymers that repeat one or more syntactic units —motifs with a characteristic fold, biological activity or physical property (e.g., elasticity, phase behavior). We review the biosynthesis and sequence-controlled behavior of protein polymers that altogether span the gap between folded proteins and unstructured polymers. Learning to speak the language of protein polymers promises to merge the science of protein design and the materials science of synthetic polymers. Paradoxically, while protein structure is largely foreign to polymer chemists, the study and synthesis of unstructured, polymer-like proteins has been—till recently—similarly foreign to structural biologists. Interesting possibilities in materials science emerge from acquiring the capacity to read, write and speak the language of protein polymers.

Introduction

A limited set of symbols or letters are arranged in natural languages—the ones we speak —in a specific order to form words that are themselves arranged in ordered strings to form sentences. Language that conveys complex ideas and information emerges from order at both the word and sentence levels. Similar to human languages, the language of proteins is characterized by the ordered arrangement of a set of 20 natural amino acids to encode complex information in the form of structural and biological properties (*1*). Because protein sequences do not always have an obvious syntactic unit (*1*)—discernable word patterns—and because our interest—and indeed that of this collection of essays—is on new approaches to sequence-controlled polymerization, this book chapter focuses on protein polymers that repeat one or more prototypical peptide motifs—the syntactic unit—with a characteristic fold, biological activity or physical property (e.g., elasticity, phase behavior). The language of protein polymers requires absolute sequence control at the letter (amino acid), word (motif) and sentence (arrangement of words) levels to encompass a complex spectrum of properties and functions as is typically observed for protein polymers in nature. Here, we review both natural and engineered protein polymers to pinpoint the role of sequence control at these hierarchical levels, as well as the tools available to the scientific community for the design and synthesis of protein polymers.

Reading: Protein Polymers in Nature

Nature's proteinogenic world is a major source of inspiration for protein polymer design. A large number of proteins with a canonical polymer-like architecture perform diverse biological functions. Here we focus on the characteristics and functions of two major and distinct types of naturally occurring protein polymers: intrinsically disordered proteins (IDPs) and repeat (folded) proteins.

Intrinsically Disordered Proteins

Proteins that are partially or entirely disordered, and lack a defined secondary structure, serve important regulatory and structural, load bearing roles in multi-cellular organisms (*2–4*). Among all proteins, IDPs most closely resemble statistical synthetic polymers. Unlike globular proteins that fold into complex structures, backbone fluctuations in IDPs conform to random coil models descriptive of synthetic polymers in a good solvent (Figure 1), and also to the collapsed structures that emerge in solvents of decreasing solvent quality. The characteristic low sequence complexity of IDPs (*5*), often dominated by a highly repetitive architecture (*6*), makes them resemble synthetic polymers.
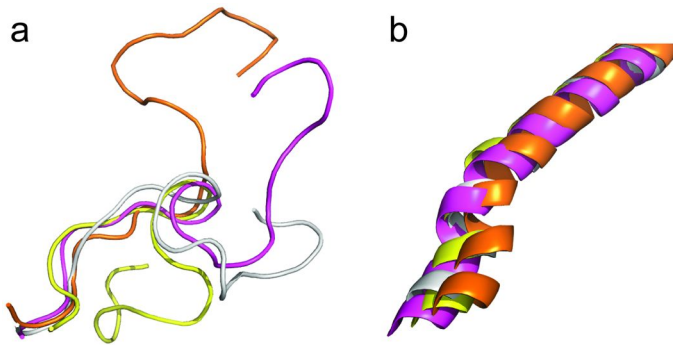
Figure 1. Structural information encoded in polymers of amino acid letters. In aqueous solution, (a) the backbone of IDPs and of other unstructured domains undergo large fluctuations and thus do not assume defined three-dimensional structures, whereas (b) the backbone of globular proteins and of ordered protein segments reproducibly adopt defined structures in the forms of helices (as shown), turns and β-strands. Variations in the color of the protein chain represent independent trajectories from a molecular dynamics simulation.

      In a structural biology dominated protein world, in which crystallography was till recently the primary mode of visualizing proteins, IDPs were ignored because their relative lack of structure made crystallography well-nigh impossible. Only recently, has their abundance, rich function and relevance to disease given them the attention they deserve (*7*). As a result, the language of IDPs, despite their low sequence complexity, has only been partially elucidated at this time (*8*). Uversky et al. first demonstrated that charged residues and residues with low hydrophobicity dominate the amino acid composition of IDPs, and they suggested thresholds of charge and hydrophobicity to identify IDPs (*9*). Recent studies have shown that a high net charge per residue forces the peptide chain into an extended conformation. As the chain length increases, the radius of gyration (R_g) of the peptide chain scales according to the power law that correlates polymer molecular weight and R_g in a good solvent (*10*). These average parameters, however, although suitable for the description of statistical polymers, fail to capture behaviors that result from a non-random amino acid distribution. Das and Pappu, for instance, used molecular dynamics simulations to demonstrate that the conformations of IDPs are modulated by the specific distribution of oppositely charged residues along the sequence (*11*). Whereas a perfectly alternating sequence of oppositely charged amino acid residues leads to random coil behavior, the clustering of like-charged residues results in collapsed globules.

      Sequence control in IDPs plays two major roles: 1) it defines the conformational ensemble (*11*), and 2) it specifies amino acid sequences capable of performing a biological function. These two roles are not necessarily independent. In their extended conformation, IDPs interact with their binding partners with high specificity but with low affinity, which has been proposed as a regulatory strategy

to facilitate rapid on/off kinetics of binding and dissociation (*12*). However, IDPs can fold upon ligand binding, which results in high affinity interactions that stabilize the bound conformation (*4*). This ligand-induced folding is a remarkable example of a sequence-controlled feature in IDPs, particularly because in some instances IDPs deviate from the one sequence, one structure paradigm and rather behave as chameleons that adopt different structures depending on the binding partner (*13*).

Besides low sequence complexity, IDPs are compositionally biased (*5*). They typically exclude order-promoting residues (e.g., C, Y, W, I and V) and favor disorder-promoting residues (e.g., R, K, E, P and S) (*5*). One interesting class of IDPs is highly enriched in two structure-breaking residues: Pro and Gly (*14*). Pro, with its side chain cyclized back into the backbone limits chain flexibility. Gly, in contrast, with a hydrogen atom as a side chain contributes a high entropy penalty to structure formation because of high chain flexibility. Major proteins of the extracellular matrix in mammalian tissues, namely collagens and tropoelastins, belong to this class of proteins. Other relevant examples include silks and resilins (*8*). Pro and Gly-rich IDPs are interesting from the perspective of sequence-controlled polymerization for a number of reasons: 1) despite the abundance of structure-breaking residues, these IDPs are capable of forming structures with long-range order upon aggregation, and 2) differences at the sequence level govern the ability of these proteins to form structured fibrils upon assembly. Collagens, for instance, are intrinsically disordered as isolated polymer chains, but form a highly ordered collagen triple helix upon trimerization and higher order aggregation of these helices leads to the formation of fibrils with remarkable mechanical properties. The assembly of collagen chains is orchestrated at the sequence level by the periodic repetition of X-Y-G tripeptides where X and Y are predominantly Pro and hydroxyproline (HPro) (*15*). The invariable occurrence of Gly every two other residues is a major contributor to the ability of these chains to pack closely together, while HPro and other common amino acid substitutions at the X and Y positions, namely oppositely charged residues, provide the polar interactions that stabilize the helix (*16*). In this regard, the precise positioning of oppositely charged residues at the X and Y position programs the formation of interchain salt bridges that are compatible with the structural requirements of the triple helix (*17, 18*). In contrast to highly ordered, crystallizable collagen nanofibrils, tropoelastins, while also highly enriched in Pro and Gly residues, assemble into amorphous aggregates (*19*). Although tropoelastins and collagens span different regions of the hydropathy space, as tropoelastins are enriched in hydrophobic residues (e.g., Val, Iso and Leu) and collagens are enriched in polar and polar charged residues, differences in Pro and Gly distribution are also likely to play a major role in the distinct assembly behavior of these two IDPs. This is particularly evident when comparing collagens with Pro and Gly-rich resilins, as they exhibit a similar compositional bias as collagens—a high content of charged residues and a nearly zwitterionic character—but do not form helical structures upon aggregation (*20*). Crosslinked resilin aggregates in fact reproduce the mechanical properties of crosslinked tropoleastin (*21*) and neither resilins nor tropoelastins exhibit a distribution of Gly in a collagen-like pattern.

Repeat Proteins

Repeat proteins in nature constitute a highly functional group of protein polymers with properties that are intermediate between those of IDPs and those of globular proteins (*22, 23*). They share a polymer-like, extended repetitive arrangement of peptide motifs, but unlike IDPs, the repeat peptides, typically 30-50 amino acids in length, assume a defined folded—mostly helices but also β-strands—conformation that propagates across the length of the polymer in the form of a common fold separated by short unstructured loops (Figure 2). Unlike compact globular proteins, repeat proteins typically exhibit a linear architecture that creates large interacting surfaces for multi-protein interactions or for the engagement of distant regions in a target (*24*). Another interesting family of repeat proteins have a circularly-closed architecture (e.g., β-propeller and β-trefoil proteins) (*25*), but because they deviate substantially from a linear polymer architecture and instead approach a globular conformation that imposes structural constraints on polymer size, we do not discuss them further.
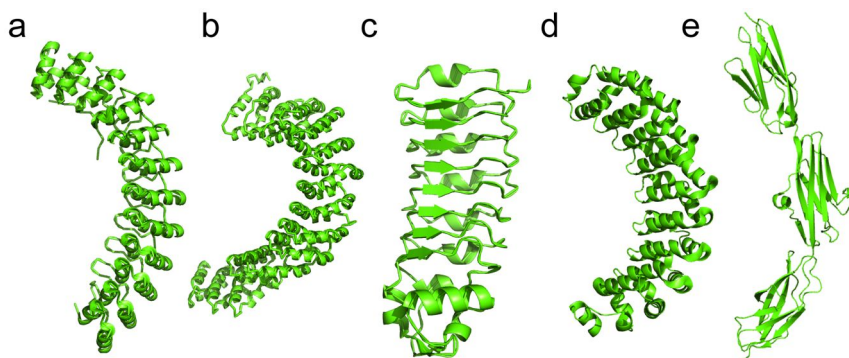
Figure 2. Structures for several naturally occurring repeat proteins. (a) Human ankyrin-R (PDB file: 1N11). (b) Giant HEAT repeat protein PR65A (PDB file: 1B3U). (c) Internalin-B leucine rich repeat domain (PDB file: 1DOB). (d) Pumilio-homology domain from human Pumilio 1 (PDB file: 1M8X). (e) Domains A168 to A170 from titin (PDB file: 2NZI). While many repeat proteins are exclusively helical forming a two (Ankyrin) or three (Arm and HEAT) helix bundle, LLRs combine one helix and one β-strand and yet others (e.g., hexapeptide repeats (26)) are exclusively composed of β-strands. The images were rendered using PyMOL (http://pymol.org/).

Members of this protein family of linear repeat proteins, namely ankyrins, HEAT-like proteins, armadillo (Arm) and Arm-like proteins, leucine-rich repeat proteins, transcription activator-like effector proteins (TALEs) and tetratricopeptide repeat proteins (*22, 26*), are outstanding examples of sequence-controlled polymerization. Here, sequence control plays three major roles: 1) programs the folding (secondary structure) of the peptide repeat, 2) stabilizes the fold of the repeat unit through the careful positioning of inter-repeat

residue interactions across the polymer, and 3) programs the binding surface by controlling surface-exposed residues that are not essential for structural stability (*27*). Because individual peptide repeats are often unable to fold in the absence of stabilizing interactions from neighboring repeats, the N-terminal and the C-terminal repeats differ from internal repeats both in structure and composition to act as capping units (*22*). To prevent aggregation these terminal repeats present two different peptide interfaces: an internal surface that forms a hydrophobic core with the neighboring repeat and a solvent-accessible surface that confers water solubility to the linear repeat protein (*28*).

Repeat proteins in nature bind protein and nuclei acid targets. In protein binding, the repetitive architecture of ankyrins provides a protein scaffold for pathway coordination through the binding of multiple target proteins (*27*). Similarly, plakophilins, a family of armadillo repeat proteins, function as scaffolds that promote multi-protein interactions to assist in the assembly of desmosomes for cell-cell adhesion (*29*). Importins, which are composed of HEAT repeats, bind cargo proteins and transport them through the nuclear pore complex into the nucleus. LLR proteins are prevalent in the innate immune system that provides defense against microbes in both the plant and animal kingdoms (*30*). Jawless vertebrates (lamprey and hagfish) present a remarkable example of the binding characteristics of these proteins as they evolved adaptive immune systems based on LLR proteins in lieu of the immunoglobulin-type antibody repertoire seen in other vertebrates.

The binding of nucleic acids by linear repeat proteins, namely TALEs and Zing fingers for double stranded DNA (*31*), and Pumilio family of proteins (PUF) for messenger RNA (*32*), demonstrates the utility of an extended, repetitive architecture and the specificity conferred by the molecular-level control of polymer sequence (*24*). The basic repeat unit in both TALEs and PUF repeat proteins is responsible for binding a single base in a nucleic acid target. The identity of two surface exposed amino acid residues per repeat is responsible for the recognition of particular nitrogenous bases. In TALEs, for instance, positions 12 and 13 form the repeat variable di-residues (RVDs) that specify each of the four DNA bases: NI= A, HD= C, NN= A or G, NH= G and NG= T (*33*, *34*). Tandem arrangements of base-specific repeat units, however, are needed to extend over the length of the nucleic acid and make possible the recognition of DNA and RNA sequences of varying length.

The folding and unfolding of repeat proteins reveals additional details of the unique properties of these proteins. Because individual repeat units may fail to fold, it has been demonstrated that there are complex interactions that determine the cooperative folding of various repeat proteins. Chemical unfolding, for instance, has been observed to proceed through two-state (i.e., all or none) and multi-state (i.e., partial unfolding of unstable segments) mechanisms. Perhaps more interesting is the repeat by repeat or multiple repeat at a time mechanical unfolding observed through single-molecule AFM studies (*22*, *26*), as these events of reversible mechanical unfolding are likely of physiological relevance for repeat proteins like β-catenin, α-catenin and other armadillo repeat proteins that connect components of adherens junctions to the actin cytoskeleton (*35*). Because some of these linker proteins modulate important signaling pathways

(e.g., Wnt signaling in the case of β-catenin), mechanical unfolding events may affect the binding of specific downstream players in the signaling cascade.

Another interesting type of repeat proteins are composed of linear arrays of stably folded protein domains, as in titin (Figure 2e), fibronectin, tenascin-C and in many proteins in signaling and regulatory networks that exhibit a multi-domain architecture (e.g., kinases) (*36*). Because the repeat units in these proteins are essentially globular proteins or small protein domains with a stable fold —without the need for inter-repeat interactions—, they differ substantially from the repeat proteins discussed previously. In essence they are polymers of globular proteins (small and large) that tolerate both N- and C-terminal fusions. It is noteworthy that multivalent interactions mediated by such repetitive protein domains may be important for the self-assembly, through phase separation, of membraneless intracellular bodies that function to orchestrate gene expression and cytoskeleton organization (*37*).

Writing: Recombinant Synthesis of Protein Polymers

Gene Synthesis

The use of recombinant DNA technology for the production of protein polymers in a cellular expression system requires the ability to synthesize plasmid-borne genes that are transcribed into mRNA by RNA polymerases and then translated into the polymer of interest by the ribosome. The repetitive nature of some of these polymers, however, typically results in highly repetitive DNA sequences that are difficult to manipulate —especially for oligonucleotides with high GC content— with conventional cloning methods that rely on polymerase chain reaction (PCR) (*38*) or concatemerization (*39*). Genes encoding protein polymers of low to moderate molecular weight and relatively high sequence diversity can be produced by PCR amplification followed by DNA concatemerization, although without any control on the final length of the oligomer (*40*). The synthesis of large genes (> 1 Kb) through concatemerization is difficult due to the tendency of large oligomers to circularize, although the use of chain-terminating capping sequences may ameliorate this problem (*41*).

Because of these limitations of PCR based assembly and concatemerization, a number of methods have been developed for the synthesis of genes encoding highly repetitive protein polymers. Iterative cloning strategies that allow for the precise control of the number of DNA repeats, such as recursive directional ligation (RDL) (*42*), are among the most widely used. McDaniel *et al*., recently reported a new recursive method for the synthesis of protein polymers that is more versatile and efficient than the first generation, conventional RDL devised by Meyer and Chilkoti (*42*). This new strategy uses plasmid reconstruction (PRe) to eliminate non-specific recombinant products created by self-ligation of the vector and is thus named PRe-RDL (*39*). Furthermore, unlike RDL, the PRe-RDL cloning steps are performed using a pET expression vector —available formerly from Novagen, and now from Merck Millipore. This has the advantage of eliminating the transfer of the gene from the cloning vector to the expression vector as is done in RDL, which is especially useful for large genes (e.g., >1.5

Kb) that can be difficult to transfer because of poor ligation efficiency. Pre-RDL is also ideal for the construction of polymers with multi-domain architecture and for the incorporation of N- and C-terminal domains. A key feature in PreRDL and other recent gene synthesis strategies is the utilization of type IIS and type III DNA restriction enzymes (*33*, *38*, *43*, *44*). Because these endonucleases cut at a distance away from their DNA binding site, their recognition sequences do not interfere with the seamless assembly of the genes of interest.

The recent development of methods for the rapid assembly of repetitive genes is fueling advances in protein polymer design. In a recent paper, we developed a new methodology, *o*verlap *ex*tension *r*olling *c*ircle *a*mplification (OERCA), for the rapid synthesis of DNA libraries encoding for highly repetitive protein polymers (*45*). OERCA is a one-pot, PCR-based approach in which a chemically synthesized single stranded (ss) DNA (~80-150 bp) is designed to encode 1-5 repeats of the motif of interest —the precise number of repeats depends upon the length of the peptide repeat unit— with a codon selection strategy that creates unique 5′ and 3′ ends suitable for specific primer binding. The ssDNA is circularized prior to the reaction to enable concurrent rolling circle and overlap extension amplification throughout the PCR reaction. By simply controlling primer concentration and the number of PCR cycles, the PCR product consists of double stranded DNA oligomers with a wide and tunable range of DNA repeats. These products are blunt ligated into an expression vector and immediately transformed into a host cell equipped for heterologous protein synthesis. A single cloning step hence effectively separates out the large pool of polydisperse ligation products into a clonally distinct population, wherein each clone contains a plasmid that encodes for a peptide polymer of a defined chain length. In a stringent test case of OERCA, we showed that it outperformed concatemerization and overlap extension PCR for the synthesis of polymers with short (5-6 residues) and long (30 residues) repeat units (*45*). This method is ideal for the rapid synthesis and screening of protein polymers with a unique repeating pattern throughout the length of the polymer.

Because of the explosion of genome editing efforts (*31*), the engineering of TALEs has independently—of the efforts of researchers in the protein polymer field— driven recent innovations in high throughput gene synthesis of repeat proteins. Despite being composed of repeats of nearly identical 34 amino acid repeat units, because each repeat unit targets a unique DNA nucleotide specified by two specific residue positions in the repeat, the iterative cloning strategies described above (e.g., PreRDL and variants of golden gate cloning) would require many cloning steps or laborious preformatting of the building blocks to complete the synthesis of TALE libraries with 8-20 repeat units per protein. Two recent advances in gene assembly, a *f*ast *l*igation-based *a*utomatable *s*olid-phase *h*igh-throughput (FLASH) system (*44*) and iterative capped assembly (ICA) (*38*), exploit a cell-free approach of iterative ligations on magnetic beads to enable rapid and high-throughput assembly of TALE monomers and oligomers into full-length TALE genes without the need for iterative cloning. These approaches should also be useful for the synthesis of other repeat proteins that demand sequence control at the repeat unit level.

Expression: From DNA Oligomers to Protein Polymers

From a materials perspective, plasmid borne genes must be translated with high yield into a protein polymer with the chemical composition of interest. This can be flawlessly accomplished using the translation machinery of a number of cellular hosts, namely *E. coli*, yeast strains (e.g., P. Pastoris), plants (e.g., tobacco leaves), and animal cells (e.g., from humans, insects, rodents, etc.). These expression systems meet the expected requirements of high yield and chemical fidelity with varying degrees of success. The demands of chemical fidelity limit host selection to cellular systems capable of introducing or mediating required post-translational modifications (e.g., disulfide bond formation, hydroxylation and glycosylation). While *E. coli* is a suitable initial host to explore the high yield expressions of protein polymers that have no post-translational modifications—or the few that E. coli is known to perform—, eukaryotic expression systems are the de facto choice if certain post-translational modifications are essential (e.g., glycosylation). Unfortunately, the influence of protein sequence on expression yield for a given host is still poorly understood, but can occur at the transcriptional level (through folding into RNA structures that interfere with processing by the ribosome), translational level (due to codon biases and relative abundance of tRNA pools), or post-translational level (e.g., inclusion body formation, misfolding and protein degradation) (*46–48*). To address issues at the first two levels, low cost high throughput gene synthesis now offers the possibility to rapidly screen a large number of codon variants all encoding a unique amino acid sequence to identify synthetic genes that maximize protein yields (*49*). Factors at the post-translational level are overcome by host selection, by adjusting growth conditions, by subtle amino acid modifications that prevent misfolding —or aberrant folding in the case of IDPs — or N-terminal leader sequences and protective mutations that prevent undesired degradation.

As an example of the wide range of protein yields and of the high yield production — from a few mg to hundreds of mg per L of culture (or Kg in the case of plants)— of protein polymers, Table 1 reports representative protein yields for the recombinant production of tropoelastin, collagen, silk-like and elastin-like protein polymers, and Ankyrin and LLR repeat proteins in different expression systems, predominantly *E. Coli*, but also *P. Pastoris* and Tobacco leaves. Collagens are particularly difficult to produce recombinantly because Pro hydroxylation demands costly mammalian expression systems armed with the required hydroxylation machinery. Despite decade long efforts to engineer yeast strains capable of performing Pro hydroxylation (*50*), and recent advances in the synthesis of full-length, mammalian-like collagens —with suitable hydroxylation levels and sequence specificity— in tobacco plants (*47*), the synthesis and use of recombinant collagens is still limited to niche applications (*51*). Progress in recombinant synthesis of proteins incorporating multiple and potentially unlimited nonstandard amino acids (NSAAs), particularly the recoding of E. coli's genome to eliminate all UAG (amber) stop codons that are instead used to encode for a NSAA in plasmid borne genes (*52*), represents an exciting and elegant potential solution to achieve absolute sequence control in protein polymers that incorporate

HPro, other post-translationally modified residues and a wide range of available NSAAs.

Speaking: Engineered Protein Polymers

Nature's protein polymers are undoubtedly a remarkable example of the advanced properties that result from accessing molecular-level sequence control over the length of a macromolecular polymeric system. Engineered protein polymers in turn provide a drawing canvas to create new material properties through the exploration of amino acid sequence space informed by nature's designs.

Inspired by the repetitive architecture of tropoelastin (*19*) and by specific peptide motifs that recur in its sequence , elastin-like polypeptides (ELPs) are designer protein polymers that —like tropoelastin— exhibit stimuli-responsive, phase transition behavior (*68*). First identified as a common tandem repeat in bovine tropoelastin but also describing many other non-perfect repeats seen in tropoleastins across evolutionary distant species (*69*), the pentapeptide motif VPGXG —where X is any amino acid but Pro— is the most extensively studied elastin-like word. The design of ELPs revolves around controlling the amino acid composition of the polymer, namely the selection of the guest residue X, specifying the number of pentapeptide repeats (i.e., molecular weight) and the specific arrangement of individual repeat units and of blocks of repeat units (*70–72*), as well as introducing N-terminal, C-terminal or inter-repeat peptide or protein domains to provide further functionality (e.g., binding sites, residues for crosslinking and bioactive domains among others) (*72*). Absolute sequence control over these design parameters in genetically encoded synthesis has been instrumental in the development of a wide variety of protein polymers with lower critical solution temperature (LCST) phase behavior that is finely tuned for specific applications in medicine —for both diagnosis (*73*) and treatment (*72, 74, 75*) — and in biotechnology —as tools for protein purification (*76, 77*) and capture (*78*).

Among Pro and Gly-rich IDPs, ELPs are undoubtedly the most extensively engineered protein polymers at the sequence level to access a broad spectrum of stimuli-responsive phase behaviors. Recently, however, resilin-like polypeptides (RLPs) composed of consensus resilin repeat sequences from various animal species, as in GGRPSDSYGAPGGGN from Drosophila Melanogaster (*79*) and AQTPSSQYGAP from *Anopheles Gambiae* (*80*), are also under investigation for the synthesis of stimuli-responsive phase transition polymers, but little is known about the sequence dependence of the LCST and upper critical solution temperature (UCST) phase behavior observed in resilin (exon 1) from *Drosophila Melanogaster* (*81, 82*). In the case of silk-like polymers, despite efforts to explore modular protein polymers with silk-like words from a number of species and silk types (e.g., dragline and flagelliform silk) (*83*), innovation has mostly occurred at the final processing stage and typically involves the use of extracted silk proteins (*84*). Much work remains to be done in exploiting sequence level determinants of the unique tenacity exhibited by silk polymers (*83*).

Table 1. Expression systems and typical production yields for intrinsically disordered and structured protein polymers. Leader amino acid sequences used for expression or purification purposes are indicated when applicable.[a]

Sequence	Leader sequence	Synthesis method/ Expression system	Purification method	Reported yield	Ref
(1) HHHHHHHDDDDK (LDGE-EIQGHIPREDVYHLYPG((VPGIG)$_2$-VPGKG(VPGIG)$_2$)$_4$)VP)$_3$LKE	MASMTGGQQMG	pET28 expression plasmid (kan). BL21(DE3)pLysS. IPTG induction. 10 L Bioflow 3000 fermentor	Adapted inverse transition cycling (ITC) protocol (pH 9)	(1) 300mg/L	(53)
(2) RKTMG[LD-+GEEIQIGHIPRED-VDYHLYP-G(VPGIG)$_{25}$VP]$_5$-LEKAAKLE				(2) 600mg/L	
ELP[KV6-(56-224)], ELP[QV6-112], and ELP[KV16-(51-204)]	SKGPVP	pET25b exp plasmid (Amp). BLR(DE3) 1L cultures with no induction at 37 °C for 24 h	ITC	200-400mg/L depending on MW	(54), (55)
ELP[5V3A2G]-90	RFPSIFTAVLFAASSALAAPVN-TTTEDETAQIPAEAVIGYSDL-EGDFDVAVLPFSNSTNNGLL-FINTTIASIAAKEEGVSLE-KREAEA (secretion signal that is cleaved)	Genomic integration of a pPIC9 (Invitrogen). P. pastoris fed-batch 2.5 L Bioflo 3000 fermentors. 48 h induction and pH 6.0 (secreted expression)	ITC	255mg/L	(56)
[Y]-[X]-[Y] [Y]={VPAVG[(IPAVG)$_4$-(VPAVG)]$_{16}$IPAVG} (1). [X] = VPGVG[(VPGVG)$_2$-VPGEG(VPGVG)$_2$]$_{30}$VPGVG (2). [X] = VPGVGVPGVG	Not reported	pET24b exp. Plasmid (Kan). BL21-Gold (DE3). Large-scale fermentation at 37 °C in TB media	ITC	(1). 614mg/L (2). 781mg/L	(57)

Table 1. (Continued). Expression systems and typical production yields for intrinsically disordered and structured protein polymers. Leader amino acid sequences used for expression or purification purposes are indicated when applicable.[a]

Sequence	Leader sequence	Synthesis method/ Expression system	Purification method	Reported yield	Ref
$\{[(VPGVG)_2$-$(VPGEG)$-$(VPGVG)_2]_{10}$-$[VGIPG]_{60}\}_2V$	ESLLP	E. Coli. (presumably a Fermentor system)	ITC	520mg/L	(58)
GFP-ELP[V5A2G3]-90	Green fluorescent protein (GFP)	pET25b exp. Vector (Amp). BLR(DE3). 1L cultures at 37 °C for 24 h in optimized media (no induction)	ITC	1620mg/L	(59)
SO1- ELP[V5A2G3]-100 (Silk-ELP) SO1: recombinant Spindroin 1 (N. clavipes MaSp1) (51.2KDa)	LeB4-ER signal peptide[b] Note: the design includes a C terminal ER retention signal	pCB301 (Kan). Tobacco (Nicotiana tabacum cv. SNN) Growth time was not reported	Extraction from leaves followed by ITC	80mg/Kg	(60)
V_H(TNF)-[SO1-ELP] V_H(TNF): variable heavy domain against TNF	LeB4-ER signal peptide[b] Note: the design includes a C terminal ER retention signal	pCB301 (Kan). Tobacco (Nicotiana tabacum cv. SNN) Growth time was not reported	Extraction from leaves followed by ITC and SEC	20 mg/Kg	(61)
Tropoelastin (SHELΔ26A)(MW=60KDa)	No leader	pET3d (Amp). E. coli. BioFlo III fermentor.	Cleared lysates after butanol and n-propanol treatment followed by RP-HPLC	~1 g/L[c]	(62), (63)[c]
Engineered silks: (QAQ)8NR3, C16NR4 Q: (GPGQQ)4 A: (GPYGPGASAAAAAG-GYGPGSGQQ) C: (GSSAAAAAAAASGPGGYG-PENQGPSGPGGYGPGGP)	ASMTGGQQMGR	pAZL (Amp). E. Coli BLR (DE3). Fermenter with fed-batch method. IPTG induction at 25-30 °C for 4-16h.	Heat-denaturation of endogenous E. coli proteins followed by a salting-out protocol.	140 mg/L, 360 mg/L	(64)

26

Sequence	Leader sequence	Synthesis method/ Expression system	Purification method	Reported yield	Ref
Heterotrimeric Collagen Type I	Vacuole signal peptide[d]	pBINPLUS (Kan). Tobacco leaves. Growth time > 1.5 months	Extraction from leaves followed by cycles of salt and pH-induced precipitation.	200-1000 g/kg dry leaves	(47), (65)
Consensus Ankyrin repeat proteins (5-6 internal repeats)	RGSHHHHHHGS	pQE30 (Amp). E. coli XL1-Blue. 1L cultures at 37 °C with IPTG induction.	Immobilized metal affinity chromatography	200 mg/L	(66)
Consensus LLR repeat proteins (2-5 internal repeats)	RGSHHHHHHGS	pQE30 (Amp). E. coli XL1-Blue. 1L cultures at 37 °C with IPTG induction.	Immobilized metal affinity chromatography	5-10 mg/L (soluble) 30-50 mg/L (refolding from insoluble fraction)	(28)

[a] ITC: Inverse Transition Cycling. Kan: Kanamycin. Amp: Ampicillin. SEC: Size exclusion chromatography. TNF: Tumor necrosis factor.   [b] LeB4 signal peptide: MASKPFLSLLSLSLLLFTSTCLA.(67)   [c] Approximate raw expression levels (Weiss, A.S., 2010, personal communication).   [d] Vacuole signal peptide: MAHARVLLLALAVLATAAVAVASSSSFADSNPIRPVTDRAASTLA.(65)

The modular nature of protein polymers is readily exploited in the design of hybrid protein polymers. Silk, elastin-like polymers (SELPs) are an interesting example. In these hybrid polymers that combine elements of the syntax of silk with that of elastin, Ala- and Gly-rich silk-like domains are interspersed with molecular precision with elastin-like VPGXG domains to combine the semi-crystallinity of silk domains with the elasticity and stimuli-responsive phase behavior of the elastin-like domains (*85*). In another example of hybrid protein polymers that combine motifs from two natural sources, polymers that alternate 1 resilin repeat (15 residues long) with one or more small, stably folded proteins domains with an immunoglobulin-like fold (GB1; 56 amino acid residues per repeat) have been synthesized (*86*). The mechanical properties of these hybrid polymers mimic the properties of titin (Figure 2e) and are dominated by the mechanical unfolding (stability) of the GB1 domains, while the short resilin repeats provide additional crosslinking sites. By using de novo design of folded domains, these studies have shown that accessing folds with reduced mechanical stability favors the tenacity of protein polymers by favoring energy dissipation through unfolding, while the ensuing aggregation in the crosslinked networks leads to unusual yet intriguing mechanical properties (*87*). However, to the best of our knowledge no work has been conducted that examines the role of sequence control at the level of the linking disordered segments (e.g., number and type of repeats). This is a rather relevant direction in the light of recent studies showing that the folding stability of the helical segments that link naturally-occurring spectrin repeats plays an important role in modulating the flexibility of these repeat proteins (*88*).

Among engineered repeat proteins, consensus-design is the most common approach and has been successful for the engineering of Ankyrin (*22*), Cys-devoid LLR (*28*) and tetratricopeptide repeat proteins (*89*). Recent work has extended this consensus approach to HEAT repeat proteins that typically exhibit high motif variability and low sequence conservation (*90*). Sequence control in these protein polymers has been almost exclusively exploited to specify and modulate their binding affinity to a wide range of targets (*91*). Consensus-designed Ankyrin repeat proteins (DARPins) are particularly popular as an alternative to antibodies (*22*). Interestingly, whereas natural ankyrin repeat proteins often accumulate in inclusion bodies during heterologous expression in *E.coli*, consensus engineered Ankyrin repeat proteins express solubly at high yields and remain soluble over weeks at 4 °C (*92*). Another notable example is the engineering of PUF repeats that bind cytosine, as natural PUF repeats only bind adenine, uracil and guanine. This has enabled the engineering of PUF repeat proteins containing 16 RNA-binding repeats that can target RNA sequences of interest (*32*).

The sequence of individual repeats can be modified to modulate the stability of a given repeat or domain of the protein to control the unfolding pathway. The extensibility of repeat proteins, which involves the reversible unfolding of individual repeats, leads to extension ratios (10-15) that are comparable to IDPs and hence significantly larger than the ratios observed in globular proteins (2-5). The flexibility of repeat proteins, however, remains intermediate between that of globular proteins and IDPs (*22*, *23*). This flexibility, as in IDPs, also appears to be important for the binding of different partners (*23*). These properties will

likely be of utility for the design of new biomaterials. In this context, material properties can be controlled by exploiting specific protein-protein interactions, as in the case of engineered modular TPRs that form physically crosslinked networks in the presence of a peptide ligand (*93*). Another interesting example of engineered material properties in repeat proteins comes from the work of Rosen's group. They demonstrated that the phase transition of a protein polymer system can be modulated by the number of repeat units in the two polymers composed of interacting protein domains, as well as by changes in their binding affinity upon phosphorylation (*37*). This work opens up the possibility of further evolving the "smart" behavior of these materials by using sequence control to tune the binding affinity between protein domains and their organization into more complex architectures.

Conclusion

Natural and engineered protein polymers with a range of interesting material properties can be accessed through absolute control of their sequence and architecture. Advances in the rapid assembly of DNA repeats will continue to spur the exploration of a broad range of amino acid motifs to construct increasingly complex protein polymers that both reproduce and reinvent nature's designs and that span the structural spectrum from intrinsic disorder to spatially defined structures. We believe that new opportunities in materials science will emerge from the acquired capacity to read, write and speak this language of protein polymers.

References

1. Gimona, M. *Nat. Rev. Mol. Cell Biol.* **2006**, *7*, 68–73.
2. Iakoucheva, L. M.; Brown, C. J.; Lawson, J. D.; Obradović, Z.; Dunker, A. K. *J. Mol. Biol.* **2002**, *323*, 573–584.
3. Guharoy, M.; Szabo, B.; Martos, S. C.; Kosol, S.; Tompa, P. *Cytoskeleton* **2013**, *70*, 550–571.
4. Dyson, H. J.; Wright, P. E. *Nat. Rev. Mol. Cell Biol.* **2005**, *6*, 197–208.
5. Romero, P.; Obradovic, Z.; Li, X.; Garner, E. C.; Brown, C. J.; Dunker, A. K. *Proteins: Struct., Funct., Bioinf.* **2001**, *42*, 38–48.
6. Jorda, J.; Xue, B.; Uversky, V. N.; Kajava, A. V. *FEBS J.* **2010**, *277*, 2673–2682.
7. Vavouri, T.; Semple, J. I.; Garcia-Verdugo, R.; Lehner, B. *Cell* **2009**, *138*, 198–208.
8. Peysselon, F.; Xue, B.; Uversky, V. N.; Ricard-Blum, S. *Mol. BioSyst.* **2011**, *7*, 3353–3365.
9. Uversky, V. N.; Gillespie, J. R.; Fink, A. L. *Proteins: Struct., Funct., Bioinf.* **2000**, *41*, 415–427.
10. Mao, A. H.; Crick, S. L.; Vitalis, A.; Chicoine, C. L.; Pappu, R. V. *Proc. Natl. Acad. Sci. U. S. A.* **2010**, *107*, 8183–8188.

11. Das, R. K.; Pappu, R. V. *Proc. Natl. Acad. Sci. U. S. A.* **2013**, *110*, 13392–13397.
12. Fuxreiter, M.; Simon, I.; Friedrich, P.; Tompa, P. *J. Mol. Biol.* **2004**, *338*, 1015–1026.
13. Uversky, V. N. *Chem. Soc. Rev.* **2011**, *40*, 1623–1634.
14. Muiznieks, L. D.; Keeley, F. W. *J. Biol. Chem.* **2010**, *285*.
15. Ricard-Blum, S. *Cold Spring Harbor Perspect. Biol.* **2011**, *3*, a004978.
16. Persikov, A. V.; Ramshaw, J. A.; Kirkpatrick, A.; Brodsky, B. *J. Mol. Biol.* **2002**, *316*, 385–394.
17. Fallas, J. A.; Dong, J.; Tao, Y. J.; Hartgerink, J. D. *J. Biol. Chem.* **2012**, *287*, 8039–8047.
18. Persikov, A. V.; Ramshaw, J. A.; Kirkpatrick, A.; Brodsky, B. *Biochemistry* **2005**, *44*, 1414–1422.
19. Yeo, G. C.; Keeley, F. W.; Weiss, A. S. *Adv. Colloid Interface Sci.* **2011**, *167*, 94–103.
20. Dutta, N. K.; Truong, M. Y.; Mayavan, S.; Roy Choudhury, N.; Elvin, C. M.; Kim, M.; Knott, R.; Nairn, K. M.; Hill, A. J. *Angew. Chem., Int. Ed.* **2011**, *50*, 4428–4431.
21. Gosline, J.; Lillie, M.; Carrington, E.; Guerette, P.; Ortlepp, C.; Savage, K. *Philos. Trans. R. Soc., B* **2002**, *357*, 121.
22. Javadi, Y.; Itzhaki, L. S. *Curr. Opin. Struct. Biol.* **2013**, *23*, 622–631.
23. Forwood, J. K.; Lange, A.; Zachariae, U.; Marfori, M.; Preast, C.; Grubmüller, H.; Stewart, M.; Corbett, A. H.; Kobe, B. *Structure* **2010**, *18*, 1171–1183.
24. Lunde, B. M.; Moore, C.; Varani, G. *Nat. Rev. Mol. Cell Biol.* **2007**, *8*, 479–490.
25. Blaber, M.; Lee, J. *Curr. Opin. Struct. Biol.* **2012**, *22*, 442–450.
26. Kloss, E.; Courtemanche, N.; Barrick, D. *Arch. Biochem. Biophys.* **2008**, *469*, 83–99.
27. Li, J.; Mahajan, A.; Tsai, M.-D. *Biochemistry* **2006**, *45*, 15168–15178.
28. Stumpp, M. T.; Forrer, P.; Binz, H. K.; Plückthun, A. *J. Mol. Biol.* **2003**, *332*, 471–487.
29. Bass-Zubek, A. E.; Godsel, L. M.; Delmar, M.; Green, K. J. *Curr. Opin. Cell Biol.* **2009**, *21*, 708–716.
30. Pancer, Z.; Cooper, M. D. *Annu. Rev. Immunol.* **2006**, *24*, 497–518.
31. Gaj, T.; Gersbach, C. A.; Barbas, C. F., III. *Trends Biotechnol.* **2013**, *31*, 397–405.
32. Filipovska, A.; Razif, M. F.; Nygård, K. K.; Rackham, O. *Nat. Chem. Biol.* **2011**, *7*, 425–427.
33. Morbitzer, R.; Elsaesser, J.; Hausner, J.; Lahaye, T. *Nucleic Acids Res.* **2011**, *39*, 5790–5799.
34. Cong, L.; Zhou, R.; Kuo, Y.-c.; Cunniff, M.; Zhang, F. *Nat. Commun.* **2012**, *3*, 968–973.
35. Valbuena, A.; Vera, A. M.; Oroz, J.; Menéndez, M.; Carrión-Vázquez, M. *Biophys. J.* **2012**, *103*, 1744–1752.
36. Han, J.-H.; Batey, S.; Nickson, A. A.; Teichmann, S. A.; Clarke, J. *Nat. Rev. Mol. Cell Biol.* **2007**, *8*, 319–330.

37. Li, P.; Banjade, S.; Cheng, H.-C.; Kim, S.; Chen, B.; Guo, L.; Llaguno, M.; Hollingsworth, J. V.; King, D. S.; Banani, S. F. *Nature* **2012**, *483*, 336–340.

38. Briggs, A. W.; Rios, X.; Chari, R.; Yang, L.; Zhang, F.; Mali, P.; Church, G. M. *Nucleic Acids Res.* **2012**, *40*, 1–10.

39. McDaniel, J.; MacKay, J.; Quiroz, F.; Chilkoti, A. *Biomacromolecules* **2010**, *11*, 944–952.

40. Girotti, A.; Reguera, J.; Rodríguez-Cabello, J.; Arias, F.; Alonso, M.; Testera, A. *J. Mater. Sci.: Mater. Med.* **2004**, *15*, 479–484.

41. Mcpherson, D.; Morrow, C.; Minehan, D.; Wu, J.; Hunter, E.; Urry, D. *Biotechnol. Progr.* **1992**, *8*, 347–352.

42. Meyer, D.; Chilkoti, A. *Biomacromolecules* **2002**, *3*, 357–367.

43. Engler, C.; Gruetzner, R.; Kandzia, R.; Marillonnet, S. *PLoS One* **2009**, *4*, e5553.

44. Reyon, D.; Tsai, S. Q.; Khayter, C.; Foden, J. A.; Sander, J. D.; Joung, J. K. *Nat. Biotechnol.* **2012**, *30*, 460–465.

45. Amiram, M.; Quiroz, F. G.; Callahan, D. J.; Chilkoti, A. *Nat. Mater.* **2011**, *10*, 141–148.

46. Andersen, D. C.; Krummen, L. *Curr. Opin. Biotechnol.* **2002**, *13*, 117–123.

47. Shoseyov, O.; Posen, Y.; Grynspan, F. *Tissue Eng., Part A* **2013**, *19*, 1527–1533.

48. O'Brien, E. P.; Vendruscolo, M.; Dobson, C. M. *Nat. Commun.* **2012**, *3*, 868–875.

49. Quan, J.; Saaem, I.; Tang, N.; Ma, S.; Negre, N.; Gong, H.; White, K. P.; Tian, J. *Nat. Biotechnol.* **2011**, *29*, 449–452.

50. Chan, S. W. P.; Hung, S.-P.; Raman, S. K.; Hatfield, G. W.; Lathrop, R. H.; Da Silva, N. A.; Wang, S.-W. *Biomacromolecules* **2010**, *11*, 1460–1469.

51. Browne, S.; Zeugolis, D. I.; Pandit, A. *Tissue Eng., Part A* **2013**, *19*, 1491–1494.

52. Lajoie, M. J.; Rovner, A. J.; Goodman, D. B.; Aerni, H.-R.; Haimovich, A. D.; Kuznetsov, G.; Mercer, J. A.; Wang, H. H.; Carr, P. A.; Mosberg, J. A. *Science* **2013**, *342*, 357–360.

53. Heilshorn, S.; DiZio, K.; Welsh, E.; Tirrell, D. *Biomaterials* **2003**, *24*, 4245–4252.

54. McHale, M.; Setton, L.; Chilkoti, A. *Tissue Eng.* **2005**, *11*, 1768–1779.

55. Trabbic-Carlson, K.; Setton, L.; Chilkoti, A. *Biomacromolecules* **2003**, *4*, 572–580.

56. Schipperus, R.; Teeuwen, R.; Werten, M.; Eggink, G.; de Wolf, F. *Appl. Microbiol. Biotechnol.* **2009**, *85*, 293–301.

57. Wright, E.; McMillan, R.; Cooper, A.; Apkarian, R.; Conticello, V. *Adv. Funct. Mater.* **2002**, *12*, 57.

58. Martín, L.; Arias, F.; Alonso, M.; García-Arévalo, C.; Rodríguez-Cabello, J. *Soft Matter* **2010**, *6*, 1121–1124.

59. Chow, D.; Dreher, M.; Trabbic-Carlson, K.; Chilkoti, A. *Biotechnol. Progr.* **2006**, *22*, 638.

60. Scheller, J.; Henggeler, D.; Viviani, A.; Conrad, U. *Transgenic Res.* **2004**, *13*, 51–57.

61. Conrad, U.; Plagmann, I.; Malchow, S.; Sack, M.; Floss, D.; Kruglov, A.; Nedospasov, S.; Rose-John, S.; Scheller, J. *Plant Biotechnol. J.* **2011**, *9*, 22–31.

62. Martin, S.; Vrhovski, B.; Weiss, A. *Gene* **1995**, *154*, 159–166.

63. Wu, W.; Vrhovski, B.; Weiss, A. *J. Biol. Chem.* **1999**, *274*, 21719.

64. Huemmerich, D.; Helsen, C. W.; Quedzuweit, S.; Oschmann, J.; Rudolph, R.; Scheibel, T. *Biochemistry* **2004**, *43*, 13604–13612.

65. Stein, H.; Wilensky, M.; Tsafrir, Y.; Rosenthal, M.; Amir, R.; Avraham, T.; Ofir, K.; Dgany, O.; Yayon, A.; Shoseyov, O. *Biomacromolecules* **2009**, *10*, 2640–2645.

66. Kohl, A.; Binz, H. K.; Forrer, P.; Stumpp, M. T.; Plückthun, A.; Grütter, M. G. *Proc. Natl. Acad. Sci. U. S. A.* **2003**, *100*, 1700–1705.

67. Scheller, J.; Guhrs, K.; Grosse, F.; Conrad, U. *Nat. Biotechnol.* **2001**, *19*, 573–577.

68. MacEwan, S. R.; Chilkoti, A. *Pept. Sci.* **2010**, *94*, 60–77.

69. He, D.; Chung, M.; Chan, E.; Alleyne, T.; Ha, K. C.; Miao, M.; Stahl, R. J.; Keeley, F. W.; Parkinson, J. *Matrix Biol.* **2007**, *26*, 524–540.

70. McDaniel, J. R.; MacEwan, S. R.; Li, X.; Radford, D. C.; Landon, C. D.; Dewhirst, M. W.; Chilkoti, A. *Nano Lett.* **2014**, *14*, 2890–2895.

71. McDaniel, J. R.; Radford, D. C.; Chilkoti, A. *Biomacromolecules* **2013**, *14*, 2866–2872.

72. MacEwan, S. R.; Chilkoti, A. *Nano Lett.* **2014**, *14*, 2058–2064.

73. Ghoorchian, A.; Chilkoti, A.; Lopez, G. P. *Anal. Chem.* **2014**, *86*, 6103–6110.

74. McDaniel, J. R.; Callahan, D. J.; Chilkoti, A. *Adv. Drug Delivery Rev.* **2010**, *62*, 1456–1467.

75. Nettles, D. L.; Chilkoti, A.; Setton, L. A. *Adv. Drug Delivery Rev.* **2010**, *62*, 1479–1485.

76. Meyer, D. E.; Chilkoti, A. *Nat. Biotechnol.* **1999**, *17*, 1112–1115.

77. Hassouneh, W.; Christensen, T.; Chilkoti, A. *Curr. Protoc. Protein Sci.* **2010**, 6.11. 1–6.11. 16.

78. Hyun, J.; Lee, W.-K.; Nath, N.; Chilkoti, A.; Zauscher, S. *J. Am. Chem. Soc.* **2004**, *126*, 7330–7335.

79. Elvin, C. M.; Carr, A. G.; Huson, M. G.; Maxwell, J. M.; Pearson, R. D.; Vuocolo, T.; Liyou, N. E.; Wong, D. C. C.; Merritt, D. J.; Dixon, N. E. *Nature* **2005**, *437*, 999–1002.

80. Lyons, R.; Nairn, K.; Huson, M.; Kim, M.; Dumsday, G.; Elvin, C. *Biomacromolecules* **2009**, *10*, 3009–3014.

81. Renner, J. N.; Cherry, K. M.; Su, R. S.-C.; Liu, J. C. *Biomacromolecules* **2012**, *13*, 3678–3685.

82. Charati, M. B.; Ifkovits, J. L.; Burdick, J. A.; Linhardt, J. G.; Kiick, K. L. *Soft Matter* **2009**, *5*, 3412–3416.

83. Tokareva, O.; Jacobsen, M.; Buehler, M.; Wong, J.; Kaplan, D. L. *Acta Biomater.* **2014**, *10*, 1612–1626.

84. Teulé, F.; Miao, Y.-G.; Sohn, B.-H.; Kim, Y.-S.; Hull, J. J.; Fraser, M. J.; Lewis, R. V.; Jarvis, D. L. *Proc. Natl. Acad. Sci. U. S. A.* **2012**, *109*, 923–928.

85. Gustafson, J. A.; Price, R. A.; Frandsen, J.; Henak, C. R.; Cappello, J.; Ghandehari, H. *Biomacromolecules* **2013**, *14*, 618–625.

86. Lv, S.; Dudek, D. M.; Cao, Y.; Balamurali, M.; Gosline, J.; Li, H. *Nature* **2010**, *465*, 69–73.

87. Fang, J.; Mehlich, A.; Koga, N.; Huang, J.; Koga, R.; Gao, X.; Hu, C.; Jin, C.; Rief, M.; Kast, J. *Nat. Commun.* **2013**, *4*, 2974–2983.

88. Autore, F.; Pfuhl, M.; Quan, X.; Williams, A.; Roberts, R. G.; Shanahan, C. M.; Fraternali, F. *PloS one* **2013**, *8*, e63633.

89. Main, E. R.; Stott, K.; Jackson, S. E.; Regan, L. *Proc. Natl. Acad. Sci. U. S. A.* **2005**, *102*, 5721–5726.

90. Urvoas, A.; Guellouz, A.; Valerio-Lepiniec, M.; Graille, M.; Durand, D.; Desravines, D. C.; van Tilbeurgh, H.; Desmadril, M.; Minard, P. *J. Mol. Biol.* **2010**, *404*, 307–327.

91. Binz, H. K.; Amstutz, P.; Plückthun, A. *Nat. Biotechnol.* **2005**, *23*, 1257–1268.

92. Binz, H. K.; Stumpp, M. T.; Forrer, P.; Amstutz, P.; Plückthun, A. *J. Mol. Biol.* **2003**, *332*, 489–503.

93. Grove, T. Z.; Osuji, C. O.; Forster, J. D.; Dufresne, E. R.; Regan, L. *J. Am. Chem. Soc.* **2010**, *132*, 14024–14026.

Chapter 3

Precision Sequence Control in Bioinspired Peptoid Polymers

Jing Sun, Caroline Proulx, and Ronald N. Zuckermann[*]

Molecular Foundry, Lawrence Berkeley National Laboratory, Berkeley, California 94720
[*]E-mail: rnzuckermann@lbl.gov

'Recent advances in solid-phase organic synthesis are shrinking the gap between biopolymers and traditional polymers. It is now possible to synthesize synthetic polymers with exact control over main chain length and monomer sequence, which is leading to a new class of information-rich materials. Peptoids are a particularly promising bio-inspired polymer platform because of their highly efficient synthesis and ready availability of starting materials. Hundreds of chemically diverse side chains can be introduced from simple building blocks, allowing their properties to be finely tuned. The peptoid platform allows the systematic investigation of new materials that are intermediate between proteins and bulk polymers, in both their structure and their properties. Here we review recent examples of peptoid polymers where the polymer properties are the direct result of the specific monomer sequence.

Introduction

During the past few decades, advances in polymer synthesis have significantly increased the degree of control over their structure. Great efforts have been made on new generations of functional polymeric materials by design at the molecular level (*1–4*). However, in comparison to biological polymers, current polymerization techniques offer a lower level of structural control. Biomacromolecules, like DNA, RNA and proteins, are distinct in that they are sequence-defined – they have precise monomer sequences, and absolute monodispersity. As a result, they often have complex tertiary folded structures,

and are capable of incredibly sophisticated functions, like information storage, molecular recognition and catalysis.

Bio-inspired polymers are an emerging class of materials that borrow from the most fundamental of design rules from nature to produce chemically diverse heteropolymers of defined length and sequence. Polypeptoids are a promising class of peptidomimetic polymers based on an N-substituted glycine backbone (*5–16*). The polypeptoid has an identical backbone to a polypeptide, but the side chain is covalently attached to the amide nitrogen. It thus lacks both chirality and hydrogen-bonding capacity in the backbone (*17*, *18*), which reduces complexity and offers tremendous advantageous properties for material studies, e.g. flexibility of the main chain (*18*, *19*), processible thermal properties (*18*), and good solubility in common solvents. The properties of the polypeptoid are highly dependent on the choice of side chains that allows for simplicity and freedom of design. The polypeptoid material is also biocompatible and exhibits potent biological activities with enhanced stability to proteolysis in comparison to a polypeptide (*20–22*).

Based on the well-established Merrifield method of solid-phase peptide synthesis (SPPS), Zuckermann et al. developed a two-step submonomer synthetic method that precludes main chain protecting groups (Figure 1) (*5, 6, 23–25*). In the first step, acylation of a resin-bound amine is performed with a haloacetic acid, with bromoacetic acid being generally preferred (*26*). The second step is an S_N2-type displacement reaction with a primary amine, which introduces the side chain. As hundreds of primary amines are readily available, a tremendous range of chemical diversity of is accessible. Both steps can be undertaken under very mild conditions that allow for facile manual or automated synthesis, with most commercial peptide synthesizers being able to accomplish the synthesis of polypeptoids. Zuckermann et al. built and optimized custom robotic synthesizers for fully automated synthesis of polypeptoids (*5, 27*). With such a synthesizer, peptoid compounds can either be made in parallel or combinatorial libraries of high complexity can be synthesized by the 'mix & split' method. Combinatorial synthesis allows a very large number of peptoid chains to be generated in a single run where each individual resin bead contains a single compound (*28–30*). They have also developed mass spectrometry-based sequencing methods to sequence the peptoid on each bead, which greatly facilitates the screening of peptoids for new functions (*31, 32*).

In general, polypeptoids exhibit high coupling efficiency (> 99% per monomer addition cycle), enabling up to 50 monomers to be added sequentially in good yields (*11, 33*). However, longer chains (> 50 monomers) are challenging. Instead, the chemical conjugation of short segments has been used for the synthesis of long chains of polypeptoids (*34*). For example, azide-alkyne click chemistry was used to obtain a chain length of 100 monomers by coupling two 50mers together (*35*). It is worth mentioning that classical bulk polymerization of N-carboxyanhydrides allows for large-scale synthesis of longer chain length peptoids on a larger scale, but with less control (*13, 14, 36*).

Polypeptoids can thus be thought of as an information-rich polymer, where the structural precision of biopolymers is combined with the chemical diversity and robustness of traditional synthetic polymers. The ability to synthesize precise sequences will greatly benefit the investigation on the relationship of

structure and properties in polymeric materials on different levels, and enable further explorations of new generations of highly functional materials. In this book chapter, we will summarize recent advances in using peptoids to address fundamental issues in both polymer science and biomimetic nanoscience.
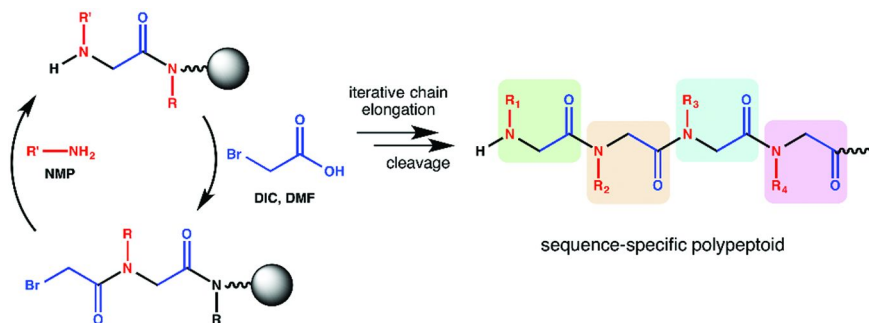
Figure 1. The solid-phase submonomer method allows the rapid synthesis of polypeptoids by a repeating two-step monomer addition cycle of acylation followed by nucleophilic S_N2 displacement with primary amines. Reproduced with permission from reference (16). Copyright (2013) American Chemical Society.

Sequence Control over Properties and Self-Assembly in Peptoid Polymers

In recent years, interest in polymer science has focused on new functional design at the molecular level (*37–40*), where precise architectural control during synthesis is key (*41–43*). Traditional polymerization techniques (e.g. radical and anionic polymerization) offer limited levels of control over chemical structures. Although many other techniques with a high-level of control have been explored (*10*, *41*, *44*, *45*), biologically inspired polymers, particularly polypeptoids, perhaps provide the most convenient platform. The sequence specificity and monodispersity of polypeptoids make them excellent candidates to elucidate the behavior of polymeric materials and the structure-property relationships.

Sequence Influence on Crystallization Behavior of Peptoid Polymers

Crystallization can strongly influence the physical properties of polymeric materials. Tunability of polymer crystallization is generally achieved through copolymerization, where comonomer content distribution in the polymer is key. Precisely controlled structure in peptoid polymers allows for different levels of control in crystallization behavior. Rosales et al. have studied the effects of comonomer compositions and distributions on crystallization behavior in series

of polypeptoids (*18*). The impact of side-chain size and comonomer distribution has been investigated. In general, it was found that increasing the side chain length induced melting temperature depression in these peptoid 15mers. For example, the addition of two carbons to the side chain depressed the melting transition by almost 15°C. Simultaneously, the crystallinity was readily controlled through the insertion of comonomers at precise locations along the polymer backbone. All of the above results are consistent with Flory's theory of crystallization (*46*). The sequence specificity leads to an increased understanding of the effects of comonomers on the crystallization behavior.

Sequence Influence on Microphase Separation of Peptoid Polymers

Microphase-separated block copolymers have a wide range of applications, such as templating, lithography and energy storage (*47*). In a diblock copolymer system A-B, the phase behavior may be controlled by three experimental parameters: the polymerization degree, the chemical composition, and the A-B Flory-Huggins parameter. All these parameters of the blocks can be readily controlled by the sequence of peptoid monomers.

One of the first microphase separation study focused on conjugates of polypeptoid with 2-methoxyethyl side chains ranging exactly from 18 to 48 monomers in length and polystyrene (*48*). These polystyrene-polypeptoid (SNme) block copolymers were shown to self-assemble into well-ordered hexagonally-packed cylinders and lamellae, as predicted by mean field theory for diblock copolymers. Furthermore, *N*-(2-phenylethyl)glycine (Npe) residues were incorporated to increase the miscibility with the polystyrene block. Despite the fact that the domain spacing of the S(Nme-Npe) diblock copolymer increased slightly, the strength of segregation decreased as the compatibility was increased.

Lately, Sun et al. designed a series of diblock co-polypeptoids with poly-*N*-2-(2-(2-methoxyethoxy)ethoxy)ethylglycine (pNte) as one of the blocks and poly-*N*-(2-ethyl)hexylglycine (pNeh) as the other block (*49*). With solid-phase synthesis, the chain length of all analogs was fixed at 36 monomers per chain, but the volume fraction of the pNte block was varied from 0.11 to 0.65 (Figure 2). This design allows the systematic investigation of the influence of side chains and monomer compositions. They are among the first groups to perform "fixed-length composition scans" on diblock copolymers that can quickly reveal interesting new phase behavior. Only lamellar and disordered morphologies were observed over the entire composition and temperature window examined. Moreover, the phase diagram of order-disorder transition temperature versus volume fraction of pNte (ϕ_{Nte}) exhibited a peak at $\phi_{Nte} = 0.24$, instead of 0.5 as expected from theory. This is possibly due to a composition-dependent parameter (χ) or the unique nature of the peptoid monomers. These results are in qualitative disagreement with all known theories of microphase separation in block copolymers that raises new questions about the intertwined roles of chemical structure of the monomer and polydispersity in the phase behavior of diblock copolymers.
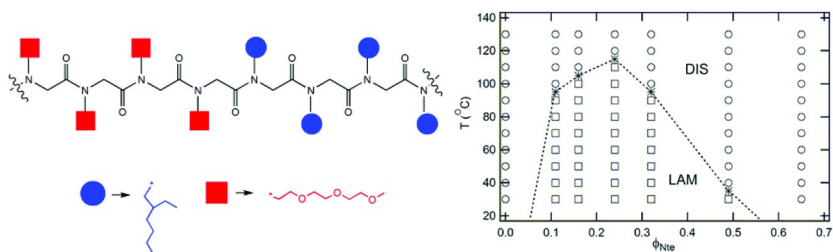
Figure 2. Structure of the diblock copolypeptoid and its phase diagram at different temperature and volume fractions, where DIS is disordered phase and LAM is lamellar phase. This unique phase diagram is different from all known theories of microphase separation in block copolymers.

Sun et al. also studied a series of crystalline diblock copolypeptoids poly-*N*-2-(2-(2-methoxyethoxy)ethoxy)ethylgly-cine (pNte)-*block*-poly-*N*-decylglycine (pNdc), where the pNdc block is crystalline (*50*). The block copolypeptoids self-assembles into a lamellar structure driven by the crystallization of the pNdc block (Figure 3). Interestingly, it is observed that the diblock copolymer can form two crystalline lamellae at room temperature, even though the pNte homopolymer is amorphous. More interestingly, the melting of both pNdc and pNte crystals is governed by the chain length of the pNdc block. This phenomenon could be due to the nearly identical molecular volumes of the side chains. The preorganization of the pNdc chains thus induces crystallization of the pNte chains. This study enhanced the understanding of block copolymer crystallization and proved that sequence-specific polypeptoid materials provide a unique platform to study the effect of composition and sequence design on physical properties and self-assembly of block copolymers.
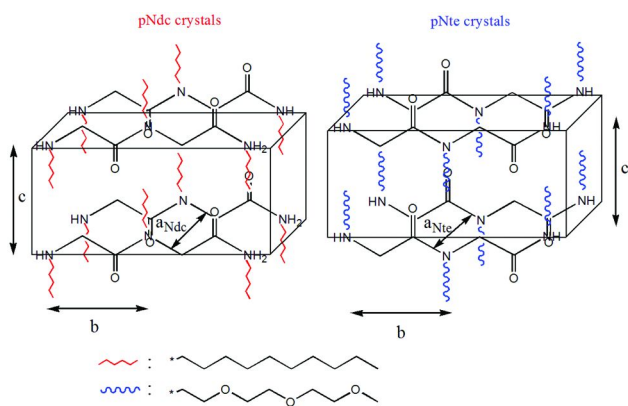
Figure 3. Two crystal structures of two blocks in diblock copolypeptoid. The formation of two crystalline lamellae at low temperatures is possible due to the nearly isosteric side chains of the two blocks. Reproduced with permission from reference (50). Copyright (2014) American Chemical Society.

Sequence Influence on Solution Self-Assembly of Peptoid Polymers

Solution self-assembly of block copolymers has been researched for years due to their potential applications in nanoscience and nanotechnology. The solid-phase synthetic approach enables highly tunable self-assembly behavior in block copolypeptoids (*51*).

Zuckermann and coworkers have developed model systems that allow controlled engineering of self-assembled structures in aqueous solution (*52*). They synthesized an amphiphilic diblock copolypeptoid system [*N*-(2-phenethyl)glycine]$_{15}$-*b*-[*N*-(2-carboxyethyl)glycine]$_{15}$ with one hydrophobic block of phenylethyl side chains and one chargeable hydrophilic block of carboxyethyl side chains. This diblock copolypeptoid first self-assembles into bilayer sheets and further twists into a superhelix structure at pH 6.5 (Fig. 4). The super helices remain remarkably robust homo-chiral structure in spite of the achiral nature of components.
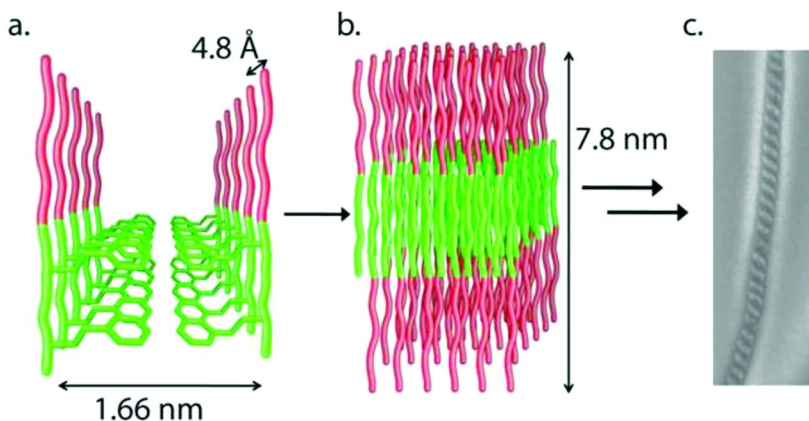
Figure 4. A model of the proposed superhelix self-assembly process. The chains initially crystallize with the aromatic groups facing each other (a). This spacing (1.66 nm) along with the distance between two chains laterally (4.8 Å) are verified in X-ray scattering. The chains further arrange into two-dimensional sheets (b) with a height of 7.8 nm as verified by AFM and X-ray scattering. The sheets are layered within the helices as evidenced by lamellar X-ray scattering of the fully formed superhelices. The green represents the hydrophobic portion of the chain while the red represents the hydrophilic block. Reproduced with permission from reference (52). Copyright (2010) American Chemical Society. (see color insert)

Solid-phase synthesis allows for facile synthesis of related analogs for investigation of the effect of ionic interactions and hydrogen bonding of the carboxyethyl side chains on the self-assembly of the superhelices. It is demonstrated that ionic interactions are critical for helix self-assembly to occur. Such systematic studies with exact structural control will benefit the study on self-assembly behavior of block copolymers in solution.

Sequence-Specific Polypeptoids for Applications in Material Science

Polypeptoid materials with precisely controlled structures and sequences are of particular interests for many applications ranging from biology to energy storage. Zoelen et al. studied tunable surface properties of polypeptoid-polystyrene block copolymers by systematically tuning the amount and sequence of fluorinated monomers for antifouling coating purposes (Figure 5) (*53*). They demonstrated that fluorinated polypeptoid chains dominated the free surface, where the presence of three fluorinated groups at the end of a 45mer peptoid chain allowed for maximal peptoid surface display. Surface reconstruction with three fluorinated groups is very fast. However, when the number of such group increases to five, it was found to be slower by an order of magnitude. They also reported a surface-exposed loop formation when fluorinated groups were located in the middle of the hydrophilic block. This study demonstrates that polypeptoid is a versatile platform for investigating surface properties of block copolymers for applications of antifouling-coating.
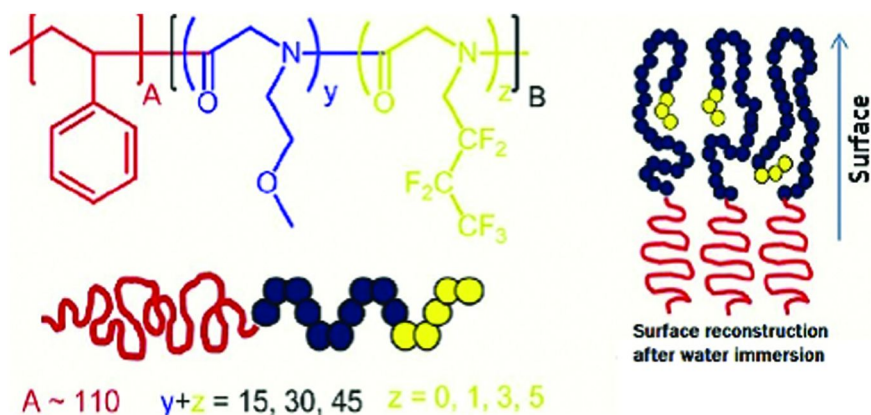
Figure 5. Schematic structures of block copolymers. Three fluorinated groups in peptoid sequences consisting of up to 45 hydrophilic monomers in length are needed to lower the surface energy of the peptoid and allow for its maximal surface segregation. Reproduced with permission from reference (53). Copyright (2012) American Chemical Society. (see color insert)

Poly(ethyleneoxide) (PEO)-based materials have received the most interest for solid polymer electrolyte application due to their high ionic conductivity. Efforts have been paid to optimize the thermal and electrical properties of such materials. Sun et al. designed a class of well-defined homopolypeptoids with controllable numbers of ethylene oxide units on the side chain (*54*). The polymer chain lengths were fixed at 20-monomers and the number of pendant (EO) units in the monomers ranged from one to three. This tunability of side chains enables the systematic study of the relationship between polymer structure and property. It was demonstrated that T_g values decreased with increasing side chain EO unit length. A very interesting crossover has been observed in the plot of T_g of

three polypeptoids versus *r* ratio (Li:EO). The ionic conductivity behavior of the complex of the polypeptoids and $Li[N(SO_2CF_3)_2]$ salt has been subsequently explored. The highest ionic conductivity of 2.6 x 10^{-4} S/cm in this study was obtained in oligo-*N*-2-(2-(2-methoxyethoxy)ethoxy)ethylglycine–Li salt complex at 100°C, which is two orders of magnitude higher than PEO-mimetic polypeptides. Moreover, it is well demonstrated that the variations in conductivity of the system at a fixed temperature and salt concentration is dominated by T_g, and not other factors such as complexation with salts or chain length of (EO) units. It is proved that polypeptoid material with fine-tuned structure will, in a long run, offer great opportunity to explore new generation materials for many applications.

Mimicking proteins and peptides, amphiphilic peptoids have been used to control growth rate and morphology of calcite as a way to sequester CO_2. In a recent study, it was found that nanomolar concentrations of amphiphilic peptoids comprised of hydrophobic and anionic monomers were capable of enhancing calcite growth by up to 23-fold (*55*). The sequence, number of acidic side-chains, main chain length, and overall hydrophobicity, all influenced the ability of peptoids to affect calcite growth rate and morphology, with a variety of unique crystal shapes being observed (e.g. elongated spindles, twisted paddles, crosses, spheres). Interestingly, closely related analogs that each contained four substituted *N*-2-phenylethyl side chains at the N-terminus and eight *N*-2-carboxyethyl side-chains at the C-terminus, exhibited dramatically different influence on calcite growth depending on the nature of the phenyl ring substituents. This illustrates that subtle changes in the side-chain chemistry are enough to tune $CaCO_3$ mineralization growth rates and crystal morphology. Given the ease of synthesis and stability of peptoids, these analogs may find utility in templating $CaCO_3$ growth for application in atmospheric CO_2 sequestration.

Sequence Control in Biomimetic Materials

Two-Dimensional Peptoid Nanosheet Synthesis and Assembly

Sequence control in solid-phase peptoid synthesis enables the rational design of peptoid polymers that have the potential to self-assemble *via* non-covalent interactions, such as ionic and aromatic interactions. Given the lack of α carbon chirality and hydrogen bond donor at the nitrogen atom, the design element in peptoids has been exclusively focused on the nature of the side-chain functional groups. The widespread commercial availability of primary amines and the automated two-step submonomer protocol for peptoid synthesis has allowed the rapid construction of combinatorial peptoid libraries, leading to the discovery of materials exhibiting interesting properties. For example, in recent efforts, the Zuckermann laboratory explored the importance of sequence patterning of polar and nonpolar residues in the peptoid chain. Hydrophobic sequence patterning is known to be one of the primary determinants of protein structure (*56*), so libraries of peptoids were prepared in which the patterns were systematically varied. Interestingly, they identified a pair of amphiphilic peptoids that self-assembled into two-dimensional, 3 nm-thick nanosheet materials that are hundreds of micrometers in length and width (Figure 6) (*57*). These complimentary sequences

alternate between ionic and hydrophobic residues, such that the hydrophilic monomers are exposed to water, whereas the aromatic monomers form the bilayer's hydrophobic core. Assembly of the nanosheets occurs under dilute physiological conditions, and produces free-floating sheets that were characterized by numerous scattering and microscopy techniques.
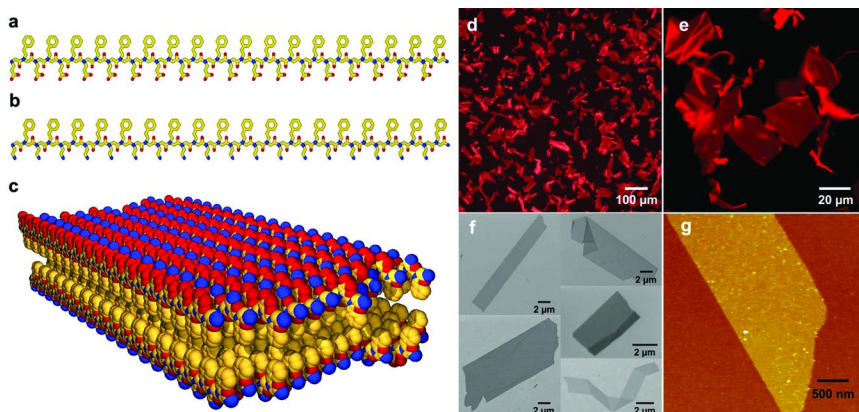
Figure 6. Two-dimensional crystalline sheets formed from two oppositely charged peptoid polymers. Atomic color scheme: carbon, yellow; nitrogen, blue; oxygen, red. (a) Chemical structure of a negatively charged periodic amphiphilic peptoid, (Nce-Npe)$_{18}$. (b) Chemical structure of a positively charged periodic amphiphilic peptoid, (Nae-Npe)$_{18}$. (c) Molecular model of the sheets assembled from (Nce-Npe)$_{18}$ and (Nae-Npe)$_{18}$. The modelled conformation shows that hydrophobic groups face each other in the interior of the sheet and oppositely charged hydrophilic groups are alternating and surface-exposed. (d) Fluorescent optical microscope image of sheets stained with Nile Red (1μM) that are free-floating in aqueous solution. (e) Fluorescent optical microscope image of individual sheets. (f) SEM images of sheets on Si substrate. (g) Height-mode AFM image of a sheet. (see color insert)

The level of precision achieved by the automated, step-wise monomer addition cycles on solid-phase enables exact control over (1) the length of the designed peptoid chains, (2) the type of side-chain functionality, and (3) the exact monomer sequence. All of these were systematically varied to elucidate the factors that govern two-dimensional nanosheet assembly (Figure 7). For example, a length series of peptoid pairs 36, 18, 12 and 6 residues in length were synthesized, demonstrated that the sheet-forming capacity of peptoids below 12 residues in length decreased significantly, and that the optimal sheet-forming motif was 36 residues in length. Similarly, varying the sequence periodicity of the polar and nonpolar monomers while fixing the main chain length to 36 gave three sets of amphiphilic peptoid pairs: twofold [(Nae-Npe)$_{18}$ and (Nce-Npe)$_{18}$], threefold [(Nae-Npe-Npe)$_{12}$ and (Nce-Npe-Npe)$_{12}$], and fourfold [(Nae-Npe-Npe-Npe)$_9$ and (Nce-Npe-Npe-Npe)$_9$] sequences. Of the three above set of peptoid pairs, only the twofold sequence pair was able to assemble into

nanosheets. Moreover, in the twofold (Nae-Npe)$_{18}$ and (Nce-Npe)$_{18}$ sheet-forming system, the polar and apolar residues were systematically substituted by a neutral hydrophilic monomer, *N*-(2-methoxyethyl)glycine (Nme), in order to elucidate the importance of the charged and aromatic residues, respectively. These control experiments confirmed the crucial role of both the electrostatic interactions of the surface-exposed residues, as well as the aromaticity of the hydrophobic core. The nature of the hydrophobic monomer was varied further to give peptoid analogs with an all-benzyl hydrophobic residue composition, conserving the aromaticity but decreasing the overall side-chain length and conformational freedom. In this case, sheets assembly was unperturbed, and the sheet thickness decreased by 2 Å as expected by X-ray diffraction (XRD).
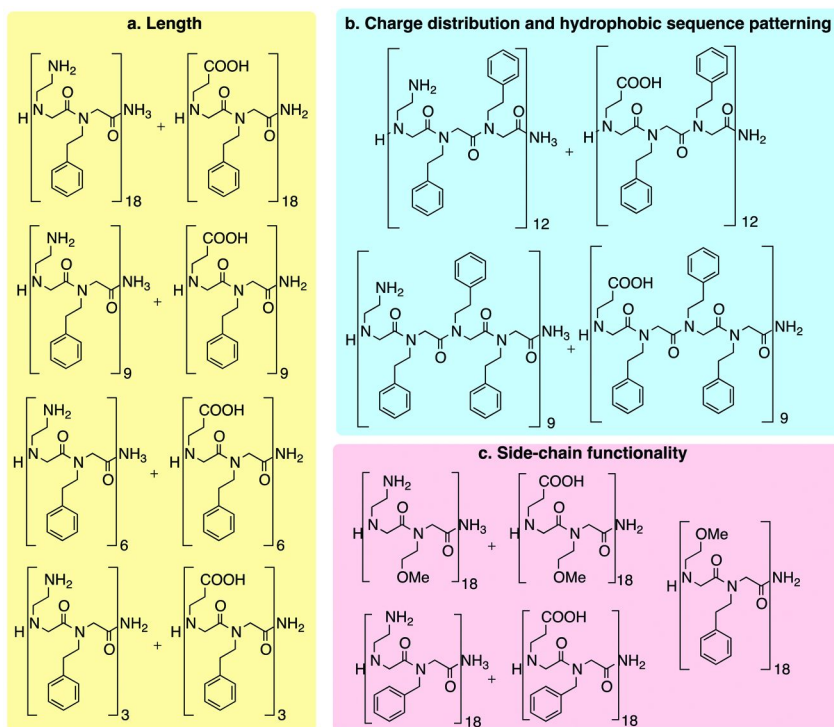
Figure 7. Peptoid sequences synthesized to study the effect of (a) length, (b) charge distribution, and (c) side-chain functionality on sheet-forming ability.

It was subsequently discovered that the nanosheet forming sequences could be simplified such that a single information-rich chain could be used to form nanosheets (*58*). A single-chain structure has a number of advantages, by avoiding the need to mix two strands, and easing the interpretation of analytical data and simplifying molecular modeling efforts. This was accomplished by combining the anionic and cationic residues into the same strand, by either (a) alternating the anionic and cationic residues in turn with the phenylethyl side-chain to give

(Nae-Npe-Nce-Npe)$_9$, or (b) by synthesizing a "block charge" peptoid, where the first half of the peptoid is positively charged and the second half is negatively charged (Nae-Npe)$_9$-(Nce-Npe)$_9$ (Figure 8).
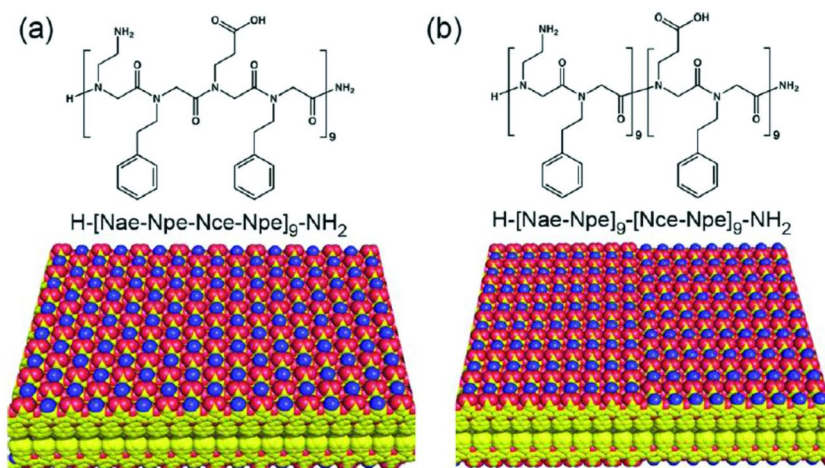
Figure 8. Single-chain peptoids that form nanosheets: (a) alternating charge and (b) block charge sequences. A model of a section of each type of sheet is shown, illustrating the differences in the proposed alignment of the chains. Although both designs can accommodate oppositely charged groups to be in close proximity, the alternating charge sheets would be expected to have less long-range order. Reproduced with permission from reference (58). Copyright (2011) Wiley. (see color insert)

Although it was found that both sequences were capable of assembling into nanosheets, differential pH and acetonitrile stability were detected in the two systems. Specifically, the nanosheets obtained from the alternating charge peptoid were less resistant to extreme pH variation and high percentage of organic solvent. The higher stability of the block charge nanosheets was rationalized by computer simulations, which showed more favorable electrostatic interactions could be achieved with this design.

Using Langmuir-trough isotherms and surface pressure measurements, a unique mechanism by which these nanosheet materials are produced was discovered (*59*). Notably, the amphiphilic peptoids were found to undergo: (1) adsorption at the air-water interface of a peptoid solution, followed by (2) compression into an ordered monolayer and (3) irreversible collapse of the monolayer to form stable, free-floating nanosheet bilayers. This process, which can occur by mechanical compression in a Langmuir-trough isotherm or by simply rotating vials from the horizontal to the vertical position using a custom-made "sheet rocker", can be repeated until over 95% of the peptoid is converted into nanosheets.

Peptoid Nanosheets as Antibody Mimetics

Given the robustness of the peptoid nanosheets, as well as the above-mentioned unique mode of assembly, it became apparent that they were ideal scaffolds for peptoid and peptide loops to be displayed on the nanosheet surface at precise intervals (*60*). As such, these materials could be designed to mimic antibodies and/or enzymes and engage in the multivalent binding of target molecules. It was envisioned that insertion of a hydrophilic sequence within a sheet-forming strand would lead to its exclusion from the bilayer scaffold during compression (Figure 9), and that positioning the loop insert in the middle would be less likely to disrupt sheet formation. In addition, a loop insert must not be too long or too hydrophobic in nature as to not hinder the adsorption at the air-water interface. Thus, precise sequence control over the position, nature, and length of the insert was an important element in designing artificial antibody mimetics.
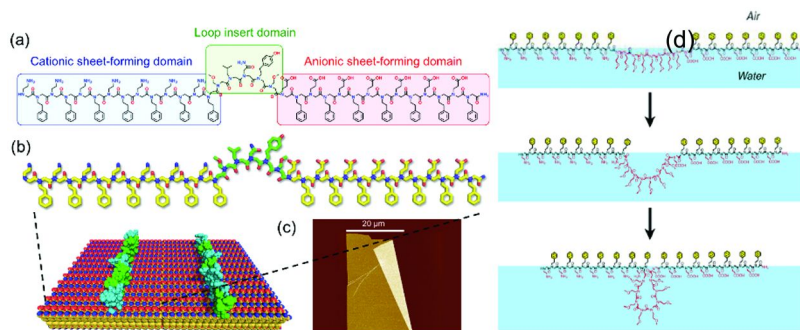
Figure 9. Peptoid nanosheets displaying a high density of conformationally constrained loops can be readily prepared by (a) flanking a random loop domain with sheet forming domains. (b) The amphiphilic pattern in the sheet-forming domains forms an extremely stable aromatic core that pushes the loop region onto the sheet surface. (c) The sheets are very uniform in structure as observed by AFM. (d) Mechanism of folding a linear peptoid sequence into a loop domain through compression of the peptoid monolayer at the air-water interface. (see color insert)

As a proof of concept, a series of 4, 8, and 12 consecutive neutral hydrophilic residues (*N*-(2-methoxyethyl)glycines, Nme) were inserted in the middle of the sheet-forming strand and tested for assembly. Expectedly, all of the above sequences formed nanosheets with predictable increases in sheet thickness and roughness detected by AFM. Using this strategy, peptidic loop-containing nanosheets could also be obtained, where the nature of the loop insert was tailored to bind protein and inorganic materials. In cases where the original

loop-containing peptoid designed was unable to form sheets, it was possible to tune the hydrophobicity of the peptoid chain by alternating biphenylethyl with phenylethyl side-chians in order to better compensate for the hydrophilic insert. The presence of peptide loops on the surface of the bilayer was confirmed by incubating the nanosheets with a mixture of proteases to selectively degrade the loop insertion, followed by AFM height measurements to corroborate a decrease in sheet thickness. Notably, the peptoid nanosheet scaffold remained intact under these harsh conditions. In addition, phosphorylation of a peptide loop substrate followed by incubation with FITC-labeled anti-phosphoserine antibody allowed fluorescent imaging of the nanosheets, thereby providing additional evidence of loop display. These materials hold great promise as molecular recognition elements for chemical and biological detection, and as templates for the growth of 2D materials. This work also highlights the importance of sequence control to predictably form a three-dimensional, antibody-like architecture from a carefully designed information-rich, linear peptoid.

Hydrophobic Sequence Patterning in Coil-to-Globule Transition

The use of peptoid polymers to study the folding process of globular proteins was recently reported, where the lack of hydrogen bond partners and chirality at the α carbon allowed for deconvolution of the hydrophobic effect from other competing factors in protein collapse (*35*). In accordance with the hydrophobic-polar (HP) protein folding model (*61*), where only two types of monomers, hydrophobic (H) and polar (P) are used, peptoid side-chains in this study were limited to either an *N*-methyl (blue, non polar) or *N*-2-carboxyethyl (red, polar) substituent (Figure 10a). Aside from the limited set of monomers used, several factors have been predicted to play important roles in globule formation, such as the H:P monomer ratio (*62*), the degree of hydrophobicity or hydrophilicity (*63*), the length of the polymer chain (*64*), the distribution of H and P monomers (*65*), as well as the ability for ionic interactions to occur. Solid phase synthesis allows precise control over all of the above parameters, with the intrinsic ability to design, synthesize, and ultimately compare peptoids with either blocky (protein-like) monomer distribution or repeating sequences (Figure 10b). Two monodisperse 50mers were ligated together to obtain a 100mer using a copper-catalyzed alkyne-azide cycloaddition reaction. The coil-to-globule transition of the two 100mers was then compared using a variety of techniques, including small angle X-ray scattering and acetonitrile titration, as well as dynamic light scattering measurements and fluorescence from environmentally sensitive dyes. These experiments revealed the formation of a tighter, more stable globule in the case of the protein-like sequence. Indeed, although both sequences appeared to form globules in aqueous solution, the protein-like sequence exhibited greater folding cooperativity by equilibrium acetonitrile titration and formed a more compact globule as determined by small-angle X-ray scattering.
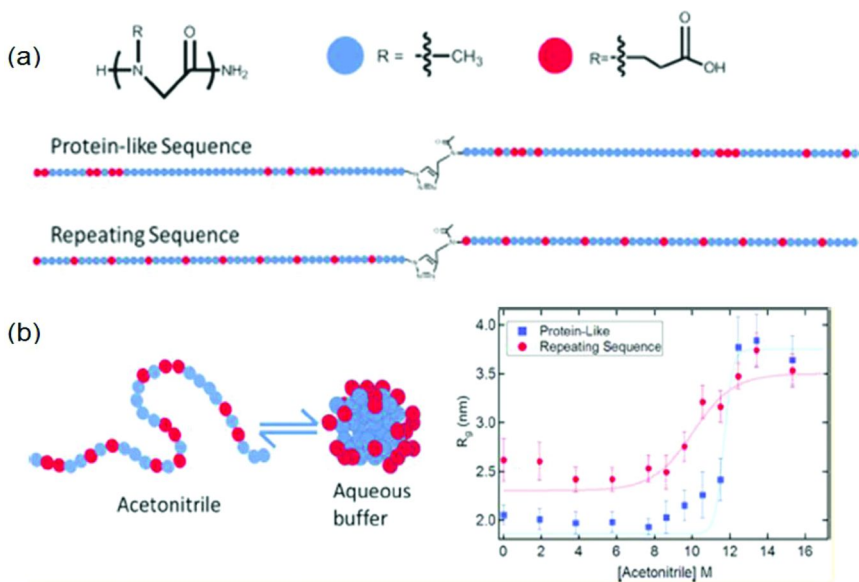
Figure 10. (a) Protein-like and repeating sequence polypeptoid 100mers. The polypeptoids were synthesized by clicking two HPLC-purified 50mers together. Each monomer is represented by a circle where the red circles are the hydrophilic and polar N-(2-carboxyethyl)glycine (P) monomer while the blue circles are non polar N-methylglycine (H) monomers. The protein-like sequence contains block sections of each type of monomer, while the repeating sequence has an even distribution of monomers. Both molecules have an identical composition of exactly 80 hydrophobic monomers and 20 hydrophilic monomers and a molecular weight of 8517 g/mol. (b) Protein-like sequence exhibited greater folding cooperativity by equilibrium acetonitrile titration and formed a more compact globule as determined by small-angle X-ray scattering. (see color insert)

Peptoid Helical Bundles

The degree of precision by which peptoid can be made has also permitted the design and synthesis of amphiphilic sequences adopting helical conformation (*51*). In this design, bulky, hydrophobic side-chains are patterned in a three-fold periodicity alternating with chiral hydrophilic monomers, and the main chain length is fixed at 15 residues to mimic the length of α helices observed in helical bundle proteins (Figure 11) (*66*). Varying the side-chain chemistry while keeping the hydrophobic patterning and main-chain length fixed, a one-bead-one compound combinatorial library was constructed using the "mix-and-split" method and a robotic synthesizer (*67*).

About 2.5% of the library in this study exhibited significant 1,8-ANS binding, which was used to assess the presence of a hydrophobic core. The MS/MS sequencing of 8 compounds revealed the importance of hydrophobic side chains with chiral α-methyl substitutions, but also found the diphenylethyl side chain to be prevalent.
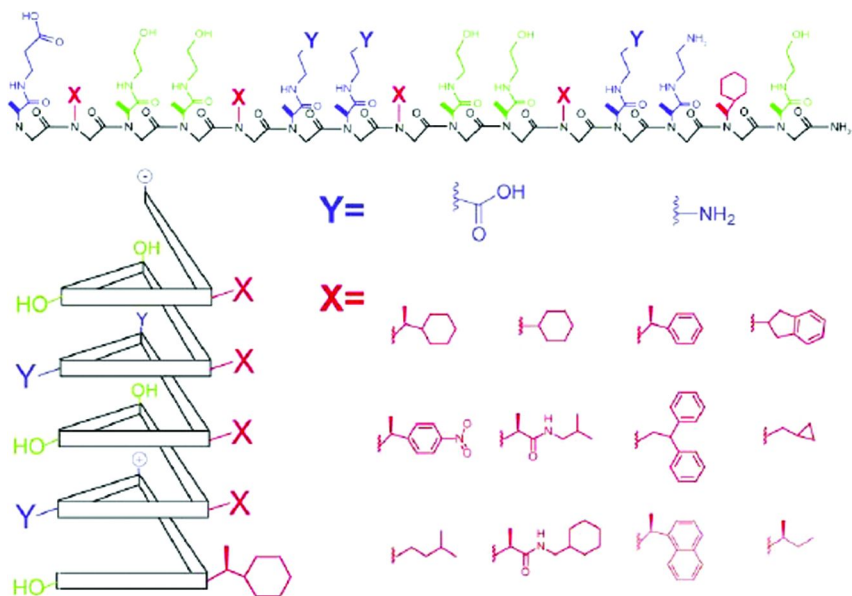
Figure 11. The 15-mer amphiphilic peptoid sequence with a 3-fold periodicity used as the combinatorial library scaffold, to screen for the assembly of helical bundles. Reproduced with permission from reference (51). Copyright (2002) Elsevier. (see color insert)

In a related study, one of the above 15mers, H-Nsace-Ndpe-Nsahe-Nsahe-Ndpe-Nsace-Nsaae-Nsch-Nsahe-Nsahe-Nspe-Nsace-Nsaae-Nsch-Nsahe-NH₂, was linked covalently together to form dimers, trimers, and tetramers *via* disulfide and oxime ligations (*34*). This approach was used to form single-chain helix bundles, where the incorporation of FRET pairs at each end facilitated the diagnosis of folded structures. It is oberved that several peptoids underwent cooperative transitions without disrupting helical secondary structure when tritrated with acetonitrile, suggesting the transitions to be a result of tertiary interactions forming a stable hydrophobic core similar to folded proteins. High affinity binding sites for zinc were later engineered into a linear peptoid sequence to obtain a functional helical bundle (*68*). Specifically, thiol and imidazole side-chains were incorporated such that zinc binding would only occur if a two-helix bundle was formed. The locations and numbers of thiols and imidazoles, as well as the monomer sequences and sizes of the loops connecting the two 15mers, were varied to enable sequence-structure-funciton relationships of zinc binding and selectivity. Some of the two-helix bundles studied were found to bind zinc with nanomolar affinity and high selectivity as compared to other divalent metal ions, such as Mg^{2+}, Mn^{2+}, Ca^{2+}, Ni^{2+}, Co^{2+}, Cu^{2+}, and Cd^{2+}.

Conclusion and Outlook

Polypeptoids are a unique, chemically diverse class of material closely related to polypeptides, in which the side-chain attachment point is shifted from the α carbon to the backbone nitrogen atom. This substitution has two major consequences: it removes chirality and a hydrogen bond donor (NH) from the backbone. Furthermore, this modification confers peptoids with an increased stability to both chemical and protease degradation. Although traditional synthetic polymers are equally robust and can be synthesized in bulk, their synthesis conditions preclude the formation of specific sequences or monodisperse polymers. Much like solid-phase peptide synthesis (SPPS), the step-wise submonomer approach for solid-phase peptoid synthesis allows polypeptoids to be synthesized with an exact length and sequence. This allows structure-properties studies to be conducted and clear design rules to be established to enforce specific behaviors and properties in peptoids (e.g. crystallization, microphase separation, self-assembly). In addition, there are hundreds of primary amines building blocks that are commercially available, enabling vast sequence diversity for the rapid discovery and tuning of novel materials.

In conjuction with experiment, tools for the predictive behavior of polypeptoids are currently being developed and have progressed tremendously in the past few years. Ramachandran plots of peptoids have been calculated and used to provide a preliminary picture of the peptoid folding landscape (*69*). The structures of several linear and cyclic peptoids have been successfully predicted using molecular dynamics simulations (*70*). Most recently, a custom forcefield derived specifically for peptoids (called MFTOID) has been developed a for CHARMM22 that enables accurate atomistic peptoid sumulations to be performed (*71*). The availability of these computational tools should begin to close the gap between experiment and prediction by dramatically enhancing the accuracy by which peptoid conformation can now be simulated. Structure prediction, in combination with the facile synthesis of peptoid polymers, sets the stage to further explore the impact of sequence-control in synthetic polymers for a wide range of applications.

Acknowledgments

References

1. Willner, I.; Zayats, M. *Angew. Chem., Int. Ed.* **2007**, *46*, 6408–6418.
2. Gomes, S.; Leonor, I. B.; Mano, J. F.; Reis, R. L.; Kaplan, D. L. *Prog. Polym. Sci.* **2012**, *37*, 1–17.
3. Shin, H.; Jo, S.; Mikos, A. G. *Biomaterials* **2003**, *24*, 4353–4364.

4. Esser-Kahn, A. P.; Iavarone, A. T.; Francis, M. B. *J. Am. Chem. Soc.* **2008**, *130*, 15820–15822.
5. Zuckermann, R. N. *Pept. Sci.* **2011**, *96*, 545–555.
6. Simon, R. J.; Kania, R. S.; Zuckermann, R. N.; Huebner, V. D.; Jewell, D. A.; Banville, S.; Ng, S.; Wang, L.; Rosenberg, S.; Marlowe, C. K. *Proc. Natl. Acad. Sci. U.S.A.* **1992**, *89*, 9367–9371.
7. Zuckermann, R. N. *Curr. Opin. Struct. Biol.* **1993**, *3*, 580–584.
8. Zuckermann, R. N.; Kodadek, T. *Curr. Opin. Mol. Ther.* **2009**, *11*, 299–307.
9. Kirshenbaum, K.; Zuckermann, R. N.; Dill, K. A. *Curr. Opin. Struct. Biol.* **1999**, *9*, 530–535.
10. Barron, A. E.; Zuckerman, R. N. *Curr. Opin. Chem. Biol.* **1999**, *3*, 681–687.
11. Murphy, J. E.; Uno, T.; Hamer, J. D.; Cohen, F. E.; Dwarki, V.; Zuckermann, R. N. *Proc. Natl. Acad. Sci. U.S.A.* **1998**, *95*, 1517–1522.
12. Lee, B. C.; Connolly, M. D.; Zuckermann, R. N. *Proc. NSTI Nanotech.* **2007**, *2*, 28–31.
13. Zhang, D.; Lahasky, S. H.; Guo, L.; Lee, C. U.; Lavan, M. *Macromolecules* **2012**, *45*, 5833–5841.
14. Luxenhofer, R.; Fetsch, C.; Grossmann, A. *J. Polym. Sci., Part A: Polym. Chem.* **2013**, *51*, 2731–2752.
15. Rosales, A. M.; Segalman, R. A.; Zuckermann, R. N. *Soft Matter* **2013**, *9*, 8400–8414.
16. Sun, J.; Zuckermann, R. N. *ACS Nano* **2013**, *7*, 4715–4732.
17. Rosales, A. M.; Murnen, H. K.; Kline, S. R.; Zuckermann, R. N.; Segalman, R. A. *Soft Matter* **2012**, *8*, 3673–3680.
18. Rosales, A. M.; Murnen, H. K.; Zuckermann, R. N.; Segalman, R. A. *Macromolecules* **2010**, *43*, 5627–5636.
19. Bradley, E. K.; Kerr, J. M.; Richter, L. S.; Figliozzi, G. M.; Goff, D. A.; Zuckermann, R. N.; Spellmeyer, D. C.; Blaney, J. M. *Mol. Divers.* **1997**, *3*, 1–15.
20. Lee, J.; Udugamasooriya, D. G.; Lim, H. S.; Kodadek, T. *Nat. Chem. Biol.* **2010**, *6*, 258–260.
21. Seo, J.; Lee, B. C.; Zuckermann, R. N. In *Comprehensive Biomaterials*; Ducheyne, P., Healy, K. E., Hutmacher, D. W., Grainger, D. W., Kirkpatrick, C. J., Eds.; Elsevier: 2011; Vol. 2, pp 53−76.
22. Fowler, S. A.; Blackwell, H. E. *Org. Biomol. Chem.* **2009**, *7*, 1508–1524.
23. Zuckermann, R. N.; Kerr, J. M.; Kent, S. B. H.; Moos, W. H. *J. Am. Chem. Soc.* **1992**, *114*, 10646–10647.
24. Zuckermann, R. N.; Figliozzi, G. M.; Banville, S. C.; Kerr, J. M.; Siani, M. A.; Martin, E. J.; Brown, E. G.; Wang, L. *Innovations and Perspectives in Solid-Phase Synthesis*; Epton, R., Ed.; Mayflower Worldwide Ltd.: Oxford, 1994; pp 397−402.
25. Uno, T.; Beausoleil, E.; Goldsmith, R. A.; Levine, B. H.; Zuckermann, R. N. *Tetrahedron Lett.* **1999**, *40*, 1475–1478.
26. Burkoth, T. S.; Fafarman, A. T.; Charych, D. H.; Connolly, M. D.; Zuckermann, R. N. *J. Am. Chem. Soc.* **2003**, *125*, 8841–8845.
27. Richter, L. S.; Spellmeyer, D. C.; Martin, E. J.; Figliozzi, G. M.; Zuckermann, R. N. *Comb. Pept. Nonpept. Libr.* **1996**, 387–404.

28. Zuckermann, R. N.; Martin, E. J.; Spellmeyer, D. C.; Stauber, G. B.; Shoemaker, K. R.; Kerr, J. M.; Figliozzi, G. M.; Goff, D. A.; Siani, M. A. *J. Med. Chem.* **1994**, *37*, 2678–2685.

29. Lam, K. S.; Lebl, M.; Krchnak, V. *Chem. Rev.* **1997**, *97*, 411–448.

30. Yu, P.; Liu, B.; Kodadek, T. *Nat. Biotechnol.* **2005**, *23*, 746–751.

31. Paulick, M. G.; Hart, K. M.; Brinner, K. M.; Tjandra, M.; Charych, D. H.; Zuckermann, R. N. *J. Comb. Chem.* **2006**, *8*, 417–426.

32. Thakkar, A.; Cohen, A. S.; Connolly, M. D.; Zuckermann, R. N.; Pei, D. *J. Comb. Chem.* **2009**, *11*, 294–302.

33. Lee, B. C.; Dill, K. A.; Zuckermann, R. N. *Polym. Prepr.* **2005**, *46*, 174–175.

34. Lee, B. C.; Zuckermann, R. N.; Dill, K. A. *J. Am. Chem. Soc.* **2005**, *127*, 10999–11009.

35. Murnen, H. K.; Khokhlov, A. R.; Khalatur, P. G.; Segalman, R. A.; Zuckermann, R. N. *Macromolecules* **2012**, *45*, 5229–5236.

36. Robinson, J. W.; Secker, C.; Weidner, S.; Schlaad, H. *Macromolecules* **2013**, *46*, 580–587.

37. Bellomo, E. G.; Wyrsta, M. D.; Pakstis, L.; Pochan, D. J.; Deming, T. J. *Nat. Mater.* **2004**, *3*, 244–248.

38. Pfeifer, S.; Zarafshani, Z.; Badi, N.; Lutz, J. F. *J. Am. Chem. Soc.* **2009**, *131*, 9195–9197.

39. Borner, H. G.; Schlaad, H. *Soft Matter* **2007**, *3*, 394–408.

40. Aida, T.; Meijer, E. W.; Stupp, S. I. *Science* **2012**, *335*, 813–817.

41. Lutz, J. F. *Nat. Chem.* **2011**, *2*, 84–85.

42. Sawamoto, M.; Kamigaito, M. *CHEMTECH (USA)* **1999**, *29*, 30–38.

43. Soeriyadi, A. H.; Boyer, C. A.; Nyström, F.; Zetterlund, P. B.; Whittaker, M. R. *J. Am. Chem. Soc.* **2011**, *133*, 11128–11131.

44. van Hest, J. C. M.; Tirrell, D. A. *Chem. Commun.* **2001**, 1897–1904.

45. Fetsch, C.; Luxenhofer, R. *Macromol. Rapid Commun.* **2012**, *33*, 1708–1713.

46. Flory, P. J. *Trans. Faraday Soc.* **1955**, *51*, 848–857.

47. Ruiz, R.; Kang, H.; Detcheverry, F. A.; Dobisz, E.; Kercher, D. S.; Albrecht, T. R.; de Pablo, J. J.; Nealey, P. F. *Science* **2008**, *321*, 936–939.

48. Rosales, A. M.; McCulloch, B. L.; Zuckermann, R. N.; Segalman, R. A. *Macromolecules* **2012**, *45*, 6027–6035.

49. Sun, J.; Teran, A. A.; Liao, X.; Balsara, N. P.; Zuckermann, R. N. *J. Am. Chem. Soc.* **2013**, *135*, 14119–14124.

50. Sun, J.; Teran, A. A.; Liao, X.; Balsara, N. P.; Zuckermann, R. N. *J. Am. Chem. Soc.* **2014**, *136*, 2070–2077.

51. Burkoth, T. S.; Beausoleil, E.; Kaur, S.; Tang, D.; Cohen, F. E.; Zuckermann, R. N. *Chem. Biol.* **2002**, *9*, 647–654.

52. Murnen, H. K.; Rosales, A. M.; Jaworski, J. N.; Segalman, R. A.; Zuckermann, R. N. *J. Am. Chem. Soc.* **2010**, *132*, 16112–16119.

53. van Zoelen, W.; Zuckermann, R. N.; Segalman, R. A. *Macromolecules* **2012**, *45*, 7072–7082.

54. Sun, J.; Stone, G. M.; Balsara, N. P.; Zuckermann, R. N. *Macromolecules* **2012**, *45*, 5151–5156.

55. Chen, C.-L.; Qi, J.; Zuckermann, R. N.; DeYoreo, J. J. *J. Am. Chem. Soc.* **2011**, *133*, 5214–5217.
56. Dill, K. A. *Biochemistry* **1990**, *29*, 7133–7155.
57. Nam, K. T.; Shelby, S. A.; Choi, P. H.; Marciel, A. B.; Chen, R.; Tan, L.; Chu, T. K.; Mesch, R. A.; Lee, B. C.; Connolly, M. D. *Nat. Mater.* **2010**, *9*, 454–460.
58. Kudirka, R.; Tran, H.; Sanii, B.; Nam, K. T.; Choi, P. H.; Venkateswaran, N.; Chen, R.; Whitelam, S.; Zuckermann, R. N. *Pept. Sci.* **2011**, *96*, 586–595.
59. Sanii, B.; Kudirka, R.; Cho, A.; Venkateswaran, N.; Olivier, G. K.; Olson, A. M.; Tran, H.; Harada, R. M.; Tan, L.; Zuckermann, R. N. *J. Am. Chem. Soc.* **2011**, *133*, 20808–20815.
60. Olivier, G. K.; Cho, A.; Sanii, B.; Connolly, M. D.; Tran, H.; Zuckermann, R. N. *ACS Nano* **2013**, *7*, 9276–9286.
61. Dill, K. A. *Biochemistry* **1985**, *24*, 1501–1509.
62. Ashbaugh, H. S. *J. Phys. Chem. B* **2009**, *113*, 14043–14046.
63. Siu, M.; Zhang, G.; Wu, C. *Macromolecules* **2002**, *35*, 2723–2727.
64. Jennings, D. E.; Kuznetsov, Y. A.; Timoshenko, E. G.; Dawson, K. A. *J. Chem. Phys.* **2000**, *112*, 7711–7722.
65. Dasmahapatra, A. K.; Nanavati, H.; Kumaraswamy, G. *J. Chem. Phys.* **2007**, *127*, 234901.
66. Presnell, S. R.; Cohen, F. E. *Proc. Natl. Acad. Sci. U.S.A.* **1989**, *86*, 6592–6596.
67. Zuckermann, R. N.; Kerr, J. M.; Siani, M. A.; Banville, S. C. *Int. J. Pept. Protein Res.* **1992**, *40*, 497–506.
68. Lee, B. C.; Chu, T. K.; Dill, K. A.; Zuckermann, R. N. *J. Am. Chem. Soc.* **2008**, *130*, 8847–8855.
69. Butterfoss, G. L.; Renfrew, P. D.; Kuhlman, B.; Kirshenbaum, K.; Bonneau, R. *J. Am. Chem. Soc.* **2009**, *131*, 16798–16807.
70. Butterfoss, G. L.; Yoo, B.; Jaworski, J. N.; Chorny, I.; Dill, K. A.; Zuckermann, R. N.; Bonneau, R.; Kirshenbaum, K.; Voelz, V. A. *Proc. Natl. Acad. Sci. U.S.A.* **2012**, *109*, 14320–14325.
71. Mirijanian, D. T.; Mannige, R. V.; Zuckermann, R. N.; Whitelam, S. *J. Comput. Chem.* **2014**, *35*, 360–370.

Chapter 4

Peptide-Polymer Conjugates as Model Systems To Explore the Functional Space of Precision Polymers

Niels ten Brummelhuis, Sebastian Wieczorek, Patrick Wilke, Thorsten Schwemmer, and Hans G. Börner*

Laboratory for Organic Synthesis of Functional Systems, Department of Chemistry, Humboldt-Universität zu Berlin, Brook-Taylor-Str. 2, D-12489 Berlin, Germany
***E-mail: h.boerner@hu-berlin.de**

Oligopeptides and peptide-polymer conjugates provide an established platform for the exploration of the influence of monomer sequence on material properties. Various methods of selecting interesting amino-acid sequences are discussed, such as bioinspired selection or exploiting phage-display and combinatorial techniques. The use of these methods in finding sequences that specifically bind to surfaces or small molecules are discussed.

Introduction

The properties of polymeric materials are strongly dependent on a wide variety of parameters, such as molecular weight, dispersity, chemical composition, stereochemistry and monomer sequence. Over the last two decades a number of methods have been developed to obtain a better control over the first three parameters, notably controlled free-radical polymerization techniques and ring-opening metathesis polymerization (*1–6*). Control over the tacticity and especially monomer sequence in synthetic polymers is still very limited, especially in chain-growth polymerizations, though a number of interesting approaches are currently being developed towards better control over these factors (*7–9*).

It might currently not be easy to produce synthetic polymers with well-defined complex monomer sequences by chain-growth polymerizations, but this goal can readily be achieved for forced step-growth polymerizations, *e.g.* via solid-phase

synthesis (*10–12*). Solid-phase synthesis methods have been widely applied to the synthesis of biopolymers (nucleic acids, peptides and sugars) but can also be applied to other monomers (*13–18*). Though limitations still exist, polymers prepared through a step-growth polymerization can therefore be used for the creation of functional materials (for applications in coatings, drug-delivery, catalysis, *etc.*) but also to evaluate the influence of monomer sequence and stereochemistry on the properties of macromolecules, thereby defining relevant goals for the control of monomer sequences in fully artificial systems.

The possibility of creating polymers with well-defined sequences faces us with the new challenge of selecting sequences that yield the properties required for a particular application. Nature has had millions of years to optimize the structure of biopolymers, something scientists typically do not have the patience for. Therefore, different methods of selection are needed. To some degree rational design can be used to introduce desired properties into a monomer sequence (*19*), but a large number of approximations and guesses are involved in this process, limiting the applicability and effectiveness.

Alternatively, one can benefit from the optimization that nature has provided by replicating certain domains from proteins with desired properties. More general methods for the development of functional sequences are phage-display (*20*) or usage of chemically prepared libraries (*21*). In both of these methods oligopeptides are displayed and sorted to find those sequences with the desired properties.

In this publication we will highlight the (dis)advantages of the various methods for the screening of monomer sequences. As examples of how such screening methods can be used to design functional materials, work focused on the binding of bioconjugates to inorganic surfaces (stainless steel and gadolinium oxide) and the drug molecule *meta*-tetra hydroxyphenyl chlorine performed in our group is compared. Some examples of the material properties that can be derived from these oligopeptides and their polymer-peptide conjugates will be discussed.

Results and Discussion

Bioinspired Design of Bioconjugates

Natural systems provide a great source of functional proteins/peptides for the development of functional materials (*22–24*). Bioinspired peptide-polymer/protein-polymer conjugates are widely used for a broad range of applications (*25*), including enzyme stabilization (*26–29*) the self-organization of bioconjugates (*30–33*), or in adhesive systems, where proteins have proved to serve as excellent interfaces between organic and inorganic materials (*34–36*).

Interesting natural adhesives are *e.g.* found in larval salivary glues used to affix the puparia of *Drosophila*, which are composed mainly of *Thr*-rich and highly glycosylated proteins (*38*). Furthermore, the sandcastle worm produces an underwater glue, in which the protein backbone is primarily composed of acidic and basic residues (*35*). Also, peptide sequences derived from adhesive proteins found in marine mussels (especially from *mytilus edulis*) are highly promising. As mussels adhere strongly to virtually any substrate under harsh conditions (high salt concentration, strong sheer conditions, *etc.*), their adhesive

proteins have been extensively studied (*39*, *40*). Figure 1a shows a simplified composition of a mussel byssus. Foot proteins mefp-3 and mefp-5 directly interact with the surface the mussel adheres to. They contain a large number of basic amino acids, *e.g.* arginine and lysine (*41*, *42*). More importantly though is a high concentration of 3,4-dihydroxyphenylalanine (Dopa) residues, which are introduced in a post-translational process from natural tyrosine (see Figure 1b). Dopa has proven to be one of the key factors for the adhesion of the mussel foot and has shown very strong adherence to metal surfaces (*43*). Nevertheless, conjugates with only Doparesidues, especially under harsh conditions, will not lead to an effective and fast coating of desired surfaces, as adhesion kinetics are strongly dependent on the peptide backbone.

Although adhesive residues are apparent throughout both mefp-3 and mefp-5, no obvious functional peptide oligomer can be extracted which is suitable for the preparation of peptide-polymer conjugates, where short peptides are desired (<15 amino acids), as proteins are expensive and solid phase peptide synthesis (SPPS) of longer peptides often proves challenging (*44*). On the other hand, mefp-1, which does not directly interact with the substrate surface but serves as a coating for the mussel byssus (*45*), contains the repetitive 10-*mer* peptide sequence AKPSYPPTYK (Y = Tyrosine, Y* = Dopa), which obviously is highly important. Therefore, conjugation of mefp-1 derived 10-mer sequence to generate peptide-polymer conjugates could very well result in efficient coating systems.

Indeed, Börner and coworkers could show that derivatives of this sequence provide excellent adhesive behavior, even resulting in efficient anti-fouling coatings (*46*, *47*). Here, the problem of dopa residues tending to side reactions, especially under basic conditions (*43*), is circumvated by *in-situ* enzymatic activation of tyrosine residues.   This can be realized by using the enzyme tyrosinase (*46*, *48*), which catalyzes the *ortho*-hydroxylation of phenols to corresponding dopa and dopa-quinone, respectively (*49*).

Although it has been shown that binding of the dopa-quinone state is weaker compared to that of dopa (*43*), peptide-polymer conjugates have proven effective in coating steel substrates. Figure 2 shows the possibility of activating the mefp-1 derived peptide polymer conjugate Pep1-PEO (AKPSYPPTYK-*block*-PEO$_{72}$) by adsorption isotherms from quartz crystal microbalance (QCM). This technique uses quartz crystals coated with *e.g.* stainless steel and measures the frequency change of the crystal during adsorption of material from a liquid phase. Whereas non-activated Pep1-PEO only adheres in a minor fashion under buffered conditions, Pep1^{Ox}-PEO (dopa-quinone state) results in an efficient coating of the steel substrate. Even more importantly, for Pep1-PEO the frequency practically returns to the initial value upon rinsing with buffer, demonstrating the full reversibility of the adhesion. By contrast, Pep1^{Ox}-PEO proved to form an irreversible coating under the experimental conditions, even withstanding extensive rinsing with model sea water solutions (599 mM NaCl). Furthermore, experiments with bovine serum albumin (BSA) and full blood serum indicate anti-fouling behavior of the coating (*46*). Therefore, an effective enzymatically triggered coating is realized.   This example highlights the potential of short peptide domains from proteins as precursors for functional peptide-polymer conjugates.

(b)

Mefp-1
261 YPPTYK **AKPSYPPTYK AKPSYPPTYK** PTYKAKPTYPSTYK
301 AKPTYPPTYK **AKPSYPPTYK AKPSYPPTYK** AKPTYI**AKPS**
341 **YPPTYK AKPSYPPTYK AKPSYPPTYK** AKSSYPPTYK AKPT
381 YKAKPTYPSYK **AKPSYPPTYK** AKPTYK

Mefp-3
1 ADYYGPNYGPPRRYGGGNYNRYNRY
26 GRRYGGYKGWNNGWNRGRRGKYW

Mefp-5
1 SSEEYKGGYYPGNAYHYHSGGSYHG
26 SGYHGGYKGKYYGKAKKYYYKYKNS
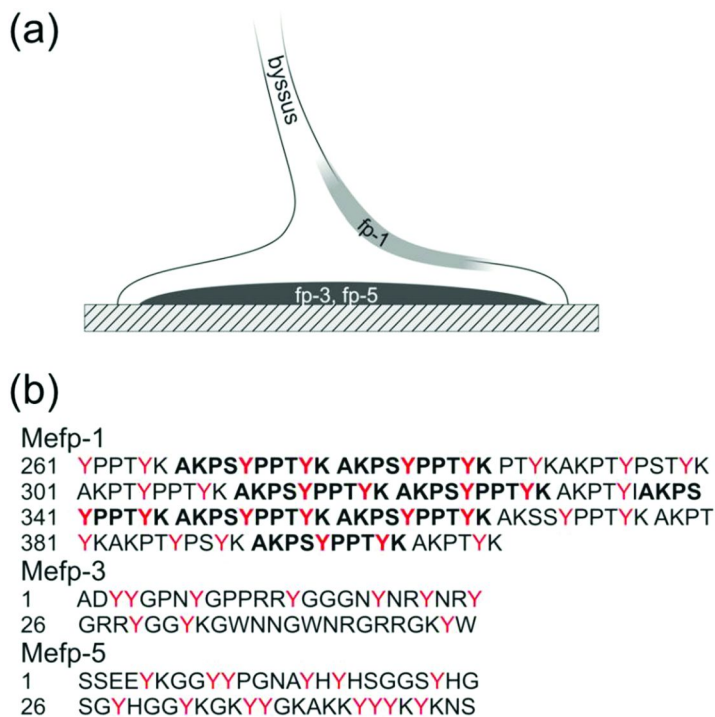
Figure 1. (a) Scheme of a mussel byssus. Foot proteins fp-3 and fp-5 directly interact with the substrate surface, whereas fp-1 serves as a protective coating for the byssal structure. (b) Excerpt from protein sequences of Mytilusedulis foot proteins mefp-1 (37), mefp-3 (41) and mefp-5 (42). Amino acid sequences printed in bold represent repeating sequences. Adapted with permission from reference (46). Copyright (2012) American Chemical Society.

Phage Display Assisted Design of Bioconjugates

Phage-display technology has been extensively used for the investigation of interactions between proteins and other biomolecules (20), but can also be utilized to find sequences interesting in material science. The technology is based on the expression of short peptides on the shell of phages. This is accomplished by introducing new DNA into the phage's genetic material, encoding an oligopeptide at the terminus of one of the coat-proteins, where it is free to interact with the target. A library of phages displaying peptides with random amino-acid sequences is exposed to a surface with *e.g.* immobilized target molecules. Phages with strongly binding domains are selected by washing cycles, a process referred to as panning (20). After elution of the phages from the surface they are typically amplified by incubation with *E. coli* and the panning process is repeated. Finally, colonies of infected *E. coli* cells are grown (each colony only multiplies one type of phage) and the amino-acid sequence of the binding peptides is deduced by evaluating the sequence of the phage DNA (Figure 3).
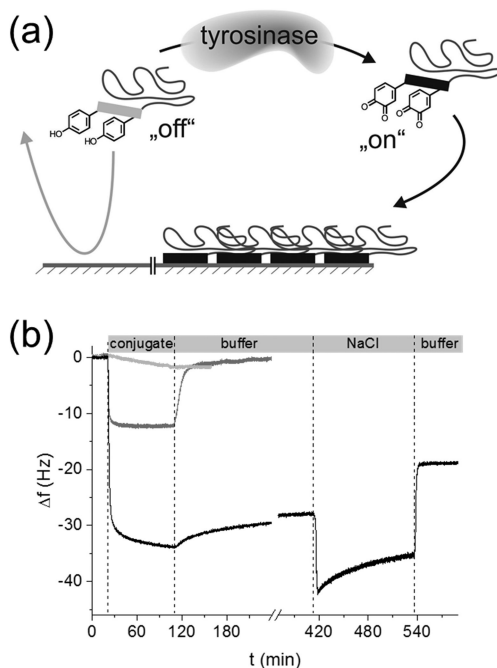
Figure 2. (a) Illustration of the mussel derived adhesive system. Whereas peptide-polymer conjugates in tyrosine-state adhere very weakly, tyrosinase processed conjugates yield an effective coating. (b) QCM adsorption of Pep1-PEO (grey), Pep1^{Ox}-PEO (black) and enzyme reference (light grey). Adapted with permission from reference (46). Copyright (2012) American Chemical Society.

In material science, phage-display technology has been used for the selection of amino-acid sequences that bind specifically to various inorganic (GaAs (*50*), AlGaAs (*50*), valerite (*51*), calcite (*52*), hydroxyapatite) and polymeric materials (*53–56*).

Recently, phage-display technology was used to find peptide sequences that specifically bind to the surface of gadolinium oxide nanoparticles (Gd$_2$O$_3$ NPs) (*57*), which present an interesting target because of their potential as contrast agents for magnetic resonance imaging (*58, 59*). Gd$_2$O$_3$ NPs with an average radius of 295 nm and an accessible surface area of ~ 16 m^2/g were obtained by fractionation from commercially available particles.

A library of M13-bacteriophages was used, which displayed randomized dodeca-peptides on the five pIII cap proteins. In this way ~ 10^9 different peptide sequences can be sampled, illustrating how many more sequences can be screened using phage-display technology as compared to *e.g.* rational design. Five panning and amplification cycles were used. Colonies of infected *E. coli* bacteria are grown and for six of these colonies the DNA was sequenced, all yielded identical amino-acid sequences: NHWSDKRAQITI.
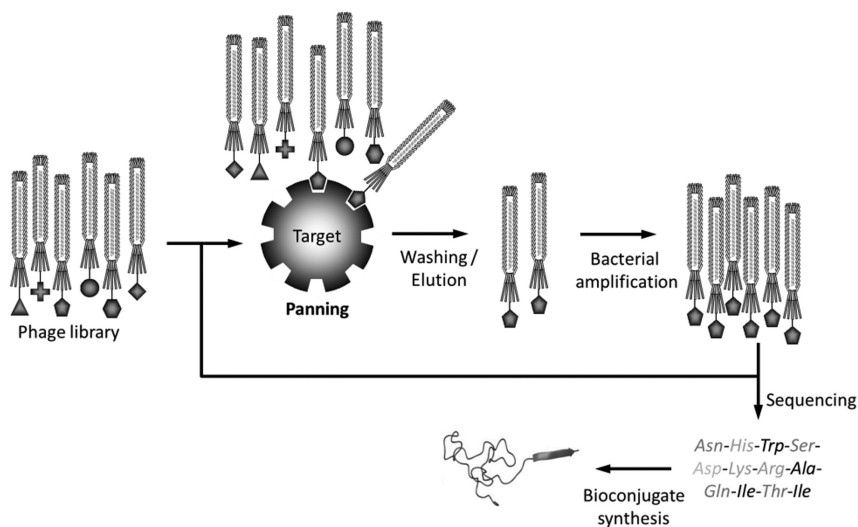
Figure 3. Generalized scheme showing phage-display technology and the synthesis of bioconjugates.

Peptides (AD, short for adhesion domain) and peptide-polymer (PEO-AD) conjugates (with a PEO block, $M_n = 3.2 \cdot 10^3$ g/mol) with this sequence were synthesized by solid-phase peptide synthesis using inverse conjugation strategies (*60*). Additionally, a fluorescent marker (carboxyfluorescein, abbreviated fam) and a spacer (two glycine residues) were incorporated, yielding fam-GG-NHWSDKRAQITI. As a control, a peptide and peptide-polymer conjugate with randomized amino-acid sequences were prepared (fam-GG-DRINASHWQTIK) (SC and PEO-SC).

Binding of these species onto Gd_2O_3 NPs was evaluated by incubation of the peptides or peptide-polymer conjugates with NPs and evaluation of the remaining fluorescence in the supernatant. After incubation the fluorescence intensity was reduced to ~43% using the peptide and ~75% for the polymer-peptide conjugate, indicating that ~57 and 25% of these species respectively absorbed onto the Gd_2O_3 surface (Figure 4). After ten washing cycles respectively 87 and 80% of the fluorescence intensity was recovered, indicating that a significant portion of the peptide could be washed of, whereas the major part of the PEO-peptide conjugate remained bound to the surface. The fact that binding of the polymer-peptide conjugates proved stronger and more specific than the binding of the native peptides might be due to a decreased tendency towards aggregation and/or changes in the conformation of the peptide. In all cases the randomized sequence resulted in far less bound material, which could be washed of quantitatively, indicating that the sequence of the peptide is key to the binding process.
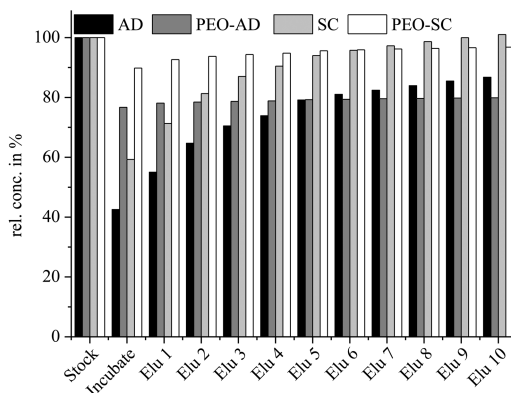
Figure 4. Cumulative adsorption/elution diagrams of peptides and bioconjugates containing the amino acid sequence found by phage display (AD and PEO-AD) and a scrambled sequence (SC and PEO-SC). Adapted with permission from reference (57). Copyright (2012) American Chemical Society.

The use of peptide-polymer conjugates allowed for the functionalization of the Gd_2O_3 NPs with a PEO layer, which can imbue the material with anti-fouling properties. This could be shown using fluorescently labeled BSA, which is known to bind to oxidic and hydrophobic surfaces. The binding of BSA could be reduced by ~80% in this way.

Though here the example of Gd_2O_3 was used, the identification of interesting peptide sequences by biocombinatorial approaches should proof a generally applicable screening method for material science applications.

Design of Bioconjugates Assisted by Combinatorial Means

Compared to natural product extracted libraries (*61*) and biocombinatorial methods such as phage display, synthetically derived compound libraries are much more widely used in pharmaceutical high-throughput screening (HTS). They can exhibit higher purity than natural extracts and a broader chemical diversity. Usually, these libraries are synthesized by combinatorial approaches (*62*), which are used to combine a set of different building blocks in all possible combinations. Solid-phase synthesis methods are very useful in this context as they allow for rapid synthesis and purification cycles compared to synthesis in solution. Especially SPOT-synthesis (where oligomers are prepared on a planar solid support (*63–65*)) and the split&mix (one-bead-one-sequence) approach are widely used.

The split&mix approach uses functionalized beads and iterative cycles of building block coupling in several batches, mixing for further processing and separation for the next coupling step. In this manner, a large number of randomized building block combinations is generated, with every bead carrying copies of only one sequence. The library size, which can be generated by split&mix synthesis is much higher than in SPOT-synthesis. Nonetheless, the immobilized compound of interest must be identified either by bead encoding techniques or by peptide cleavage from selected beads followed by downstream analysis, which is not necessary for SPOT-synthesis.

The split&mix method was exploited to identify appropriate peptide sequences for the solubilization of poorly soluble small molecules (*66*). A strong sequence specific binding between the small molecule and the peptide sequence is required for this application. To identify peptide sequences capable of binding a small molecule of interest, a screening method was established using a solid-phase bound peptide library (Figure 5). This library was prepared by standard Fmoc-strategy solid-phase peptide synthesis, providing a broad spectrum of different peptides with varying amino acid sequences. The library was composed of a set of randomized 7-*mer* peptide sequences containing hydrophobic (Leu), aromatic (Phe), polar (Ser, Gln), negatively (Glu) and positively charged (Lys) amino acids, as well as Gly, which adds flexibility to the peptide backbone. The chosen methodology yielded $\sim 8.23 \cdot 10^5$ peptide sequences.
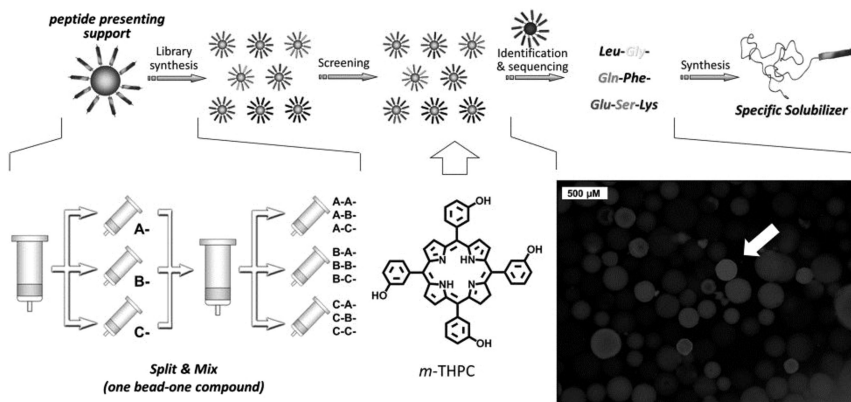
Figure 5. Schematic representation of the screening process to identify peptides sequences with high affinity for m-THPC. Adapted with permission from reference (66). Copyright (2013) American Chemical Society.

The library was screened against the binding of *meta*-tetra hydroxyphenyl chlorine (*m*-THPC), one of the most powerful second generation photosensitizers for photodynamic cancer therapy (*67–71*). *m*-THPC was partially approved for the palliative treatment of advanced head and neck cancer, but due to its strong tendency towards aggregation in aqueous media, accompanied by unpredictable pharmacokinetics, application is challenging (*72–74*).

By incubating the peptide library with *m*-THPC, enrichment of the drug on polymer beads carrying high affinity peptide sequences was followed by fluorescence microscopy, utilizing the intrinsic fluorescence of the drug (*66*). Highly fluorescent beads were collected and the peptide material was cleaved from individual beads for sequencing by MALDI-MS/MS. The peptide sequences found by screening contained, as expected, a high number of aromatic phenylalanine residues, which seem to be favorable for binding of *m*-THPC. Furthermore, hydrophobic leucine or negatively charged glutamic acid residues were found between three to four aromatic amino acids. In addition, this core motif was flanked by polar residues like glutamine or serine. Glycine and positively charged lysine were rarely included.

These findings were used to design three 7-*mer* amino acid sequences of which peptide-PEO conjugates (PI – PIII; Figure 6a) were synthesized. The PEO block was used to render the small molecules water soluble. The capacity of the conjugate for the solubilization of *m*-THPC, release behavior and drug activity were investigated.
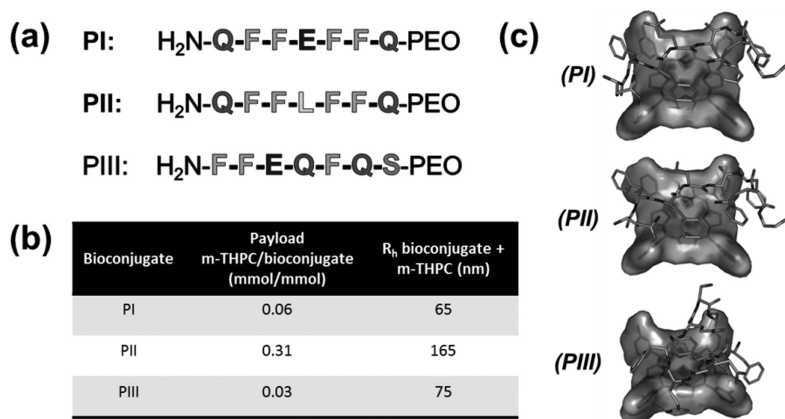
Figure 6. (a) Peptide sequences of conjugate transporters, (b) amount of m-THPC bound by each bioconjugate molecule and the hydrodynamic radius of the bioconjugate/m-THPC aggregates and (c) modeling of idealized 1:1 drug/carrier complexes (m-THPC: surface, peptides: sticks) visualizing non-covalent interactions. Adapted with permission from reference (66). Copyright (2013) American Chemical Society.

The amount of solubilized drug was determined by absorption spectroscopy of each supernatant after loading of the conjugates with *m*-THPC (Figure 6b). Conjugate PII, with the central hydrophobic leucine residues exhibited the highest payload capacity. PI and PIII, containing a central charged or a charged and a polar amino acid residue showed lower solubilization efficiency.

Drug activity, measured in terms of toxic singlet oxygen generation, is associated with fluorescence emission. Surprisingly, *m*-THPC solubilized by the selected peptide conjugates showed no fluorescence emission in aqueous

solution. The absence of drug activity was confirmed by direct singlet oxygen luminescence measurements. This effect is likely caused by aggregation (Figure 7a), which was verified by light scattering (Figure 6b). The solubilization of *m*-THPC in an aggregated and quenched state can be highly beneficial for a drug transporter systems, as the drug is silenced and inactive until it is released from the carrier. This release can take place upon transfer to proteins such as serum albumin and lipoproteins in blood (*75*). BSA was used as a model system to test the release of *m*-THPC from the conjugate carriers. The successful release could be shown by time-resolved fluorescence emission spectroscopy (Figure 7b) and the activation of the drug was confirmed by singlet oxygen luminescence (data not shown) (*66*).
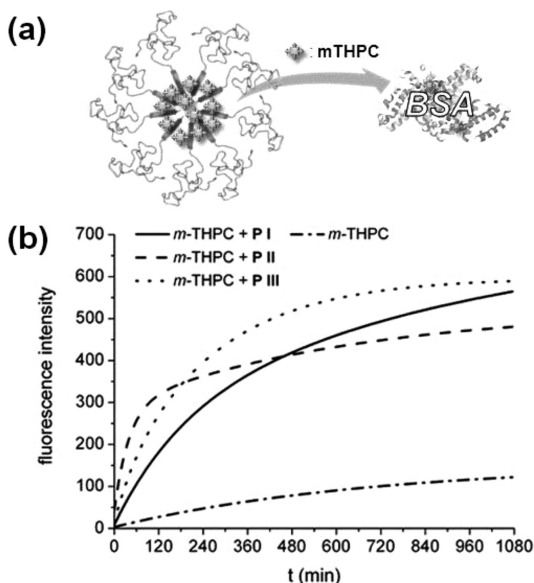
Figure 7. (a) Schematic illustration of peptide-PEO conjugates forming aggregates with m-THPC and trans-solubilization of drug to BSA. (b) Increasing fluorescence of m-THPC/solubilizer complex solutions in the presence of BSA. Adapted with permission from reference (66). Copyright (2013) American Chemical Society.

Discussion

Various methods for the selection of oligo-peptides for designing bioconjugates usefull for material science applications have been presented. Which one of these methods is most suitable depends strongly on the type of application envisioned.

If suitable, natural proteins can be found that display the property of interest, sequences from such proteins may be adopted and translated into functional oligo-

peptides in a 'top-down' approach. The challenge lies in the selection of suitable oligo-peptides from the target proteins. Unless repetitive sequences occur in the protein, identification of the relevant sequence can be extremely tedious and time consuming. Even if the relevant sequence can be identified the question remains if the fragment is still functional, as secondary and tertiary structures strongly influence the functionality.

These problems are circumvented in (bio)combinatorial ('bottom-up') approaches, where there is no need for the thorough analysis of complex biomolecules and their interactions. Furthermore, the influence of the support is minimal, as the selection is, ideally, performed in the absence of moieties that influence the 3D-structure of the peptide in solution.

There are significant differences between biocombinatorial approaches like phage display and combinatorial methods based on synthetically derived compound libraries like split&mix synthesis.

First of all, in split&mix libraries there is no need to immobilize and therefore modify the small molecule target chemically, which may alter the molecular behavior and hamper the accessibility of the target. For a split&mix library a suitable read-out signal is necessary, e.g. a colored or fluorescent probe is needed. Though such a probe can be introduced by chemical modification, this would again change the target and possibly its behavior.

The size of synthetically derived split&mix libraries that can be handled in a standard laboratory is considerably smaller regarding peptide length and numbers of amino acid combinations compared to biocombinatorial libraries, limiting the usefulness of the split&mix method to shorter sequences. Phage display requires more specialized labs with expertise and certification in handling of bacteria cultures and phage viruses though, whereas solid-phase synthesis methods can be performed in standard labs.

Another advantage of the split&mix method is that a much broader range of building blocks can be used, including unnatural amino acids, nucleobases, oligosaccharides or synthetic molecules, compared to biocombinatorial methods. In phage display, only canonical amino acids can be readily expressed by the bacterial host.

A difference can also be the number and density of peptides displayed on the particle: for phage-display systems typically only a limited number of peptides are displayed, whereas a higher density and number can be introduced on a synthetic particle. Another difference imposed by the support (*e.g.* phage or synthetic support) is the solvent and temperature compatibility. As phage capsules are protein based they can easily be denatured, a property that can be tuned for synthetic support, depending on the application.

Determining the amino acid sequence of positive hits from split&mix libraries can be accomplished rapidly and with relatively low amounts of peptide material using mass spectroscopy peptide sequencing, which is advantageous compared to Edman degradation. Still, access to a powerful MALDI-MS/MS spectrometer and expertise in peptide sequencing and proteomics analysis is necessary. Furthermore, sequencing in mass spectroscopy requires a suitable amount of sample, limiting particle size and demanding highly loaded particles. The smaller size of phages and the relative ease with which they can be multiplied

by bacteria makes larger libraries more practicable than with synthetic supports, therefore allowing quicker screening.

Additionally, repeating cycles of screening/panning steps can be realized much more easily in phage display, as it is based on a natural selection and amplification strategy. The expressed phage library is refined more towards very specific binding events with every cycle. Therefore, it is much more likely in phage display to find a distinct, specifically binding peptide sequence, whereas split&mix screening gives a broader idea of suitable binding motifs embedded in several sequences.

Conclusion

In conclusion, oligo-peptides and peptide-polymer conjugates present an interesting class of materials to investigate the influence of monomer sequence on the properties of materials. Various methodologies, such as bioinspired selection, phage-display and combinatorial methods, can be used to find amino-acid sequences with desired properties, *e.g.* for binding to surfaces or the binding of small molecules.

The use of such techniques to find sequences for a wide variety of applications has only just begun, and the potential is nearly endless. Simultaneously, the sequences that are found present promising targets for the design of synthetic equivalents with interesting properties.

Acknowledgments

References

1. Matyjaszewski, K.; Xia, J. *Chem. Rev.* **2001**, *101*, 2921–2990.
2. Moad, G.; Rizzardo, E.; Thang, S. H. *Aust. J. Chem.* **2009**, *62*, 1402–1472.
3. Hawker, C. J.; Bosman, A. W.; Harth, E. *Chem. Rev.* **2001**, *101*, 3661–3688.
4. Grubbs, R. B. *Polym. Rev.* **2011**, *51*, 104–137.
5. Braunecker, W. A.; Matyjaszewski, K. *Prog. Polym. Sci.* **2007**, *32*, 93–146.
6. Bielawski, C. W.; Grubbs, R. H. *Prog. Polym. Sci.* **2007**, *32*, 1–29.
7. Badi, N.; Lutz, J.-F. *Chem. Soc. Rev.* **2009**, *38*, 3383–3390.
8. Ouchi, M.; Badi, N.; Lutz, J.-F.; Sawamoto, M. *Nat. Chem.* **2011**, *3*, 917–924.
9. Lutz, J.-F.; Börner, H. G. *Macromol. Rapid Commun.* **2011**, *32*, 113.
10. Merrifield, B. *Methods Enzymol.* **1997**, *289*, 3–13.

11. Maude, S.; Tai, L. R.; Davies, R. P. W.; Liu, B.; Harris, S. A.; Kocienski, P. J.; Aggeli, A. *Top. Curr. Chem.* **2012**, *310*, 27–70.
12. Reese, C. B. *Org. Biomol. Chem.* **2005**, *3*, 3851–3868.
13. Franz, N.; Kreutzer, G.; Klok, H.-A. *Synlett* **2006**, *12*, 1793–1815.
14. Ponader, D.; Wojcik, F.; Beceren-Braun, F.; Dernedde, J.; Hartmann, L. *Biomacromolecules* **2012**, *13*, 1845–1852.
15. König, H. M.; Gorelik, T.; Kolb, U.; Kilbinger, A. F. M. *J. Am. Chem. Soc.* **2007**, *129*, 704–708.
16. Hartmann, L.; Börner, H. G. *Adv. Mater.* **2009**, *21*, 3425–3431.
17. Seeberger, P. H. *Chem. Soc. Rev.* **2008**, *37*, 19–28.
18. *Pseudo-peptides in Drug Discovery*; Nielsen, P. E., Ed.; Wiley-VCH: Weinheim, 2004.
19. Hirsch, A. K. H.; Diederich, F.; Antonietti, M.; Börner, H. G. *Soft Matter* **2010**, *6*, 88–91.
20. Smith, G. P.; Petrenko, V. A. *Chem. Rev.* **1997**, *97*, 391–410.
21. Kennedy, J. P.; Williams, L.; Bridges, T. M.; Daniels, R. N.; Weaver, D.; Lindsley, C. W. *J. Comb. Chem.* **2008**, *10*, 345–354.
22. Vincent, F. F. V.; Bogatyreva, O. A.; Bogatyrev, N. R.; Bowyer, A.; Pahl, A. K. *J. R. Soc. Interface* **2006**, *3*, 471–482.
23. Broyer, R. M.; Grover, G. N.; Maynard, H. D. *Chem. Commun.* **2011**, *47*, 2212–2226.
24. Lazaris, A.; Arcidiacono, S.; Huang, Y.; Zhou, J. F.; Duguay, F.; Chretien, N.; Welsh, E. A.; Soares, J. W.; Karatzas, C. N. *Science* **2002**, *295*, 472–476.
25. Börner, H. G. *Prog. Polym. Sci.* **2009**, *34*, 811–851.
26. Ryan, S. M.; Mantovani, G.; Wang, X.; Haddleton, D. M.; Brayden, D. J. *Expert Opin. Drug Delivery* **2008**, *5*, 371–383.
27. Zarafshani, Z.; Obata, T.; Lutz, J.-F. *Biomacromolecules* **2010**, *11*, 2130–2135.
28. Li, H.; Bapat, A. P.; Li, M.; Sumerlin, B. S. *Polym. Chem.* **2010**, *2*, 323–327.
29. Wilke, P.; Brooks, W. L. A.; Kühnle, R.; Sumerlin, B.; Börner, H. G. In *Progress in Controlled Radical Polymerization*; ACS Symposium Series; American Chemical Society: Washington, DC, 2012; Vol. 1101; pp 271−285.
30. Hentschel, J.; Krause, E.; Börner, H. G. *J. Am. Chem. Soc.* **2006**, *128*, 7722–7723.
31. Kühnle, H.; Börner, H. G. *Angew. Chem., Int. Ed.* **2009**, *48*, 6431–6434.
32. Kühnle, R. I.; Börner, H. G. *Angew. Chem.* **2011**, *50*, 4499–4502.
33. Börner, H. G.; Sütterlin, R. I.; Theato, P.; Wiss, K. T. *Macromol. Rapid Commun.* **2014**, *35*, 180–185.
34. Freeman, C. L.; Harding, J. H.; Quigley, D.; Rodger, P. M. *Angew. Chem.* **2010**, *122*, 5261–5263.
35. Stewart, R. J.; Wang, C. S.; Shao, H. *Adv. Colloid Interface Sci.* **2011**, *167*, 85–93.
36. Lee, B. P.; Messersmith, P. B.; Israelachvili, J. N.; Waite, J. H. *Annu. Rev. Mater. Res.* **2011**, *41*, 99–132.

37. Silverman, H. G.; Roberto, F. F. (BattelleEnergy Alliance, Llc., USA). Cloning and expression of recombinant adhesive protein Mefp-1 of the blue mussel, Mytilus edulis. US Patent 6987170-B, January, 17, 2006.
38. Lanio, W.; Swida, U.; Kress, H. *Biochim. Biophys. Acta* **1994**, *1219*, 576–580.
39. Waite, J. H.; Tanzer, M. L. *Science* **1981**, *212*, 1038–1040.
40. Lee, H.; Dellatore, S. M.; Miller, W. M.; Messersmith, P. B. *Science* **2007**, *318*, 426–430.
41. Papov, V. V.; Diamond, T. V.; Biemann, K.; Waite, J. H. *J. Biol. Chem.* **1995**, *270*, 20183–20192.
42. Hwang, D. S.; Yoo, H. J.; Jun, J. H.; Moon, W. K.; Cha, H. J. *Appl. Environ. Microbiol.* **2004**, *70*, 3352–3359.
43. Lee, H.; Scherer, N. F.; Messersmith, P. B. *Proc. Natl. Acad. Sci. U.S.A.* **2006**, *103*, 12999–13003.
44. Bray, B. L. *Nat. Rev. Drug Discovery* **2003**, *2*, 587–593.
45. Lin, Q.; Gourdon, D.; Sun, C.; Holten-Andersen, N.; Anderson, T. H.; Waite, J. H.; Israelachvili, J. N. *Proc. Natl. Acad. Sci. U.S.A.* **2007**, *104*, 3782–3786.
46. Wilke, P.; Börner, H. G. *ACS Macro Lett.* **2012**, *1*, 871–875.
47. Dalsin, J. L.; Hu, B. H.; Lee, B. P.; Messersmith, P. B. *J. Am. Chem. Soc.* **2003**, *125*, 4253–4258.
48. Burzio, L. A.; Waite, J. H. *Biochemistry* **2000**, *39*, 11147–11153.
49. Sizer, I. *Adv. Enzymol.* **1953**, *14*, 129–171.
50. Whaley, S. R.; English, D. S.; Hu, E. L.; Barbara, P. F.; Belcher, A. M. *Nature* **2000**, *405*, 665–668.
51. Roy, M. D.; Stanley, S. K.; Amis, E. J.; Becker, M. L. *Adv. Mater.* **2008**, *20*, 1830–1836.
52. Sarikaya, M.; Tamerler, C.; Schwartz, D.; Baneyx, F. *Annu. Rev. Mater. Res.* **2004**, *34*, 373–408.
53. Kase, D.; Kulp, J. L.; Yudasaka, M.; Evans, J. S.; Iijima, S.; Shiba, K. *Langmuir* **2004**, *20*, 8939–8941.
54. So, C. R.; Kulp, J. L.; Oren, E. E.; Zareie, H.; Tamerler, C.; Evans, J. S.; Sarikaya, M. *ACS Nano* **2009**, *3*, 1525–1531.
55. Weiger, M. C.; Park, J. J.; Roy, M. D.; Stafford, C. M.; Karim, A.; Becker, M. L. *Biomaterials* **2010**, *31*, 2955–2963.
56. Serizawa, T.; Matsuno, H.; Sawada, T. *J. Mater. Chem.* **2011**, *21*, 10252–10260.
57. Schwemmer, T.; Baumgartner, J.; Faivre, D.; Börner, H. G. *J. Am. Chem. Soc.* **2012**, *134*, 2385–2391.
58. Bridot, J. L.; Faure, A. C.; Laurent, S.; Rivière, C.; Billotey, C.; Hiba, B.; Janier, M.; Josserand, V.; Coll, J. L.; Elst, L. V.; Muller, R.; Roux, S.; Perriat, P.; Tillement, O. *J. Am. Chem. Soc.* **2007**, *129*, 5076–5084.
59. Na, H. B.; Song, I. C.; Hyeon, T. *Adv. Mater.* **2009**, *21*, 2133–2148.
60. Meszynska, A.; Badi, N.; Börner, H. G.; Lutz, J.-F. *Chem. Commun.* **2012**, *48*, 3887–3889.
61. Koehn, F. E.; Carter, G. T. *Nat. Rev. Drug Discovery* **2005**, *4*, 206–220.

62. Macarron, R.; Banks, M. N.; Bojanic, D.; Burns, D. J.; Cirovic, D. A.; Garyantes, T.; Green, D. V. S.; Hertzberg, R. P.; Janzen, W. P.; Paslay, J. W.; Schopfer, U.; Sittampalam, G. S. *Nat. Rev. Drug Discovery* **2011**, *10*, 188–195.

63. Frank, R. *J. Immunol. Methods* **2002**, *267*, 13–26.

64. Frank, R. *Tetrahedron* **1992**, *48*, 9217–9232.

65. Kramer, A.; Schneider-Mergener, J. In *Combinatorial Peptide Library Protocols*; Cabilly, S., Ed.; Humana Press: 1998; Vol. 87, pp 25−39.

66. Wieczorek, S.; Krause, E.; Hackbarth, S.; Röder, B.; Hirsch, A. K. H.; Börner, H. G. *J. Am. Chem. Soc.* **2013**, *135*, 1711–1714.

67. van Geel, I. P. J.; Oppelaar, H.; Oussoren, Y. G.; van Valk, M. A. D.; Stewart, F. A. *Int. J. Cancer* **1995**, *60*, 388–394.

68. Ma, L.; Moan, J.; Berg, K. *Int. J. Cancer* **1994**, *57*, 883–888.

69. Yow, C. M. N.; Chen, J. Y.; Mak, N. K.; Cheung, N. H.; Leung, A. W. N. *Cancer Lett.* **2000**, *157*, 123–131.

70. Mitra, S.; Foster, T. H. *Photochem. Photobiol.* **2005**, *81*, 849–859.

71. Bonnett, R.; Charlesworth, P.; Djelal, B. D.; Foley, S.; McGarvey, D. J.; Truscott, T. G. *J. Chem. Soc., Perkin Trans. 2* **1999**, 325–328.

72. Glanzmann, T.; Hadjur, C.; Zellweger, M.; Grosjean, P.; Forrer, M.; Ballini, J.-P.; Monnier, P.; van den Bergh, H.; Lim, C. K.; Wagnières, G. *Photochem. Photobiol.* **1998**, *67*, 596–602.

73. Braichotte, D.; Savary, J.-F.; Glanzmann, T.; Westermann, P.; Folli, S.; Wagnieres, G.; Monnier, P.; van den Bergh, H. *Int. J. Cancer* **1995**, *63*, 198–204.

74. Triesscheijn, M.; Ruevekamp, M.; Out, R.; Berkel, T. C.; Schellens, J.; Baas, P.; Stewart, F. *Cancer Chemother. Pharmacol.* **2007**, *60*, 113–122.

75. Sasnouski, S.; Zorin, V.; Khludeyev, I.; D'Hallewin, M.-A.; Guillemin, F.; Bezdetnaya, L. *Biochim. Biophys. Acta* **2005**, *1725*, 394–402.

Chapter 5

DNA-Templated Chemistries for Sequence Controlled Oligomer Synthesis

P. J. Milnes and R. K. O'Reilly*

Department of Chemistry, University of Warwick, Coventry, CV4 7AL, U.K.
***E-mail: r.k.o-reilly@warwick.ac.uk**

The development of new methods for the synthesis of sequence controlled materials is of great current interest to polymer scientists. An interesting methodology which takes inspiration from the codon-anti-codon recognition of nucleobases in the ribosome is the utilization of DNA templating synthesis. In recent years this method has been applied towards the preparation of sequence controlled oligomers. The key advances in these methods rely on the development of new DNA mechanisms and also robust chemistries which are compatible with DNA and an overview of these developments is presented in this Chapter.

Introduction

DNA achieves well-defined controlled chemistry that is at the heart of the operation of all biological systems. DNA is made of only 4 components but achieves a wide diversity of structure and activation at appropriate times in the cell cycle. Proteins similarly, though with a more complex library of *ca.* 20 components, achieve analogous diversity and control. Both of these biopolymers have complex functions and properties as a result of their specific monomer sequence. In contrast synthetic polymers can be prepared from a much broader range of monomers to afford polymers with a variety of structures and architectures, and hence a vast range of properties and diversity of applications. However, a primary limitation of current synthetic polymers is their lack of precise structure (*i.e.* sequence control) and hence complex function (*i.e.* replication and evolution).

Biological sequence controlled polymers draw important functional features and macroscopic properties from both their backbones and the specific sequence of distinct monomers. Indeed, the ordered monomer sequence of biopolymers such as DNA and polypeptides (Figure 1) is responsible for the diversity, complexity, and adaptability of life. In polypeptides (or proteins), both the choice and sequence of amino acid monomers determine macroscopic superstructure and function. Important contributions arise from the rotational flexibility and aromatic rigidity along the peptide backbone (a characteristic that is key in the formation of α-helices and β-sheets), as well as the chemical diversity of the 20 amino acid monomers (a characteristic that controls inter- and intra-molecular interactions). The potent functionalities and higher order architectures that arise from the relatively simple monomers found in biology inspire us to search for similar structures that might serve technological roles, rather than biological ones. In biology, only limited sets of monomers are utilized, consequently forming limited classes of sequence controlled polymers. The expansion of this repertoire to include diverse, synthetic monomers that are not limited to those found in nature will result in new classes of macromolecules that have extraordinarily tunable properties (*1*, *2*).
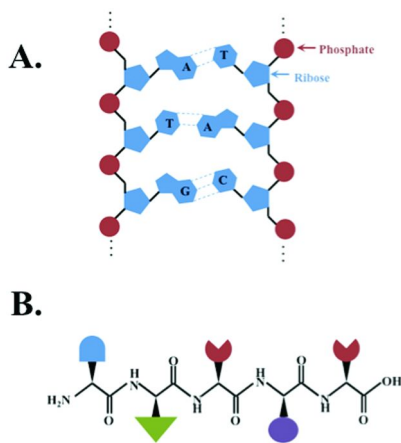
Figure 1. A. Nucleic acids are sequence controlled polymers, where the backbone and sequence endow the capacities to store, recall, and propagate information. B. Proteins are sequence controlled polymers of amino acids.

In contrast to biological polymers, chemical polymers, despite having access to a wide range of building blocks (*3*, *4*), currently give rise either to unordered structures or to a narrow range of high-order structures. We and others hypothesize that the lower level of structural sophistication and complexity displayed by synthetic polymers is, in part, because perfect sequence control has yet to be achieved (*5*). Researchers have tried to gain control of polymerization processes by inventing an incredible spectrum of polymerization processes,

initiators, monomers and precious catalysts. Yet, all of these processes have failed to produce polymers with exact compositions and sequences of functionality in a scalable manner. While bio-inspired coupling strategies have led to a variety of advanced material properties (*6–9*) and biohybrid materials (*10–14*), the inability to precisely control the order of monomer addition in a tractable manner synthetically has limited the preparation of man-made materials as complex and functional as biological assemblies. In fact, there is growing interest in the preparation of sequence controlled polymers from polymer and material scientists; indeed, it has been suggested to be the "Holy Grail" of polymer synthesis (*5*, *6*). Recently, Sawamoto has used chain-end templating and also inter-monomer templating methods to allow for access to a limited number of programmable sequence controlled materials (*7*, *8*). Pioneering work by Thomas has explored using metal catalysts to achieve alternation (*9*) and work by Lutz has explored using a kinetic strategy for controlling the microstructure of polymers to achieve good sequence control (*10*, *11*). Recent work, from Whittaker has shown that efficient controlled radical polymerization methods can be used to prepare sequence controlled polymers with good control (*12*). However, perhaps the most successful route to prepare perfect sequence defined oligomers, so far, involves using DNA templating (*15–19*) and more recently using molecular machines (*13*). This approach is efficient and whilst not currently scalable represents a key step towards achieving the goal of sequence specificity in polymer science.

DNA as a Functional Material

There is significant current interest in bio-mimetic synthesis as technologies to underpin the development of processes which are modular, scalable and crucially accessible to the broad materials community. The state of the art research, such as DNA nanotechnology (nanoscale fabrication using DNA building blocks) and DNA templated synthesis (*in vitro* replication, transcription and translation using DNA templates) currently all have a complete reliance on biological polymers. These approaches are primarily biokleptic wherein biological polymers such as nucleic acids are harvested directly from nature's toolbox in pursuit of controlled synthesis or replication. Ultimately, such a templating approach is limiting, especially when one considers inherent constraints in biological polymers such as limited building block functionality, instability in synthetic media such as non-native pH and/or ion concentrations, limited bioavailability, possible immunogenicity issues in therapeutic applications limited scalability and thus accessibility. Surprisingly, this feature of replication is almost completely absent in the chemical universe; hence, we propose expanding the scope of replication to include synthetic materials.

There are few polymers that have the same capabilities as DNA: DNA has the ability to faithfully replicate and also incorporate mutations in a quantized fashion (for example, the few peptide replicators that are known are resistant to mutation). DNA also has the ability to form sequence-dependent structures that have immense functionality, including the ability to undergo ligand-dependent conformational changes and to catalyze reactions (*14*). If other materials besides biological materials could be embedded with the same properties as DNA then

it is not unreasonable that they would be able to perform in the same ways as biological entities; not only would their morphologies be encoded in the information within, but they could repair themselves, be rebuilt or even replicate. To improve the materials interface between the chemical and biological worlds we should forego our over-reliance on natural macromolecules and embrace concepts which combine salient features of both worlds. This has been explored in recent years towards the development of materials capable of replication. However, most of the previous work in the area of self-replicating materials has not demonstrated broad scope and applicability in materials science. It has often focused on single system replication rather than on a more universal approach to make replication an achievable feature in a range of materials. Furthermore, no previous approaches have been able to generate synthetic materials with inbuilt sequence, sequence recognition, and therefore replication and evolution abilities. There has been one key report, in 2009 by Sleiman (20), on the transfer of polymerization degree from a synthetic parent to a daughter polymer using nucleobases and orthogonal polymerization. This highlights the feasibility of our proposal, but this system does not display sequence recognition. Recent work from our group, in 2012, highlights that through a combination of nucleobase templating and active site segregation high molecular weight polymers could be synthesized (15). Once again whilst this system is elegant it does not currently incorporate or enable sequence recognition.

Synthesis of Sequence Specific Oligomers

The most common strategy used by chemists to execute ordered multistep synthesis is to divide the construction of the desired molecule into a sequence of isolated reaction steps, involving: addition of reagents, purification, isolation of intermediate products and the utilization of protecting group chemistry. Standard chemical reactions are generally carried out in mM to M concentrations using particular reactants. However, in nature, specific reactions take place in the nM to µM range despite the presence of numerous reactive species. These lower concentrations minimize random intermolecular reactions and favour only those either brought into close contact with or those catalyzed by biomolecules. Multistep synthesis in single solutions is achieved by increasing the effective molarity of specific sets of reactants at precise moments during synthesis. This approach is not only remarkably elegant and efficient but also sufficiently selective to eliminate the need for protecting groups. This principle has been exploited to control the reactivity of chemical groups attached to oligonucleotide adaptors in DNA-templated organic synthesis (DTS) by modulating the effective molarity and proximity of the reactive species through DNA hybridization (for recent reviews see Li and Liu and Grossmann et al.) (17, 18) In addition, there are many chemical and biological applications related to DTS that are not possible with normal organic synthesis, such as nucleic acid sensing, sequence specific DNA modifications, the creation and assessment of molecular libraries, as well as directed evolution of molecules linked to DNA (19).

DNA-Templated Chemistry

In living organisms, DNA does not usually exist as a single molecule, but instead as a pair of molecules that are held tightly together (*20*). These two long strands entwine like vines, in the shape of a double helix (duplex). Similarly, DNA oligonucleotides with complimentary base pair sequences align themselves to form the energetically favourable duplex structure. Hybridized complementary oligonucleotide sequences are important in a number of molecular biology and chemistry applications including polymerase chain reaction (PCR) primers (*21*), nucleotide probes (*22*), gene arrays (*23*), silencing RNA (*24*), single nucleotide polymorphisms (*25*), oligonucleotide microarrarys (*26*) and DNA templated reactions (*17, 27, 28*).

It has been shown that DNA adapters linked to reactants can direct small-molecule chemical synthesis. The use of DNA hybridization to modulate the effective molarity of DNA tagged reactants allows the synthesis of molecules that cannot be accessed using traditional synthetic methods. If two reactants are linked to complementary oligonucleotides tags then hybridization of the tags ties them closely together and this can greatly increase the reaction rate (*29*).The rate enhancement can be sufficient to ensure that cross-reactions with other molecules present in the same vessel but not connected by DNA tags can be neglected (*30*). Our approach towards the synthesis of ordered oligomers is based upon a synthetic version of the ribsome. Through attaching reagents to DNA the various mechanisms of DNA have been explored to control the order and timing in which reactants are in close proximity to one another.

Many advances have been made towards this approach using the concept of DNA templated synthesis (DTS). Sequential multistep DNA templated syntheses have been controlled by stepwise addition of reagents followed by purification at each step (*28, 31*), and by controlling stepwise changes in the secondary structure of the template DNA by increasing the temperature (*32*). In order to bring the reactants in close proximity for multistep synthesis two DNA architectures are commonly employed, the end-of-helix and omega architectures (Figure 2a). Both architectures utilize short DNA sequences with reactive groups that bind to different portions of a linear template with a chemically modified end (Figure 2b). In the end-of-helix architecture the reactive ends are separated by a single-stranded sequence, with every new DNA adaptor being increasingly separated from the reactive end of the template strand. The longer distance between the reactant and the reaction center on the template can decrease the reaction efficiency after every step (*33, 34*).

This problem was addressed by Liu and co-workers by developing the omega architecture, which contains a three to five constant base pair region for all the oligonucleotide adaptors which are complementary to the end of the template strands with an intervening unbound single-stranded DNA loop. This way, every oligonucleotide adaptor has a complementary portion to the end of the template and is therefore in reactive proximity, even if it is located on a distal position in the template (*27*). However, the single-stranded loop and single-stranded portions of the template can fold into undesired secondary structures, affecting the DNA-templated reactivity (*35*). A recent approach by Hansen *et al.* utilizes

DNA three-way junctions to overcome the problems associated with using linear templates (Figure 2b) (*36*). Although this DNA system provides distance independence and constant sequence environments for the oligonucleotide adaptors, it is limited by the number of building blocks that can be employed. It would require more complicated DNA junctions to generate additional steps than the current three building block synthesis.

In all cases the current mechanisms impose a limit on the length of the multistep product oligomer. Hence, in 2010 we developed a new strategy for the synthesis of ordered functional oligomeric materials by means of sequential DNA-templated reactions, without the need for addition of reagents or the purification of intermediates (*37*). In principle this mechanism allows for the synthesis of products without a length restriction. The general mechanism is depicted in Figure 3, and involves oligonucleotide adaptors with a constant complementary region and a unique single-stranded toehold end. The reactive groups alternate between the 5′ and 3′ ends of the oligonucleotides, and annealing brings them in close proximity for the reaction to take place. The next step is the removal of the waste reagent-DNA by the addition of a fully complementary 'remover' DNA strand which forms a more energetically favorable duplex. The product which is attached to the second DNA strand now exists as a single strand and can hybridize and react with a third adaptor strand. The second adaptor is then removed by strand displacement with its complementary remover strand, allowing the cycle to be repeated for the desired number of steps to build up the targeted oligomeric sequence.
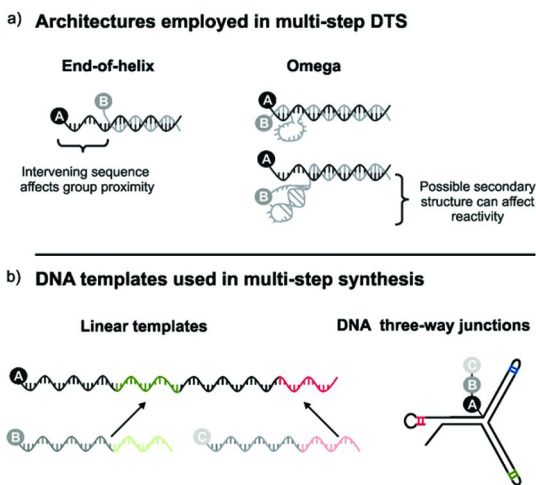
Figure 2. DNA systems employed in multi-step synthesis influence reaction efficiency. a) Distance between reactive groups and secondary structure in the end-of-helix and omega architectures affect reactivity. b) Linear templates and three-way junctions currently employed in multi-step DTS have a limit on oligomer synthesis length.
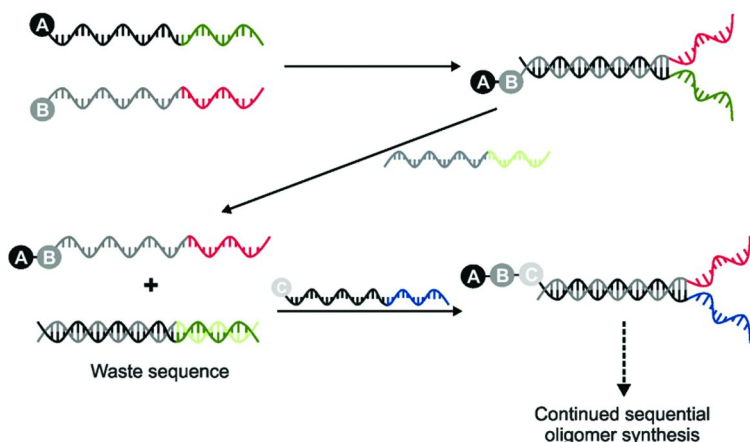
Figure 3. DNA mechanism allows for continued stepwise addition of building block units

To test if this mechanism was viable for oligomer synthesis, a series of olefin 4-mers were synthesized from three sequential DNA-templated Wittig reactions. This coupling chemistry was chosen because of its robustness in aqueous solution (*38*) and because it has been successfully used to synthesize triolefin substrates using phosphine modified oligonucleotides (*32*). The overall design for the DNA adapters used in this work is shown in Figure 4. All of the reactive oligonucleotides strands were modified with a bifunctional adapter containing both a phosphine ylide and a masked aldehyde moiety, except for the first and last adaptors of the multistep synthesis; the first adaptor contains only a phosphine modification whereas the last contains only the aldehyde moiety. The adaptor was also designed to include a tuneable handle (R) that allows for the introduction of additional functionality.
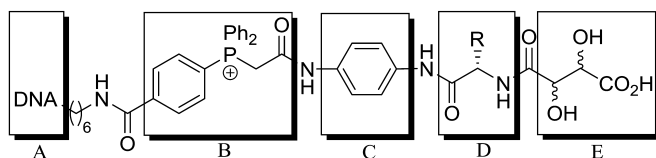
Figure 4. Design of functional DNA adapter unit. A) DNA for template control of Wittig reaction, B) triphenylphosphosphonium (ylide precusor), C) para-phenyl spacing unit (to minimize intramolecular Wittig reaction, D) function unit (amino acid), E) masked aldehyde.

The overall group transfer efficiency of the oligonucleotides adapters were assayed by synthesizing one-step olefin dimers. The desired products were observed by ESI-MS only when the aldehyde moiety was unmasked or when the

complementary adaptor was used. The main limitation to this transfer chemistry is the possible oxidation of the adaptor prior to the Wittig reaction. However, yields of around 80% for the single transfer reaction were observed. Any number of intermediate bifunctional oligonucleotide adaptors alternating between 5′ and 3′ ends can be used in the overall synthesis to make longer oligomers. In this work we explored the formation of two internal steps for the synthesis of two different olefin 4mers. In each synthesis cycle the reactants were brought together by hybridization of the oligonucleotides and the functionalities attached to the phosphine ylide were transferred to the aldehyde group of the adjacent adaptor. After the transfer reaction took place (following the 2 hr incubation per step in 0.1 M TAPS, 1M NaCl pH 8.5), the strand left with the unreactive phosphine oxide was displaced by addition of its complementary remover strand. The reaction was terminated by the addition of the final mono-aldehyde functionalized adaptor. This strand was longer in length than the rest of the DNA adaptors to facilitate analysis by PAGE. Because strand displacement is sufficient to direct the desired reactive groups in close proximity, there was no need for purification of the intermediate coupling steps. The final products were isolated from waste products by using a biotinylated remover strand fully complementary to the final sequence and purified using Streptavidin coated magnetic beads. Densitometric analysis showed 42% overall fluorescent group transfer and ESI-MS analysis confirmed the formation of the desired oligomers. However, note the scale these reactions are performed on, often yield to picomolar amounts of oligomer product.

This new DNA-templated mechanism utilizes very selective and robust templated Wittig chemistry, using bifunctional (ylide and aldehyde) adapters for the synthesis of sequence controlled oligomers. Using this new approach the introduction of additional chemical (or functional) groups into the resultant oligomers has also been demonstrated. A key feature of the mechanism involves the synthesis proceeding *via* sequential addition of templated-monomer strands; this facilitates the synthesis of oligomers which have exact control over monomer unit order. In 2012 we demonstrated that this mechanism can be extended and provides an opportunity to prepare long and functional oligomers using DNA-templated chemistries (Figure 5) (*39*).

In this report the method was adapted to be more efficient, high-yielding, quicker and more accessible for longer oligomer synthesises. This was achieved by removing the annealing steps from the DNA duplex formation, but instead relying upon spontaneous hybridization of complimentary DNA; it gave us higher average yields (88% and 85% per step) thereby making large macromolecule products a realistic target. Furthermore, removing the annealing step also allows us to use the same DNA adapter multiple times in the sequence of reactions, thus making the generation of larger products more accessible as two adapters can be added alternately to lengthen the material. We have also demonstrated that the system can carry orthogonal functionality (such as an alkyne group), which leads to the opportunity to prepare macromolecules with further product diversity. This revised method was utilized to synthesize two sequentially defined 10mers. To our knowledge these macromolecules represented the longest sequence controlled macromolecules prepared by DTS chemistries, furthermore the products are designed to allow for additional side-chain functionalization.
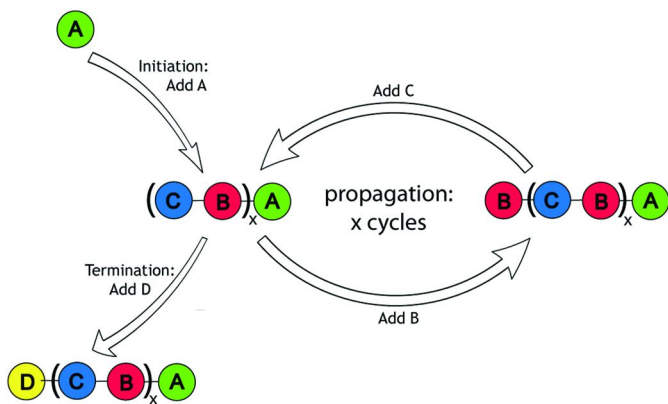
*Figure 5. Sequence-controlled synthesis of decamer **1**. Once initiated by the addition of monomer A the chain is extended by the alternating addition of B and C monomers (propagation: x = 4 cycles). The process is terminated by addition of D.*

In 2012 we reported a new DNA-templated mechanism that retains identical reaction environments for each successive coupling step but unlike our previous system, permits all reactive species to be present simultaneously in one-pot (*40*). The method also permits programmable parallel synthesis of multiple products. The system consists of oligonucleotide adapters modified with reactive groups at either the 5′ or 3′ end. Each adapter has a unique address domain and one of two short, complementary universal domains adjacent to the chemical modification. Two adapters can be linked through hybridization of their address domains to a template strand to form a three-way DNA junction: formation of this complex triggers the reaction (Figure 6). Once the reaction is complete, the template strand is removed by strand displacement using a fully complementary 'remover' strand. Coupling of further subunits are programmed by the addition of subsequent template and remover strands. Even when all of the reactive adapters are present in the same solution, they will not react until they hybridize to the correct template because the universal sequence is insufficient in length to promote stable interaction in the absence of template. The technique can therefore be applied to parallel multistep reactions, and has the potential to create complex oligomer libraries.

The mechanism can be used to synthesize oligomers using adapters with chemical modifications at either the 5′ or 3′ ends. The Wittig adapters used in this work carry either phosphonium ylide or aldehyde modification (start/stop adapters), or have both functionalities within the same adapter as described previously. An interesting aspect of the system is that the multistep reactions can be programmed to begin with either the phosphonium ylide or the aldehyde adapter as the chain starter. The choice affects the manner in which the growing oligomer is produced. When the ylide is used as the chain starter there is a transfer of the growing chain between adjacent adapters, alternating between 3′ and 5′ ends. On the other hand, if the synthesis is started with the aldehyde

adapter, the oligomer product remains covalently attached to the start adaptor throughout the series of reactions. Switching between the two mechanisms can be achieved simply by adding different template instructions strands to the same pot of reactants. Any number of intermediate steps can be programmed by using the bifunctional adapters. The reaction is ended by adding the opposing monofunctional chain terminator.

Both mechanisms were tested by programming the synthesis of two olefin 4-mers using the DNA junctions system. To facilitate polyacrylamide gel analysis, adapters varying in size from 20 to 32 nucleotides were used. In both mechanisms the final product is attached to the longest adapter, and the first adaptor contains the fluorescent group (FAM) attached as a phosphonium ylide to allow reaction progress to be monitored. Transfer of the fluorescent tag was observed between adapters in the alternating strand mechanism after the first step (by PAGE) whereas there was no change in motility of the fluorescent band until the last step using the same strand mechanism. This indicates that either mechanism can be successfully executed if the corresponding instruction set is provided. The identity of the products was confirmed by mass spectroscopy. Although incomplete products were observed in the alternating strand mechanism, no incorrect building blocks were added to the final product purified by streptavidin bead capture. Incomplete and truncated products did arise from the same strand mechanism, but again, no incorrect building blocks were added to the desired olefin (as determined by ESI-MS analysis). The main cause of the formation of truncated products is oxidation of the ylide adapters during reaction conditions.
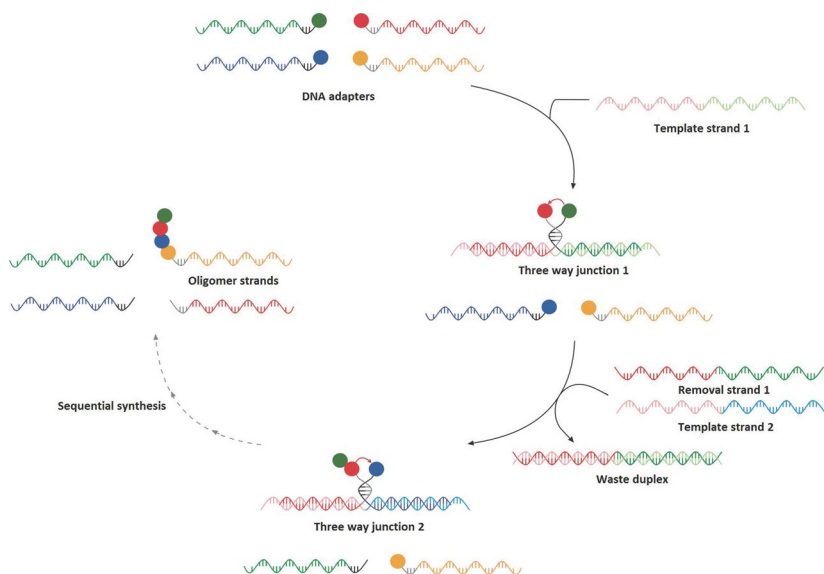
Figure 6. One-pot mechanism for templated synthesis of oligomers.
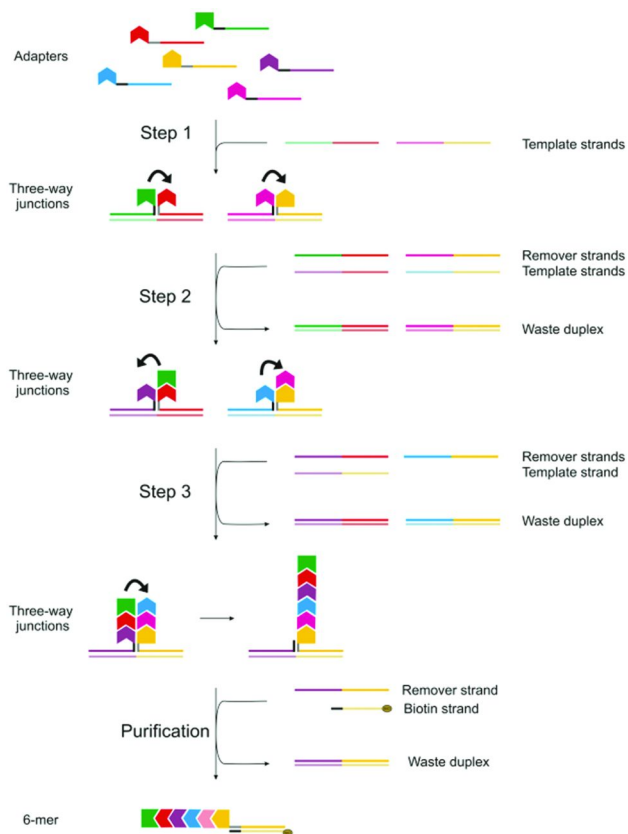
Figure 7. Two mechanisms for the synthesis of oligomers and the coupling of products generated by the same strand and alternating strand mechanism.

The programmed reaction of intermediate products can half the number of reaction steps required to make an oligomer of a given length. This feature could greatly increase the complexity of overall products being synthesized, minimizing time and steps involved required for the overall synthesis. As proof of principle a 6-mer oligomer was synthesized in 3 reaction steps. Two trimers were synthesized simultaneously, one using the alternate strand, and another the same strand mechanism. The two intermediate products were then brought together with a third template strand triggering the formation of the 6-mer olefin (Figure 7). A useful feature of the system is that it is possible to run parallel one-pot reactions, this is possible because there is no reaction between adaptors in the absence of template strands. This was demonstrated by the parallel multistep chemistry using a mixture of six different adapter strands and a series of template and remover instructions. The synthesis of two different 4-mers was programmed over 3 coupling steps in the same solution. The resulting products were purified by streptavidin bead purification and analyzed by PAGE and ESI-MS.

More recent work by Liu has demonstrated the design and implementation of a DNA-templated translation system which accurately utilises the code of a DNA template to produce biopolymers of unprecedented length and sequence specificity (*41*). Indeed, the authors have been able to close the cycle of translation to allow for the *in vitro* selection of sequence defined synthetic polymers without using enzymes. The authors use well-established copper(I) click chemistry for the coupling of building blocks through an AA/BB strategy. Previous work has demonstrated the applicability of these chemistries for efficient polymer synthesis, however, Liu's work through combination with DNA templated chemistries, shows its true potential through the introduction of sequence control. Impressively the authors report the coupling of 16 consecutive substrates to afford a synthetic polymer containing 90 β-amino acid residues in a specific sequence. Impressively, the resultant polymers have no structural relationship with nucleic acids and hence the elegance of this artificial translation system is its ready applicability to any building block unit (that is compatible with the coupling chemistries used).

Conclusions

The potential of DNA templated chemistries has been realised in recent years allowing access to oligomeric materials through a range of organic chemistries. It can be used to create intricate macromolecule libraries that can be used to select and evolve novel bioactive compounds. Indeed, perhaps this multi-step chemistry can also be adapted to make functional synthetic autonomous DNA machines and DNA motors. However, these approaches are currently somewhat limited by the scale and length of products that can be prepared. Compared to the conventional polymer synthesis approach towards sequence controlled polymers, the DNA templated approach is very different. It draws inspiration from the ribosome with its use of nucleobase code recognition combined with simple coupling chemistries for the polymer synthesis. Whereas controlled polymer synthesis strategies often utilise well-established polymerisation methods implementing control through kinetics or the chain end. The concept of DNA template chemistry is very simple and elegant but faces challenges of lack of scalability, poor atom efficiency and cost. However, developments in synthetic biology and system biology may address these challenges and enable DTS to realize its full potential as a robust and precise mechanism for the synthesis of sequence controlled materials.

References

1. Brudno, Y.; Liu, D. R. *Chem. Biol.* **2009**, *16*, 265–276.
2. Lutz, J. F. *Polym. Chem.* **2010**, *1*, 55–62.
3. Liu, C. C.; Schultz, P. G. *Annu. Rev. Biochem.* **2010**, *79*, 413–444.
4. Wang, L.; Xie, J.; Schultz, P. G. *Annu. Rev. Biophys. Biomol. Struct.* **2006**, *35*, 225–249.
5. Badi, N.; Lutz, J. F. *Chem. Soc. Rev.* **2009**, *38*, 3383–3390.
6. Hartmann, L.; Börner, H. G. *Adv. Mater.* **2009**, *21*, 3425–3431.

7. Hibi, Y.; Ouchi, M.; Sawamoto, M. *Angew. Chem., Int. Ed.* **2011**, *50*, 7434–7437.
8. Hibi, Y.; Tokuoka, T.; Terashima, M.; Ouchi, M.; Sawamoto, M. *Polym. Chem.* **2011**, *2*, 341–347.
9. Kramer, J. W.; Treitler, D. S.; Dunn, E. W.; Castro, P. M.; Roisnel, T.; Thomas, C. M.; Coates, G. W. *J. Am. Chem. Soc.* **2009**, *131*, 16042–16044.
10. Lutz, J. F. *Macromol. Rapid Commun.* **2011**, *32*, 127–135.
11. Zamfir, M.; Lutz, J. F. *Nat, Commun.* **2012**, *3*, 1138.
12. Soeriyadi, A. H.; Boyer, C.; Nystrom, F.; Zetterlund, P. B.; Whittaker, M. R. *J. Am. Chem. Soc.* **2011**, *133*, 11128–11131.
13. Lewandowski, B.; Bo, G. D.; Ward, J. W.; Papmeyer, M.; Kuschel, S.; Aldegunde, M. J.; Gramlich, P. M. E.; Heckmann, D.; Goldup, S. M.; D'Souza, D. M.; Fernandes, A. E.; Leigh, D. A. *Science* **2013**, *339*, 189–193.
14. Boersma, A. J.; Megens, R. P.; Feringa, B. L.; Roelfes, G. *Chem. Soc. Rev.* **2010**, *39*, 2083–2092.
15. Sleiman, H. F.; Lo, P. K. *J. Am. Chem. Soc.* **2009**, *131*, 4182–4183.
16. McHale, R.; Patterson, J. P.; Setterland, P.; O'Reilly, R. K. *Nat. Chem.* **2012**, *4*, 491–497.
17. Grossmann, T. N.; Strohbach, A.; Seitz, O. *Chem. Biol. Chem.* **2008**, *9*, 2185–2192.
18. Li, X.; Liu, D. R. *Angew. Chem., Int. Ed.* **2004**, *43*, 4848–4870.
19. Rozenman, M. M.; McNaughton, B. R.; Liu, D. R. *Curr. Opin. Chem. Biol.* **2007**, *11*, 259–268.
20. Watson, J. D.; Crick, F. H. C. *Nature* **1953**, *171*, 737–738.
21. Bulat, S. A.; Mironenko, N. V. *Genetika* **1996**, *32*, 165–183.
22. Jung, K. H.; Marx, A. *Cell. Mol. Life Sci.* **2005**, *62*, 2080–2091.
23. Brentani, R. R.; Carraro, D. M.; Verjovski-Almeida, S.; Reis, E. M.; Neves, E. J.; de Souza, S. J.; Carvalho, A. F.; Brentani, H.; Reis, L. F. L. *Crit. Rev. Oncology Hematology* **2005**, *54*, 95–105.
24. Csorba, T.; Pantaleo, V.; Burgyan, J. *Adv. Virus Res.* **2009**, *75*, 35–71.
25. Drago, F.; Karpasitou, K.; Poli, F *Transfusion Med. Hemother.* **2009**, *36*, 157–160.
26. Auburn, R. P.; Kreil, D. P.; Meadows, L. A.; Fischer, B.; Matilla, S. S.; Russell, S. *Trends Biotechnol.* **2005**, *23*, 374–379.
27. Gartner, Z. J.; Grubina, R.; Calderone, C. T.; Liu, D. R. *Angew. Chem., Int. Ed.* **2003**, *42*, 1370–1375.
28. Gartner, Z. J.; Tse, B. N.; Grubina, R.; Doyon, J. B.; Snyder, T. M.; Liu, D. R. *Science* **2004**, *305*, 1601–1605.
29. Gartner, Z. J.; Liu, D. R. *J. Am. Chem. Soc.* **2001**, *123*, 6961–6963.
30. Calderone, C. T.; Puckett, J. W.; Gartner, Z. J.; Liu, D. R. *Angew. Chem., Int. Ed.* **2002**, *41*, 4104–4108.
31. Gartner, Z. J.; Kanan, M. W.; Liu, D. R. *J. Am. Chem. Soc.* **2002**, *124*, 10304–10306.
32. Snyder, T. M.; Liu, D. R. *Angew. Chem., Int. Ed.* **2005**, *44*, 7379–7382.
33. McKee, M. L.; Evans, A. C.; Gerrard, S. R.; O'Reilly, R. K.; Turberfield, A. J.; Stulz, E. *Org. Biomol. Chem.* **2011**, *9*, 1661–1666.

34. Gartner, Z. J.; Kanan, M. W.; Liu, D. R. *Angew. Chem., Int. Ed.* **2002**, *41*, 1796–1800.
35. Snyder, T. M.; Tse, B. N.; Liu, D. R. *J. Am. Chem. Soc.* **2008**, *130*, 1392–1401.
36. Hansen, M. H.; Blakskjaer, P.; Petersen, L. K.; Hansen, T. H.; Hojfeldt, J. W.; Gothelf, K. V.; Hansen, N. J. V. *J. Am. Chem. Soc.* **2009**, *131*, 1322–1327.
37. McKee, M. L.; Milnes, P.; Bath, J.; Stulz, E.; Turberfield, A. J.; O'Reilly, R. K. *Angew. Chem., Int. Ed.* **2010**, *49*, 7948–7951.
38. Dambachera, J.; Zhaoa, W.; El-Battaa, A.; Annessa, R.; Jianga, C.; Bergdahl, M. *Tetrahedron Lett.* **2005**, *46*, 4473–4477.
39. Milnes, P. J.; McKee, M. L.; Bath, J.; Song, L.; Stulz, E.; Turberfield, A. J.; O'Reilly, R. K. *Chem. Commun.* **2012**, 5614–5616.
40. McKee, M.; Milnes, P.; Bath, J.; Stulz, E.; O'Reilly, R. K.; Turberfield, A. J. *J. Am. Chem. Soc.* **2012**, *134*, 1446–1449.
41. Niu, J.; Hili, R.; Liu, D. R. *Nat. Chem.* **2013**, *5*, 282–292.

Chapter 6

Recent Advances in Solid Phase Polymer Synthesis: Polyamides from Tailor-Made Building Blocks

Felix Wojcik, Daniela Ponader, Simone Mosca, and Laura Hartmann*

Max Planck Institute of Colloids and Interfaces, Department of Biomolecular Systems, Research Campus Golm, 14424 Potsdam, Germany
***E-mail: laura.hartmann@mpikg.mpg.de**

In this chapter, we discuss the use of solid phase synthesis for the preparation of monodisperse, sequence-defined polymers. Special focus is devoted to the synthesis of polyamides from tailor-made building blocks using standard peptide coupling protocols. This strategy allows for the straightforward and fully automated synthesis of polymers with varying properties and functionalities. As examples of a bioactive, highly functional polymer classes, the solid phase synthesis of so-called precision glycomacromolecules and peptidomimetics will be discussed in detail.

Introduction

Many of the advanced functionalities of synthetic polymers are inspired by their natural analogues, the biopolymers. However, synthetic polymers still cannot reach the level of complexity e.g. of an enzyme or an antibody. The limiting factor is not the functional groups that can be introduced into a polymer chain, but rather the precise positioning of these functionalities. While biopolymers only use a small library of functional building blocks, e.g. amino acids, they can build up structures with defined chain length and sequence-defined positioning of the functional groups. Such precision is not yet achievable for synthetic polymers but, if realized, it can be expected to lead to novel materials with superior properties, in particular in biomaterials and biomedicine. As of yet, the interactions of a synthetic polymer with a biological surrounding are not well understood and most systems so far are empirically optimized. In this regard,

well defined, monodisperse or even sequence-defined polymers could help to gain a deeper insight into the structure-property correlation for synthetic materials in biology and medicine.

Solid Phase Synthesis in Bioorganic Chemistry

While the synthesis of monodisperse, sequence-defined *synthetic* polymers remains a challenging task (*1*, *2*) their natural analogues, the biopolymers, are synthesized with perfect monodispersity and sequence-control: In bioorganic chemistry, peptides (*3*), oligonucleotides (*4*, *5*) and an increasing amount of oligosaccharides (*6*, *7*) are commonly accessed *via* solid phase synthesis as this synthetic strategy allows for precise positioning of building blocks within a polymer chain. Furthermore, solid phase synthesis can be fully automated and traditional bottlenecks in work up and purification have been successfully addressed. Introduced in the 1960s by Merrifield et al (*3*), the solid phase peptide synthesis (SPPS) has since developed as the standard synthetic procedure to obtain peptides, not only on lab-scale but also in industry, e.g. for the synthesis of Enfuvirtide or Fuzeon® (Roche), a 36mer, used in combination therapy for the treatment of HIV-1 infection (*8*). The key component for SPPS is the solid phase, often a polystyrene based resin, functionalized with specifically cleavable linkers and functional groups. This solid support allows for the stepwise addition of the monomers or building blocks, the straightforward removal of excess reagents *via* filtration and fully automated handling *via* a simple set-up of pumps and valves. The second key component is the monomer or building block along with a highly sophisticated set of protecting groups. For SPPS an Fmoc-based strategy has developed as standard protocol for peptide synthesis, where Fmoc-groups are used as temporary protecting groups during activation and coupling of the amino acid to the resin (*9*). After complete addition of the first monomer, the Fmoc-group is cleaved and the second monomer can be added. All other functional groups in the side chains of the monomer must carry protecting groups that are only released during the final cleavage of the desired product from the resin. The third and final key component of SPPS is the coupling reagent. Since every coupling step has to proceed with > 99.9% efficiency in order to obtain the desired monodisperse, sequence-defined product in the end, activation reagents have to maximize conjugation and minimize undesired side reactions. These requirement are readily fulfilled for the amide bond formation in SPPS and there exists a large variety of activation reagents which are commercially available guaranteeing high coupling efficiencies (*10*, *11*).

Solid Phase Polymer Synthesis

Inspired by the solid phase synthesis of natural macromolecules (e.g. peptides, DNA), automated solid phase technology has since been applied also for the synthesis of artificial macromolecular structures that are monodisperse and sequence-defined. The most developed material in this respect are peptidomimetics. Another important class of synthetic macromolecules obtained *via* solid phase synthesis are precision polycations. Firstly introduced by

ourselves (*12–14*) and advanced by Wagner et al (*15*, *16*), it could be shown that in dependence of the number, type and position of cationic groups within the macromolecule, their potential as non-viral vectors for gene delivery can dramatically be altered – from toxic compounds to highly effective yet non-toxic transfection agents (*14*, *17*, *18*). There are also other examples for artificial solid phase synthesized macromolecules, however the synthetic procedure is often related to a single target structure and is not necessarily applicable for the synthesis of a variety of macromolecules (*19–21*). We believe that solid phase synthesis has the potential for the synthesis of a large variety of synthetic macromolecules and thus introduced the term solid phase polymer synthesis. In this chapter we will present our recent progress in the fundamental development of the solid phase polymer synthesis (SPPoS) of functional polyamides including the design of building blocks, automated solid phase coupling protocols and applications of the obtained precision macromolecules.

Before we present the chemistry, we shortly discuss nomenclature. Both, the term 'precision' as well as 'sequence-defined' can be used for the molecules obtained *via* solid phase assembly. However, the term polymer might lead to controversies. Usually polymers are defined by their chain length (> 3 repeating units) (*22*, *23*). Indeed, the solid phase approach allows for the assembly of chains with up to 20 repeating units and molecular weights of about 10 kDA. Depending on the molecular weight and number of repeating units, we can differentiate between oligomers or polymers. However, these systems additionally are monodisperse, lacking any molecular weight distribution. Therefore they do not follow a second part of the definition of a polymer, where a polymer is "less than a simple weight majority of molecules of the same molecular weight" (*22*) and thus not monodisperse. Therefore, we name the products obtained by solid phase assembly of artificial building blocks *precision macromolecules*, pointing at both, their chemical precision and macromolecular structure ranging from 1-10 kDa. However, in order to stress the difference between solid phase peptide chemistry and the solid phase synthesis of precision macromolecules, the simpler term solid phase polymer synthesis (SPPoS) is maintained.

Solid Phase Polymer Synthesis: Building Blocks and Coupling Strategies

Our first approach towards the synthesis of precision macromolecules was based on coupling symmetric diamines and symmetric diacids on solid support inspired by the classical polycondensation reactions (*12–14*, *24*, *25*). The major advantage of this approach is the straightforward use of commercially available diamine and diacid building blocks without the requirement for protecting groups. However, this synthetic protocol is limited to the synthesis of shorter oligomers, as during the synthesis of longer chains, chain-chain coupling resulting dimer formation occurs in the diamine coupling step. Therefore, we introduced an improved method based on the introduction of temporary protected diamines (*e.g.* Fmoc protected diamine HCl salts), which also allows for the use of non-symmetric diamines and diacids (*26*). As of yet, this approach is still limited

to the use of PyBop (or other phosphonium based coupling agents) as coupling reagent during the diamine coupling step and activation of the carboxy group on solid support.

To enable the use of non phosphonium based reagents and further improve coupling efficiency, we recently introduced the so-called dimer building block approach (*27*, *28*) The following subchapter will discuss the design and synthesis of suitable dimer building blocks *via* the coupling of diamine and diacid units in solution prior to solid phase synthesis. This coupling approach can be combined with a broad range of peptide coupling chemistry protocols and thus ensures higher coupling efficiency, reduced byproduct formation and accessibility of longer structures, in combination with a large variety of main and side chain functionalities (*27–34*).

Dimer Building Blocks

In general, dimer building blocks suitable for SPPoS have to meet four criteria. They should contain one free carboxylate group for selective activation and coupling onto the resin. They should contain one Fmoc-protected amine group that allows for orthogonal deprotection on solid support and addition of the next building block. All other side chains, functional groups or spacer units need to be inert or carry a protecting group during coupling and deprotection cycles. Ideally deprotection should be realized in a one-step procedure upon acidic cleavage from the resin. Additionally, for fully automated procedures, the buildings blocks as well as the activated species have to be well soluble in DMF or NMP even in high concentrations.

As solid phase synthesis applies high excess of building blocks to achieve complete conversion in each coupling step, building blocks need to be accessible on gram scale in high purity. In order to allow for a large variety in building blocks, the synthetic procedures ideally allow for simple exchange of functional side chains or are adoptable for different starting material. Overall, building block synthesis should be cost efficient, thus starting from readily available materials and without laborious and expensive chromatographic clean-up.

In order to establish a library of building blocks with functional side chains diethylenetriamine, a commercially available simple triamine and building block for organic synthesis, was chosen as starting material. Besides its suitable chemical structure, the diethylentriamine subunit has been shown to be biocompatible and highly suitable for several biomedical applications. It has been widely applied for gene delivery studies (*35*), RNA/PNA conjugates (*36*) and imaging agents (*37*) making diethylenetrimaine highly attractive as functionalizable diamine unit. Figure 1 shows the synthetic approach starting by differentiating the two primary amine groups *via* selective introduction of the bulky trityl group just on one of the primary amine groups. The second primary amine can then be selectively functionalized with a trifluoro acetic acid protecting group. This molecule already is the key intermediate to a first group of functional building blocks. The secondary amine can then be used for the attachment of various side chains or protecting groups *via* amide coupling e.g. with pentynoic acid or pentenoyl acid chloride (*27*, *32*). In the final step, the trityl group is

cleaved releasing again a free primary amine that is used for the condensation with succinic anhydride leading to the final building block. All building blocks obtained can be isolated on a large scale (up to 30 g of final building block) and without the use of any chromatographic purification (*27, 32*). The nomenclature for the obtained building blocks follows a three letter code indicating the side group, diamine and diacid components. For example, the building blocks are functionalized with **A**lloc, **B**oc, a terminal **D**ouble or **T**riple bond on the secondary amine and contain **D**iethylentriamine as the diamine unit and **S**uccinic acid the diacid unit giving ADS, BDS, DDS and TDS, respectively (see Figure 1).

Building blocks with functional side chains:
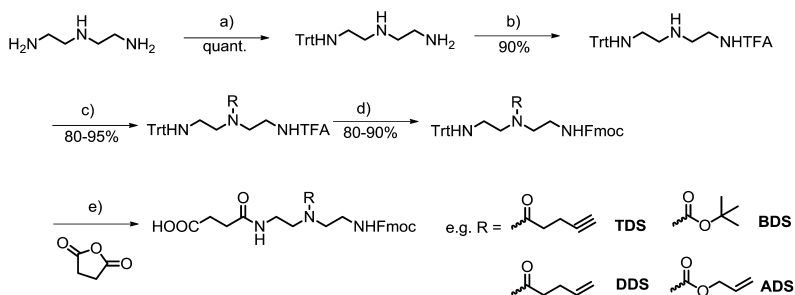
Spacer building blocks:
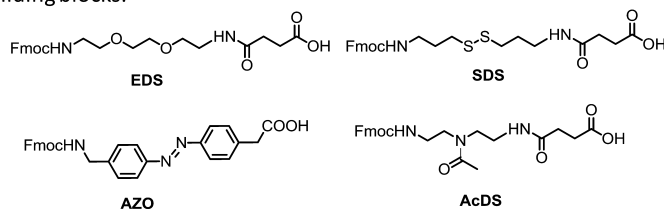
Figure 1. Synthesis, structures and nomenclature of functional building blocks suitable for solid phase coupling applying standard peptide chemistry protocols. Reaction conditions: a) Trt-Cl/DCM, quant.; b)TFAEt/THF, 90%; c) e.g. Alloc-Cl or Boc₂O/DCM/NEt₃, 70-90%; d) K₂CO₃, MeOH/H₂O, Fmoc-Cl, THF/H₂O e) 5%TFA, DCM, TIS, Succinic anydride, Et₃N, DCM (27, 28, 33).

Figure 1 also shows a set of so-called spacer building blocks. These building blocks are obtained following similar synthetic protocols starting from their diamine structure. These building blocks do not obtain functional side chains, but introduce different main chain motifs such as a hydrophilic ethylene glycol unit (EDS) or light sensitive azobenzene moiety (AZO). The choice of spacer building blocks during synthesis will therefore strongly influence the overall properties of the polymeric backbone i.e. flexibility or degradability.

Branched Precision Macromolecules

With this building block library in hand, we can now perform solid phase polymer synthesis. As previously discussed, all building blocks are compatible

with standard peptide Fmoc coupling chemistry e.g. using HBTU or HATU as activation reagents. Therefore, it is also possible to perform all coupling steps on a fully automated peptide synthesizer. Additionally, the Fmoc cleavage allows for the *in situ* monitoring of the coupling efficiency *via* measuring the UV signal after cleavage. Overall, we could show that up to 20 building blocks can be efficiently coupled on solid support (*28*). Final products can be isolated as crude products directly after cleavage from the resin in high purity and high yield (*27*, *28*, *31*, *34*).

Besides the comparatively straightforward coupling of dimer building blocks in a linear fashion, we can also introduce specific branching points to a growing oligomer chain. Symmetrically branched poly(amidoamines) synthesized *via* SPPoS have been already described and were accessible by applying Fmoc-Lys(Fmoc)-OH as amino acid building block as symmetrical branching unit. After Fmoc cleavage from this building block the main chain can grow in two directions *via* attachment to the two primary amine groups and thus lead to a symmetrical branching point (*16*). Theoretically, the exchange of one Fmoc group towards a different temporary protecting group with orthogonal cleavage conditions should allow for a differentiation of the two branching sites and thus lead to so-called asymmetrical branching.

In order to obtain such asymmetrical branching, allyloxycarbonyl (Alloc) as orthogonal protecting group was chosen and installed on the secondary amine group of the dimer building block (ADS, see Figure 1) (*28*). An oligomeric backbone was synthesized by attaching a sequence of ADS building blocks linearly *via* standard Fmoc-coupling protocols. Only after completing the sequence, all Alloc protecting groups were cleaved on solid support releasing secondary amine groups that could then be used for the further attachment of building blocks, e.g. BDS for introduction of cationic charged side chains. Due to the sequence-specific positioning of the ADS building block during solid phase polymer synthesis, it is now possible to vary the position and number of side chains as well as the composition of side chains and to increase the degree of branching e.g. by introducing ADS building blocks in the side chains as well.

In the following two subchapters we will now discuss the potential of SPPoS based on our tailor-made building blocks for the synthesis and application of two classes of functional macromolecules –glycomacromolecules and ß3R3-peptides. While the glycomacromolecules are based on the combination of a polyamide backbone with pendant sugar ligands in the side chains, the ß3R3-peptides are based on the sequence-specific introduction of chiral side chains to our precision macromolecules. Thus these two classes of precision macromolecules adequately show the synthetic diversity of SPPoS as well as our building block library.

Precision Glycomacromolecules as Novel Glycomimetics

Natural Sugar Ligands and Sugar Mimetics

Carbohydrates are essential for numerous biological and biomedical processes such as inflammation and immune response, viral and bacterial infection or protein folding and stability (*38*, *39*). In most of these processes, the carbohydrates act as ligands binding to specific protein receptors. Although

monosaccharides generally only exhibit a very low affinity, nature is able to obtain sugar ligands with a higher affinity and specificity by assembling several monosaccharides into an oligosaccharide. This is also known as the glycocluster effect or multivalency of sugar ligands (*40*). Indeed, this strategy can also be applied for the synthesis of sugar mimetics, where several sugar ligands are attached to a non-natural scaffold mimicking the multivalent structure of oligosaccharides or glycoconjugates (*41*, *42*). Today, there exists a large variety of multivalent sugar-functionalized materials ranging from small molecules to macromolecules and μm-sized objects, from inorganic materials to organic and from synthetic to biological scaffolds. Although direct comparisons are limited, some very general structure-property-correlations have been identified for the design of such multivalent glycomimetics: It has been shown that the number, density and distancing of the sugar ligands along the scaffold has a strong influence on the resulting binding properties. Furthermore, there are strong indications that also the chemical properties of the scaffold as well as the linker between scaffold and sugar ligand have tremendous influence on the resulting binding affinity as well as selectivity (*43*, *44*). However, most systems so far are optimized empirically and very little is known about the underlying structure-property relations of glycomimetics. This is especially true for multivalent sugar ligands based on polymers or polymeric materials such as hydrogels. Due to their inherent polydisperse nature and the limitation in controlling precise positioning of functionalities along the backbone, polymer scaffolds make it especially difficult to correlate their chemical structure with the resulting binding properties. Despite these difficulties they remain a highly important class of scaffolds regarding the large variability of polymer synthesis: Through polymer-analogue reactions as well as the functionalization of suitable monomers, glycopolymers presenting various sugar ligands have been synthesized and proved to be able to recognize and bind protein receptors with high affinities. Moreover, different architectures and functionalities are accessible and a large number of polymeric systems were shown to be non-toxic and biocompatible. These attributes are especially interesting for biomedical applications employing glycopolymeric drugs or drug delivery systems (*44–48*).

Overall, having access to monodisperse, sequence-defined glycopolymers would allow for direct structure-activity relation studies, a more detailed understanding of multivalent effects as well as improved design rules for novel sugar mimetics and further promote their application in biomedicine and biotechnology. In the following subchapter we will discuss our recent advances on using solid phase polymer synthesis for the preparation of precision glycomacromolecules.

Monodisperse, Sequence-Defined Glycomacromolecules via Solid Phase Polymer Synthesis

The most common strategy for the sugar functionalization of polymers is their so-called polymer analogue functionalization where firstly the polymer backbone carrying several functional groups is synthesized that is and then conjugated by of multiple sugars units in a second step. In a similar fashion, the SPPoS

allows for the synthesis of precision macromolecules carrying functional groups at defined positions along the polymer backbone. After assembly of the desired backbone, those functional groups are then reacted in a polymer analogue fashion with the desired sugar ligand and the final sugar oligo/polymer is cleaved from the resin (Figure 2b) (*27*, *33*). In general, different functionalization strategies can be applied for the conjugation of sugars to the scaffold. In order to obtain a monodisperse, sequence-defined product, conjugations should lead to complete conversion, be compatible with the solid phase synthesis and lead to stable products under cleavage conditions. So far we have applied two strategies – Copper-Catalyzed Azide-Alkyne Cycloaddition (CuAAc) (*27*, *34*) and thiol-ene conjugation (TEC) (*32*, *33*). The CuAAc or click chemistry uses sugar azides that can be selectively coupled to alkyne moieties introduced *via* the TDS building block (Figure 1 and 2b). TEC conjugation applies thiol sugars and their radical addition to double bond presenting DDS building blocks (Figure 1 and 2a). CuAAc conjugation to the alkyne presenting polymer is performed on solid support and the final product is obtained without further purification in high purity and yield directly after cleavage from the resin (*27*, *34*). TEC is performed using a dedicated flow reactor that was developed for the efficient conjugation of sugar ligands to our polymeric scaffolds (*32*, *33*). Both methods rely on the use of only small excess of sugar ligands (1.5-3 eq. per functional side chain) and thus also allow for the introduction of more complex and valuable oligosaccharides.

So far, the presented combination of SPPoS and different conjugation methods allows for the synthesis of sugar mimetics with controlled variations in the chain length, scaffold properties and geometry, number and spacing of sugar ligands attached to the scaffold as well as the combination with peptide segments. While the sequence-control of solid phase synthesis is applied during the assembly of the oligo/polymer backbone, only one type of sugar ligand is introduced at the multiple conjugation sites leading to so-called homomultivalent structures. However, recent studies suggested that the combination of different binding or non-binding sugars and their simultaneous multivalent presentation on a single scaffold can influence the resulting binding properties in both affinity and selectivity *e.g.* towards a specific protein receptor (*49*, *50*). Thus it would be highly relevant to obtain and study sequence-defined heteromultivalent glycomacromolecules presenting different sugar ligands at defined positions along the scaffold.

The most straightforward approach towards heteromultivalent glycomacromolecules is the use of sugar functionalized building blocks. Therefore, double-bond presenting building block DDS was functionalized with different thiol sugars using a flow reactor. A first library of sugar building blocks was obtained introducing mono- as well as disaccharides. These building blocks were then successfully applied for the synthesis of heteromultivalent glycomacromolecules (*33*). However, in order to introduce more complex oligosaccharides and to minimize the amount of required sugar ligands, alternative strategies have been developed. One option is the combination of the different conjugation strategies, as this is also common practice in standard polymer functionalization strategies. Here TDS and DDS building blocks can be combined within one polymer segment. Functionalization with sugar ligand

A then first proceeds *via* CuAAc with the according sugar azide. The second sugar ligand B is then introduced in a second functionalization step *via* thiol-ene coupling with the according thiol sugar. However, this strategy is limited in the number of different sugar ligands that can be introduced and the different functionalization steps cannot be performed fully automated and continuously on the peptide synthesizer.

Figure 2. Examples for synthetic strategies towards glycomacromolecules using solid phase polymer synthesis: a) homomultivalent glycomacromolecules via TEC of sugar ligands to double-bond presenting macromolecules (32), b) heteromultivalent glycomacromolecules via sequential CuAAc of sugar azides to alkyne presenting building blocks (34).

Table 1. Examples for homo- and heteromultivalent precision glycomacromolecules and their structure dependent binding affinity towards ConA lectin receptor determined by inhibition/competition assay. Dark grey spheres represent Mannose, light grey spheres represent Galactose, EDS was used exclusively as spacer building block, all sugars were conjugated via CuAAC. (* value from literature (51))

	IC_{50} [µM]		IC_{50} [µM]		IC_{50} [µM]
Methyl-α-D-Mannoside	620 ± 20	Man(3)-5	6.1 ± 0.7	Man,Gal,Man(1,3,5)-5	0.8 ± 0.1
Mannotrioside	3.7*	Man(1,3,5)-5	0.8 ± 0.1	Man,Man,Gal(1,3,5)-5	0.7 ± 0.1
Man(1,3)-5	3.9 ± 0.3	Man(1-5)-5	0.4 ± 0.1	Gal,Man,Gal(1,3,5)-5	1.0 ± 0.1
Man(1,5)-5	3.4 ± 0.5	Man(1-10)-10	0.3 ± 0.1	e.g. controls	n.b.

Therefore, a new strategy was developed based on the sequential CuAAc coupling and chain elongation on solid support (34). Figure 2b shows the general principle: The chain is assembled up to the position of the first sugar ligand, here a TDS building block is introduced and immediately functionalized with the according sugar azide. In contrast to the polymer analogue reaction, the sugar ligands have to carry acetyl protecting groups on all hydroxyl moieties. Only then the terminal Fmoc group is cleaved, allowing for further chain elongation up to the position of the next sugar ligand. Again, TDS is introduced and functionalized with the sugar azide of choice, now enabling introduction of a different sugar as on the first position. This approach not only allows for the synthesis of heteromultivalent sugar mimetics but also gives straightforward access to a library of differently functionalized scaffolds, as for every functionalization step a split-and-mix strategy can be applied.

Overall, the combination of functional building blocks and solid phase synthetic protocols now gives a toolbox or assembly kit that allows for the straightforward synthesis of a large variety of monodisperse, sequence-defined glycomacromolecules. Indeed, we have applied our toolbox to synthesize both, homo- and heteromultivalent glycomacromolecules and use them as model compounds to study multivalent sugar ligand/receptor interactions. Table 1 shows some examples for Mannose and Galactose functionalized oligomers that were characterized as glycomimetic ligands binding to Concanavalin A (ConA) lectin receptor.

ConA is a highly selective binder of mannose residues and an extensively studied model receptor for lectin binding assays as it presents a tetrameric structure that is quite typical for lectins (*52*). Table 1 shows the results for the affinity obtained in an inhibition/competition assay using soft colloidal probe reflection interference contrast microscopy (SCP-RICM) (*29*, *30*) and surface plasmon resonance (SPR), expressed as half maximal inhibitory concentration (IC$_{50}$) (*27*, *34*) Importantly, all control structures presenting no sugar ligand or only non-binding sugar ligands show no binding to ConA, therefore the polymer backbone does not interact non-specifically with the protein receptor. Interestingly, the attachment of a single mannose ligand already results an increase in affinity in comparison to the free monosaccharide of a factor of 100. This could be due to a secondary effect of the oligomeric backbone, namely the release of structured water from the receptor upon binding of the hydrophilic ligand also known as the effect of water as molecular mortar. This hypothesis is currently under further investigation by thermodynamic studies of the binding with isothermal calorimetry (ITC) and surface plasmon resonance (SPR). An increase in the number of ligands while keeping the scaffold length constant leads to a further increase in affinity based on statistically enhanced binding. Overall, all ligands tested so far show affinities in the low μM to nM range which is comparably high considering the low number of attached sugar ligands (N≤10) and in comparison to values known from literature for similar structures. Our studies show that there is no linear correlation between the number of sugar ligands attached and the resulting binding affinity. Rather, there seems to be an optimal number of sugar ligands (for ConA we found this to be three to five sugar ligands) that will lead to the most effective glycomacromolecule. We also found that the backbone itself can strongly influence binding, e.g. glycomacromolecules with the same number of sugar residues but larger spacings between the sugars result in higher affinity. The effects of the backbone on the ligand binding affinity are currently under investigation for a series of precision glycomacromolecules with varying backbone properties such as hydrophobicity and flexibility.

In order to investigate the influence of the sugar ligands in more detail, a set of heteromultivalent ligands was synthesized combining the high affinity mannose ligands with intermediate affinity glucose and non-binding galactose residues (*34*). To our surprise, in the competition/inhibition assay we observed that trivalent structures presenting a decreasing number of binding and increasing number of non-binding sugars resulted in similar affinities. This could be explained by a monovalent binding mode for all trivalent structures but would be in contradiction to the trends observed previously for the homomultivlent ligands. In order to gain a deeper insight into the molecular interactions of the heteromultivalent ligands, saturation-transfer difference (STD) NMR and Dual Focus Fluorescence Correlation Spectroscopy (2fFCS) measurements were performed (*34*). Indeed, STD-NMR confirmed that the non-binding galactose residues do not show any unspecific or subsite binding while the mannose ligands associated to ConA binding sites. Interestingly, 2fFCS results showed a clear difference for the binding of trivalent homo- vs. heteromultivalent ligands. In solution the trivalent all mannose ligand is able to intermolecularly crosslink two ConA receptors whereas the heteromultivalent structures only bind to one

ConA molecule. Again, through the controlled variation of specific molecular parameters e.g. the presented sugar ligands we were able to directly correlate the chemical structure with the resulting binding properties and to identify the underlying binding mechanism.

Thus, precision glycomacromolecules have proven to be a suitable platform for the systematic study of multivalent effects in glycopolymer binding. Furthermore all glycomacromolecules based on precision polyamides studied so far show a reduced immunogenicity and no cytotoxicity. Overall they have a great potential for biomedical applications and are currently investigated e.g. for targeted gene delivery and novel antimicrobial treatments.

Novel Peptidomimetics by Combining Peptide and Polymer Chemistry

While solid phase synthesis was originally developed for the synthesis of natural peptides, in the last decades it also has been extensively used for the synthesis and development of peptidomimetics – structures that show similar biological activity but exhibit a higher proteolytic stability then their natural analogues (*52–55*). One of the most established classes of peptidomimetics are the β-peptides introducing a methylene group in the peptide backbone (*56, 57*). These systems offer a higher conformational and proteolytic stability in comparison to the natural peptides and thus have a great potential especially in the area of biomedicine and as peptide-based drugs. Nevertheless, peptidomimetics show limited variability in secondary structures, for example β-peptides predominantly form helical structures and only very few examples for strand and sheet conformations are known. Additionally many β-peptides still exhibit cytotoxic side effects *in vitro* and *in vivo* (*58, 59*).

Inspired by the use of solid phase synthesis for the synthesis of non-natural polyamides, we combined the class of β-peptides with features from the polyamides – namely an inversion of the orientation of every second amide bond (*26, 31*). This leads to changes in the intra- as well as intermolecular hydrogen bonding patterns with a higher potential to form extended strand and sheet-like structures and also alters the proteolytic stability and cytotoxicity of these systems. According to their additional methylene group and the position of side chains along the polyamide backbone, these systems are named $β^{3R3}$-peptides (*31*).

In order to investigate the ability of $β^{3R3}$-peptides to form secondary structures and higher order aggregates, their folding and aggregation behavior at the air/water interface was characterized (*31*). The Langmuir film balance technique provides a unique and accurate methodology to investigate biomacromolecules at the air/water interface and establish relationships between chemical properties and assembly behavior (*60*).

Again, the synthesis of these structures starts from preparing suitable building blocks: In similarity to the previously discussed dimer building blocks, diamine and diacid subunits were synthesized separately and then coupled in solution

to give the final dimer building blocks (*26, 31*). As functional side chains, the hydrophobic and chiral side chains of the amino acid alphabet were targeted. Thus natural amino acids were chosen as starting materials. Several synthetic strategies have been presented for the synthesis of mono Fmoc-protected vicinal diamines derived from L-α-amino acids. However, the relatively low solubility of Fmoc-protected α-amino acids does not allow for large scale synthesis and laborious purification methods such as column chromatography are required. Therefore a novel versatile route was developed using Boc-protected L-α-amino acids as starting material for the synthesis of the Fmoc-protected enantiomerically pure vicinal diamines with proteinaceous side chains (*26, 31*). These diamine units were then combined with different diacid units to give the final dimer building blocks in high quantity and yield. With these building blocks at hand, a set of chiral, hydrophobic precision macromolecules or β3R3-peptides was synthesized varying their monomer sequence, their chain length as well as introducing different end groups (*31*).
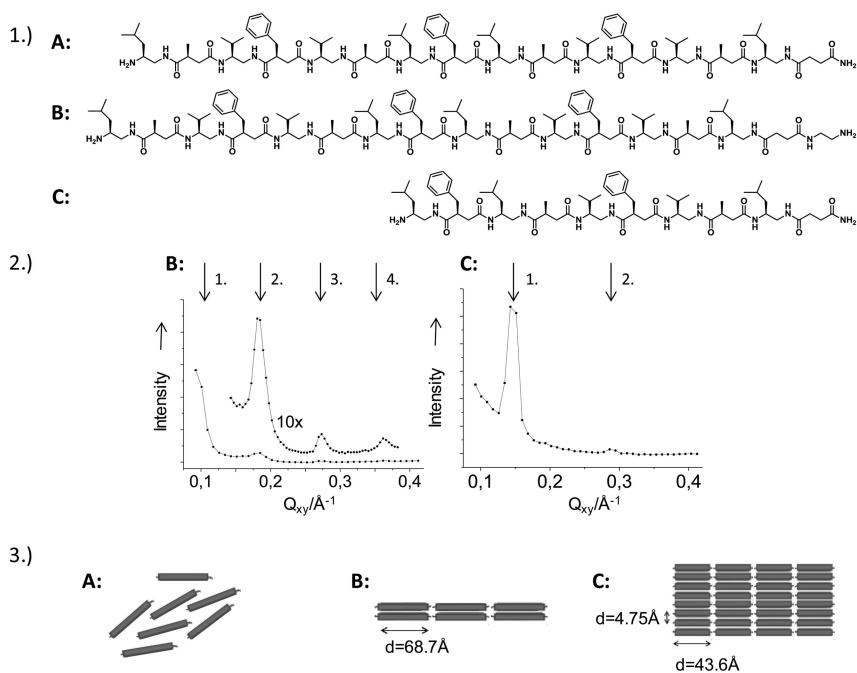
*Figure 3. 1.) Examples for three β3R3-peptides and their structure formation as analyzed by IRRAS and GIXD. 2. Corrected X-ray intensities versus the in-plane scattering vector component Q_{xy} for **B** and **C**. 3.) Schematic representation of the self-assembly properties of oligomers **A-C**, where **A** forms strands, **B** forms amorphous sheets and **C** crystalline sheet (31).*

Analysis by means of Infrared Reflection Absorption Spectroscopy (IRRAS), Grazing Incidence X-Ray Diffraction (GIXD) and X-ray Reflectivity (XR) showed the potential of β^{3R3}-peptides presenting specific monomer sequences of hydrophobic side chains to form extended β-sheet assemblies (*31*). Figure 3 shows the chemical structure of three β^{3R3}-peptides differing in their overall chain length (A and C) or endgroup (A and B). While oligomer A forms strands, oligomer B forms amorphous sheets and C crystalline sheet. These results show that *via* alternating directions of the amide bonds along β-peptide sequences, the β^{3R3}-peptides have the potential to extend the structural space of β-peptides and to form strands with particular self-assembling properties. Due to this finding, and due to their proteolytic stability, β^{3R3}-peptides can be considered new class of peptidomimetic foldamers. Ongoing studies further evaluate the structural space of β^{3R3}-peptides as well as their potential for various biomedical applications e.g. as antimicrobial agents and for targeted drug delivery.

Conclusion

Overall this chapter presented our recent advances in the field of solid phase polymer synthesis – from the development of a building block library to the synthesis and application of precision polycations, glycomacromolecules and peptidomimetics. Through the use of solid phase synthesis, we are now able to combine the sequence control of biopolymers with the vast range of functional groups that synthetic polymers offer. Therefore we believe that solid phase polymer synthesis has a great potential in various areas of science and will help to promote the fundamental understanding of structure-property correlations for synthetic macromolecules.

Acknowledgments

References

1. Badi, N.; Lutz, J.-F. *Chem. Soc. Rev.* **2009**, *38*, 3383–3390.
2. Ouchi, M.; Badi, N.; Lutz, J.-F.; Sawamoto, M. *Nat. Chem.* **2011**, *3*, 917–924.
3. Merrifield, R. B. *J. Am. Chem. Soc.* **1963**, *85* (14), 2149–2154.
4. Froehler, B. C.; Ng, P. G.; Matteucci, M. D. *Nucleic Acids Res.* **1986**, *14* (13), 5399–5407.
5. Garegg, P. J.; Lindh, I.; Regberg, T.; Stawinski, J.; Stromberg, R.; Henrichson, C. *Tetrahedron Lett.* **1986**, *27* (34), 4051–4054.

6. Danishefsky, S. J.; McClure, K. F.; Randolph, J. T.; Ruggeri, R. B. *Science* **1993**, *260* (5112), 1307–1309.

7. Plante, O. J.; Palmacci, E. R.; Seeberger, P. H. *Science* **2001**, *291* (5508), 1523–1527.

8. Bray, B. L. *Nat. Rev. Drug Discovery* **2003**, *2* (7), 587–593.

9. Guy, C. A.; Fields, G. B. *Solid-Phase Peptide Synthesis*; Fields, G. B., Ed.; Methods in Enzymology; Academic Press: New York , 1997; Vol. 289, pp 67−83.

10. Klausner, Y. S.; Bodansky, M. *Synthesis* **1972**, *9*, 453–463.

11. Han, S. Y.; Kim, Y. A. *Tetrahedron* **2004**, *60* (11), 2447–2467.

12. Hartmann, L.; Häfele, S.; Peschka-Süss, R.; Antonietti, M.; Börner, H. G. *Macromolecules* **2007**, *40* (22), 7771–7776.

13. Hartmann, L.; Krause, E.; Antonietti, M.; Börner, H. G. *Biomacromolecules* **2006**, *7* (4), 1239–1244.

14. Hartmann, L.; Häfele, S.; Peschka-Süss, R.; Antonietti, M.; Börner, H. G. *Chem. Eur. J.* **2008**, *14* (7), 2025–2033.

15. Schaffert, D.; Badgujar, N.; Wagner, E. *Org. Lett.* **2011**, *13* (7), 1586–1589.

16. Schaffert, D.; Troiber, C.; Salcher, E. E.; Froehlich, T.; Martin, I.; Badgujar, N.; Dohmen, C.; Edinger, D.; Klaeger, R.; Maiwald, G.; Farkasova, K.; Seeber, S.; Jahn-Hofmann, K.; Hadwiger, P.; Wagner, E. *Angew. Chem., Int. Ed.* **2011**, *50* (38), 8986–8989.

17. Froehlich, T.; Edinger, D.; Klaeger, R.; Troiber, C.; Salcher, E.; Badgujar, N.; Martin, I.; Schaffert, D.; Cengizeroglu, A.; Hadwiger, P.; Vornlocher, H.-P.; Wagner, E. *J. Controlled Release* **2012**, *160* (3), 532–541.

18. Troiber, C.; Wagner, E. *Bioconjugate Chem.* **2011**, *22* (9), 1737–1752.

19. König, H. M.; Gorelik, T.; Kolb, U.; Kilbinger, A. F. M. *J. Am. Chem. Soc.* **2006**, *129* (3), 704–708.

20. Santiago-Garcia, J. L.; Aguilar-Vega, M. *Eur. Polym. J.* **2009**, *45* (11), 3210–3216.

21. Zhang, Z.; Pickens, J. C.; Hol, W. G.; Fan, E. *Org. Lett.* **2004**, *6* (9), 1377–1380.

22. *Official Journal of the European Union*, L 396 of 30 December 2006, REACH, Chapter 2, Article 3.5.

23. Hiorns, R. C.; Boucher, R. J.; Duhlev, R.; Hellwich, K. H.; Hodge, P.; Jenkins, A. D.; Jones, R. G.; Kahovec, J.; Moad, G.; Ober, C. K.; Smith, D. W.; Stepto, R. F. T.; Vairon, J. P.; Vohlídal, J. *Colloid Polym. Sci.* **2013**, *291* (3), 457–458.

24. Hartmann, L. *Macromol. Chem. Phys.* **2011**, *212* (1), 8–13.

25. Hartmann, L.; Boerner, H. G. *Adv. Mater.* **2009**, *21* (32−33), 3425–3431.

26. Mosca, S.; Wojcik, F.; Hartmann, L. *Macromol. Rapid Commun.* **2011**, *32* (2), 197–202.

27. Ponader, D.; Wojcik, F.; Beceren-Braun, F.; Dernedde, J.; Hartmann, L. *Biomacromolecules* **2012**, *13* (6), 1845–1852.

28. Wojcik, F.; Mosca, S.; Hartmann, L. *J. Org. Chem.* **2012**, *77* (9), 4226–4234.

29. Pussak, D.; Behra, M.; Schmidt, S.; Hartmann, L. *Soft Matter* **2011**, *8*, 1664–1672.

30. Pussak, D.; Ponader, D.; Mosca, S.; Vargas Ruiz, S.; Hartmann, L.; Schmidt, S. *Angew. Chem., Int. Ed.* **2013**, *52*, 6084–6087.

31. Mosca, S.; Dannehl, C.; Möginger, U.; Brezesinski, G.; Hartmann, L. *Org. Biomol. Chem.* **2013**, *11* (33), 5399.

32. Wojcik, F.; O'Brien, A. G.; Goetze, S.; Seeberger, P. H.; Hartmann, L. *Chem. Eur. J.* **2013**, *19* (9), 3090–3098.

33. Wojcik, F.; Lel, S.; O'Brien, A.G.; Seeberger, P.H.; Hartmann, L. *Beilstein J. Org. Chem.* **2013**, *9*, 2395–2403.

34. Ponader, D.; Maffre, P.; Aretz, J.; Pussak, D.; Ninnemann, N. M.; Schmidt, S.; Seeberger, P. H.; Rademacher, C.; Nienhaus, G. U.; Hartmann, L. *J. Am. Chem. Soc.* **2014**, *136* (5), 2008–2016.

35. Miyata, K.; Oba, M.; Nakanishi, M.; Fukushima, S.; Yamasaki, Y.; Koyama, H.; Nishiyama, N.; Kataoka, K. *J. Am. Chem. Soc.* **2008**, *130* (48), 16287–16294.

36. Verheijen, J. C.; Deiman, B. A. L. M.; Yeheskiely, E.; van der Marel, G. A.; van Boom, J. H. *Angew. Chem., Int. Ed.* **2000**, *39* (2), 369–372.

37. Svenson, S.; Tomalia, D. A. *Adv. Drug Delivery Rev.* **2005**, *57* (15), 2106–2129.

38. Lindhorst, T. Artificial Multivalent Sugar Ligands to Understand and Manipulate Carbohydrate-Protein Interactions. In *Host-Guest Chemistry*, Penadés, S., Ed.; Springer Berlin Heidelberg: 2002; Vol. 218, pp 201−235;

39. Stallforth, P.; Lepenies, B.; Adibekian, A.; Seeberger, P. H. *J. Med. Chem.* **2009**, *52* (18), 5561–5577.

40. Fasting, C.; Schalley, C. A.; Weber, M.; Seitz, O.; Hecht, S.; Koksch, B.; Dernedde, J.; Graf, C.; Knapp, E.-W.; Haag, R. *Angew. Chem., Int. Ed.* **2012**, *51* (42), 10472–10498.

41. Deniaud, D.; Julienne, K.; Gouin, S. G. *Org. Biomol. Chem.* **2011**, *9* (4), 966–979.

42. Lepenies, B.; Lee, J.; Sonkaria, S. *Adv. Drug Delivery Rev.* **2013**, *65* (9), 1271–1281.

43. Gestwicki, J. E.; Cairo, C. W.; Strong, L. E.; Oetjen, K. A.; Kiessling, L. L. *J. Am. Chem. Soc.* **2002**, *124* (50), 14922–14933.

44. The reader is referred to themed collection on 'Multivalent scaffolds in glycosciences': Renaudet, O.; Roy, R. *Chem. Soc. Rev.* **2013**, *42* (11), 4515–4517.

45. Eissa, A. M.; Cameron, N. R. *Bio-Synth. Polym. Conjugates* **2013**, *253*, 71–114.

46. Kiessling, L. L.; Grim, J. C. *Chem. Soc. Rev.* **2013**, *42* (10), 4476–4491.

47. Miura, Y. *Polym. J.* **2012**, *44* (7), 679–689.

48. Becer, C. R. *Macromol. Rapid Commun.* **2012**, *33* (9), 742–752.

49. Jimenez Blanco, J. L.; Ortiz Mellet, C.; Garcia Fernandez, J. M. *Chem. Soc. Rev.* **2013**, *42* (11), 4518–4531.

50. Ortega-Muñoz, M.; Perez-Balderas, F.; Morales-Sanfrutos, J.; Hernandez-Mateo, F.; Isac-García, J.; Santoyo-Gonzalez, F. *Eur. J. Org. Chem.* **2009**, *2009* (15), 2454–2473.

51. Brewer, F.; Bhattacharyya, L.; Brown Iii, R. D.; Koenig, S. H. *Biochem. Biophys. Res. Commun.* **1985**, *127* (3), 1066–1071.

52. Ahmad, E.; Naeem, A.; Javed, S.; Yadav, S.; Khan, R. H. *J. Biochem.* **2007**, *142* (3), 307–315.

53. Huc, I. *Eur. J. Org. Chem.* **2004**, *2004* (1), 17–29.

54. Goodman, C. M.; Choi, S.; Shandler, S.; DeGrado, W. F. *Nat. Chem. Biol.* **2007**, *3* (5), 252–62.

55. Matson, J. B.; Stupp, S. I. *Chem. Commun.* **2012**, *48* (1), 26–33.

56. Seebach, D.; Gardiner, J. *Acc. Chem. Res.* **2008**, *41* (10), 1366–1375.

57. Horne, W. S.; Gellman, S. H. *Acc. Chem. Res.* **2008**, *41* (10), 1399–1408.

58. Raguse, T. L.; Porter, E. A.; Weisblum, B.; Gellman, S. H. *J. Am. Chem. Soc.* **2002**, *124* (43), 12774–12785.

59. Chongsiriwatana, N. P.; Miller, T. M.; Wetzler, M.; Vakulenko, S.; Karlsson, A. J.; Palecek, S. P.; Mobashery, S.; Barron, A. E. *Antimicrob. Agents Chemother.* **2011**, *55* (1), 417–420.

60. Brezesinski, G.; Mohwald, H. *Adv. Colloid Interface Sci.* **2003**, *100*, 563–584.

Chapter 7

Solid-Phase Synthesis as a Tool for the Preparation of Sequence-Defined Oligomers Based on Natural Amino Acids and Synthetic Building Blocks

Delphine Chan-Seng[*] and Jean-François Lutz

Institut Charles Sadron, UPR22/CNRS, 23 rue du Loess, BP 84047, 67034 Strasbourg Cedex 2, France
[*]E-mail: delphine.chan-seng@ics-cnrs.unistra.fr

Nature has demonstrated a high level of control of the primary structure of their macromolecules, control that chemists have attempted to reach through the development of different synthetic routes. Here a iterative strategy for the preparation of relatively long sequence-defined oligomers constituted of natural α-amino acids and synthetic blocks achieved through a three-steps repeating cycle introducing three types of building blocks, i.e. natural α-amino acid, spacer and linker, on the oligomer chain is reported. Oligomers comprising up to seventeen building blocks were elaborated from a standard solid support used for peptide synthesis employing orthogonal and quantitative reactions, i.e. formation of amide bonds and copper-assisted alkyne-azide cycloaddition, which permitted to synthesize sequence-defined oligomers without requiring constraining purification steps after each reaction step.

Introduction

The complexity of macromolecules existing in nature is a source of interest for the scientific community to understand it and learn from it to design and create new materials with specific properties adapted to targeted applications. In this perspective, polymer chemists have been looking for new synthetic strategies to

approach the level of control of the primary structure of oligomers and polymers mimicking the control of sequences found for proteins (*1*). Techniques developed for the synthesis of sequence-controlled polymers relies on kinetic control (*2*, *3*), (macro)monomer design (*4*, *5*), templated chemistry (*6–8*), catalysis (*9*, *10*), and iterative synthesis (*11*, *12*).

Solid-phase synthesis is a method that have been developed for the preparation of organic compounds and peptides from a solid support, also called resin, by performing step-by-step reactions from its surface (*13*, *14*). Concerning the synthesis of peptides from a resin, i.e. crosslinked polystyrene beads bearing a large number of functional groups at its surface, the most common approach involves the repetition of two steps consisting in 1) the addition of a Fmoc-protected amino acid and 2) the removal of the Fmoc protecting group until the targeted peptide is synthesized at the surface of the resin and then cleaved from the resin to isolate the peptide as depicted in Figure 1. This technique permits to perfectly control the sequence of each amino acid on the oligomer backbone and simplify the purification step after each amino acid addition since it is simply achieved through washing the resin multiple times with the adequate solvent, which renders solid-phase synthesis an attractive approach for the elaboration of sequence-defined oligomers.
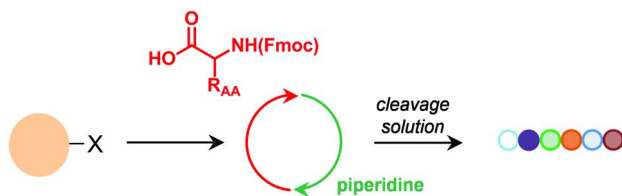
Figure 1. Solid-phase peptide synthesis schematic representation.

Solid-phase synthesis has been an inspiration for the synthesis of unnatural sequence-defined oligomers with a large panel of chemical structures as illustrated in Table 1. Fmoc-based solid phase synthesis as used for peptide synthesis has been applied to the elaboration of various sequence-defined oligomers such as oligoureas (*15*), oligocarbamates (*16*), α-amino phosphonic acid oligomers (*17*), and oligosulfanamides (*18*) consisting in the replacement of the amide moiety by the corresponding moiety of interest through the use of different chemistry reactions from a solid support.

Table 1. Examples of sequence-defined oligomers prepared by solid-phase synthesis and the structure of their repeat units.

oligomers	repeat unit structures
oligourea	
oligocarbamate	
α-amino phosphonic acid oligomer	
oligosulfanamide	
peptoid	
oligoamide	
oligo(amidotriazole)	
triazolomer	
thiolactone-based oligomer	
oligothiophene	
oligo(1,3-phenylene ethynylene)	

Zuckermann and coworkers have developed a solid-phase synthesis method to prepare oligo(*N*-substituted glycine)s, also called peptoids, where the substituents are attached to the nitrogen instead of the carbon in alpha of the carbonyl (*19*, *20*). The synthesis relies on repeating cycles from the surface of the resin consisting in an acylation reaction with bromacetic acid followed by a displacement reaction with a primary amine as depicted in Figure 2a. This synthetic platform has been demonstrated to offer the ability to design a vast variety of materials and tune their properties due to a large library of primary amines available. The influence of the primary structure of peptoids has been investigated to evaluate their potential as materials as illustrated by the work of the group of Kodadek evaluating a library of peptoids as mammalian coactivator CREB-binding protein ligands and demonstrating that among the hexameric peptoids studied the ligand based on Nlys-Ntrp-Nser-Nbsa-Nser-Nleu exhibited the best ability for binding affinity, selectivity and cell permeability (*21*).

a) peptoid synthesis

b) oligoamide synthesis

c) oligo(amidotriazole) synthesis
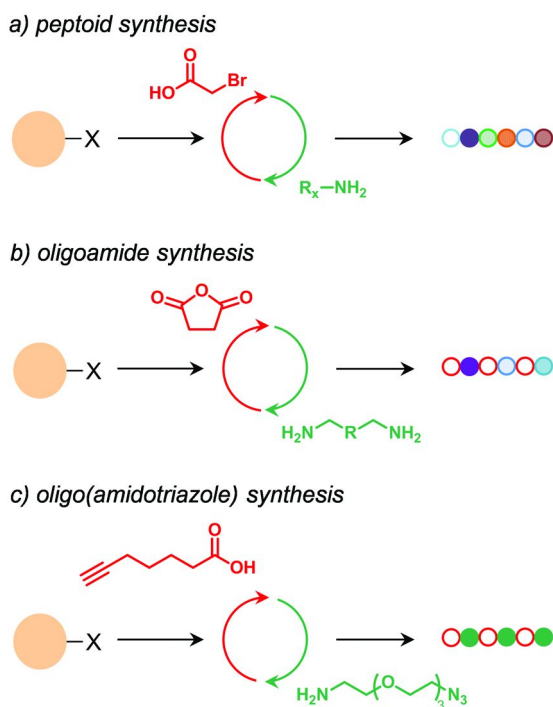
Figure 2. Schematic representation of solid-phase synthesis of some sequence-defined oligomers: a) peptoids, b) oligoamides and c) oligo(amidotriazole)s.

The preparation of oligoamides by solid-phase synthesis without requiring the need of using protected building blocks and thus involving an deprotection step has been investigated by few research groups (Figure 2b). Rose et al. have proposed to prepare sequence-defined oligoamides through a repeating cycle based on three steps from a resin involving an acylation reaction using succinic anhydride, an activation step in the presence of carbonyldiimidazole and an aminolysis reaction with PEG-based diamine (*22*). More recently Börner and Hartmann have explored a series of diamine building block bearing various functionalized moieties using a similar synthetic strategy (*23*, *24*). Hartmann et al. reported the introduction of mannose units as side chains along the sequence-defined oligoamide backbone and demonstrated that the affinity of these glycooligomers to bind to the lectin Concanavalin A was not only dependent on the number of mannose units present on the backbone but also the chemical composition and spacing between the mannose units, parameters controlled through iterative synthesis from the solid support (*25*).

The use of orthogonal syntheses has been also investigated on solid support for the preparation of sequence-defined oligomers. For example, the group of Lutz has reported the elaboration of sequence-controlled oligo(amidotriazole)s from a Wang resin as shown in Figure 2c using two building blocks bearing two different functional groups at each end that can not react with each other but can react orthogonally with the functional groups present on the other building block, i.e. 6-heptynoic acid as AB building block and 11-azido-3,6,9-trioxaundecane-1-amine as CD building block where B can react solely with C and A with D (*26*, *27*).

The variety of sequence-defined oligomers that can be synthesized is not restricted to oligomers bearing amide linkages. Few research groups have described the solid-phase synthesis of sequence-defined oligomers exempt of amide moieties such as triazolomers (*28*), thiolactone-based oligomers (*29*), oligothiophene (*30*) and oligo(1,3-phenylene ethynylene) (*31*).

Sequence-Defined Oligomers Based on Natural Amino Acids and Synthetic Spacers

Fmoc-based solid-phase synthesis offers the ability to synthesize peptides and peptidomimetic compounds from a library of natural and unnatural amino acids with different spacing between the amide linkages such as α-, β- and γ-amino acids and/or bearing various functional groups on their side chains like primary amine, thiol and propargyl moieties (*32*, *33*). Few research groups have reported the introduction of building blocks that could act as spacers, however the insertion of building blocks such as 6-aminohexanoic acid (*34*) requires as for natural α-amino acids employing their Fmoc-protected form and performing a deprotection step after the addition of each building block on the oligomer chain growing on the resin, factors that could induce a higher cost value of the final product even though some of these building blocks are commercially available.

The development of a synthetic strategy to prepare sequence-defined oligomers keeping the advantages of solid-phase peptide synthesis, i.e. synthesis of perfectly monodisperse molecules and access to commercially available building blocks possessing a wide range of functional groups on their side chains, but introducing synthetic building blocks without requiring protection and deprotection reactions for each step makes the use of orthogonal reactions highly valuable. To achieve this goal a repeating cycle based on three steps consisting in the iterative insertion of i) one amino acid, ii) one azidocarboxylic acid acting as a spacer, and iii) propargylamine as a linker (Figure 3) was proposed.
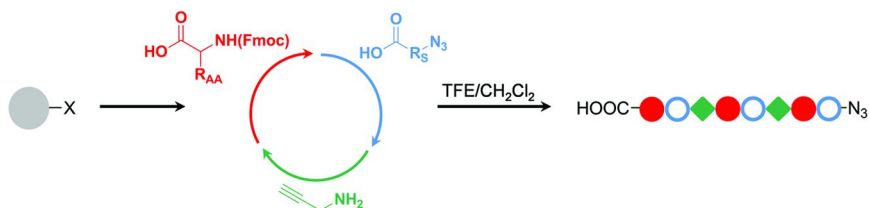
Figure 3. Synthetic route adopted for the preparation of sequence-defined oligomers based on natural α-amino acids and synthetic building blocks from a solid support through the iterative addition of 1) Fmoc-protected amino acid, 2) azidocarboxylic acid and 3) propargylamine for each repeating cycle.

We previously reported the use of this iterative approach to synthesize sequence-defined oligomers obtained through the reiteration of cycles based on these three steps, i.e. insertion of one protected natural α-amino acid, one spacer and one linker, up to three cycles (*35*). The final building block introduced on the oligomer growing from the resin was an azidocarboxylic acid to prepare an oligomer bearing at one extremity a carboxylic acid and at the other an azide once cleaved from the solid support. The viability and versatility of this iterative approach was demonstrated for the preparation of a panel of sequence-defined oligomers obtained through the use of a variety of spacers of different lengths and bearing various degrees of substitution, but also for a selection of natural α-amino acids. The synthetic strategy was validated and did not reveal to be more constraining as performing solid-phase peptide synthesis.

We propose to describe here the synthesis of larger sequence-defined oligomers prepared using this synthetic approach and obtained through the reiteration of a larger number of these repeating cycles. Model sequence-defined oligomers were prepared by considering Fmoc-Lys(Boc)-OH

as Fmoc-protected amino acid, 6-azidohexanoic acid as azidocarboxylic acid and propargylamine as building blocks. The solid-phase synthesis was realized from a chlorotrityl chloride resin. The insertion of each Boc-protected lysine residue and 6-azidohexanoic acid through the formation of amide bonds on the surface of the resin was performed using as coupling agent O-(benzotriazol-1-yl)-N,N,N',N'-tetramethyluronium hexafluorophosphate (HBTU) in the presence of 1-hydroxybenzotriazole hydrate (HOBt) and diisopropylethylamine in N,N-dimethylformamide, while the introduction of propargylamine by copper-assisted alkyne-azide cycloaddition was conducted in the presence of copper bromide and N,N,N',N',N''-pentamethyldiethylenetriamine in dichloromethane under an atmosphere of argon. The oligomers were synthesized by reiterating this repeating cycle ensuring that the last step of each cycle consisted in the insertion of 6-azidohexanoic acid permitting to obtain after cleavage from the resin an oligomer bearing at one extremity a carboxylic acid and at the other an azide. The step-by-step construction of each sequence-defined oligomer was monitored by Fourier transform infrared (FT-IR) spectroscopy demonstrating the insertion of 6-azidohexanoic acid on the growing oligomer chain from the surface of the resin by the presence on the spectrum of the characteristic absorption band at 2100 cm$_{-1}$ corresponding to the asymmetric stretching vibration of azide functional groups and the disappearance of this absorption band after performing the copper-assisted alkyne-azide cycloaddition reaction indicating the full conversion of the azide functional groups into triazole moieties as shown in Figure 4 for the synthesis of a model oligomer based on six cycles.

The synthesized oligomers were cleaved from the resin with a solution of 2,2,2-trifluoroethanol (TFE) in dichloromethane and isolated in good yields, i.e. around 70 %. The structural integrity of the oligomers was confirmed by nuclear magnetic resonance (NMR) exhibiting the characteristics peaks of each building block as illustrated in Figure 5 for the preparation of a sequence-defined oligomer elaborated from the repetition of six cycles. The lysine residues were easily identified on the ^{1}H NMR spectrum especially the protons in alpha position of the carbonyl on the main chain at 4.29 ppm and the protons of the methylene next to the amide of the Boc protecting group at 2.85 ppm. All the spacers exhibited their expected peaks and were easily observed in view of the methylene next to the amide moiety at 2.11 ppm on the ^{1}H NMR spectrum. The incorporation of the linkers was determined due to the presence of the triazole that was detected on the ^{13}C NMR spectrum at 123 and 145 ppm. The end- functionalization of the oligomer with an azide functional group was confirmed by the observation of the methylene next to the azide as a triplet at 3.27 ppm on the ^{1}H NMR spectrum permitting to validate the overall composition of the oligomer by comparing the integration of this peak to other characteristic peaks from each building block constituting the oligomer.

The model sequence-defined oligomers were further characterized by mass spectrometry. The determination of the molecular weight of these oligomers by electrospray ionization mass spectrometry (ESI-MS) permitted to confirm obtaining the targeted sequence-defined oligomers as the mass found for each oligomer adduct matched the calculated value as shown in Table 2.
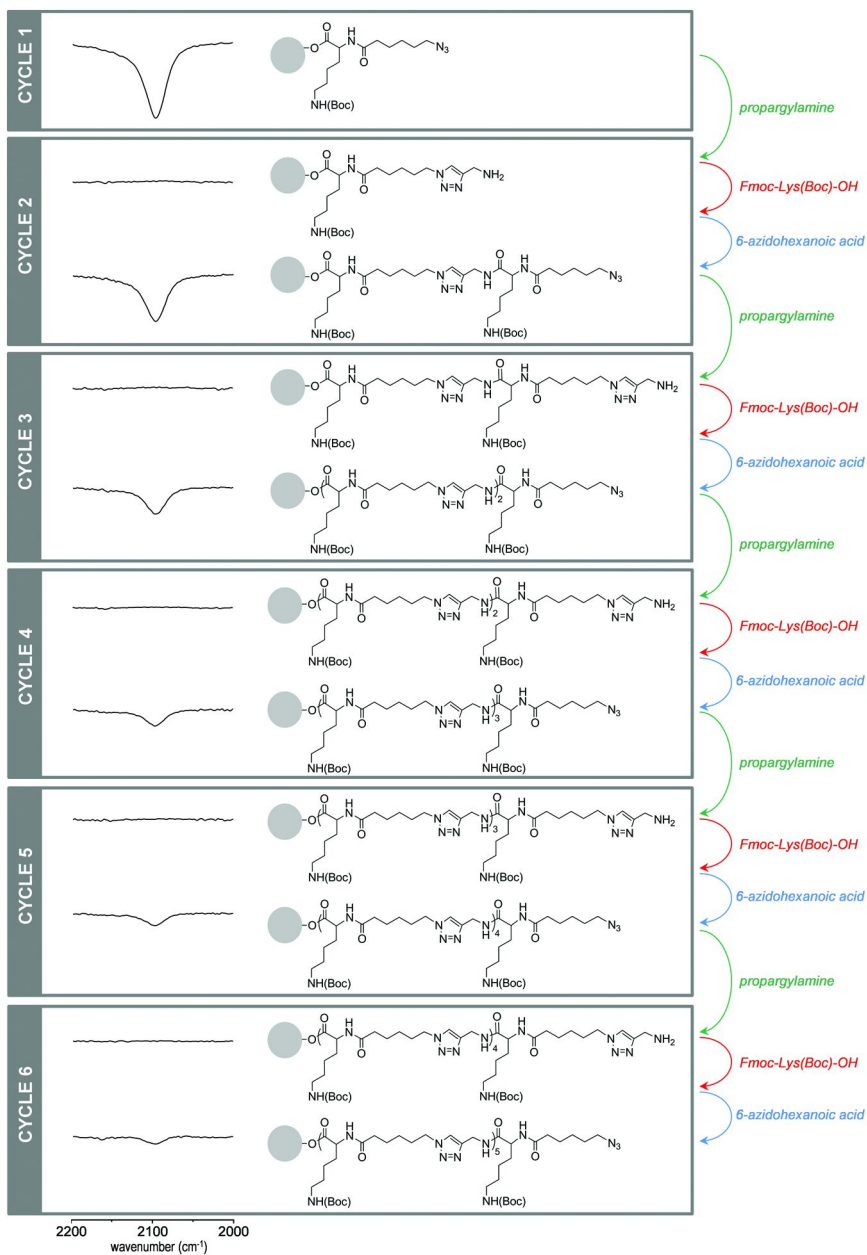
Figure 4. Monitoring of the iterative synthesis of sequence-defined oligomers prepared from Fmoc-Lys(Boc)-OH, 6-azidohexanoic acid and propargylamine on a chlorotrityl chloride resin up to six cycles by FT-IR spectroscopy.
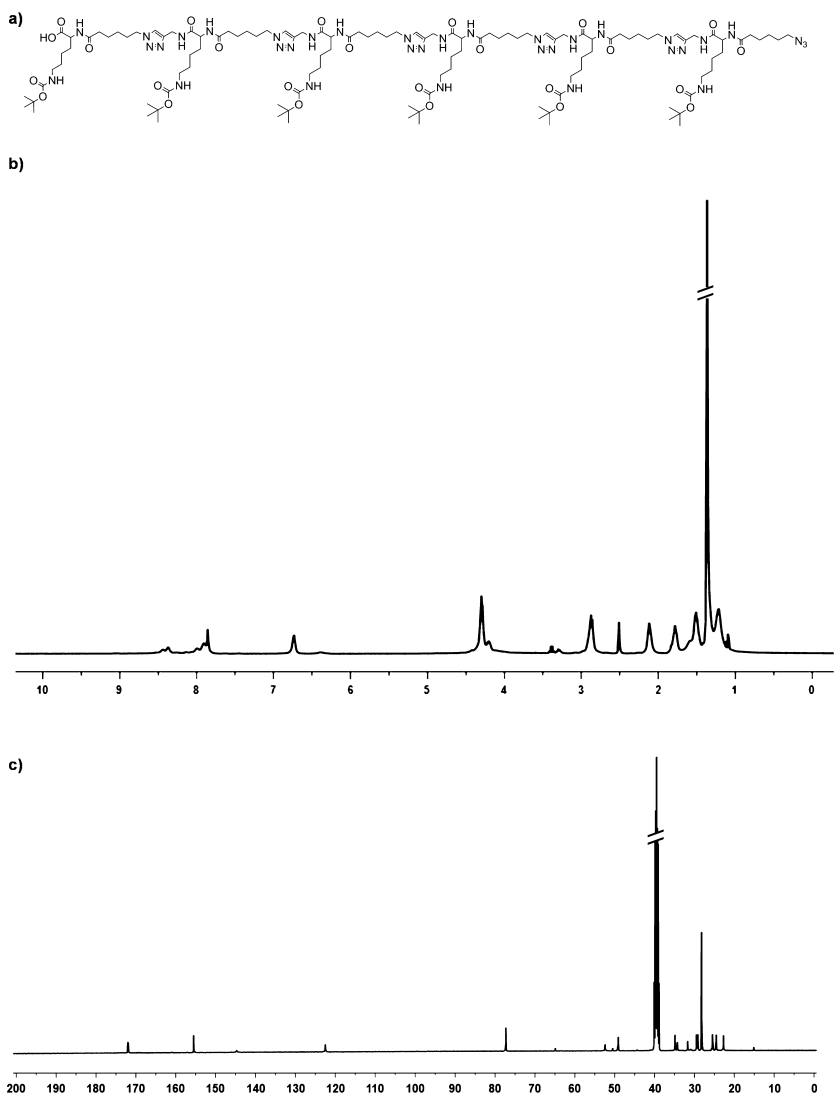
Figure 5. a) Structure, b) ^1H and c) ^{13}C NMR in DMSO-d_6 of a model sequence-defined oligomer synthesized through the reiteration of six repeating cycles using as building blocks Fmoc-Lys(Boc)-OH, 6-azidohexanoic acid and propargylamine on a chlorotrityl chloride resin.

Table 2. ESI-MS characterization of the model oligomers synthesized from Fmoc-Lys(Boc)-OH, 6-azidohexanoic acid and propargylamine on a chlorotrityl chloride resin for different number of repeating cycles.

cycle	[M+Na]$^+$	
	Cald.	*Found*
1	408.22	408.22
2	830.49	830.49
3	1252.74	1252.75
4	1675.01	1675.01
5	2097.28	2097.30
6	2519.54	2519.56

Conclusions and Future Prospects

Solid-phase synthesis was demonstrated to be a viable synthetic tool for the preparation of sequence-defined oligomers and able to handle multiple types of chemistry without requiring more constraining conditions as those employed for the synthesis of peptides. We have reported here the access to relatively long sequence-defined oligomers based on natural α-amino acids and synthetic building blocks through the use of orthogonal reactions, namely, formation of amide bonds and copper-assisted alkyne-azide cycloadditions. These synthetic building blocks can be simple alkyl linkers as reported here, but the use of building blocks providing further functionalities to the oligomers could be also considered contributing in tuning the design of the oligomers and their properties.

Experimental

Materials

Chlorotrityl chloride resin (1.6 mmol·g^{-1}, 100-200 mesh), 2-(1H-benzo-triazol-1-yl)-1,1,3,3-tetramethyluronium hexafluorophosphate (HBTU, 99%), and Fmoc-L-Lys(Boc)-OH (>99%) were purchased from Iris Biotech GmbH. 1-Hydroxybenzotriazole hydrate (HOBt, >97%), piperidine (99%), copper(I) bromide (CuBr, 98%), acetic acid (99.8%), *N,N,N′,N′,N″*-pentamethyldiethyl-enetriamine (PMDETA, 99%), hydrochloric acid (concentrated HCl, 37% in water), anhydrous dichloromethane (CH$_2$Cl$_2$, anhydrous, >99.8%), anhydrous *N,N*-dimethylformamide (DMF, anhydrous, 99.8%), and *N,N*-dimethylformamide (DMF, >99%) were purchased from Aldrich. 6-Bromohexanoic acid (98+%), *N*-ethyldiisopropylamine (DIPEA, 99%), propargylamine (>95%), and 2,2,2-tri-fluoroethanol (TFE, 99+%) were purchased from Alfa Aesar. Dichloromethane (CH$_2$Cl$_2$, RE, pure stabilized with amylene), methanol (RPE, for analysis,

ACS reagent), diethyl ether (RE, pure stabilized with BHT) and acetone (RE, pure) were purchased from Carlo Erba. All the reagents were used as received except if otherwise noted. Copper(I) bromide was purified by stirring in acetic acid overnight, washing with methanol, and drying under vacuum at room temperature. 6-Azidohexanoic acid was synthesized as reported previously (*35*). All the syntheses on solid support were performed in solid-phase extraction (SPE) tubes (12 mL polypropylene SPE tubes with polyethylene frits, 20 μm porosity purchased from SUPELCO®) and shaken using a modified IKA KS 130 basic shaker.

Characterization

Nuclear magnetic resonance (NMR) spectra were recorded in DMSO-*d$_6$* on a Bruker Avance 400 MHz spectrometer equipped with Ultrashield magnets.

Fourier transform infrared (FTIR) spectra were recorded on a Bruker Vertex 70 spectrometer using the attenuated total reflectance (ATR) technique.

Electrospray ionization mass spectrometry (ESI-MS) experiments were performed on a Bruker Daltonics microTOF spectrometer equipped with an orthogonal electrospray (ESI) interface. Calibration was performed using a solution of 10 mM sodium formiate. Sample solutions were introduced into the spectrometer source with a syringe pump (Harvard type 55 1111: Harvard Apparatus Inc., South Natick, MA, USA) with a flow rate of 4 μL·min^{-1}.

Synthesis of Sequence-Defined Oligomers Based on Natural Amino Acids and Synthetic Building Blocks

Sequence-defined oligomers based on three repeating cycles were prepared as previously reported (*35*) and the longer ones were synthesized similarly. In brief, 1.28 g of chlorotrityl chloride resin (2.0 mmol of functional groups) was weighted in a SPE vessel, swollen in CH$_2$Cl$_2$ for 10 min and washed 3 times with CH$_2$Cl$_2$. Fmoc-Lys(Boc)-OH (2.9 g, 6.1 mmol) was added to the vessel, which was then degased by performing 3 vacuum/argon cycles. 7 mL of anhydrous CH$_2$Cl$_2$ was added to the vessel followed by 2.1 mL of DIPEA (12.1 mmol). The solution was agitated for 1 h under argon. The solution was filtered and the resin was washed 6 times with DMF. 7 mL of a 80/15/5 CH$_2$Cl$_2$/methanol/DIPEA solution was agitated for 10 min (twice), and the resin was subsequently washed with DMF 6 times. The Fmoc-protecting groups were removed by agitation for 3 min with 7 mL of a 25% piperidine cleavage solution in DMF followed by filtration and agitation with a fresh cleavage solution for 20 min. The resin was then washed 6 times with DMF, 6 times with CH$_2$Cl$_2$, 3 times with methanol and 3 times with CH$_2$Cl$_2$. The resin was dried overnight under vacuum at room temperature. The loading density of lysine residues grafted on the resin was determined by gravimetric analysis (typically 1.0 to 1.4 mmol·g^{-1}).

The sequence-defined oligomers were synthesized from successive additions of 6-azidohexanoic acid, propargylamine and Fmoc-Lys(Boc)-OH following the procedure described below until the desired sequence was obtained.

i) Addition of 6-azidohexanoic acid. 6-Azidohexanoic acid (3 eq. relative to the loading), HBTU (3 eq. relative to the loading), HOBt (3 eq. relative to the loading), DIPEA (6 eq. relative to the loading) and anhydrous DMF (5 mL per mmol of functional groups on the resin) were added to the peptide vessel, and agitated for 30 min. After filtration, the resin was washed 6 times with DMF and 6 times with CH_2Cl_2.

ii) Copper-assisted alkyne-azide cycloaddition with propargylamine. CuBr (0.2 eq. relative to the loading) was added to the peptide vessel, which was then degased through 3 vacuum/argon cycles. Anhydrous CH_2Cl_2 (7 mL per mmol of functional groups on the resin) were added to the peptide vessel, followed by PMDETA (0.4 eq. relative to the loading) and propargylamine (3 eq. relative to the loading). The solution was agitated under argon for 1 h. After filtration, the resin was washed 6 times with DMF and 6 times with CH_2Cl_2.

iii) Addition of Fmoc-Lys(Boc)-OH. Fmoc-Lys(Boc)-OH (3 eq. relative to the loading), HBTU (3 eq. relative to the loading), HOBt (3 eq. relative to the loading), DIPEA (6 eq. relative to the loading) and anhydrous DMF (5 mL per mmol of functional groups on the resin) were added to the peptide vessel, and agitated for 30 min. After filtration, the resin was washed 6 times with DMF. The Fmoc-protecting group was removed by agitation for 3 min with a 25% piperidine cleavage solution in DMF followed by filtration and agitation with a fresh cleavage solution for 20 min. The resin was then washed 6 times with DMF and 6 times with CH_2Cl_2.

The oligomer was cleaved from the resin by adding a 4/1 CH_2Cl_2/TFE solution to the peptide vessel for 45 min (twice). The resin was filtered, washed three times with CH_2Cl_2, and the filtrates were collected in a clean round-bottom flask. The solution was concentrated by rotary evaporation and precipitated in diethyl ether. The product was recovered by filtration and dried under vacuum at room temperature.

Acknowledgments

References

1.   Lutz, J.-F.; Ouchi, M.; Liu, D. R.; Sawamoto, M. *Science* **2013**, *341*, 1238149.
2.   Pfeifer, S.; Lutz, J.-F. *J. Am. Chem. Soc.* **2007**, *129*, 9542–9543.
3.   Satoh, K.; Matsuda, M.; Nagai, K.; Kamigaito, M. *J. Am. Chem. Soc.* **2010**, *132*, 10003–10005.

4. Zhang, J.; Matta, M. E.; Hillmyer, M. A. *ACS Macro Lett.* **2012**, *1*, 1383–1387.

5. Stayshich, R. M.; Meyer, T. Y. *J. Am. Chem. Soc.* **2010**, *132*, 10920–10934.

6. Ida, S.; Terashima, T.; Ouchi, M.; Sawamoto, M. *J. Am. Chem. Soc.* **2009**, *131*, 10808–10809.

7. Milnes, P. J.; McKee, M. L.; Bath, J.; Song, L.; Stulz, E.; Turberfield, A. J.; O'Reilly, R. K. *Chem. Commun.* **2012**, *48*, 5614–5616.

8. Hibi, Y.; Ouchi, M.; Sawamoto, M. *Angew. Chem., Int. Ed.* **2011**, *50*, 7434–7437.

9. Kramer, J. W.; Treitler, D. S.; Dunn, E. W.; Castro, P. M.; Roisnel, T.; Thomas, C. M.; Coates, G. W. *J. Am. Chem. Soc.* **2009**, *131*, 16042–16044.

10. Satoh, K.; Ozawa, S.; Mizutani, M.; Nagai, K.; Kamigaito, M. *Nat. Commun.* **2010**, *1*, 6.

11. Soth, M. J.; Nowick, J. S. *Curr. Opin. Chem. Biol.* **1997**, *1*, 120–129.

12. Tong, X.; Guo, B.-H.; Huang, Y. *Chem. Commun.* **2011**, *47*, 1455–1457.

13. Früchtel, J. S.; Jung, G. *Angew. Chem., Int. Ed.* **1996**, *35*, 17–42.

14. Feuerbacher, N.; Vögtle, F. Iterative Synthesis in Organic Chemistry. In *Dendrimers*; Springer: Berlin, Heidelberg: 1998; Vol. 197, pp 1−18.

15. Boeijen, A.; van Ameijde, J.; Liskamp, R. M. J. *J. Org. Chem.* **2001**, *66*, 8454–8462.

16. Cho, C. Y.; Moran, E. J.; Cherry, S. R.; Stephans, J. C.; Fodor, S. P. A.; Adams, C. L.; Sundaram, A.; Jacobs, J. W.; Schultz, P. G. *Science* **1993**, *261*, 1303–1305.

17. Ishibashi, Y.; Kitamura, M. *Chem. Commun.* **2009**, 6985–6987.

18. Moree, W. J.; van der Marel, G. A.; Liskamp, R. J. *J. Org. Chem.* **1995**, *60*, 5157–5169.

19. Zuckermann, R. N.; Kerr, J. M.; Kent, S. B. H.; Moos, W. H. *J. Am. Chem. Soc.* **1992**, *114*, 10646–10647.

20. Sun, J.; Zuckermann, R. N. *ACS Nano* **2013**, *7*, 4715–4732.

21. Alluri, P.; Liu, B.; Yu, P.; Xiao, X.; Kodadek, T. *Mol. BioSyst.* **2006**, *2*, 568–579.

22. Rose, K.; Vizzavona, J. *J. Am. Chem. Soc.* **1999**, *121*, 7034–7038.

23. Hartmann, L.; Krause, E.; Antonietti, M.; Börner, H. G. *Biomacromolecules* **2006**, *7*, 1239–1244.

24. Hartmann, L. *Macromol. Chem. Phys.* **2011**, *212*, 8–13.

25. Ponader, D.; Wojcik, F.; Beceren-Braun, F.; Dernedde, J.; Hartmann, L. *Biomacromolecules* **2012**, *13*, 1845–1852.

26. Pfeifer, S.; Zarafshani, Z.; Badi, N.; Lutz, J.-F. *J. Am. Chem. Soc.* **2009**, *131*, 9195–9197.

27. Trinh, T. T.; Oswald, L.; Chan-Seng, D.; Lutz, J.-F. *Macromol. Rapid Commun.* **2014**, *35*, 141–145.

28. Angelo, N. G.; Arora, P. S. *J. Org. Chem.* **2007**, *72*, 7963–7967.

29. Espeel, P.; Carrette, L. L. G.; Bury, K.; Capenberghs, S.; Martins, J. C.; Du Prez, F. E.; Madder, A. *Angew. Chem., Int. Ed.* **2013**, *52*, 13261–13264.

30. Malenfant, P. R. L.; Fréchet, J. M. J. *Chem. Commun.* **1998**, 2657–2658.

31. Young, J. K.; Nelson, J. C.; Moore, J. S. *J. Am. Chem. Soc.* **1994**, *116*, 10841–10842.

32. Seebach, D.; Gardiner, J. *Acc. Chem. Res.* **2008**, *41*, 1366–1375.
33. Liu, C. C.; Schultz, P. G. *Annu. Rev. Biochem.* **2010**, *79*, 413–444.
34. Green, B. R.; Catlin, P.; Zhang, M.-M.; Fiedler, B.; Bayudan, W.; Morrison, A.; Norton, R. S.; Smith, B. J.; Yoshikami, D.; Olivera, B. M.; Bulaj, G. *Chem. Biol.* **2007**, *14*, 399–407.
35. Chan-Seng, D.; Lutz, J.-F. *ACS Macro Lett.* **2014**, *3*, 291–294.

Chapter 8

Synthesis of Sequence-Controlled Copolymers Using Time-Regulated Additions of *N*-Substituted Maleimides in Styrenic Radical Polymerizations

Nathalie Baradel, Olga Shishkan, Sansanee Srichan, and Jean-François Lutz***

Precision Macromolecular Chemistry, Institut Charles Sadron, BP 84047, 23 rue du Loess, 67034 Strasbourg Cedex 2, France
***E-mail: jflutz@unistra.fr**

The present chapter describes the preparation of sequence-controlled copolymers by a free-radical polymerization process. Over the last years, our group has shown that controlled/living radical polymerization mechanisms offer interesting advantages for sequence regulation. In such mechanisms, polymer chains form gradually over time, and their microstructure can, therefore, be tuned using time-controlled monomer additions. For instance, the addition of small amounts of acceptor comonomers, such as *N*-substituted maleimides, during the controlled radical polymerization of a large excess of donor monomer, such as styrene, allows the writing of information onto polymer chains. This strategy is not perfect and exhibits some of the drawbacks of chain-growth polymerizations, such as the formation of chain-to-chain sequence defects. On the other hand, this approach is experimentally easy, rapid, scalable and very versatile.

Introduction

Free-radical copolymerizations lead in most cases to statistical copolymers (i.e. macromolecules containing ill-defined comonomer sequences). Thus, during the last decades, many studies have been conducted in order to prepare

copolymers containing ordered sequences of monomers by radical chain-growth polymerization (*1–4*). It has been known, for example, since the 1940's (see the introduction chapter of this volume for historical context) that the free-radical copolymerization of donor and acceptor comonomers leads often to AB alternating copolymers (*5*). It has also been reported that more elaborated microstructures such as AAB repeating sequences can be attained using very specific comonomers, however such examples remain the exception rather than the norm (*6*).

The discovery of controlled radical polymerizations (CRP) techniques two decades ago has opened up new options for preparing sequence-controlled copolymers (*7–9*). For instance, Matyjaszewski and coworkers have pointed out the relevance of these methods for preparing gradient copolymers (*10*). Yet, until a few years ago, block, statistical, alternating and gradient copolymers were the only types of copolymers that could be prepared by radical polymerization (*3*). In order to change that situation, some research groups have attempted to develop iterative free-radical growth-processes, in which comonomers are incorporated in the chains using succesive insertion steps (*11*, *12*). However, these approaches require in general time-consuming purification steps and remain therefore limited to the incorporation of a few monomer units. The group of Sawamoto has also reported very elegant template radical polymerization approaches that are summarized in another chapter of the present volume of the ACS Symposium Series (*13–15*).

In 2007, our group reported a new method for 'writing' local functional information in the microstructure of styrenic polymers prepared by a controlled/living radical polymerization process (*16*). This method utilizes donor/acceptor comonomers, such as *N*-substituted maleimides (MIs) and styrenics, that were classically used in alternating free-radical copolymerizations. However, in our strategy, these monomers are used in a non-stoichiometric ratio (*17*). In particular, the time-controlled addition of tiny amounts of functional *N*-substituted maleimides (i.e. acceptor comonomers) in the controlled/living radical polymerization of a large excess of a styrenic monomer (i.e. donor monomer) allows preparation of unprecedented aperiodic copolymers. This method does not allow synthesis of perfectly sequence-defined copolymers but present the advantage of being easy and versatile. Recent achievements obtained with this method are summarized herein. It should be noted that large portions of the text of this chapter were already used in a recent Account (*18*). This text is used with permission of the American Chemical Society.

Description of the Concept

The concept for monomer sequence-control that we introduced in 2007 is based on the 'living' copolymerization of donor and acceptor comonomers (*16*). A comprehensive analysis of the field of donor/acceptor copolymerization was reported in a previous feature article and will therefore not be described in details herein (*17*). In brief, our concept requires two different types of

unsaturated monomers, a donor and an acceptor comonomer. Due to the opposite polarity of their double bonds, these monomers exhibit usually a stronger tendency to copolymerize than to homopolymerize. Typical examples of donor monomers include isobutylene, vinyl ethers, stilbene, styrene and many styrenic derivatives. Frequently-used acceptor comonomers are, for example, maleic anhydride, MIs and pentafluorostyrene. The radical or cationic copolymerization of a donor/acceptor comonomer pair leads in general to regular alternating microstructures. However, the obtained microstructure depends on the initial donor/acceptor comonomer feed and on the monomer conversion at which the copolymer was isolated. For instance, when a large excess of donor monomer is used in the initial feed, copolymerization usually takes place at the beginning of the reaction (i.e. until the acceptor comonomer is consumed) followed by the homopolymerization of the excess of donor. Such a two-stage behavior is particularly interesting in the case of a 'living' polymerizations mechanism, e.g. in CRP processes such as atom transfer radical polymerization (ATRP) or nitroxide mediated polymerization (NMP) (7, 8). In such polymerizations, all chains are initiated and grown simultaneously and therefore variations in comonomer consumption are 'encrypted' in the microstructure of the formed polymer. Thus, non-stoichiometric donor/acceptor living copolymerizations containing an excess of donor lead generally to the formation of block copolymers containing a donor/acceptor copolymer segment connected and a donor homopolymer segment (19–21). The main originality of our approach was to exploit this interesting behavior in extreme conditions (Figure 1), in particular in the presence of very small amounts of acceptor comonomers (e.g. 1 molar eq. per chain). In such conditions, the zones encrypted in the polymer chains cannot be described anymore as 'blocks' but as short functional patches positioned in a donor homopolymer chain. This concept was first demonstrated by ATRP using styrene as the donor monomer and various MIs as acceptor comonomers (16). It was shown that, although tiny amounts of acceptor comonomer are used, donor/acceptor copolymerization remains kinetically favored compared to donor homopolymerization. Consequently, the MI is rapidly consumed and included in short regions of the copolymer chain. For instance, if the copolymerization is started in the presence of both donor and acceptor comonomers, the MI is fully integrated at the beginning of the chain (22). Interestingly, when the polymerization is started in the presence of the sole donor monomer and the MI is added later in the process as described in Figure 1, the MI-containing zone is formed inside the chain.

Such a time-controlled addition is actually one of the main strengths of our approach because it allows placement of the MI at different chain-locations (22). The chain-positioning can be extremely precise as described in the third section of this chapter. However, it should be clearly explained that the MI placement is not uniform in all chains. The zones created in such a copolymerization process are still, to some degree, statistical. In fact, as depicted in Figure 1, two different types of chain-to-chain variations occur. Firstly, differences in chain placement exist. The localization of a MI in a chain is estimated by comparing the kinetics of consumption of the donor and acceptor comonomers during a given time interval (i.e. the amount of time needed for reaching complete conversion of the acceptor

comonomer). Generally, while a single molar equivalent of MI is polymerized, a comparatively higher amount of styrene is consumed. Thus, during the time interval required for full MI consumption, a short PS 'patch' is formed and it is therefore not possible to assess precisely the location of the MI is in this region. In fact, the placement slightly varies from chain to chain as depicted in Figure 1. The MI can be located at the beginning of the patch, at the end, or anywhere between these two extremes. The second type of deviations that exists in our systems is the chain-to-chain variation in composition. When 1 molar eq. of MI is used as compared to initiator, the formed chains contain in average 1 MI. However, a chain-to-chain distribution of composition exists (i.e. some chains contain no MI, whereas other contains 1, 2, or more MIs as shown in Figure 1). Nevertheless, recent MALDI-TOF MS (*17*, *22*) studies indicate that this distribution is usually rather narrow.
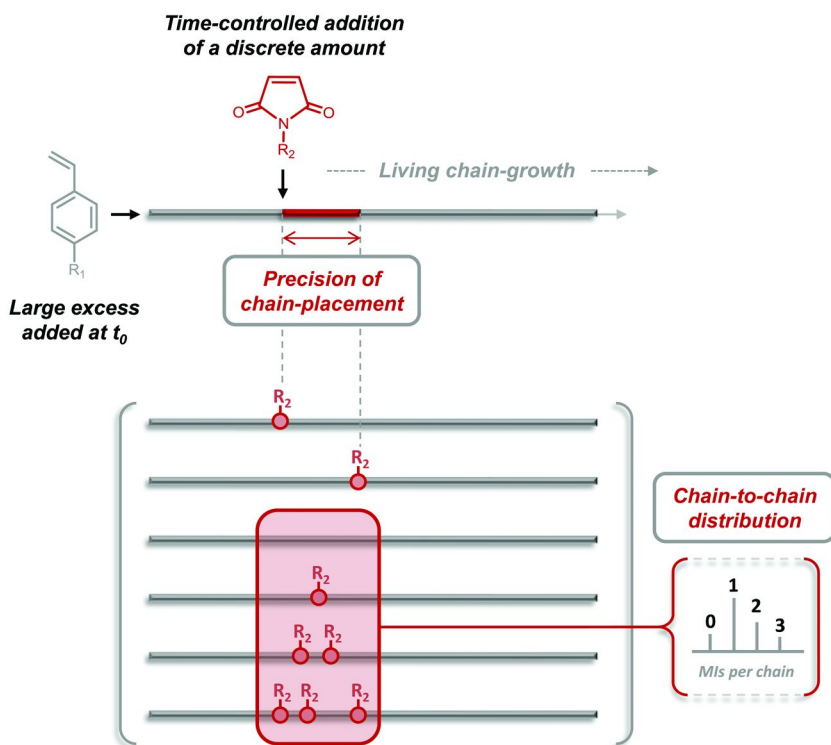
Figure 1. Main concept: local chain-installation of a discrete amount of an acceptor monomer during the controlled radical polymerization of a large excess of a donor monomer. Reprinted with permission form reference (18). Copyright 2013 American Chemical Society.

Donor Comonomers

In the concept described above, two types of monomers are mandatory, i.e. a donor and an acceptor comonomer. The donor comonomer is used in large excess and is therefore the main constitutive unit of the polymer backbone, whereas the acceptor comonomer is used for local encryption (see the following section). The molecular structure of this main building-block is important since it determines the properties (e.g. chain rigidity, solubility, and reactivity) of the formed backbones. In our early studies, styrene was always used as a donor comonomer (*16*, *22*). This monomer is indeed a convenient model because its reactivity in radical polymerization has been extensively studied and therefore many kinetic parameters (i.e. rate constants, reactivity ratios) have been reported. In addition, optimized CRP conditions have been identified for styrene homopolymerizations and copolymerizations (*23*, *24*). This aspect is actually crucial. Indeed, the concept described in Figure 1 is only valid if the homopolymerization of the donor monomer is perfectly controlled (i.e. all living polymerization criteria should be verified). Still, styrene is not the only donor monomer, which can be used in our concept. For instance, *para*-substituted styrene derivatives can also be utilized. The chemical nature of the *para*-substituent may lead to interesting backbone properties such as water-solubility, side-chain crystallinity or reactivity. However, not all types of substituents lead to sequence-controlled copolymerization with MIs. Another mandatory criterion in our approach is that the donor/acceptor copolymerization is kinetically highly favored as compared to homopolymerization. Roughly speaking, the concept works well for donor/acceptor comonomer pairs with reactivity ratios below 0.05. Above this value, copolymerization starts to be too slow as compared to homopolymerization and therefore MIs are imprecisely incorporated in the chains. For example, although interesting for post-polymerization modifications strategies (*25*), monomers such as vinyl benzyl chloride or pentafluorophenyl 4-vinylbenzoate (*26*) are not suitable for our concept, probably because of the electron-withdrawing nature of the *para*-subsitutents that decrease the electron donor properties of these monomers. The *tert*-butyl ester of vinylbenzoic acid is an example of *para*-substituted monomer that can be used in our approach (*27*). This monomer can be copolymerized with MIs and afterwards deprotected to afford sequence-controlled polyelectrolytes. In this strategy, the *tert*-butyl esters are cleaved in acidic conditions that do not affect succinimide units incorporated in the copolymer chains. However, due to the electron-withdrawing character of the *tert*-butyl ester substituent, the reactivity ratios measured for this monomer in the presence of various MIs were found to be slightly too high for a perfect sequence regulation. Sequence-controlled water-soluble polymers with more precise microstructures can be synthesized using donor monomers such as 4-acetoxystyrene or 4-*tert*-butoxystyrene (*28*). Indeed, both monomers have donor substituents in *para*-aromatic position and lead therefore to extremely favored copolymerization behaviors with MIs. After copolymerization, the ether functions can be selectively cleaved in acidic conditions to afford hydrophilic polymers. Very precise copolymerization trends with MIs were also observed for donor monomers such as 4-methylstyrene (*28*) or 4-octadecylstyrene (*29*). In

the latter case, sequence-controlled copolymers with interesting semi-crystalline behaviors were obtained.

Acceptor Comonomers

As shown in Figure 1, MIs are the molecular units used for chain encryption in our approach. MIs are not the only type of acceptor comonomers that can be used in our concept but they present the great advantage of being easily functionalized at their *N*-site. Indeed, the synthesis of these monomers is, in general, relatively easy (*22*). Moreover, a large number of functional MIs are commercially available since this class of compounds is also widely used for protein modification via Michael addition. It is therefore possible to create a full 'alphabet' of MIs (*17, 18*). However, not all MIs are suitable for our technique. Firstly, it is necessary to check, for each MI, whether the reactivity ratios are sufficiently low for an accurate sequence-control. In general, the chemical nature of a *N*-substituent does not influence considerably MI double bond reactivity. For instance, the electronic nature (i.e. electron donating/withdrawing character) of a *N*-substituent in a MI is less critical in our approach than the one of a *para*-substituent in a donor monomer (see discussion in the previous section). Nevertheless, different MIs exhibit different reactivities. For example, monomers with strong electron-withdrawing substituents, such as pentafluorophenyl 4-maleimidobenzoate, work very well in our concept and can be positioned extremely precisely in polystyrene chains (*30*). In comparison, MIs with alkyl chain substituents, such as *N*-propyl maleimide, are usually incorporated in broader regions (*31*). However, despite these small differences, most MIs have suitable reactivities for being used in our concept. Yet, the chemical reactivity of the *N*-substituent is another limitation. Indeed, some substituents may disturb the polymerization reaction. For instance, phenols inhibit radical polymerization (*22*). Similarly, terminal alkynes interfere with polymerization radicals and shall be protected in our technique (*22, 32, 33*). Some substituents may also interact with polymerization catalysts. For instance, carboxylic acids and primary amines shall be protected in sequence-controlled ATRP (*22*). Another important aspect is the solubility of MIs in the polymerization medium. Indeed, our concept requires that MIs are homogenously solubilized in the reaction medium (i.e. bulk donor monomer) at the temperature at which the copolymerization is conducted (i.e. typically above 90°C). Some MIs are not well-soluble in styrene or other donor monomers at room temperature but can be dissolved at higher temperature and therefore used in our approach. This aspect is unproblematic when MIs are added at the beginning of the reaction but more critical when time-controlled additions are performed as shown in Figure 1. In such cases, a solution of MI in a minimal amount of solvent is added via a syringe. For some particular MIs (e.g. pentafluorophenyl 4-maleimidobenzoate), hot solutions or solvent dispersions are also sometimes used. Another important point is that, after each syringe addition, the MIs should be rapidly dispersed in the reaction medium in order to avoid local copolymerization effect. This aspect is in fact not really critical when CRP conditions are used. Indeed, in styrene CRP, the polymer chains are predominantly in a 'dormant' state and are

therefore not consuming MIs directly after addition. The chain incorporation of a single molar equivalent of MI requires, in general, more than 20 minutes to be completed. Thus, under vigorous stirring conditions, the influence of diffusion can be neglected. In some rare cases, MIs are not soluble in the polymerization medium even at high temperature. For example, some biotin-functionalized MIs cannot be dissolved in styrene (*22*). In such cases, the copolymerization can be performed using a cosolvent. However, the kinetics of copolymerization are slower in solution than in the bulk. To bypass such limitations, problematic functions can be attached to positioned MI sites using post-polymerization modification strategies (*25*). For instance, we have recently reported the biotin functionalization of a pentafluorophenyl-modified sequence controlled polymer (*30*). Besides pentafluorophenyl 4-maleimidobenzoate, other types of reactive MIs can also be used in post-polymerization modification strategies. For instance, MIs containing protected alkyne functions can be modified after polymerization by copper-catalyzed azide-alkyne cycloaddition, Glaser coupling or Sonogashira coupling (*32–35*).

Recent Optimization of the Concept

The concept for MI positioning shown in Figure 1 is, of course, not limited to one addition. Successive time-controlled additions can be performed in order to install several MI zones in the chains. In our first publication, it was demonstrated that 4 functional MIs can be added sequentially during the bulk ATRP of styrene. It should be noted that, when multiple additions are performed, it is recommended to use more than 1 molar eq. of MI per addition (e.g. 2-3 molar eq. as compared to initiator). Due to chain-to-chain discrepancies in composition, the repeated utilization of a single equivalent of MI leads to a high level of chain defects (*17*). It should be also specified that copolymerizations employing successive time-controlled additions are experimentally demanding and require a detailed kinetic monitoring. For instance, when such experiments are conducted manually, it is challenging to install more than 4 MIs zones in a chain. This situation can be improved by using synthetic robotic platforms that allows rapid screening and optimization of experimental conditions. For instance, we have recently reported that a large density of information can be incorporated in polystyrene chains using automated protocols (*31*). Using *N*-benzyl maleimide as a model MI, we have explored the boundaries of our concept. It was shown that 4, 7 and 8 non-overlapping MI zones can be positioned in polystyrene chains with an average chain length of 20, 50 and 100, respectively. These results open interesting avenues in terms of information storage. Indeed, more than 65000 microstructural arrangements can be potentially created on a chain of *DP*100 using a 4-letter alphabet of MIs. This number rises up to 100 million if 10 different MIs would be used. This is undoubtedly the highest level of chain-encoding reported to date for chain-growth polymers. It should be however clearly reminded that our concept is not leading to perfectly controlled monomer sequences. However, it was observed that the precision of MI incorporation increase with styrene conversion. MIs added at the end of the polymerization (i.e. at high styrene conversion) are

much more precisely installed in the chains than MIs added at the beginning. A simple explanation of this behavior was reported in a recent communication (*35*). In fact, the precision of incorporation depends on the donor/acceptor comonomer ratio present in the reaction medium at the time the MI is added. If this ratio is high, donor-donor propagation competes with donor-acceptor cross-propagation, thus leading to broad uncertainty regions. On the other hand, when this ratio is low a very precise incorporation is observed. In fact, at high styrene conversions (e.g. above 70%), an almost perfect MI monoinsertion is observed (i.e. only 1 or 2 styrene units are incorporated in the chains during the interval of time needed for full MI consumption). We have shown that this interesting situation can be restored at different moments of a polymerization if the donor monomer is used in starved conditions (Figure 2) (*35*). In this 'ultra-precise' strategy, a partial amount of the donor monomer is added at the beginning of the reaction (feed 1 in Figure 2b) instead of the full amount that is usually introduced in the conventional procedure. When this partial amount reaches high conversion, MI comonomer is added in the copolymerization medium (feed 2 in Figure 2b). In these conditions, the donor/acceptor comonomer ratio is low and therefore the MI is precisely incorporated in the chains.
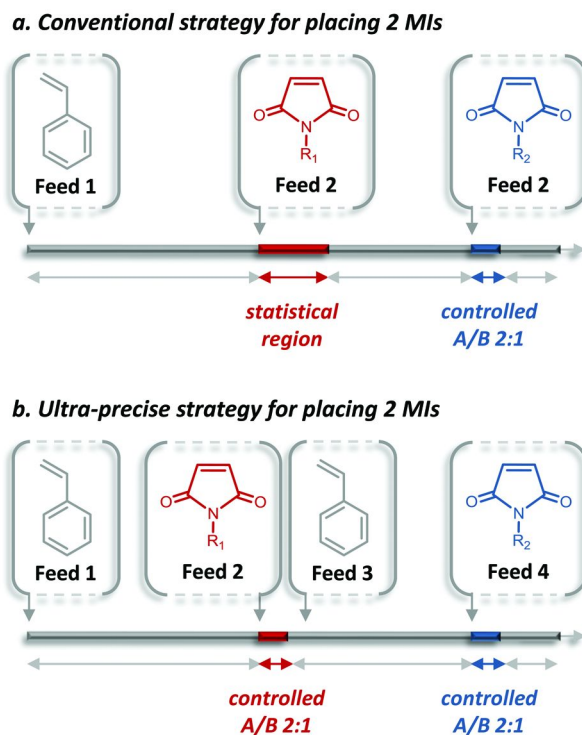
Figure 2. Chain-positioning of functional N-substituted maleimides using (a) a conventional strategy or (b) an ultra-precise strategy.

Afterwards, a new batch of donor monomer is added in the copolymerization medium (feed 3 in Figure 2b). This should be rapidly done before the experiment loses its living character. Indeed, if the polymerization reaches too high donor monomer conversions, side reactions such as elimination or termination become kinetically dominant. However, if the addition of the second donor monomer feed is done in optimal conditions, the polymerization restarts. When this new batch reaches high conversion in its turn, a second MI can be then installed in the chains (feed 4 in Figure 2b). This simple strategy can be repeated 2 or 3 times and leads in all cases to ultra-precise MI insertions.

Synthesis of Complex Copolymers

The sequence-controlled polymers described in the previous sections of this Account are not only interesting in terms of polymer synthesis but also open up interesting opportunities in the field of materials science. Indeed, the possibility to 'write' local functional patches on synthetic polymer chains is an important step-forward. However, it is important at this stage to discuss the molecular structures of our polymers. These macromolecules possess an atactic flexible backbone and are, in most cases, amorphous. Thus, it is not possible to form secondary structures using the same principles as those that govern protein folding (i.e. Anfinsen's dogma that links primary, secondary, and tertiary structures). However, other principles may be applicable (36). For instance, it was recently proposed that a certain degree of order (i.e. pseudo-crystalline state) can be attained with atactic polymers in confined conditions (37). Non-natural secondary structures can also be created in atactic polymers using synthetic supramolecular motifs. For instance, Meijer, Palmans and coworkers have recently shown that side-chain supramolecular moieties induce order in atactic polymer chains (38). Moreover, controlled covalent interactions can be used to organize atactic chains. Our group has reported that the donor/acceptor sequence-controlled copolymerization approach can be used to create precisely positioned covalent bridges (32, 39, 40). In a first study, alkyne-containing MIs were positioned in polystyrene chains and were involved, after deprotection, in intramolecular reactions in dilute conditions (32). Different macromolecular topologies, such as α-, P-, Q- or 8-shapes, were prepared using either azide-alkyne cycloaddition with azide chain-ends or alkyne-alkyne Glaser coupling. In a following work, more complex bio-hybrid topologies were synthesized using a peptide motif as shown in Figure 3 (40). In this approach, an oligomer containing the cysteine-arginine-cysteine (CRC) sequence was attached at specific locations on atactic polystyrene backbones and used to form intramolecular covalent bridges. These results are just a beginning. In future, the combination of spatially controlled covalent and supramolecular interactions should lead to the development of single chain objects with controllable functions (41). Such a vision opens up interesting options in the field of catalysis and molecular transport (42). The possibility to form local regions in polymeric microstructures is also an appealing strategy for preparing single-chain functional arrays (i.e. chain regions containing specific

information). The simplest version of such a design is a periodic copolymer containing a functional group regularly spaced along the polymer backbone. We reported the preparation of periodic structures containing repeating primary amines, carboxylic acids or alkyne functions (*43*). In this work, short reactive prepolymers were first synthesized by sequence-controlled copolymerization of styrene and MIs and afterwards polymerized by step-growth polymerization to afford periodic functional copolymers. The next step in terms of complexity is the preparation of microstructures containing different functional regions (*33, 44*). For instance, we have reported very recently the synthesis of single-chain sugar-arrays (*33*). In this work, different monosaccharides were installed on a well-defined polystyrene chain using a multistep post-polymerization modification approach. It was demonstrated that the formed sugar-arrays were recognized by complementary lectins. Such new types of sequence-controlled glycopolymers constitute interesting mimics of glycoproteins since the amount of sugar functions and their placement in the chain can be precisely controlled.
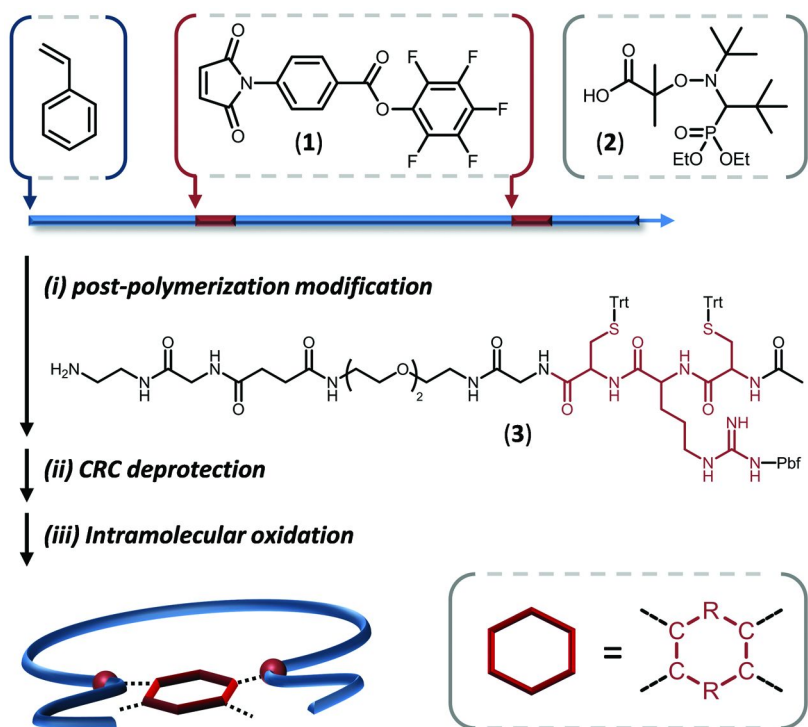
Figure 3. General strategy studied for folding well-defined linear polymers, prepared by sequence-controlled nitroxide mediated copolymerization, into defined bicyclic topologies. In this concept, a twin disulfide cycle is formed by oxidation of two cysteine-arginine-cysteine (CRC) peptide motifs.

Outlook

The aim of this chapter was to summarize our recent achievements in the preparation of synthetic polymers with controlled primary structures by radical chain-growth polymerization. After five years of research, it is obvious that the controlled radical copolymerization of styrenic derivatives and MIs is a versatile approach for preparing tailor-made microstructures. One of the main advantages of this strategy is certainly its applicability to a large number of donor and acceptor comonomers. In particular, the library of MIs that we developed in recent years can be considered as a true 'molecular alphabet' that allows chain-encryption. These different letters can be placed and spaced at desired locations in polymer chains. As described herein, this versatile concept opens up interesting opportunities for design of encoded microstructures, single-chain functional arrays and complex cyclic topologies. It should, however, always be kept in mind that our approach is a chain-growth copolymerization process and, therefore, that chain-to-chain sequence defects exist. Nevertheless, the 'ultra-precise' concept, that we reported very recently, clearly shows that these imperfections can be minimized to a very low level.

Acknowledgments

References

1. Lutz, J.-F.; Ouchi, M.; Liu, D. R.; Sawamoto, M. *Science* **2013**, *341*, 1238149.
2. Badi, N.; Lutz, J.-F. *Chem. Soc. Rev.* **2009**, *38*, 3383–3390.
3. Lutz, J.-F. *Polym. Chem.* **2010**, *1*, 55–62.
4. Lutz, J.-F. *Nat. Chem.* **2010**, *2*, 84–85.
5. Cowie, J. M. G. *Alternating Copolymers*; Plenum Press: New York, 1985.
6. Satoh, K.; Matsuda, M.; Nagai, K.; Kamigaito, M. *J. Am. Chem. Soc.* **2010**, *132*, 10003–10005.
7. Matyjaszewski, K.; Tsarevsky, N. V. *Nat. Chem.* **2009**, *1*, 276–288.
8. Ouchi, M.; Terashima, T.; Sawamoto, M. *Chem. Rev.* **2009**, *109*, 4963–5050.
9. Satoh, K.; Kamigaito, M. *Chem. Rev.* **2009**, *109*, 5120–5156.
10. Matyjaszewski, K.; Ziegler, M. J.; Arehart, S. V.; Greszta, D.; Pakula, T. *J. Phys. Org. Chem.* **2000**, *13*, 775–786.
11. Tong, X.; Guo, B.-h.; Huang, Y. *Chem. Commun.* **2011**, *47*, 1455–1457.
12. Vandenbergh, J.; Reekmans, G.; Adriaensens, P.; Junkers, T. *Chem. Commun.* **2013**, *49*, 10358–10360.
13. Ida, S.; Terashima, T.; Ouchi, M.; Sawamoto, M. *J. Am. Chem. Soc.* **2009**, *131*, 10808–10809.

14. Ida, S.; Ouchi, M.; Sawamoto, M. *J. Am. Chem. Soc.* **2010**, *132*, 14748–14750.

15. Hibi, Y.; Ouchi, M.; Sawamoto, M. *Angew. Chem., Int. Ed.* **2011**, *50*, 7434–7437.

16. Pfeifer, S.; Lutz, J.-F. *J. Am. Chem. Soc.* **2007**, *129*, 9542–9543.

17. Lutz, J.-F.; Schmidt, B. V. K. J.; Pfeifer, S. *Macromol. Rapid Commun.* **2011**, *32*, 127–135.

18. Lutz, J.-F. *Acc. Chem. Res.* **2013**, *46*, 2696–2705.

19. Benoit, D.; Hawker, C. J.; Huang, E. E.; Lin, Z.; Russell, T. P. *Macromolecules* **2000**, *33*, 1505–1507.

20. Harrisson, S.; Wooley, K. L. *Chem. Commun.* **2005**, *0*, 3259–3261.

21. Bapat, A. P.; Ray, J. G.; Savin, D. A.; Hoff, E. A.; Patton, D. L.; Sumerlin, B. S. *Polym. Chem.* **2012**, *3*, 3112–3120.

22. Pfeifer, S.; Lutz, J.-F. *Chem. Eur. J.* **2008**, *14*, 10949–10957.

23. Lacroix-Desmazes, P.; Lutz, J.-F.; Boutevin, B. *Macromol. Chem. Phys.* **2000**, *201*, 662–669.

24. Lutz, J.-F.; Matyjaszewski, K. *J. Polym. Sci., Part A: Polym. Chem.* **2005**, *43*, 897–910.

25. Günay, K. A.; Theato, P.; Klok, H.-A. *J. Polym. Sci., Part A: Polym. Chem.* **2013**, *51*, 1–28.

26. Nilles, K.; Theato, P. *Eur. Polym. J.* **2007**, *43*, 2901–2912.

27. Srichan, S.; Oswald, L.; Zamfir, M.; Lutz, J.-F. *Chem. Commun.* **2012**, *48*, 1517–1519.

28. Srichan, S.; Chan-Seng, D.; Lutz, J.-F. *ACS Macro Lett.* **2012**, *1*, 589–592.

29. Srichan, S.; Kayunkid, N.; Oswald, L.; Lotz, B.; Lutz, J.-F. *Macromolecules* **2014**, *47*, 1570–1577.

30. Kakuchi, R.; Zamfir, M.; Lutz, J.-F.; Theato, P. *Macromol. Rapid Commun.* **2012**, *33*, 54–60.

31. Chan-Seng, D.; Zamfir, M.; Lutz, J.-F. *Angew. Chem., Int. Ed.* **2012**, *51*, 12254–12257.

32. Schmidt, B. V. K. J.; Fechler, N.; Falkenhagen, J.; Lutz, J.-F. *Nat. Chem.* **2011**, *3*, 234–238.

33. Baradel, N.; Fort, S.; Halila, S.; Badi, N.; Lutz, J.-F. *Angew. Chem., Int. Ed.* **2013**, *52*, 2335–2339.

34. Lutz, J.-F. *Angew. Chem., Int. Ed.* **2007**, *46*, 1018–1025.

35. Zamfir, M.; Lutz, J.-F. *Nat. Commun.* **2012**, *3*, 1138.

36. Lutz, J.-F. *Kobunshi* **2013**, *62*, 509–510.

37. Distefano, G.; Suzuki, H.; Tsujimoto, M.; Isoda, S.; Bracco, S.; Comotti, A.; Sozzani, P.; Uemura, T.; Kitagawa, S. *Nat. Chem.* **2013**, *5*, 335–341.

38. Mes, T.; van der Weegen, R.; Palmans, A. R. A.; Meijer, E. W. *Angew. Chem., Int. Ed.* **2011**, *50*, 5085–5089.

39. Zamfir, M.; Theato, P.; Lutz, J.-F. *Polym. Chem.* **2012**, *3*, 1796–1802.

40. Shishkan, O.; Zamfir, M.; Gauthier, M. A.; Borner, H. G.; Lutz, J.-F. *Chem. Commun.* **2014**, *50*, 1570–1572.

41. Ouchi, M.; Badi, N.; Lutz, J.-F.; Sawamoto, M. *Nat. Chem.* **2011**, *3*, 917–924.

42. Giuseppone, N.; Lutz, J.-F. *Nature* **2011**, *473*, 40–41.

43. Berthet, M. A.; Zarafshani, Z.; Pfeifer, S.; Lutz, J.-F. *Macromolecules* **2010**, *43*, 44–50.
44. Baradel, N.; Gok, O.; Zamfir, M.; Sanyal, A.; Lutz, J.-F. *Chem. Commun.* **2013**, *49*, 7280–7282.

Chapter 9

RAFT for the Control of Monomer Sequence Distribution – Single Unit Monomer Insertion (SUMI) into Dithiobenzoate RAFT Agents

Graeme Moad,[*] Carlos Guerrero-Sanchez, Joris J. Haven, Daniel J. Keddie, Almar Postma, Ezio Rizzardo, and San H. Thang

CSIRO Materials Science and Engineering, Bag 10, Clayton, Victoria 3168, Australia
[*]E-mail: graeme.moad@csiro.au

In this paper we explore RAFT (reversible addition-fragmentation chain transfer) single unit monomer insertion (SUMI) into dithiobenzoates. Styrene and N-isopropylacrylamide (NIPAm) were successfully inserted into 2-cyanopropan-2-yl dithiobenzoate. Attempted SUMI of methyl methacylate (MMA) provided an oligomeric insertion product due to the low transfer constant of the dithiobenzoate in MMA polymerization. A very low yield with maleic anhydride (MAH) reflects the low reactivity of MAH towards 2-cyanopropan-2-yl radicals. We also examined insertion of MAH, styrene and NIPAm into the styrene SUMI product. Insertion of MAH was rapid and efficient. SUMI with styrene and NIPAm was slower, which is attributed both to the low monomer concentrations used and the poor leaving group ability of the propagating species. The reaction with NIPAm is additionally complicated by initiator-derived by-products.

Precisely controlled compositions, well-defined architectures and narrow molecular weight distributions are now an expected (though not always achieved) outcome when applying techniques for reversible-deactivation radical polymerization (RDRP) (*1*), such as reversible addition-fragmentation chain transfer (RAFT) polymerization (*2–9*). However, precise control over

sequence distribution at the monomer level, as is achieved by nature in protein or polynucleotide biosynthesis, remains an elusive goal in the field of radical polymerization (*10–12*).

Zard and coworkers (*13*) first performed selective single unit monomer insertion (SUMI) in the late 80s for an *N*-alkylmaleimide or a vinyl sulfone into a xanthate. They (*14–19*) have subsequently provided many examples of this chemistry mainly in the context of organic synthesis. The noted the reaction was not effective with more-activated monomers (MAMs). In 2004, Chen and coworkers (*20*) applied SUMI in their synthesis of light harvesting polymers when they prepared new dithiobenzoate macro-RAFT agents by selectively inserting a single unit of a styrene derivatives. SUMI has since been applied to a wider range of examples involving styrene or vinylthiophene derivatives [all (MAMs) (*21*)] and either trithiocarbonate or dithiobenzoates RAFT agents (*22–25*).

SUMI into macro-RAFT agents has also been developed as a method of chain-end functionalization with monomers such as maleic anhydride (MAH) (*26–29*), *N*-alkylmaleimide derivatives (*30*, *31*) or β-pinene (*31*). Success in these experiments was attributed to the monomers not readily undergoing homopolymerization. This meant that the monomer could be used in excess with respect to the macro-RAFT agent (*e.g.* macro-RAFT agent:monomer>1:20 (*30*)) with little risk of multiple insertion (oligomerization).

McLeary, Klumperman and colleagues (*29*, *32–37*) observed that complete conversion of the initial RAFT agent to a species incorporating a single monomer unit is common to many well-behaved RAFT polymerizations (including those of styrene (*32*, *35*), methyl acrylate (MA) (*34*, *37*), *N*-vinylpyrrolidone (*36*) and vinyl acetate (VAc) (*36*)). They termed the behavior selective initialization. However, no similar selectivity was seen for subsequent monomer insertions. We have made similar observations for styrene polymerization and found that the phenomenon was strongly dependent on the specific RAFT agent and the polymerization conditions (*38*). Specifically, with 4.3 M styrene and 0.5 M RAFT agent, selective initialization is observed with 2-cyanopropan-2-yl and cumyl dithiobenzoates but not with benzyl dithiobenzoate or 2-cyanopropan-2-yl dodecyl trithiocarbonate. Selective initialization may be observed with 2-cyanopropan-2-yl dodecyl trithiocarbonate only when higher RAFT agent to styrene ratios are used (*25*).

Quiclet-Sire et al. (*19*) found that two sequential SUMI for a xanthate could be achieved where the first monomer is the electron poor less activated monomer (LAM), specifically *N*-vinylphthalimide, and the second monomer is an electron-rich LAM (a functional propene).

In a recent paper (*25*), we explored the scope and limitations for performing (two) successive SUMI for MAMs (styrene or *N*-isopropylacrylamide (NIPAm)) into a trithiocarbonate RAFT agent. We also made predictions with respect to the scope of the process and pointed out some of the limitations.

Recently, a number of reports of the synthesis of multiblock copolymers (meth)acrylates or acrylamides by sequential RAFT (*39–42*) (or atom transfer radical polymerization (ATRP (*43*))) steps have appeared. In that a single unit can be considered as a block with length unity, many of the factors important to the success of these experiments are also important in forming polymers through multiple SUMI steps. However, an additional criteria for successful SUMI is a

very high transfer constant for the RAFT agent for the monomer being inserted (*25*).

Vandenbergh et al. (*44*) performed four consecutive SUMI of acrylate monomers into a trithiocarbonate RAFT agent. Excess (10-fold) monomer was used in the experiments and the degree of oligomerization was controlled by limiting the monomer conversion through short (10 min) reaction times. Automated recycle size exclusion chromatography (SEC) was developed to provide a pure SUMI product after each step. A goal in designing our experiments has been to obtain achieve sufficient selectivity to render complex purification procedures unnecessary.

In principle, higher selectivities for single unit insertion of MAMs might be expected with the use dithiobenzoates because of their higher transfer constants in RAFT polymerization (*45*). In this paper we explore single unit insertion of styrene, NIPAm, methyl methacylate (MMA) and MAH into 2-cyanopropan-2-yl dithiobenzoate (**1**). We then examine insertion of styrene, NIPAm and MAH into the so-formed styrene single unit insertion product.

Results and Discussion

RAFT Single Unit Monomer Insertion into 2-Cyanopropan-2-yl Dithiobenzoate (1)

The initial RAFT agent used in the present work was 2-cyanopropan-2-yl dithiobenzoate (**1**). The use of azobis(isobutyronitrile) (AIBN) as initiator then ensured there would be no initiator-derived insertion products in the first SUMI step. SUMI experiments with styrene, NIPAm, MMA and MAH were carried out as *in situ* NMR experiments as described in our previous study (*25*). For these experiments used solutions were prepared in a nominal 5:5:1 [Monomer]:[RAFT agent (**1**)]:[AIBN] ratio with the exact ratios being determined by 1H NMR (see Table 1 in Experimental). Difficulties experienced in maintaining the tuning of the nuclear magnetic resonance (NMR) spectrometer (with MMA) and inconvenient peak overlaps precluded a detailed kinetic analysis.

SUMI of styrene (Figure 1) or NIPAm (Figure 2) into **1** provided **2** or **3**, respectively (Scheme 1). The reaction with styrene showed a higher degree of specificity than the similar reaction previously carried out with dodecyl 2-cyanopropan-2-yl trithiocarbonate (*25*) to the extent that "dimers" or higher oligomers from multiple monomer insertion were not detected at all. The products from cage reaction of the initiator-derived radicals, TMSM, IBN and KB (Scheme 2), were observed in the anticipated amounts.

For the reactions with styrene, NIPAM and MAH the rate determining step, that limiting the rate of disappearance of monomer and the initial RAFT agent, is the rate of cyanoisopropyl adding to monomer. This increases in the series MAH<<NIPAM<<styrene. The SUMI with styrene provide complete consumption of **1** within 9 h (Figure 1), SUMI with NIPAM is only ~60% complete after 15 h (Figure 2). The rate of disappearance of MMA is high because of the oligomerization of the monomer. Consistent with this hypothesis,

the rate of SUMI of styrene and NIPAM appears similar for both dithiobenzoate and trithiocarbonate RAFT agents (*25*).
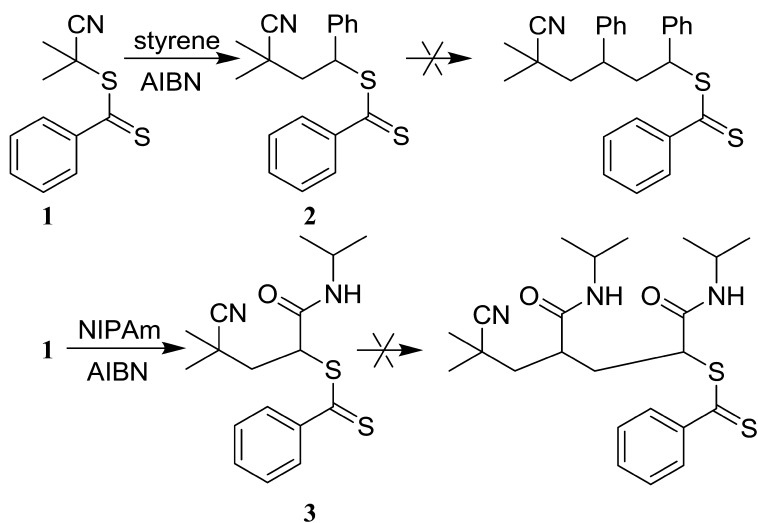
*Scheme 1. Processes for insertion of styrene and N-isopropylacrylamide (NIPAm) into 2-cyanopropan-2-yl dithiobenzoate (**1**).*
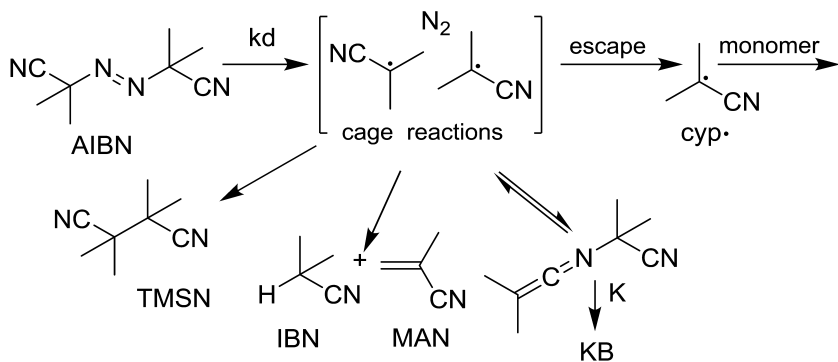
Scheme 2. Mechanism for decomposition of AIBN.
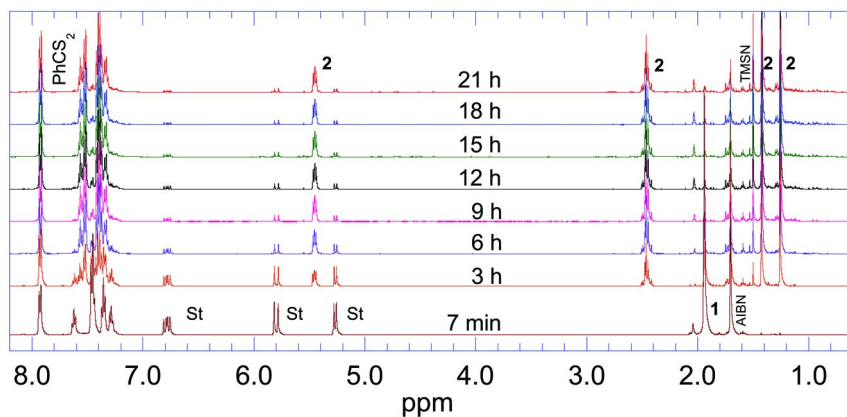
*Figure 1. Region 0.7-8.2 ppm of ^1H NMR spectra (CD₃CN) for reaction mixture for SUMI of styrene into 2-cyanopropan-2-yl dithiobenzoate (**1**) at 70 °C. Experiments were conducted real time in probe of NMR spectra were obtained at ~2 min intervals and results at 3 h time intervals are shown above (initial at time 7 min (lower), final after 21 h (upper)). For experimental conditions see Experimental.*
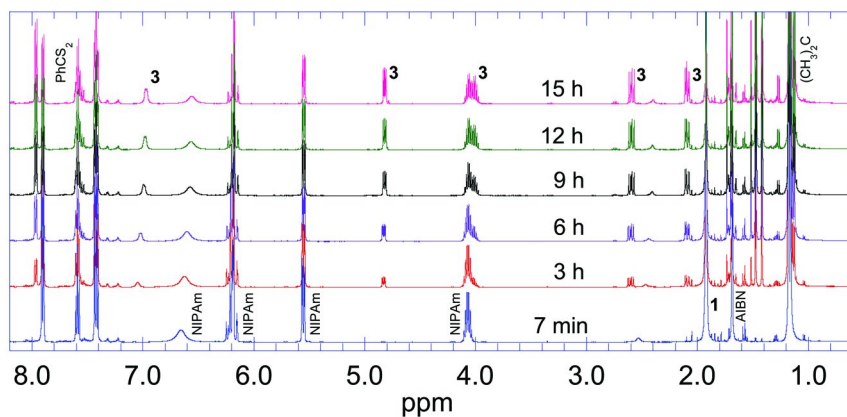
*Figure 2. Region 0.7-8.2 ppm of ^1H NMR spectra (CD₃CN) for reaction mixtures for SUMI of NIPAM into 2-cyanopropan-2-yl dithiobenzoate (**1**) at 70 °C. Results shown for 3h time intervals (initial at time 7 min (lower), final after 15 h (upper)) Other details as for Figure 1.*

For experiments with MAH (Scheme 3), only ~15% of the RAFT agent and MAH was consumed after 24 h and little **4** was formed even though the appropriate amount of AIBN had been consumed and converted to initiator derived by-products (TMSN, KB). The very slow reaction was ascribed to the electron-deficient monomer MAH being relatively unreactive towards the weakly nucleophilic (*46*) 2-cyanopropan-2-yl radical. While, some literature data (*47*) suggest that MAH should be reactive, the finding is consistent with the results of van den Dungen et al (*29*).
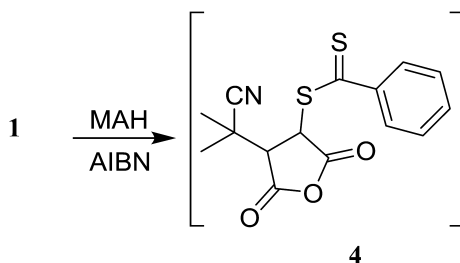
Scheme 3. Processes for insertion of maleic anhydride (MAH) into 2-cyanopropan-2-yl dithiobenzoate (1).

In experiments with MMA (Scheme 4), an oligomeric product with average degree of polymerization ~4 from multiple unit insertion and little of the SUMI product **5** were observed. Analysis by electrospray ionization (ESI) mass spectrometry revealed the presence of oligomer series attributable to **6** (with m/z = 221.03 + (n × 100) +1) and **7**, formed from **6** by elimination of dithiobenzoic acid (with 167.09 + (n × 100) +1) most likely during analysis. Several further oligomer series were observed in minor amounts. These are not yet fully identified but might correspond to the products from "missing step" reactions (*48*) and oligomers with thionoketone or sulfine ends (the latter also formed post-RAFT polymerization during analysis). 2-cyanopropan-2-yl dithiobenzoate (**1**) has a relatively low transfer constant in MMA polymerization (*45, 49*) such that multiple units of MMA are inserted per activation cycle under the present conditions.
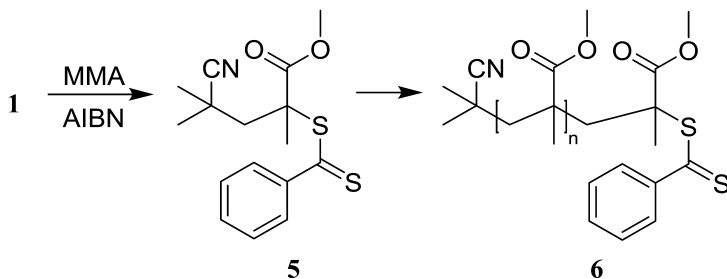
Scheme 4. Processes for insertion of methyl methacrylate (MMA) into 2-cyanopropan-2-yl dithiobenzoate (1).

7
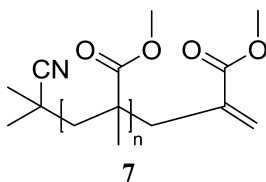
Preparative SUMI of styrene with **1** and azobis(isobutyronitrile) (AIBN) initiator at 70 °C in dichloroethane solvent for 18 h resulted in formation of the adduct (**2**) as the major product in high isolated yield. The procedure used a mole ratio of **1**:styrene of 1:1 and **1**:AIBN of ~5:1. The main contaminants in the product (**2**) were a small amount of the initial RAFT agent and the expected by-products from AIBN decomposition (mainly TMSN). The purity and structure of the isolated product **2** was confirmed by mass spectrometry and ^{1}H, ^{13}C NMR.

RAFT Monomer Single Unit Monomer Insertion into 3-Cyano-3-methyl-1-phenylbutyl Dithiobenzoate (2)

The styrene SUMI product **2** was used in further SUMI experiments. These involved adding the appropriate monomer directly to the reaction mixture after 7.5 h, which was degassed and heated at 70 °C for 6, 12 or 18 h (see Experimental). No additional initiator was added. An initial ratio of monomer to **2** of ~ 2:1 was used in these experiments to compensate for the low reaction rate.

SUMI of styrene into **2** was successful though slow providing about 50% conversion after 12 h (Scheme 5). Longer reaction times are precluded by initiator depletion (though it may be possible to add additional initiator). Under the reaction conditions, there was no evidence of the formation of higher oligomers (Figure 3). In this case, initiator-derived by-products are not an issue since the initiator-derived insertion product is **2.**

SUMI of NIPAm into **2** (Scheme 5) gave the initiator-derived product **3** in addition to the desired styrene-NIPAm "co-dimer" **9**. The outcome of the reaction was ascertained by examining the region 3.8-4.3 ppm of the ^{1}H NMR spectrum (Figure 4). Signals attributable to the SCH(X)CH$_2$ and (CH$_3$)$_2$CHN-hydrogens of **3** and **9** were assigned by analogy those of the corresponding dodecyl trithiocarbonates (*25*). The signals for the SCH(CONH(CH$_3$)$_2$)CH$_2$ hydrogens of **9** were largely obscured by those for the (CH$_3$)$_2$CHN- of NIPAm.

The relatively slow reaction observed for SUMI of styrene or NIPAm into **2** is a consequence of the intermediate formed by addition of 2-cyanopropan-2-yl radical partitioning strongly in favor of starting materials (Scheme 6). The tertiary, 2-cyanopropan-2-yl, radical is a substantially better homolytic leaving group than the substituted phenylethyl radical **10a** in the case of styrene or **10b** in the case of NIPAm. For the reaction to proceed, we require that 2-cyanopropan-2-yl radical first add to monomer. The intermediate formed by addition of this radical to a RAFT agent then can partition to the substituted phenylethyl radical, which may then add a single unit of monomer and provide after further reaction with RAFT agent the desired product (**8** or **9**). This pathway also provides initiator-derived by-products; **2** in the case of styrene and by-product **3** in the case of NIPAm.
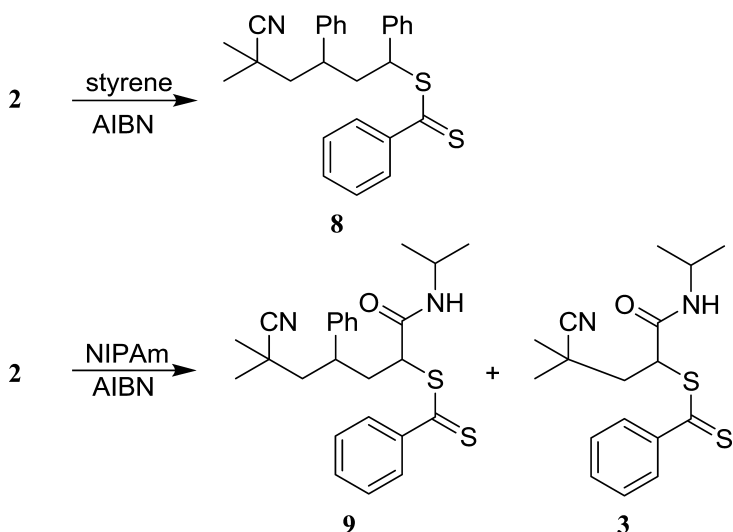
Scheme 5. Processes for insertion of styrene or N-isopropylacrylamide (NIPAm) into the styrene single unit insertion product **2**.
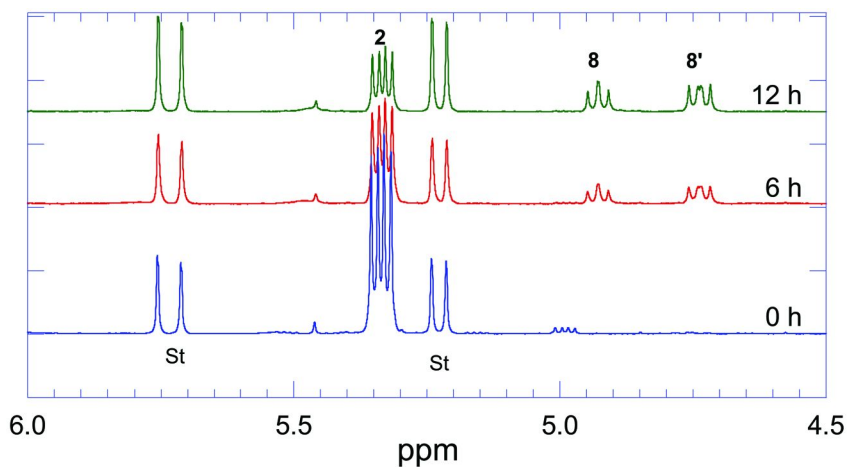
Figure 3. Region 4.5-6.0 ppm of ^1H NMR spectra (CDCl$_3$) for reaction mixture at time 0 (lower) and after 6 and 12 h (middle and upper respectively) showing the signals corresponding to the SCH(X)CH$_2$ hydrogens corresponding to single unit styrene adduct **2** and two unit styrene adduct **8** (two diastereomers). Signals labelled 'St' are due to styrene monomer.
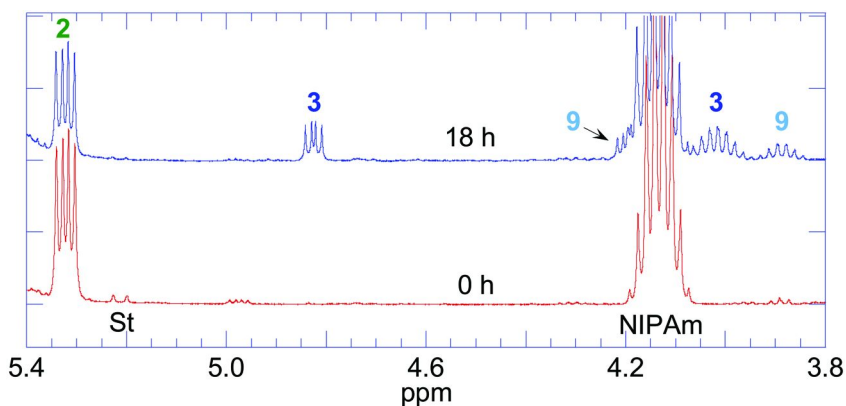
*Figure 4. Region 3.8-5.4 ppm of the ^{1}H NMR spectra (CDCl$_3$) for reaction mixture at time 0 h (lower) and after 18 h (upper) showing (from left to right) the signals corresponding to the SCH(X)CH$_2$ hydrogens corresponding to single unit styrene adduct **2** and the single unit NIPAm adduct **3**. Signals for the two diastereomers of the desired product **9** are largely obscured by the (CH$_3$)$_2$CHN- of NIPAm. Signals in the region 3.8-4.0 ppm are attributable to the (CH$_3$)$_2$CHN- hydrogens of **3** and **9**.*

10 a X=Ph
b X=CO$_2$NH*i*Pr

2 X=Ph
3 X=CO$_2$NH*i*Pr
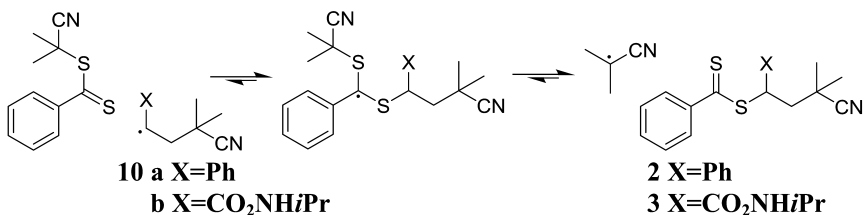
Scheme 6. RAFT equilibria.

SUMI of MAH into **2** (Scheme 7) provided essentially complete conversion of **2** to two diastereomers the desired product **11** and consumption of the appropriate amount of MAH at the first time point (6 h reaction time; see Figure 5). Several factors favor a rapid and selective reaction in this case. The 2-cyanopropan-2-yl radical reacts with MAH only slowly such that there are little, if any, initiator-derived insertion products formed (*vide infra*). The radical formed by addition of MAH propagates very slowly, if at all, thus oligomeric products are not expected. The ^{1}H NMR (Figure 6) showed that the major products isolated from the SUMI reaction mixture, by preparative HPLC with CH$_3$CN/H$_2$O eluent, are two diastereomers of the maleic acid insertion product formed by hydrolysis of **11** (Scheme 8).
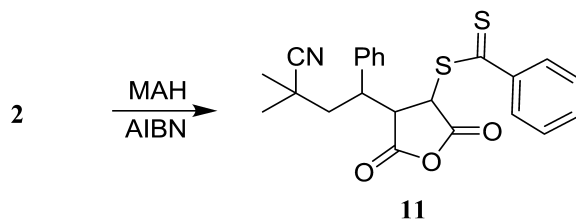
Scheme 7. *Process for insertion of maleic anhydride (MAH) into the styrene single unit insertion product* **2**.
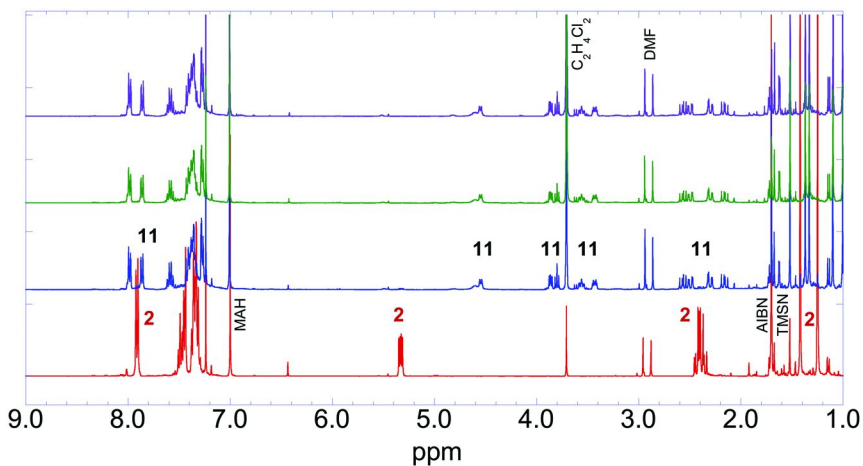
Figure 5. *Region 1.0-9.0 ppm of the ^1H NMR spectra (CD$_3$CN) of the reaction mixture after 0 (lower), 6, 12, and 18 h (upper) from insertion of MAH into single unit styrene insertion product* **2**.

Conclusions

SUMI of monosubstituted monomers, styrene and NIPAm, into 2-cyanopropan-2-yl dithiobenzoate (**1**) was successful providing high yields and no evidence of oligomer formation. In contrast, attempted SUMI of methyl methacylate (MMA) into **1** under similar conditions provided only an oligomeric product. The result is attributed to the much lower transfer constant of **1** in MMA polymerization. We also examined SUMI of MAH, styrene and NIPAm into the styrene SUMI product (**2**) formed in a 'one pot' process. Insertion of MAH is rapid and efficient. However, SUMI with styrene and NIPAm, while selective, is slow, and in the case of NIPAm, complicated by the formation of an initiator-derived by-product (**3**). The slow rate of reaction can be traced to the poor leaving group ability of the propagating species vs. the 2-cyanopropan-2-yl radical.
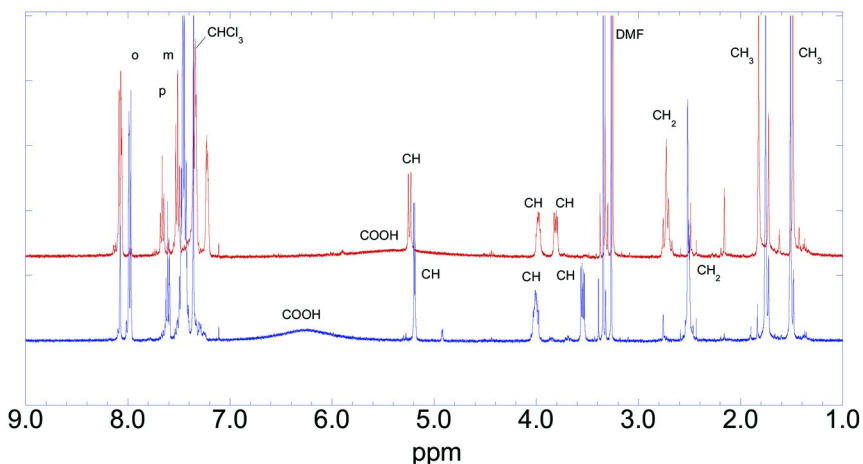
Figure 6. Region 1.0-9.0 ppm of the ¹H NMR spectra (CDCl₃) of the two diastereomers of 12 isolated as the major products by preparative HPLC from insertion of MAH into single unit styrene insertion product 2.

11   **12**
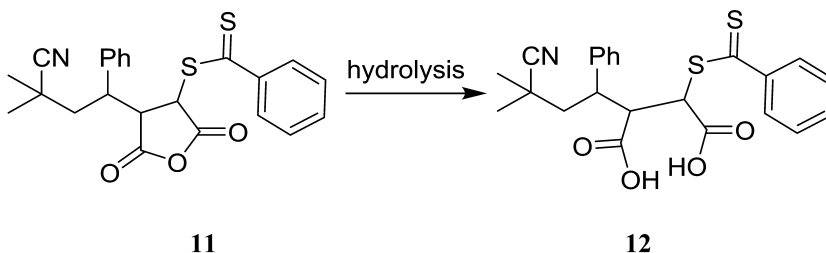
Scheme 8. Hydrolysis of maleic anhydride (MAH) insertion product 11.

SUMI can be an effective method of macro-RAFT agent synthesis and in this context dithiobenzoate RAFT agents can offer better selectivity than the similar trithiocarbonates (*25*). However, results are very much dependent on the specific monomers and the polymerization conditions.

Experimental

The procedures and instrumentation used for SUMI are described in our previous paper (*25*).

Materials

Monomers were obtained from Aldrich. Styrene and MMA were purified by stirring with inhibitor remover and flash distillation before use. NIPAm was purified by recrystallization from hexane/Et₂O 4:1. MAH was used as received.

2-cyanopropan-2-yl dithiobenzoate (**1**) was obtained from Aldrich and, with purity confirmed by ^{1}H NMR, was used without purification. AIBN (VAZO64) was obtained from DuPont and was recrystallized from methanol/chloroform.

SUMI into 2-Cyanopropan-2-yl Dithiobenzoate (1) by Real Time Nuclear Magnetic Resonance

^{1}H-NMR spectra for real time SUMI experiments in real time experiments were recorded on a Bruker BioSpin Av500 NMR spectrometer with a 5 mm inverse ^{13}C/^{15}N resonance probe operating at 500.13 MHz for ^{1}H. Data were acquired using a standard single pulse experiment with a 30° excitation pulse and a total recycle time of 27.2 s (2.2 s acquisition time and 25 s delay), summed over 8 scans. The recycle time was chosen to be longer than 5× the longest measured T_1 of the components of the reactions when using a 30° pulse. The data were processed using a line broadening of 0.3 Hz. The sample temperature was corrected using the 80% ethylene glycol in DMSO-d_6 method described by Berger and Braun (*50*). The tube containing monomer, RAFT agent **1** and AIBN in CD$_3$CN (reagent concentrations shown in Table 1) was inserted into the NMR probe at 25 °C, the magnet was fully shimmed and a spectrum acquired. The sample was then removed from the probe and the probe temperature was raised to 70 °C. Once the temperature had stabilized at 70 °C the sample was reinserted into the probe (time zero). The sample was allowed to equilibrate for *ca* 7 min before acquisition commenced. NMR data were processed via a multiple integration macro in Bruker Topspin 3.1. Integrated ^{1}H-NMR data were processed in Microsoft Office Excel 2007 or Kaleidagraph 4.5.

Table 1. Composition of polymerization mixtures for real time ^{1}H NMR experiments in CD$_3$CN[a]

Monomer	[Monomer] M	[1] M	[AIBN] M
Styrene	1.00	0.89	0.20
N-isopropyl acrylamide (NIPAm)	1.00	0.95	0.20
Methyl methacrylate (MMA)	1.00	0.97	0.22
Maleic anhydride (MAH)	1.00	1.00	0.22

[a] Relative concentrations were determined by ^{1}H NMR (t$_0$, 25 °C). Solutions were prepared in 5:5:1 (Monomer:**1**:AIBN) ratio.

Synthesis of 3-Cyano-3-methyl-1-phenylbutyl Dithiobenzoate (2)

A stock solution of **2** was prepared as follows. A 15 mL ampoule was charged with a solution of AIBN (156.7 mg, 0.954 mmol), styrene (496 mg, 4.77 mmol) and RAFT agent **1** (1.056 g, 4.77 mmol) in dichloroethane (2.40 mL). (The ratio AIBN:styrene:**1** determined by NMR was 0.23:1.06:1 which compares

with 0.2:1:1 based on the amounts reagents added) The solution was degassed through four freeze-pump-thaw cycles and flame sealed. The ampoule was placed in an oil bath at 70 °C for 7.5 h. At this time conversions of AIBN, styrene and 1 determined by NMR were 36, 93 and 100% respectively. This reaction solution was used directly as the stock solution of **2** in the second unit insertion experiments. ^{1}H-NMR (400 MHz, CDCl$_3$, signals attributable to **2**): δ7.88-7.86 (2H, m, Ar-*H*), 7.58-7.10 (m, Ar-*H*), 6.30 (1H, d, *J* = 7.35 Hz, N-*H*), 4.85-4.80 (1H, dd, *J* = 5.00; 8.12 Hz, S-*H*), 4.07-3.96 (1H, septet, *J* = 6.65 Hz, (CH$_3$)$_2$-C*H*), 3.13-3.04 (1H, m, CH$_2$-C*H*-CH$_2$), 3.03-2.96 (2H, m, CH-C*H*$_2$-CH), 2.69-2.60 (2H, m, C$_{quat}$-C*H*$_2$), 1.41, 1.24 (2 x 3H, s, C$_{quat}$-C*H*$_3$), 1.17, 1.15 (2 x CH3, s, (C*H*$_3$)$_2$-CH).

SUMI into 3-Cyano-3-methyl-1-phenylbutyl Dithiobenzoate (2)

The following procedure is typical. Three 5 mL ampoules charged with the above reaction solution (0.4 mL) and styrene (60.22 mg, 0.578 mmol, 2 molar equivalents) which were degassed through four freeze-pump-thaw cycles and flame sealed. The ampoules were placed in an oil bath at 70 °C for 6, 12 and 18 h. The reaction were quenched by cooling and analyzed by ^{1}H NMR, HPLC and mass spectrometry.

References

1. Jenkins, A. D.; Jones, R. I.; Moad, G. *Pure Appl. Chem.* **2010**, *82*, 483–491.
2. Moad, G.; Rizzardo, E.; Thang, S. H. *Aust. J. Chem.* **2005**, *58*, 379–410.
3. Moad, G.; Rizzardo, E.; Thang, S. H. *Aust. J. Chem.* **2006**, *59*, 669–692.
4. Moad, G.; Rizzardo, E.; Thang, S. H. *Acc. Chem. Res.* **2008**, *41*, 1133–1142.
5. Moad, G.; Rizzardo, E.; Thang, S. H. *Aust. J. Chem.* **2009**, *62*, 1402–1472.
6. Moad, G.; Rizzardo, E.; Thang, S. H. *Aust. J. Chem.* **2012**, *65*, 985–1076.
7. Boyer, C.; Bulmus, V.; Davis, T. P.; Ladmiral, V.; Liu, J.; Perrier, S. *Chem. Rev.* **2009**, *109*, 5402–5436.
8. Moad, G.; Rizzardo, E.; Thang San, H. Fundamentals of RAFT Polymerization. In *Fundamentals of Controlled/Living Radical Polymerization*; Tsarevsky, N. V., Sumerlin, B. S., Eds.; Royal Society of Chemistry: Cambridge, 2013; pp 205−249.
9. Moad, G.; Rizzardo, E.; Thang, S. H. *Chem. Asian J.* **2013**, *8*, 1634–1644.
10. Lutz, J.-F. *Polym. Chem.* **2010**, *1*, 55–62.
11. Lutz, J.-F. *Acc. Chem. Res.* **2013**, *46*, 2696–2705.
12. Ouchi, M.; Badi, N.; Lutz, J.-F.; Sawamoto, M. *Nat. Chem.* **2011**, *3*, 917–924.

13. Delduc, P.; Tailhan, C.; Zard, S. Z. *J. Chem. Soc., Chem. Commun.* **1988**, 308–310.

14. Zard, S. Z. *Angew. Chem., Int. Ed. Engl.* **1997**, *36*, 672–685.

15. Quiclet-Sire, B.; Zard, S. Z. *Top. Curr. Chem.* **2006**, *264*, 201–236.

16. Quiclet-Sire, B.; Zard, S. Z. *Chem. Eur. J.* **2006**, *12*, 6002–6016.

17. Quiclet-Sire, B.; Zard, S. Z. *Org. Lett.* **2008**, *10*, 3279–3282.

18. Lebreux, F.; Quiclet-Sire, B.; Zard, S. Z. *Org. Lett.* **2009**, *11*, 2844–2847.

19. Quiclet-Sire, B.; Revol, G.; Zard, S. Z. *Tetrahedron* **2010**, *66*, 6656–6666.

20. Chen, M.; Ghiggino, K. P.; Mau, A. W. H.; Rizzardo, E.; Sasse, W. H. F.; Thang, S. H.; Wilson, G. J. *Macromolecules* **2004**, *37*, 5479–5481.

21. In a more-activated monomer, or MAM, the double bond is conjugated to an aromatic ring, a carbonyl group, a nitrile, or another double bond (e.g. styrene, acrylates, acrylonitrile, butadiene). In a less-activated monomer, or LAM, an oxygen or nitrogen lone pair or saturated carbon is in the adjacent position (e.g. vinyl acetate, *N*-vinylpyrrolidone) [Benaglia, M.; Chiefari, J.; Chong, Y. K.; Moad, G.; Rizzardo, E.; Thang, S. H. *J. Am. Chem. Soc.* **2009**, *131*, 6914−6915]. *N*-Vinylcarbazole is an Intermediate-activated monomer or IAM [Keddie, D. J.; Guerrero-Sanchez, C.; Moad, G. *Polym. Chem.* **2013**, *4*, 3591−-3601].

22. Chen, M.; Ghiggino, K. P.; Rizzardo, E.; Thang, S. H.; Wilson, G. J. *Chem. Commun.* **2008**, 1112–1114.

23. Chen, M.; Haeussler, M.; Moad, G.; Rizzardo, E. *Org. Biomol. Chem.* **2011**, *9*, 6111–6119.

24. Tanaka, S.; Nishida, H.; Endo, T. *Macromolecules* **2009**, *42*, 293–298.

25. Houshyar, S.; Keddie, D.; Moad, G.; Mulder, R.; Saubern, S.; Tsanaktsidis, J. *Polym. Chem.* **2012**, *3*, 1879–1889.

26. Feng, X. S.; Pan, C. Y. *Macromolecules* **2002**, *35*, 4888–4893.

27. Shi, G. Y.; Tang, X. Z.; Pan, C. Y. *J. Polym. Sci., Part A: Polym. Chem.* **2008**, *46*, 2390–2401.

28. Sasso, B.; Dobinson, M.; Hodge, P.; Wear, T. *Macromolecules* **2010**, *43*, 7453–7464.

29. van den Dungen, E. T. A.; Rinquest, J.; Pretorius, N. O.; McKenzie, J. M.; McLeary, J. B.; Sanderson, R. D.; Klumperman, B. *Aust. J. Chem.* **2006**, *59*, 742–748.

30. Henry, S. M.; Convertine, A. J.; Benoit, D. S. W.; Hoffman, A. S.; Stayton, P. S. *Bioconjugate Chem.* **2009**, *20*, 1122–1128.

31. Zhou, C.; Qian, S.; Zhang, A.; Xu, L.; Zhu, J.; Cheng, Z.; Kang, E.-T.; Yao, F.; Fu, G. D. *RSC Adv.* **2014**, *4*, 8144–8156.

32. McLeary, J. B.; Calitz, F. M.; McKenzie, J. M.; Tonge, M. P.; Sanderson, R. D.; Klumperman, B. *Macromolecules* **2004**, *37*, 2383–2394.

33. McLeary, J. B.; Calitz, F. M.; McKenzie, J. M.; Tonge, M. P.; Sanderson, R. D.; Klumperman, B. *Macromolecules* **2005**, *38*, 3151–3161.

34. McLeary, J. B.; McKenzie, J. M.; Tonge, M. P.; Sanderson, R. D.; Klumperman, B. *Chem. Commun.* **2004**, 1950–1951.

35. McLeary, J. B.; Tonge, M. P.; Klumperman, B. *Macromol. Rapid Commun.* **2006**, *27*, 1233–1240.

36. Pound, G.; McLeary, J. B.; McKenzie, J. M.; Lange, R. F. M.; Klumperman, B. *Macromolecules* **2006**, *39*, 7796–7797.

37. van den Dungen, E. T. A.; Matahwa, H.; McLeary, J. B.; Sanderson, R. D.; Klumperman, B. *J. Polym. Sci., Part A: Polym. Chem.* **2008**, *46*, 2500–2509.

38. Moad, G.; Chong, Y. K.; Mulder, R.; Rizzardo, E.; Thang, S. H. New Features of the Mechanism of RAFT Polymerization. In *Controlled/Living Radical Polymerization: Progress in RAFT, NMP & OMRP*; Matyjaszewski, K., Ed.; American Chemical Society: Washington, DC, 2009; Vol. 1024, pp 3−18.

39. Haven, J. J.; Guerrero-Sanchez, C.; Keddie, D. J.; Moad, G. *Macromol. Rapid Commun.* **2014**, *35*, 492–497.

40. Haven, J. J.; Guerrero-Sanchez, C.; Keddie, D. J.; Moad, G.; Thang, S. H.; Schubert, U. S. *Polym. Chem.* **2014**, *5*, 5236–5246.

41. Vandenbergh, J.; de Moraes Ogawa, T.; Junkers, T. *J. Polym. Sci., Part A: Polym. Chem.* **2013**, *51*, 2366–2374.

42. Gody, G.; Maschmeyer, T.; Zetterlund, P. B.; Perrier, S. *Macromolecules* **2014**, *47*, 639–649.

43. Anastasaki, A.; Waldron, C.; Wilson, P.; Boyer, C.; Zetterlund, P. B.; Whittaker, M. R.; Haddleton, D. *ACS Macro Lett.* **2013**, *2*, 896–900.

44. Vandenbergh, J.; Reekmans, G.; Adriaensens, P.; Junkers, T. *Chem. Commun.* **2013**, *49*, 10358–10360.

45. Moad, G. *Macromol. Chem. Phys.* **2014**, *215*, 9–26.

46. De Vleeschouwer, F.; Van Speybroeck, V.; Waroquier, M.; Geerlings, P.; De Proft, F. *Org. Lett.* **2007**, *9*, 2721–2724.

47. Markevich, I. N.; Borisova, G. S.; Glebova, N. N.; Sharaev, O. K.; Ostrovskaya, I. Y.; Gol'berg, A. I. *Russ. Chem. Bull.* **1989**, *38*, 789–792.

48. Sidoruk, A.; Buback, M.; Meiser, W. *Macromol. Chem. Phys.* **2013**, *214*, 1738–1748.

49. Chong, Y. K.; Krstina, J.; Le, T. P. T.; Moad, G.; Postma, A.; Rizzardo, E.; Thang, S. H. *Macromolecules* **2003**, *36*, 2256–2272.

50. Berger, S.; Braun, S. *200 and More NMR Experiments*; Wiley-VCH: Weinheim, 2004; pp 145−148.

Chapter 10

Selective Single Monomer Radical Addition via Template-Assisted Ring Closure: A Feasibility Study toward Sequence Control in Vinyl Polymers with Peptide Templates

Makoto Ouchi,[*,1,2] **Yusuke Hibi,**[1] **Takahiro Arima,**[1] **Daisuke Hayata,**[1] **and Mitsuo Sawamoto**[*,1]

[1]**Department of Polymer Chemistry, Graduate School of Engineering, Kyoto University, Katsura, Nishikyo-ku, Kyoto 615-8510, Japan**
[2]**Precursory Research for Embryonic Science and Technology (PRESTO), Japan Science and Technology Agency (JST), 4-1-8 Kawaguchi, Saitama 332-0012, Japan**
[*]**E-mail: ouchi@living.polym.kyoto-u.ac.jp**
[*]**E-mail: sawamoto@star.polym.kyoto-u.ac.jp**

A feasibility study has demonstrated sequence-controlled radical polymerization with peptide templates, where an acrylic monomer and a radical initiating site were embedded in a dipeptide template framework. The close vicinity of the two components enhanced a selective radical "single monomer" addition via ring-closure catalyzed by a ruthenium complex.

Introduction

Sequence control in synthetic polymers has increasingly been attracting attention (*1–12*), because the order of constitutional repeat units, or functionality sequence along a backbone, is among the most essential structural factors in expressing elaborate functions, as abundantly seen in enzymes, genes, peptides, and other naturally occurring macromolecules. In nature, precision sequence regulation is based on templates that regulate and in turn ensure the fidelity in transcription and translation of sequence information.

The development of resin-assisted solid-phase synthesis (*13*) has allowed a similar sequence-control for synthetic peptides via repeated step-wise amidations

with protected amino acids. Technically, this method replaces transcription and translation of repeat-unit sequence in natural peptides with one-by-one substrate feeding of protected amino acids. Such an iterative "single monomer addition", however, would be quite difficult in chain-growth polymerization, because the propagation involves a collision-dependent statistical reaction between a monomer (M) and a chain carrier (~P*), even with an equimolar injection free from side-reactions. Thus, attempts often result in dimeric and higher homo-enchainments [~P–(M)n; n = 2, 3, ...] with leftover intact growing ends.

We have been interested in sequence control in chain-growth polymerization of alkene (vinyl) monomers, with a belief that this will lead to a new family of carbon-chain based sequence-controlled macromolecules contrasting peptides, enzymes, and related biopolymers, all based on condensation-type hetero-chain backbones. To overcome the inherent difficulty in chain-growth sequence control, as discussed above, this communication is to introduce a new approach, "templated" polymerization (Figure 1). Herein it should be noted that the "templated" approach conceptually differs from "template"(-assisted) polymerization hitherto examined (*14–17*). Whereas the latter method utilizes a template for recognizing and aligning monomers via non-covalent interaction in a predetermined order, the "templated" polymerization involves a prefabricated polymer chain as a "template framework" where an initiating site and "monomers" (alkene-containing pendent groups) are covalently attached in a predetermined order defined by the framework backbone. With a catalyst, the aligned monomers may be polymerized intramolecularly along the framework, by iterative chain-growth single monomer addition (ring-closure) of the pendent alkenes; thus, in Figure 1 propagation may proceed from the left end (the initiating site) to the right end along the framework.

Results and Discussion

Design of Dipeptide Template

In this feasibility study, we employed a dipeptide (**11**, Scheme 1) as the template framework for templated polymerization, in which one amino acid residue carries an acrylic monomer (from **4**) and the other an initiating site (initiator; from **9**) for a metal-catalyzed living radical polymerization (*18–20*). As with our previous study (*21–23*), this new template with a rigid and well-defined amide framework may secure the close vicinity of the two components that may in turn facilitate the intended selective intramolecular ring-closure single-monomer addition. The metal-mediated addition is suitable in that it is precision controlled, free from side reactions, and highly tolerant of polar functionalities. The established step-wise peptide synthesis will ensure precision construction of the amide framework of **11**.
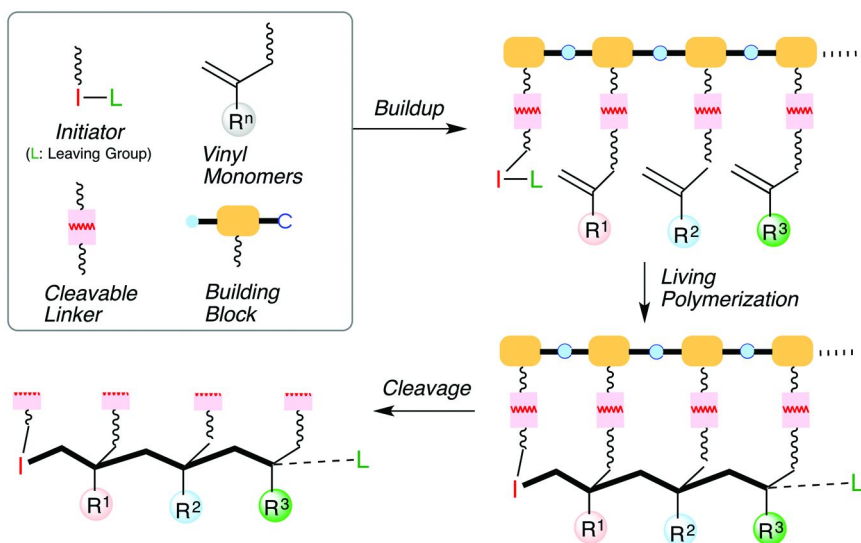
Figure 1. Concept of templated polymerization to obtain sequence-controlled vinyl polymer. Template is prepared via step-wise reaction from building blocks carrying an initiator for living polymerization and comonomers via cleavable linker on the side chains.

As the monomer, an α-substituted acrylate [methyl 2-(hydroxymethyl)acrylate; MHMA] was selected; the pendent ester may be employed for introducing a functional group, while the α-hydroxymethyl for a junction point to the template. This template–monomer linkage should be cleavable, so that the resulting polymers may readily be detached from the template after the ring-closure polymerization; herein an acetal bond was selected, readily cleavable under mild acidic conditions without deteriorating the pendent functionalized esters.

To build up the template framework, we carefully examined reactions and their order along with protection/deprotection procedures, so as not to interfere base-sensitive esters in the initiator and the monomer components, as well as the acid-sensitive acetal in **6** (Scheme 1). The *t*-Boc-protected cysteine (**1**) and the Fmoc-protected serine (**7**) were used as the starting amino acids. The thiol in **1** and the hydroxyl in **7**, respectively, were decorated to introduce the α,α-disubstituted monomer (MHMA) and the radical initiator; for the monomer fragment, alkyne **3** from **1** and azide **6** from **4** was first combined by a Click reaction, before the final coupling with the initiator fragment **9** from **7** by amidation, to give the templated initiator–monomer pair **11**.
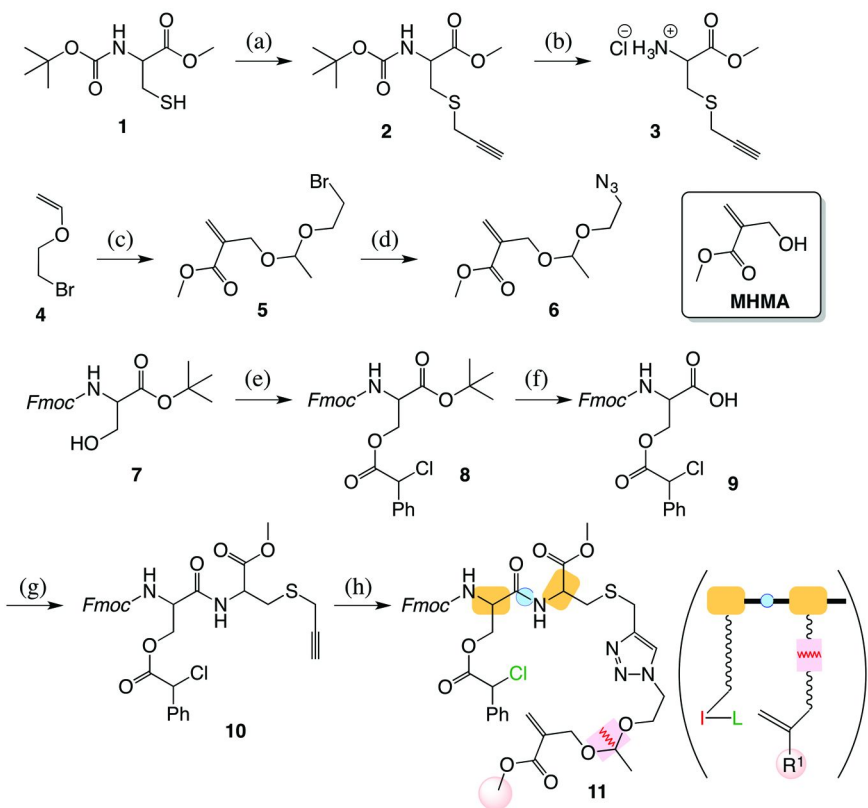
Scheme 1. Reagents and conditions: (a) propargyl bromide, Cs₂CO₃, DMF, r.t. (b) TFA, DCM, r.t. (c) MHMA, pyridium p-toluenesulfonate, r.t. (d) NaN₃, DMF, r.t. (e) 2-chloro-2-phenylacetyl chloride, DIPEA, THF, r.t. (f) TFA, DCM r.t. (g) 3, EDC, BOHt, 4-ehylmorphorine, DCM, 0 °C, (h) 6, CuI, DIPEA, DMF, r.t.

Metal-Catalyzed Radical Addition on Dipeptide Template

When combined with this templated system, a transition metal catalyst (Ru^{II} complex) for living radical polymerization will activate the C–Cl bond therein to generate a carbon-centered radical (C–Cl + Ru^{II} ↔ C• + ClRu^{III}). The radical species could intramolecularly react onto the nearby double bond of the monomer moiety to complete ring-closure. The reaction under diluted conditions would selectively allow the intramolecular reaction without intermolecular radical addition or oligomerization. Note that control of such a single monomer radical addition is not so straightforward even under controlled generation of radical species, since the catalyst would further activate the resultant C–Cl bond within the cyclized product, to give a new radical species. The templated reaction was expected to be selective enough without inducing any intermolecular reactions between different template molecules, either before or after the ring-closure.

With these considerations and the template synthesis, we then examined the ruthenium-catalyzed radical addition within **11** for the single monomer addition.

The extent and the selectivity therein was monitored by following the parallel consumption of the initiator and the monomer moieties by in-situ time-lapse ^{1}H NMR spectroscopy: (initiator) the methyne proton –CH(Ph)Cl; (monomer) the alkene protons CH_2=C– (Figure 2, bottom center inset). The obtained data were also employed for optimization of reaction conditions in terms of catalyst and ligand structures, catalyst and substrate concentrations, and reaction temperature, eventually leading to the following. Substrate **11**: 20 mM; catalyst: [(pentamethylcyclopentadiene)-ruthenium iodide with PPh$_2$CH$_2$P(=O)Ph$_2$ (Ph = phenyl)], 2.0 mM or 1/10 eq to **11**, without any cocatalyst; in toluene at 40 °C. Under these optimized conditions, the initiator and the monomer/alkene moieties were consumed smoothly in parallel nearly at the same rates, reaching almost 100 % conversion in 120 hr (Figure 2, bottom left inset).
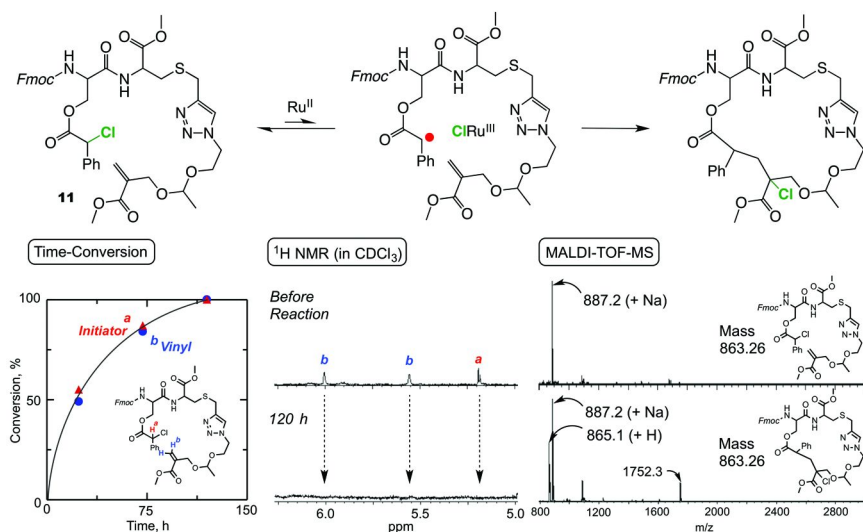
*Figure 2. Ru-catalyzed intramolecular radical addition of **11** in toluene at 40 °C: [**11**]$_0$ = 20 mM; [Ru]$_0$ = 2 mM. The ruthenium catalyst was prepared via aging of [Cp*Ru(μ_3-I)]$_4$ with PPh$_2$CH$_2$P(=O)Ph$_2$ in toluene at 60°C, and the resultant complex was directly employed as the catalyst. Consumption of initiator and monomer were determined through ^{1}H NMR analysis of the reaction solution for methyne proton (a) of the former and vinyl group protons (b) of the latter. ^{1}H NMR and MALDI-TOF-MS were directly measured with the reaction solutions without any purification.*

To examine controlling effects of the dipeptide template, similar but now intermolecular "cutout" model reactions were examined under otherwise the same conditions without intervention of a template; namely, 1:1 radical reactions of ethyl 2-chloro-2-phenylacetate (ECPA; initiator) with methyl methacrylate (MMA) or methyl 2-(hydroxymethyl)acrylate (MHMA); ECPA/monomer/Ru = 40/40/2.0 mM in toluene at 40 °C (Figure 3). In sharp contrast to the intermolecular reaction, either the initiator or the monomer hardly or only

sluggishly reacted, without forming a recoverable trace of expected adducts, with the initiator consumed slightly faster. These results indicate that the templated system effectively facilitates intramolecular single monomer addition both in rate and in selectivity, even under extremely diluted conditions where the corresponding intermolecular processes hardly proceed.
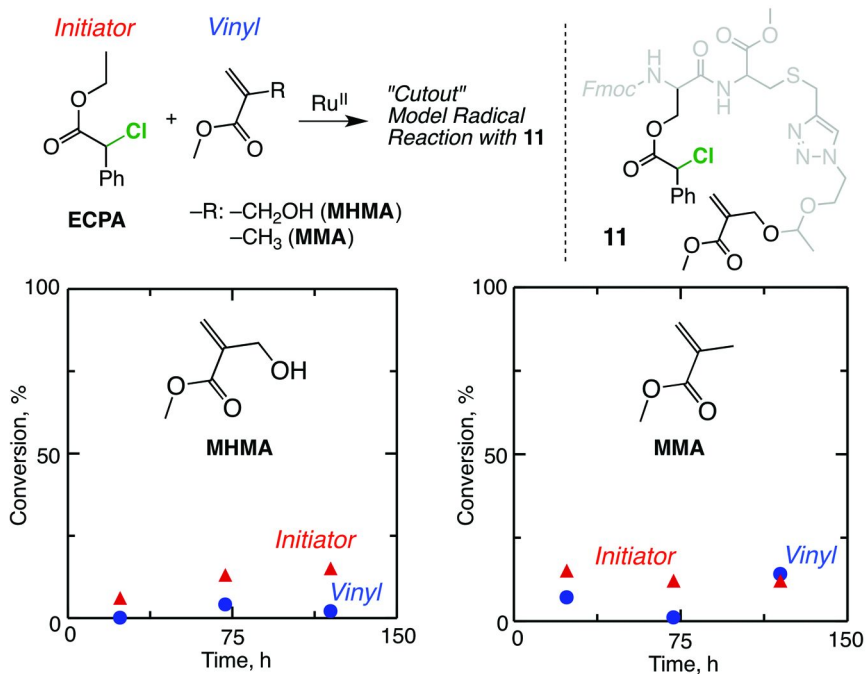
Figure 3. Ru-catalyzed radical addition without peptide template in toluene at 40 °C: $[ECPA]_0 = 20$ mM; $[MHMA]_0$ or $[MMA]_0 = 20$ mM; $[Ru]_0 = 2$ mM. Reactions were performed totally same as with 11 (see Figure 2).

The products obtained at ~100% for 11 were directly analyzed by MALDI-TOF-MS without purification (Figure 2, bottom right inset). While the starting compound 11 (theoretical mass: 863.26) gave a single peak at m/e 865.1 for the protonated form (+1), the products exhibited two main peaks, one at m/e 865.1 (+1) and the other at m/e 887.2 most likely from the Na^+-adduct (+23). Thus, molecular weight did not change before and after the reaction, nevertheless the initiator and the alkene units were quantitatively consumed at same rates. However, a minor mass peak at m/e 1752.3 attributed to a dimeric product, was also observed, indicating that some intermolecular radical addition supervened, though not extensively. These data are consistent with that intramolecular ring-closure single addition was successfully controlled on the templated system, although the reaction proceeded via chain-growth mechanism while giving active carbon-chlorine bond.

Selective Cleavage of Acetal Linker

Finally, the acid-catalysed cleavage of the acetal bond in the product was tested. The mass after acidolysis decreased by 26, consistent with the expected open-chain product via the formation of α,ω-diol and the loss of ethylene, though the small amount of the product did not allow further characterization by NMR and other methods (Figure 4). The clean cleavage suggests that it proceeded without damaging other parts and functionalities in the product and that an acetal linker is suitable for our templated systems.
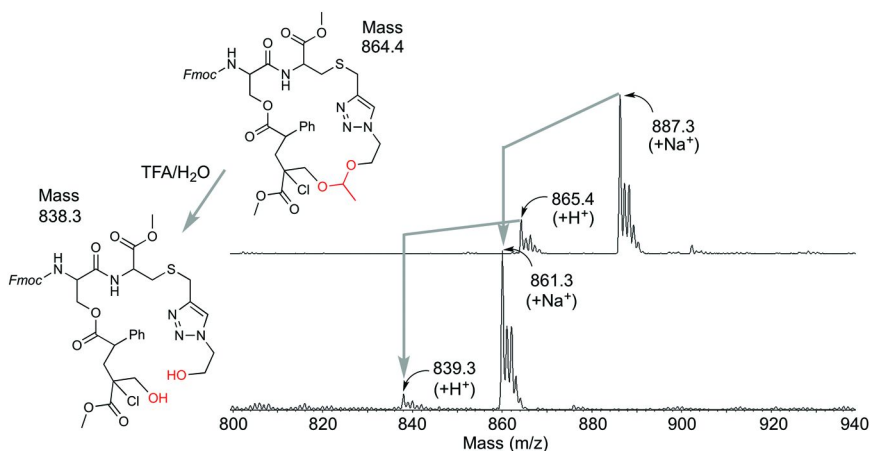
Figure 4. MALDI-TOF-MS specta of 11 (top) and the product after TFA treatment (bottom). See experimental section for the condition.

Experimental

Materials and Measurement

All the solvents were purchased from Wako Pure Chemical Industries and used without further purification. 2-Chloroethyl vinyl ether (TCI, > 97%), bromoethane (TCI, > 98 %), NaBr (Wako, > 99.0%), methyl 2-(hydroxymethyl)acrylate (MHMA (**4**); Gift from Nippon Shokubai, > 98%), pyridinium *p*-toluenesulfonate (TCI, > 98%), *N*-fmoc-L-serine tert-butyl ester (TCI, > 98%), trifluoroactic acid (TFA; Wako > 98%), 1-hydroxybenzotriazole monohydrate (HOBt; TCI, > 97%), 1-ehyl-3-(3-dimethylaminopropyl)carbodiimide hydrochloride (EDC·HCl; TCI, > 98%), 4-ethylmorpholine, *N,N*-diisopropylethylamine (DIPEA; TCI, > 98.0%), CuBr (Aldrich, > 98.0%), bis(diphenylphosphino)methane monooxide (PPh$_2$CH$_2$P(=O)Ph$_2$; Strem, > 97%) were used as received. Methacryloyl chloride (TCI, > 80%), 2-chloro-2-phenylacetyl chloride (Aldrich, > 90%), triethylamine (TCI, > 99%) and 1,2,3,4-tetrahydrousnaphthalene (tetralin; internal standard for ^{1}H NMR) were distilled before use. Toluene (Kishida Kagaku; purity 99.5%) was dried and purified by passing through purification columns (Solvent Dispensing System, SG Water USA, Nashua, NH; Glass Contour)

and bubbled with dry nitrogen for more than 15 min immediately before use. *S*-Propargyl-*N*-Boc-cysteine methyl ester (**2**) and *S*-propargyl-cysteine methyl ester hydrochloride (**3**) were synthesized as described in the literature (*24*). Column chromatography was carried out using Wakosil C300 (Wako) as the stationary phase.

^{1}H and ^{13}C NMR spectra were recorded on a JEOL JNM-ECA500 spectrometer, operating at 500 and 125 MHz, respectively. MALDI-TOF-MS analysis was performed on a Shimadzu AXIMA-CFR instrument equipped with 1.2-m linear flight tubes and a 337-nm nitrogen laser. Dithranol was used as matrix.

Synthesis of 2-Bromoethyl Vinyl Ether (4)

The mixture of 2-chloroethyl vinyl ether (30 mL, 297 mmol), ethyl bromide (EtBr, 220 mL, 297 mmol), NaBr (6.08 g, 59.4 mmol) and *N*-methyl-2-pyrrolidone (NMP; 295 mL) was heated at reflux for 72 h. The reaction mixture was then poured into ice-water (300 mL) and combined with brine (250 mL). The EtBr phase was washed with ice-water and then dried over sodium sulfate. After the solvent was removed under reduced pressure, the crude product was purified by distillation over CaH2 to give colorless liquid (**4**, ^{1}H NMR: Figure 5 top).
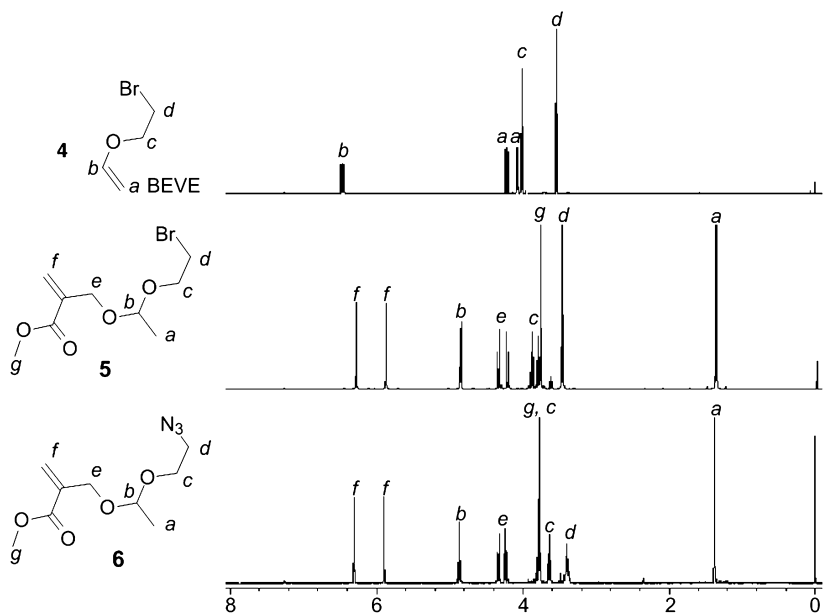
Figure 5. ^{1}H NMR spectra of 4, 5 and 6 in CDCl$_3$

Synthesis of Methyl 2-((1-(2-Bromoethoxy)ethoxy)methyl)acrylate (5)

Pyridinium *p*-toluenesulfonate was placed in round-bottom-flask under argon and dissolved in DCM (220 mL). To the resultant solution, MHMA (8.34 g, 72.0 mmol) and **4** (10.8 g, 72.0 mmol) were added at 0°C and subsequently stirred for 18 hours. The reaction was quenched with NaHCO$_3$ saturated aqueous solution and then the aqueous layer was extracted with ethyl acetate 3 times. The organic layer was combined and washed with brine, dried over Na$_2$CO$_3$, and then concentrated under reduced pressure to give crude product. It was then purified by silica column chromatography (ethyl acetate : hexane = 1:9 as eluent: ^{1}H NMR: Figure 5 middle)

Synthesis of Methyl 2-((1-(2-Azidoethoxy)ethoxy)methyl)acrylate (6)

NaN$_3$ (1.83 g, 28 mmol) was placed in round-bottom-flask under argon and dissolved in DMF (100 mL). To the resultant solution, **5** (5 g, 18.8 mmol) was added and subsequently stirred for 24 hours. After the reaction, the reaction mixture was diluted with diethyl ether and washed with water. After the aqueous layer was extracted with diethyl ether 3 times, the ether layer was combined, washed with brine, and then dried over Na$_2$CO$_3$ to give **6** (^{1}H NMR: Figure 5 bottom).

Synthesis of *N*-fmoc-*O*-(2-Chloro-2-phenylacetoxy)-L-serine-*S*-propargyl-cysteine Methyl Ester (10)

To a solution of *S*-propargyl-cysteine methyl ester hydrochloride (**3**; 1.46 g, 6.96 mmol) and HOBt (1.88 g, 13.9 mmol) in DCM (40 mL), a solution of **9** in DCM (10 mL) and 4-ethylmorpholine (0.88 mL, 6.96 mmol) were added. A solution of EDC·HCl in DCM was added at 0 °C and the resultant solution was stirred for 24 hours. The reaction mixture was then diluted with ethyl acetate and washed with saturated aqueous Na$_2$CO$_3$, 2 M aqueous citric acid, water and brine in this order. The organic phase was dried over Na$_2$SO$_4$, and the solvent was removed under reduced pressure. The crude product was purified by silica column chromatography (DCM : MeOH = 100 : 2 as eluent) to yield **10** (2.63 g, 4.15 mmol, yield 60%, ^{1}H NMR: Figure 6 bottom).

Synthesis of Initiator-Monomer Dipeptide Molecule (11)

10 (1.0 g, 1.57 mmol) and CuBr (0.0587 g, 0.41 mmol) were placed in round-bottom flask under argon and treated with a solution of **6** (2.36 mmol) in DMF (10 mL) and DIPEA (0.07 mL, 0.41 mmol) at r.t. for 17 hours. The reaction mixture was concentrated under reduced pressure and the crude product was purified by silicagel column chromatography (DCM:MeOH = 100:2 as eluent) to yield initiator-monomer dipeptide molecule **11** (yield 24%, ^{1}H NMR: Figure 7 bottom).
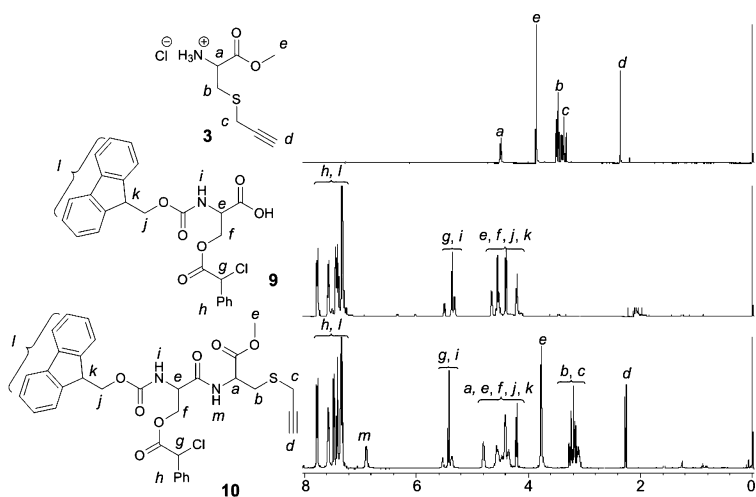
Figure 6. ¹H NMR spectra of **3**, **9** and **10** in CDCl₃
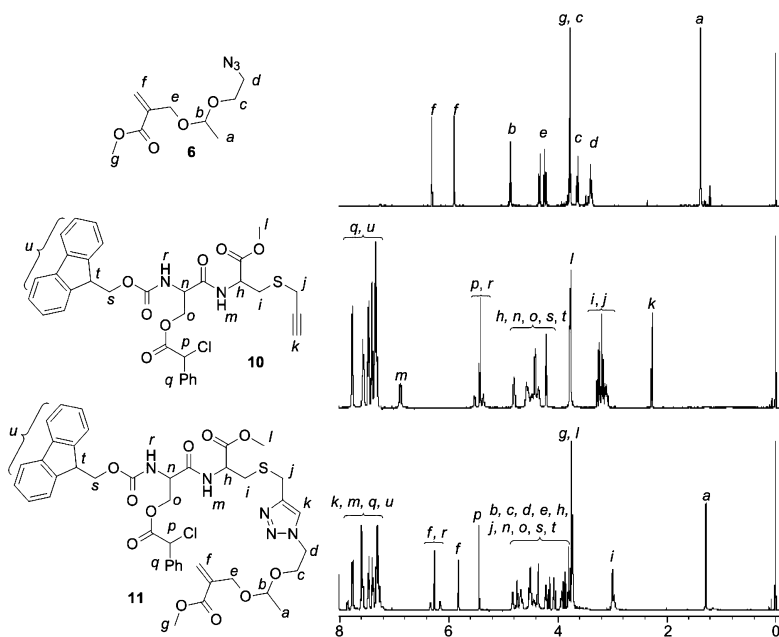
Figure 7. ¹H NMR spectra of **6**, **10** and **11** in CDCl₃

Synthesis of [Cp*Ru(μ₃-I)]₄

A chlorine-based ruthenium precursor [Cp*Ru(μ₃-Cl)]₄ (0.52 g, 0.48 mmol) (*25*) was placed in round-bottom flask under argon and dissloved in CH₃CN (15 mL). This resultant solution was treated with sodium iodide (0.36 g, 2.4 mmol)

at r.t. for 1 hour (*26*). After the reaction, the mixture was passed through a filter under argon and the filtrate was concentrated under reduced pressure to yield the crude product, which was washed with diethyl ether (1.0 mL) 3 times to yield brown solid ([Cp*Ru(μ_3-I)]$_4$; 0.47g, 68%). The halogen exchange was confirmed with ^{1}H NMR.

Preparation of a Ruthenium Complex

[Cp*Ru(μ_3-I)]$_4$ (3.6 mg, 2.5μmol) and PPh$_2$CH$_2$P(=O)Ph$_2$ (4.0 mg, 10μmol) were placed in schlenk-flask under argon and dissolved in toluene (1 mL). The solution was heated at 80°C for 1 hour, and the solution color was changed from black-brown to yellow-brown likely due to phosphine coordination. The in-situ formed ruthenium complex was directly used for the radical addition.

Ru-Catalyzed Intramolecular Radical Addition of 11

Radical addition was carried out by the syringe technique under dry argon in baked glass tubes equipped with a three-way stopcock. The dipeptide **11** (17.4 mg, 20 μmol) was placed in schlenk-flask and dissolved in 0.8 mL of toluene under argon. To this solution were added one droplet of tetralin and a solution of the ruthenium complex (0.2 mL; 10 mM), which was prepared as above. The resultant mixture was heated at 40°C. In predetermined intervals, the reaction was terminated by cooling the reaction mixtures to –78°C. The reaction conversion was determined from the concentration of residual vinyl group and 2-chloro-2-phenylacetyl group respectively measured by ^{1}H NMR (CDCl$_3$) from integrated peak area of the olefinic and benzyl protons of the **11** (5.82 ppm and 5.70 ppm respectively) with tetraline (2.77 ppm) as an internal standard.

Cleavage Reaction of Acetal Bond after Radical Addition

The radical reaction mixture with **11** (17.4 mg, 20 μmol) (reaction time: 120 h) was concentrated under reduced pressure. Then, the crude product was treated with TFA (0.4 mL) and water (0.1 mL) at r.t. for 24 hours. Saturated Na$_2$CO$_3$ aqueous solution was added and the water layer was extracted with dichloromethane 3 times. The organic phase were combined, washed with brine and dried over Na$_2$SO$_4$. After removal of solvents under reduced pressure, the product was directly measured with MALDI-TOF-MS without further purification (Figure 4 bottom).

Conclusion

In conclusion, one alkene monomer and one radical initiator were incorporated onto the pendent groups of a dipeptide framework to construct "templated" monomer–initiator systems. Assisted by this design, the single monomer addition therein, or intramolecular radical ring-closure, was well controlled, far better than the corresponding template-free systems. The

control of single monomer radical addition keeping active carbon–halogen bond is significant, and this design concept suggests sequence control via templated-radical polymerization. The control requires diluted condition and the productivity is low, but more active catalyst of high turnover frequency would enhance the reaction efficiency.

References

1. Lutz, J. F.; Ouchi, M.; Liu, D. R.; Sawamoto, M. *Science* **2013**, *341*, 1238149.
2. Ouchi, M.; Badi, N.; Lutz, J. F.; Sawamoto, M. *Nat. Chem.* **2011**, *3*, 917–924.
3. Lutz, J. F. *Acc. Chem. Res.* **2013**, *46*, 2696–2705.
4. Pfeifer, S.; Lutz, J.-F. *J. Am. Chem. Soc.* **2007**, *129*, 9542–9543.
5. Lutz, J. F. *Polym. Chem.* **2010**, *1*, 55–62.
6. Satoh, K.; Ozawa, S.; Mizutani, M.; Nagai, K.; Kamigaito, M. *Nat. Comm.* **2010**, *1*, 6.
7. Niu, J.; Hili, R.; Liu, D. R. *Nat. Chem.* **2013**, *5*, 282–292.
8. Lewandowski, B.; De Bo, G.; Ward, J. W.; Papmeyer, M.; Kuschel, S.; Aldegunde, M. J.; Gramlich, P. M.; Heckmann, D.; Goldup, S. M.; D'Souza, D. M.; Fernandes, A. E.; Leigh, D. A. *Science* **2013**, *339*, 189–193.
9. Rosales, A. M.; Segalman, R. A.; Zuckermann, R. N. *Soft Matter* **2013**, *9*, 8400–8414.
10. McKee, M. L.; Milnes, P. J.; Bath, J.; Stulz, E.; Turberfield, A. J.; O'Reilly, R. K. *Angew. Chem., Int. Ed.* **2010**, *49*, 7948–7951.
11. Zamfir, M.; Lutz, J. F. *Nat. Commun.* **2012**, *3*, 1138.
12. Meyer, T. Y.; Stayshich, R. M. *J. Am. Chem. Soc.* **2010**, *132*, 10920–10934.
13. Merrifield, R. B. *J. Am. Chem. Soc.* **1963**, *85*, 2149–2154.
14. Melville, H. W.; Watson, W. F. *J. Polym. Sci.* **1953**, *11*, 299–305.
15. Szwarc, M. *J. Polym. Sci.* **1954**, *13*, 317–318.
16. Tan, Y. Y. *Prog. Polym. Sci.* **1994**, *19*, 561–588.
17. Polowinski, S. *Prog. Polym. Sci.* **2002**, *27*, 537–577.
18. Kamigaito, M.; Ando, T.; Sawamoto, M. *Chem. Rev.* **2001**, *101*, 3689–3745.
19. Ouchi, M.; Terashima, T.; Sawamoto, M. *Chem. Rev.* **2009**, *109*, 4963–5050.
20. Matyjaszewski, K.; Xia, J. H. *Chem. Rev.* **2001**, *101*, 2921–2990.
21. Ida, S.; Terashima, T.; Ouchi, M.; Sawamoto, M. *J. Am. Chem. Soc.* **2009**, *131*, 10808–10809.
22. Ida, S.; Ouchi, M.; Sawamoto, M. *J. Am. Chem. Soc.* **2010**, *132*, 14748–14750.
23. Ida, S.; Ouchi, M.; Sawamoto, M. *Macromol. Rapid Comm.* **2011**, *32*, 209–214.
24. Struthers, H.; Spingler, B.; Mindt, T. L.; Schibli, R. *Chem. Eur. J.* **2008**, *14*, 6173–6183.
25. Fukuzaki, Y.; Tomita, Y.; Terashima, T.; Ouchi, M.; Sawamoto, M. *Macromolecules* **2010**, *43*, 5989–5995.
26. Fagan, P. J.; Mahoney, W. S.; Calabrese, J. C.; Williams, I. D. *Organometallics* **1990**, *9*, 1843–1852.

Chapter 11

Sequence-Controlled Polymers by Ruthenium-Mediated Ring-Opening Metathesis Polymerization

Alice B. Chang, Garret M. Miyake, and Robert H. Grubbs*

Arnold and Mabel Beckman Laboratory of Chemical Synthesis, Division of Chemistry and Chemical Engineering, California Institute of Technology, Pasadena, California 91125, United States
***E-mail: rhg@caltech.edu**

In sequence-controlled polymers, repeat units of different chemical composition are arranged in a well-defined order. Due to its living characteristics and functional group tolerance, ruthenium-mediated ring-opening metathesis polymerization (ROMP) is a powerful strategy for sequence control. Catalysts for ROMP can be tuned to achieve polymers with highly controlled sequences, thereby encoding structural information in the structure of the catalyst itself. The study of sequence-cotrolled polymerization offers both mechanistic insights and routes to new materials with precise structure–property relationships. This chapter will review design strategies for ruthenium-mediated sequence-controlled ROMP. Structural control in terms of *cis/trans*-selectivity and tacticity will first be discussed to illustrate the key principles of catalyst design. This framework will then be extended to sequence control for alternating copolymerization, with the goal of motivating continued progress in this area.

Introduction

Polymers can access many levels of structural order, depending on the identity of the monomers and on the polymerization method employed. The configuration of the polymer backbone, orientation of side groups, and (in copolymers) distribution of repeat units along the chain can all be tuned, enabling

control over polymer structure and properties. The focus of this chapter will be on sequence-controlled polymers, in which repeat units of different chemical composition are arranged in a well-defined order (*1, 2*).

The most basic level of structural control governs the homopolymerization of one monomer to produce one polymer microstructure among multiple possible configurations. As a result, the stereochemistry of any double bonds and/or chiral sp^3-hybridized centers in the polymer backbone is highly controlled. The copolymerization of two or more monomers introduces new opportunities for sequence control: in addition to the stereochemical factors involved in homopolymerization, the *order* of monomer incorporation becomes important. Copolymerization can proceed in either a statistical or sequence-controlled fashion (Figure 1). In a statistical copolymerization, the distribution of monomers in the polymer chain is determined by the reactivity ratios of the system (*3*). This statistical dependence typically results in a non-uniform distribution of polymer microstructures. Sequence control offers an increased level of control over polymer structures and properties, opening routes to the design and synthesis of new materials.
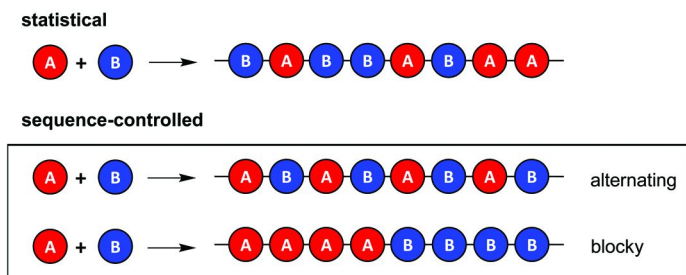
Figure 1. The polymerization of a mixture of A and B monomers can produce either statistical or sequence-controlled copolymers.

In the production of polymer-based materials, sequence control is often crucial to obtaining desired macroscopic properties. To a large extent, properties such as thermal transition temperatures, crystallinity, toughness, and conductivity all depend on the uniformity of polymer microstructures. The close relationship between polymer structure and properties is also illustrated in biological systems. In biopolymers such as proteins and nucleic acids, the precise sequence of monomers (amino acids and nucleotides, respectively) determines the structure of the polymer. The structure, in turn, determines many of the functions of biopolymers that are essential to life, such as self-assembly, substrate recognition, catalysis, and the storage and high-fidelity transmission of genetic information. Synthetic polymers with well-defined sequences can be developed for similar applications and new functional materials. Nature's ability to develop systems with precise structure–property relationships is a source of inspiration for sequence-controlled polymerization.

The first (and most direct) approach to the synthesis of sequence-controlled polymers involved connecting monomer units one by one. This iterative approach, which entailed cycles of coupling and deprotection, was introduced in the 1950s to synthesize oligopeptides (*4*). Although it has since been optimized for solid-phase peptide synthesis (*5*, *6*), this strategy is limited in general by low yields and demanding purification steps. Subsequent approaches to sequence control involved the step-growth copolymerization of bifunctional monomers (*7*), but these methods were restricted to certain co-monomer pairs and typically produced statistical sequences. Living methods such as ionic polymerization (*8*), radical polymerization (*9*, *10*), and ring-opening metathesis polymerization (ROMP) (*11*, *12*) have also been explored for sequence control. Various catalyst systems have been developed for each of these methods, and ruthenium-mediated ROMP has emerged as a powerful strategy for sequence control (*13–15*). The living characteristics of ROMP enable the synthesis of polymers with controlled molecular weights and narrow molecular weight distributions. Furthermore, the high functional group tolerance of ruthenium-based initiators allows the direct incorporation of a wide variety of functional groups from the monomers, enabling the synthesis of new materials.

In biological systems, sequence-controlled polymers like proteins and nucleic acids are synthesized by a highly sophisticated system of cellular machinery. Large complexes like ribosomes (the sites of protein synthesis) template sequences by enforcing controlled physical and chemical environments around the monomers and growing chains. An important challenge for chemistry is to design synthetic catalysts that can achieve similarly precise sequence control. For both biological and synthetic catalysts, the structure of the catalyst determines its function and the properties of the polymers produced. Ruthenium (Ru) ROMP catalysts, which are typically based on a [$L_2X_2Ru=CHR$] scaffold, cannot template sequence control in the same way as large complexes like ribosomes. However, by varying the L, X, and R groups on the catalyst scaffold, the steric and electronic properties of the catalyst can be tuned to achieve sequence-controlled polymerization.

The structure of the catalyst and mechanism of polymerization determine the type and extent of sequence control. The goal of this chapter is to review design strategies for ruthenium-mediated sequence-controlled ROMP. To illustrate the key principles of catalyst design, structural control in terms of *cis/trans*-selectivity and tacticity will first be discussed. This framework will then extended to sequence control for alternating copolymerization, with the goal of motivating continued progress in this area.

Stereochemistry of ROMP

The field of sequence-controlled polymerization aims toward both improving the mechanistic understanding of relevant reactions and synthesizing new materials with precise structure–property relationships. Polymer microstructures can be controlled on many levels, allowing polymers to be tuned for a wide variety of specific functions. Overall, ROMP (mediated by a transition metal catalyst) breaks and reforms carbon–carbon double bonds, while at the same time

opening strained cyclic monomers (Figure 2). The release of ring strain provides the driving force to overcome the unfavorable entropy of polymerization (*3*), and as a consequence of ring-opening, the backbones of polymers prepared by ROMP contain carbon–carbon double bonds.
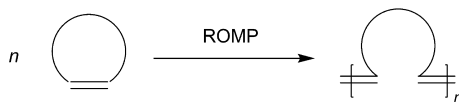
Figure 2. ROMP of a cyclic olefin produces polymers that possess double bonds along the main chain.

In ROMP, the first and most basic level of structural control concerns the *cis/trans*-selectivity of main-chain double bonds. In the case of bicyclic and/or substituted monomers, a second element, the tacticity of the side groups, becomes relevant. Lastly, sequence control through the copolymerization of a mixture of monomers provides additional opportunities for polymer design. In line with the historical development of the field, this review will introduce ROMP in terms of *cis/trans*-selectivity and controlled tacticity, highlighting interactions between the monomer and catalyst in the mechanism of metathesis. Based on the design principles outlined, this review will then explore ruthenium-mediated ROMP for the synthesis of sequence-controlled copolymers.

Due to their high ring strain (*16, 17*), norbornene-based monomers are efficiently polymerized through ROMP (*18*). Norbornene-based polymers prepared by ROMP contain carbon–carbon double bonds flanked by chiral sp^3-hybrizdized carbon atoms. As a result, the backbone of polynorbornene can adopt any of four stereoregular configurations, based on the arrangement of the double bonds and chiral carbons (Figure 3a). In the case of unsymmetrically substituted norbornene monomers, different relative orientations of the substituents create additional possible microstructures (Figure 3b). NMR spectroscopy enables the identification of different microstructures (*19–22*).

Controlling these microstructures is essential to preparing polymers with well-defined physical and mechanical properties. For example, the melting temperature of polymers prepared by ROMP depends both on the double-bond density (which is determined by the ring size of the monomer) and on the *cis/trans* ratio: the melting temperature decreases linearly as the *cis* content of the polymer increases (*23*). The same trend has been observed for the glass transition temperature (*24*) and rate of crystallization (*25*). Because ROMP is an equilibrium process that exhibits a thermodynamic preference for *trans* products, sequence control for *cis*-selectivity represents a significant challenge. Developing routes to sequence-controlled ROMP paves the way for understanding both the mechanism of olefin metathesis and the relationship between polymer structure and properties.
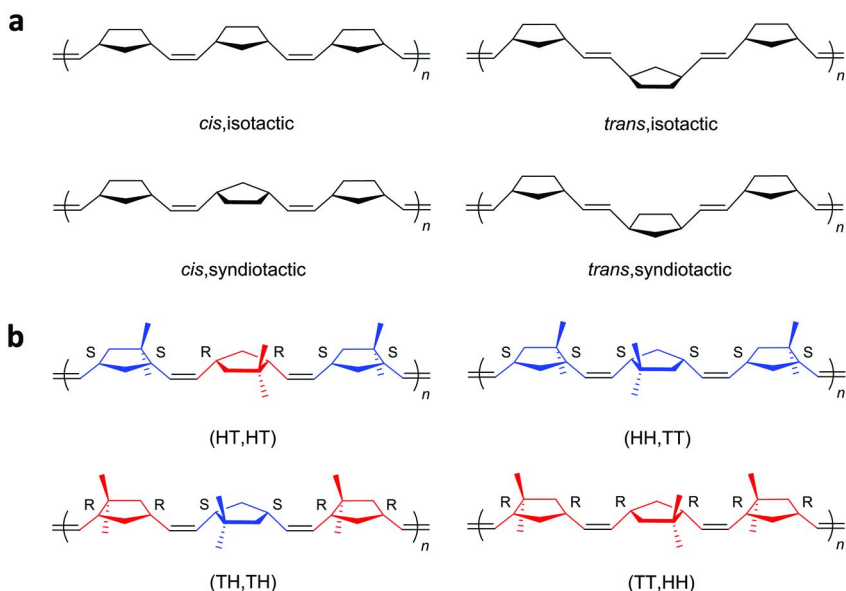
Figure 3. (a) The stereoregular microstructures of polynorbornene are determined by the configurations of the double bond and chiral centers. (b) In polymers of racemic 5,5-dimethylnorbornene, additional microstructures exist due to the possible orientations of the substituents. The four possible orientations of the substituents for cis,syndiotactic polymers are shown.

Principles of Rational Catalyst Design

Rational design strategies for sequence-controlled ROMP focus on tuning the catalyst for selectivity. Catalyst design requires an understanding of the mechanism of metathesis. In 1971, Chauvin and coworkers proposed a metathesis mechanism involving [2+2] cycloaddition between an olefin and a metal carbene, forming a metallacyclobutane intermediate (*26*). In a productive metathesis step, this intermediate subsequently cycloreverts to a new olefin and metal carbene, propagating ROMP (Figure 4).
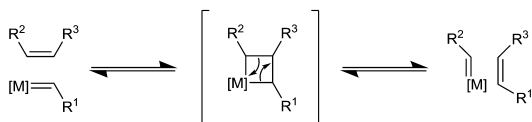
Figure 4. Olefin metathesis proceeds by [2+2] cycloaddition of an olefin to a metal carbene, forming a metallacyclobutane intermediate that undergoes subsequent cycloreversion.

Early studies by Basset and coworkers examined the Chauvin mechanism and speculated that bulky ligands in the metal sphere could influence stereochemistry by directing the approach of the olefin to the metal carbene (*27*). They proposed that different modes of olefin coordination result in different configurations of the metallacyclobutane intermediate. In general, since metathesis is an equilibrium process, cycloreversion of the most stable metallacyclobutane favors certain configurations of the double bond in the products. This concept—that metathesis can be tuned for stereoselectivity by modifying ligands on the metal center—motivates catalyst design for sequence-controlled ROMP.

Early examples of olefin metathesis employed catalyst systems involving transition metal salts, often combined with main-group alkylating agents or deposited on solid supports. In particular, halides of late metals like rhenium, ruthenium, osmium, and iridium were shown to be effective ROMP catalysts (*13*). These classical catalyst systems, however, relied on the *in situ* generation of an ill-defined metathesis-active metal carbene species, complicating the control over the molecular weight and molecular weight distributions of the polymer products. Despite such disadvantages, these early systems introduced the foundation for rational catalyst design (Chart 1).
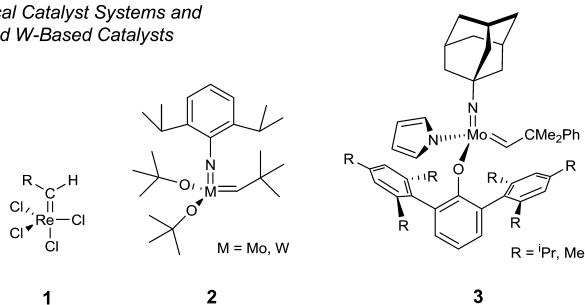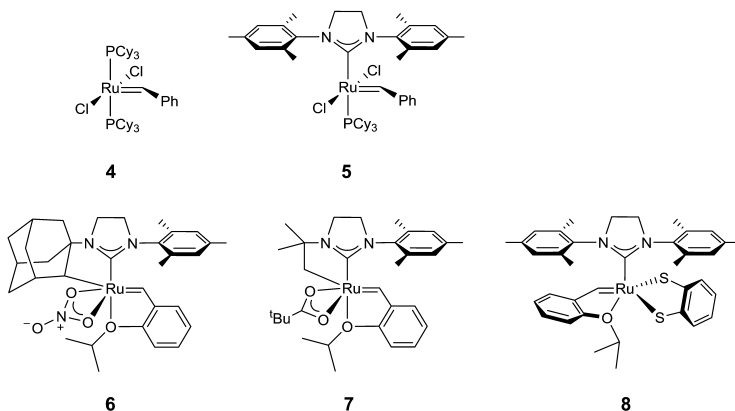
Chart 1. Catalysts for cis-selective and/or stereospecific ROMP.

Cis/*Trans*-Selectivity and Tacticity

Classical Catalyst Systems and Molybdenum- and Tungsten-Based Catalysts

In the first known syntheses of stereoregular polymers by ROMP, Rooney and coworkers achieved highly controlled microstructures through the regioselective polymerization of cyclopentene and norbornene monomers (*28*, *29*). A variety of transition metal halides (including RuCl$_3$, WCl$_6$, and ReCl$_5$) were screened in the ROMP of substituted norbornenes, and ReCl$_5$ was identified as the most *cis*-selective catalyst (*30*). In subsequent studies, Ivin, Rooney, and coworkers reported highly *cis*, syndiotactic, HT structures from the ROMP of racemic 1-methylnorbornene using ReCl$_5$. Under the reaction conditions, a catalytically active rhenium carbene complex was generated *in situ* (**1**) (*31*). *Cis*-selectivity and tacticity control were attributed to alternating chiral forms of the propagating carbene, in tandem with the unfavorable steric interactions associated with forming the *cis*-metallacyclobutane intermediates that led to other polymer microstructures (Figure 5). Because each of the two enantiomeric carbene species only reacts with one enantiomer of 1-methylnorbornene, the polymer can be considered an alternating copolymer of the two enantiomers (compare Figure 3b).
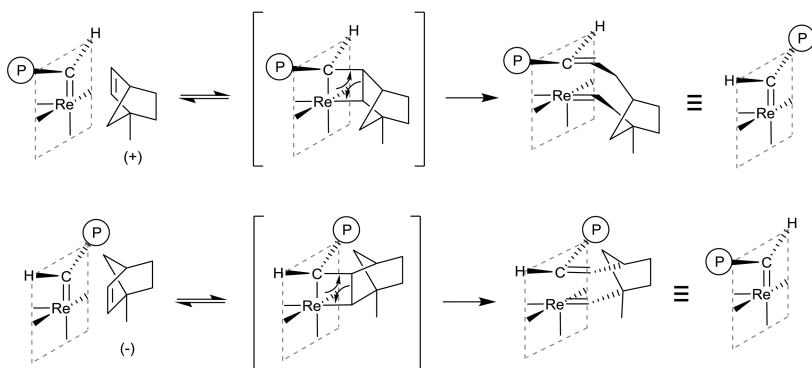
*Figure 5. Rhenium carbene **1** affords cis-selective and stereospecific ROMP. The alternating forms of the chiral carbene each incorporate only one enantiomer of 1-methylnorbornene. P represents the growing polymer chain. Reproduced with permission from reference (31). Copyright (1983) Royal Society of Chemistry.*

In agreement with the mechanism of olefin metathesis, these early reports identified the geometry of the metal carbene and metallacyclobutane intermediates as integral to structural control. Although non-living systems were able to afford structural control, catalysts such as **1** that rely on the *in situ* generation of the active metal carbene species were limited by (a) the formation of other complexes that were not metathesis-active; (b) slow initiation relative to the rate of propagation; and (c) chain-transfer processes such as backbiting (*18*). Progress in controlled ROMP came with the discovery of discrete transition metal alkylidene catalysts (*11*, *32*, *33*). Pioneering work by Schrock and coworkers reported the synthesis of discrete molybdenum (Mo) and tungsten (W) alkylidenes that catalyzed the

living ROMP of norbornene and norbornadiene derivatives (*34–36*). Subsequent studies demonstrated the ability of certain Mo and W alkylidene species (*e.g.*, **2**) to promote *cis*-selective metathesis by forcing the monomer to approach different faces of the chiral tetrahedral carbene (*37–39*). The recent development of monoaryloxide pyrrolide (MAP) complexes (*e.g.*, **3**) has improved the selectivity of Mo alkylidene species to afford remarkable control over polymer microstructures (*40–42*). The *cis*-selectivity afforded by the MAP ligands has been attributed to the presence of a relatively large, bulky aryloxide and a relatively small imido group on the stereogenic Mo center. This steric contrast favors olefin coordination to yield an all-*cis* metallacyclobutane intermediate in which all substituents point away from the axial aryloxide and toward the axial imido group (Figure 6) (*43*). Cycloreversion of this metallacyclobutane results in the formation of *cis*-alkenes.
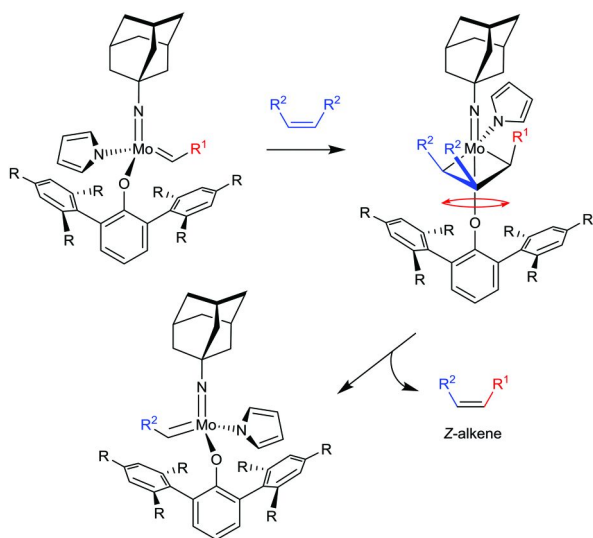
Figure 6. In Mo MAP catalysts, the size difference between the large aryloxide ligand and small imido ligand promotes high Z-selectivity in metathesis reactions. Reproduced with permission from reference (41). Copyright (2009) American Chemical Society.

Well-defined Mo and W alkylidene catalysts (*e.g.*, **2** and **3**) differ from classical catalyst systems (*e.g.*, **1**) in both their metal centers and ligand environments. Despite these differences, both types of catalysts have achieved selectivity in ROMP by directing monomer approach to the propagating carbene. In general, different orientations of monomer approach lead to different metallacyclobutane intermediates that can vary widely in stability due to the steric constraints imposed by the ligands. Productive metathesis generally proceeds via the formation of the most stable metallacyclobutane intermediate. Cycloreversion of this metallacycle leads to polymers with controlled microstructures. These principles of sequence control also operate in ruthenium-mediated ROMP. Further

treatment of the mechanism of *cis/trans*-selectivity and tacticity control in ROMP by classical catalyst systems and Mo- and W-based alkylidenes can be found in recent reviews (*18*, *21*, *43*, *44*), but remains outside the scope of this chapter.

Ruthenium-Based Catalysts

Although Mo- and W-based ROMP catalysts have demonstrated control over polymer microstructures, they are sensitive to air, moisture, and polar functional groups. Ru alkylidene metathesis catalysts offer alternatives that combine activity and functional group tolerance. Ru-based catalysts were first developed in the 1990s (*45*) and continue to be optimized today. The increased stability of Ru-based catalysts arises from differences in the interactions between the ligand and metal center: whereas Mo- and W-based alkylidene catalysts are typically high oxidation state d^0 complexes in which ligands increase the electrophilicity of the metal center, Ru-based alkylidenes are typically d^4 complexes with large, Lewis-basic ligands. Rather than increasing the inherent reactivity of the metal, the ligands promote the dissociation of an L-type ligand to generate a reactive low-valent intermediate. The stability and functional group tolerance of Ru catalysts expands the scope of ROMP by enabling the direct incorporation of a wide variety of functional groups, facilitating the synthesis of new materials.

As early as 1965, the ROMP of functionalized norbornene monomers by Ru salts in aqueous emulsions was reported (*46*). The comparatively low activity of Ru salts, however, discouraged research on Ru-mediated metathesis until the late 1980s. In 1995, Grubbs and coworkers developed **4**, the most active metathesis catalyst among the early series of discrete Ru-based alkylidenes. The mechanism of metathesis by **4** proceeds via initial dissociation of the phosphine ligand to form a 14-electron intermediate (*47*, *48*). In the next step, the olefinic substrate coordinates to the metal center, forming a 16-electron complex. As described previously with classical systems and Mo- and W-based catalysts, subsequent steps involve [2+2] cycloaddition to form a metallacyclobutane intermediate, followed by cycloreversion to generate a new olefin and metal carbene species. Olefin coordination can occur either *cis* or *trans* to the L ligand, leading to side-bound or bottom-bound metallacyclobutanes, respectively. The preferred geometry of the metallacyclobutane determines the configuration of the product (Figure 7) (*49*).

Cis/trans-selectivity and tacticity control have been sought after with Ru-based catalysts. Although they have advantages such as high tolerance to air, moisture, and functional groups, catalyst **4** and similar Ru-based ROMP initiators are unable to afford the high *cis* content of polymers prepared with Mo- or W-based catalysts (*50*, *51*). Ru initiators also suffer from the degradation of *cis*-content at high conversions. Many metathesis catalysts based on the [L₂X₂Ru=CHR] scaffold of **4** have been synthesized in efforts to optimize stability, activity, and selectivity. With the introduction of the second-generation catalyst **5** (*52*, *53*), modified with a bulky N-heterocyclic carbene (NHC) ligand, the *cis*-selectivity of the Ru-mediated ROMP of norbornene was improved to 75% (*54*, *55*). Grubbs and coworkers subsequently developed catalysts in which the NHC is cyclometalated

via C-H activation (*e.g.*, **6**) (*56, 57*). This family of catalysts has demonstrated up to 95% *cis*-selectivity in the ROMP of norbornene-based monomers (*58*).

Despite advances in *cis*-selective Ru-mediated ROMP, until recently, no highly tactic polymers had been prepared with Ru-based catalysts (*59–62*). In comparison to Mo- and W-based catalysts, Ru-based catalysts experience readier rotation about the metal–carbon double bond (*19*). For example, the barrier to rotation in a Ru-based NHC catalyst such as **5** has been calculated to be less than 3 kcal mol^{-1} (*63*). Due to facile rotation about the Ru=C bond, it was suggested that the propagating carbene in Ru-based initiators might be unable to enforce the steric environment required for controlled tacticity. However, the cyclometalated catalysts (*e.g.*, **7**) recently reported by Grubbs and coworkers afford polymers that are not only highly *cis* (>95%) but also highly syndiotactic (>95%) (*64*). As for classical systems and Mo- and W-based catalysts, the mechanistic model is expected to involve steric constraints imposed by the ligands. In general, by directing monomer approach to the propagating metal carbene, the ligands favor the formation of *syn*-metallacyclobutane intermediates, creating a preference for *cis*-olefins (Figure 7). Hoveyda and coworkers have employed this principle to synthesize catalysts (*e.g.*, **8**) in which a bidentate dithiolate ligand inhibits the formation of *anti*-metallacyclobutane species, leading to highly *cis* (>98%) polymers of norbornene or cyclooctadiene (*65*).
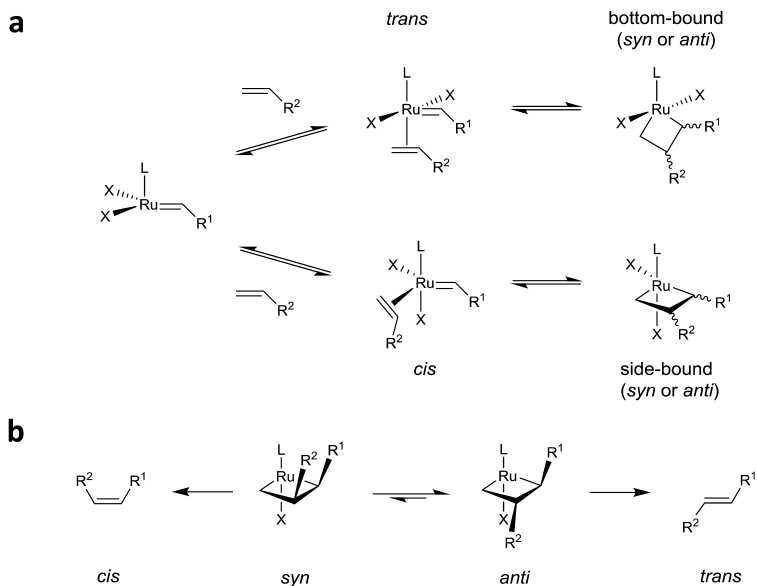
Figure 7. Approach of the olefin to the metal center determines the geometry of the metallacyclobutane intermediate. (a) The metallacyclobutane can be either bottom- or side-bound, and (b) substituents can be either syn or anti. The syn and anti structures of bottom-bound metallacycles are omitted here.

The themes developed for catalyst design for *cis/trans*-selectivity and controlled tacticity can also be applied to develop a more advanced form of controlled ROMP: the alternating copolymerization of A and B monomers. The presence of certain substituents on the metal center (or on the growing polymer chain) can restrict access to the catalytic site and favor incorporation of one monomer over another. The catalyst can be tuned by modifying ligands on the metal to create different steric and electronic environments, thereby encoding sequence information in the structure of the catalyst itself.

Alternating Copolymers

Catalyst-Controlled Approaches

Early work on alternating ROMP reported alternating sequences of enantiomers from the regioselective homopolymerization of strained olefins, catalyzed by **1** (*31*) or **2** (*38*). The copolymerization of two different olefin monomers, A and B, to alternating A,B-sequences presents new challenges. The similar polarities of most olefins makes it difficult to achieve sequence alternation; typically, blocky or statistical copolymers result (Figure 1). To overcome these challenges, various catalyst-controlled approaches to the synthesis of alternating copolymers have been developed (Chart 2 and Table I).

In parallel to the development of *cis*-selective and stereospecific ROMP, early studies of alternating ROMP employed classical catalyst systems and reported sequences based on norbornene and cyclopentene monomers. In 1982, Castner and Calderon synthesized copolymers of cyclopentene and 5-norbornene-2,3-dicarboxylic anhydride by WCl_6-catalyzed ROMP (Table I, Entry 1) (*66*). Based on the disparity between the monomer feed ratio and the polymer composition, as well as thermal transition data, the authors speculated that the copolymerization had an alternating tendency. Later, Hamilton and coworkers developed a catalyst-controlled method for the alternating ROMP of norbornene and cyclopentene (*67, 68*). Catalysts were prepared *in situ* from Ru, Os, and Ir chlorides in phenolic solvent, generating active carbene species analogous to **1** (Table I, Entry 2). The phenolic solvent was proposed to create a cage around each active metal center, enhancing steric interactions between approaching monomers and polymer chain ends (Figure 8).

The cage effect biases monomer interactions with the different forms of the metal carbene generated in each metathesis step (Figure 9). In structure P_N, the last monomer incorporated into the growing polymer chain is norbornene. The proximity of the cyclopentane ring to the metal center, due to facile rotation about the Ru=C bond, inhibits the approach of the bulky norbornene monomer. However, due to its smaller size, cyclopentene can access the catalytic site and be incorporated into the polymer chain, generating carbene P_C. P_C, which is less sterically hindered than P_N, can be accessed by both monomers, but it reacts preferentially with the more reactive norbornene monomer to generate P_N, and so forth. This cage effect for the alternating copolymerization of norbornene and cyclopentene has also been cited in systems catalyzed by Ru initiators, such as **4** and **5**, in the presence of $MoCl_5$ or WCl_5 (*69*).

Catalyst-controlled approaches to alternating ROMP have focused on modifying the [L$_2$X$_2$Ru=CHR] scaffold of **4** and **5**. Varying the ligands L and X, in particular, creates new steric and electronic environments around the metal center, tuning the relative energies of all intermediate species in the catalytic cycle. Chen and coworkers have studied the alternating ROMP of norbornene and cyclooctene by modifying the steric environment around catalyst **4** with chelating phosphine phenoxide ligands (*70–72*). Their previous work on the mechanism of metathesis motivated the design concept for catalysts **9**, **10**, and **11** (Chart 2).

Ru Catalysts for Catalyst Control
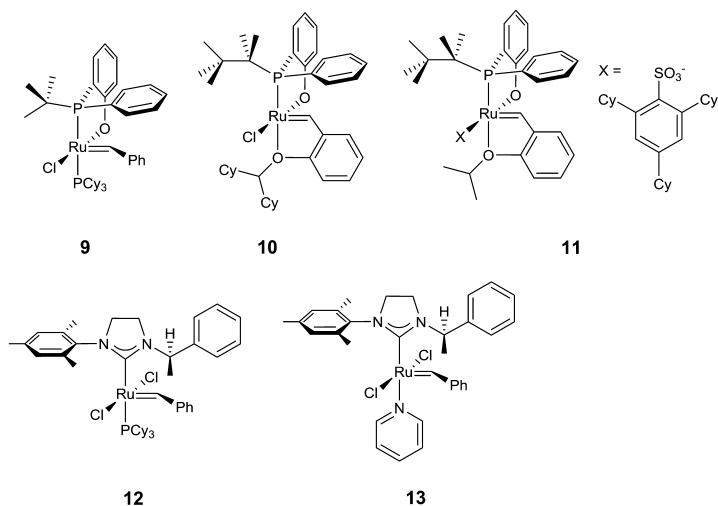
Ru Catalysts for Monomer Control
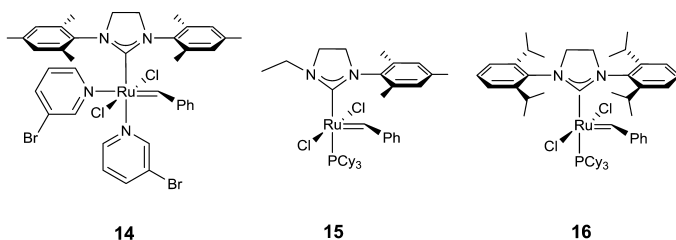
Chart 2. Catalysts for alternating ROMP.

Table I. Catalyst-controlled systems for alternating copolymers.

Entry	Catalyst	Monomer A	Monomer B	[A] : [B]	A,B-Dyads[a] (%)	Ref.
1	WCl$_6$ / Et$_3$Al			1 : 1	—	66
2	RuCl$_3$ / PhOH			1 : 8	—	67, 68
3	**9**			1 : 200	67	70, 71
4	**10**			1 : 20	97	72
5	**11**			1 : 20	97	72, 79
6	**12**			1 : 50	97	80, 81
7	**13**			1 : 50	97	80, 81
8	**13**			1 : 7	90	80, 81
9	**12**			1 : 1	72	80
10	**12**			1 : 1	48	80

[a] Determined by ^{1}H NMR.
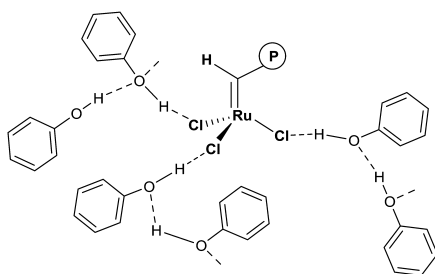
Figure 8. A solvent cage around the propagating carbene (bold) enhances steric interactions. P represents the polymer chain. Reproduced with permission from reference (68). Copyright (2000) Elsevier.
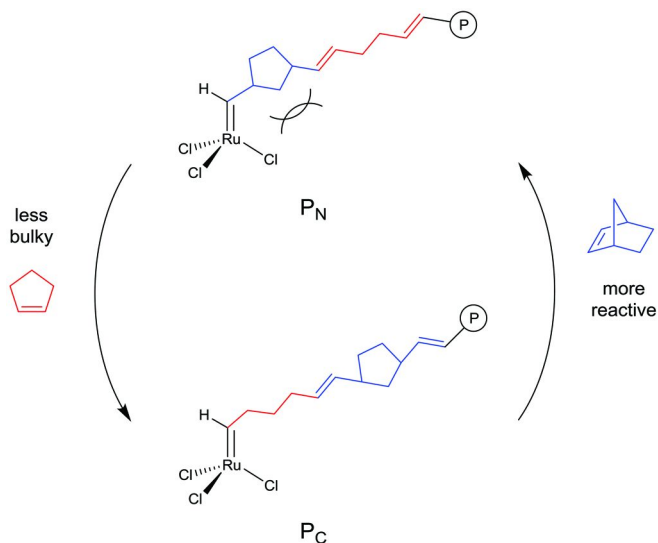
Figure 9. The two forms P_N and P_C of the metal carbene, determined by the last-incorporated monomer, favor the incorporation of cyclopentene and norbornene, respectively. P represents the growing polymer chain. Reproduced with permission from reference (68). Copyright (2000) Elsevier.

Early kinetic isotope studies of near-thermoneutral cross metathesis by **4** appeared to support a metallacyclobutane transition state (*73*). This observation, however, contradicted DFT calculations, which identified the metallacyclobutane species as an intermediate (*74–77*). This contradiction was resolved by the observation that, for near-thermoneutral metathesis, the first-generation complex **4** requires rotation of the tricyclohexylphosphine ligand (*74*). A rate-limiting

rotation of the phosphine ligand at the metallacyclobutane would result in a rate-determining step whose transition state connected two intermediates, both of which were metallacyclobutanes. As a result, with each productive metathesis step, the carbene unit swings between two faces of the complex. Indeed, this oscillation between two forms of the propagating carbene was invoked earlier by Ivin, Rooney, and coworkers to explain the alternating copolymerization of enantiomers of 1-methylnorbornene (Figure 5) (31). This mechanistic insight was identified as a potential element to exploit in sequence-controlled ROMP. In catalyst **9**, the initial platform developed by Chen and coworkers (70), the chelating phosphine phenoxide ligand bears two different substituents and suppresses rotation in the transition state. As a consequence of frustrated rotation, the active site swings between two diastereomeric carbene states with each productive metathesis step.

In mixtures of norbornene and cyclooctene monomers, the parent Ru catalyst **4** forms predominantly norbornene homopolymer until norbornene is consumed. The catalyst then polymerizes cyclooctene, leading to block copolymers. This lack of sequence control can be attributed to degenerate rotation of the phosphine ligand. Modifying **4** with a chelating phosphine phenoxide obtains catalyst **9**, which favors the alternating ROMP of norbornene and cyclooctene (Table I, Entry 3). Alternation was attributed to the different groups on the chelating phosphine phenoxide, which could be tuned to create different steric interactions in each diastereomer of the propagating carbene. Crystal structures of metathesis intermediates and variable-temperature NMR studies provided further mechanistic insight (70). Figure 10 depicts the proposed dual-site catalytic cycle for the alternating ROMP of norbornene and cyclooctene. Species **A** and **D** are diastereomeric metallacarbene intermediates, which differ in the position of the propagating chain (*trans* or *cis*, respectively) relative to the bulky *t*-butyl substituent on the phosphine phenoxide ligand. Species **A** experiences less steric crowding than **D**. In the catalytic cycle, the pathway **A→B→C** only occurs if norbornene is incorporated. Release of the high ring strain in norbornene favors cycloreversion of the *trans*-metallacyclobutane intermediate **B** to species **C** rather than collapse to **A**. However, due to the low ring strain of cyclooctene, in the event of cyclooctene addition, **B** readily collapses to **A**. The pathway **D→E→F**, however, can incorporate any cycloalkene, since the strained *trans*-metallacyclobutane intermediate **E** favors ring-opening to the less hindered **F** over collapse to **D**. As a result, **D→E→F** proceeds for either monomer, but favors incorporation of cyclooctene due to its higher concentration relative to norbornene.

Dilute norbornene in solutions of cyclooctene undergo ROMP by **9** to largely 1:1 alternating copolymers. The preference for alternating copolymerization increases as the [norbornene]:[cyclooctene] ratio decreases, as monitored by ^{13}C NMR (70). As a negative control, in order to support the hypothesis of dual-site catalysis, the authors prepared an analogue of **9** with symmetrical substitution (*i.e.*, two *t*-butyl groups on the chelating phosphorus rather than one *t*-butyl and one phenyl group). This analogue, like the parent catalyst **4**, homopolymerizes norbornene well and cyclooctene poorly, displaying no tendency toward alternating copolymerization.
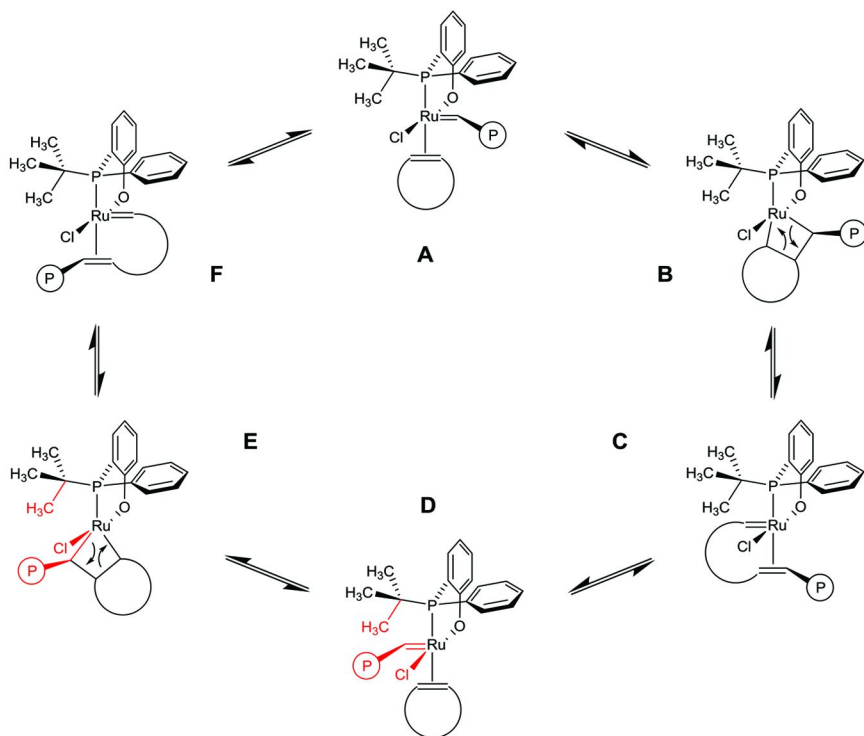
*Figure 10. Dual-site catalytic cycle for the alternating ROMP of norbornene and cyclooctene by catalyst **9**. P represents the growing polymer chain. Reproduced with permission from reference (70). Copyright (2005) John Wiley and Sons.*

Decomposition of **9** in solution leads to the formation of **4**. The loss of dual-site control upon decomposition, together with the large excess of cyclooctene, results in considerable amounts (~20%) of polycyclooctene blocks. In subsequent studies (*71*), to test whether the comparatively low selectivity of **9** was in fact due to decomposition (rather than insufficient discrimination between the two diastereomeric carbenes **A** and **D**), Chen and coworkers prepared catalysts (*e.g.*, **10**) with a Hoveyda-type (*78*) chelating benzylidene (Table I, Entry 4). Introducing the Hoveyda-type carbene stabilized the scaffold of **9**, improving selectivity for alternation. Replacing the *t*-butyl substituent on the chelating phosphine of **9** with a bulkier alkyl group also improved selectivity. With **10**, up to 97% alternating dyads were obtained from the ROMP of norbornene and cyclooctene, even at higher [norbornene]:[cyclooctene] feed ratios (Table I, Entry 4) (*72*). In related studies, the structure of **10** was modified by a sulfonate ligand in an effort to improve *cis*-selectivity as well as alternation. With catalyst **11**, highly alternating copolymers with up to 51% cis double bonds were achieved (Table I, Entry 5) (*79*).

Another strategy for catalyst-controlled alternating copolymerization has been developed by the Blechert and Buchmeiser groups. Whereas Chen and coworkers modified the steric environment around catalyst **4** by introducing chelating phosphine phenoxide ligands, Blechert, Buchmeiser, and coworkers modified **5** by introducing unsymmetrical NHCs and/or pseudohalides (*80–82*). Catalyst **12** affords up to 97% alternating dyads in the ROMP of norbornene and cyclooctene (Table I, Entry 6) (*80*). Replacing the axial phosphine ligand with a more labile pyridine ligand gives catalyst **13**, which retains the selectivity of **12** but improves the initiator efficiency (Table I, Entry 7) (*83–85*). The observation that only one pyridinecoordinates to the Ru center, rather than two, indicates that the NHC ligand is highly sterically demanding. Catalyst **13** also displays selectivity for alternation (~90%) in the ROMP of norbornene and cyclopentene, despite the limited affinity of cyclopentene for ROMP (Table I, Entry 8) (*22*).

To obtain mechanistic insight into sequence control, Blechert, Buchmeiser, and coworkers performed temperature-dependent NMR experiments (*80*). By measuring the coalescence temperature of the alkylidene proton, they estimated the rate constant of rotation (k_{rot}) of the NHC ligand to be 260 s^{-1}. As a consequence of rapid NHC rotation, catalysts **12** and **13** do not afford the diastereomeric dual-site control possible with catalysts **9**, **10**, or **11**. NMR experiments also enabled the calculation of reactivity ratios for the ROMP of norbornene and cyclooctene catalyzed by **12** or **13**. According to the calculated reactivity ratios, the rate of cyclooctene insertion into the copolymer is slightly enhanced, relative to the rate of cyclooctene homopolymerization, by the presence of a norbornene-initiator-derived terminus. Meanwhile, the rate of norbornene insertion is dramatically accelerated, relative to the rate of norbornene homopolymerization, by a cyclooctene-initiator-derived terminus. Therefore, the copolymerization of norbornene and cyclooctene by **12** or **13** favors alternation. It was proposed that the steric crowding introduced by the NHC ligand disfavors the incorporation of two consecutive norbornene monomers (compare Figure 9). The possible metallacyclobutane intermediates that result from successive norbornene insertion are too severely strained to compete with cyclooctene insertion (Figure 11). However, after cyclooctene has been incorporated into the growing chain (**D→E→F**), the catalytic site is sufficiently free from steric strain to incorporate either cyclooctene or norbornene, through either bottom-bound or side-bound metallacyclobutane intermediates (Figure 7). Since norbornene is more reactive, **F** favors incorporation of norbornene over consecutive incorporation of cyclooctene.

In sum, steric interactions between a norbornene-derived terminus and the bulky 1-phenylethyl group on the NHC ligand are the key to sequence control. For catalysts **12** and **13**, these interactions promote the alternating copolymerization of various mixtures of A and B monomers (Table I, Entries 6–10). In comparison to cyclooctene (Entries 6 and 7), sterically more demanding (*i.e.*, less reactive) co-monomers such as substituted cyclooctenes and norbornene derivatives (Entries 9 and 10) undergo ROMP with norbornene even at a 1:1 feed ratio to afford alternating (50–75%) copolymers. The scope of alternation in these systems is of particular interest, suggesting that alternating copolymers can be achieved for monomer pairs other than cyclooctene or cyclopentene.
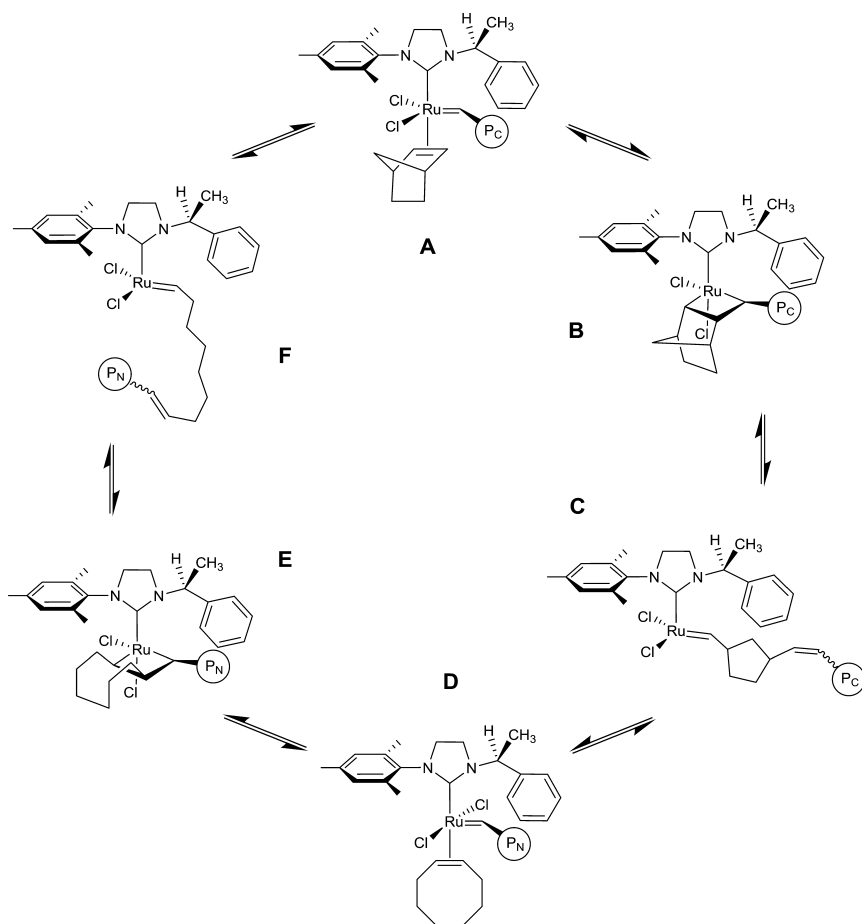
Figure 11. Catalytic cycle for the alternating ROMP of norbornene and cyclooctene by catalyst 12 or 13. P_N represents a polymer chain with a norbornene-derived terminus, and P_C represents a chain with a cyclooctene-derived terminus. Reproduced with permission from reference (80). Copyright (2008) John Wiley and Sons.

Monomer-Controlled Approaches

Balancing Sterics and Reactivity

Norbornene and cyclooctene constitute the most studied monomer pair for catalyst-controlled alternating copolymerization. The highly reactive, yet sterically demanding norbornene monomer and the less reactive, more flexible cyclooctene monomer are considered a model pair. Norbornene and cyclopentene can also be copolymerized by ROMP, yielding polymers with up to 90% alternating dyads (Table I, Entry 8) (*80*). Other monomer pairs, however, typically result in lower selectivity for sequence alternation. Future directions in this

area may explore other monomer pairs that yield highly alternating copolymers, inspired by mechanistic considerations and catalyst-controlled systems.

For the alternating copolymerization of olefins with similar double-bond polarity (*e.g.*, norbornene and cyclooctene), sequence selectivity must be catalyst-dependent. Monomer control can operate, however, for monomer pairs with sufficiently different functional groups and electronic character proximate to the carbon–carbon double bond. In this sense, monomer control can also be considered an extension of catalyst control, with the coordinating monomer acting as a template or other ligand. Many different monomer pairs have been studied, encompassing a wide range of approaches to monomer control for alternating copolymerization (Table II). In general, many approaches rely on pairing a bulky, strained monomer with an unhindered, less strained monomer, and/or on employing a significant excess of one co-monomer. Other strategies will also be discussed.

In 2002, Ilker and Coughlin reported highly alternating polymers from the ROMP of an equimolar mixture of polar 2,3-difunctionalized 7-oxanorbornene derivatives with a series of nonpolar cycloalkenes (Table II, Entries 1–3) (*86*). From a catalyst control perspective, this system is remarkable both because it uses an equimolar mixture of the two monomers and because it employs catalyst **4**, which displays no selectivity for alternation in the copolymerization of cyclic olefins with similar double-bond polarity (*70*). For the copolymerization of *endo*-*N*-ethyl-7-oxanorbornene-2,3-dicarboximide and cyclooctene, Ilker and Coughlin reported 98% alternating dyads (Table II, Entry 1). Copolymerizing the *exo*-oxanorbornene isomer with cyclooctene decreased the amount of alternating dyads to 80% (Table II, Entry 2), suggesting that the monomer approaches the propagating carbene from the *endo* face of the double bond. As a result, the more hindered *endo*-isomer undergoes slower homopolymerization relative to cross-propagation with cyclooctene, enabling more precise sequence control.

The effects of ring strain were also explored in this system. Copolymers of norbornene and a polar norbornene derivative (Table II, Entry 3) display a moderate tendency toward alternation (40%), despite the fact that the two monomers experience similar ring strain. In copolymers with norbornene, the selectivity for alternating dyads decreases as the ring strain in the cyclic olefin increases (from cyclooctene to cyclooctadiene, cyclopentene, or norbornene), indicating that the balance between ring strain and steric hindrance is a crucial factor in monomer control.

Alternating copolymers have also been synthesized from the ROMP of highly strained cyclobutene-1-esters with cyclohexene derivatives, catalyzed by **14** (*87*). Catalyst **14**, a bispyridine adduct of **5**, increases the initiation rate due to extremely rapid dissociation of the electron-deficient 3-bromopyridine ligand (*83*, *84*). From the ROMP of a 1:2 mixture of cyclobutene methyl ester and cyclohexene, Sampson and coworkers reported 91% alternating dyads (Table II, Entry 4). Although the linear polymer was completely alternating, the system was contaminated by cyclic polymers resulting from intramolecular backbiting. Sequence control was attributed to two factors. First, cyclohexene is inactive in ROMP, but it readily undergoes cross metathesis with acrylates. Second, the cyclobutene ester does not homopolymerize, due to the instability

of the enoic carbene intermediate (*88*). A mixture of the two monomers, each unable to homopolymerize, readily undergoes ROMP to afford highly alternating copolymers.

Noncovalent Templates

Other approaches to monomer control employ noncovalent interactions between monomers to template alternation. Weck and coworkers have reported segments of alternation in copolymers of norbornene- and cyclooctene-based monomers functionalized with charge transfer units (Table II, Entry 5) (*89*). Norbornene and cyclooctene were functionalized with donor and acceptor groups, respectively, and copolymerized with **15**, an unsymmetrical NHC-ligated Ru complex (*81*).   Addition of a phosphine scavenger like CuCl or AlCl$_3$ was required to increase the initiation rate. The aromatic charge transfer units aligned in a face-to-face geometry, favoring alternation to maximize donor-acceptor interactions. In the first report of such systems (Table II, Entry 5), a large excess of the acceptor-functionalized cyclooctene monomer resulted in copolymers with highly alternating segments amid a gradient of increasing cyclooctene. After consumption of the donor-functionalized norbornene monomer, polycyclooctene blocks formed. While NMR methods demonstrated the presence of alternating segments in the copolymers, the tendency toward gradient or blocky sequences prevented the reliable calculation of the percent of alternating dyads. Subsequent studies, in collaboration with Sampson and coworkers, improved the percent alternation in similar charge-transfer systems based on cyclobutene and cyclohexene monomers (Table II, Entry 6) (*90*). ^{1}H NMR analysis demonstrated that the sequences were purely alternating, and in agreement with expectations, UV-Vis spectroscopic measurements displayed a charge-transfer absorbance signal that confirmed the face-to-face alignment of side chains. In this system, however, molecular weights are moderate: synthesizing copolymers with more than ten repeating units presents a challenge.

Another monomer-controlled approach has taken advantage of acid-base interactions to template alternation. For example, Sanda and coworkers have reported the alternating copolymerization of amino-acid-derived norbornene monomers (*91*).   Because NMR chemical shifts for the homopolymers and copolymers are almost identical, the percent of alternating dyads could not be measured.   Instead, the selectivity for alternation was determined by calculating monomer reactivity ratios (*3*, *92*) Reactivity ratios calculated for the copolymerization of unprotected carboxyl- and amino-functionalized norbornenes (Table II, Entry 7) suggested that the copolymerization is highly alternating. When the carboxyl-functionalized monomer is protected, acid-base interactions are disrupted, and statistical or blocky copolymers result. Whereas the monomer-controlled approaches discussed previously (compare Table II, Entry 3) require the monomers to display significantly different ROMP activity, this amino-acid-inspired approach achieves highly alternating sequences when both monomers are based on norbornene. Since the difference in electronic characters between the monomers is negligible, the authors proposed that

acid-base interactions instead enabled sequence control (Figure 12). Alternation could be templated by acid-base interactions, either between carboxyl and amino groups on the monomers (increasing local monomer concentration), or between the propagating carbene species and the incoming monomer.
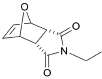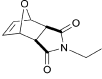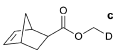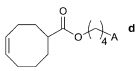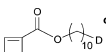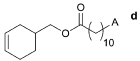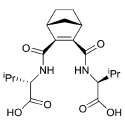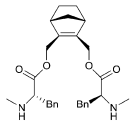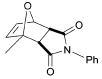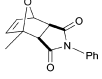
Sequence Editing

A third class of monomer-controlled approaches to the synthesis of alternating copolymers operates by an insertion or "sequence editing" mechanism. In 2002, Grubbs and coworkers reported copolymers with up to 99% alternating dyads from the ROMP of an equimolar mixture of a diacrylate and a cycloalkene, initiated by **5** (Table II, Entries 8 and 9) (*93*). In addition to displaying high ROMP activity, **5** promotes the cross-metathesis of α,β-unsaturated olefins (*94*, *95*). Mixtures of a diacrylate and a cycloalkene undergo rapid and complete ROMP to form homopolymers of the cycloalkene. The diacrylate does not undergo metathesis, due to the instability of the enoic carbene intermediate (*88*). Instead, diacrylate monomers selectively insert into the unsaturated polycyloalkene backbone, affording highly alternating copolymers (Figure 13). Highly alternating (>95%) sequences can be achieved with a wide variety of cycloalkenes, even with low-strain rings like cyclopentene and cycloheptene. Functional groups such as protected alcohols can also be incorporated into the alternating copolymers (Table II, Entry 9), opening a new class of polymers that can be synthesized by ROMP.

The insertion mechanism has also been described for other systems. ROMP of an equimolar mixture of a bulky 1-substituted oxanorbornene and cyclooctene yields alternating polymers (Table II, Entries 10 and 11) (*96*). The extent of alternation depends on the catalyst. Reactivity ratios calculated for initiator **4** were close to 0 ($r_A r_B = 0.003$), indicating that the copolymerization of a 1-substituted oxanorbornene and cyclooctene has strongly alternating character (Table II, Entry 10). In contrast, the copolymerization of norbornene and cyclooctene by **4** displays no tendency for alternation (*70*). This disparity can be explained as a consequence of 1-substitution of the monomer, which discourages oxanorbornenene homopolymerization. At the same time, the high ring strain of oxanorbornene relative to cyclooctene favors incorporation of oxanorbornene after cyclooctene (compare Figure 9).

While this mechanism explains the activity of **4**, it does not explain the higher selectivity for alternation displayed by **16**, an NHC-functionalized catalyst based on **5**. Reactivity ratios could not be calculated for catalyst **16** (Table II, Entry 11), due to rapid and complete homopolymerization of cyclooctene. The authors suggested that **16** operates by the insertion mechanism proposed in previous studies by Grubbs and coworkers (*93*). The homopolymerization of cyclooctene precedes ring-opening cross metathesis with oxanorbornene, which inserts oxanorbornene selectively into the polycyclooctene chains (compare Figure 13). This result demonstrates that multiple mechanisms for alternating copolymerization can operate in the same system, depending on the catalyst and monomer pair.

Table II. Monomer-controlled systems for alternating copolymers.

Entry	Catalyst	Monomer A	Monomer B	[A] : [B]	A,B-Dyads [a] (%)	Ref.
1	**4**			1 : 1	98	86
2	**4**			1 : 1	80	86
3	**4**			1 : 1	40	86
4	**14**			1 : 2	91	87
5	**15** [b]			1 : 50	—	89
6	**14**			2 : 1	—	90
7	**5**			1 : 1	—	91
8	**5**			1 : 1	99	93
9	**5**			1 : 1	95	93
10	**4**			1 : 1	56	96
11	**16**			1 : 1	73	96

[a] Determined by ^{1}H NMR.

[b] Addition of a phosphine scavenger is necessary.

[c] D (donor) = 1,5-dialkoxynaphthalene

[d] A (acceptor) = 1,2,4,5-benzenetetracarboxylic dianhydride

a

b
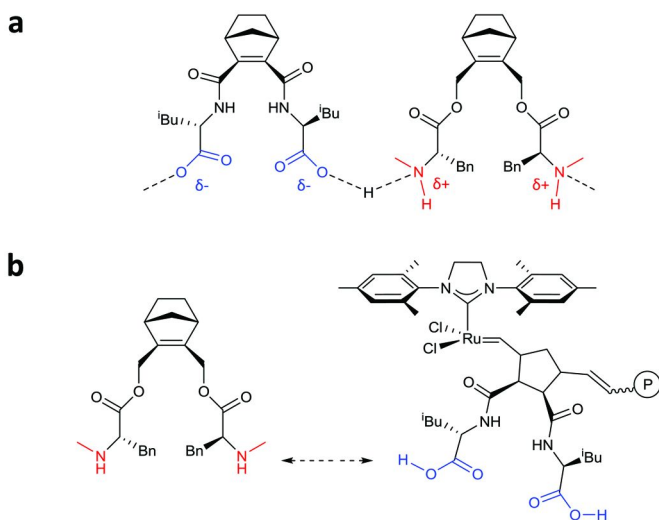
Figure 12. In the ROMP of amino-acid-functionalized norbornene monomers, acid-base interactions were proposed to template sequence alternation (a) between carboxyl and amino groups, or (b) between the propagating carbene and the incoming monomer. Reproduced with permission from reference (91). Copyright (2009) American Chemical Society.
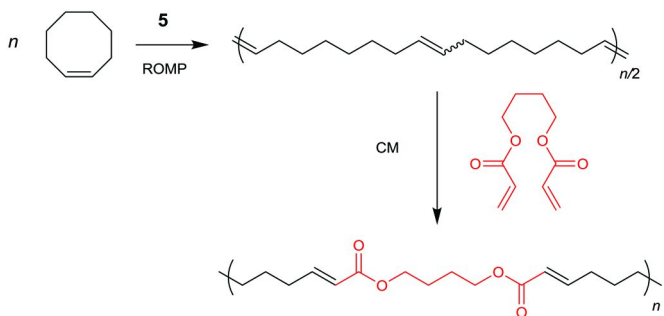
Figure 13. Alternating copolymers can be synthesized by an insertion mechanism, involving ROMP of the cycloalkene followed by cross metathesis (CM) to insert the diacrylate.

Conclusion

ROMP affords many levels of structural and sequence control, and a variety of factors affect control at each level. The most basic level of structural control is stereocontrol of the *cis/trans*-geometry of ring-opened double bonds in the polymer backbone (Figure 3). A second level of control (*i.e.*, the tacticity of side groups) becomes relevant with bicyclic and/or substituted olefins. A third level of control is possible for mixtures of two or more monomers: the order of

monomer incorporation becomes a dominant concern, posing new challenges and opportunities for sequence control. The structure of the catalyst determines its function and the properties of the polymers it produces. For Ru-based initiators, which are generally based on a [$L_2X_2Ru=CHR$] scaffold, the L, X, and R groups can be varied to tune the steric and electronic properties of the catalyst, thereby encoding sequence information in the structure of the catalyst itself.

Early studies of ROMP developed classical catalyst systems (*e.g.*, **1**) capable of producing highly *cis*, tactic polymers through the homopolymerization of norbornene- or cyclopentene-based monomers. The development of discrete Mo and W alkylidene catalysts (*e.g.*, **2**) introduced living characteristics to ROMP. By manipulating the ligand environment to discriminate between different orientations of monomer approach to the propagating carbene, subsequent studies extended the selectivity of Mo-based initiators (*e.g.*, **3**) to obtain remarkably stereoregular microstructures. Ru-based initiators (*e.g.*, **4** and **5**) have further expanded the scope of sequence-controlled ROMP by improving functional group tolerance and stability to air and moisture. Despite concerns that facile rotation about the Ru=C bond would limit the ability of Ru-based catalysts to enforce the steric environment necessary for structural control, recent work has demonstrated the ability of Ru alkylidenes (*e.g.*, **6–8**) to afford stereoregular microstructures.

The themes developed for catalyst design for *cis/trans*-selectivity and controlled tacticity also apply to design strategies for alternating copolymerization. Approaches to alternating copolymerization can be considered either catalyst-controlled or monomer-controlled. In catalyst-controlled approaches, due to the similar double-bond polarity of the co-monomers, selectivity for alternation is determined by steric interactions between the catalyst, monomers, and polymer chain end (Table I). In general, for a certain metathesis step, reactivity favors the incorporation of one monomer over another. In the next step, steric interactions, together with a concentration difference between the monomers, favor incorporation of the other monomer. Due to the oscillating preference for incorporating different monomers with each productive metathesis step, alternating copolymers result. Different strategies have been developed to create selective catalysts. Chen and coworkers have modified catalyst **4** with chelating phosphine phenoxide ligands, developing catalysts **9–11**. Blechert, Buchmeiser, and coworkers have modified catalyst **5** with bulky, unsymmetrical NHCs, obtaining **12** and **13**.

Monomer control can be considered an extension of catalyst control, with the coordinating monomer acting as a template or another ligand. In monomer-controlled systems (Table II), ROMP of an equimolar mixture of monomers can obtain highly alternating sequences due to chemical, steric, and/or electronic interactions between the monomers. Polymers produced by monomer-controlled alternating ROMP illustrate the power of sequence-controlled polymerization to produce new materials.

Fundamental mechanistic understanding paves the way for designing sequence-controlled polymerizations. Ru-mediated ROMP enables the design and synthesis of polymers with new materials properties and applications. Examples of sequence-controlled polymers by Ru-mediated ROMP remain rare, but design strategies developed in previous studies open the field for continued progress.

References

1. Lutz, J.-F. *Polym. Chem.* **2009**, *1*, 55–62.
2. Lutz, J.-F.; Ouchi, M.; Liu, D. R.; Sawamoto, M. *Science* **2013**, *341*, 628–637.
3. Odian, G. *Principles of Polymerization*, 4th ed.; Wiley-Interscience: Hoboken, New Jersey, 2004.
4. du Vigneaud, V.; Ressler, C.; Swan, J. M.; Roberts, C. W.; Katsoyannis, P. G. *J. Am. Chem. Soc.* **1954**, *76*, 3115–3121.
5. Merrifield, R. B. *J. Am. Chem. Soc.* **1963**, *85*, 2149–2154.
6. *Solid-Phase Synthesis: A Practical Guide*; Kates, S. A., Albericio, F., Eds.; Marcel Dekker, Inc.: New York, 2000.
7. Ueda, M. *Prog. Polym. Sci.* **1999**, *24*, 699–730.
8. Szwarc, M. *Nature* **1956**, *178*, 1168–1169.
9. Patten, T. E.; Xia, J.; Abernathy, T.; Matyjaszewski, K. *Science* **1996**, *272*, 866–868.
10. Ouchi, M.; Terashima, T.; Sawamoto, M. *Chem. Rev.* **2009**, *109*, 4963–5050.
11. Schrock, R. R. *Acc. Chem. Res.* **1990**, *23*, 158–165.
12. Bielawski, C. W.; Grubbs, R. H. *Prog. Polym. Sci.* **2007**, *32*, 1–29.
13. Trnka, T. M.; Grubbs, R. H. *Acc. Chem. Res.* **2001**, *34*, 18–29.
14. Bielawski, C. W.; Grubbs, R. H. Living Ring-Opening Metathesis Polymerization. In *Controlled and Living Polymerizations: From Mechanisms to Applications*; Müller, A. H. E., Matyjaszewski, K., Eds.; Wiley-VCH: 2009; pp 297−342.
15. Leitgeb, A.; Wappel, J.; Slugovc, C. *Polymer* **2010**, *51*, 2927–2946.
16. Benson, S. W.; Chruickshank, F. R.; Golden, D. M.; Haugen, G. R.; O'Neal, H. E.; Rodgers, A. S.; Shaw, R.; Walsh, R. *Chem. Rev.* **1969**, *69*, 279–324.
17. Schleyer, P. v. R.; Williams, J. E.; Blanchard, K. R. *J. Am. Chem. Soc.* **1970**, *92*, 2377–2386.
18. Black, G.; Maher, D.; Risse, W. Living Ring-Opening Metathesis Polymerization. In *Handbook of Olefin Metathesis*; Grubbs, R. H., Ed.; Wiley-VCH: Weinheim, 2003; Vol. 3.
19. Amir-Ebrahimi, V.; Hamilton, J. G.; Rooney, J. J. Blockiness and Tacticity in Ring-Opened Metathesis Polymers. In *NATO Sci. Ser., II*; Khosravi, E., Szymanska-Buzar, T., Eds., 2002; Vol. 56, pp 45−67.
20. Hamilton, J. G. *Polymer* **1998**, *39*, 1669–1689.
21. Hamilton, J. G. Stereochemistry of Ring-Opening Metathesis Polymerization. In *Handbook of Metathesis*; Grubbs, R. H., Ed.; Wiley-VCH: Weinheim, 2003; Vol. 3.
22. Ivin, K. J.; Mol, J. C. *Olefin Metathesis and Metathesis Polymerization*; Academic Press: San Diego, 1997.
23. Dounis, P.; Feast, W. J.; Kenwright, A. M. *Polymer* **1995**, *36*, 2787–2796.
24. Ofstead, E. A. *Encylopedia of Polymer Science and Engineering*; John Wiley & Sons: New York, 1988; Vol. 11.
25. Edwards, J. H.; Feast, W. J.; Bott, D. C. *Polymer* **1984**, *25*, 395–398.
26. Hérisson, J.-L.; Chauvin, Y. *Makromol. Chem.* **1971**, *141*, 161–176.

27. Bilhou, J. L.; Basset, J. M.; Mutin, R.; Graydon, W. F. *J. Am. Chem. Soc.* **1977**, *99*, 4083–4090.

28. Ivin, K. J.; Laverty, D. T.; Rooney, J. J. *Makromol. Chem.* **1977**, *178*, 1545–1560.

29. Ivin, K. J.; Łapienis, G.; Rooney, J. J. *Polymer* **1980**, *21*, 436–443.

30. Thoi, H. H.; Ivin, K. J.; Rooney, J. J. *J. Mol. Catal.* **1982**, *15*, 245–270.

31. Hamilton, J. G.; Ivin, K. J.; Rooney, J. J.; Waring, L. C. *J. Chem. Soc., Chem. Commun.* **1983**, *4*, 159–161.

32. Schrock, R. R.; Rocklage, S.; Wengrovius, J.; Rupprecht, G.; Fellmann, J. *J. Mol. Catal.* **1980**, *8*, 73–83.

33. Bazan, G. C.; Khosravi, E.; Schrock, R. R.; Feast, W. J.; Gibson, V. C.; O'Regan, M. B.; Thomas, J. K.; Davis, W. M. *J. Am. Chem. Soc.* **1990**, *112*, 8378–8387.

34. Feast, W. J.; Gibson, V. C.; Marshall, E. L. *J. Chem. Soc., Chem. Commun.* **1992**, *16*, 1157–1158.

35. Schrock, R. R.; Feldman, J.; Cannizzo, L. F.; Grubbs, R. H. *Macromolecules* **1987**, *20*, 1169–1172.

36. Schrock, R. R. *Chem. Rev.* **2002**, *102*, 145–179.

37. McConville, D. H.; Wolf, J. R.; Schrock, R. R. *J. Am. Chem. Soc.* **1993**, *115*, 4413–4414.

38. Wu, Z.; Grubbs, R. H. *Macromolecules* **1995**, *28*, 3502–3508.

39. Schrock, R. R.; Lee, J.-K.; O'Dell, R.; Oskam, J. H. *Macromolecules* **1995**, *28*, 5933–5940.

40. Malcolmson, S. J.; Meek, S. J.; Sattely, E. S.; Schrock, R. R.; Hoveyda, A. H. *Nature* **2008**, *456*, 933–937.

41. Ibrahem, I.; Yu, M.; Schrock, R. R.; Hoveyda, A. H. *J. Am. Chem. Soc.* **2009**, *131*, 3844–3845.

42. Flook, M. M.; Ng, V. W. L.; Schrock, R. R. *J. Am. Chem. Soc.* **2011**, *133*, 1784–1786.

43. Schrock, R. R. *Dalton Trans.* **2011**, *40*, 7484–7495.

44. Buchmeiser, M. R. *Chem. Rev.* **2000**, *100*, 1565–1604.

45. Nguyen, S. T.; Johnson, L. K.; Grubbs, R. H. *J. Am. Chem. Soc.* **1992**, *114*, 3974–3975.

46. Michelotti, F. W.; Keaveney, W. P. *J. Polym. Sci., Part A* **1965**, *3*, 895–905.

47. Dias, E. L.; Nguyen, S. T.; Grubbs, R. H. *J. Am. Chem. Soc.* **1997**, *119*, 3887–3897.

48. Romero, P. E.; Piers, W. E. *J. Am. Chem. Soc.* **2005**, *127*, 5032–5033.

49. Correa, A.; Cavallo, L. *J. Am. Chem. Soc.* **2006**, *128*, 13352–13353.

50. Delaude, L.; Demonceau, A.; Noels, A. F. *Macromolecules* **1999**, *32*, 2091–2103.

51. Amir-Ebrahimi, V.; Corry, D. G.; Hamilton, J. G.; Thompson, J. M.; Rooney, J. J. *Macromolecules* **2000**, *33*, 717–724.

52. Scholl, M.; Ding, S.; Lee, C. W.; Grubbs, R. H. *Org. Lett.* **1999**, *1*, 953–956.

53. Vougioukalakis, G. C.; Grubbs, R. H. *Chem. Rev.* **2010**, *110*, 1746–1787.

54. Lee, J. C.; Parker, K. A.; Sampson, N. S. *J. Am. Chem. Soc.* **2006**, *128*, 4578–4579.

55. Teo, P.; Grubbs, R. H. *Organometallics* **2010**, *29*, 6045–6050.

56. Endo, K.; Grubbs, R. H. *J. Am. Chem. Soc.* **2011**, *133*, 8525–8527.

57. Keitz, B. K.; Endo, K.; Herbert, M.; Grubbs, R. H. *J. Am. Chem. Soc.* **2011**, *133*, 9686–9688.

58. Keitz, B. K.; Federov, A.; Grubbs, R. H. *J. Am. Chem. Soc.* **2012**, *134*, 2040–2043.

59. Yang, H.-C.; Lin, S.-Y.; Yang, H.-C.; Lin, C.-L.; Tsai, L.; Huang, S.-L.; Chen, I. W.-P.; Chen, C.-H.; Jin, B.-Y.; Luh, T.-Y. *Angew. Chem., Int. Ed.* **2006**, *45*, 726–730.

60. Song, A.; Lee, J. C.; Parker, K. A.; Sampson, N. S. *J. Am. Chem. Soc.* **2010**, *132*, 10513–10520.

61. Kobayashi, S.; Pitet, L. M.; Hillmyer, M. A. *J. Am. Chem. Soc.* **2011**, *133*, 5794–5797.

62. Zhang, J.; Matta, M. E.; Martinez, H.; Hillmyer, M. A. *Macromolecules* **2013**, *46*, 2535–2543.

63. Straub, B. F. *Adv. Synth. Catal.* **2007**, *349*, 204–214.

64. Rosebrugh, L. E.; Marx, V. M.; Keitz, B. K.; Grubbs, R. H. *J. Am. Chem. Soc.* **2013**, *135*, 10032–10035.

65. Khan, R. K. M.; Torker, S.; Hoveyda, A. H. *J. Am. Chem. Soc.* **2013**, *135*, 10258–10261.

66. Castner, K. F.; Calderon, N. *J. Mol. Catal.* **1982**, *15*, 47–59.

67. Al Samak, B.; Carvill, A. G.; Hamilton, J. G.; Rooney, J. J.; Thompson, J. M. *Chem. Commun.* **1997**, *21*, 2057–2058.

68. Al Samak, B.; Amir-Ebrahimi, V.; Corry, D. G.; Hamilton, J. G.; Rigby, S.; Rooney, J. J.; Thompson, J. M. *J. Mol. Catal. A* **2000**, *160*, 13–21.

69. Amir-Ebrahimi, V.; Rooney, J. J. *J. Mol. Catal. A* **2004**, *2008*, 115–121.

70. Bornand, M.; Chen, P. *Angew. Chem., Int. Ed.* **2005**, *44*, 7909–7911.

71. Bornand, M.; Torker, S.; Chen, P. *Organometallics* **2007**, *26*, 3585–3596.

72. Torker, S.; Müller, A.; Sigrist, R.; Chen, P. *Organometallics* **2010**, *29*, 2735–2751.

73. Adlhart, C.; Hinderling, C.; Baumann, H.; Chen, P. *J. Am. Chem. Soc.* **2000**, *122*, 8204–8214.

74. Adlhart, C.; Chen, P. *Angew. Chem. Int. Ed.* **2002**, *41*, 4484–4487.

75. Adlhart, C.; Chen, P. *J. Am. Chem. Soc.* **2004**, *126*, 3496–3510.

76. Cavallo, L. *J. Am. Chem. Soc.* **2002**, *124*, 8965–8973.

77. Vyboishchikov, S. F.; Bühl, M.; Thiel, W. *Chem. Eur. J.* **2002**, *8*, 3962–3975.

78. Kingsbury, J. S.; Harrity, J. P. A.; Bonitatebus, P. J.; Hoveyda, A. H. *J. Am. Chem. Soc.* **1999**, *121*, 791–799.

79. Torker, S.; Müller, A.; Chen, P. *Angew. Chem., Int. Ed.* **2010**, *49*, 3762–3766.

80. Vehlow, K.; Wang, D.; Buchmeiser, M. R.; Blechert, S. *Angew. Chem., Int. Ed.* **2008**, *47*, 2615–2618.

81. Lichtenheldt, M.; Wang, D.; Vehlow, K.; Reinhardt, I.; Kühnel, C.; Decker, U.; Blechert, S.; Buchmeiser, M. R. *Chem. Eur. J.* **2009**, *15*, 9451–9457.

82. Buchmeiser, M. R.; Ahmad, I.; Gurram, V.; Kumar, P. S. *Macromolecules* **2011**, *44*, 4098–4106.

83. Love, J. A.; Morgan, J. P.; Trnka, T. M.; Grubbs, R. H. *Angew. Chem., Int. Ed.* **2002**, *41*, 4035–4037.
84. Choi, T.-L.; Grubbs, R. H. *Angew. Chem., Int. Ed.* **2003**, *42*, 1743–1746.
85. Sanford, M. S.; Love, J. A.; Grubbs, R. H. *Organometallics* **2001**, *20*, 5314–5318.
86. Ilker, M. F.; Coughlin, E. B. *Macromolecules* **2002**, *35*, 54–58.
87. Song, A.; Parker, K. A.; Sampson, N. S. *J. Am. Chem. Soc.* **2009**, *131*, 3444–3445.
88. Choi, T.-L.; Lee, C. W.; Chatterjee, A. K.; Grubbs, R. H. *J. Am. Chem. Soc.* **2001**, *123*, 10417–10418.
89. Romulus, J.; Patel, S.; Weck, M. *Macromolecules* **2012**, *45*, 70–77.
90. Romulus, J.; Tan, L.; Weck, M.; Sampson, N. S. *ACS Macro Lett.* **2013**, *2*, 749–752.
91. Sutthasupa, S.; Shiotsuki, M.; Masuda, T.; Sanda, F. *J. Am. Chem. Soc.* **2009**, *131*, 10546–10551.
92. Fineman, M.; Ross, S. D. *J. Polym. Sci.* **1950**, *5*, 259–262.
93. Choi, T.-L.; Rutenberg, I. M.; Grubbs, R. H. *Angew. Chem., Int. Ed.* **2002**, *41*, 3839–3841.
94. Chatterjee, A. K.; Morgan, J. P.; Scholl, M.; Grubbs, R. H. *J. Am. Chem. Soc.* **2000**, *122*, 3783–3784.
95. Choi, T.-L.; Chatterjee, A. K.; Grubbs, R. H. *Angew. Chem., Int. Ed.* **2001**, *40*, 1277–1279.
96. Daeffler, C. S.; Grubbs, R. H. *Macromolecules* **2013**, *46*, 3288–3292.

Chapter 12

Synthesis of Side-Chain-Sequenced Copolymers Using Vinyl Oligomonomers via Sequential Single-Monomer ATRA

Takamasa Soejima, Kotaro Satoh,* and Masami Kamigaito*

Department of Applied Chemistry, Graduate School of Engineering, Nagoya University, Nagoya 464-8603, Japan
***E-mail: satoh@apchem.nagoya-u.ac.jp**
***E-mail: kamigait@apchem.nagoya-u.ac.jp**

This study was conducted to synthesize novel vinyl copolymers bearing specific side-chain sequences via the radical copolymerization of allyl-functionalized sequence-regulated oligomers (oligomonomers) containing the common vinyl monomer, methyl acrylate (MA). The allyl-functionalized oligomonomers were successfully prepared via the sequential single-monomer radical addition of vinyl monomers such as acrylate and styrene via the Kharasch addition reaction to α-haloester followed by cationic allylation with allyltrimethylsilane. During the free radical copolymerization of the oligomonomer and MA, the use of fluoroalcohol [PhC(CF$_3$)$_2$OH] as the solvent enhanced the incorporation ratio of the oligomonomers into the produced copolymers, with the highest value reaching up to 40 mol%. The effects of the regulated side-chain sequences on the thermal properties of the produced copolymers were also evaluated.

Introduction

Metal-catalyzed atom transfer living radical polymerization using ruthenium- or copper-based metal complexes was first discovered in the mid-1990s and began a new era of precision polymer synthesis (Scheme 1) (*1–5*). This controlled/living polymerization system was originally based on the metal-catalyzed atom transfer radical addition (ATRA) or Kharasch addition reaction, a carbon–carbon bond-

forming radical reaction where a radical derived from an alkyl halide adds to a vinyl compound to generate the 1:1 adduct (*6–8*).

(A) Single-Monomer Addition for Sequence-Regulated Vinyl Polymer (Previous Work)
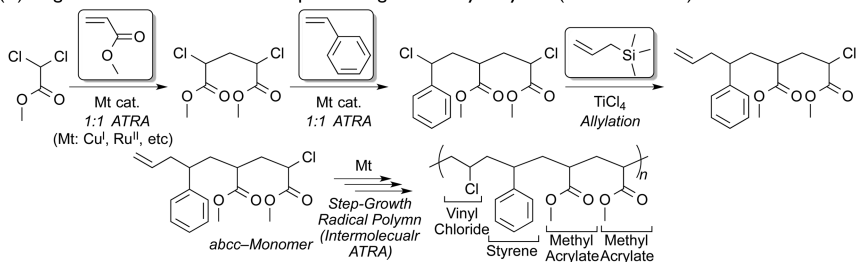
(B) Single-Monomer Addition for Side-Chain Sequence-Regulated Copolymer (This Work)
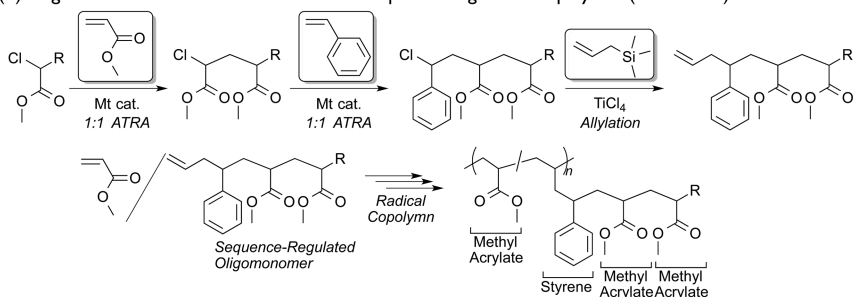
Scheme 1. Sequential Single-Monomer ATRA for Sequence-Regulated (Co)polymers

We recently found that ATRA is applicable to the sequential single addition of vinyl monomers, such as acrylate and styrene, to prepare unprecedented sequence-regulated vinyl oligomers where multiple monomer additions, i.e., polymerization, are diminished under the optimized reaction conditions (*9*). In addition, when the sequence-regulated oligomer is designed to possess a reactive carbon–halogen bond (C–Cl) and an unconjugated carbon–carbon double bond (C=C) within a single molecule, ATRA reaction can be conducted again for these sequence-regulated vinyl oligomers as the AB-type monomers in their step-growth radical polymerization (*10, 11*) (Scheme 1A). The AB-type step-growth monomers are synthesized using a dihalide as the starting material. After the sequential single monomer ATRA, one of the C–Cl bonds adjacent to the phenyl group is selectively activated using $TiCl_4$ to form a carbocation adjacent to the phenyl group. The vinyl group was introduced via allylation with allyltrimethylsilane, whereas the other C–Cl bonds remain intact and are used for the step-growth radical polymerization (*12*).

Unconjugated α-olefin monomers, such as 1-hexene, are hard to homopolymerize via radical polymerizations, while their copolymerizations with electron-withdrawing monomers, such as acrylonitrile and acrylates, yield copolymers with low unconjugated monomer incorporation. Lewis acids are known to enhance the copolymerizability during such copolymerizations and

increase olefin incorporation (*13–16*).   Recently, we found that using protic fluoroalcohols, such as PhC(CF$_3$)$_2$OH and (CF$_3$)$_2$CHOH, as the solvent also significantly enhances the olefin incorporation into the copolymer during the radical copolymerization of methyl acrylate (MA) and 1-hexene (Hex) (*17, 18*).   The coordination of the fluorinated alcohol to the MA carbonyl groups and growing radical species decreased their electron densities and enhanced the cross-propagation between the MA and the relatively electron-donating unconjugated monomer, 1-Hex.

In this study, allyl-functionalized oligomonomers were prepared via the sequential single-monomer-addition of various vinyl monomers using the Kharasch reaction followed by a cationic allylation with allyltrimethylsilane. The obtained oligomonomers were subsequently radically copolymerized in toluene and PhC(CF$_3$)$_2$OH with MA to afford copolymers possessing specific side-chain sequences (Scheme 1B).

Results and Discussion

Synthesis of Allyl-Functionalized Sequence-Regulated Oligomers

A series of allyl-functionalized sequence-regulated oligomers was prepared via the sequential ATRA of various monomers to alkyl halides. We first conducted a Cu-catalyzed ATRA between methyl α-bromobutanoate and styrene, with the former eventually containing a methyl acrylate unit.   The reaction proceeded smoothly to form the 1:1 adduct in relatively good yield although the mono-halide reactivity was much lower than that of the dihalide employed in the previous study.   The C–Br bond adjacent to the phenyl group in the resultant adduct was subsequently activated by TiCl$_4$ to generate the carbocation, which was reacted with allyltrimethylsilane to form an allyl-functionalized oligomonomer bearing a styrene (St)-methyl acrylate (MA) sequence (**2**) (Scheme 2A).
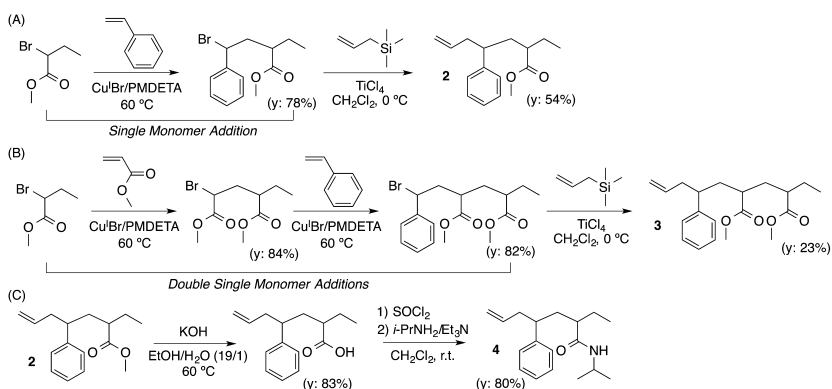
Scheme 2. Synthesis of Allyl-functionalized Oligomonomers by Sequential Single-Monomer ATRA and Subsequent Allylation

A trimeric oligomonomer consisting of one St and two MA units (**3**) was further synthesized by the sequential additional via the Cu-catalyzed single monomer ATRA of MA followed by St to methyl α-bromobutanoate. Because these ATRAs were not quantitative, the obtained dimer and trimer were purified via distillation. These sequential single-monomer additions were followed by an allylation on the terminal styrene unit to form the allyl-St-MA-MA sequence-regulated oligomonomer (Scheme 2B). For the dimeric oligomonomer containing St and *N*-isopropylacrylamide (NIPAM) sequences, the ester group in **2** was converted into an amide group via a traditional amidation process (Scheme 2C).

It was noteworthy that both these final products and the intermediate compounds were successfully isolated via distillation and/or purified via column chromatography (*9, 19*). Figure 1 shows the ^{1}H NMR spectra for the purified sequence-regulated vinyl oligomonomers obtained via a single monomer ATRA. Allyl or vinyl peaks (*a* and *b*) were observed in all of the spectra at 5.0 and 5.6 ppm, respectively, in addition to peaks attributed to the corresponding vinyl monomer units, which indicates the quantitative conversion of the halides within the oligomers into allyl groups without the loss of the sequence-regulated oligomonomer structure.
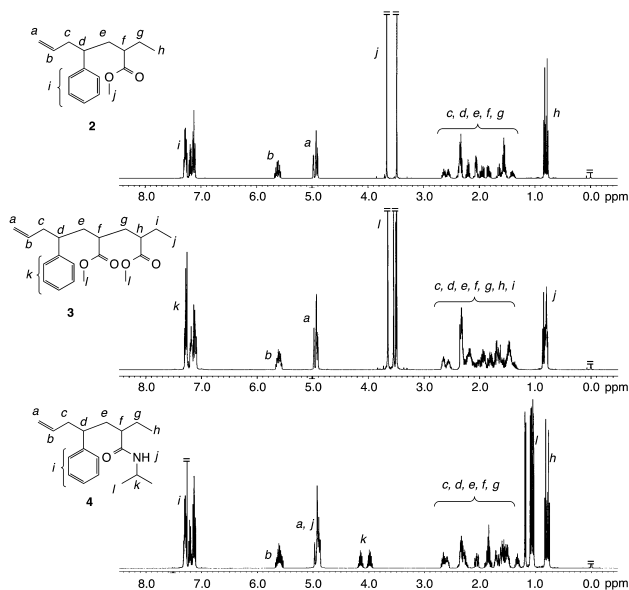
*Figure 1. ^{1}H NMR spectra (CDCl$_3$, 55 °C) of allyl-functional oligomonomers (**2**: allyl-St-MA; **3**:allyl-St-MA-MA; **4**: allyl-St-NIPAM)*

Copolymerization of Sequence-Regulated Oligomonomers with Methyl Acrylate

The obtained allyl-functionalized oligomonomer (**2**: allyl-St-MA), a commercially available monomeric model (**1**: allyl-St), and 1-Hex were copolymerized with MA, a typical electron-withdrawing monomer, in toluene using AIBN as the initiator at 60 °C. The initial charge ratios for the two monomers were [MA]$_0$/[allyl compound]$_0$ = 1/1. Figure 2 shows the time-conversion and SEC curves for the radical copolymerization of both **2** with MA and the other unconjugated compounds (**1** and 1-Hex). The conversion of the oligomonomer was determined by the C=C bond consumption analyzed via ^{1}H NMR.
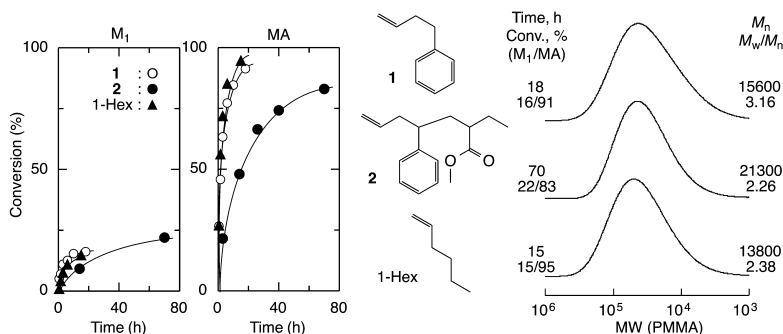
Figure 2. Copolymerization of sequence-regulated oligomonomer 1, 2, or 1-hexene (M_1) with MA by AIBN in toluene at 60 °C; $[M_1]_0 = [MA]_0$, $([M_1]_0+[MA]_0)/[AIBN]_0 = 100$.

The copolymerization proceeded smoothly even though the unconjugated monomer consumption ceased after the near depletion of the MA. The monomeric model **1** showed nearly the same reactivity as 1-Hex, which nearly quantitatively consumed the MA within 24 hours. Although the copolymerization using the dimeric oligomonomer **2** proceeded at a slightly slower rate than the other reactions, the C=C bond consumption for **2** reached a higher conversion (>20%) than for the other reactions (15–16%), and a relatively high-molecular-weight copolymer (M_n > 10^4) was formed. Despite the tendency of allyl compounds to induce chain-transfer during their radical homopolymerization, these copolymerizations yielded high-molecular-weight copolymers in the presence of the acrylic comonomer similarly to the case of 1-Hex (*17*).

All of the dimeric and trimeric oligomonomers (**1–4**) were similarly copolymerized with MA. Figure 3 shows the time-conversion and SEC curves for the copolymerization of these oligomonomers and MA in toluene (A) and fluoroalcohol [PhC(CF$_3$)$_2$OH] (B) using AIBN as the initiator at 60 °C.

As in the 1-Hex and MA copolymerization, using the fluoroalcohol solvent enhanced copolymerizability of the oligomonomers and MA and accelerated the copolymerization. While the effects of the fluoroalcohol solvent on the copolymerization with MA were smaller for the sequence-regulated oligomonomers than for 1-Hex, the copolymerization proceeded to produce copolymers possessing sequence-regulated side chains with oligomonomer consumption rates in the following order: $1 > 2 > 4 > 3$. This result was probably due to the interaction of PhC(CF$_3$)$_2$OH not only with the carbonyl in the MA monomer but also with the MA units in the oligomonomers. In addition, all of the copolymers exhibited relatively high molecular weights ($M_n > 20000$), irrespective of the solvent and side-chain sequences of their oligomonomer.
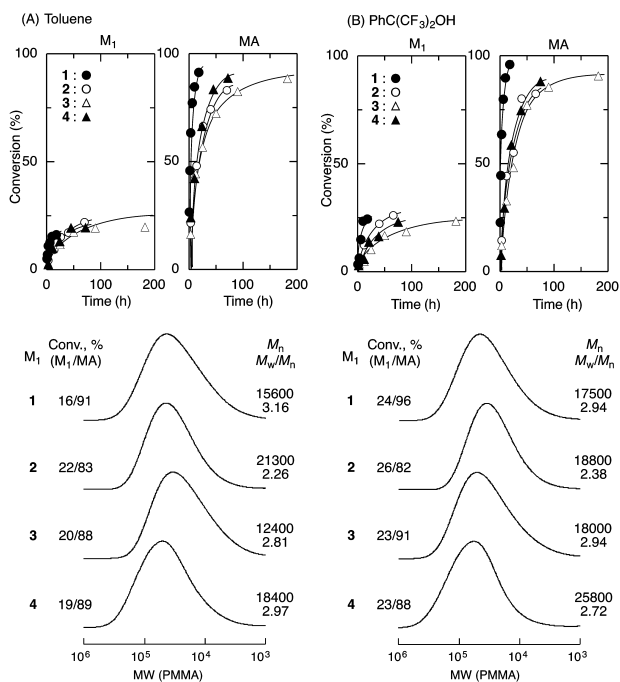
Figure 3. Copolymerization of sequence-regulated oligomonomer 1–4 (M$_1$) with MA by AIBN in toluene (A) and PhC(CF$_3$)$_2$OH (B) at 60 °C; [M$_1$]$_0$ = [MA]$_0$, ([M$_1$]$_0$+[MA]$_0$)/[AIBN]$_0$ = 100.

The copolymer structures obtained from oligomonomers **1–4** and MA were analyzed by ^{1}H NMR. Figure 4 shows the ^{1}H NMR spectra for the copolymers obtained in toluene. The signals assigned to the main chain poly(MA-*co*-olefin) protons; i.e., the methyl ester (*c*), methylene (*a*), and methine (*b*) protons in the MA units and both methylene (*d*) and methine (*e*) protons in the olefin units,

showed peaks at 3.7, 1.4–2.0, and 2.2–2.6 ppm. In addition, the protons from the side-chain vinyl monomer units, i.e., styrene (*f*, *g*), MA (*a'*, *a''*, *b'*, *b''*, *c'*, *c''*), and NIPAM (*k–o*), can be seen along with the terminal group (*i*, *i'*, *j*, *j'*). The composition ratio of the vinyl monomer units estimated from the intensity ratios for these main-chain and side-chain peaks agreed well with the theoretical values calculated from the MA and oligomonomer conversions. These results suggest novel sequence-regulated copolymers with a well-defined side-chain sequence formed via the copolymerization of the oligomonomers.
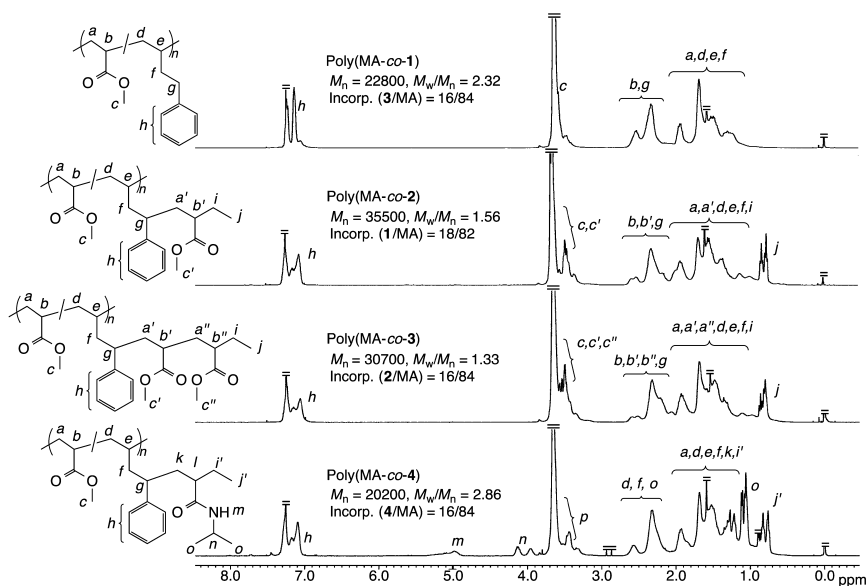
Figure 4. ^1H *NMR spectra (CDCl₃, 55 °C) of side-chain sequence-regulated copolymers obtained with allyl-functionalized oligomonomers.*

To further investigate the effects of the sequence on the copolymerizability, the oligomonomers (M_2) and MA (M_1) were copolymerized with various comonomer feed compositions $[([MA]_0 + [oligomonomer]_0)/[AIBN]_0 = 100]$ in PhC(CF₃)₂OH and toluene at 60 °C. Figure 5 shows the copolymer composition curve for these copolymerizations with the comonomer composition in the product as a function of the MA feed ratio. The plots best fit the Kelen-Tüdõs method for determining the monomer reactivity ratios (*20*), where M_1 and M_2 represent the oligomonomers and MA, respectively. In all cases, using PhC(CF₃)₂OH as the solvent lowered the r_2 values relative to toluene, whereas the r_1 values were zero irrespective of the side-chain sequence. The cross-propagation enhancement rendered by the decreased r_2 values also depended on the number of carbonyl groups in the oligomonomer. These results support the hydrogen-bonding

interactions of the fluoroalcohol to the carbonyl groups in the MA monomer changing the monomer reactivity ratio and enhancing cross propagation (*17*).
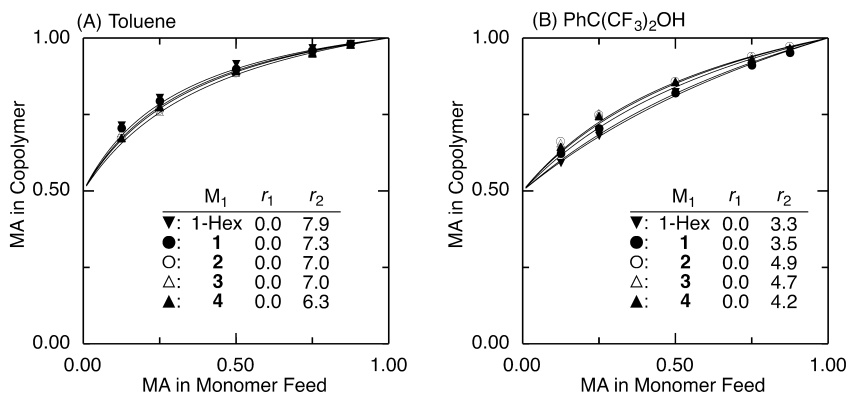
*Figure 5. Copolymer composition curves for the copolymerization of oligomonomers (**1-4**) by AIBN with MA in toluene (A) and PhC(CF$_3$)$_2$OH (B) at 60 °C; ([M$_1$]$_0$+[MA]$_0$)/[AIBN]$_0$ = 100.*

Table 1 summarizes the molecular weight and thermal properties of the copolymers obtained from **1-4** and MA under various conditions. The glass transition temperature (T_g) of the copolymers increased with the oligomonomer content, which most likely reflects the side-chain monomer units such as MA, St, and NIPAM [T_g = 10 °C (poly(MA)), 100 °C (polystyrene), 134 °C (poly(NIPAM))]. Also, all of the copolymers showed relatively high thermal durabilities with T_{d5}> 300 °C. A copolymerization with a higher oligomonomer feed ratio was also conducted ([MA]$_0$/[oligomonomer]$_0$ = 1/7) to increase the sequence-regulated oligomonomer incorporation ratio. At the higher initial feed, the oligomonomer content determined by ^{1}H NMR reached approximately 40% in all cases, which indicates the nearly alternating copolymers formed from the oligomonomers and MA with perfect side-chain oligomer sequencing; however, a large amount of the oligomonomers remained in the polymerization system and the molecular weights decreased to <10[4].

In conclusion, novel copolymers with perfect side-chain sequences were obtained via the radical copolymerization of various allyl-functionalized sequence-regulated oligomonomers prepared by sequential single-monomer ATRA followed by allylation. The fluoroalcohol solvent proved highly effective for copolymerizing allyl-oligomonomers with the acrylic monomer to enhance the oligomonomer incorporation in the resultant copolymer. In addition, copolymers with 40% of the sequenced oligomonomer incorporated into the main chain were obtained under the optimized conditions.

Table 1. Side-Chain-Sequenced Copolymers Obtained from Sequence-Regulated Oligomonomers and MA

M_1	Solvent	$M_n{}^c$	$M_w/M_n{}^c$	Incorp. M_1/MA (%)[d]	T_g (°C)[e]	T_{d5} (°C)[e]
1	toluene[a]	22800	2.32	16/84	20.5	311
1	PhC(CF$_3$)$_2$OH[a]	22900	2.33	24/76	21.6	321
1	PhC(CF$_3$)$_2$OH[b]	12100	2.10	39/61	23.4	304
2	toluene[a]	35500	1.56	18/82	26.6	328
2	PhC(CF$_3$)$_2$OH[a]	34100	1.55	19/81	28.3	351
2	PhC(CF$_3$)$_2$OH[b]	8900	1.40	38/62	32.4	317
3	toluene[a]	30700	1.33	16/84	23.6	319
3	PhC(CF$_3$)$_2$OH[a]	50500	1.28	20/80	24.8	336
3	PhC(CF$_3$)$_2$OH[b]	6100	1.86	40/60	27.1	318
4	toluene[a]	20200	2.86	16/84	45.4	309
4	PhC(CF$_3$)$_2$OH[a]	27800	2.52	21/79	57.6	331
4	PhC(CF$_3$)$_2$OH[b]	9400	2.45	39/61	84.9	333

[a] $[M_1]_0/[MA]_0 = 1/1$ ($[M]_{total}/[AIBN]_0 = 100$) at 60 °C.   [b] $[M_1]_0/[MA]_0 = 7/1$ at 60 °C.
[c] Determined by SEC.   [d] Determined by ^{1}H NMR.   [e] Determined by DSC and TGA.

Experimental

Materials

Methyl acrylate (TCI, >99%), styrene (Kishida, 99.5%), 4-phenyl-1-butene (**1**; TCI, >98%), N,N,N',N'',N''-pentamethyldiethylenetriamine (PMDETA; Aldrich, 99%), methyl 2-bromobutylate (TCI, >97%), and PhC(CF$_3$)$_2$OH (Wako, >99%) were distilled from calcium hydride under reduced pressure before use. CuBr (Aldrich, 99.999%) was used as received and handled in a glove box (MBRAUN LABmaster sp) under a moisture- and oxygen-free argon atmosphere (O$_2$, <1 ppm). Toluene (Kanto, >99.5%; H$_2$O <10 ppm) was dried and deoxygenized by passage through columns of Glass Contour Solvent Systems before use. α,α-Azobisisobutyronitrile (AIBN) (Kishida, >99%) was purified by recrystallization from methanol.

Synthesis of Allyl-Functionalized Sequence-Regulated Oligomers

Allyl-functionalized dimeric oligomer (**2**) was synthesized by Kharasch addition and allylation as follows. In a 500 mL round-bottomed flask were placed CuBr (2.16 g, 15.0 mmol), toluene (15.0 mL), PMDETA (3.14 mL, 15.0 mmol), styrene (69.2 mL, 0.600 mol), and methyl 2-bromobutyrate (214 mL,

1.66 mol) at room temperature. The flask was placed in an oil bath maintained at 60 °C under vigorous stirring. The conversion of styrene was determined from the concentration of the residual styrene measured by ^{1}H NMR. After 3 h, the conversion of styrene reached 83% to from the 1:1 adduct almost quantitatively (78%). To remove the Cu complex, the reaction mixture was led to pass through a silica-gel column eluted with *n*-hexane and ethyl acetate, and then evaporated in vacuum to yield the crude 1:1 adduct (104 mL). To a dichloromethane solution of the adduct (104 mL) and allyltrimethylsilane (111 mL, 0.698 mol) was added 25.6 mL of TiCl$_4$ dropwise at −78 °C under dry nitrogen. The mixture was kept stirred for 4.5 h at −78 °C, and then over 10 h at 0 °C. The reaction was terminated with methanol and the mixture was washed with aqueous HCl and NaOH solutions, and finally with water. The organic layer was evaporated to remove the solvents. Oligomonomer **2** was purified by distillation and column chromatography to yield pure **2** as clear and colorless viscous oil (total yield 54%, purity > 99%).

Trimeric oligomer (**3**) was also prepared by Kharasch addition and allylation as follows. In a 500 mL round-bottomed flask were placed CuBr (2.88 g, 20.0 mmol), toluene (20.0 mL), PMDETA (4.20 mL, 20.0 mmol), MA (109 mL, 1.20 mol), and methyl 2-bromobutyrate (269 mL, 2.10 mol) at room temperature. The flask was placed in an oil bath maintained at 60 °C under vigorous stirring. The conversion of MA was determined from the concentration of the residual styrene measured by ^{1}H NMR. After 4 h, the conversion of MA reached 97% to from the 1:1 adduct almost quantitatively (84%). To remove the Cu complex, the reaction mixture was led to pass through a silica-gel column eluted with *n*-hexane and ethyl acetate, and then evaporated in vacuum to yield the crude 1:1 adduct (186 mL). The Kharasch addition reaction between styrene and the adduct was carried out similarly. In a 300 mL round-bottomed flask were placed CuBr (1.89 g, 13.2 mmol), toluene (11.0 mL), PMDETA (2.60 mL, 13.6 mmol), styrene (50.6 mL, 0.174 mol), and the adduct (186 mL) at room temperature. The flask was placed in an oil bath maintained at 60 °C under vigorous stirring. The conversion of styrene was determined from the concentration of the residual styrene measured by ^{1}H NMR. After 6 h, the conversion of styrene reached 97% to from the 1:1 adduct almost quantitatively (82%). To remove the Cu complex, the reaction mixture was led to pass through a silica-gel column eluted with *n*-hexane and ethyl acetate, and then evaporated in vacuum to yield the crude 1:1 adduct (186 mL). To a dichloromethane solution of the adduct (186 mL) and allyltrimethylsilane (103 mL, 0.650 mol) was added 23.8 mL of TiCl$_4$ dropwise at −78 °C under dry nitrogen. The mixture was kept stirred for 2 h at −78 °C, and then over 140 h at 0 °C. The reaction was terminated with methanol and the mixture was washed with aqueous HCl and NaOH solutions, and finally with water. The organic layer was evaporated to remove the solvents. Oligomonomer **3** was purified by distillation and column chromatography to yield pure **3** as clear and colorless viscous oil (total yield 23%, purity > 99%).

Dimeric oligomer with NIPAM (**4**) was prepared by amidation of the ester group in **2** as follows. In a 50 mL were placed KOH (7.29 g, 0.130 mol), EtOH (76 mL), H$_2$O (4.0 mL), and **2** (18.0 mL, 72.9 mmol) at room temperature. The flask was placed in an oil bath kept at 60 °C under stirring. After 6 h at ambient temperature, to the mixture was added HCl aqueous solution, and the mixture was

washed with water. The organic layer was evaporated to yield the carboxylic acid form of **2** (14.1 g, 60.7 mmol, 83%). To a CH_2Cl_2 solution of the product and DMF (0.5 mL) was added $SOCl_2$ (8.83 mL, 0.122 mol). The mixture was stirred for 2 h at room temperature. To remove the unreacted $SOCl_2$, the mixture was evaporated in vacuum to yield the product. The acyl halide was diluted with CH_2Cl_2 and added dropwise to a solution of isopropylamine (10.4 mL, 0.122 mol) and Et_3N (10.2 mL, 72.9 mmol) in CH_2Cl_2 at 0 °C. The mixture was stirred for 1 h at 0 °C, and then for 2 h at room temperature. The mixture was washed with water. The crude product was purified by column chromatography to give **4** (total yield 80%, purity > 99%).

Copolymerization

Copolymerization was carried out by the syringe technique under dry nitrogen in sealed glass tubes. A typical example for **2** and MA copolymerization with AIBN in $PhC(CF_3)_2OH$ is given below. In a 50 mL round-bottomed flask were placed $PhC(CF_3)_2OH$ (0.38 mL), **2** (1.5 mL, 6.0 mmol), MA (0.54 mL, 6.0 mmol), and $PhC(CF_3)_2OH$ solution of AIBN (0.60 mL of 200 mM solution, 0.12 mmol) at room temperature. The total volume of the reaction mixture was 3.0 mL. Immediately after mixing, aliquots (0.4 mL each) of the solution were distributed via syringe into baked glass tubes, which were then sealed by flame under nitrogen atmosphere. The tubes were immersed in thermostatic oil bath at 60 °C. In predetermined intervals, the polymerization was terminated by the cooling of the reaction mixtures to –78 °C. Monomer conversion was determined from the concentration of residual monomer measured by ^{1}H NMR with $PhC(CF_3)_2OH$ as internal standard. The quenched reaction solutions were evaporated to dryness to give the product polymers.

Measurements

^{1}H NMR spectra were recorded in $CDCl_3$ at room temperature on a JEOL ESC-400 spectrometer, operating at 400 MHz. The number-average molecular weight (M_n) and molecular weight distribution (M_w/M_n) of the product polymers were determined by SEC in THF at 40 °C on two polystyrene gel columns [Tosoh Multipore H_{XL}-M (7.8 mm i.d. × 30 cm) × 2; flow rate 1.0 mL/min] connected to a JASCO PU-2080 precision pump and a JASCO RI-2031 detector. The columns were calibrated against standard poly(MMA) samples (Varian; M_p = 202-1677000, M_w/M_n = 1.02-1.23). Glass transition temperatures (T_g) of the polymers were recorded on Q200 differential scanning calorimeter (TA Instruments Inc.). Samples were first heated to 150 °C at 10 °C/min., equilibrated at this temperature for 10 min, and cooled to –50 °C at 5 °C/min. After being held at this temperature for 5 min, the samples were then reheated to 150 °C at 10 °C/min. All T_g values were obtained from the second scan, after removing the thermal history. Thermogravimetric analyses (TGA) were performed on Q500 system (TA Instruments Inc.) at 5 °C/min under N_2 gas flow.

Acknowledgments

References

1. Kato, M.; Kamigaito, M.; Sawamoto, M.; Higashimura, T. *Macromolecules* **1995**, *28*, 1721–1723.
2. Wang, J.-S.; Matyjaszewski, K. *J. Am. Chem. Soc.* **1995**, *117*, 5614–5615.
3. Percec, V.; Barboiu, B. *Macromolecules* **1995**, *28*, 7970–7972.
4. Granel, C.; Dubois, P.; Jérôme, R.; Teyssié, P. *Macromolecules* **1996**, *29*, 8576–8582.
5. Haddleton, D. M.; Jasieczek, C. B.; Hannon, M. J.; Shooter, A. J. *Macromolecules* **1997**, *30*, 2190–2193.
6. Kharasch, M. S.; Jensen, E. V.; Urry, W. H. *Science* **1945**, *102*, 128.
7. Minisci, F. *Acc. Chem. Res.* **1975**, *8*, 165–171.
8. Iqbal, J. P.; Bhatia, B.; Nayyar, N. K. *Chem. Rev.* **1994**, *94*, 519–564.
9. Satoh, K.; Ozawa, S.; Mizutani, M.; Nagai, K.; Kamigaito, M. *Nat. Commun.* **2010**, *1*, 6.
10. Satoh, K.; Mizutani, M.; Kamigaito, M. *Chem. Commun.* **2007**, 1260–1262.
11. Mizutani, M.; Satoh, K.; Kamigaito, M. *Macromolecules* **2009**, *42*, 472–480.
12. Dau-Schmidt, J.-P.; Mayr, H. *Chem. Ber.* **1994**, *127*, 205–212.
13. Cowie, J. M. G. *Alternating Copolymers*; Plenum Press: New York, 1985.
14. Hagiopol, C. *Copolymerization: Toward a Systematic Approach*; Kluwer Academic/Plenum Publishers: New York, 1999.
15. Hirooka, M.; Yabuuchi, H.; Morita, S.; Kawasumi, S.; Nakaguchi, K. *J. Polym. Sci., Part B: Polym. Lett.* **1967**, *5*, 47–55.
16. Hirai, H. *J. Polym. Sci., Macromol. Rev.* **1976**, *11*, 47–91.
17. Koumura, K.; Satoh, K.; Kamigaito, M. *Macromolecules* **2009**, *42*, 2497–2504.
18. Satoh, K.; Matsuda, M.; Nagai, K.; Kamigaito, M. *J. Am. Chem. Soc.* **2010**, *132*, 10003–10005.
19. Houshyar, S.; Keddie, D. J.; Moad, G.; Mulder, R. J.; Saubern, S.; Tsanaktsidis, J. *Polym. Chem.* **2012**, *3*, 1879–1889.
20. Kelen, T.; Tüdõs, F. *J. Macromol. Sci. Chem.* **1957**, *A9*, 1–27.

Chapter 13

Cu(0)-Mediated Controlled/Living Radical Polymerization: A Tool for Precise Multiblock Copolymer Synthesis

Cyrille Boyer,[1] Michael R. Whittaker,[2,*] and Per B. Zetterlund[1]

[1]Centre for Advanced Macromolecular Design (CAMD), School of Chemical Engineering, University of New South Wales, Sydney, NSW 2052 Australia
[2]ARC Centre of Excellence in Convergent Nano-Bio Science & Technology, Monash University, ParkVille Campus, Melbourne, VIC 3052, Australia
***E-mail: Michael.whittaker@monash.edu**

In this chapter, we introduce the concept of a highly efficient and versatile one-pot iterative strategy for the synthesis of multiblock copolymers. Critical to this approach is the unprecedented maintenance of end-group fidelity afforded by controlled/living radical polymerization (CLRP) in the presence of zero-valent copper. We have applied this approach to the synthesis of multiblock systems in high yield and purity. To demonstrate the unique utility of this approach for the synthesis of these materials, we have synthesized multiblock copolymers exhibiting a range of block numbers (up to a maximum of ten), and with low (~3-4) and high DPn (>100), with specific examples in linear and star polymers.

Introduction

There is widespread impetus to translate the sophisticated control over biopolymer synthesis that is demonstrated in biological organisms to purely synthetic systems. These biopolymer chains which are essential for all life - peptides, proteins, RNA and DNA - obtain their critical structure-function relationships through the precisely controlled placement of individual structural repeat units (or monomers), such as amino acids (proteins) and nucleotide bases

(RNA and DNA). DNA chain-encodes the recipe for a human being utilising the precise placement of only 4 nucleotide bases. Importantly, for the synthetic polymer chemist these biological molecules may be described as a multiblock copolymer, containing many blocks, where each block is only a single controlled monomer insertion (DPn = 1).

While there have been significant advances in the last decade in CLRP methods (e.g. transition metal mediated polymerization (atom transfer radical polymerization; ATRP) (*1*, *2*), radical addition-fragmentation chain transfer polymerization (RAFT) (*3*, *4*) or nitroxide mediated polymerization (NMP) (*5*)), biological-like control of synthetic polymer synthesis has remained elusive. These approaches have however allowed increased control over the functionality, molecular weight, molecular weight distribution and chain architecture, including important advances in the synthesis of block polymers (*6*). Typically, while it is relatively simple to synthesise polymers using CLRP where each block usually comprises 10-250 monomers units, up until recently the reports of block numbers >3 are scarce. However even with this limited structural control, these block copolymer materials have found widespread application in self-assembled systems such as micelles, vesicles, etc., in solution, and various morphologies in the solid state (*7–9*).

This lack of progress using CLRP to synthesise complex multiblock materials with control of monomer insertion largely reflects both the inherent kinetic (where monomers have differing tendencies to homo- or cross-propagate) and mechanistic constraints (involving highly reactive radical species, complex methodology specific reaction pathways) of radical polymerization. Counter-intuitively a number of researchers have exploited these caveats to their advantage, and have been able to demonstrate increased, although limited, control of monomer insertion and multiblock copolymer synthesis: for examples see work by Lutz and coworkers (*10–16*), Kamigaito and coworkers (*17*, *18*), Sawamoto and co-workers (*2*, *17*, *19–22*) , Klumperman and coworkers (*23*), Tsanaktsidis and co-workers (*24*), Junkers and co-workers (*25*) and Perrier and co-workers (*26–29*). However, generally, all these reports have failed to address one of the significant mechanistic drawbacks of radical polymerization: i.e. loss of chain end functionality which generally increases at high conversion (*30*, *31*). As a result of this fact the synthesis of multiblock copolymers, where each block needs to be carried out to low/intermediate conversion, is extremely time consuming as each block formation cycle involves an intermediate purification step to remove excess monomer (Note: This does not apply to the recent work of Perrier and co-workers (*26–29*) using iterative RAFT polymerization under carefully considered conditions based on the same principle as the present Cu(0)-mediated radical polymerization technique). The precise control of the conversion of each block is also experimentally challenging and therefor the targeting of a specific block length remains difficult. The maintenance of chain end functionality or livingness is therefore a critical barrier to the full translation of biological-like control to synthetic polymer synthesis.

However, one of the most recent incarnations of CLRP, Cu(0)-mediated radical polymerization, has revolutionised the synthesis of block copolymers: it features extremely high livingness to full conversion (*32–38*). As first demonstrated by us (*9*, *37*, *39*, *40*), by applying this technique it is possible to carry out each step of a multiblock copolymer synthesis to full conversion, allowing access to both stoichiometric control of block DP and structurally complex high order multiblock copolymers. In this chapter we explore the use of this technique to the synthesis of functional multiblock materials that were previously inaccessible via other CRLP processes.

Results and Discussion

The principles of Cu(0)-mediated radical polymerization have been reviewed elsewhere but briefly (*41–45*); it refers to a CLRP system that comprises a number of components including monomer, solvent, an initiator (alkyl halide species), a ligand (most commonly Me6Tren), Cu(0) source (either in the form of Cu wire (*34*, *46*), or "nascent" (*47*) formed via in-situ disproportionation of Cu(I)) and sometimes also a Cu(II) complex. It has been found that careful optimisation of initiator, ligand and deactivator (if used) concentrations are important to obtain optimal results (*37*, *48–50*). This versatile technique can be carried out at room temperature or below, in a range of polar solvents such as DMSO, DMF, ionic liquids, water (including blood serum) and alcohols. The high polymerization rate and high livingness that is characteristic of this technique have mainly been demonstrated successfully for acrylate monomers (*51*), but recent works reported successful polymerization for methacrylates (*52*) and acrylamides (*53*, *54*).

Original works by both Percec (*33*, *34*, *36*, *55*, *56*), Haddleton (*37*, *38*, *57*, *58*) and coworkers have demonstrated that Cu(0)-mediated radical polymerization displays near perfect end group fidelity at high monomer conversion (typically >80%) for various monomers. Inspired by these works, we investigated the maintenance of livingness under post polymerization conditions, where the "polymerization" is continued in the absence of monomer (*59*). Surprisingly, we found that under specific conditions, i.e. in the presence of a small amount of added deactivator, the livingness could be conserved over a period of three days (*59*). We postulated therefore that a one pot iterative technique could be employed for multiblock polymer synthesis (*39*). In this approach, each block could be taken to full conversion, without the significant loss of end-group fidelity, and then further monomer added to continue the multiblock synthesis. Using this process the muliblock copolymer can therefore be continuously built as shown in Scheme 1. Importantly, this method does not require the time consuming purification steps at the end of each block formation cycle.
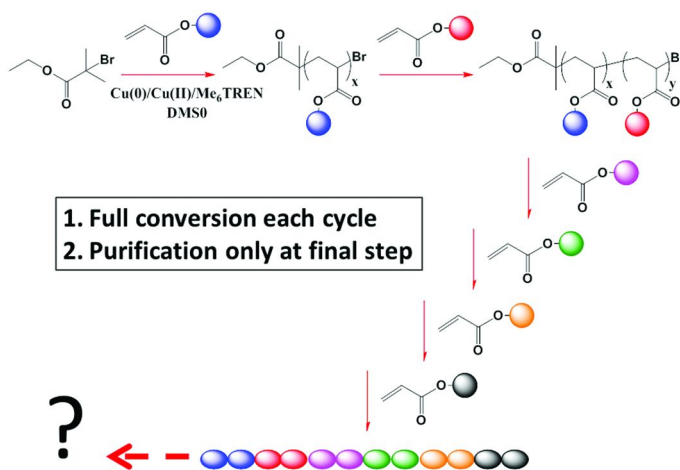
Scheme 1. Schematic representation of the synthesis of multi-block copolymer by sequential addition of monomers without purification. Adapted from reference (39). (see color insert)

Low Block DPn System

To demonstrate the robustness of this approach we initially undertook the synthesis of a model "hexablock" homopolymer (*39*) P[(MA)2-5]6, where each block was comprised of 2-5 monomer units, using [CuBr2]:[Me6Tren] = [0.05]:[0.18] in DMSO at room temperature. Each cycle was allowed to reach full monomer conversion, as confirmed by NMR (24 h), before the addition of further monomer (and solvent) in the one-pot approach. The widespread utility of this approach was further demonstrated using a range of on-hand commercially available acrylate monomers, including n-buyl acrylate (BA), ethyl acrylate (EA), tert-butyl acrylate (tert-BuA) and 2-ethylhexyl acrylate (2-EHA) to successfully synthesise a hexa-block copolymer P(PMA-b-PBA-b-PEA-b-P2EHA-b-PEA-b-PBA) on a multigram scale in high yield. The evolution of the molecular weight distributions revealed the expected systematic increase in molecular weight on the completion of each block for both materials (Figure 1).

Both NMR and ESI-MS data confirmed the structure of the two multiblock polymers synthesised, and in combination with model chemical modification of the bromine chain ends (nitroxide capping, thiol-ene and nucleophilic substitution), confirmed that a high degree of livingness was maintained throughout the iterative process (*39*). More recently, we have expanded our monomer library to include tetrahydrofurfuryl acrylate acrylate (THFA), diethylene glycol ethyl ether acrylate (DEGA), 2-hydroxyethyl acrylate (2HEA) and solketal acrylate (solKA) as building blocks for structurally controlled hexablocks with low DPn for each block (Figure 2).
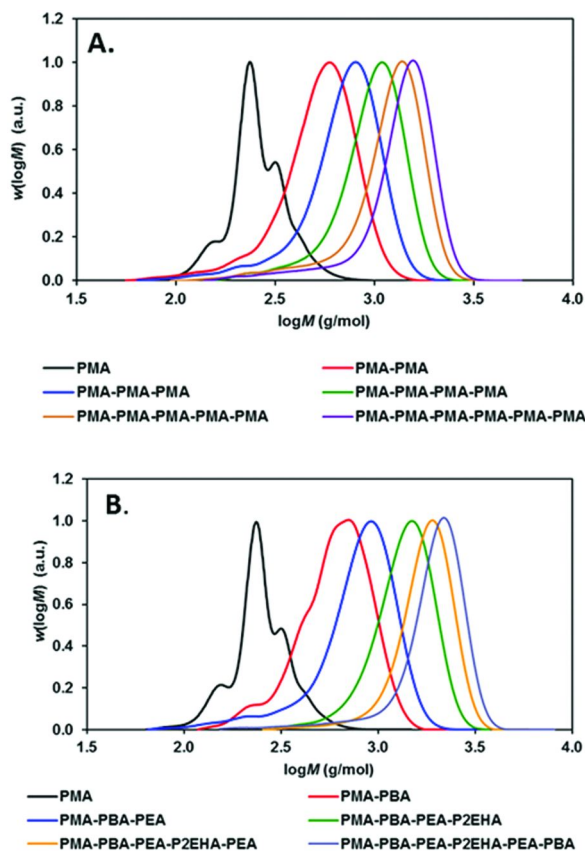
Figure 1. Molecular weight distributions of; A) multi-block homo-polymer and B) multi-block copolymer obtained via Cu(0)-mediated polymerization via iterative chain extension. Reproduced with permission from reference (39). Copyright (2011) American Chemical Society. (see color insert)

Using the methodology described in our earlier work we set about the successful synthesis of P(P2HEA-b-PMA-b-PtBA-b-PMA-b-PsolKA-b-PMA) and P(PTHF-b-PMA-b-P2HEA-b-PMA-b-PDEGA-b-PMA). Evolution of the molecular weight distributions as the multiblock polymers are iteratively built are shown in Figure 2 (blocks 1 to 6). The block copolymers synthesised showed good agreement between theoretical and experimental molecular weight and PDIs in all cases were below 1.25 (Figure 3).

While the hydrophilic PEG component imparts interesting "bio-stealth" properties, the PtertBA and PsolkA blocks could be deprotected to reveal acid and diol moieties respectively, increasing the functional complexity of these predesigned hexablock copolymers with low block DPn. This iterative approach to multiblock copolymer synthesis has now been widely exploited by Haddleton and coworkers in the synthesis of structurally complex multiblock glycopolymers (*60*, *61*).

In an effort to introduce further architectural complexity the above approach was applied to the synthesis of a 5-arm star polymers where each arm contained a multiblock copolymer, where each block was constituted by 3-4 monomer units (on average) with a total of up to five blocks (*9*). Using a multifunctional core first approach, we employed a 5-arm core macroinitiator (1,2,3,4,6-penta-O-isobutyryl bromide-α-D-glucose) to initiate a Cu(0)-mediated polymerization. In our preliminary optimisation experiments, we found that to limit star-star coupling and improve PDI the previous ratio of [Cu(II)]:[CH–Br] had to be increased from 0.04:1 to 0.16:1: with the same amount of Cu(0) in the presence of Me6Tren (*39*, *40*). Using these modified parameters a model pentablock P(MA)5 star was prepared in high yield and very low PDI (<1.1). Using these optimised parameters, we then demonstrated the synthesis of two "true" five arm star multiblock copolymer systems and introduced the new monomers dodecyl acrylate (DOA) and dimethylaminoethyl acrylate (DMAEA) to our monomer library. We successfully prepared P(PMA-b-PHEA-b-PDMEA-b-PDA) and P(PMA-b-PnBA-b-PEA-b-PEHA-b-PtBA) five arm star copolymers with very low PDI (all <1.1). More recently Haddleton and Qiao and coworkers have expanded on this approach to produce stars of higher arm number (*60*) and using an arm first approach (*62*), respectively, but with limited block numbers.

High Block DPn Systems

Larger individual block lengths are required to take advantage of the physico-chemical differences between the blocks for self-driven assembly of these materials in solution and the solid state. In this context we then applied the methodology above to the successful preparation of initially an octablock poly(PMA-b-PnBA-b-PEA-b-PEHA-b-PEA-b-PnBA-b-PnBA-b-PMA) and then a decablock poly(PMA-b-PEA-b-PnBA-b-PtBA-b-PMA-b-PEA-b-PnBA-b-PtBA-b-PMA-b-PEA), where each block DPn was 5 and 20, respectively (*40*). To ensure full conversion in the later cycles we increased the cycle time from 24 h up to a maximum of 72 h (we attribute this to dilution effects). The evolution of the molecular weight distributions for the iterative synthesis of the octablock poly(PMA-b-PnBA-b-PEA-b-PEHA-b-PEA-b-PnBA-b-PnBA-b-PMA) copolymer is shown in Figure 4. In collaboration with the group of Haddleton (*37*), we have now successfully prepared both a model MA pentablock copolymer, (poly(PMA-b-PMA-b-PMA-b-PMA-b-PMA) and a tri-block copolymer poly(PMA-b-PtBA-b-PMA) where each block is constituted by 100 monomer units in DMSO.
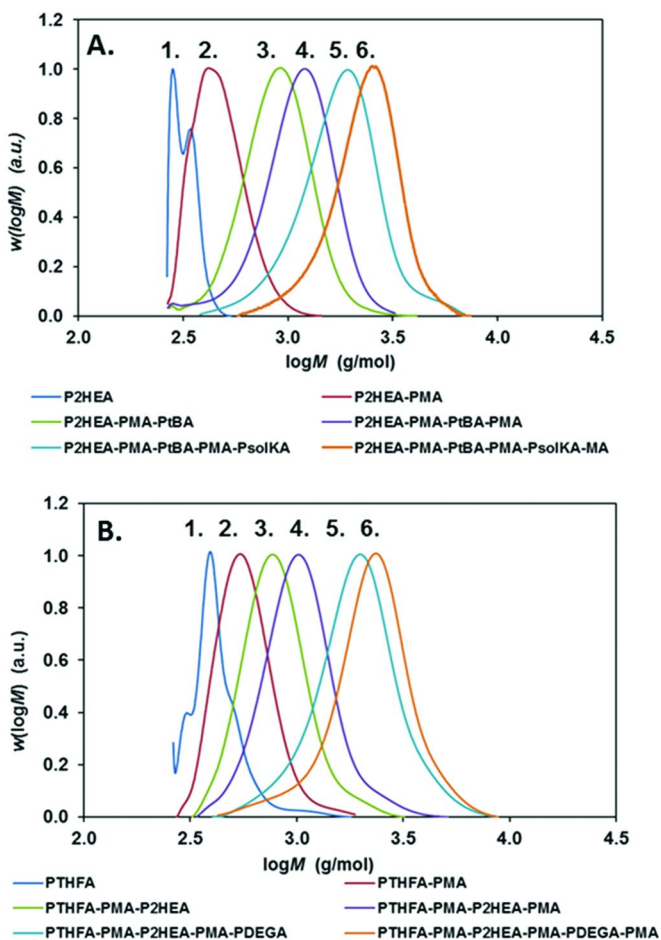
Figure 2. Molecular weight distributions of; A) P[(2HEA)-b-(MA)-b-(tBA)-b-(MA)-b-(solKA)-b-(MA)]and B) P[(THFA)-b-(MA)-b-(2HEA)b-(MA)-b-(DEGA)-b-(MA)]multi-block copolymer obtained via Cu(0)-mediated polymerization via iterative chain extension (see color insert)

In an alternate approach, Haddleton *et al.* (*53*) have also explored the use of nascent Cu(0) produced from Cu(I) in water for the synthesis of multiblock water soluble polymers and block copolymers. They demonstrated the successful homopolymerization of N-isopropyl acrylamide (NIPAAm) 2-hydroxyethyl acrylate 2(HEA), dimethylacrylamide (DMA), glucose acrylamide and oligoethylene glycol acrylate (OEGA) in water for molecular weights of approximately 10,000 g/mol. The successful synthesis of a water soluble multiblock copolymer P(PNIPAAm$_{20}$-b-P2HEA$_{40}$-b-POEGA$_{10}$) using successive chain extensions via iterative addition of monomers was demonstrated.
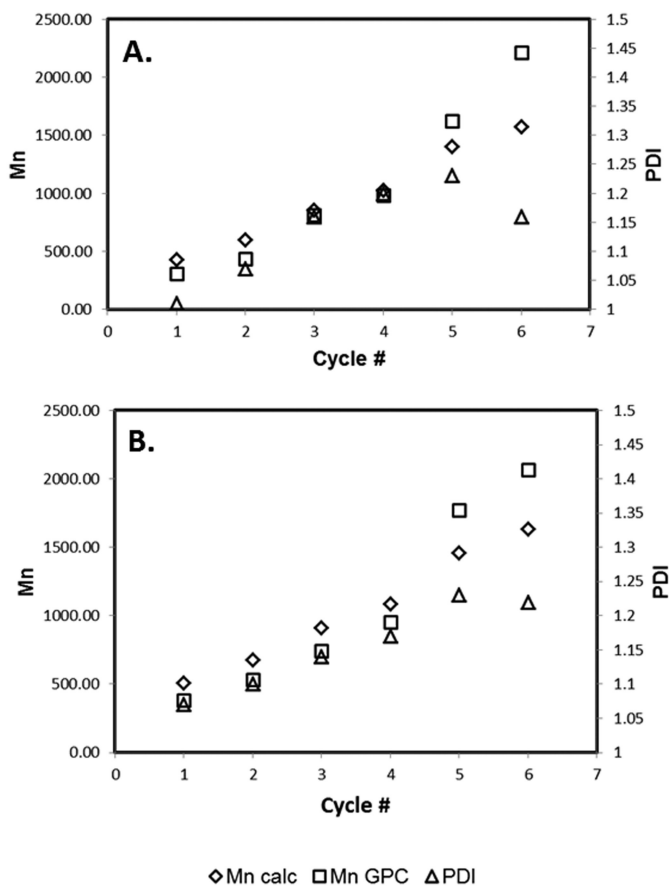
Figure 3. Molecular weight (experimental and theoretical) and PDI of; A) P[(2HEA)-b-(MA)-b-(tBA)-b-(MA)-b-(solKA)-b-(MA)] and B) P[(THFA)-b-(MA)-b-(2HEA)b-(MA)-b-(DEGA)-b-(MA)] multi-block copolymer obtained via Cu(0)-mediated polymerization via iterative chain extension

While this approach has now been demonstrated for multiblock polymers with a range of individual block DPn , the successful translation to a multiblock system where each individual block DPn = 1 may not be possible. In an ideal living polymerization there will be a Poisson distribution of chain lengths, however in CLRP the distribution will inevitably be broader than a Poisson distribution. As such, when targeting very low degrees of polymerization during synthesis of multiblock copolymers, it is likely that some fraction of chains will contain blocks of zero monomer units, i.e. a given block may be missing. This represents an intrinsic limitation of multiblock copolymer synthesis using CLRP, regardless of the specific CLRP system. For a comprehensive critique of the utility of this approach we refer the readers to a Highlight Article (*63*) recently published by the authors.
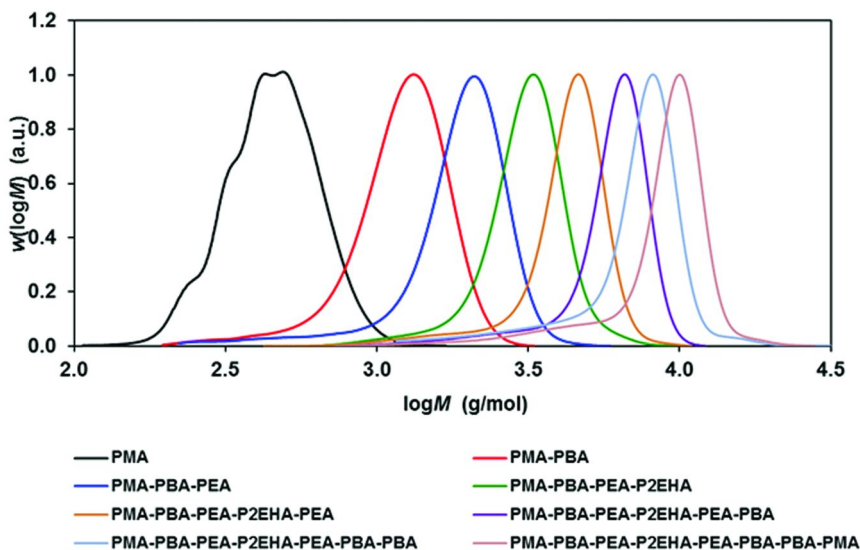
Figure 4. Molecular weight distributions of poly(MA-b-nBA-b-EA-b-EHA-b-EA-b-nBA-b-nBA-b-MA) multi-block copolymer obtained via Cu(0)-mediated polymerization via iterative chain extension. Reproduced with permission from reference (40). Copyright (2011) American Chemical Society. (see color insert)

Conclusions

The application of CLRP in the presence of zero-valent copper has become an important tool for the synthesis of structurally complex polymers. Critical to its widespread application is the maintenance of end-group fidelity at ultra-high monomer conversions. This aspect has been exploited by us to develop a one-pot iterative approach for the synthesis of structurally complex multiblock systems that can be synthesised in high yield and with purification only required at the final step. These important features cannot be easily achieved via most other CLRP techniques (we note the recent work of Perrier and our co-author Zetterlund for the application of the RAFT process (*26–29*)). Not only will these new materials find application in self-assembly but we believe that the opportunity to build predesigned and functional multiblock copolymers with low individual block DPn provides new opportunities to develop new synthetic polymeric materials with truly biologically inspired properties.

References

1. Tsarevsky, N. V.; Matyjaszewski, K. *RSC Polym. Chem. Ser.* **2013**, *4*, 287–357.
2. Ouchi, M.; Terashima, T.; Sawamoto, M. *Chem. Rev.* **2009**, *109*, 4963–5050.
3. Moad, G.; Rizzardo, E.; Thang, S. H. *Chem. - Asian J.* **2013**, *8*, 1634–1644.

4. Boyer, C.; Stenzel, M. H.; Davis, T. P. *J. Polym. Sci., Part A: Polym. Chem.* **2011**, *49*, 551–595.

5. Gigmes, D.; Marque, S. R. A. In *Encyclopedia of Radicals in Chemistry, Biology and Materials*; Chatgilialoglu, Ch., Studer, A., Eds; John Wiley & Sons Ltd.: 2012; Vol. 4, pp 1813−1850.

6. Kahveci, M. U.; Yagci, Y.; Avgeropoulos, A.; Tsitsilianis, C. In *Polymer Science: A Comprehensive Reference*; Matyjaszewski, K., Müller, M., Eds.; Elsevier B.V.: Oxford, 2012; Vol. 6, pp 455−509.

7. Abetz, V.; Boschetti-de-Fierro, A.; Gohy, J.-F. In *Controlled and Living Polymerizations*; Matyjaszewski, K., Müller, A. H. E., Eds; Wiley-VCH Verlag GmbH & Co. KGaA: 2009; pp 493−554.

8. Hayward, R. C.; Pochan, D. J. *Macromolecules* **2010**, *43*, 3577–3584.

9. Boyer, C.; Derveaux, A.; Zetterlund, P. B.; Whittaker, M. R. *Polym. Chem.* **2012**, *3*, 117–123.

10. Baradel, N.; Gok, O.; Zamfir, M.; Sanyal, A.; Lutz, J.-F. *Chem. Commun.* **2013**, *49*, 7280–7282.

11. Chan-Seng, D.; Zamfir, M.; Lutz, J.-F. *Angew. Chem., Int. Ed.* **2012**, *51*, 12254–12257.

12. Lutz, J.-F.; Ouchi, M.; Liu, D. R.; Sawamoto, M. *Science* **2013**, *341*, 628–636.

13. Lutz, J.-F.; Schmidt, B. V. K. J.; Pfeifer, S. *Macromol. Rapid Commun.* **2011**, *32*, 127–135.

14. Pfeifer, S.; Lutz, J.-F. *Chem. - Eur. J.* **2008**, *14*, 10949–10957.

15. Zamfir, M.; Lutz, J.-F. *Nat. Commun.* **2012**, *3*, 1138.

16. Zamfir, M.; Theato, P.; Lutz, J.-F. *Polym. Chem.* **2012**, *3*, 1796–1802.

17. Satoh, K.; Matsuda, M.; Nagai, K.; Kamigaito, M. *J. Am. Chem. Soc.* **2010**, *132*, 10003–10005.

18. Matsuda, M.; Satoh, K.; Kamigaito, M. *Macromolecules* **2013**, *46*, 5473–5482.

19. Hibi, Y.; Tokuoka, S.; Terashima, T.; Ouchi, M.; Sawamoto, M. *Polym. Chem.* **2011**, *2*, 341–347.

20. Hibi, Y.; Ouchi, M.; Sawamoto, M. *Angew. Chem., Int. Ed.* **2011**, *50*, 7434–7437.

21. Ida, S.; Ouchi, M.; Sawamoto, M. *J. Am. Chem. Soc.* **2010**, *132*, 14748–14750.

22. Ida, S.; Terashima, T.; Ouchi, M.; Sawamoto, M. *J. Am. Chem. Soc.* **2009**, *131*, 10808–10809.

23. McLeary, J. B.; Calitz, F. M.; McKenzie, J. M.; Tonge, M. P.; Sanderson, R. D.; Klumperman, B. *Macromolecules* **2004**, *37*, 2383–2394.

24. Houshyar, S.; Keddie, D. J.; Moad, G.; Mulder, R. J.; Saubern, S.; Tsanaktsidis *J. Polym. Chem.* **2012**, *3*, 1879–1889.

25. Vandenbergh, J.; Reekmans, G.; Adriaensens, P.; Junkers, T. *Chem. Commun.* **2013**, *49*, 10358–10360.

26. Gody, G.; Maschmeyer, T.; Zetterlund, P. B.; Perrier, S. *Nat. Commun.* **2013**, *4*, 2505.

27. Zetterlund, P. B.; Gody, G.; Perrier, S. *Macromol. Theory Simul.* **2014**, *23*, 331–339.

28. Gody, G.; Maschmeyer, T.; Zetterlund, P. B.; Perrier, S. *Macromolecules* **2014**, *47*, 639–649.
29. Gody, G.; Maschmeyer, T.; Zetterlund, P. B.; Perrier, S. *Macromolecules* **2014**, *47*, 3451–3460.
30. Rodlert, M.; Harth, E.; Hawker, C. J. *J. Polym. Sci., Part A: Polym. Chem.* **2000**, *38*, 4749–4763.
31. Jakubowski, W.; Kirci-Denizli, B.; Gil, R. R.; Matyjaszewski, K. *Macromol. Chem. Phys.* **2008**, *209*, 32–39.
32. Percec, V.; Guliashvili, T.; Ladislaw, J. S.; Wistrand, A.; Stjerndahl, A.; Sienkowska, M. J.; Monteiro, M. J.; Sahoo, S. *J. Am. Chem. Soc.* **2006**, *128*, 14156–14165.
33. Nguyen, N. H.; Levere, M. E.; Percec, V. *J. Polym. Sci., Part A: Polym. Chem.* **2012**, *50*, 860–873.
34. Jiang, X.; Rosen, B. M.; Percec, V. *J. Polym. Sci., Part A: Polym. Chem.* **2010**, *48*, 2716–2721.
35. Lligadas, G.; Rosen, B. M.; Monteiro, M. J.; Percec, V. *Macromolecules* **2008**, *41*, 8360–8364.
36. Lligadas, G.; Percec, V. *J. Polym. Sci., Part A: Polym. Chem.* **2007**, *45*, 4684–4695.
37. Anastasaki, A.; Waldron, C.; Wilson, P.; McHale, R.; Haddleton, D. M. *Polym. Chem.* **2013**, *4*, 2672–2675.
38. Levere, M. E.; Willoughby, I.; O'Donohue, S.; de Cuendias, A.; Grice, A. J.; Fidge, C.; Becer, C. R.; Haddleton, D. M. *Polym. Chem.* **2010**, *1*, 1086–1094.
39. Soeriyadi, A. H.; Boyer, C.; Nystrom, F.; Zetterlund, P. B.; Whittaker, M. R. *J. Am. Chem. Soc.* **2011**, *133*, 11128–11131.
40. Boyer, C.; Soeriyadi, A. H.; Zetterlund, P. B.; Whittaker, M. R. *Macromolecules* **2011**, *44*, 8028–8033.
41. Wang, W.; Zhao, J.; Zhou, N.; Zhu, J.; Zhang, W.; Pan, X.; Zhang, Z.; Zhu, X. *Polym. Chem.* **2014**, *5*, 3533–3546.
42. Rosen, B. M.; Percec, V. *Chem. Rev.* **2009**, *109*, 5069–5119.
43. Ouchi, M.; Terashima, T.; Sawamoto, M. *Chem. Rev.* **2009**, *109*, 4963–5050.
44. Konkolewicz, D.; Wang, Y.; Zhong, M.; Krys, P.; Isse, A. A.; Gennaro, A.; Matyjaszewski, K. *Macromolecules* **2013**, *46*, 8749–8772.
45. Guliashvili, T.; Mendonça, P. V.; Serra, A. C.; Popov, A. V.; Coelho, J. F. *Chem. - Eur. J.* **2012**, *18*, 4607–4612.
46. Nguyen, N. H.; Percec, V. *J. Polym. Sci., Part A: Polym. Chem.* **2011**, *49*, 4756–4765.
47. Jiang, X.; Rosen, B. M.; Percec, V *J. Polym. Sci., Part A: Polym. Chem.* **2010**, *48*, 403–409.
48. Lligadas, G.; Rosen, B. M.; Bell, C. A.; Monteiro, M. J.; Percec, V. *Macromolecules* **2008**, *41*, 8365–8371.
49. Nguyen, N. H.; Rosen, B. M.; Lligadas, G.; Percec, V. *Macromolecules* **2009**, *42*, 2379–2386.
50. Levere, M. E.; Nguyen, N. H.; Leng, X.; Percec, V. *Polym. Chem.* **2013**, *4*, 1635–1647.

51. Samanta, S. R.; Anastasaki, A.; Waldron, C.; Haddleton, D. M.; Percec, V. *Polym. Chem.* **2013**, *4*, 5555–5562.
52. Samanta, S. R.; Anastasaki, A.; Waldron, C.; Haddleton, D. M.; Percec, V. *Polym. Chem.* **2013**, *4*, 5563–5569.
53. Zhang, Q.; Wilson, P.; Li, Z. D.; McHale, R.; Godfrey, J.; Anastasaki, A.; Waldron, C.; Haddleton, D. M. *J. Am. Chem. Soc.* **2013**, *135*, 7355–7363.
54. Nguyen, N. H.; Rosen, B. M.; Percec, V. *J. Polym. Sci., Part A: Polym. Chem.* **2010**, *48*, 1752–1763.
55. Lligadas, G.; Percec, V. *J. Polym. Sci., Part A: Polym. Chem.* **2008**, *46*, 2745–2754.
56. Nguyen, N. H.; Percec, V. *J. Polym. Sci., Part A: Polym. Chem.* **2011**, *49*, 4227–4240.
57. Zhang, Q.; Li, Z.; Wilson, P.; Haddleton, D. M. *Chem. Commun.* **2013**, *49*, 6608–6610.
58. Levere, M. E.; Willoughby, I.; O'Donohue, S.; Wright, P. M.; Grice, A. J.; Fidge, C.; Becer, C. R.; Haddleton, D. M. *J. Polym. Sci., Part A: Polym. Chem.* **2011**, *49*, 1753–1763.
59. Nystrom, F.; Soeriyadi, A. H.; Boyer, C.; Zetterlund, P. B.; Whittaker, M. R. *J. Polym. Sci., Part A: Polym. Chem.* **2011**, *49*, 5313–5321.
60. Zhang, Q.; Su, L.; Collins, J.; Chen, G.; Wallis, R.; Mitchell, D. A.; Haddleton, D. M.; Becer, C. R. *J. Am. Chem. Soc.* **2014**, *136*, 4325–4332.
61. Zhang, Q.; Collins, J.; Anastasaki, A.; Wallis, R.; Mitchell, D. A.; Becer, C. R.; Haddleton, D. M. *Angew. Chem., Int. Ed.* **2013**, *52*, 4435–4439.
62. Wong, E. H. H.; Blencowe, A.; Qiao, G. G. *Polym. Chem.* **2013**, *4*, 4562–4565.
63. Boyer, C.; Zetterlund, P. B.; Whittaker, M. R. *J. Polym. Sci., Part A: Polym. Chem.* **2014**, *52* (15), 2083–2098.

Chapter 14

The Rationale Behind Sequence-Controlled Maleimide Copolymers

Bert Klumperman*

Department of Chemistry and Polymer Science, Stellenbosch University, Private Bag X1, Matieland 7602, South Africa
***E-mail: bklump@sun.ac.za**

The rationale behind sequence-controlled maleimide copolymers is discussed. To that end, two specific features of styrene – maleic anhydride copolymerizations are highlighted. Maleic anhydride (MAnh) is chosen as a mimic of *N*-substituted maleimide monomers since they both represent electron-poor species. The alternating tendency of styrene (STY) with MAnh is discussed in light of the penultimate unit model. On the basis of reactivity ratios it can be assessed that the probability for MAnh addition to a STY-centered growing polymer radical is two to four times larger in the case of a STY penultimate unit compared to a MAnh penultimate unit. The expected initialization behavior of a polySTY macro-RAFT agent with maleic anhydride (or maleimide) is highly beneficial for the precise introduction of a single unit in a PSTY chain at a predetermined location. The kinetic/mechanistic features discussed in this contribution provide a rationale for the successful sequence control in styrene – maleimide copolymerizations.

Introduction

Recent years have witnessed various attempts to induce sequence control during chain growth processes such as living radical polymerization (*1*, *2*). A traditional method to achieve sequence control is by templated copolymerization,

which somewhat mimics the sequence control in protein synthesis (*3*). Older versions of templated copolymerization largely suffer from the difficulty of separating the newly formed chain from the template. In order to overcome this complication, one would need to mimic the role of tRNA as a vehicle to introduce the next monomer without the monomer itself being bound to the template. This would be very elegant, but the synthetic efforts to make the tRNA mimics are quite significant. A much simpler and currently quite successful method turns out to be the precise incorporation of maleic anhydride or maleimide moieties in a polystyrene chain (*4*, *5*). Two major characteristics of the RAFT-mediated copolymerization of styrene and maleimides are expected to play an important role. The first characteristic is the strong alternating tendency of electron rich and electron poor monomers such as styrene and maleic anhydride or maleimides, respectively, which has received significant attention throughout the history of radical copolymerization (*6*). This tendency towards alternation is equally observed for living radical polymerization techniques (*7*) as it is for conventional radical copolymerization (*8*). The other characteristic that may play an important role is the process of initialization in Reversible Addition–Fragmentation Chain Transfer (RAFT) mediated polymerization that was investigated and described in literature a number of years ago (*9*, *10*). Initialization has only been investigated for low molar mass RAFT agents. In the present contribution, the potential application of initialization towards macro-RAFT agents will be discussed.

The Mechanism Behind Alternating Copolymerization

It has been known for a long time that electron-rich monomers such as styrene and electron-poor monomers like maleimides and maleic anhydride have a strong tendency towards alternating copolymerization (*6*). The underlying mechanism has long been a point of debate, where some studies would conclude that the alternating tendency was due to normal terminal or penultimate unit model with a high rate of cross-propagation (*8*), and others would conclude that the addition of charge-transfer complexes was responsible for the alternating tendency (*11*). It turns out that on the basis of copolymer composition and/or monomer sequence distribution measurements, it is impossible to distinguish between the two models. However, when accurate measurements of the propagation rate coefficient are combined with the composition measurements, model discrimination strongly favors the conclusion that the penultimate unit model is the only model that can adequately describe the copolymerization (*8*). Just as an example for the case of the copolymerization of styrene (STY) and maleic anhydride (MAnh), all rate parameters according to the penultimate unit model (PUM) could be determined with reasonable accuracy, except for the addition rate of styrene to a maleic anhydride chain end radical. The fit of the model to the experimental data was good as long as that addition rate constant was larger than 10^5 L·mol^{-1}·s^{-1} (*8*).

Figure 1 shows the average propagation rate coefficient as a function of the fraction of MAnh in the STY/MAnh copolymerization. The curves are based on a combined fit to the propagation rate constant and composition data (latter not

shown). The copolymerization model is a restricted PUM in which all MAnh homopropagation events have been set to zero. The high value of the average propagation rate coefficient at high fraction MAnh ($f_{MAnh} \approx 0.9$) is due to the previously indicated rate constant $k_{SMS} > 10^5$ L·mol^{-1}·s^{-1} (8).
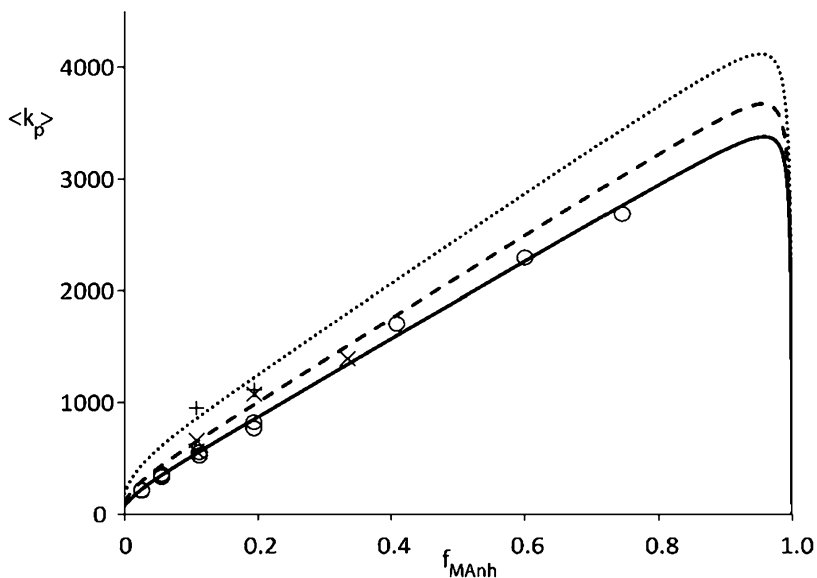
Figure 1. Average propagation rate coefficient ($<k_p>$) as a function of fraction MAnh in STY-MAnh copolymerization (f_{MAnh}) at 25 °C (○), 35 °C (×) and 50 °C (+). Curves are calculated on the basis of the PUM. Reprinted with permission from reference (8). Copyright (2010) Royal Society of Chemistry.

On the basis of the rate constants, conditional probabilities for propagation events can be defined. A STY-centered propagating chain-end radical can either add a STY monomer or a MAnh monomer. The conditional probability is dependent on the penultimate unit, and can be written as in Equations 1 and 2.

$$p_{SSM} = \frac{1}{1 + r_{SS}\frac{[STY]}{[MAnh]}} \qquad \text{Equation 1}$$

$$p_{MSM} = \frac{1}{1 + r_{MS}\frac{[STY]}{[MAnh]}} \qquad \text{Equation 2}$$

The probabilities for MAnh addition increase with a decrease in the product of reactivity ratio (r_{SS} or r_{MS}) and ratio of [STY]/[MAnh]. The reactivity ratios have been determined experimentally from intermediate conversion continuous copolymerizations at 60 °C (*12*). The values are r_{SS} = 0.023 and r_{MS} = 0.148, respectively. Effectively this means that the probability for MAnh addition to a STY-centered growing polymer radical is two to four times larger in the case of a STY penultimate unit compared to a MAnh penultimate unit if the fraction MAnh in the monomer mixture is in the range of 0.02 < f_{MAnh} < 0.10. In other words, in a living polymerization system, where all polymer chains have equal probability of chain growth, there is as much chance that all chains will add one MAnh unit as compared to a few chains adding a larger number of MAnh units. Obviously, this discussion neglects the effect of activation and deactivation reactions in living radical polymerization. However, for the reactivity of the propagating radical and for the conditional probabilities in copolymerization reactions this is a legitimate approach. Nevertheless, it is known from previous work that living radical copolymerization kinetics may show deviations from conventional copolymerization reactions. Especially in those cases where the stability of the radical is strongly dependent on the nature of the terminal monomer unit in a propagating chain, these deviations may occur. Our group previously reported a modest example of this phenomenon (*13*).

Initialization in RAFT-Mediated Polymerization

In 2004, kinetic studies on the initial stages of RAFT-mediated polymerization led to understanding of what is now known as *initialization* (*9*). During the initialization process, the original RAFT-agent is converted into its single monomer adduct. Several examples of efficient initialization have been reported. The polymerization of styrene mediated by cyanoisopropyl dithiobenzoate (CiPDB) shows a very clean initialization in a reasonably short reaction time (Figure 2A) (*9*). In Figure 2A, AD represents the CiPDB RAFT agent, ASD is the single monomer (STY) adduct and AS_2D is the two-monomer adduct. If CiPDB is replaced by cumyl dithiobenzoate (CDB), the initialization is equally selective, but it takes much longer (Figure 2B) (*14*). In Figure 2B, CD represents the CDB RAFT agent and CSD, CS_2D, ASD and AS_2D are the monomer adducts similar to previously explained for Figure 2A, where C represents the cumyl leaving group of CDB. The much longer initialization time is assigned to the slower re-initiation rate of the cumyl radical compared to the cyanoisopropyl radical in the case of styrene polymerization.

When maleic anhydride is added to this polymerization, a very interesting phenomenon is observed (*10*). In the case of the AIBN initiated CiPDB-mediated polymerization, it is almost as if the maleic anhydride is not present. The duration of the initialization period is identical to the styrene homopolymerization, and the styrene adduct is virtually exclusively formed in the early stages of

the reaction (Figure 3A). Conversely, in the AIBN initiated CDB-mediated polymerization, the addition of the cumyl radical to maleic anhydride is extremely fast. Under specific conditions where the initialization in CDB-mediated styrene polymerization would take 240 minutes, initialization in the CDB-mediated copolymerization of styrene and maleic anhydride is over in less than five minutes for the polymerization at 70 °C (results not shown). Only upon lowering the reaction temperature to 60 °C, initialization can be properly observed (Figure 3B). The underlying feature in these polymerizations is the nature of initiating radical and added monomer. In the case of the cyanoisopropyl radical, even though it has been reported as being weakly nucleophilic (*15*), the radical is fairly electron poor as compared to the cumyl radical, which is electron rich. Styrene as a monomer is electron rich, whereas maleic anhydride is electron poor. It is known from the early days of copolymerization that the combination of an electron rich and an electron poor monomer leads to a strong tendency towards alternation. The same effect leads to fast or slow initialization when electron poor and electron rich radicals, respectively, add to styrene.

If then the case of a macromolecular radical is considered, it is quite likely that the same rules apply. A styrene-centered chain-end radical (of a growing polystyrene chain) is electron rich due to the nature of the constituting monomers. Although to the author's knowledge the experiment has never been performed, it is highly likely that an initialization experiment with a polystyrene macro-RAFT agent would lead to a very short initialization time when the monomer to add is electron poor such as maleic anhydride or most of the maleimide derivatives. In the initialization experiments for styrene – maleic anhydride, it almost seemed as if two initialization steps were taking place. The first one, highly selective, would only add maleic anhydride in the case of the cumyl radical or styrene in the case of the cyanoisopropyl radical. After that selective first monomer addition, a second monomer addition would take place with slightly less specificity. If the radical chain end is maleic anhydride, exclusively styrene would add, whereas if styrene is the chain-end radical, the majority of chains would subsequently add maleic anhydride. Some further monomer addition would be witnessed before the "second initialization" was complete. However, if the concept of initialization with macro-RAFT agents is extrapolated to the site-specific insertion of maleimide monomers in a polystyrene chain, the similarities are obvious.

The addition of an equimolar amount of maleimide relative to the number of polystyrene chains will start a process that very much resembles initialization. As soon as a chain is reactivated, the styrene-centered chain-end radical will have a great preference for the addition of a maleimide over a styrene. After subsequent chain transfer, it is likely that the maleimide-centered leaving group is a worse leaving group than a styrene-centered one. In other words, if an asymmetrical intermediate radical is formed with a styrene-centered radical on one side and a maleimide-centered one on the other side, the styrene-centered radical is the one that will have the highest probability of being released. Hence, there is an effective process by which all the chains add exactly one maleimide unit as opposed to some chains adding an alternating sequence of styrene and maleimide units and other chains adding no maleimide at all. Obviously, after all the maleimide has been consumed, further styrene homopolymerization will continue.
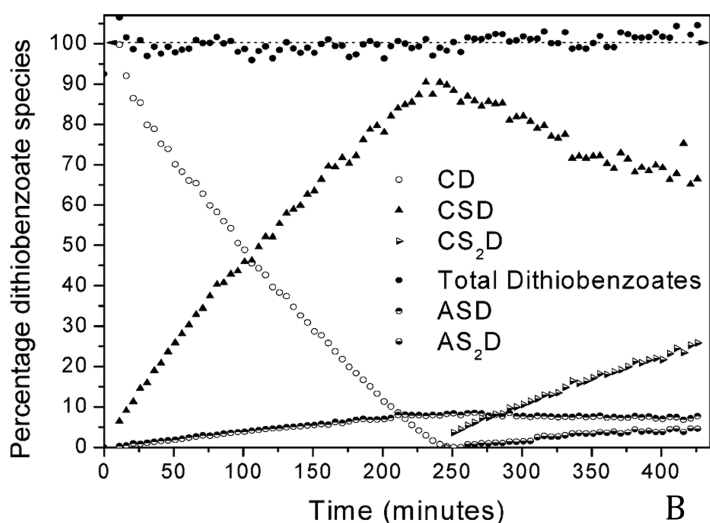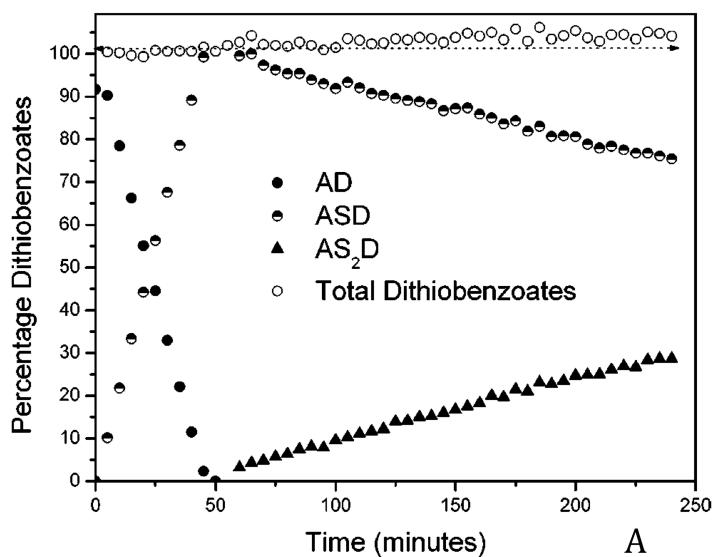
Figure 2. A: Relative concentrations of methyl protons of dithiobenzoate species versus time in the AIBN initiated, cyanoisopropyl dithiobenzoate (AD)-mediated polymerization of styrene at 70 °C. Reproduced with permission from reference (9). Copyright (2004) American Chemical Society. B: Relative concentrations of methyl protons of dithiobenzoate species versus time in the AIBN initiated, cumyl dithiobenzoate (CD)-mediated polymerization of styrene at 70 °C. Reproduced with permission from reference (14). Copyright (2005) American Chemical Society.
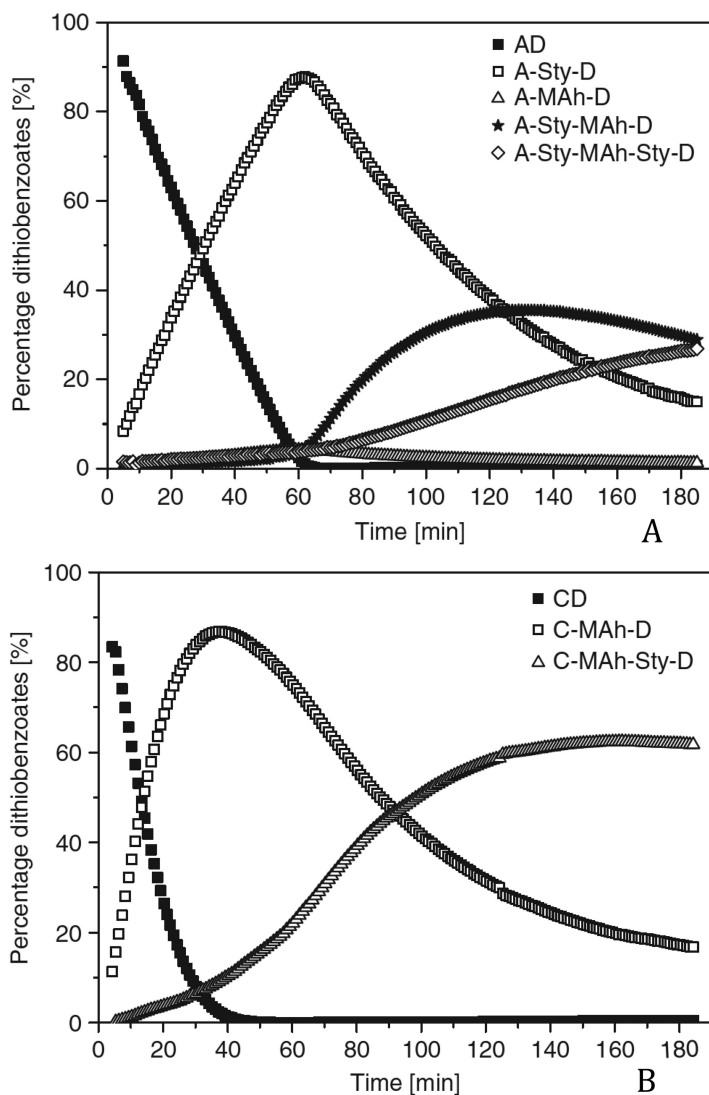
Figure 3. A: Conversion of the initial RAFT agent and the formation of the first, second and third monomer adducts for a AIBN initiated, cyanoisopropyl dithiobenzoate-mediated STY-MAnh copolymerization at 70 °C. B: Conversion of the initial RAFT agent and the formation of the first and second monomer adducts for a AIBN initiated, cumyl dithiobenzoate-mediated STY-MAnh copolymerization at 60 °C. Reproduced with permission from reference (10). Copyright (2006) CSIRO.

Conclusions

The precise incorporation of maleimides in a polystyrene chain is currently one of the most promising techniques for sequence controlled chain growth polymerization. Two specific phenomena for the copolymerization of electron rich and electron poor comonomers are discussed in this contribution. The penultimate unit effect in the copolymerization of styrene (STY) and maleic anhydride (MAnh) leads to a preference single MAnh insertion over alternating sequences. Specifically for RAFT-mediated living radical polymerization, the initialization behavior of STY/MAnh copolymerization is also likely to favor the selective addition of one MAnh unit to a growing polystyrene chain. Confirmation of this behavior for a polySTY macro-RAFT agent should still be carried out. However, based on initialization studies with low molar mass RAFT agents, the expectation is that initialization is playing a large role in the single monomer insertion. Based on the large similarity between MAnh and maleimides, it is expected that the phenomena investigated for MAnh will also apply for maleimides. It must be taken into account that the nature of the *N*-subtitution may influence the electron-poor character of the maleimide. This will also have a consequence on the initialization behavior, and therefore on the precision of sequence control.

References

1. Badi, N.; Lutz, J.-F. *Chem. Soc. Rev.* **2009**, *38*, 3383–3390.
2. Lutz, J.-F.; Ouchi, M.; Liu, D. R.; Sawamoto, M. *Science* **2013**, *341*, 1238149.
3. Challa, G.; Tan, Y. Y. *Pure Appl. Chem.* **1981**, *53*, 627–641.
4. Zamfir, M.; Lutz, J.-F. *Nat. Commun.* **2012**, *3*, 1138.
5. Pfeifer, S.; Lutz, J.-F. *J. Am. Chem. Soc.* **2007**, *129*, 9542–9543.
6. Hill, D. J. T.; O'Donnell, J. H.; O'Sullivan, P. W. *Macromolecules* **1985**, *18*, 9–17.
7. Chen, G.-Q.; Wu, Z.-Q.; Wu, J.-R.; Li, Z.-C.; Li, F.-M. *Macromolecules* **2000**, *33*, 232–234.
8. Klumperman, B. *Polym. Chem.* **2010**, *1*, 558–562.
9. McLeary, J. B.; Calitz, F. M.; McKenzie, J. M.; Tonge, M. P.; Sanderson, R. D.; Klumperman, B. *Macromolecules* **2004**, *37*, 2383–2394.
10. van den Dungen, E. T. A.; Rinquest, J.; Pretorius, N. O.; McKenzie, J. M.; McLeary, J. B.; Sanderson, R. D.; Klumperman, B. *Aust. J. Chem.* **2006**, *59*, 742–748.
11. Tsuchida, E.; Tomono, T. *Makromol. Chem.* **1971**, *141*, 265–298.
12. Klumperman, B. Free radical copolymerization of styrene and maleic anhydride – Kinetic studies at low and intermediate conversion, PhD thesis, Eindhoven University of Technology, Eindhoven, The Netherlands, 1994, p 72.
13. Chambard, G.; Klumperman, B.; Brinkhuis, R. H. G. *Advances in Controlled/ Living Radical Polymerization*; ACS Symposium Series; Matyjaszewski, K.,

Ed.; American Chemical Society: Washington, DC, 2003; Vol. 854, pp 180−192.

14. McLeary, J. B.; Calitz, F. M.; McKenzie, J. M.; Tonge, M. P.; Sanderson, R. D.; Klumperman, B. *Macromolecules* **2005**, *38*, 3151–3161.

15. De Vleeschouwer, F.; Van Speybroeck, V.; Waroquier, M.; Geerlings, P.; De Proft, F. *Org. Lett.* **2007**, *9*, 2721–2724.

Chapter 15

Sequence-Regulated Polymers via Combination of Orthogonal Passerini Three-Component Reaction and Thiol-ene Reaction

Jian Zhang, Xin-Xing Deng, Fu-Sheng Du, and Zi-Chen Li*

Key Laboratory of Polymer Chemistry & Physics of Ministry of Education, Department of Polymer Science & Engineering, College of Chemistry and Molecular Engineering, Peking University, Beijing 100871, China
*E-mail: zcli@pku.edu.cn

The present work describes a facile approach to sequence-regulated polymers via a combination of orthogonal Passerini three-component reaction and thiol-ene reaction. The first step was the synthesis of an α,ω-diene compound via the Passerini three-component reaction of 1, 6-diisocyanohexane with 10-undecylenic acid and a monoaldehyde. In the second step, thiol-ene reaction of this diene compound with 3-mercaptopropionic acid converted the dienes to dicarboxylic acids. Finally, these dicarboxylic acid monomers were copolymerized with 1, 6-diisocyanohexane and another monoaldehyde to get polymers, each repeating unit of which contains four different side groups in an AABB sequence.

Introduction

The past two decades have witnessed a great progress in precise synthesis of polymers with controlled molecular weights, end groups and defined complex architectures (*1*, *2*). This was largely enabled by the development of controlled living radical polymerization and orthogonal click reactions (*1*, *2*). One of the remaining challenges for polymer chemists is to develop simple synthetic methods for polymers with well-defined monomer sequence (*3–6*). It is expected that these polymers will exhibit unique properties and functions as biomacromolecules do, for example chain folding and catalytic properties of proteins (*3–6*). A number of techniques have been developed to address this

challenge. Sequence-defined oligomers by the classical Merrifield solid-phase synthetic method is perhaps the most well-established approach (*7*). Recently, this approach has been extended to the simple synthesis of other types of sequence-defined oligomers by using orthogonal efficient organic reactions (*8–11*). Step-wise polymerization of monomers with encoded monomer sequence is another approach to get sequence-defined copolymers, but the sequence is only limited to periodic microstructure (*12–14*). Chain polymerization of special monomer pairs can produce sequence-regulated polymers in a more simple way (*15–22*). Controlled polymerization can tune the side groups in a programmed manner along a defined polymer chain. In our previous paper, we developed a facile synthetic method that can simultaneously construct the backbone and side group sequence of segmented multi-block copolymers (*23*). The technique involves the polymer supported liquid phase synthesis of PEG diacid macromonomers via stepwise Passerini three-component reaction (P-3CR) with *tert*-butyl isocyanoacetate and a functional aldehyde followed by selective hydrolysis, and the final multicomponent polymerization of these diacid monomers with phenylacetaldehyde and 1, 6-diisocyanohexane. One drawback of the procedure is that the carboxylic groups for P-3CR and the final multi-component polymerization needs to be protected and deprotected, thus making the synthesis not so straightforward. In this report, we developed a more straightforward approach to sequence-regulated polymers via combination of orthogonal P-3CR and thiol-ene reaction. As shown in Scheme 1, starting from 1, 6-diisocyanohexane, the P-3CR of which with an aldehyde and 10-undecylenic acid leads to an α, ω-diene with two side chain groups originated from the aldehyde. Then, the dienes were transformed into dicarboxylic acids by the photo-catalyzed thiol-ene reactions with 3-mercaptopropionic acid. This step does not add more side chains, but increase the chain length with end carboxylic acid groups which can be used for another circle of P-3CR and thiol-ene reaction to add more side groups. P-3CR polymerization of these dicarboxylic acids with 1, 6-diisocyanohexane and another monoaldehyde generates final polymers with four side groups in a defined AABB sequence. Noteworthy, in the course of our work, Meier et al reported a similar approach for the synthesis of sequence-defined tetramer and block copolymer via iterative application of the P-3CR and the thiol-ene reaction (*11*).

Experimental

Materials

1, 6-Diisocyanohexane (Sigma-Aldrich; >98%), 10-undecylenic acid (Alfa Aesar; 98%), 3-mercaptopropionic acid (Alfa Aesar; 99%), 2, 2-dimethoxy-2-phenylacetophenone (DMPA, Alfa Aesar; >98%), and *o*-nitrobenzaldehyde (Beijing Chem. Works) were used as received. Phenylacetaldehyde (Alfa Aesar; >95%) and 2-methylpropanal (Beijing Chem. Works) and all the solvents were redistilled before use.
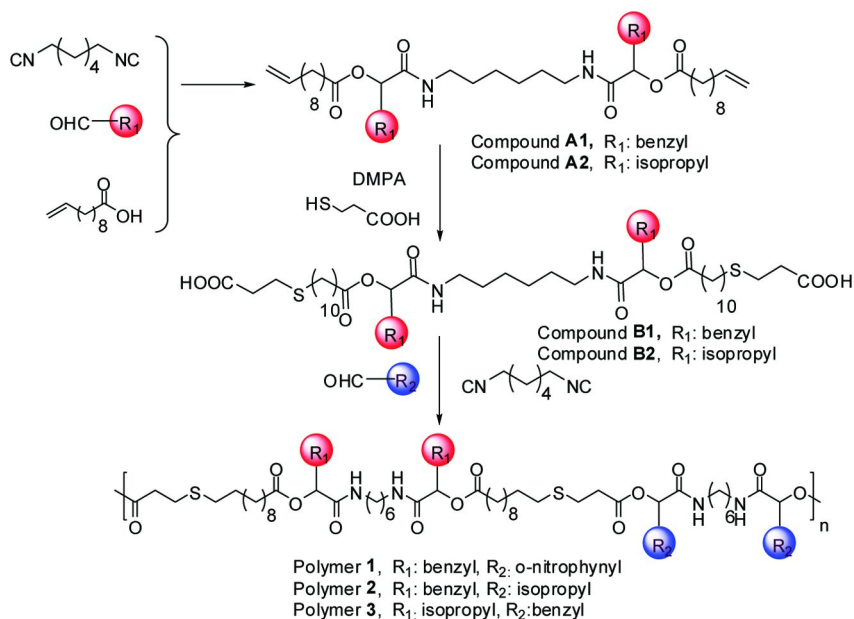
Scheme 1. Synthesis of sequence-regulated polymers by combination of Passerini reaction, thiol-ene reaction and Passerini polymerization.

Measurements

Average molecular weights and the polydispersities (PDI) of the polymers were measured by gel permeation chromatography (GPC). The GPC instrument was equipped with a Waters 1525 binary HPLC pump, a Waters 2414 refractive index detector, and three Waters Styragel HT columns (HT2, HT3, HT4) thermostated at 35 °C. THF was used as the eluent at a flow rate of 1.0 mL/min for a total time of 36 minutes. Calibration was made against linear polystyrene standards. The obtained data were processed on professional software. ^{1}H NMR (400 MHz) and ^{13}C NMR (100 MHz) spectra were obtained on a Bruker Avance-400 spectrometer. NMR chemical shifts are reported in ppm with tetramethylsilane (TMS) as the internal reference. Matrix-assisted laser desorption ionization time-of-flight (MALDI-TOF) mass spectra were obtained on a Bruker Autoflex III mass spectrometer equipped with a 355 nm nitrogen laser. α-Cyano-4-hydroxycinnamic acid was used as the matrix and reflective and linear positive ion modes were used.

Synthesis of Diene Compounds A1 and A2

To a 25 mL round bottom flask containing 10-undecylenic acid (2.208 g, 12 mmol) in THF or CH_2Cl_2 (2 mL) was added 1, 6-diisocyanohexane (0.680 g, 5 mmol) and phenylacetaldehyde (1.440g, 12 mmol). The mixture was stirred at 30°C for 24 h. The reaction mixture was then concentrated by removing the solvent under reduced pressure, the yellow viscous residue was purified by column

chromatography (EtOAc: petroleum ether, 1:5). Compound **A1** was obtained in 85% yield as a white solid. ^{1}H NMR (400 MHz, CDCl$_3$), δ (TMS, ppm): 7.15-7.29 (m, 10H), 5.95 (s, 2H), 5.81 (m, 2H), 5.37 (t, 2H), 4.96 (m, 4H), 3.08-3.25 (m, 8H), 2.31 (m, 4H), 2.04 (q, 4H), 1.55 (m, 4H), 1.15-1.41 (m, 28H).

Compound **A2** was synthesized in a similar way except that 2-methylpropanal (0.865g, 12 mmol) was used instead of phenylacetaldehyde. This compound was obtained as a white solid in 87% yield after column purification. ^{1}H NMR (400 MHz, CDCl$_3$), δ (TMS, ppm): 6.05 (s, 2H), 5.81 (m, 2H), 5.05 (m, 2H), 4.96 (m, 4H), 3.26 (m, 4H), 2.42 (t, 4H), 2.30 (m, 2H), 2.04 (q, 4H), 1.66 (m, 4H), 1.50 (m, 4H), 1.25-1.41 (m, 24H), 0.94 (t, 12H).

Synthesis of Monomers B1 and B2

To a 25 mL round bottom flask containing compound **A1** (2.232g, 3 mmol) in THF (1 mL) was added 3-mercaptopropionic acid (3.184g, 30 mmol) and DMPA (0.0308g, 0.12 mmol). The mixture was exposed to a UV lamp (365nm) for 3 h. After that, the reaction mixture was concentrated by removing the solvent under reduced pressure, the brown residue was purified by gradient column chromatography (EtOAc: petroleum ether: acetic acid, from 1:7:0.45 to 1:2:0.17). Monomer **B1** was obtained as a yellow viscous liquid in 94% yield. ^{1}H NMR (400 MHz, CDCl$_3$), δ (TMS, ppm): 7.15-7.28 (m, 10H), 6.09 (s, 2H), 5.38 (s, 2H), 3.08-3.25 (m, 8H), 2.78 (t, 4H), 2.65 (t, 4H), 2.53 (t, 4H), 2.32 (m, 4H), 2.10 (s, HOAc), 1.50-1.62 (m, 4H), 1.50 (m, 4H), 1.25-1.41 (m, 24H), 0.94 (t, 12H). MALDI-TOF-MS: M/z calcd for C$_{52}$H$_{80}$N$_2$O$_{10}$S$_2$ [M+Na]$^+$, 979.53; Found [M+Na]$^+$, 979.5.

Monomer **B2** was synthesized in a similar way except that compound **A2** (1.944g, 3 mmol) was used instead of compound **A1**. This compound was obtained in 86% yield as a pale yellow viscous liquid. ^{1}H NMR (400 MHz, CDCl$_3$), δ (TMS, ppm): 6.14 (s, 2H), 5.05 (m, 2H), 3.27 (m, 4H), 2.79(t, 4H), 2.65 (t, 4H), 2.54 (t, 4H), 2.42 (t, 4H), 2.30 (m, 2H), 2.10 (s, HOAc), 1.46-1.71 (m, 12H), 6.98, 1.43 (s, BHT), 1.25-1.41 (m, 28H), 0.94 (t, 12H). MALDI-TOF-MS: M/z calcd for C$_{44}$H$_{80}$N$_2$O$_{10}$S$_2$ [M+Na]+, 883.53; Found [M+Na]$^+$, 883.6.

Passerini Polymerization and Synthesis of Polymers

To a 10 mL round bottom flask containing monomer **B1** (0.287 g, 0.3 mmol) in CH$_2$Cl$_2$ (3.3 mL) was added 1, 6-diisocyanohexane (0.0408 g, 0.3 mmol) and *o*-nitrobenzaldehyde (0.0997 g, 6.6 mmol). The mixture was stirred at 30°C for 48 h. and then was precipitated into cold diethyl ether (30 mL). This procedure was repeated for two more times to get a yellow solid, which was further vacuum dried to get polymer **P1** in 65% yield.

Polymer **P2** was synthesized in a similar way by using monomer **B1** (0.287 g, 0.3 mmol), 1, 6-diisocyanohexane (0.0408 g, 0.3 mmol) and 2-methylpropanal (0.0476 g, 6.6 mmol). After three precipitations in diethyl ether and vacuum dry, a yellow solid was obtained in 65% yield.

Similarly, Polymer **P3** was synthesized by using monomer **B2** (0.258 g, 0.3 mmol), 1, 6-diisocyanohexane (0.0408 g, 0.3 mmol) and phenylacetaldehyde

(0.0792 g, 6.6 mmol). After three precipitations in diethyl ether and vacuum dry, a yellow solid was obtained in 67% yield.

Results and Discussion

Synthesis of Two α, ω-Diene Compounds by P-3CR Reaction

P-3CR reaction of an isocyanide with an aldehyde and a carboxylic acid forms an α-acyloxy carboxamide (*24*). This reaction can tolerate many functional groups like alkyne, alkene or azide groups. This reaction was recently developed as a polymerization method to prepare polyesters, polyamides and poly(ester-amide)s by using two components as bifunctional compounds (*25–27*). In our previous report, we used a polymer supported dicarboxylic acid for the preparation of sequence-regulated macromonomers *via* consecutive P-3CR with a protected isocyanide (*23*). Though separation is easy, it needs deprotection to liberate the terminal carboxylic acid for further P-3CR. To overcome this limit, we selected the thiol-ene reaction to transfer the terminal alkylene groups into carboxylic acids (*28*, *29*). First, we prepared compound **A1** by the P-3CR of 10-undecylenic acid, 1, 6-diisocyanohexane and phenylacetaldehyde at room temperature. The reaction was followed by NMR, and after 12 h, all the 1, 6-diisocyanohexane had been converted. After column purification, compound **A1** was obtained as a white solid in 90% yield. It has two side chain benzyl groups originated from phenylacetaldehyde. The ^{1}H NMR spectrum of compound **A1** is shown in Figure 1. All the expected proton signals can be well resolved, and the integration ratio of these peaks also confirmed the integrity of the expected structure. Alternatively, compound **A2** was obtained in a similar way by the P-3CR of 10-undecylenic acid, 1, 6-diisocyanohexane and 2- methylpropanal. The ^{1}H NMR spectrum of compound **A2** (Figure 1B) also confirmed the expected structure. This compound has two isopropyl side groups from 2-methylpropanal.

Synthesis of Two Monomers by Thiol-ene Reaction

The thiol-ene reaction is an efficient click reaction that has been widely used in polymer science (*28*, *29*). First, we carried out the reaction of compound **A1** and 3-mercaptopropionic acid with DMPA as an UV initiator. To ensure that all the terminal alkylene groups in compound **A1** can be transferred, 3-mercaptopropionic acid was used in a 1.5-fold excess. In addition, low concentration of photo-initiator (4 mol% of compound **A1**) was used to suppress any side reactions (*30*). The final product was separated by column chromatography; however, due to the existence of two carboxylic acid groups, the absorption of this compound on silica column is very strong which makes the separation very difficult. Finally, by using a mixture of eluent and also change the composition of the eluent gradually, we successfully got the desired compound. The ^{1}H NMR spectrum of monomer **B1** is shown in Figure 2, it can be seen that the terminal alkylene protons at δ=5.81 and 5.96 ppm in compound **A1** disappeared completely, indicating the full conversion of the alkylene groups. Meanwhile, other expected signals were all clearly resolved and the integration ratio was also in accordance with the expected structure.
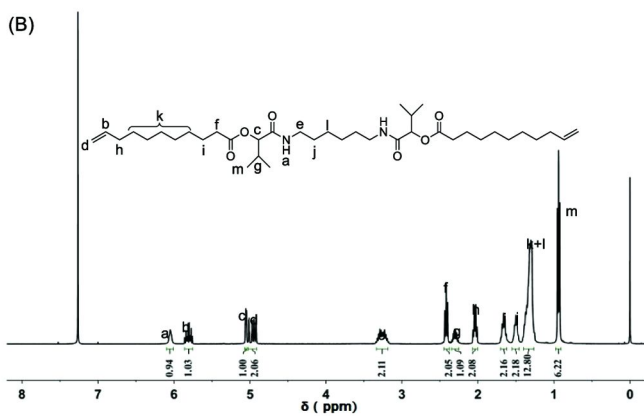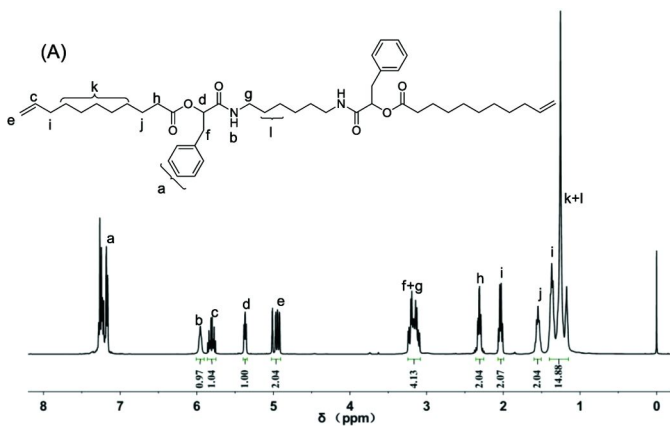
Figure 1. ¹H NMR spectra of compounds **A1** and **A2** in CDCl₃
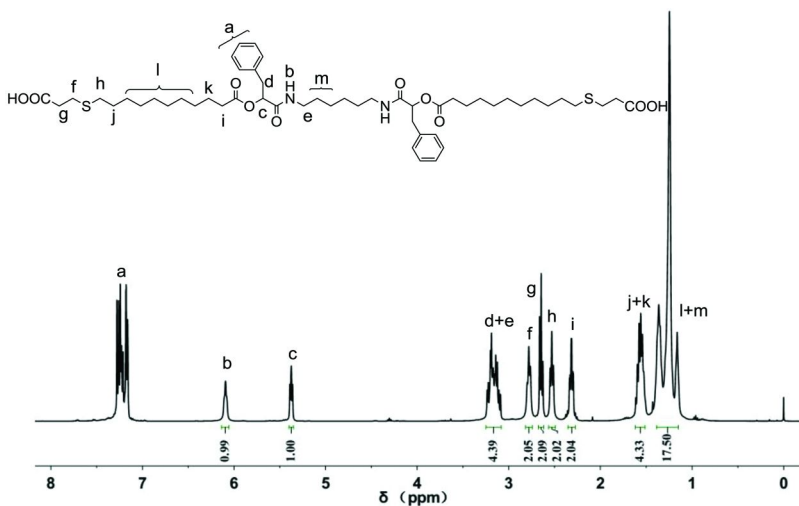
Figure 2. ¹H NMR spectrum of monomer **B1** in CDCl₃.

Monomer **B2** was obtained in a similar way and the NMR spectrum shown in Figure 3 confirmed the structure.
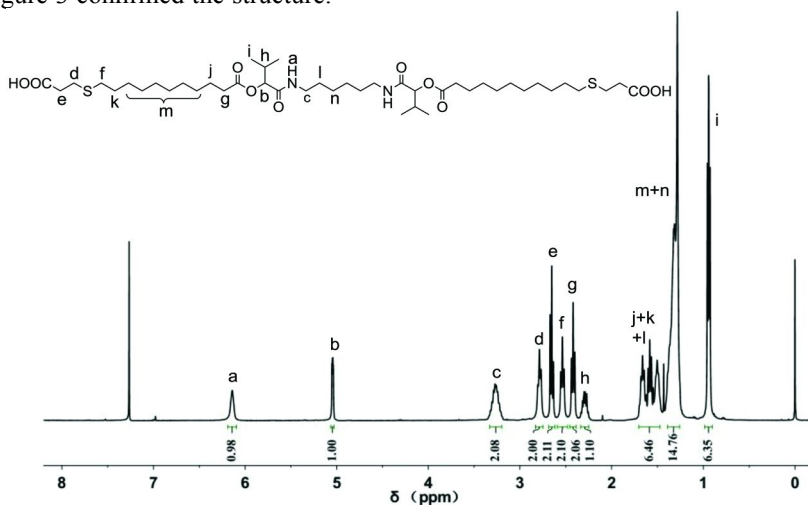
*Figure 3. ^1H NMR spectrum of monomer **B2** in CDCl3.*

P-3CR Polymerization of Monomers

With the two monomers in hand, we studied the Passerini multi-component polymerization (MCP) of the two diacid monomers with 1, 6-diisocyanohexane in the presence of different monoaldehydes. As already revealed in our previous paper (*26*), the Passerini MCP is a step-wise polymerization, the two difunctional monomers should be in a 1:1 stoichiometry, but the monoaldehyde component can be in an excess to both increase the polymerization rate and the molecular weights of the final polymers. Other conditions, like solvents and monomer concentrations may also affect the polymerization. Therefore, we studied in detail the Passerini MCP of monomer **B1**, with 1, 6-diisocyanohexane and *o*-nitrophenyl benzaldehyde.

Initially, the polymerization was carried out in CH_2Cl_2, and the concentration of monomer **B1** was 0.5 M, 1.0 M, and 2.0 M respectively (Table 1, entry 1, 2, 5). The crude GPC traces of the three polymerizations are shown in Figure 4. It can be concluded that when the polymerization was conducted at 1.0 M, polymers with the highest molecular weights can be obtained. This is reasonable, because at higher monomer concentration, the viscosity of the polymerization system is rather high, thus limiting the final conversion of the end groups. The polymerizations at 1.0 M were also conducted in THF and $CHCl_3$ (Table 1, entry 3, 4), the molecular weights of the polymers obtained in these two solvents were all lower than that in CH_2Cl_2. These results were all in accordance with our previous report, thus further confirming that the Passerini MCP should be carried out in less polar solvent at an appropriate monomer concentration to afford high molecular weight polymers. From the GPC traces (Shown in Figure 4) , we could

see the existence of oligomers; this is also the feature of step-wise polymerization. Nevertheless, after three precipitations in ethyl ether, polymer **P1** was recovered as a white solid in 66% yield due to the removal of oligomers. Polymer yields for these polymerizations are quite similar. The highest molecular weight of polymer **P1** was 16.5 kDa (Table 1, entry 2).

Table 1. Synthesis of Sequence Regulated Polymers[a]

Entry	Polymer	Conc. /M[b]	Solvent	Yield/%[d]	Mn/kDa[c]	PDI[c]
1	**P1**	0.5	CH_2Cl_2	66	10.1	1.59
2	**P1**	1.0	CH_2Cl_2	64	16.5	1.75
3	**P1**	1.0	$CHCl_3$	63	9.2	1.56
4	**P1**	1.0	THF	62	8.2	1.50
5	**P1**	2.0	CH_2Cl_2	65	9.1	1.59
6	**P2**	1.0	CH_2Cl_2	68	12.6	1.61
7	**P3**	1.0	CH_2Cl_2	58	15.5	1.66

[a] At 30 °C in CH_2Cl_2 for 48h;   [b] the concentration of monomer **B1** or **B2**. Concentration of 1, 6-diisocyanohexane was equal to the monomer, while that of the aldehyde was 2.4 times in molar ratio.   [c] Molecular weights and PDIs were measured by GPC with THF as eluent and calibrated with PS standards.   [d] Yields were determined after precipitation and vacuum dryness.
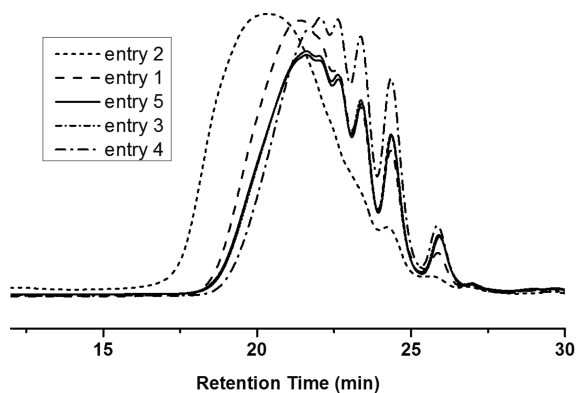
*Figure 4. GPC traces for the Passerini MCP of monomer **B1** with 1, 6-diisocyanohexane and o-nitrophynyl aldehyde.*

One polymer sample **P1** was characterized by [^1]H NMR (Figure 5). The peak g is a newly formed peak after polymerization. The integration ratio of this peak with peak i (one of the characteristic of monomer **B1**) is 1.01:1.00, demonstrating the integrity of the repeating unit of the expected polymer. Thus, this polymer **P1** contains an AABB side group sequence in the repeating units, where A is a benzyl group and B is an *o*-nitrophenyl group.
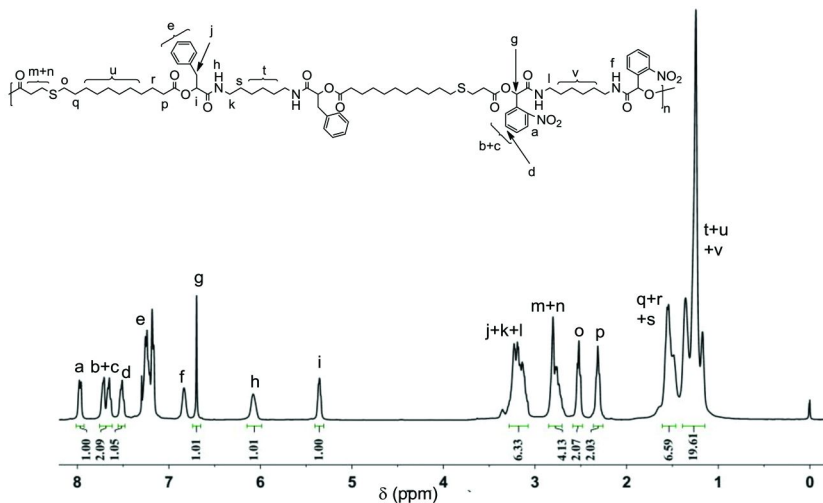
Figure 5. [^1]*H NMR spectrum of polymer **P1** in CDCl₃*

To regulate the side groups of polymers, monomer **B1** was polymerized with 1, 6-diisocyanohexane and 2-methylpropanal to get another polymer **P2** in a similar way. This polymer was obtained in 68% yield with a molecular weight of 12.6 kDa (Table 1, entry 6). The [^1]H NMR spectrum of polymer **P2** is shown in Figure 6. Again, the newly formed characteristic peak (peak e) was clearly resolved, and the integration ratio of this peak to the characteristic peak in the monomer (peak d) was 1.00:1.02, demonstrating the integrity of the structure. Thus, this polymer **P2** contains an AABB side group sequence in the repeating units, where A is a benzyl group and B is an isopropyl group.

Furthermore, by polymerizing monomer **B2** with 1, 6-diisocyanohexane and phenylacetaldehyde, we obtained polymer **P3** in 58% yield with an average molecular weight of 15.5 kDa (Table 1, entry 7). The [^1]H NMR spectrum of polymer **P3** is shown in Figure 7. It contains an AABB side group sequence in the repeating units, where A is a benzyl group and B is an isopropyl group.
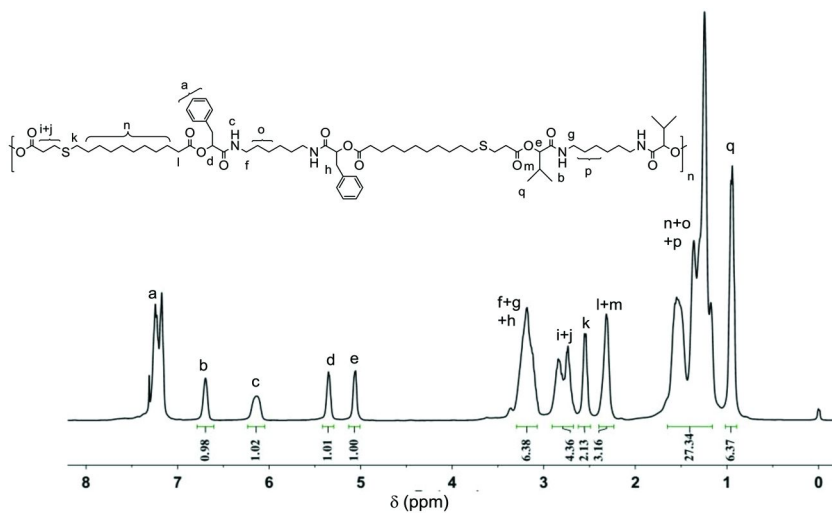
*Figure 6. ^{1}H NMR spectrum of polymer **P2** in CDCl$_3$.*
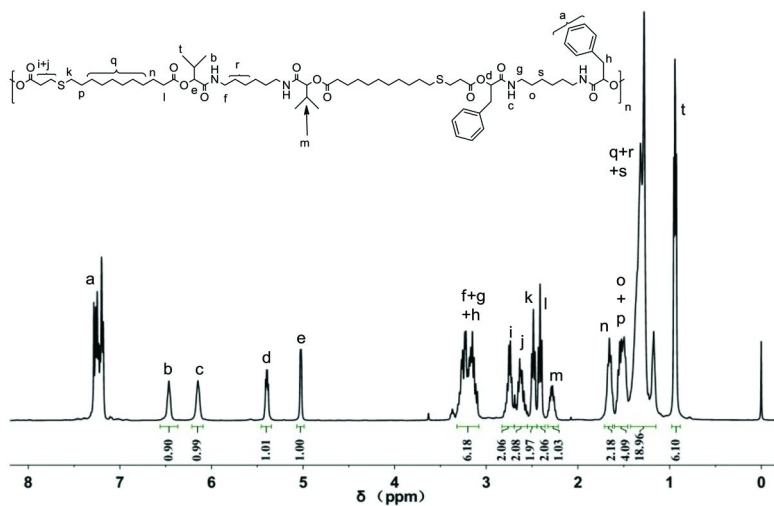
*Figure 7. ^{1}H NMR spectrum of polymer **P3** in CDCl$_3$.*

Conclusions

We demonstrated that orthogonal Passerini three-component reaction, thiol-ene reaction and Passerini MCP can be a facile synthetic strategy toward polymers containing poly(ester-amide) segments with ordered side group sequence. The Passerini three-component reaction was used to introduce side chains, the thiol-ene reaction was used to extend the main chain and transfer the dienes to dicarboxylic acid groups. The final Passerini MCP was used to synthesize a polymer, and at

the same time add two more side groups in a controlled way. In principle, this method can be extended to sequence-regulated polymers with more side groups via repeating the Passerini three-component reaction and the thiol-ene reaction.

Acknowledgments

References

1. Hawker, C. J.; Wooley, K. L. *Science* **2005**, *309*, 1200–1205.
2. Matyjaszewski, K.; Tsarevsky, N. V. *J. Am. Chem. Soc.* **2014**, *136*, 6513–6533.
3. Badi, N.; Lutz, J.-F. *Chem. Soc. Rev.* **2009**, *38*, 3383–3390.
4. Lutz, J.-F. *Polym. Chem.* **2010**, *1*, 55–62.
5. Ouchi, M.; Badi, N.; Lutz, J.-F.; Sawamoto, M. *Nat. Chem.* **2011**, *3*, 917–924.
6. Lutz, J.-F.; Ouchi, M.; Liu, D. R. *Science* **2013**, *341*, 1238149.
7. Merrifield, R. B. *J. Am. Chem. Soc.* **1963**, *85*, 2149–2154.
8. Pfeifer, S.; Zarafshani, Z.; Badi, N.; Lutz, J.-F. *J. Am. Chem. Soc.* **2009**, *131*, 9195–9197.
9. Espeel, P.; Carrette, L. L. G.; Bury, K.; Capenberghs, S.; Martins, J. C.; Du Prez, F. E.; Madder, A. *Angew. Chem., Int. Ed.* **2013**, *52*, 13261–13264.
10. Yan, J. J.; Wang, D.; Wu, D. C.; You, Y. Z. *Chem. Commun.* **2013**, *49*, 6057–6059.
11. Solleder, S. C.; Meier, M. A. R. *Angew. Chem., Int. Ed.* **2014**, *53*, 711–714.
12. Zhang, C. Y.; Ling, J.; Wang, Q. *Macromolecules* **2011**, *44*, 8739–8743.
13. Li, Z.-L.; Li, L.; Deng, X.-X.; Zhang, L.-J.; Dong, B.-T.; Du, F.-S.; Li, Z.-C. *Macromolecules* **2012**, *45*, 4590–4598.
14. Wang, C.-H.; Song, Z.-Y.; Deng, X.-X.; Zhang, L.-J.; Du, F.-S.; Li, Z.-C. *Macromol. Rapid Commun.* **2014**, *35*, 474–478.
15. Lutz, J.-F. *Acc. Chem. Res.* **2013**, *46*, 2696–2705.
16. Schmidt, B. V. K. J.; Fechler, N.; Falkenhagen, J.; Lutz, J.-F. *Nat. Chem.* **2011**, *3*, 234–238.
17. Pfeifer, S.; Lutz, J.-F. *J. Am. Chem. Soc.* **2007**, *129*, 9542–9543.
18. Baradel, N.; Fort, S.; Halila, S.; Badi, N.; Lutz, J. F. *Angew. Chem., Int. Ed.* **2013**, *52*, 2335–2339.
19. Zamfir, M.; Lutz, J. F. *Nat. Commun.* **2012**, *3*, 1138.
20. Hibi, Y.; Tokuoka, S.; Terashima, T.; Ouchi, M.; Sawamoto, M. *Polym. Chem.* **2011**, *2*, 341–347.
21. Hibi, Y.; Ouchi, M.; Sawamoto, M. *Angew. Chem., Int. Ed.* **2011**, *50*, 7434–7437.
22. Satoh, K.; Matsuda, M.; Nagai, K.; Kamigaito, M. *J. Am. Chem. Soc.* **2010**, *132*, 10003–10005.

23. Lv, A.; Deng, X.-X.; Li, L.; Li, Z.-L.; Wang, Y.-Z.; Du, F.-S.; Li, Z-C. *Polym. Chem.* **2013**, *4*, 3659–3662.
24. Passerini, M.; Simone, L. *Gazz. Chim. Ital.* **1921**, *51*, 126–129.
25. Kreye, O.; Toth, T.; Meier, M. A. R. *J. Am. Chem. Soc.* **2011**, *133*, 1790–1792.
26. Deng, X.-X.; Li, L.; Li, Z.-L.; Lv, A.; Du, F.-S.; Li, Z.-C. *ACS Macro Lett.* **2012**, 1300–1303.
27. Wang, Y.-Z.; Deng, X.-X.; Li, L.; Li, Z.-L.; Du, F.-S.; Li, Z.-C. *Polym. Chem.* **2013**, *4*, 444–448.
28. Hoyle, C. E.; Lowe, A. B.; Bowman, C. N. *Chem. Soc. Rev.* **2010**, *39*, 1355–1387.
29. Hoyle, C. E.; Bowman, C. N. *Angew. Chem., Int. Ed.* **2010**, *49*, 1540–1573.
30. Derboven, P.; D'hooge, D. R.; Stamenovic, M. M.; Espeel, P.; Marin, G. B.; Du Prez, F. E.; Reyniers, M.-F. *Macromolecules* **2013**, *46*, 1732–1742.

Sequence-Controlled Polymerization Guided by Aryl-Fluoroaryl π-Stacking

Clément Mugemana, Sarah Almahdali, and Valentin O. Rodionov[*]

KAUST Catalysis Center and Division of Physical Sciences and Engineering, King Abdullah University of Science and Technology, Thuwal 23955-6900, Kingdom of Saudi Arabia
[*]E-mail: valentin.rodionov@kaust.edu.sa; Tel: +966 (12) 8084592

The ability to control monomer sequences is essential in macromolecular chemistry. Better sequence control leads to better control over macromolecular folding and self-assembly, which, in turn, would enable control over bulk properties (such as thermal behavior, conductivity and rigidity), as well as mimicking the properties of globular proteins. Here, we present a three-part synopsis of recent advances in research on sequence-controlled polymerization guided by aryl-perfluoroaryl π-π stacking of monomer pairs. We also show that for monomers that are capable of strong associative interactions, the classical reactivity ratio analysis based on Fineman-Ross/terminal reactivity models may lead to an imprecise determination of the monomer alternation mode.

Introduction

Aromatic π-stacking interactions have been studied extensively and are responsible for a wide array of phenomena in chemistry and biology, including organic transformations (*1*), molecular recognition (*2*) and the organization of molecular solids (*3*). Although a considerable amount of work related to the stacking of aromatic rings has focused on phenyl-phenyl interactions, there is a growing interest in the π-stacking interactions between phenyl and perfuoroaryl groups. The first observations of such phenomena were reported by Patrick and Prosser (*4*), who noted that an equimolar mixture of benzene (MP 5.5 °C) and hexafluorobenzene (MP 4 °C) is a crystalline solid with a melting point of 24

°C. The crystalline structure of the adduct is formed by columns of alternating benzene and hexafluorobenzene molecules stacked in a slightly offset parallel manner, with a face-to-face arrangement and a distance of 3.7 Å (*5*, *6*).

The strength of π-π-stacking interactions between perfluoroaryls and aromatic hydrocarbons is similar to that of weak hydrogen bonds, as determined by heat capacity measurements in n-heptane (*7*). Although these interactions are relatively weak, they have been widely used in polymer chemistry and materials science. For example, the addition of octafluoronaphtalene (OFN) to a telechelic polyethylene glycol (PEG) di-functionalized with pyrene yielded a hydrogel cross-linked through OFN-pyrene π-π-stacking interactions. Rheology and fluorescence measurements detected a dramatic increase in the viscosity and the characteristic fluorescence emission of the pyrene-OFN complex, respectively (*8*). Recently, Weck and co-workers reported a linear polystyrene-*b*-poly(dimethylacrylamide)-*b*-poly(2,3,4,5,6-pentafluorostyrene) triblock copolymer prepared by reversible addition-fragmentation chain-transfer (RAFT) polymerization that reproduced, on a basic level, the RNA hairpin turn motif by exploiting π-π-stacking interactions between the electron-rich styrene (St) and the electron-deficient 2,3,4,5,6-pentafluorostyrene (FSt) blocks (*9*). They showed that intramolecular single-chain folding of these polymers occurred in chloroform due to π-π-stacking, while larger aggregates formed via intermolecular interactions in DMF. Similar π-π-stacking interactions were used for crystal structure engineering (*3*, *10*, *11*), for directing solid-state photodimerization reactions (*12*), for the generation of one-dimensional ribbon structures (*13*), and for the stabilization of liquid crystalline phases (*14*).

This chapter highlights recent works that demonstrate the ability of aryl and fluoroaryl monomers to form complexes through π-π stacking; it also shows how this ability can be exploited to generate sequence-controlled copolymers. We discuss several modes, both controlled (RAFT and ATRP) and conventional, of free radical copolymerization of styrenic monomers. Models that could be used to describe the kinetics of these copolymerizations are briefly discussed. Finally, we highlight the application of π-stacking self-assembly to sequence-controlled photopolymerization.

Conventional Free Radical Copolymerization

The free radical copolymerization of styrene (St) and 2,3,4,5,6-pentafluorostyrene (FSt) was first described by Pryor and Huang in 1969. Based on a classical analysis of monomer reactivity ratios, it was suggested that the resulting polymer was alternating (*15*).

More recently, Pugh and coworkers reported a way to tune the strength and extent of π-π interactions by making a copolymer of St and one of two fluorinated styrenes (*16*). The investigated fluoroaryl monomers, FSt and 4-fluorostyrene (4FSt), were chosen as they exist at the two extremes of aromatic fluorination. The copolymers were first synthesized in bulk at 70 °C in the presence of benzoyl peroxide (BOP), an efficient initiator for FSt. The monomer conversion and copolymer composition were determined by ^{1}H NMR. The

alternating nature of the resulting copolymers was supported by two-dimensional HMQC NMR analysis. The monomer reactivity ratios were determined from the copolymer compositions at low comonomer conversions using Fineman-Ross (*17*), Kelen-Tudos (*18*) and nonlinear least-squares methods (*19*). The products of the reactivity ratios of 4FSt and St were found to be close to 1 at 70 °C, as the comonomer units were distributed randomly under these conditions (Table 1). However, the products of the reactivity ratios of St and FSt were found to be close to zero at 70 °C. These results are in agreement with the expected tendency of FSt and St to form π-π complexes during copolymerization. The importance of the π-π stacking interactions between St and FSt was found to decrease with increasing temperature, while the individual and product reactivity ratios were almost constant. The impact of the solvent was also investigated by adding toluene. Little influence was noticed, even though a higher effect was expected, given the competition between toluene and St for π-π complexation with FSt. The influence of these interactions on the thermal behavior of the copolymer was studied through measuring glass transition temperature (T_g). Due to strong π-π interactions, the St-FSt copolymers had high T_g values relative to the mole-averages of each monomer and the miscibility of the corresponding homopolymer blends. On the other hand, St-4FSt's glass transition occurred at the mole-average temperatures typical of immiscible homopolymer blends. At these two extreme levels of fluorination, the authors demonstrated that the strength and/or the extent of π-π stacking interactions between aromatic fluorocarbons and aromatic hydrocarbons correlates with the tendency of their vinyl analogs to alternate ($r_1 = r_2 = r_1 \times r_2 = 0$) in free radical copolymerizations.

Because of the ability of 1-vinylnapthalene (1VN) and 2-vinylnaphtalene (2VN) to form a stable π-π complex with PFSt, these monomers were investigated and the results were compared to the St/FSt system (*20*). The monomer reactivity ratios from free radical copolymerizations of FSt with 1VN and 2VN obtained by ^{1}H NMR revealed that both comonomer pairs have a tendency to alternate in the same manner as the St-FSt copolymer. With decreasing temperatures, the products of the reactivity ratio of the 1VN-FSt system decreased slightly, as was observed in the case of the St-FSt system. This decrease in the reactivity ratio was attributed to the low tendency of 1VN to homopropagate at low temperatures. Although the temperature did not significantly affect the copolymerization reactivity ratios of the 1VN-FSt system, the propensity to alternate was primarily attributed to the influence of the aromatic rings on the frontier molecular orbitals of the vinyl groups (*21*). Nevertheless, the thermal behavior of the resulting copolymers of fluorinated and non-fluorinated styrene derivatives was found to be more appropriate for a qualitative evaluation of the strength and the extent of π-π stacking interactions between aromatic fluorocarbons and aromatic hydrocarbons. The T_g values were elevated relative to their mole-average values, evidently due to stiffening of the polymer backbone by the intramolecular π-π stacking interactions between alternating aromatic fluorocarbon and aromatic hydrocarbon rings. As can be seen in Figure 1, the elevation of the T_g values from their mole-average values correlates with the strength and/or the extent of their π-π stacking interactions. The elevation increases in the following order: St-FSt < 2VN-FSt < 1VN-FSt.

Table 1. Comonomer reactivity ratios (r_{St}, r_{FSt}) and their products determined by the nonlinear least-squares curve-fitting method in the radical copolymerizations of styrene (St) with 2,3,4,5,6-pentafluorostyrene (FSt) and 4-fluorostyrene (4FSt). Adapted from reference (20).

	Reactivity ratios		
Conditions	r_{St}	r_{FSt}	$r_{St} \times r_{FSt}$
St-FSt			
70 °C, bulk	0.62	0.28	0.17
70 °C, toluene	0.47	0.30	0.14
60 °C, bulk	0.43	0.22	0.095
25 °C, bulk	0.22	0.22	0.048
25 °C, toluene	0.30	0.23	0.069
St-4FSt			
70 °C, bulk	0.84	0.74	0.62
25 °C, redox	1.0	0.69	0.69

Weck and co-workers reported an original pathway for making a library of copolymers with varying degrees of alternation by tuning the electron density of the styrenic monomer functionalized in the para-position (22). To that end, 2,3,4,5,6-pentafluorostyrene (FSt) was copolymerized with propargyl styrene derivatives by free radical polymerization. Nucleophilic addition of amines and thiols onto FSt and copper-catalyzed azide-alkyne cycloaddition (CuAAC) were selected for functionalization of the resulting alternating copolymers. Several propargyl-containing styrenes were used as comonomers, including propargyl 4-vinylbenzoate (PVB), propargyl 4-vinylbenzyl ether (PVBE), 4-propargyloxystyrene (POS), N-propargyl 4-vinylaniline (PVA), *N,N*-dipropargyl 4-vinylaniline (DPVA) and *N,N*-propargylmethyl 4-vinylaniline (PMVA) (Scheme 1). The syntheses of the copolymers were performed in 1,4-dioxane at 65 °C, using AIBN as the radical initiator. The reactivity ratios for each monomer pair were determined using the Fineman-Ross (17) and Kelen-Tüdos (18) models (Table 2). The copolymerization of PVB and PVBE with FSt led to random copolymers because these monomers have higher reactivity ratios with FSt relative to styrene. Conversely, POS, DPVA, and PMVA yielded highly alternating copolymers due to very low reactivity ratios. The differences in the degree of alternation were attributed to the electron-withdrawing/donating properties of the substituent on the aromatic ring of the styrene derivatives. As previously mentioned, alternating copolymerization is driven by the electron-deficient nature of FSt and the electron-rich nature of the styrene derivatives. ^{1}H NMR analysis showed that,

for each monomer, the chemical shifts of the vinyl groups were in agreement with the electron-withdrawing/donating influence of the substituents. As a proof of principle, the PPOS-*co*-PFSt copolymer was functionalized with methyl 2-azidoacetate and 6-mercapto-1-hexanol in a two-step procedure *via* CuAAC and then a nucleophilic addition onto the FSt moieties. As expected, both reactions proceeded with excellent conversion and selectivity.
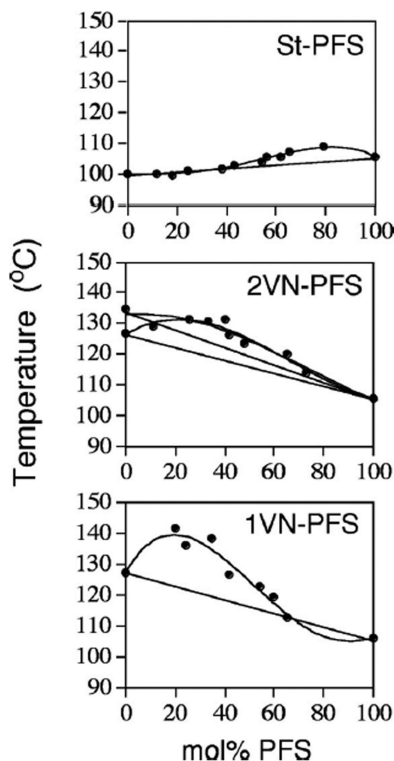
Figure 1. Comparison of the glass transition temperatures of poly(styrene-co-2,3,4,5,6-pentafluorostyrene), poly(2-vinylnaphthalene-co-2,3,4,5,6-pentafluorostyrene), and poly(1-vinylnaphthalene-co-2,3,4,5,6-pentafluorostyrene) copolymers produced by radical copolymerizations in bulk as a function of composition. Reproduced with permission from reference (20). Copyright (2008) Wiley & Sons.
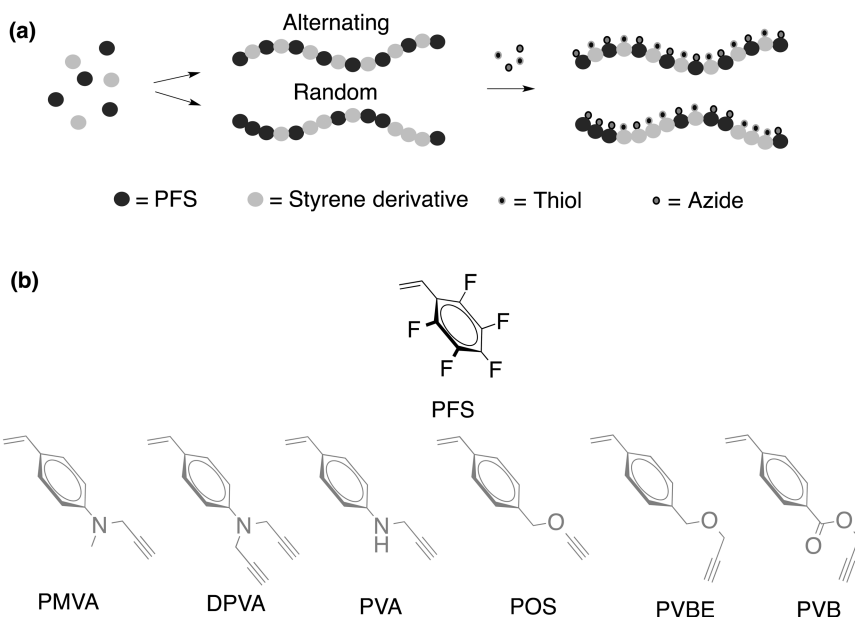
Scheme 1. (A) The strategy for producing functional random and alternating copolymers; (B) Structures of FSt and propargyl-containing styrene derivatives and their abbreviations. Reproduced with permission from reference (22). Copyright (2012) American Chemical Society.

Table 2. Reactivity ratios for different copolymerizations with FSt obtained through the Fineman-Ross and Kelen-Tüdos methods. Reproduced with permission from reference (*22*). Copyright (2012) American Chemical Society.

		Fineman-Ross			Kelen-Tüdos		
M_1	M_2	r_1	r_2	$r_1.r_2$	r_1	r_2	$r_1 r_2$
PVB	PFS	1.66	0.59	0.99	1.39	0.49	0.68
PVBE	PFS	0.58	0.49	0.29	0.69	0.50	0.35
S	PFS	0.52	0.45	0.23	0.53	0.48	0.25
POS	PFS	0.41	0.41	0.17	0.41	0.42	0.17
DPVA	PFS	0.31	0.37	0.11	0.29	0.34	0.10
PMVA	PFS	0.20	0.09	0.02	0.20	0.09	0.02

Controlled Radical Polymerization

In this section, we begin with a short overview describing how π-π stacking interactions impact the rate of polymerization and the tacticity of the polymer, followed by a description of the synthesis of alternating copolymers. The effect of π-π stacking on the atom-transfer radical-polymerizaiton (ATRP) of styrene (St) was explored by Tillman and coworkers (*23*). The range of interaction between the electron-deficient face of the hexafluorobenzene (HFB) and the electron-rich face of the styrenic or polystyrenic phenyl rings was investigated as a function of the polymerization solvent. The solvents explored included both non-aromatic (hexanes and THF) and aromatic (benzene and toluene) solvents. The authors reported that the polymerization rate of St was slowed by the addition of HFB, leading to a decrease in the monomer conversion as compared with analogous reactions in bulk. In addition, when aromatic solvents were used instead of hydrocarbons, the effect of HFB on the rate of the ATRP was minimized, in line with the solvent itself competing with the styrenic phenyl groups for π-π stacking interactions with HFB. The decrease in the polymerization rate in the presence of HFB was attributed to the reduced ability of the terminal phenyl group on the polystyrene chain to stabilize the active polymer radical, pushing the equilibrium further towards the dormant alkyl halide. The ATRP reactions of non-aromatic vinyl monomers, e.g., butyl acrylate and methyl methacryate, were not as sensitive to the presence of HFB due to their lower propensity to participate in π-π stacking interactions.

Extending this work further (*24*), St was polymerized by ATRP in the presence of octafluorotoluene (OFT) (Scheme 2). The presence of one equivalent of OFT nearly halved the rate at which St was consumed, as compared with St polymerized in bulk. Interestingly, this decline occured even when the polymerization solvent was benzene, itself capable of stacking interactions with OFT and HFB. Mechanistic studies revealed that the π-π stacking agent preferentially interacts with St at the early stages of the reaction. As St is consumed, the interaction of HFB or OFT with the polymer phenyl groups becomes more important. Even though the rate of polymerization is not affected by the interactions with the mid-chain phenyl groups, interactions with dormant chain ends alter their ability to form active radicals and lower the k_{ATRP}. The difference between the HFB and OFT as π-π stacking agents can be clearly seen in Figure 2 in which it is clear that 0.5 equivalents of OFT affect the monomer conversion to a greater extent than does HFB at the same concentration. On the other hand, at 1 equivalent of either, the effects become similar. This variation of effect was attributed to stronger π-π stacking interactions of OFT, allowing interactions with more aromatic faces. OFT was able to interact with the dormant chain even in the presence of excess St. The effects of π-π stacking on KATRP were overcome by choosing a stronger Cu ligand, such as is Me6TREN. Under this condition, the presence of HFB did not affect the monomer conversion due to the more active ligand-metal complex. ATRP of FSt in the presence of benzene or toluene, both π-π stackers, exhibited increased monomer conversion as compared with reactions in their absence. This observation is consistent with the idea that π-π stacking interactions are able to increase the stability of the active radical.
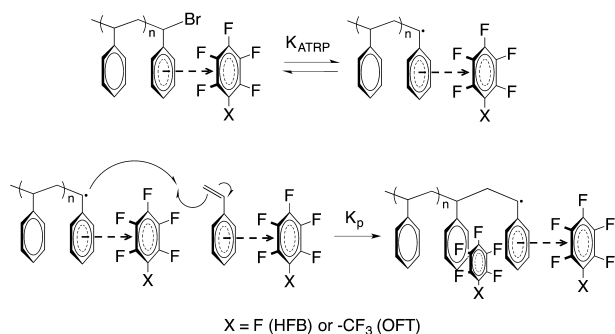
Scheme 2. Proposed effects of π-π stacking on the ATRP of St. Top: effect on K_{ATRP}; Bottom: effect on k_p; Inset: interaction with the BEB initiator. Reproduced with permission from reference (24). Copyright (2012) Wiley & Sons.
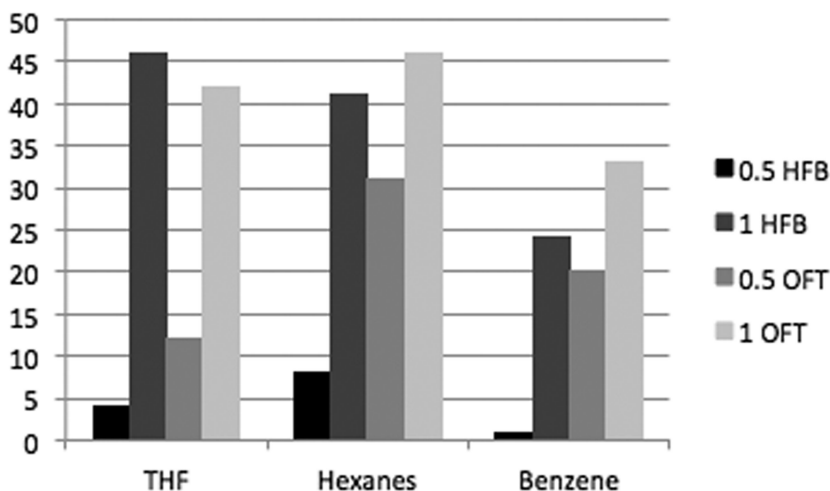
Figure 2. Decrease in monomer conversion in ATRP reactions performed with 0.5 or 1 eq OFT and HFB as compared to reactions run in their absence. Figure reproduced with permission from Wiley. Reproduced with permission from reference (24). Copyright (2012) Wiley & Sons.

Recently, Weck and coworkers investigated a novel strategy of making alternating copolymers by reversible addition-fragmentation chain-transfer (RAFT) polymerization of St and FSt (*25*). Control over the monomer sequence was optimized by changing the polymerization temperature and solvent. Initially, three different chain-transfer agents (CTAs) were investigated (Scheme 3). Among them, CTA **3** was selected because the polymerization proceeded faster without a significant impact on polydispersity. Using the Fineman-Ross (*17*) method to estimate the reactivity ratios and the Kelen-Tudos (*18*) method as a proof of reproducibility, the authors also investigated whether the polymerization reaction proceeded via alternating, random, or block polymerization routes. They

found that polymerizations performed at room temperature led to a higher degree of alternation with a lower polydispersity as compared to RAFT polymerization performed at 65 or 90 °C. The impact of solvent selection was studied by performing the polymerization in DMF and in toluene. In both cases, good control over the molecular weight was reached. In toluene, higher values of reactivity ratios were obtained, which were attributed to an increase of the rate of St homopolymerization relative to the rate of the addition of FSt to a St-terminal growing polymer chain. The lower r_2 (r_{PFS}) value indicated that the FSt homopolymerization was slowed relative to the addition of St onto a FSt-terminal growing polymer chain. This result indicated that the FSt monomer is less reactive, possibly due to π-π stacking interactions with the solvent.
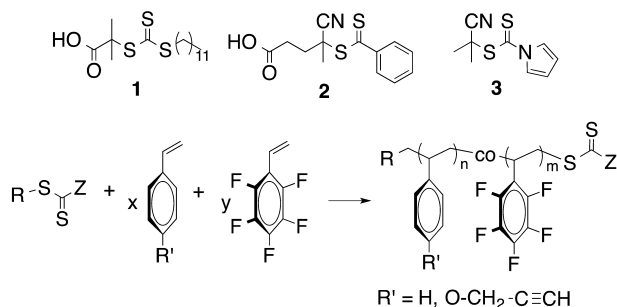
Scheme 3. CTAs 1-3 for the RAFT copolymerization of PFSt and styrenic monomers. Reproduced with permission from reference (25). Copyright (2014) Wiley & Sons.

A related pathway to alternating "clickable" copolymers was reported by Rodionov and coworkers (26). They used a combination of sequence-controlled copolymerization with reliable click reactions to decorate a soluble polymer support efficiently and selectively with co-catalytic groups. A strictly alternating co-polymer of St and FSt was synthesized by ATRP (Scheme 4). The study was further extended to a 4-azidomethylstyrene (N₃St)/FSt system.
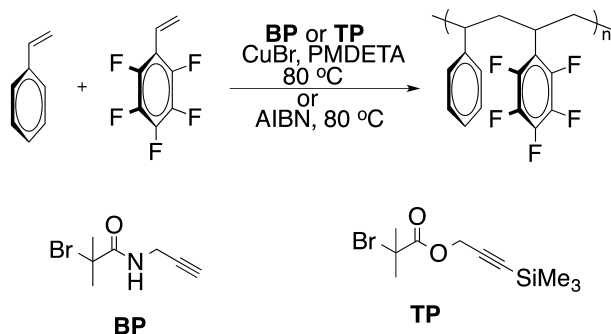
Scheme 4. Copolymerization of St and FSt. Reproduced with permission from reference (26). Copyright (2014) Royal Society of Chemistry.

In contrast to earlier work, in which the copolymerization of St/FSt was performed with conventional free radical polymerization (Section 2), the use of ATRP allowed for better control over the degree and nature of monomer alternation as a function of the polymerization initiator (BP and TP), and of the solvent (trifluorotoluene (TFT), chlorobenzene (CB) dimethyformamide (DMF)). In bulk, the BP and TP initiators led to equal consumption rates for both St/FSt and N_3St/FSt comonomer pairs. The kinetics became much more complex in the presence of solvents. When using BP as the initiator, FSt reacted faster than did St in CB and DMF, while the reverse was observed in TFT. With TP as the initiator, the consumption rates of St and FSt were close in all solvents.

Reactivity ratios for the St/FSt and N_3St/FSt pairs were determined under both controlled polymerization (ATRP) and conventional free radical polymerization (FRP) conditions, where the initiators and solvents were systematically varied. Based on previous work in the field (*16*, *20*, *22*), the assumption that terminal-model kinetics are applicable was initially made (*27*). The terminal model assumes that reactivity depends solely on the identity of the last reactive monomer group and is unaffected by the composition of the remainder of the growing chain (*28*). Subsequently, the reactivity ratios were determined through a Fineman-Ross graphical solution method of the copolymerization equation (*17*). By comparing the obtained values of reactivity ratios in different solvents, only a loose correspondence with observed reaction kinetics was found. While the reaction kinetics indicated wildly variant copolymerization behaviors and preferential monomer incorporation depending on the solvent and the initiator, the differences in apparent reactivity ratios across these conditions were much smaller than expected. Consequently, a Karad-Schneider complex-addition model (*29*) was applied. This model extends the terminal-model by assuming that a 1:1 comonomer complex can be added to a propagating radical. In choosing this model, it was assumed that the existence or disruption of comonomer complexes is related to (and incorporates effects due to) variations in the local monomer concentration, for instance formation of monomer domains in the polymerization solvent.

The mode of monomer alternation in copolymers has been established unambiguously using heteronuclear multiple bond correlation (HMBC) NMR. A ^{1}H-^{13}C HMBC NMR experiment establishes multiple-bond correlations between ^{1}H and ^{13}C nuclei. The carbon in the polymer CH backbone happened to have a well-defined and isolated cross peak with the aromatic ^{1}H of the St ring (Figure 3a and b). By using a ^{13}C projection of this HMBC cross peak, the ^{13}C resonances could be completely filtered out from the CH_2 backbone and from CH groups belonging to FSt moieties (Figure 3c). The resonances at 40.6, 42.0, and 42.8 ppm were then assigned to St-St-St, FSt-St-St, and FSt-St-FSt triads, respectively. Analysis of the ^{13}C projections (Figure 3c) demonstrated that the FSt-St alternation mode in the copolymers was indeed highly variable and depended on both the solvent and the nature of the free radical initiator. Both ATRP and FRP of FSt and St in bulk led to almost perfectly alternating copolymers, P(St$_{50\%}$-*co*-FSt$_{50\%}$) and P(St$_{47\%}$-*co*-FSt$_{53\%}$). Similarly, an alternating polymer (albeit with more randomness) resulted from the ATRP of FSt and N_3St in bulk. ATRP of FSt and St in TFT yielded the P(St$_{60\%}$-*co*-FSt$_{40\%}$)

copolymer, which was almost perfectly random, while FRP in DMF yielded the P(St$_{40\%}$-co-FSt$_{60\%}$) block-copolymer incorporating ~10% (FSt)$_n$ homo-sequences and ~90% alternating (St-FSt)$_n$ sequences. Thus, it was concluded that the best route to alternating (N$_3$)St/FSt copolymers is bulk copolymerization.

While solvent effects can be substantial in radical mechanisms (*30*), in the case of FSt/St copolymerization, it was expected that such effects will influence the PDI and degree of polymerization significantly. This prediction is the opposite of what was found (Figure 4). Furthermore, the structure of the copolymers was significantly influenced by the nature of the free-radical initiator used (that is, by *how* and *where* the polymer chain starts growing) – even though the end of the growing chain should be similar for both ATRP initiators used. This observation led the authors to conclude that the mode of copolymerization of St and FSt was primarily guided by the pre-organization of the monomers. Thus, the customary Fineman-Ross treatment of the copolymerization equation, which relies on the terminal model of reactivity, is *not* the best way to describe reactivity in the St/FSt system. Fineman-Ross reactivity ratios for FSt and St were determined for both ATRP and conventional FRP. As expected, there was only a loose correspondence between these values and NMR structural data.

Strong FSt-St interactions persisted in the polymers. The authors examined the T$_g$ of a range of copolymers with similar number-average molecular weights (M$_n$). T$_g$ values for alternating St-FSt copolymers prepared in bulk were lower than the corresponding values for more random copolymers (such as P(St$_{60\%}$-co-FSt$_{40\%}$)) or block-copolymers. In a perfectly alternating copolymer, each of the St or FSt moieties is coordinatively saturated, which discourages inter-chain interactions. Random copolymers, and especially block-copolymers, are expected to have a much higher degree of chain "stickiness". To test this hypothesis, a P(St$_{20}$-block-FSt$_{19}$) diblock-copolymer was prepared by sequential ATRP. The weight-average molecular weight (M$_w$) of this polymer determined by vapor pressure osmometry (VPO) was a staggering 51900 Da, which is an order of magnitude higher than its M$_n$ estimated from SEC (5800 Da). An alternating copolymer of similar M$_n$ (4800 Da by SEC and NMR) had a VPO-determined M$_w$ of 11500 Da, which suggests a considerably lower propensity for aggregation as compared with the diblock.

The alternating copolymer of N$_3$St/FSt was used as a bifunctional organocatalyst support for a Henry reaction between benzaldehyde and nitromethane (*26*). To that end, the above-described N$_3$St/FSt copolymer was functionalized using orthogonal "click" chemistry: CuAAC and fluoroarene–thiol coupling (FTC). The N$_3$St/FSt copolymer was decorated with amine moieties in the presence of cysteamine and K$_2$CO$_3$ under mild conditions (Scheme 5). The amine-decorated polymer was then reacted with sodium propargylsulfonate using a standard CuAAC protocol. While the reaction was slow in the absence of a catalyst (only 10% conversion after 12 hours), as well as in the presence of an equimolar mixture of P2 and P3, the alternating bifunctional polymer was found to be a competent organocatalyst for the Henry reaction between benzaldehyde and nitromethane. A yield of 76% nitroaldol product was reached in 12 hours with excellent selectivity.
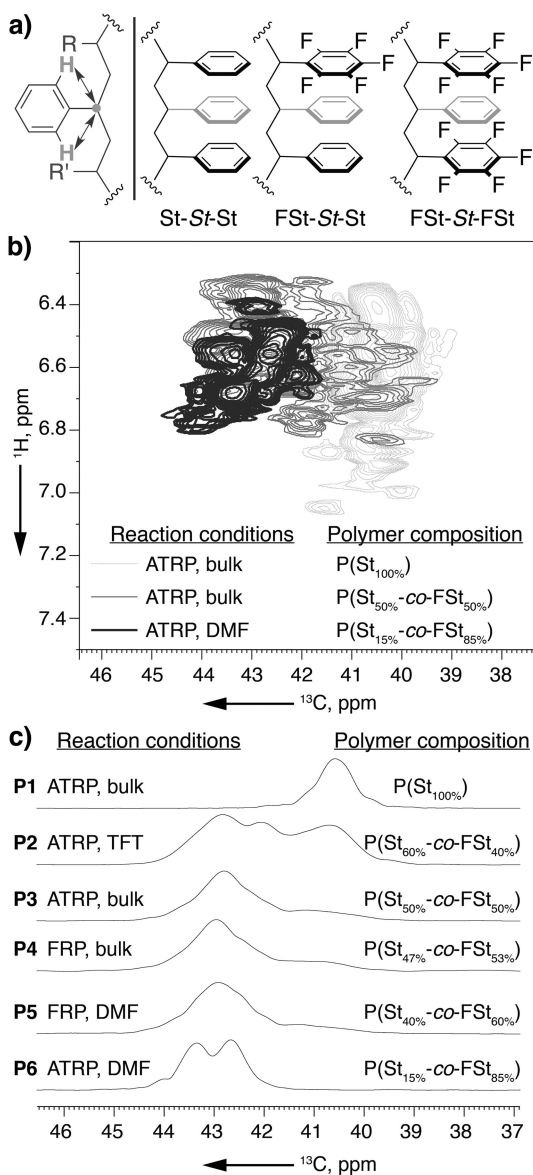
Figure 3. a) The ^{1}H-^{13}C HMBC correlation used in the monomer triad analysis and in three types of St-centered monomer triads. b) Truncated ^{1}H-^{13}C HMBC spectra of polystyrene (light gray) and copolymers (P(St$_{15\%}$-co-FSt$_{85\%}$)) prepared in DMF (black) and P(St$_{50\%}$-co-FSt$_{50\%}$) polymerized in bulk (gray). All three were prepared by ATRP with BP as the initiator. c) ^{13}C projections of ^{1}H-^{13}C HMBC spectra for select copolymers in our study. All ATRP reactions were performed with BP as the initiator and all FRP reactions used AIBN. The P6 polymer was isolated at ~15% monomer conversion. Reproduced with permission from reference (26). Copyright (2014) Royal Society of Chemistry.
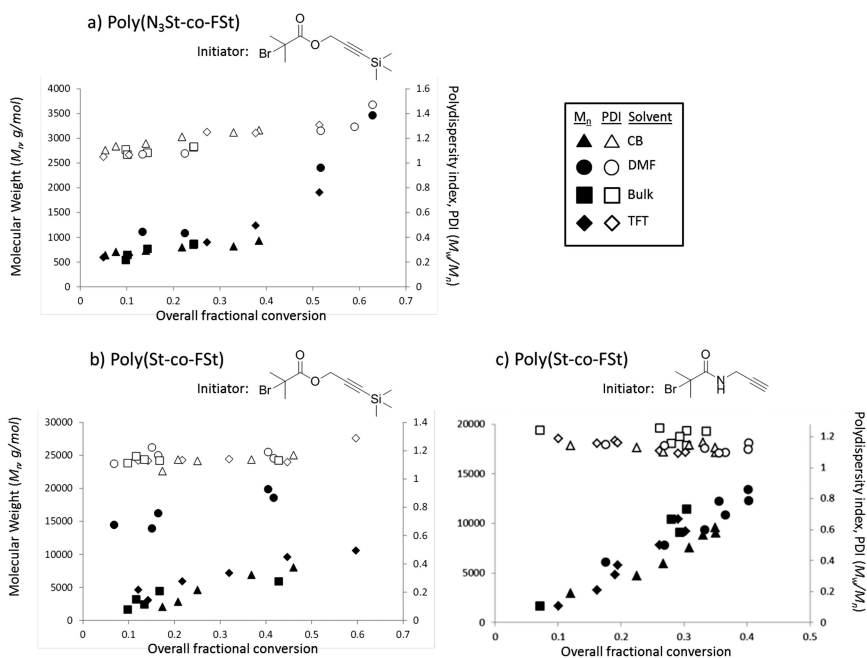
Figure 4. Molecular weight and polydispersity of copolymerization of FSt with N₃St and St at 80°C under various conditions: a) P(N₃St-co-FSt) initiated with TP; b) P(St-co-FSt) initiated with TP; c) P(St-co-FSt) initiated with BP. Reproduced with permission from reference (26). Copyright (2014) Royal Society of Chemistry.
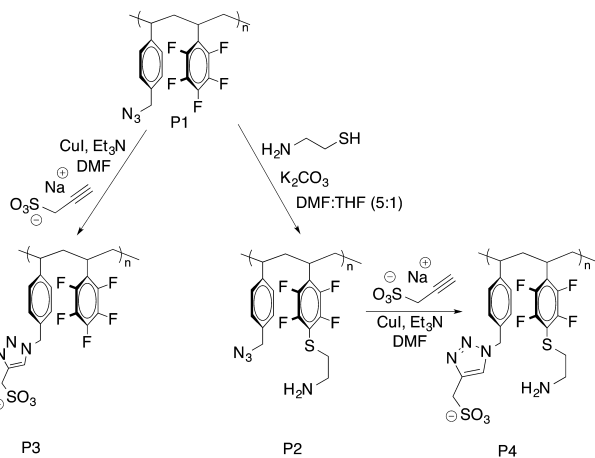
Scheme 5. Synthesis of a bifunctional organocatalyst based on a N₃St-alt-FSt copolymer. Adapted from reference (26).

Photopolymerization

Dougherty and Grubbs reported that the phenyl-perfluorophenyl stacking interactions can be used to align diyne molecules for reactions in the crystalline state (*3*). The required condition for efficient topochemical polymerization of 1,3-diynes is a distance range, "d", between the diyene centers of 4.7-5.2 Å and an angle, Φ, between the molecular and stacking axes of about 45° (Scheme 6). Polymerization in these systems, typically indicated by a color change, can be induced by exposure to heat, UV-light, or γ-rays or by application of pressure to the crystal. Trans-polybutadiyne is the commonly observed product of diyne polymerization, and no examples of cis-polymers in which the diacetylene monomers are packed in a ladder-type structure (Φ= 45°) have been reported so far. π-π stacking interactions between hexafluorobenzene and aromatic hydrocarbons were used, because the observed interplanar distances corresponding to 3.4-3.6 Å were close to the calculated (3.4 Å) optimal diacetylene separation for this kind of polymerization. Fluorinated diphenyldiacetylenes might thus stack in the required geometry for a cis-specific polymerization.
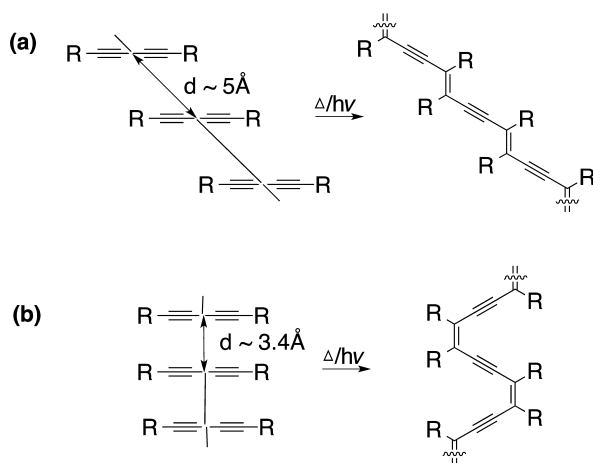
Scheme 6. a) Commonly observed diyne polymerization to yield a trans-polybutadiyene. b) Unprecedented synthesis of a cis-polybutadiyne. Reproduced with permission from reference (3). Copyright (1997) Wiley & Sons.

Diynes **4** and **5** (Figure 5) were used in this fashion as the phenyl-perfluorophenyl stacking interaction motifs (*3*). X-ray structural analysis of **4-5** cocrystals revealed that the di-acetylenes pack alternately in well-ordered stacked columns similar to the benzene/hexafluorobenzene complex. Diyne **6** was expected to stack in a similar manner as the **4-5** cocrystals and then adopt the arrangement required for a cis polymerization. A solid-state, photochemically induced polymerization occurred in crystals **4-5** and **6**. After irradiation with UV light, the unconverted monomer was removed via sublimation, leading to

18% and 50% conversion after 18 and 24 hours of irradiation, respectively. Such diphenylbutadiynes are structurally among the simplest diynes that undergo a polymerization reaction, and they are packed in the crystal to yield novel alternating copolymers (poly(**4-5**)) and regioregular, head-to-tail homopolymers (poly(**6**)).
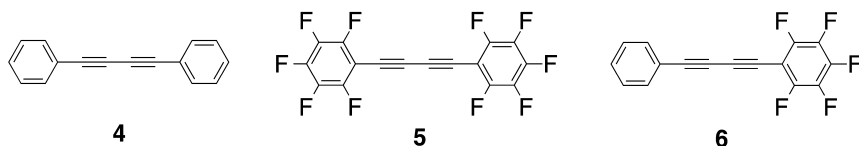
Figure 5. Diphenylbutadiyne 4, decafluorodiphenylbutadiyne 5 and 2,3,4,5,6-pentafluorodiphenydiacetylene 6. Reproduced with permission from reference (3). Copyright (1997) Wiley & Sons.

The same group also reported the use of phenyl-perflurophenyl interactions for the topochemical photocycloaddition of olefins and photopolymerization of diolefins (Figure 6) (*12*). Since the discovery of the first topochemical photopolymerization of a diolefinic molecule, many reports have revealed that the geometrical parameters that dictate reactivity in diolefin systems are the same as those of the monoalkenes. To determine whether the phenylperfluorophenyl interaction could be used to design crystals for photocycloaddition polymerizations, diolefins containing these groups were synthesized and their photoreactivity was investigated. Diene **7** was synthesized by a Heck coupling of the corresponding 1,4-diiodobenzene and styrene to form a colorless crystalline solid. Photolysis of **7** for 20 h yielded a white powder that was virtually insoluble in typical organic solvents. ^{1}H NMR analysis showed that the shift of the cyclobutene protons matched those of the model compound, suggesting that **7** packs in slanted stacks as shown in Figure 6. This conclusion is in agreement with single-crystal X-ray structure analysis. Thus, these stacked phenyl-perfluorophenyl arrangements are responsible for the orientation of the reactive moieties, such that a photochemical cycloaddition reaction is possible for olefins in parallel, separated by less than 4.2 Å.

In 2009, π-π stacking interactions were effectively utilized to control the photoreactions of diphenylhexatrienes in the crystalline state by Sonoda's group (*31*). Irradiation of the crystals of **8**, **9/10**, and **10** induced [2+2] photodimerization and photopolymerization (Figure 7). The order of reactivity was **8** > **9/10** >> **10**. The reaction of **8** was relatively efficient compared with that of typical organic crystals and 100 % conversion was reached after 3 hours of irradiation. In each case, the regio- and stereo-selectivities of the photodimerization were high. On the other hand, the selectivity was much lower for the formation of trimer and higher oligomers. The photoproducts from **8** and **9/10** were amorphous due to the non-planar and bulky structures of the cyclobutane products, as evidenced by powder XRD and polarizing optical microscopy. The high reaction efficiency of **8** was attributed to much easier molecular movements in amorphous solids than

in ordinary rigid crystals. The high selectivity in the dimerization clearly results from the anti-parallel pre-alignment of the molecules in the original crystal. The formation of trimers and higher oligomers occurred randomly in the disordered crystal structure produced by the dimer formation, which explained the low selectivity in the trimer formation relative to that in the dimer formation.
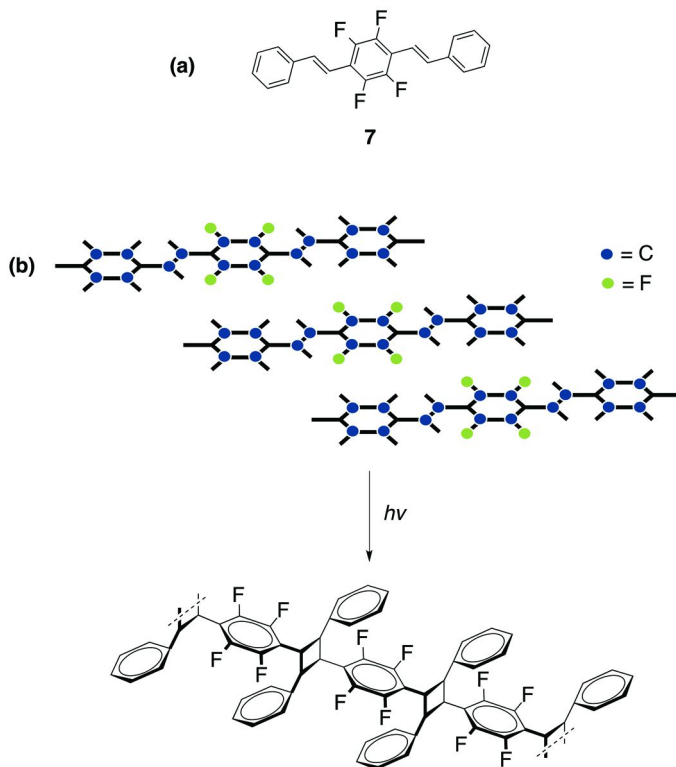
Figure 6. (a) Trans, trans-1,4-bis(2-phenyllethenyl)-2,3,5,6-tetrafluorobenzene. (b) Molecular packing diagram of diolefin 9 and the proposed structure of poly(9). Reproduced with permission from reference (12). Copyright (1998) American Chemical Society.
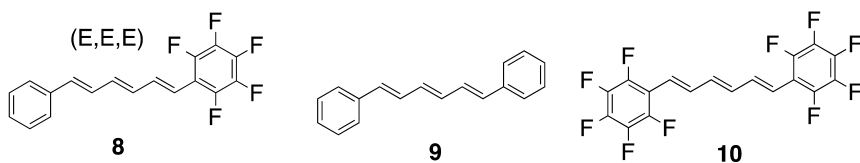
Figure 7. (E,E,E)-1-Perfluorophenyl-6-phenyl-1,3,5-hexatriene 8; (E,E,E)-1,6-Diphenyl-1,3,5-hexatriene 9; (E,E,E)-1,6-Bis(perfluorophenyl)-1,3,5-hexatriene 10. Reproduced with permission from reference (31). Copyright (2009) Elsevier.

Conclusion

A three-part overview of recent advances in sequence-controlled polymerization guided by π-stacking was presented. Free radical polymerization, both controlled and conventional, was described as a straightforward route to alternating copolymers. It is suggested that for monomers that are capable of strong associative interactions (such as FSt and St), the classical reactivity ratio analysis based on Fineman-Ross/terminal reactivity models may lead to an imprecise determination of the monomer alternation mode.

The possibility of controlling monomer sequences in macromolecular chemistry is of great use and paves the way for versatile and highly attractive possibilities. Among them, we can imagine precise control over macromolecular folding and self-assembly, with the possibility of mimicking the properties of globular proteins such as enzymes and transporters. In addition, monomer sequence control will allow for perfect control over bulk properties of materials, including thermal behavior, conductivity, rigidity, and elasticity.

Abbreviations

^{1}H NMR	^{1}H-Nuclear Magnetic Resonance
1VN	1-vinylnapthalene
2VN	2-vinylnaphtalene
4FSt	4-fluorostyrene
AIBN	Azobisisobutyronitrile
ATRP	Atom transfer radical polymerization
BOP	Benzoyl peroxide
BP	2-bromo-2-methyl-N-(prop-2-yn-1-yl) propanamide
CB	Chlorobenzene
CTA	Chain-transfer agent
CuAAC	Copper(I)-catalyzed alkyne-azide cycloaddition
DMAA	Dimethylacryl amide
DMF	Dimethylformamide
DVPA	N,N-dipropargyl 4-vinylaniline
FRP	Free radical polymerization
FSt	2,3,4,5,6-pentafluorostyrene
FTC	Fluoroarene–thiol coupling
HFB	Hexafluorobenzene
HMBC	Heteronuclear multi bond correlation
N$_3$St	4-azidomethylstyrene
OFN	Octafluoronaphtalene
OFT	Octafluorotoluene
PDI	Polydispersity index
PEG	Polytheylene glycol
PMVA	N,N-propargylmethyl 4-vinylaniline
POS	N-propargyl 4-vinylaniline
PVA	N-propargyl 4-vinylaniline
PVB	Propargyl 4-vinylbenzoate

PVBE	Propargyl 4-vinylbenzyl ether
RAFT	Reversible addition fragmentation chain transfer
St	Styrene
TFT	Trifluorotoluene
T_g	Glass transition temperature
THF	Tetrahydrofuran
TP	3-(trimethylsilyl)prop-2-yn-1-yl 2-bromo-2-methylpropanoate
UV	Ultraviolet
PSt	Polystyrene
PFSt	Poly(2,3,4,5,6-pentafluorostyrene)
XRD	X-ray diffraction

References

1. Trost, B. M.; Okrongly, D.; Belletire, J. L. *J. Am. Chem. Soc.* **1980**, *102*, 7595–7596.
2. Benzing, T.; Tjivikua, T.; Wolfe, J.; Rebek, J. *Science* **1988**, *242*, 266–268.
3. Coates, G. W.; Dunn, A. R.; Henling, L. M.; Dougherty, D. A.; Grubbs, R. H. *Angew. Chem., Int. Ed.* **1997**, *36*, 248–251.
4. Patrick, C. R.; Prosser, G. S. *Nature* **1960**, *187*, 1021–1021.
5. Gabbaï, F. P.; Gardinier, J. R. *J. Chem. Soc., Dalton Trans.* **2000**, 2861–2865.
6. Bartsch, E.; Bertagnolli, H.; Chieux, P. *Ber. Bunsen Phys. Chem.* **1986**, *90*, 34–46.
7. Perez-Casas, S.; Hernandez-Trujillo, J.; Costas, M. *J. Phys. Chem. B.* **2003**, *107*, 4167–4174.
8. Kilbinger, A. F. M.; Grubbs, R. H. *Angew. Chem., Int. Ed.* **2002**, *41*, 1563–1566.
9. Lu, J.; Ten Brummelhuis, N.; Weck, M. *Chem. Commun.* **2014**, *50*, 6225–6227.
10. Knapp, C.; Lork, E.; Mews, R.; Zibarev, A. V. *Eur. J. Inorg. Chem.* **2004**, *2004*, 2446–2451.
11. Feast, W. J.; Lovenich, P. W.; Puschmann, H.; Taliani, C. *Chem. Commun.* **2001**, 505–506.
12. Coates, G. W.; Dunn, A. R.; Henling, L. M.; Ziller, J. W.; Lobkovsky, E. B.; Grubbs, R. H. *J. Am. Chem. Soc.* **1998**, *120*, 3641–3649.
13. Messina, M. T.; Metrangolo, P.; Pappalardo, S.; Parisi, M. E.; Pilati, T.; Resnati, G. *Chem. Eur. J.* **2000**, *6*, 3495–3500.
14. Weck, M.; Dunn, A. R.; Matsumoto, K.; Coates, G. W.; Lobkovsky, E. B.; Grubbs, R. H. *Angew. Chem, Int. Ed.* **1999**, *38*, 2741–2745.
15. Pryor, W. A.; Huang, T.-L. *Macromolecules* **1969**, *2*, 70–77.
16. Pugh, C.; Tang, C. N.; Paz-Pazos, M.; Samtani, O.; Dao, A. H. *Macromolecules* **2007**, *40*, 8178–8188.
17. Fineman, M.; Ross, S. D. *J. Polym. Sci.* **1950**, *5*, 259–262.
18. Kelen, T.; Tudos, F. *J. Macromol. Sci. Chem.* **1975**, *9*, 1–27.
19. Tidwell, P. W.; Mortimer, G. A. *J. Polym. Sci., Part A* **1965**, *3*, 369–387.

20. Pugh, C.; Paz-Pazos, M.; Tang, C. N. *J. Polym. Sci., Polym. Chem.* **2008**, *47*, 331–345.

21. Fleming, I. *Frontier Orbitals and Organic Chem Reactions*; Wiley: London, 1976.

22. ten Brummelhuis, N.; Weck, M. *ACS Macro Lett.* **2012**, *1*, 1216–1218.

23. Pickett, P. D.; Tillman, E. S.; Voter, A. F. *Polymer* **2011**, *52*, 55–62.

24. Pickett, P. D.; Radzinski, S. C.; Tillman, E. S. *J. Polym. Sci., Polym. Chem.* **2012**, *50*, 156–165.

25. ten Brummelhuis, N.; Weck, M. *J. Polym. Sci., Polym. Chem.* **2014**, *52*, 1555–1559.

26. O'Shea, J. P.; Solovyeva, V.; Guo, X. R.; Zhao, J. P.; Hadjichristidis, N.; Rodionov, V. O. *Polym. Chem.* **2014**, *5*, 698–701.

27. Mayo, F. R.; Lewis, F. M. *J. Am. Chem. Soc.* **1944**, *66*, 1594–1601.

28. Odian, G. G. *Principles of polymerization*, 4th ed.; Wiley-Interscience: Hoboken, NJ, 2004.

29. Karad, P.; Schneider, C. *J. Polym. Sci., Polym. Chem.* **1978**, *16*, 1137–1145.

30. Litwinienko, G.; Beckwith, A. L. J.; Ingold, K. U. *Chem. Soc. Rev.* **2011**, *40*, 2157–2163.

31. Sonoda, Y.; Goto, M.; Tsuzuki, S.; Akiyama, H.; Tamaoki, N. *J. Fluorine Chem.* **2009**, *130*, 151–157.

Sequence-Regulated Polymers via Living Radical Polymerization: From Design to Properties and Functions

Takaya Terashima* and Mitsuo Sawamoto*

Department of Polymer Chemistry, Graduate School of Engineering, Kyoto University, Katsura, Nishikyo-ku, Kyoto 615-8510, Japan
*E-mail: terashima@living.polym.kyoto-u.ac.jp (T.T.)
*E-mail: sawamoto@living.polym.kyoto-u.ac.jp (M.S.)

Sequence-regulated polymers have been recently designed and synthesized via ruthenium-catalyzed living radical polymerization for unique physical properties and functions. This chapter summarizes the recent advances on the following topics: 1) gradient copolymers via concurrent tandem catalysis of living radical polymerization and in situ transesterification of methacrylates with alcohols; 2) cyclopolymers comprising in-chain large poly(ethylene glycol) (PEG) rings via cation template-assisted cyclopolymerization of PEG dimethacrylates for cation recognition; 3) single-chain folding of amphiphilic random copolymers into compact unimer micelles in water with intramolecular hydrophobic interaction.

Introduction

Polymers consist of monomer units that are consecutively connected and *"sequenced"* along a chain. Thus, the sequence of monomers and functional groups is no doubt an essential factor on primary structure control of polymers to modulate properties and create functions (*1*). Protein and enzymes in natural polymers have perfectly controlled primary structure (molecular weight, tacticity, sequence) to form specific higher-order (secondary, tertiary) structures, actually performing selective recognition and catalysis. Thanks to recent advances of precision polymerization systems, several factors of primary structure (molecular weight, composition and sequences of monomers and

functional groups, terminal structure, and tacticity etc.) can be controlled. In particular, living radical polymerization (*2–10*) is a powerful tool to design well-controlled functional polymers owing to high functionality tolerance. For unique physical properties and functions, we have recently investigated the synthesis of various sequence-controlled polymers via ruthenium-catalyzed living radical polymerization (*2, 3*).

In this chapter, we review recent advances on the design, properties, and functions of the following sequence-controlled polymers (Figure 1).

1. **Gradient Sequence-Regulated Copolymers via Tandem Catalysis.** Concurrent and/or sequential tandem catalysis of living radical polymerization and in situ monomer transesterification with alcohols was developed as a versatile strategy to synthesize various gradient sequence-controlled copolymers in one-pot (*11–13*). Importantly, the gradient sequence can be catalytically controlled on demand.
2. **Cyclopolymers via Cation Template-Assisted Cyclopolymerization.** Cyclopolymers comprising in-chain large poly(ethylene glycol) rings were directly prepared by cation template-assisted living radical cyclopolymerization for unique and selective cation recognition (*14*).
3. **Single-Chain Folding of Amphiphilic Random Copolymers in Water.** Well-controlled amphiphilic random copolymers self-folded in water with intramolecular hydrophobic interaction to be compact, dynamic unimer micelles (*15*).
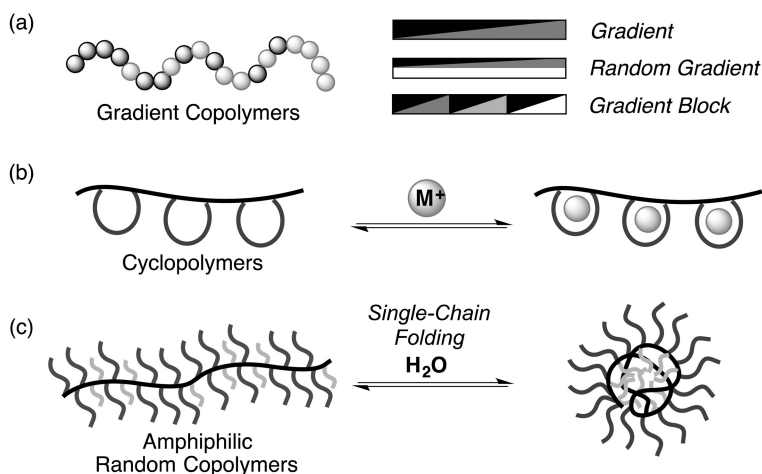
Figure 1. Sequence-regulated polymers via living radical polymerization: (a) gradient sequence-regulated copolymers; (b) cyclopolymers for cation recognition; (c) self-folding of amphiphilic random copolymers in water.

1. Gradient Sequence-Regulated Copolymers via Tandem Catalysis

Gradient Copolymers

Gradient copolymers are one kind of sequence-controlled copolymers with instantaneous comonomer composition that gradually changes from one monomer rich at an initiating terminal (α-end) to another at a growing terminal (ω-end) along a chain (Figure 1a). As a result of the characteristic monomer sequence, gradient copolymers afford physical properties different from random and block copolymers (16). In general, gradient copolymers are obtained from the two methodologies: 1) living polymerization of two monomers with different reactivity; 2) continuous addition of a second monomer into living polymerization of a monomer. The former is easy and convenient but involves the limitation of sequence control and monomer combination (e.g. living radical polymerization of methacrylates and acrylates). The latter is in turn controllable and versatile (applicable to various monomers) but requires the complicated set-up in laboratory level (syringe pump etc.) to keep and control monomer addition. All methacrylate gradient copolymers are often obtained from the latter method since the copolymerization reactivity of methacrylates (r_1, r_2) is generally independent of the pendant structures. Thus, methacrylate gradient copolymers have been not so accessible.

Potential of Living Radical Polymerization for Tandem Catalysis

Tandem catalysis is an intriguing one-pot synthetic approach much more efficient and convenient than multi-step synthesis, in which different two or more reactions simultaneously and/or sequentially undergo in a single vessel to directly give products without any purification and/or isolation of intermediates (17–23). The key for efficient tandem catalysis is the compatibility of respective active intermediates and chemical reagents (catalysts, substrates) in different reactions; if one component deactivates another, tandem catalysis never proceeds. Metal catalysts, even in a single component, induce various different reactions dependent on conditions and substrates to be often utilized for tandem reactions (21, 22).

Transition metal-catalyzed living radical polymerization including atom transfer radical polymerization (ATRP) is typically mediated by metal complexes of ruthenium, copper, iron, and nickel in conjunction with alkyl halide initiators (2–5). Among them, ruthenium-catalyzed system is applicable to the direct polymerization of polar functional monomers (hydroxyl group, amine, acid, ionic groups etc.) without any protection even in alcohols and/or water owing to the high tolerance of both the neutral propagating radicals and ruthenium complexes to the functional groups (24, 25). Thus, ruthenium-catalyzed living radical polymerization is potentially suitable as one reaction for tandem catalysis

coupled with non radical-mediated reactions. Additionally, metal alkoxide cocatalysts (aluminum or titanium isopropoxides) are also often employed in ruthenium-mediated polymerization to efficiently promote catalytic cycles (*3, 26, 27*). The diverse catalysis of metal alkoxides is also a potential advantage of this polymerization system for tandem catalysis.

Gradient Copolymers via Concurrent Tandem Catalysis with in Situ Transesterification

Aluminum or titanium isopropoxides [Al(O*i*-Pr)$_3$, Ti(O*i*-Pr)$_4$] are effective not only as cocatalysts for ruthenium-catalyzed living radical polymerization but also as catalysts for transesterification with alcohols (*28*). Focusing on the dual activities, we have developed concurrent tandem catalysis of ruthenium-catalyzed living radical polymerization and metal alkoxide-mediated transesterification of methacrylates with alcohols to synthesize various gradient copolymers in one pot (Figure 2) (*11–13*).
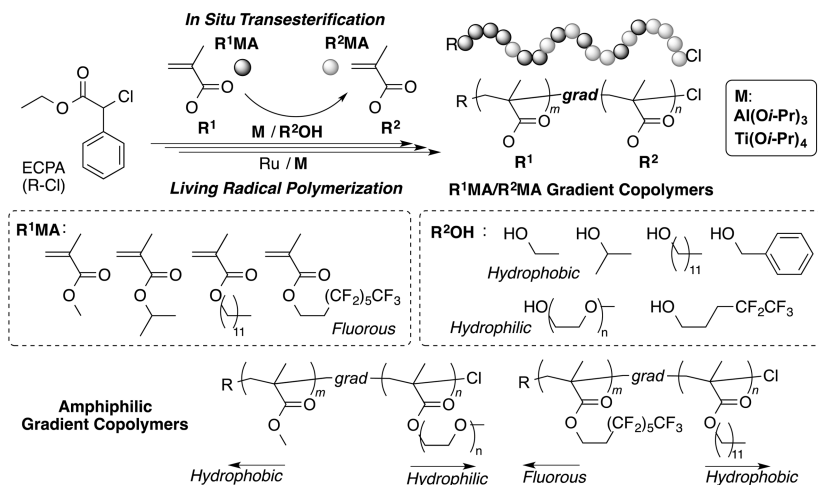
Figure 2. Gradient copolymers via concurrent tandem catalysis of living radical polymerization and in situ monomer transesterification with alcohols.

Typically, methyl methacrylate (MMA) was polymerized with a ruthenium catalyst [Ru(Ind)Cl(PPh$_3$)$_2$] and a chloride initiator (ECPA) in the presence of Al(O*i*-Pr)$_3$ and ethanol at 80 °C (*11, 12*). The aluminum alkoxide efficiently and simultaneously induced in situ transesterification of MMA with ethanol into ethyl methacrylate (EMA) during living polymerization; monomer composition in the solution gradually changes from MMA alone to EMA rich mixture. Importantly, the transesterification was selective for monomers (not for the copolymers). As

a result, the concurrent tandem catalysis provides gradient copolymers from MMA at the initiating terminal (α-end) to EMA at growing (chlorine) terminal (ω-end) along a chain, where the gradient sequence along a chain directly reflects the change of instantaneous monomer composition in polymerization solutions. Importantly, in situ transesterification never interfered with ruthenium-catalyzed polymerization.

Compared with conventional synthetic methods for gradient copolymers, this tandem catalysis has lots of advantages. First, diverse, common alcohols and methacrylates easily leads to a wide variety of gradient copolymers without monomer preparation (*11*, *12*). Except for tertiary alcohols (e.g. *t*-BuOH), various primary and secondary alcohols such as ethanol, 2-propanol, 1-dodecanol, benzyl alcohol, poly(oligo)(ethylene glycol) methyl ethers [PEG-OH: $CH_3(OCH_2CH_2)_nOH$; n = 1 – 12], and fluoroalcohols are available in this system. Amphiphilic gradient copolymers from MMA (hydrophobic) to PEGMA (hydrophilic) are also directly obtained with MMA, PEG-OH, and Ti(O*i*-Pr)$_4$.

Next, the gradient sequence can be catalytically controlled by the reaction conditions to be freely tunable (*12*). In MMA/EMA gradient copolymers obtained with MMA, ethanol, and Al(O*i*-Pr)$_3$, the instantaneous gradient composition (gradient slope) of EMA increased with increasing aluminum (10-40 mM) and ethanol (2.0-6.5 M) concentration, and temperature (40-80 °C).

Molecular sieves further enhanced the efficiency and yield of in situ transesterification of MMA with alcohols by the removal of generating methanol (*13*). Typically, the combination of molecular sieves 4A and a small amount of titanium isopropoxide (5 mM) with 1-dodecanol fully synchronized in situ transesterification of MMA into DMA and the copolymerization to give a gradient copolymer with the sequence distribution almost linearly changing from MMA to DMA. Owing to the gradient sequence, the MMA/DMA gradient copolymer exhibited extremely broad range of glass transition temperature (~170 °C), different from MMA/DMA random or block copolymers (*13*).

Multi-Sequence Control via Tandem Catalysis

Multi-sequence-controlled copolymers are also directly synthesized by this tandem polymerization (Figure 3) (*12*). Because of the steric hindrance of the pendant, tert-butyl methacrylate (*t*-BuMA) was inert for titanium-mediated transesterification with alcohols. Fortunately, this trend afforded unique random gradient copolymers as a new category of sequence-controlled polymers. For example, tandem copolymerization of MMA and *t*-BuMA with ethanol gives copolymers comprising both gradient distribution from MMA to EMA and random incorporation of *t*-BuMA. Iterative process of concurrent tandem polymerization of MMA with different alcohols in turn successfully leads to gradient block copolymers, demonstrating that in situ transesterification never deactivates the propagating radicals and the terminal carbon-halogen bond.
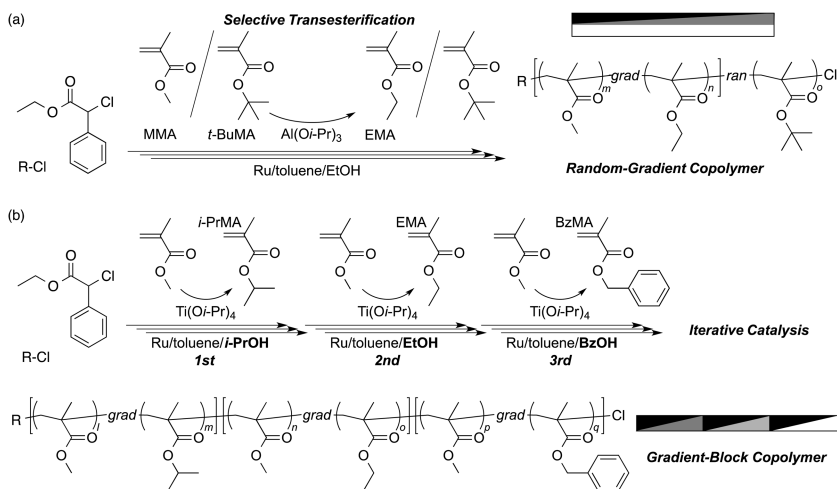
Figure 3. (a) Random gradient copolymers via concurrent tandem polymerization with in situ selective transesterification of monomers. (b) Gradient block copolymers via iterative concurrent tandem polymerization.

Additionally, random or block copolymerization is achieved by changing the starting period of monomer transesterification (*12*). Typically, MMA/EMA random copolymers are obtained from living copolymerization of MMA and EMA after the equilibrium state of prior transesterification of MMA into EMA, whereas MMA/EMA block-like copolymers are formed via the in situ fast transesterification of MMA into EMA after the middle stage of polymerization.   Thus, tandem living radical polymerization coupled with monomer transesterification is one of the most convenient and versatile strategies to access sequence-controlled copolymers in one-pot.

2. Cyclopolymers via Cation Template-Assisted Cyclopolymerization

Cyclopolymerization

In chain polymerization, divinyl monomers potentially undergo various reaction routes including not only propagation (intermolecular addition) as well as common monovinyl monomers but also inter and/or intra-molecular crosslinking and intramolecular cyclization (Figure 4). A major role of divinyl compounds is as a linking agent to produce macroscopic gels, soluble and/or dispersed microgels, and hyperbranched polymers. In this case, the propagation of divinyl monomers for olefin-bearing polymers and the intermolecular crosslinking of the polymers through the pendant olefin simultaneously and competitively proceed (Figure 4a,b) (*29–32*).
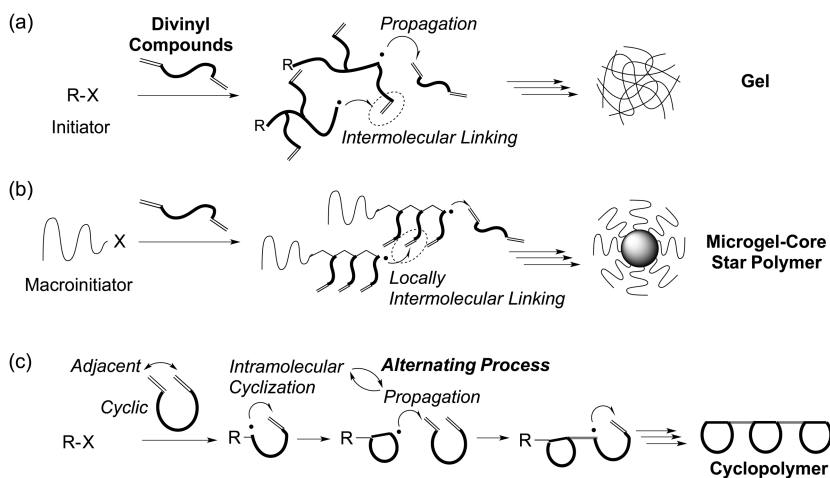
Figure 4. Polymerization of divinyl compounds: (a) gelation; (b) microgel-core star polymers via the linking reaction of macroinitiators (arms); (c) cyclopolymers via the alternating process of intermolecular addition (propagation) and intramolecular cyclization.

In contrast, cyclopolymerization of divinyl compounds via the precisely alternating process of intramolecular cyclization and intermolecular addition gives cyclopolymers, i.e. soluble linear polymers comprising consecutive in-chain rings (Figure 4c) (*33–40*). Selective cyclopolymerization without gelation involves efficient intramolecular cyclization of divinyl monomers so as to incorporate both of the two olefins into a main chain without dangling olefins in polymers. The key is to select and/or design divinyl monomers that carry two olefins at originally adjacent location through a spacer. Thus, cyclopolymerization has been generally investigated with divinyl monomers consisting of short (for 5 or 6-membered rings), rigid, and elaborate spacer units (*38–40*). Cyclopolymers are attractive polymeric materials for unique functions originating from the in-chain cyclic units (molecular recognition etc.) (*35*, *36*). However, the direct incorporation of large and functional cyclic units into polymers is difficult in principle.

Potassium Template-Assisted Cyclopolymerization

Poly(ethylene glycol) (PEG) and crown ethers interact with metal cations such as sodium and potassium (*41*). Focusing on the cation recognition properties (*42*), we have developed cation template-assisted cyclopolymerization of PEG dimethacrylates with a precision PEG spacer [PEGnDMA, PEG spacer: -$O(CH_2CH_2O)_n$-; n = 4, 5, 6, 8]. This is a one-pot approach to produce cyclopolymers with in-chain large cyclized PEGs (PPEGnDMAs), "polymeric pseudo-crown ethers", for efficient and selective cation recognition (Figure 5) (*14*).
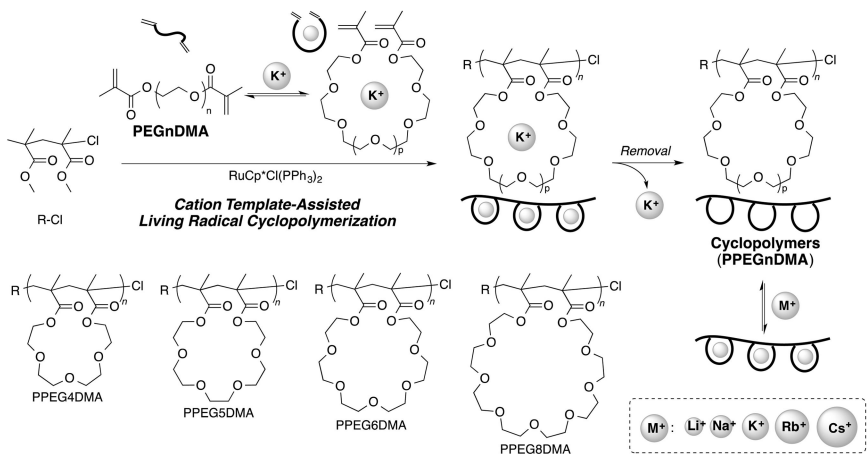
Figure 5. Potassium template-assisted living radical cyclopolymerization of PEGnDMAs for cyclopolymers (PPEGnDMA).

The point is to select a size-fit metal cation for PEGnDMA, assuming that the PEG spacer interacts with a metal cation to dynamically form pseudo cyclic monomers bringing two olefins at close position. Typically, potassium cation (KPF$_6$) interacted with PEG6DMA at 1:1 mole ratio in cyclohexanone/acetone-d_6 (confirmed by ^{1}H NMR measurement and Job plots), to be employed as a template for PEG6DMA cyclopolymerization.

In the presence of KPF$_6$, PEG6DMA was efficiently and homogeneously polymerized with a ruthenium catalyst [RuCp*Cl(PPh$_3$)$_2$/n-Bu$_3$N] and a chloride initiator [H-(MMA)$_2$-Cl] in cyclohexanone under diluted conditions ([PEG6DMA] = 25 - 100 mM) to give well-controlled cyclopolymers with in-chain 24-membered PEG rings (PPEG6DMA) in high cyclization efficiency (>90%). In contrast, non-template PEG6DMA led to high molecular weight products and insoluble gels via intermolecular polymer linking. The potassium template was further effective for PEG6DMA-random or block copolymers and PEG5DMA and PEG8DMA cyclopolymers.

Properties and Cation Recognition

CycloPEG-polymers (PPEGnDMAs) showed unique properties and cation recognition. The thermal mobility of cyclic PEG units decreased with decreasing the spacer length (n), confirmed by ^{13}C NMR spin-lattice relaxation time (T_1) measurements. Thanks to amphiphilic and thermosensitive PEGs, PPEG6DMA and PPEG8DMA were soluble in water at room temperature and reversibly showed lower critical solution temperature (LCST)-type phase separation without hysteresis [LCST = ~35 (PPEG6DMA), ~50 (PPEG8DMA) °C].

PPEG6DMA exhibited 1:1 recognition for Li$^+$, Na$^+$, K$^+$, and Rb$^+$ with the in-chain PEG rings, more efficiently than the original monomer (Figure 6). The efficiency to bind a potassium cation (K_a: association constant) increased as the

following: PEG6DMA (~70 M^{-1}) < PPEG6DMA (~130 M^{-1}) ~ PEG6DMA/MMA random copolymer (~140 M^{-1}) < PPEG8DMA (~460 M^{-1}). The large K_a for PPEG8DMA indicates that relatively long and flexible cyclized PEG8 units adaptively fit and thereby more efficiently bind K$^+$ than cyclized PEG6 units. Owing to the consecutive cycloPEG units, PPEG6DMA recognized one large Cs$^+$ with two PEG rings (1:2 recognition) in contrast to PEG6DMA and 18-crown-6 (1:1 recognition). More importantly, PPEG6DMA selectively recognized Na$^+$ over Li$^+$ or Bu$_4$N$^+$ and in turn did K$^+$ over Na$^+$ in competitive experiments, directly confirmed by ^{23}Na NMR. Such selectivity was never observed for PEG linear pendant polymers (PPEG3MA).
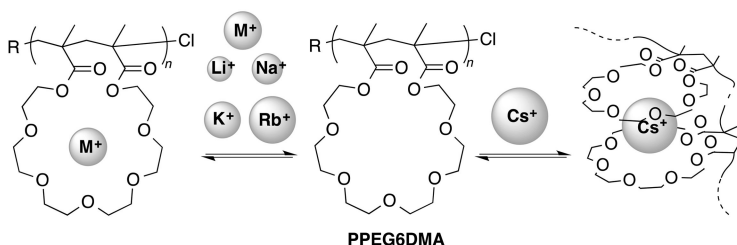
PPEG6DMA

Figure 6. Recognition of metal cations with PPEG6DMA.

3. Single Chain-Folding of Amphiphilic Random Copolymers in Water

Single Chain-Folding Spaces

With precisely controlled primary structure and/or functionalization (amphiphilic properties), polymers form three-dimensional compartments via chemical crosslinking or physical association. The representatives are given: 1) microgel-core star polymers via the intermolecular crosslinking of linear arm polymers (living polymers or macroinitiators) with bifunctional linking agents (divinyl compounds) (Figure 4b) (*29–32*); 2) micelles, vesicles, and polymersomes via the intermolecular association of amphiphilic (functional) block copolymers with physical interaction (hydrophobic, hydrogen-bonding, ionic etc.) (*43*, *44*); 3) unimer micelles and single-chain polymeric nanoparticles (SCPNs) via the "intramolecular" single-chain folding of amphiphilic (functional) random copolymers with physical interaction or chemical crosslinking (*15*, *45–55*).

Among them, unimer micelles and SCPNs (the third category) uniquely afford single-chain compartments and thereby are often designed as artificial mimics of natural proteins and enzymes (*49–54*). Typically, amphiphilic PEGMA/BTAMA random copolymers carrying hydrophilic poly(ethylene glycol) chains and hydrophobic, chiral benzene-1,3,5-tricarboxamide (BTA) units efficiently self-fold in water via the helical self-assembly of the BTA pendants with hydrogen bond (Figure 7) (*50*, *52–54*). The folding compartments with

catalysts were further applicable as enzyme-mimic nanoreactors in water (*50, 53, 54*).
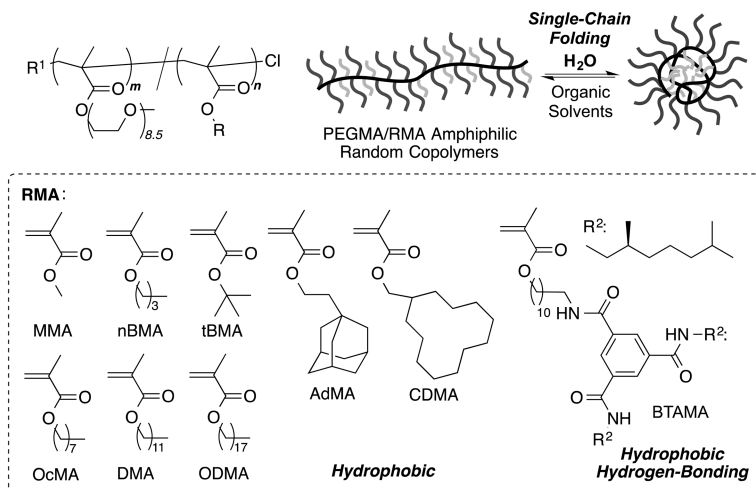
Figure 7. Single-chain folding of PEGMA/RMA amphiphilic random copolymers in water.

More importantly, unimer micelles and SCPNs directly reflect the primary structure (molecular weight, composition of monomers and functional groups, end-functional groups etc.) of linear precursor polymers to be much more precisely designable and controllable as desired than conventional multi-chain compartments. However, the design scope of precursor polymers for single-chain folding has been not established yet.

Self-Folding Polymers with Hydrophobic Interaction in Water

Given these backgrounds, we synthesized various amphiphilic PEGMA/RMA random copolymers with hydrophilic PEG chains and hydrophobic alkyl pendants [R: -$(CH_2)_nH$; n = 1 - 18] via ruthenium-catalyzed living radical polymerization (Figure 7) (*15*). The random copolymers are designed as one of the simplest precursors that self-fold with only hydrophobic interaction in water. Monomer composition (PEGMA/RMA = 200/0 – 80/120) and RMA (MMA, nBMA, tBMA, OcMA, DMA, AdMA, CDMA, ODMA) were systematically varied to clarify the effects of polymer structures on folding properties.

PEGMA/RMA random copolymers below 40 mol% hydrophobic RMA (PEGMA/RMA = 180/20, 160/40, 120/80) selectively self-folded in water to be compact unimer micelles, while those over 50 mol% RMA induced multi-chain aggregation. In detail, unimer micelles gradually became compact as RMA content increased from 0 to 40 mol% (e.g. R = -$C_{12}H_{25}$: DMA) or carbon numbers (n) of R increased from 1 to 18. In contrast, PEGMA/DMA block copolymers (DMA: 20 mol%) formed large aggregates like micelles. Thus,

efficient single-chain folding involves the random incorporation of RMA with appropriate local concentration (20-40 mol%) and hydrophobicity. The folding structures in water were unfolded via methanol addition, and more mobile up on heating to be phase-separated over LCST. Self-folding polymers can be also fixed via the intramolecular crosslinking of the inner hydrophobic spaces.

Conclusion

Various sequence-controlled copolymers including gradient copolymers (random-gradient, gradient-block), cyclopolymers, and amphiphilic random copolymers were successfully synthesized via tandem living radical polymerization with in-situ monomer transesterification, cation template-assisted living radical cyclopolymerization, and living radical random copolymerization, respectively. The resulting copolymers performed unique solid and folding properties and selective functions (cation recognition) on the basis of the inherent sequence of monomers and functional groups. But, the precision of their primary structures is still far from the perfection seen in natural polymers. In the future, development of precision sequence and stereo-regulated living polymerization systems would be a key to create innovative functional materials of polymers.

Acknowledgments

References

1. Lutz, J.-F.; Ouchi, M.; Liu, D. R.; Sawamoto, M. *Science* **2013**, *341*, 1238149.
2. Ouchi, M.; Terashima, T.; Sawamoto, M. *Acc. Chem. Res.* **2008**, *41*, 1120–1132.
3. Ouchi, M.; Terashima, T.; Sawamoto, M. *Chem. Rev.* **2009**, *109*, 4963–5050.
4. Matyjaszewski, K.; Tsarevsky, N. V. *Nature Chem.* **2009**, *1*, 276–288.
5. Matyjaszewski, K. *Macromolecules* **2012**, *45*, 4015–4039.
6. Satoh, K.; Kamigaito, M. *Chem. Rev.* **2009**, *109*, 5120–5156.
7. Hawker, C. J.; Bosman, A. W.; Harth, E. *Chem. Rev.* **2001**, *101*, 3661–3688.
8. Rosen, B. M.; Percec, V. *Chem. Rev.* **2009**, *109*, 5069–5119.
9. Moad, G.; Rizzardo, E.; Thang, S. H. *Polymer* **2008**, *49*, 1079–1131.
10. Yamago, S. *Chem. Rev.* **2009**, *109*, 5051–5068.
11. Nakatani, K.; Terashima, T.; Sawamoto, M. *J. Am. Chem. Soc.* **2009**, *131*, 13600–13601.
12. Nakatani, K.; Ogura, Y.; Koda, Y.; Terashima, T.; Sawamoto, M. *J. Am. Chem. Soc.* **2012**, *134*, 4373–4383.

13. Ogura, Y.; Terashima, T.; Sawamoto, M. *ACS Macro Lett.* **2013**, *2*, 985–989.
14. Terashima, T.; Kawabe, M.; Miyabara, Y.; Yoda, H.; Sawamoto, M. *Nat. Commun.* **2013**, *4*, 2321.
15. Terashima, T.; Sugita, T.; Fukae, K.; Sawamoto, M. *Macromolecules* **2014**, *47*, 589–600.
16. Matyjaszewski, K.; Ziegler, M. J.; Arehart, S. V.; Grenzta, D.; Pakula, T. *J. Phys. Org. Chem.* **2000**, *13*, 775–786.
17. Wasilke, J.-C.; Obrey, S. J.; Baker, R. T.; Bazan, G. C. *Chem. Rev.* **2005**, *105*, 1001–1020.
18. Pàmies, O.; Bäckvall, J.-E. *Chem. Rev.* **2003**, *103*, 3247–3261.
19. Zhou, J. *Chem. Asian J.* **2010**, *5*, 422–434.
20. Mecerreyes, D.; Moineau, G.; Dubois, P.; Jérôme, R.; Hedrick, J. L.; Hawker, C. J.; Malmström, E. E.; Trollsås, M. *Angew. Chem., Int. Ed.* **1998**, *37*, 1274–1276.
21. Bielawski, C. W.; Louie, J.; Grubbs, R. H. *J. Am. Chem. Soc.* **2000**, *122*, 12872–12873.
22. Terashima, T.; Ouchi, M.; Ando, T.; Sawamoto, M. *J. Am. Chem. Soc.* **2006**, *128*, 11014–11015.
23. Van Buijtenen, J.; Van As, B. A. C.; Meuldijk, J.; Palmans, A. R. A.; Vekemans, J. A. J. M.; Hulshof, L. A.; Meijer, E. W. *Chem. Commun.* **2006**, *30*, 3169–3171.
24. Yoda, H.; Nakatani, K.; Terashima, T.; Ouchi, M.; Sawamoto, M. *Macromolecules* **2010**, *43*, 5595–5601.
25. Fukae, K.; Terashima, T.; Sawamoto, M. *Macromolecules* **2012**, *45*, 3377–3386.
26. Ando, T.; Kato, M.; Kamigaito, M.; Sawamoto, M. *Macromolecules* **1996**, *29*, 1070–1072.
27. Takahashi, H.; Ando, T.; Kamigaito, M.; Sawamoto, M. *Macromolecules* **1999**, *32*, 3820–3823.
28. Otera, J. *Chem. Rev.* **1993**, *93*, 1449–1470.
29. Gao, H.; Matyjaszewski, K. *Prog. Polym. Sci.* **2009**, *34*, 317–350.
30. Terashima, T.; Sawamoto, M. In *Progress in Controlled Radical Polymerization: Materials and Applications*; ACS Symposium Series 1101; Matyjaszewski, K., Sumerlin, B. S., Tsarevski, N. V., Eds.; American Chemical Society: Washington, DC, 2012; pp 65−80.
31. Blencowe, A.; Tan, J. F.; Goh, T. K.; Qiao, G. G. *Polymer* **2009**, *50*, 5–32.
32. Gao, H. *Macromol. Rapid Commun.* **2012**, *33*, 722–734.
33. Butler, G. B. *J. Polym. Sci., Part A: Polym. Chem.* **2000**, *38*, 3451–3461.
34. Yokota, K.; Haba, O.; Satoh, T.; Kakuchi, T. *Macromol. Chem. Phys.* **1995**, *196*, 2383–2416.
35. Tunca, U.; Yagci, Y. *Prog. Polym. Sci.* **1994**, *19*, 233–286.
36. Alexandratos, S. D.; Stine, C. L. *React. Funct. Polym.* **2004**, *60*, 3–16.
37. Kodaira, T. *Prog. Polym. Sci.* **2000**, *25*, 627–676.
38. Ochiai, B.; Ootani, Y.; Endo, T. *J. Am. Chem. Soc.* **2008**, *130*, 10832–10833.
39. Nakano, T.; Okamoto, Y.; Sogah, D. Y.; Zheng, S. *Macromolecules* **1995**, *28*, 8705–8706.
40. Coates, G. W.; Waymouth, R. M. *J. Am. Chem. Soc.* **1993**, *115*, 91–98.

41. Pedersen, C. J. *J. Am. Chem. Soc.* **1967**, *89*, 7017–7036.

42. Marsella, M. J.; Maynard, H. D.; Grubbs, R. H. *Angew. Chem., Int. Ed.* **1997**, *36*, 1101–1103.

43. van Dongen, S. F. M.; de Hoog, H.-P. M.; Peters, R. J. R.; Nallani, M.; Nolte, R. J. M.; Van Hest, J. C. M. *Chem. Rev.* **2009**, *109*, 6212–6274.

44. Elsabahy, M.; Wooley, K. L. *J. Polym. Sci., Part A: Polym. Chem.* **2012**, *50*, 1869–1880.

45. Ouchi, M.; Badi, N.; Lutz, J.-F.; Sawamoto, M. *Nat. Chem.* **2011**, *3*, 917–924.

46. Altintas, O.; Barner-Kowollik, C. *Macromol. Rapid Commun.* **2012**, *33*, 958–971.

47. Croce, T. A.; Hamilton, S. K.; Chen, M. L.; Muchalski, H.; Harth, E. *Macromolecules* **2007**, *40*, 6028–6031.

48. Cherian, A. E.; Sun, F. C.; Sheiko, S. S.; Coates, G. W. *J. Am. Chem. Soc.* **2007**, *129*, 11350–11351.

49. Foster, E. J.; Berda, E. B.; Meijer, E. W. *J. Am. Chem. Soc.* **2009**, *131*, 6964–6966.

50. Terashima, T.; Mes, T.; de Greef, T. F. A.; Gillissen, M. A. J.; Besenius, P.; Palmans, A. R. A.; Meijer, E. W. *J. Am. Chem. Soc.* **2011**, *133*, 4742–4745.

51. Giuseppone, N.; Lutz, J.-F. *Nature* **2011**, *473*, 40–41.

52. Gillissen, M. A. J.; Terashima, T.; Meijer, E. W.; Palmans, A. R. A.; Voets, I. K. *Macromolecules* **2013**, *46*, 4120–4125.

53. Huerta, E.; Stals, P. J. M.; Meijer, E. W.; Palmans, A. R. A. *Angew. Chem., Int. Ed.* **2013**, *52*, 2906–2910.

54. Artar, M.; Terashima, T.; Sawamoto, M.; Meijer, E. W.; Palmans, A. R. A. *J. Polym. Sci., Part A: Polym. Chem.* **2014**, *52*, 12–20.

55. Schmidt, B. V. K. J.; Fechler, N.; Falkenhagen, J.; Lutz, J.-F. *Nat. Chem.* **2011**, *3*, 234–238.

Engineering Hydrolytic Degradation Behavior of Poly(lactic-*co*-glycolic acid) through Precise Control of Monomer Sequence

Jian Li,[1] Michael A. Washington,[1] Kerri L. Bell,[1] Ryan M. Weiss,[1] Sam N. Rothstein,[2] Steven R. Little,[2,3,4] Harry M. Edenborn,[5] and Tara Y. Meyer*,[1,4]

[1]Department of Chemistry, University of Pittsburgh, Pittsburgh, Pennsylvania 15260
[2]Department of Chemical Engineering, University of Pittsburgh, Pittsburgh, Pennsylvania 15260
[3]Department of Bioengineering, Department of Immunology, University of Pittsburgh, Pittsburgh, Pennsylvania 15260
[4]McGowan Institute for Regenerative Medicine, University of Pittsburgh, Pittsburgh Pennsylvania 15260
[5]National Energy Technology Laboratory, U.S. Department of Energy, Pittsburgh, Pennsylvania 15236
*E-mail: tmeyer@pitt.edu

The hydrolytic degradation behavior of biodegradable poly (lactic-*co*-glycolic acid) (PLGA) copolymers is shown to depend on monomer sequence. Although polymer properties would be expected to correlate with monomer sequence there are relatively few examples outside of biological polymers to substantiate this assertion. PLGA, one of the most widely used biodegradable polymers, was prepared with repeating sequences, e.g., $(LLG)_n$ (L = lactic unit; G = glycolic unit). All properties related to hydrolytic degradation including molecular weight, lactic acid release, mass loss, water uptake, morphology, and *in vitro* release of encapsulated rhodamine-B were shown to depend on sequence. In contrast with random copolymers, sequenced PLGAs were found to exhibit a steady hydrolysis profile without abrupt changes in properties release rates.

Introduction

While there has been an increasing interest in developing methodologies for control of sequence in copolymers (*1–24*), there are few examples of systematic correlation between sequence and properties in synthetic copolymers or oligomers (*18, 25–45*). Indeed, the majority of studies that document the effect of monomer order compare a single application-specific property for no more than 2 or 3 candidate structures. Few studies involve wider sets of structural variants and fewer yet attempt to draw conclusions that whose relevance extends beyond the focus of the particular study. In considering what might be expected in synthetic systems, however, valuable guidance can be gleaned from the studies of biological polymers such as proteins and nucleic acids (*46–48*) for which extensive structure/function studies have been conducted:

1) *Fundamental properties are sequence dependent.* In the case of proteins, for example, it has been unequivocally established by controlling the arrangement of a limited set of monomers a tremendous range of properties can be accessed. For example, the mechanical stiffness (E) and extensibility (ε_{max}) of fibers produced by spiders, ranges from E = 3 GPa, ε_{max} = 270% for Araneus Flag to E = 10^4 GPa, εmax = 27% for Araneus MA silk. These differences can be traced directly to the presence and relative ratio of specific amino acid sequences (*49*).

2) *Behaviors can be extremely sensitive to sequence.* Complex behaviors such as catalysis and degradation often depend on more than one fundamental property and can therefore exhibit an enhanced correlation with monomer order. Enzymatic catalysis can, for example, be turned off or on in some cases by shifting the position of a single amino acid.

3) *Some sequences are special.* A subset of all possible sequences have been found to confer specific characteristics upon the polymer, e.g., α-turns or recognition motifs. The presence of these special sequences can disproportionately contribute to the polymer properties and behaviors.

4) *Perfect sequence fidelity and exact homology between chains is not a requirement for the manifestation of sequence-dependent behaviors.* The properties and functions of many biological molecules are relatively insensitive to changes in sequence below a certain threshold of substitution or within regions that do not contain "special" sequences with unique functions.

5) *The effect of sequence on intra- and interchain interactions is a crucial component of nearly all sequence-dependent behavior.* Intra- and interchain interactions are of primary importance because the properties of macromolecules necessarily depend on the tertiary and quaternary structure in solution and/or the packing of the chains in the bulk.

6) *The effect of sequence on the interaction of the material with external chemical agents, e.g., water is a crucial contributor to many sequence-dependent behaviors.* As complex behaviors usually involve the interaction of the polymer with external chemical agents or surfaces,

the effect of sequence on those interactions, e.g. hydrophobicity vs. hydrophilicity, can be extraordinarily important in determining function.

We are interested in studying the effects of sequence on properties and behaviors in the synthetic copolymer, poly (lactic-*co*-glycolic acid) (PLGA) and determining to what degree the generalizations described above are relevant. PLGAs are of practical interest because, the random copolymer PLGAs are amongst the most commonly used materials in absorbable medical devices and drug carriers in the United States and Europe; they are key components in several FDA- and EMA-approved microparticle formulations, drug-eluting stents and surgical sutures (*50–58*). Although significant study of these materials has revealed that factors such as temperature (*59–61*), media composition (*62–64*), local pH (*65, 66*), and the copolymer composition (L:G ratio) (*67*) affect both the primary properties and the degradation behavior of these copolymers, little is known about the effect of the sequence of L and G units in the chain (*68–71*).

In the past few years we have developed new synthetic protocols for the creation of a substantial library of PLGAs that encode both structural sequences (L/G) and stereosequence (*R,S, rac*) and we have recently begun a systematic study to correlate the sequences present in these polymers with their properties (*41, 42, 44, 45, 72, 73*). Herein, we review our synthetic approach to these copolymers, discuss sequence/property correlations, and report on sequence-dependent degradation behaviors.

Sequence Controlled PLGAs

Naming Conventions

The following naming conventions are adopted for the oligomers and polymers described herein. The four repeating units, L-lactic, D-lactic, racemic lactic, and glycolic are abbreviated as L, L_R, L_{rac} and G, respectively (Table 1). Oligomeric units (segmers) are named by listing the order of each individual repeating unit from the C-side to the O-side, and the polymer is named with the prefix "Poly". Thus, **Poly $L_{rac}G$**, is the polymer prepared from the segmer with a sequence of a racemic lactic unit followed by a glycolic unit. Random PLGAs prepared by SAP (see below) are named with prefix **R-SAP** followed by the percent of lactic content.

Synthesis of Sequenced Polymers

Using segmer assembly polymerization (SAP), we were able to prepare a wide variety of repeating sequence copolymers of PLGA. Unlike the more commonly used ring-opening polymerization (ROP) of cyclic lactides and glycolides which yield blocky, random copolymers, the SAP approach produces polymers with exact control over both structural- and stereo-sequence in the chain. Targeted sequences were first encoded into heterotelechelic monodisperse sequenced segmers which were prepared using standard methods and protecting group strategies (Figure 1). Polymers with Mn = 15-50 kDa were synthesized by condensation of these

segmers using N,N'-diisopropylcarbodiimide as the coupling reagent (Table 2). A control "random" copolymer was produced under the same conditions by the copolymerization of the LL, LG, GL and GG dimers.

Sequence Dependent Degradation Properties

Sample Preparation and Experiment Design

Two different sample preparation methods were used to study the sequence-dependent behavior of the PLGAs. The studies involving molecular weight loss, morphology, lactic acid release, and rhodamine-B release utilized 2-5 μm microparticles prepared by a standard double emulsion method (*51*). The studies focused on erosion and swelling employed compressed cylindrical pellets (3 x 3 mm) prepared by heated compression molding.

For the microparticle degradation studies the samples were incubated in phosphate buffered saline (PBS) (pH 7.4, 37 °C) in individual micro-centrifuge tubes, with frequent exchange of buffer (every two days) and fixed sampling time (2, 4, 7, 10, 14 days, then once per week until 8th week). For the mass loss and water uptake studies, the cylinders were incubated using the same conditions as the microparticle degradation studies. The buffer was exchanged every two days for the first 10 days, then once per week until the 5th week.

Molecular Weight Change

The number average molecular weight (M_n) loss profiles of the sequence controlled and random PLGAs are shown in Figure 2. After an initial Mn loss, which can be correlated primarily to the shedding of surface coatings and/or rapid cleavage of surface bonds when wetting the freeze-dried microparticles, hydrolytic degradation rates were strongly sequence dependent. The sequenced PLGAs degrade more slowly with a more constant rate of hydrolysis when compared to random PLGAs with the same ratio of L:G. Random PLGAs, **R-SAP 50** and **R-ROP 50**, both have 1:1 ratio of L:G. As expected they both exhibited exponential-decay-type M_n-loss profiles. **R-ROP 50** degraded more quickly than **R-SAP 50** because the polymer is both racemic and more blocky in structure (*42*, *74*). The alternating copolymers **Poly LG (26k)** and **Poly LG (16k)** both degraded slowly and showed nearly linear hydrolysis rates after the initial M_n loss until the end of the degradation. (Figure 2b). After the initial drop in M_n (35% for **Poly LG (26k)** and 20% for **Poly LG (16k)**) the rate of molecular weight loss is independent of initial M_n.

The relationship of degradation rate to the percentage of L units in the copolymer is well-established (*75*, *76*); higher weight fractions of L monomers correlate with slower degradation times. The two random controls, **R-ROP 75** and **R-ROP 50**, exhibited rate differences consistent with this trend (Figure 2a). Likewise, the hydrolysis rates of sequenced PLGAs clearly are dependent on L content. **Poly GLG** degrades faster than **Poly LG (16k)**, and **Poly LG (16k)** degrades faster than **Poly LLG**.

Symbol	Definition
L	L-Lactic acid unit (S configuration)
L_{rac}	Racemic lactic acid unit
G	Glycolic acid unit
Bn	Terminal benzyl protecting group
Si	Terminal silyl protecting group (*tert*-butyldiphenylsilyl group)
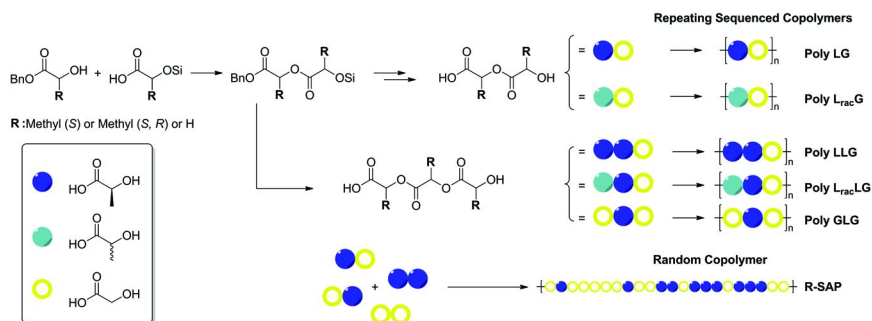
Figure 1. Segmer assembly polymerization (SAP) approach for preparation of sequence controlled PLGA copolymers. Reproduced with permission from reference (41). Copyright (2012) American Chemical Society.

The stereochemistry of L units in the sequenced PLGAs were also a factor in their hydrolysis behavior. **Poly $L_{rac}G$** and **Poly $L_{rac}LG$** hydrolyze faster than the stereopure analogues, **Poly LG** and **Poly LLG** (Figure 2b, d).

Size exclusion chromatography (SEC) traces of random and sequenced PLGAs showed distinct differences in dispersity and sample composition over an 8-week degradation period (Figure 3). The fraction of low molecular weight oligomers in **R-ROP 50** was much smaller than that observed for **Poly LG (26k)**.

Lactic Acid Release

The hydrolytic degradation of PLGAs produces soluble oligomers and monomers including lactic acid and glycolic acid. The release of these small molecules is expected to correlate to sequence.

Table 2. Properties of PLGA copolymers (*42, 44*).

Polymer	M_n (kDa)[a]	Đ[a]	L:G	T_g (°C)[b]	T_m (°C)[c]
Poly LG (16k)[d]	16	1.6	1:1	52	ND
Poly LG (24k)[e]	24	1.3	1.1	50	ND
Poly LG (26k)[d]	26	1.3	1:1	57	ND
Poly L$_{rac}$G[d]	49	2.1	1:1	55	ND
Poly LLG[d]	33	1.6	2:1	57	118
Poly L$_{rac}$LG[d]	35	1.3	2:1	53	ND
Poly GLG[d]	16	1.3	1:2	50	ND
R-SAP 50[d]	31	1.3	1:1	55	ND
R-ROP 50[d,e,f]	32	1.3	1:1	55	ND
R-ROP 75[d,f]	55	1.2	3:1	59	ND

[a] Molecular weights and dispersities were determined by SEC in THF vs. polystyrene standards. [b] Transitions were determined in the second heating cycle. [c] Transitions were determined in the first cycle. [d] These polymers were used in hydrolytic degradation study. [e] Polymers used in the erosion and swelling studies. [f] PLGAs purchased commercially as racemic materials (prepared using ROP) with 50% and 75% lactic units.

The cumulative amount of lactic acid released from random and sequenced PLGAs over an 8-week degradation period was determined and is shown in Figure 4. The presence of lactic acid in the buffer was determined using a well-established enzymatic assay (*77, 78*). **R-ROP 50**, unsurprisingly released the highest total lactic acid. All other PLGAs including the random copolymer **R-SAP 50**, released significantly less lactic acid over the same time period. This slower release of monomers likely corresponds to a much slower degradation of those copolymers. It should be noted that only in the later stages of the degradation process would soluble oligomers degrade to monomeric lactic acid and become detectable by the assay.

Lactic acid release from the PLGA copolymers exhibited a significant sequence-dependent trend, and the trend corresponds well with the M_n-loss profiles. The polymers with a 1:1 L:G ratio were determined to have an order of lactic acid release of **R-ROP 50** >> **R-SAP 50** > **Poly L$_{rac}$G** ~ **Poly LG (26k)**. The release of lactic acid was also dependent on the ratio of L:G: **Poly GLG** >> **Poly LG (26k)** > **Poly LLG**. Despite having lower L content, **Poly GLG** released lactic acid at a rate greater than copolymers with a higher fraction of L, e.g. **Poly LG**. This behavior is indicative of a significant enhancement in hydrolysis rate for copolymers with high G content. Lactic acid release rates were also found to depend on stereoregularity: **Poly L$_{rac}$G** > **Poly LG (26k)** and **Poly L$_{rac}$LG** > **Poly LLG**.
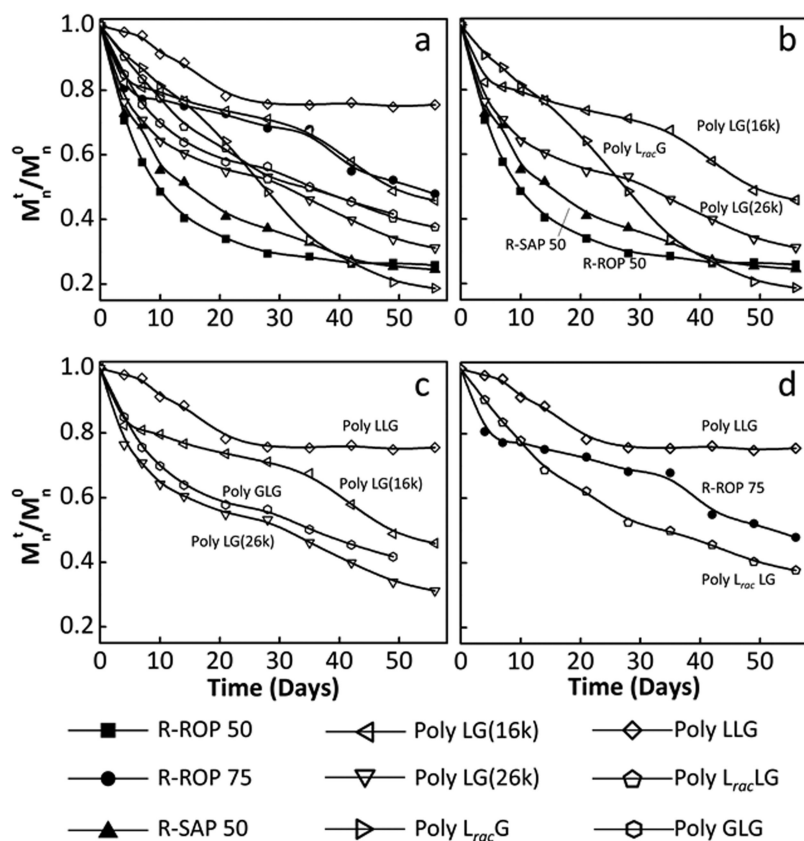
Figure 2. Relative number average molecular weight loss as a function of hydrolytic degradation time for the repeating sequenced and random PLGAs (a) plots of all polymers; (b) Comparison of all polymers with a 1:1 L:G ratio; (c) Comparison of sequenced polymers with varying L:G ratios; (d) Comparison of LLG polymers with varying stereochemistry. Reproduced with permission from reference (41). Copyright (2012) American Chemical Society.

Thermal Properties

Differences in sample morphology over the course of the hydrolysis can be seen by examination of the differential scanning calorimetry (DSC) thermograms of the PLGA copolymers (Figure 5) (*79*). The first heating cycle was used in this case because it reflects the *in situ* thermal history of microparticles after hydrolysis (*80*, *81*). Nearly all of the PLGA microparticles have a single phase transition after formulation, with T_gs of 50-60 °C.
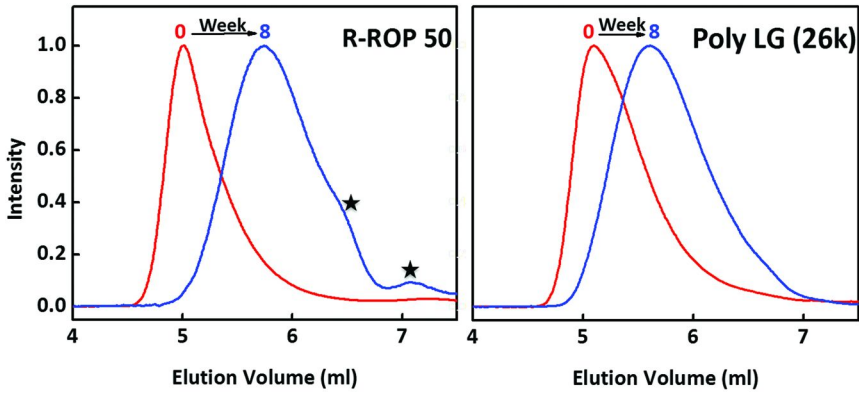
Figure 3. SEC traces for random and sequenced PLGA copolymers with 1:1 ratio of lactic and glycolic acid. Asterisks denote low-molecular weight oligomers. Reproduced with permission from reference (41). Copyright (2012) American Chemical Society.
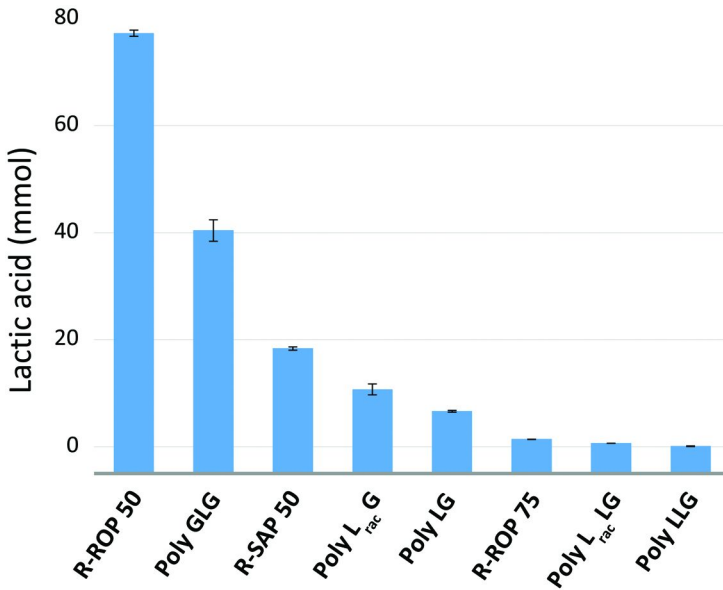
Figure 4. Cumulative amount of lactic acid released from random and sequenced PLGAs during an 8-week degradation period. (Data taken from reference (41).)
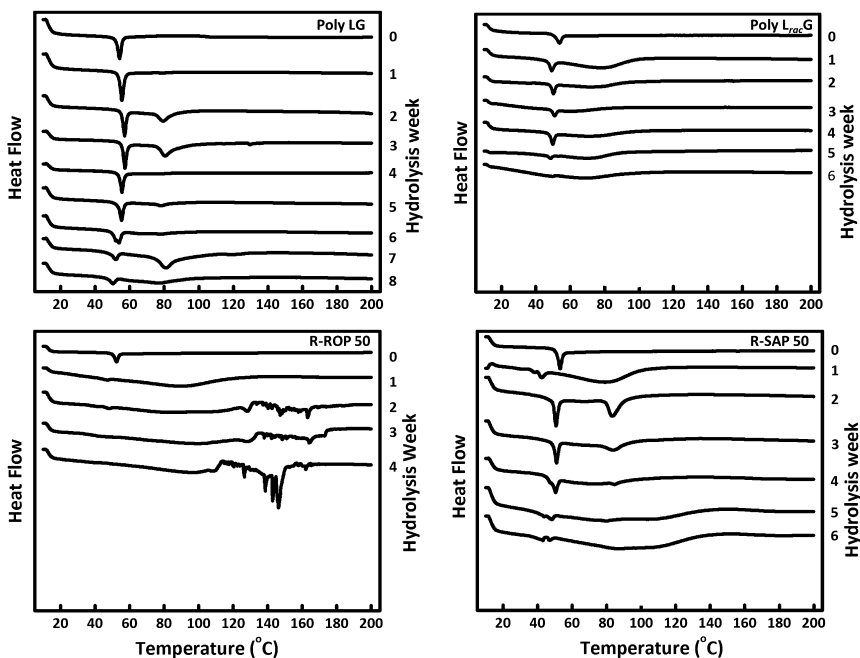
Figure 5. DSC thermograms of selected PLGAs over an 8-week hydrolysis period. Reproduced with permission from reference (41). Copyright (2012) American Chemical Society.

The T_g of the fast-degrading random PLGA, **R-ROP 50**, broadened and disappeared by week 2. By week 3, multiple T_m peaks were observed in the region spanning from 80 to 160 °C. These transitions have been previously assigned to crystallized oligomers with high lactic acid content (*80*). By week 4 there was insufficient material available for a reliable analysis. The T_g for the sequenced copolymers, broadened and shifted slightly but did not disappear over the course of the hydrolysis. A small amount of oligomeric crystallization was also observed but the temperature of the T_m is consistent with oligomers that have a similar 1:1 L:G composition (*42*). The thermal behavior of **Poly L$_{rac}$G** was similarly well-behaved although the degradation rate was faster. Interestingly, **R-SAP 50**, the random copolymer with a less blocky structure than **R-ROP 50**, exhibits an intermediate behavior. Although much of the material undergoes a shift in morphology before the sample is completely degraded, a portion of the material still exhibits the distinctive Tg observed in the original sample. Moreover, the fact that the broad transition between 80 to 160 °C is centered at a lower temperature suggests that the oligomers do not have as high an L content as those observed in the **R-ROP 50** copolymer degradation.

We propose that the differences in both molecular weight loss and morphology observed between the random and sequenced copolymers are due, in part, to the differences in relative water reaction rates between G-G, L-L and G-L/L-G linkages. It has been shown previously that G-rich regions of random PLGA copolymers degrade at a faster rate than L-rich regions (*76*). As a result, random copolymers will be expected to lose G blocks quickly, leaving L-oligomers to crystallize. These crystalline L oligomers then hydrolyze at a slower rate and therefore persist long after the structure of the particle has failed. Sequenced PLGAs are, in contrast, inherently homogeneous along the chain and therefore exhibit a more gradual loss of molecular weight and a retention of essential morphology.

Erosion and Swelling

The dependence on sequence of PLGA behavior was also examined by measuring *in vitro* water uptake (swelling) and sample mass loss (erosion) as a function of hydrolysis time. As described above, these studies were performed on cylindrical pellets fabricated by compression molding. To determine water uptake, water swollen pellets that had been agitated in PBS at 37 °C, were weighed after a brief blotting to remove surface liquid. To determine mass loss due to polymer erosion, pellets were freeze-dried prior to weighing.

Sequenced **Poly LG** was found to erode slowly and showed no significant swelling (Figure 6). Random **R-ROP 50**, in contrast, exhibited a water-swollen mass gain of nearly 200% despite having lost 40% of the dry polymer weight. **Poly LG** also retained both shape and volume over the course of the degradation studies while **R-ROP 50** became misshapen and enlarged before losing structural integrity after 21 days (Figure 7).
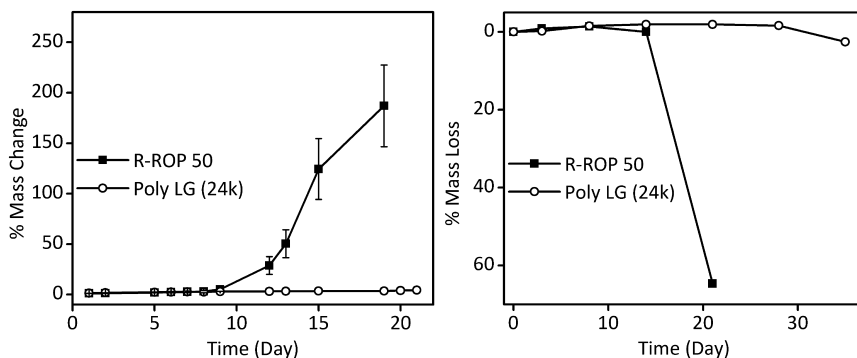
Figure 6. Mass change due to water uptake in PBS-buffer-swollen samples (left) and mass loss due to polymer erosion of samples after freeze-drying (right). Samples were 3 × 3 mm cylindrical pellets.
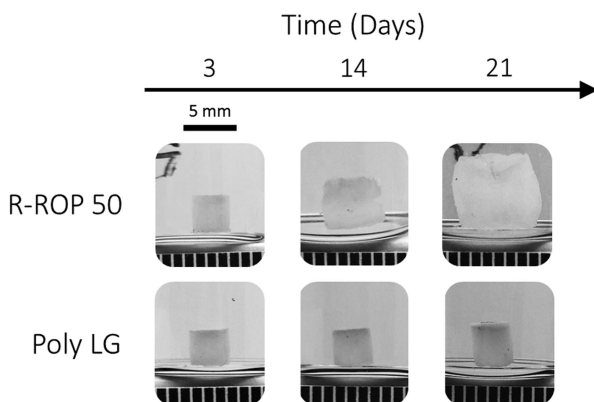
*Figure 7. Visual comparison of the cylindrical pellets of random PLGA (**R-ROP 50**) and sequenced PLGA (**Poly LG**) subjected to hydrolysis in PBS buffer at 37°C.*

Rhodamine-B Release

As drug delivery represents one of the major applications of PLGA, it is of interest to examine the release of encapsulated guests from PLGA microparticles. Rhodamine-B (RhB) has been used as a low-molecular weight hydrophilic drug model in *in vitro* drug delivery studies (*82*). Two alternating PLGAs, **Poly LG** and **Poly L$_{rac}$G**, and the random PLGA, **R-ROP 50**, were selected for the *in vitro* release study of RhB. The encapsulation of RhB into PLGA microparticles was accomplished using a standard double emulsion protocol (*51*).

A significant difference in loading capacity was observed between the random and sequenced copolymers. Specifically, the random copolymers could be loaded with twice as much RhB by weight under the same conditions (Table 3). Data were therefore acquired both for the high load microparticles and for a sample that was purposefully loaded with the same amount of RhB (**R-ROP 50-RhB 2**) as that loaded into the particles made from the alternating copolymers.

RhB release from both sequenced PLGAs is more gradual than that from the random PLGAs (Figure 8). Moreover, RhB release from the random PLGAs has the same profile despite the drastically different loadings. Interestingly, the release rates from **Poly LG** and **Poly L^{rac}G** were nearly the same despite the known differences in their hydrolytic degradation rates.

While the difference in release rates between the random and alternating LG copolymers cannot be attributed to a single factor, e.g., chain degradation in the polymers, there is no doubt that the more homogeneous sequenced copolymers give a more gradual release of the RhB guest in these *in vitro* conditions.

Table 3. PLGA polymer and loading properties. Reproduced with permission from reference (*41*). Copyright (2012) American Chemical Society.

Polymer	$M_n{}^a$ (kDa)	$Đ^a$	RhB (mg)	RhB Loading[b] (mg x 10⁻⁴ / mg)	Loading rate (%)
Poly LG	37.2	1.4	1.0	2.7	5.4
Poly L^{rac}G	38.2	1.4	1.0	2.8	5.6
R-ROP 50-RhB 1	32.0	1.3	0.1	2.9	58
R-ROP 50-RhB 2	32.0	1.3	1.0	5.9	12

[a] Molecular weights and dispersities were determined by SEC in THF vs. polystyrene standards. [b] Based on 200 mg polymer sample size, calculated by the mass of RhB loaded in 1 mg of microparticles.
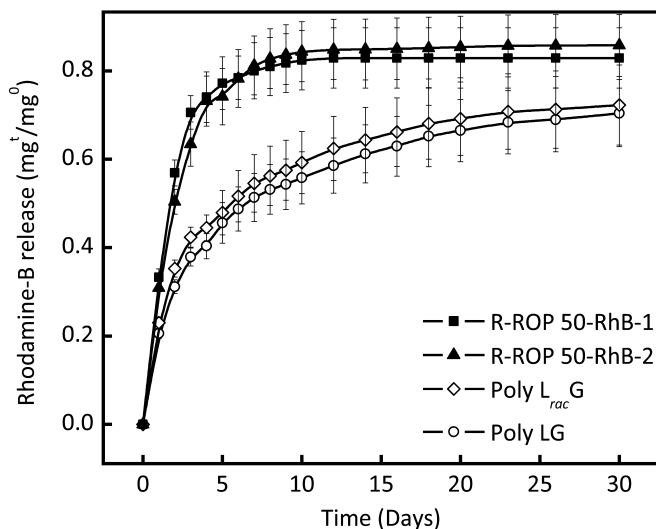
Figure 8. In vitro release profiles of rhodamine-B from random and sequenced PLGA microparticles. Reproduced with permission from reference (41). Copyright (2012) American Chemical Society.

Outlook and Conclusions

As the study of sequenced copolymers expands, it will be necessary not only to create new methods for their synthesis but also to create a body of knowledge and theory, similar to that which exists for block copolymers, that will serve as a guide to how sequence can be used to tune properties. To create such a database it will necessary to not only study sequence in the context of the optimization of an application-specific attribute but also to study sequence from a fundamental perspective. It will be necessary, for example, to determine by which mechanisms

sequence contributes to behaviors and bulk properties, what degree of sequence homogeniety is required to convey the information, and what design elements should be present in a monomer to facilitate sequence-dependent behavior.

In the studies discussed herein as well as our prior studies (*44*) on these PLGA copolymers, we have attempted to address some of these issues. We have thusfar determined that in nearly every measure of hydrolytic degradation, a strong correlation between sequence and behavior can be identified. Furthermore, starting from the premise outlined in the introduction that principles learned from the study of biological polymers will apply to our sytems, we can claim the demonstration of principles 1, 2, 5, and 6. Swelling, erosion, degradation, and guest release were all correlated to sequence and the origin of these differences can be related to sequence effects on interchain interactions and interactions with external agents (water). Future work on this system will focus on demonstrating principles 4 & 5 and on using these principles to custom tune polymers for bioengineering applications.

Acknowledgments

References

1. Atallah, P.; Wagener, K. B.; Schulz, M. D. *Macromolecules* **2013**, *46*, 4735–4741.
2. Brule, E.; Guo, J.; Coates, G. W.; Thomas, C. M. *Macromol. Rapid Commun.* **2011**, *32*, 169–185.
3. Hartmann, L.; Boerner, H. G. *Adv. Mater.* **2009**, *21*, 3425–3431.
4. Hibi, Y.; Tokuoka, S.; Terashima, T.; Ouchi, M.; Sawamoto, M. *Polym. Chem.* **2011**, *2*, 341–347.
5. Houshyar, S.; Keddie, D. J.; Moad, G.; Mulder, R. J.; Saubern, S.; Tsanaktsidis, J. *Polym. Chem.* **2012**, *3*, 1879–1889.
6. Leibfarth, F. A.; Mattson, K. M.; Fors, B. P.; Collins, H. A.; Hawker, C. J. *Angew. Chem., Int. Ed.* **2013**, *52*, 199–210.
7. Lewandowski, B.; De Bo, G.; Ward, J. W.; Papmeyer, M.; Kuschel, S.; Aldegunde, M. J.; Gramlich, P. M. E.; Heckmann, D.; Goldup, S. M.; D'Souza, D. M.; Fernandes, A. E.; Leigh, D. A. *Science (Washington, D.C.)* **2013**, *339*, 189–193.
8. Lo, P. K.; Sleiman, H. F. *J. Am. Chem. Soc.* **2009**, *131*, 4182–4183.
9. McHale, R.; Patterson, J. P.; Zetterlund, P. B.; O'Reilly, R. K. *Nat. Chem.* **2012**, *4*, 491–497.
10. Minoda, M.; Sawamoto, M.; Higashimura, T. *J. Polym. Sci., Part A: Polym. Chem.* **1993**, *31*, 2789–2797.

11. Satoh, K.; Matsuda, M.; Nagai, K.; Kamigaito, M. *J. Am. Chem. Soc.* **2010**, *132*, 10003–10005.

12. Spijker, H. J.; van Delft, F. L.; van Hest, J. C. M. *Macromolecules* **2007**, *40*, 12–18.

13. Tong, X.; Guo, B.-h.; Huang, Y. *Chem. Commun.* **2011**, *47*, 1455–1457.

14. Yu, T.-B.; Bai, J. Z.; Guan, Z. *Angew. Chem., Int. Ed.* **2009**, *48*, 1097–1101.

15. Zamfir, M.; Lutz, J.-F. *Nat. Commun.* **2012**, *3*, 1138.

16. Zhang, J.; Matta, M. E.; Hillmyer, M. A. *ACS Macro Lett.* **2012**, *1*, 1383–1387.

17. Norris, B. N.; Pan, T. Q.; Meyer, T. Y. *Org. Lett.* **2010**, *12*, 5514–5517.

18. Chen, W.; Schuster, G. B. *J. Am. Chem. Soc.* **2013**, *135*, 4438–4449.

19. Ida, S.; Ouchi, M.; Sawamoto, M. *J. Am. Chem. Soc.* **2010**, *132*, 14748–14750.

20. Kramer, J. W.; Treitler, D. S.; Dunn, E. W.; Castro, P. M.; Roisnel, T.; Thomas, C. M.; Coates, G. W. *J. Am. Chem. Soc.* **2009**, *131*, 16042–16044.

21. Ouchi, M.; Terashima, T.; Sawamoto, M. *Acc. Chem. Res.* **2008**, *41*, 1120–1132.

22. Satoh, K.; Ozawa, S.; Mizutani, M.; Nagai, K.; Kamigaito, M. *Nat. Commun.* **2010**, *1*, 1–6.

23. Lutz, J.-F. *Acc. Chem. Res.* **2013**, *46*, 2696–2705.

24. Lutz, J.-F.; Ouchi, M.; Liu, D. R.; Sawamoto, M. *Science (Washington, D.C.)* **2013**, *341*, 1238149.

25. Aitken, B. S.; Buitrago, C. F.; Heffley, J. D.; Lee, M.; Gibson, H. W.; Winey, K. I.; Wagener, K. B. *Macromolecules* **2012**, *45*, 681–687.

26. Baradel, N.; Fort, S.; Halila, S.; Badi, N.; Lutz, J.-F. *Angew. Chem., Int. Ed.* **2013**, *52*, 2335–2339.

27. Börner, H. G. *Prog. Polym. Sci.* **2009**, *34*, 811–851.

28. Copenhafer, J. E.; Walters, R. W.; Meyer, T. Y. *Macromolecules* **2008**, *41*, 31–35.

29. Hao, Z.; Li, G.; Yang, K.; Cai, Y. *Macromol. Rapid Commun.* **2013**, *34*, 411–416.

30. Hill, D. J.; Mio, M. J.; Prince, R. B.; Hughes, T. S.; Moore, J. S. *Chem. Rev.* **2001**, *101*, 3893–4012.

31. Kantor, S. W.; Sung, T. C.; Atkins, E. D. T. *Macromolecules* **1992**, *25*, 2789–2795.

32. Murnen, H. K.; Khokhlov, A. R.; Khalatur, P. G.; Segalman, R. A.; Zuckermann, R. N. *Macromolecules* **2012**, *45*, 5229–5236.

33. Norris, B. N.; Zhang, S. P.; Campbell, C. M.; Auletta, J. T.; Calvo-Marzal, P.; Hutchison, G. R.; Meyer, T. Y. *Macromolecules* **2013**, *46*, 1384–1392.

34. Rojas, G.; Inci, B.; Wei, Y.; Wagener, K. B. *J. Am. Chem. Soc.* **2009**, *131*, 17376–17386.

35. Smith, J. A.; Brzezinska, K. R.; Valenti, D. J.; Wagener, K. B. *Macromolecules* **2000**, *33*, 3781–3794.

36. Ward, R. E.; Meyer, T. Y. *Macromolecules* **2003**, *36*, 4368–4373.

37. Weiss, J.; Li, A.; Wischerhoff, E.; Laschewsky, A. *Polym. Chem.* **2012**, *3*, 352–361.

38. Ayala, V.; Muñoz, D. M.; Lozano, Á. E.; de la Campa, J. G.; de Abajo, J. *J. Polym. Sci., Part A: Polym. Chem.* **2006**, *44*, 1414–1423.
39. Choe, E.-W.; Borzo, M. *J. Appl. Polym. Sci.* **1994**, *53*, 621–632.
40. Kang, E.-C.; Kaneko, T.; Shiino, D.; Akashi, M. *J. Polym. Sci., Part A: Polym. Chem.* **2003**, *41*, 841–852.
41. Li, J.; Rothstein, S. N.; Little, S. R.; Edenborn, H. M.; Meyer, T. Y. *J. Am. Chem. Soc.* **2012**, *134*, 16352–16359.
42. Li, J.; Stayshich, R. M.; Meyer, T. Y. *J. Am. Chem. Soc.* **2011**, *133*, 6910–6913.
43. Rosales, A. M.; Segalman, R. A.; Zuckermann, R. N. *Soft Matter* **2013**, *9*, 8400–8414.
44. Stayshich, R. M.; Meyer, T. Y. *J. Am. Chem. Soc.* **2010**, *132*, 10920–10934.
45. Weiss, R. M.; Jones, E. M.; Shafer, D. E.; Stayshich, R. M.; Meyer, T. Y. *J. Polym. Sci., Part A: Polym. Chem.* **2011**, *49*, 1847–1855.
46. Anfinsen, C. B. Studies on the principles that govern the folding of protein chains. In *Nobel Lectures, Chemistry 1971-1980*; World Scientific Publishing Co.: 1972.
47. Bloomfield, V. A.; Crothers, D. M.; Tinoco, I. *Nucleic Acids: Structures, Properties, and Functions*; University Science Books: Sausalito, CA, 2000.
48. Whitford, D.: *Proteins: Structure and Function*; John Wiley & Sons: Hoboken, NJ, 2005.
49. Guthold, M.; Liu, W.; Sparks, E. A.; Jawerth, L. M.; Peng, L.; Falvo, M.; Superfine, R.; Hantgan, R. R.; Lord, S. T. *Cell Biochem. Biophys.* **2007**, *49*, 165–181.
50. Dechy-Cabaret, O.; Martin-Vaca, B.; Bourissou, D. *Chem. Rev.* **2004**, *104*, 6147–6176.
51. Jain, R. A. *Biomaterials* **2000**, *21*, 2475–2490.
52. Jagur-Grodzinski, J. *Polym. Adv. Technol.* **2006**, *17*, 395–418.
53. Puranik, A. S.; Dawson, E. R.; Peppas, N. A. *Int. J. Pharm.* **2013**, *441*, 665–679.
54. Campolongo, M. J.; Luo, D. *Nat. Mater.* **2009**, *8*, 447–448.
55. Malyala, P.; O'Hagan, D. T.; Singh, M. *Adv. Drug Delivery Rev.* **2009**, *61*, 218–225.
56. Putnam, D. *Nat. Mater.* **2008**, *7*, 836–837.
57. Allen, T. M.; Cullis, P. R. *Science (Washington, D.C.)* **2004**, *303*, 1818–1822.
58. Anderson, J. M.; Shive, M. S. *Adv. Drug Delivery Rev.* **1997**, *28*, 5–24.
59. Deng, M.; Zhou, J.; Chen, G.; Burkley, D.; Xu, Y.; Jamiolkowski, D.; Barbolt, T. *Biomaterials* **2005**, *26*, 4327–4336.
60. Andersson, S. R.; Hakkarainen, M.; Inkinen, S.; Södergård, A.; Albertsson, A. C. *Biomacromolecules* **2012**, *13*, 1212–22.
61. Weir, N. A.; Buchanan, F. J.; Orr, J. F.; Farrar, D. F.; Dickson, G. R. *Proc. Inst. Mech. Eng., Part H* **2004**, *218*, 321–330.
62. Zhong, S. P.; Doherty, P. J.; Williams, D. F. *Clin. Mater.* **1993**, *14*, 138–189.
63. Perron, J. K.; Naguib, H. E.; Daka, J.; Chawla, A.; Wilkins, R. *J. Biomed. Mater. Res., Part B* **2009**, *91B*, 876–886.
64. Valimaa, T.; Laaksovirta, S. *Biomaterials* **2004**, *25*, 1225–1232.
65. Chu, C. C. *Ann. Surg.* **1982**, *195*, 55–59.

66. Tomihata, K.; Suzuki, M.; Ikada, Y. *J. Biomed. Mater. Res.* **2001**, *58*, 511–518.
67. Giteau, A.; Venier-Julienne, M. C.; Aubert-Pouessel, A.; Benoit, J. P. *Int. J. Pharm.* **2008**, *350*, 14–26.
68. Dong, C. M.; Qiu, K. Y.; Gu, Z. W.; Feng, X. D. *J. Polym. Sci., Part A: Polym. Chem.* **2000**, *38*, 4179–4184.
69. Dong, C.-M.; Guo, Y.-Z.; Qiu, K.-Y.; Gu, Z.-W.; Feng, X.-D. *J. Controlled Release* **2005**, *107*, 53–64.
70. Dong, C.-M.; Qiu, K.-Y.; Gu, Z.-W.; Feng, X.-D. *J. Polym. Sci., Part A: Polym. Chem.* **2001**, *39*, 357–367.
71. Rebert, N. W. *Macromolecules* **1994**, *27*, 5533–5535.
72. Stayshich, R. M.; Meyer, T. Y. *J. Polym. Sci., Part A: Polym. Chem.* **2008**, *46*, 4704–4711.
73. Stayshich, R. M.; Weiss, R. M.; Li, J.; Meyer, T. Y. *Macromol. Rapid Commun.* **2011**, *32*, 220–225.
74. Kasperczyk, J. *Polymer* **1996**, *37*, 201–203.
75. Li, S. *J. Biomed. Mater. Res.* **1999**, *48*, 342–353.
76. Vey, E.; Rodger, C.; Booth, J.; Claybourn, M.; Miller, A. F.; Saiani, A. *Polym. Degrad. Stab.* **2011**, *96*, 1882–1889.
77. Takagi, M.; Fukui, Y.; Wakitani, S.; Yoshida, T. *J. Biosci. Bioeng.* **2004**, *98*, 477–481.
78. Yorita, K.; Janko, K.; Aki, K.; Ghisla, S.; Palfey, B. A.; Massey, V. *Proc. Natl. Acad. Sci. U. S. A.* **1997**, *94*, 9590–9595.
79. Fredenberg, S.; Wahlgren, M.; Reslow, M.; Axelsson, A. *Int. J. Pharm.* **2011**, *415*, 34–52.
80. Park, T. G. *Biomaterials* **1995**, *16*, 1123–1130.
81. Viswanathan, N. B.; Patil, S. S.; Pandil, J. K.; Lele, A. K.; Kulkarni, M. G.; Mashelkar, R. A. *J. Microencapsulation* **2001**, *18*, 783–800.
82. Balmert, S. C.; Little, S. R. *Adv. Mater.* **2012**, *24*, 3757–3778.

Gradient Sequence π-Conjugated Copolymers

Edmund F. Palermo and Anne J. McNeil*

Department of Chemistry and Macromolecular Science and Engineering Program, University of Michigan, 930 North University Avenue, Ann Arbor, Michigan 48109-1055
***E-mail: ajmcneil@umich.edu**

Gradient sequence copolymers exhibit a gradual change in comonomer composition along the polymer chain. These novel materials are interesting because they exhibit unique properties compared to their random, alternating and block copolymer counterparts. We describe herein the synthesis and characterization of the first π-conjugated gradient sequence copolymers, which have only recently been accessible via a controlled, chain-growth synthetic method. We demonstrate that the gradient sequence copolymers exhibit unique thermal, optical and morphological properties compared to the analogous block and random copolymers. In addition, we show that gradient sequence copolymers can act as additives to modulate the thin film morphologies and phase separation behavior of polymer/polymer and polymer/fullerene blends. The impact of gradient sequence copolymer-based additives in stabilizing bulk heterojunction organic solar cells is also described.

Introduction

Naturally-occurring biopolymers perform sophisticated functions due to their precisely defined chemical structure, which dictates their folding and assembly into complex molecular machinery. Inspired by nature, the precise control of synthetic polymer structures represents a challenging goal for modern polymer science (*1–5*). Precise control over copolymer sequence can be obtained through iterative, step-wise approaches that are labor-intensive, expensive and impractical on the large scale. Alternatively, living polymerization methods (*6–9*) provide

some level of sequence control with substantially less effort and can be quite scalable.

In 2004, Yokozawa (*10*, *11*) and McCullough (*12*) independently reported Ni-catalyzed polymerizations of thiophene-based monomers that proceed in a pseudo-living, chain-growth fashion to give regioregular poly(3-hexylthiophene) (P3HT) with low dispersities (Đ ≥ 1.15). This synthetic method, now known as catalyst transfer polycondensation (CTP) (*13–19*), paved the way for synthesizing all-conjugated diblock copolymers (*20–27*), star polymers (*28*, *29*) and surface-grafted polymers (*30–32*). CTP also provides access to all-conjugated gradient sequence copolymers (*33–36*). These studies have demonstrated that the copolymer sequence and architecture can dramatically influence the optical, electronic, thermal, and mechanical properties of the material. Nevertheless, the monomer scope remains quite narrow, ultimately limiting the diversity of new materials that can be made (*13*).

Gradient copolymers are characterized by a compositional drift – a gradual change in the copolymer composition along the polymer chain length. This microstructure differs from block copolymers, which exhibit a sharp compositional discontinuity, and random or alternating copolymers, which exhibit a uniform composition (Scheme 1).

gradient

block

random

alternating
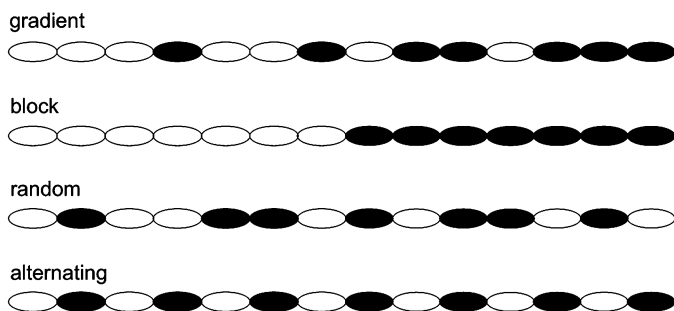
Scheme 1. Copolymer sequences.

To date, most gradient sequence copolymers have been synthesized from vinyl-containing monomers (*37–40*). These reports have demonstrated that the gradient sequence materials exhibit unique properties compared to their block, random and alternating counterparts. For example, Torkelson and co-workers showed that macrophase separated polymer/polymer blends can be rendered thermally stable by including a gradient copolymer as an additive (*41–44*). This effect has been attributed to the gradient copolymer localizing at the interface, lowering the interfacial tension, and as a result, suppressing the phase separation process. These studies motivated us to pursue π-conjugated gradient copolymers and examine their impact on phase separation in polymer/polymer and polymer/fullerene blends. The latter goal is aimed at understanding the impact of phase separation on the performance of bulk heterojunction solar cells. This chapter reviews our work in this area over the past five years, where we have focused on identifying pairs of comonomers that can undergo controlled CTP,

synthesizing gradient sequence copolymers with a linear change in copolymer composition, and understanding the impact of these sequences on their properties and ultimately, their performance in various applications (*33–36*).

Synthesis and Characterization of Gradient Copolymers

The first example of an intentionally synthesized π-conjugated gradient copolymer was reported in 2010 (*36*). This copolymer was composed of thiophene-based repeating units with different side chain identities (i.e., poly(3-hexylthiophene-*grad*-3-((hexyloxy)methyl)thiophene)). This proof-of-concept paper laid the foundation for our future studies by establishing a protocol for the semi-batch synthesis of these novel materials. In 2012, we reported the second example of a π-conjugated gradient sequence copolymer, this time with varying heteroatoms in the backbone (i.e., poly(3-hexylthiophene-*grad*-3-hexylselenophene) (*35*). These gradient copolymers exhibited sequence-dependent physical properties; for example, their extent of microphase separation was between that of the analogous random and block copolymers. These early papers demonstrated that π-conjugated gradient sequence copolymers can be prepared using CTP and that their sequence plays a role in the solid-state properties.

McNeil and co-workers (2010)   McNeil and co-workers (2012)
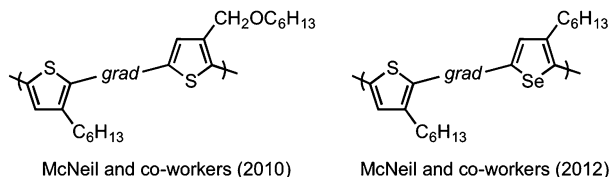
We next turned our focus to synthesizing gradient copolymers that can be used to determine the impact of phase separation in polymer/polymer and polymer/fullerene blends. To overcome some synthetic limitations of the CTP method, we targeted gradient copolymers that could be further modified in a post-polymerization step. Specifically, the copolymerization of monomers **1** and **2** were pursued (*34*). Although monomer **1** was known to homopolymerize under CTP conditions (*10*, *12*), monomer **2** was largely untested (*45*, *46*). Thus, the synthesis of poly(3-(6-bromohexyl)thiophene) (P3BrHT) was attempted via CTP. The resulting homopolymers exhibited number-average molecular weights (M_n) consistent with the [monomer]/[catalyst] ratios, low Đ, and high regioregularities. Importantly, the alkyl bromide side chains were inert to the CTP reaction conditions. Based on these promising results, the synthesis of gradient, random and block copolymers containing monomers **1** and **2** were pursued (Scheme 2). The sequence was controlled by the method of comonomer addition: To obtain a random copolymer, monomers **1** and **2** were first added, followed by precatalyst **3** (a "batch" process). To obtain a block copolymer, **1** was first polymerized to high conversion with precatalyst **3**, and then monomer **2** was injected (a "sequential addition" process). To obtain a gradient copolymer, a stock solution of monomer **2** was gradually added to the reaction mixture containing monomer **1** and precatalyst **3** using a syringe pump (a "semibatch" process).
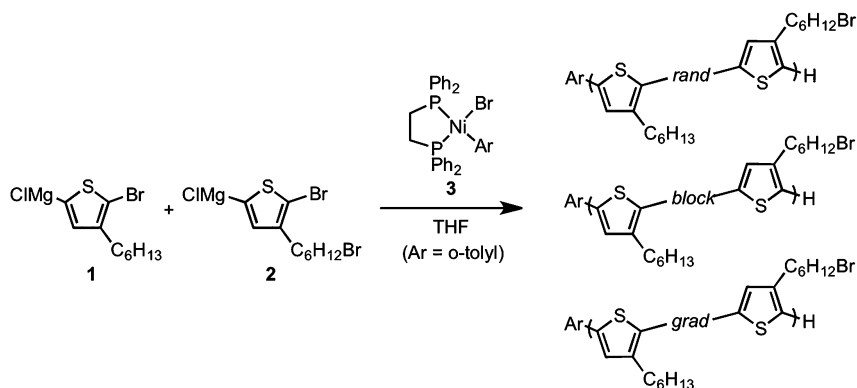
Scheme 2. Synthesis of random, block, and gradient copolymers via CTP.

The copolymer sequences were elucidated by plotting the copolymer composition (as determined by ^{1}H NMR spectroscopy) as a function of the normalized chain length (as determined by gel permeation chromatography (GPC)) using aliquots withdrawn throughout the polymerization. The three copolymers were shown to possess similar molecular weights and dispersities (Figure 1B), as well as high regioregularities (>99%). Hence, the only salient structural difference between the three copolymers was their sequence, rendering these polymers suitable for identifying sequence-dependent properties in π-conjugated polymers. As evident in Figure 1C, the melting temperatures vary from the random copolymer (T_m = 198 °C) to the gradient copolymer (T_m = 206 °C) to the block copolymer (T_m = 235 °C). These results suggest that the sequence with the large bromine atoms distributed uniformly (in the random copolymer) forms the least stable crystallites. In contrast, when all the bromine atoms are concentrated on one chain end (in the block copolymer), it forms the most stable crystallites. Intermediate between these extremes resides the gradient copolymer. The impact of these copolymers on phase-separated P3HT/P3BrHT blend morphologies will be discussed in a later section.
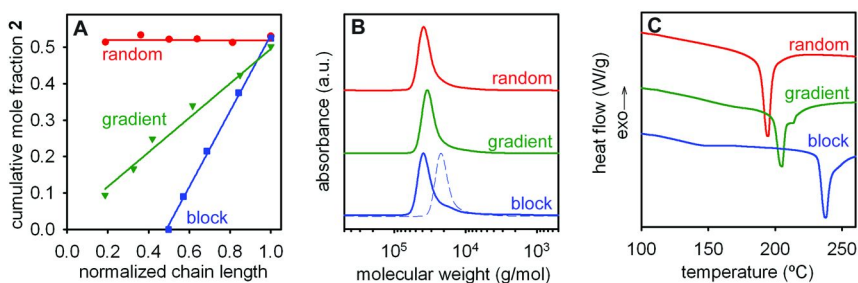
*Figure 1. Characterization data for the random (red), gradient (green) and block (blue) copolymers containing monomers **1** and **2**. (A) Plot of the copolymer composition as a function of the normalized chain length, (B) GPC data, and (C) DSC data. (see color insert)*

We next pursued post-polymerization functionalization of these copolymers to incorporate an electron-acceptor fullerene derivative (*33*). Although there have been examples of random and block copolymers bearing pendant fullerenes (*47–52*), there were no examples of gradient sequence copolymers with such functionality. To access such copolymers, the side chain bromines in the gradient copolymer were quantitatively converted to azides. A subsequent copper-catalyzed azide-alkyne cycloaddition (CuAAC) reaction was used to covalently attach a fullerene derivative (Scheme 3) (*33*). Using an excess of the fullerene, maintaining strictly oxygen-free conditions, and rigorously purifying the PMDETA ligand were all required to avoid deleterious side-reactions. We also found that elongating the linker between the polymer and fullerene (from a C_1 to a C_9 linkage) reduced the extent of intra- and interpolymer crosslinking. A gradient copolymer with approximately 10 mol% of the side chains bearing a fullerene group was prepared with this method. It is worth noting that a higher percentage fullerene loading could not be achieved due to increased crosslinking. With these materials, the impact of gradient copolymers on phase separation in polymer/fullerene blends was examined.
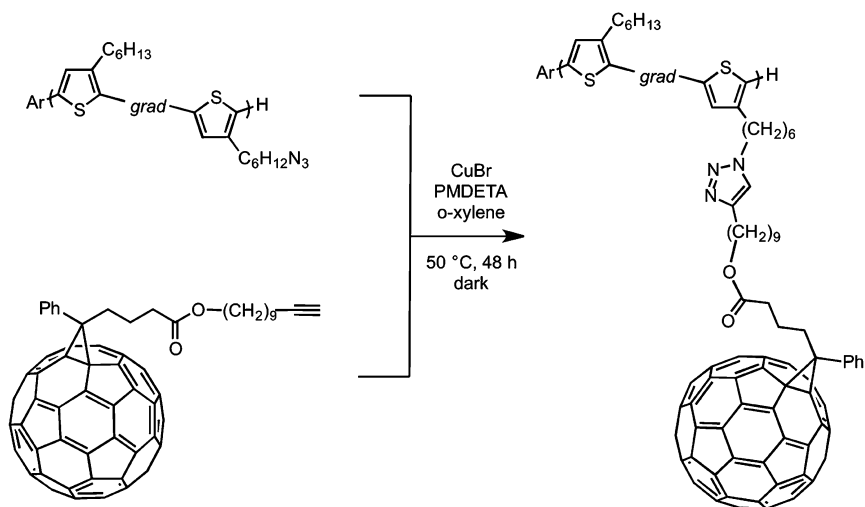
Scheme 3. Synthethic route for the fullerene-functionalized gradient copolymer.

Impact of Gradient Copolymers on Polymer/Polymer Phase Separation

The motivation for synthesizing the gradient copolymer of monomers **1** and **2** was to assess its impact on the morphology of phase separated blends composed of the two homopolymers (P3HT and P3BrHT). Without any copolymer additive, the physical blend of P3HT and P3BrHT undergoes micron-scale phase separation during the spin-coating process as evidenced by scanning transmission electron microscopy with high angle annular dark field detection (STEM/HAADF, Figure 2A). Strong contrast can be observed between isolated domains dispersed in

a continuous matrix. Energy dispersive spectroscopy (EDS) was performed on selected areas, which revealed the presence of bromine atoms in the bright regions (P3BrHT-rich domains) and their absence in the dark regions (P3HT-rich domains).
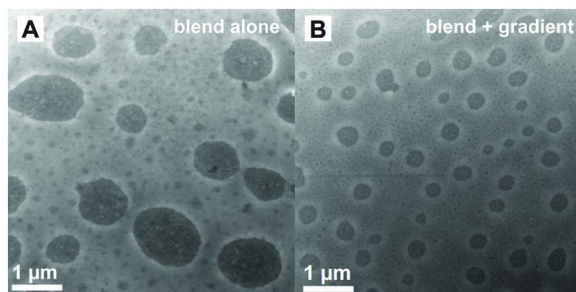
Figure 2. STEM/HAADF images of the as-cast blend of P3HT and P3BrHT with (A) 0 wt% and (B) 20 wt% gradient copolymer additive.

Next, physical blends of the homopolymers in a 1:1 volume ratio (which is based on the solvent excluded molecular volume of the corresponding repeat unit structures) were prepared with the gradient copolymer as an additive, ranging from 0–20 wt%. Spin-casting these solutions gave rise to thin films that were analyzed by STEM/HAADF to determine the domain sizes. As evident in Figure 2B, the domain sizes decreased when gradient copolymer additive was included in the blend. Measurements of domain size from randomly selected regions revealed that the average domain size decreased from 0.9 ± 0.3 μm to 0.27 ± 0.08 μm when the gradient copolymer concentration was increased from 0 to 20 wt%. Further studies revealed that the gradient copolymer out-performed the random and block copolymer analogues with smaller domain sizes and distributions. Overall, these studies revealed that semicrystalline π-conjugated gradient copolymers can influence the morphology of polymer/polymer blends, and that the effect is sequence-dependent.

It is important to note that the influence of the semicrystalline gradient copolymer described herein is different than what was reported for amorphous gradient copolymers. Specifically, Torkelson and co-workers showed that the amorphous copolymer additives suppressed a thermodynamically-driven phase separation process during thermal annealing, and suggested the mechanism involved the gradient copolymer localizing at the domain interface and lowering the interfacial tension (44). In contrast, the semicrystalline gradient copolymers described herein modulate the blend morphology during a kinetically-driven spin-coating process. Though the mechanism is unclear at this time, one rationale is that the gradient copolymer localizes at the interface and mediates the aggregation/crystallization process.

The role of thermal annealing in the P3HT/P3BrHT blends was complicated by the fact that thin films of P3BrHT undergo crosslinking with annealing above its melting temperature ($T_m = 168$ °C). Nevertheless, annealing the thin films for

1 h at 150 °C avoids the crosslinking. Processing films in this manner revealed an intriguing and novel morphology (Figure 3). Fibrils of crystalline P3BrHT were observed in the continuous matrix and appear to align parallel to the P3HT/ P3BrHT interface. Interestingly, this morphology appears regardless of whether any copolymer additive is used. The similarity of this morphology to the stars depicted in van Gogh's famous painting have led us to name it the "Starry Night morphology". That the nanofibrils appear to be preferentially oriented around the P3HT domains suggests that P3BrHT fibril growth process is influenced by the interface. Evaluating this new morphology in the context of bulk heterojunction devices represents an exciting avenue for future exploration.
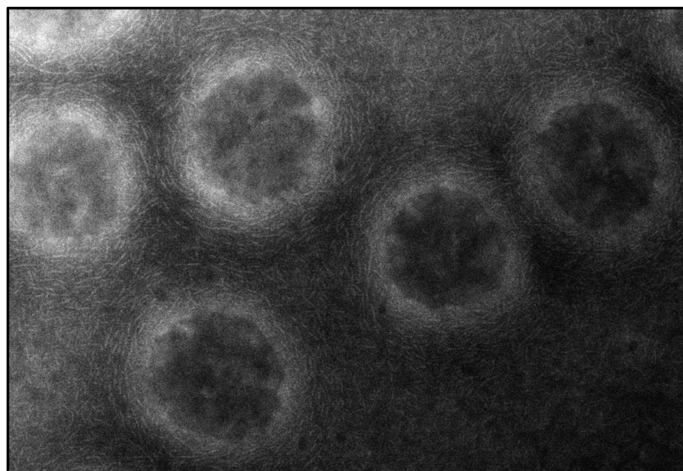
Figure 3. STEM/HAADF image of the P3HT/P3BrHT blend with 10 wt% block copolymer additive after annealing at 150 °C for 1 h.

Impact of Gradient Copolymers on Polymer/Fullerene Phase Separation

Thin films of P3HT/[6,6]-phenyl-C_{61}-butyric acid methyl ester (PCBM) undergo crystallization-induced phase separation when thermally annealed for 1 h at 150 °C, as evidenced by the micron-sized needle-shaped domains of PCBM observed under an optical microscope (Figure 4A). This process is known to be detrimental to photovoltaic device performance as the donor/acceptor domains need to be on the nanometer length scale to enable efficient exciton dissociation (*53*). Motivated by the fact that π-conjugated gradient copolymers suppress phase separation in polymer/polymer blends, we next examined their impact on P3HT/PCBM blends. When the gradient copolymer (at 10 wt%) is added to the blend, this undesirable process is completely suppressed (Figure 4B). Thus, the gradient copolymer bearing side-chain fullerenes acts as a phase compatibilizer for this polymer/fullerene blend.
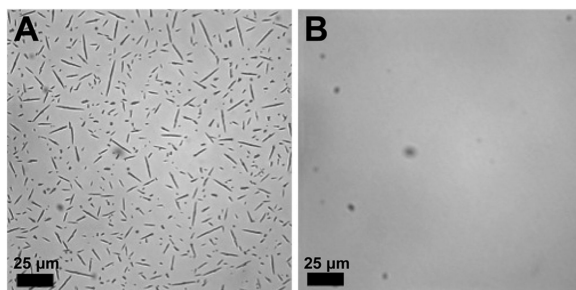
Figure 4. Optical microscope images of P3HT/PCBM (60:40 wt ratio) blends after annealing at 150 °C for 1 h (A) without and (B) with gradient copolymer additive (10 wt%).

Photoluminescence measurements were used to further support the conclusion that this novel gradient copolymer is suppressing micron-scale phase separation in the P3HT/PCBM physical blend (Figure 5). With spin-cast films, PCBM efficiently quenches the P3HT emission due to the efficient charge transfer from donor to acceptor in the film. On thermal annealing, the P3HT-based emission is typically recovered because the micron-scale domains minimize the chances of the exciton finding a PCBM molecule within its diffusion length. Excitingly, when a gradient copolymer additive was included in the blend, the P3HT emission remained quenched regardless of annealing time. These results are consistent with the notion that the donor/acceptor domains maintain intimate contact at the nanometer length scale when gradient copolymer is present.

The ultimate test of the gradient copolymer additive involved fabricating and testing solar cells based on the traditional P3HT/PCBM bulk heterojunction. In the control device, annealing for 10 min at 150 °C improves the short-circuit current (J_{sc}) and leads to a higher overall power conversion efficiency (PCE, Figure 6). Annealing for longer times reduces the J_{sc}, leading to a decrease in PCE, presumably due to the micron-scale phase separation. When 10 wt% gradient copolymer is included in the blend, an S-shaped curve was observed in the current density versus voltage plot (Figure 6A). As a result, the fill factor (FF) is reduced, leading to a lower overall PCE (Figure 6B). Related S-shaped distortions have been previously observed and attributed to an imbalance of electron/hole charge transport rates (53–58). We speculate that the gradient copolymer may be inhibiting growth of P3HT fibrils within the blend, which would restrict hole transport and increase the likelihood of non-geminate recombination (59–61). Indeed, when the gradient copolymer was added, the P3HT/PCBM blend exhibited some modest changes in the solid-state organization as evident in the powder X-ray diffraction and differential scanning calorimetry. When the gradient copolymer additive was reduced to just 1 wt%, the S-shaped distortion was minimized, leading to an improved PCE (compared to 10 wt%), albeit still with sub-optimal FF.
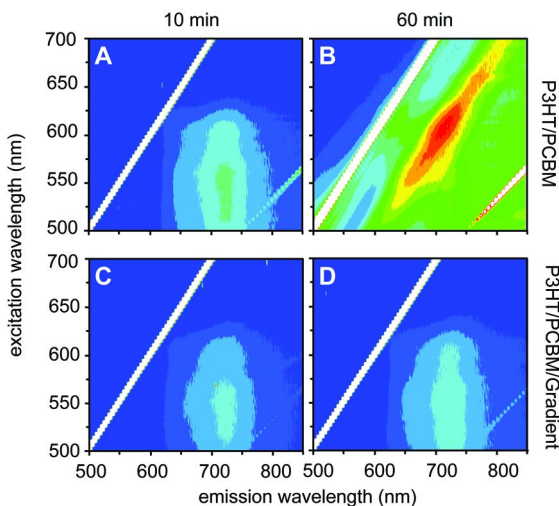
Figure 5. Contour maps of PL intensity as a function of the emission and excitation wavelengths for (A and B) P3HT/PCBM and (C and D) P3HT/PCBM + 10 wt% gradient copolymer. Each film was annealed at 150 °C for either 10 min (A and C) or 60 min (B and D). The color represents the relative PL intensity with red as the maximum. (see color insert)
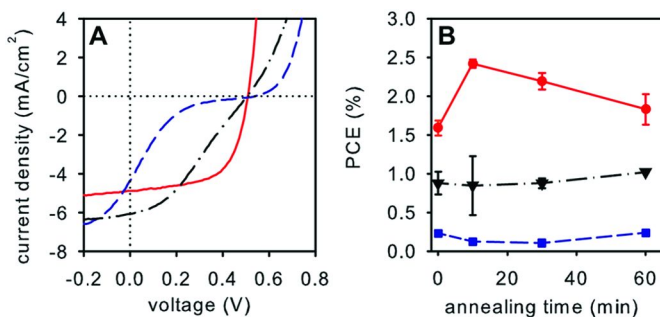
Figure 6. (A) Plot of the short-circuit current density (J_{sc}) versus voltage (V) for blends of P3HT/PCBM after 60 min of annealing at 150 °C. (B) Plot of the power conversion efficiency (PCE) versus annealing time (min) for blends of P3HT/PCBM. (0 wt% gradient copolymer (red solid line), 1 wt% gradient copolymer (black dot-dash line), and 10 wt% gradient copolymer (blue dashed line)). (see color insert)

The main advantage of a gradient copolymer additive is evident at longer annealing times. While the conventional device (no additive) undergoes phase separation, which results in lower PCEs, the devices containing gradient copolymer additive showed virtually no change in PCE even after annealing at 150 °C for 60 min (Figure 6B). Because the overall PCE in the gradient-containing devices was lower than the conventional device, we plan to synthesize a library of

gradient copolymers with systematically tuned structural parameters (e.g., mole fraction fullerene loading, gradient sequence distribution and molecular weight) to identify a gradient structure that achieves high PCE while maintaining the thermal stability.

Conclusions and Future Outlook

With just a few structurally similar monomers, a broad range of sequence-dependent properties have been observed. For example, copolymer sequence has been shown to influence both the physical and optical properties of random, block and gradient π-conjugated copolymers. Excitingly, gradient copolymers were shown to modulate and suppress phase separation in polymer/polymer and polymer/fullerene blends. The impact of these novel copolymers as additives in photovoltaic devices was shown to improve long-term thermal stability, albeit at the expense of reducing the fill factor. Future efforts will focus on modifying the gradient structure to obtain both high power conversion efficiencies and long term stabilities.

To date, we have been limited to thiophene- and selenophene-based monomers due to limitations of the CTP method. As a consequence, we have barely scratched the surface of what may be achievable with gradient sequence π-conjugated copolymers. As new catalysts are discovered and the monomer scope is broadened, we anticipate that additional unique, sequence-dependent properties will emerge from the synthesis and characterization of gradient π-conjugated copolymers. The utility of these gradient copolymers should also be expanded to include a more diverse range of applications, such as chemical/biological sensors and biomaterials (*62–66*). With much excitement in a rapidly growing field, there are many potential applications for these new sequence-controlled macromolecules.

References

1. Badi, N.; Chan-Seng, D.; Lutz, J.-F. *Macromol. Chem. Phys.* **2013**, *214*, 135–142.
2. Lutz, J.-F.; Ouchi, M.; Liu, D. R.; Sawamoto, M. *Science* **2013**, *341*, 1238149.
3. Lutz, J.-F. *Polym. Chem.* **2010**, *1*, 55–62.
4. Badi, N.; Lutz, J.-F. *Chem. Soc. Rev.* **2009**, *38*, 3383–3390.
5. Ober, C. K.; Cheng, S. Z. D.; Hammond, P. T.; Muthukumar, M.; Reichmanis, E.; Wooley, K. L.; Lodge, T. P. *Macromolecules* **2009**, *42*, 465–471.
6. Nicolas, J.; Guillaneuf, Y.; Leafy, C.; Bertin, D.; Gigmes, D.; Charleux, B. *Prog. Polym. Sci.* **2013**, *38*, 63–235.
7. Matyjaszewski, K. *Macromolecules* **2012**, *45*, 4015–4039.
8. Moad, G.; Rizzardo, E.; Thang, S. H. *Aust. J. Chem.* **2012**, *65*, 985–1076.
9. Sutthasupa, S.; Shiotsuki, M.; Sanda, F. *Polym. J.* **2010**, *42*, 905–915.

10. Yokoyama, A.; Miyakoshi, R.; Yokozawa, T. *Macromolecules* **2004**, *37*, 1169–1171.
11. Miyakoshi, R.; Yokoyama, A.; Yokozawa, T. *Macromol. Rapid Commun.* **2004**, *25*, 1663–1666.
12. Sheina, E. E.; Liu, J. S.; Iovu, M. C.; Laird, D. W.; McCullough, R. D. *Macromolecules* **2004**, *37*, 3526–3528.
13. Bryan, Z. J.; McNeil, A. J. *Macromolecules* **2013**, *46*, 8395–8405.
14. Yokozawa, T.; Nanashima, Y.; Ohta, Y. *ACS Macro Lett.* **2012**, *1*, 862–866.
15. Marrocchi, A.; Lanari, D.; Facchetti, A.; Vaccaro, L. *Energy Environ. Sci.* **2012**, *5*, 8457–8474.
16. Stefan, M. C.; Bhatt, M. P.; Sista, P.; Magurudeniya, H. D. *Polym. Chem.* **2012**, *3*, 1693–1701.
17. Kiriy, A.; Senkovskyy, V.; Sommer, M. *Macromol. Rapid Commun.* **2011**, *32*, 1503–1517.
18. Okamoto, K.; Luscombe, C. K. *Polym. Chem.* **2011**, *2*, 2424–2434.
19. Geng, Y.; Huang, L.; Wu, S.; Wang, F. *Sci. China Chem.* **2010**, *53*, 1620–1633.
20. Wang, J.; Ueda, M.; Higashihara, T. *J. Polym. Sci., Part A: Polym. Chem.* **2014**, *52*, 1139–1148.
21. Chen, W. C.; Lee, Y. H.; Chen, C. Y.; Kau, K. C.; Lin, L. Y.; Dai, C. A.; Wu, C. G.; Ho, K. C.; Wang, J. K.; Wang, L. *ACS Nano* **2014**, *8*, 1254–1262.
22. Kudret, S.; Van den Brande, N.; Defour, M.; Van Mele, B.; Lutsen, L.; Vanderzande, D.; Maes, W. *Polym. Chem.* **2014**, *5*, 1832–1837.
23. Willot, P.; Govaerts, S.; Koeckelberghs, G. *Macromolecules* **2013**, *46*, 8888–8895.
24. Bryan, Z. J.; Smith, M. L.; McNeil, A. J. *Macromol. Rapid Commun.* **2012**, *33*, 842–847.
25. Ono, R. J.; Kang, S. S.; Bielawski, C. W. *Macromolecules* **2012**, *45*, 2321–2326.
26. Sui, A.; Shi, X.; Wu, S.; Tian, H.; Geng, Y.; Wang, F. *Macromolecules* **2012**, *45*, 5436–5443.
27. Verswyvel, M.; Koeckelberghs, G. *Polym. Chem.* **2012**, *3*, 3203–3216.
28. Yuan, M. J.; Okamoto, K.; Bronstein, H. A.; Luscombe, C. K. *ACS Macro Lett.* **2012**, *1*, 392–395.
29. Senkovskyy, V.; Beryozkina, T.; Bocharova, V.; Tkachov, R.; Komber, H.; Lederer, A.; Stamm, M.; Severin, N.; Rabe, J. P.; Kiriy, A. *Macromol. Symp.* **2010**, *291-292*, 17–25.
30. Kang, S.; Ono, R. J.; Bielawski, C. W. *J. Am. Chem. Soc.* **2013**, *135*, 4984–4987.
31. Huddleston, N. E.; Sontag, S. K.; Bilbrey, J. A.; Sheppard, G. R.; Locklin, J. *Macromol. Rapid Commun.* **2012**, *33*, 2115–2120.
32. Senkovskyy, V.; Senkovska, I.; Kiriy, A. *ACS Macro Lett.* **2012**, *1*, 494–498.
33. Palermo, E. F.; Darling, S. B.; McNeil, A. J. *J. Mater. Chem. C* **2014**, *2*, 3401–3406.
34. Palermo, E. F.; van der Laan, H. L.; McNeil, A. J. *Polym. Chem.* **2013**, *4*, 4606–4611.
35. Palermo, E. F.; McNeil, A. J. *Macromolecules* **2012**, *45*, 5948–5955.

36. Locke, J. R.; McNeil, A. J. *Macromolecules* **2010**, *43*, 8709–8710.

37. Chen, J.; Li, J.-J.; Luo, Z.-H. *J. Polym. Sci., Part A: Polym. Chem.* **2013**, *51*, 1107–1117.

38. Chen, Y.; Zhang, Y.; Wang, Y.; Sun, C.; Zhang, C. *J. Appl. Polym. Sci.* **2013**, 1485–1492.

39. Zhou, Y.-N.; Li, J.-J.; Luo, Z.-H. *J. Polym. Sci., Part A: Polym. Chem.* **2012**, *50*, 3052–3066.

40. Milonaki, Y.; Kaditi, E.; Pispas, S.; Demetzos, C. *J. Polym. Sci., Part A: Polym. Chem.* **2012**, *50*, 1226–1237.

41. Kim, J.; Sandoval, R. W.; Dettmer, C. M.; Nguyen, S. T.; Torkelson, J. M. *Polymer* **2008**, *49*, 2686–2697.

42. Tao, Y.; Kim, J.; Torkelson, J. M. *Polymer* **2006**, *47*, 6773–6781.

43. Kim, J.; Zhou, H.; Nguyen, S. T.; Torkelson, J. M. *Polymer* **2006**, *47*, 5799–5809.

44. Kim, J.; Gray, M. K.; Zhou, H.; Nguyen, S. T.; Torkelson, J. M. *Macromolecules* **2005**, *38*, 1037–1040.

45. Although the homopolymerization of monomer **2** was reported under similar conditions, there was no evidence supporting (or refuting) a living, chain-growth mechanism. For reference, see: Zhai, L.; Pilston, R. L.; Zaiger, K. L.; Stokes, K. K.; McCullough, R. D. *Macromolecules* **2003**, *36*, 61–64.

46. See also: Iraqi, A.; Crayston, J. A.; Walton, J. C. *J. Mater. Chem.* **1998**, *8*, 31–36.

47. For a recent review, see: Yassara, A.; Miozzoa, L.; Girondaa, R.; Horowitza, G. *Prog. Polym. Sci.* **2013**, *38*, 791–844.

48. Miyanishi, S.; Zhang, Y.; Hashimoto, K.; Tajima, K. *Macromolecules* **2012**, *45*, 6424–6437.

49. Miyanishi, S.; Zhang, Y.; Tajima, K.; Hashimoto, K. *Chem. Commun.* **2010**, *46*, 6723–6725.

50. Lee, J. U.; Jung, J. W.; Emrick, T.; Russell, T. P.; Jo, W. H. *Nanotechnology* **2010**, *21*, 105201.

51. Gernigon, V.; Leveque, P.; Brochon, C.; Audinot, J.-N.; Leclerc, N.; Bechara, R.; Richard, F.; Heiser, T.; Hadziioannou, G. *Eur. Phys. J. Appl. Phys.* **2011**, *56*, 34107.

52. Sivula, K.; Ball, Z. T.; Watanabe, N.; Fréchet, J. M. J. *Adv. Mater.* **2006**, *18*, 206–210.

53. Finck, B. Y.; Schwartz, B. J. *Appl. Phys. Lett.* **2013**, *103*, 053306.

54. Tress, W.; Inganas, O. *Sol. Energy Mater. Sol. Cells* **2013**, *117*, 599–603.

55. Ecker, B.; Egelhaaf, H. J.; Steim, R.; Parisi; von Hauff, J. E. *J. Phys. Chem. C* **2012**, *116*, 16333–16337.

56. Wagner, J.; Gruber, M.; Wilke, A.; Tanaka, Y.; Topczak, K.; Steindamm, A.; Hormann, U.; Opitz, A.; Nakayama, Y.; Ishii, H.; Pflaum, J.; Koch, N.; Brutting, W. *J. Appl. Phys.* **2012**, *111*, 054509.

57. Wang, J. C.; Ren, X. C.; Shi, S. Q.; Leung, C. W.; Chan, P. K. L. *Org. Electron.* **2011**, *12*, 880–885.

58. Wagenpfahl, A.; Rauh, D.; Binder, M.; Deibel, C.; Dyakonov, V. *Phys. Rev. B: Condens. Matter Mater. Phys.* **2010**, *82*, 115306.

59. Groves, C. *Energy Environ. Sci.* **2013**, *6*, 3202–3217.

60. Lyons, B. P.; Clarke, N.; Groves, C. *Energy Environ. Sci.* **2012**, *5*, 7657–7663.
61. Yan, H. P.; Swaraj, S.; Wang, C.; Hwang, I.; Greenham, N. C.; Groves, C.; Ade, H.; McNeill, C. R. *Adv. Funct. Mater.* **2010**, *20*, 4329–4337.
62. Feng, L.; Zhu, C.; Yuan, H.; Liu, L.; Lv, F.; Wang, S. *Chem. Soc. Rev.* **2013**, *42*, 6620–6633.
63. Lin, P.; Yan, F. *Adv. Mater.* **2012**, *24*, 34–51.
64. Otero, T. F.; Martinez, J. G.; Arias-Pardilla, J. *Electrochim. Acta* **2012**, *84*, 112–128.
65. Kim, H. N.; Guo, Z.; Zhu, W.; Yoon, J.; Tian, H. *Chem. Soc. Rev.* **2011**, *40*, 79–93.
66. Bendrea, A. D.; Cianga, L.; Cianga, I. *J. Biomater. Appl.* **2011**, *26*, 3–84.

Sequence-Controlled Radical Copolymerization for the Design of High-Performanced Transparent Polymer Materials

Akikazu Matsumoto*

Department of Applied Chemistry, Graduate School of Engineering, Osaka Prefecture University, 1-1, Gakuen-cho, Naka-ku, Sakai, Osaka 599-8531, Japan
*E-mail: matsumoto@chem.osakafu-u.ac.jp

The precise control of polymer sequence structures for the design of high-performance transparent polymer materials with excellent thermal, optical, and mechanical properties is described in this article. We investigated the 1:1 alternating and 2:1 sequence-controlled copolymerizations of N-substituted maleimides (RMIs) with various olefin and styrene derivatives. The monomer reactivity ratios were determined for the copolymerizations of the RMIs with various electron-donating olefins and styrenes based on the analysis of the comonomer-copolymer composition curves using terminal and penultimate unit models. The penultimate unit and solvent effects on the precise chain structure control during the sequence-controlled radical copolymerization were discussed. The thermal, optical, and mechanical properties of the alternating and 2:1 sequence-controlled copolymers of the RMIs with the olefins and styrenes were also investigated. We demonstrated the rational design of the thermally stable and transparent maleimide copolymers with tunable glass transition temperatures varying over the wide temperature range.

Introduction

Sequence-controlled polymerization is one of the most challenging topics for polymer synthesis during recent years because naturally-occurring polymers

with complicated and well-defined sequences exhibit smart performances (*1*, *2*). Many attempts to fabricate artificial polymers with highly controlled sequence structures have been made using solid-state synthesis (*3*), genetic engineering (*4*), template polymerization (*5*, *6*), topochemical polymerization (*7*), regio-specific polymerization (*8*, *9*), alternating copolymerization (*10*), preorganized oligomers (*11*), and post-polymerization approaches (*12*). The N-substituted maleimides (RMIs) polymerize in the presence of a radical initiator to give a polymer with excellent thermal stability (*13–15*). A high glass transition temp- erature (T_g) originated in the rigid poly(substituted methylene) structure of the poly(RMI)s, which has no methylene spacer as a flexible joint in their main chain (*16–18*), and a high onset temperature of decomposition arose from a robust imide-ring structure included in the repeating units of the polymers (*15, 19, 20*). The RMIs also copolymerize with electron-donating monomers, such as styrene, vinyl ethers, and olefins, to give alternating copolymers with excellent thermal stability and high T_g values (*21, 22*). Especially, the copolymerization of the RMIs with isobutene provided an alternating copolymer in a high yield with excellent thermal stability, high transparency, and high modulus and strength (*23–25*). The introduction of polar groups and cyclic structures into the olefin repeating units led to further increases in the thermally stability and the T_g values of the copolymers (*26, 27*). Recently, it was demonstrated that the RMIs were useful for the sequence regulated radical copolymerization with various olefin and styrene derivatives in 1:1 alternating and 2:1 sequence-controlled fashions (Scheme 1) (*28–30*). The mechanism of the sequence-controlled radical copolymerization has attracted significant attention in research fields of polymer synthesis and radical polymerization (*31–38*). In this chapter, the synthesis of the RMI copolymers with controlled sequence structures and their thermal, optical, and mechanical properties are reviewed.
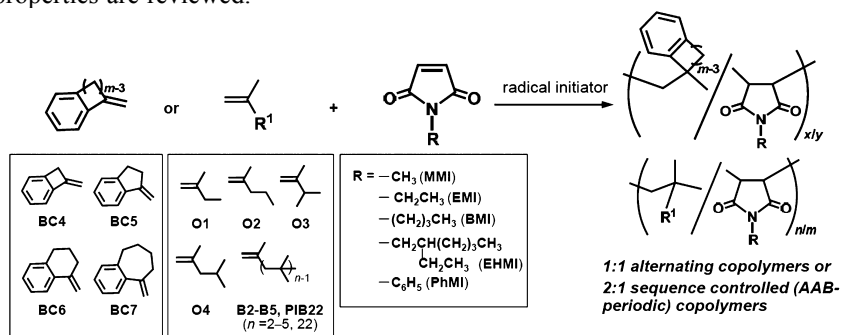
Scheme 1. Radical copolymerization of N-substituted maleimides (RMIs) with various olefin and styrene derivatives.

1:1 Alternating and 2:1 Sequence-Controlled Radical Copolymerization

The radical copolymerization of the RMIs with 1-methylenebenzocyclo-alkanes (BCms, *m* = 4–7) was carried out in the presence of a radical initiator

(Scheme 1) (*28*). The BCm monomers are α-substituted styrene derivatives with a reactive exomethylene group (*39, 40*). During the course of studies on the copolymerization of the RMIs with the BCms, we found that the sequence-controlled radical copolymerization occurred and the copolymers consisting of the AB- and AAB-repeating units (1:1 alternating and 2:1 sequence controls, respectively) were produced depending on the m number of the BCms (*28*). As shown in Table 1, the yield and the M_n value of the obtained copolymers with N-methylmaleimide (MMI) varied in the ranges of 0.5–90% and 1–25×10^3, respectively, and the both values drastically decreased with an increase in the ring size of the BCms. Similar results were observed for the homopolymeriza-tion. The obtained copolymers exhibited excellent thermal properties. The onset and maximum decomposition temperatures (T_{d5} and T_{max}) were over 345 and 365 °C, respectively. The T_g value was 143 °C for the copolymer with BC4 and over 200 °C for the copolymers with BC5 and BC6 in spite of their decreased molecular weights. The effect of the α-substituents on the copolymerization reactivity was also investigated for the alternating copolymerization of the RMIs with noncyclic α-substituted styrene derivatives (*29*). Similar suppressed copolymerization process was observed by the introduction of bulky α-substituents.

Table 1. Synthesis and Thermal Properties of Poly(MMI-*co*-BCm)s and Poly(BCm)s[a]

BCm	Co-monomer	Yield (%)	$M_n/10^3$	M_w/M_n	BCm mol%	T_{d5} (°C)	T_{max} (°C)	T_g (°C)
BC4	MMI	89.9	24.9	2.7	48.2	346	368	143
BC5	MMI	36.6	10.3	1.6	51.3	345	385	212
BC6	MMI	1.4	2.6	1.3	47.3	–	–	200
BC7	MMI	0.5	1.0	1.7	25.6	–	–	–
BC4	None	10.3	4.6	1.4		305	397	133
BC5	None	4.0	9.5	2.1		228	339	119
BC6	None	0						
BC7	None	0						

[a] Copolymerization conditions: [MMI] = [BCm] = 0.2 mol/L, [A IBN] = 10 mmol/L in 1,2-dichloroethane at 60 °C for 20 h. Homopolymerization conditions: [BCm] = 1.0 mol/L, [A IBN] = 10 mmol/L in 1,2-dichloroethane at 60 °C for 5 h.

The copolymerization of the RMIs with olefins was carried out over various compositions in the feed, and the monomer reactivity ratios were determined based on the analysis of the obtained comonomer-copolymer composition curves (Figure 1) (*30*). For the copolymerizations of *N-n*-butyl-maleimide (BMI) with BC5 and BC6, the monomer reactivity ratios, r_1 and r_2, were successfully determined by the terminal unit model. Both the determined r_1 and r_2 values were close to zero; $r_1 = 0.046$ and $r_2 = 0.0043$ for BC5 and $r_1 = 0.019$ and $r_2 = 0.047$ for BC6, as

summarized in Table 2. On the other hand, the monomer reactivity ratios were determined using the penultimate unit model for the BMI–BC7 copolymerization, while appropriate values were not obtained using the terminal model (*28*); $r_{11} = r_{21} = 0$, $r_{12} = 2.92$, and $r_{22} = 0.252$. The radical copolymerization of the RMIs was also carried out using various olefins (O1–O4) and the isobutene oligomers (B2–B5 and PIB22) with a well-defined structure (Scheme 1). The bulkier olefins provided 2:1 sequence-controlled copolymers under the penultimate unit control (*30*).
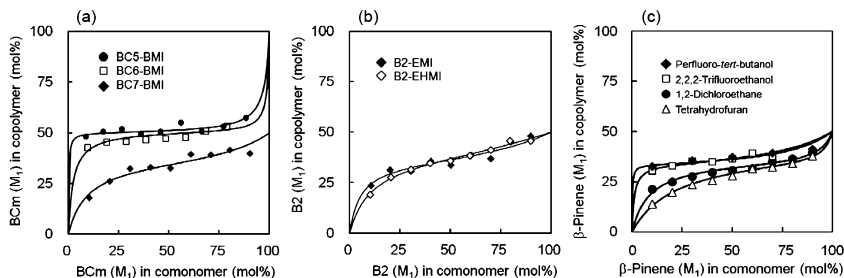
Figure 1. Comonomer-copolymer composition curves for the radical copolymerization of (a) BCms and BMI in 1,2-dichloroethane, (b) B2 and EMI or EHMI in 1,2-dichloroethane, and (c) β-pinene and PhMI in various solvents.

The olefin and styrene monomers can be classified into three types according to their conjugated structure and the bulkiness of the substituents on the vinyl moiety (Figure 2) (*30*). The 1:1 alternating copolymers are produced during the copolymerization with the A-type monomers as planar and conjugated styrene monomers, as well as the copolymerization with less-hindered and non-conjugated olefins such as isobutene (type B). The olefin O1 served as the type B. On the other hand, hindered and non-conjugated olefins with the saturated or unsaturated substituents are classified as the C-type and exhibited the 2:1 sequence-controlled copolymerizations by the penultimate unit effect. The sequence-controlled copolymerization of the RMIs with the BCms occurred in the 1:1 alternating and 2:1 sequence-controlled fashions according to the BCm monomer reactivity, which significantly depended on the coplanarity of the exomethylene moiety and the benzene ring (*28*). For the olefins with a non-cyclic structure, the penultimate unit effects were observed during the copolymerization with O3 and O4 (*30*). The inverse of the r_{12} ($1/r_{12}$) values, which represents the reactivity of the RMI radical to the olefin monomers, were 2.0 and 0.25 for the O3 and O4, respectively. This suggested that the O4 structure played a greater role as the penultimate unit than that of O3. The bulkier and stiff substituents tend to induce more significant penultimate unit effects, resulting in the greater r_{12} values, as shown in the results for the copolymerization of the olefins (Table 2).

Table 2. Monomer Reactivity Ratios for Radical Copolymerization of Various Olefins (M_1) and the RMIs (M_2) at 60 °C under Terminal and Penultimate Unit Control[a]

Olefin	RMI[b]	Solvent[c]	r_1	r_2	r_{11}	r_{12}	r_{21}	r_{22}
BC5	BMI	DCE	0.046	0.0043				
BC6	BMI	DCE	0.019	0.047				
BC7	BMI	DCE			0	2.92	0	0.252
O1	BMI	DCE	0.013	0.17				
O3	PhMI	DCE			0	0.49	0	0.49
O4	PhMI	DCE			0	3.94	0	0.17
B2	PhMI	DCE	0.0076	0.16				
B2	EMI	DCE			0	1.33	0	0.26
B2	EHMI	DCE			0	1.95	0	0.15
CH1[d]	PhMI	PhC(CF$_3$)$_2$OH			0	1.9	0	0.21
CH2[d]	PhMI	PhC(CF$_3$)$_2$OH			0	56	0	0.47
CH3[d]	PhMI	PhC(CF$_3$)$_2$OH			0	2.8	0	0.030
CH4[d]	PhMI	PhC(CF$_3$)$_2$OH			0	30	0	0.25
β-Pinene	PhMI	THF			0	15	0	0.53
β-Pinene	PhMI	DCE			0	10	0	0.24
β-Pinene	PhMI	TFE			0	2.5	0	0.032
β-Pinene	PhMI	PFTB			0	3.2	0	0.0058

[a] $r_1 = k_{11}/k_{12}$ and $r_2 = k_{22}/k_{21}$ for the terminal control. $r_{11} = k_{111}/k_{112}$, $r_{12} = k_{122}/k_{121}$, $r_{21} = k_{211}/k_{212}$, and $r_{22} = k_{222}/k_{221}$ for the penultimate unit control. [b] BMI: *N-n*-butylmaleimide, PhMI: *N*-phenylmaleimide, EMI: *N*-ethylmaleimide, and EHMI: *N*-(2-ethylhexyl)maleimide. [c] DCE: 1,2-dichloroethane, THF: tetrahydrofuran, TFE: 2,2,2-trifluoroethanol, PFTB: perfluoro-*tert*-butanol. [d] Ref. (*35*). See Figure 2 for the structures of CH1 to CH4.
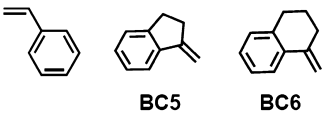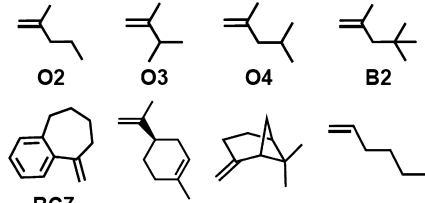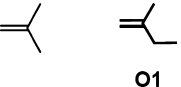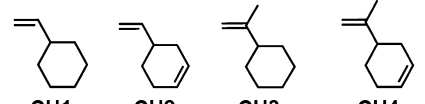
1:1 Alternating copolymerization under terminal control	2:1 Sequence-controlled copolymerization under penultimate unit control
Type A: conjugated olefins BC5 BC6	**Type C**: hindered/non-conjugated olefins O2 O3 O4 B2 BC7 CH1 CH2 CH3 CH4
Type B: non-conjugated olefins (less-hindered) O1	

Figure 2. Classification of the olefins and styrenes used for 1:1 alternating and 2:1 sequence-controlled copolymerizations of the RMIs.

In order to more discuss the copolymerization behavior of the BCms, we estimated the activation energies (E_{act}) and energy differences between the reactant and the product (ΔE) by the DFT calculations using model reactions for the homo- and cross-propagations of MMI and the BCms (Scheme 2) (*28*). The results shown in Table 3 indicated that the cross-propagation of the MMI radical predominantly occurred rather than the homo-propagation of MMI for the cases of BCms (m = 4–6). In contrast, the MMI homo-propagation was preferred to the cross-propagation for the BC7 case. The calculated E_{act} and ΔE values were closely related to each other; i.e., the lower E_{act} values, the negatively larger the ΔE values. The formation of the copolymers with the 2:1 sequence was based on the reduced reactivity of the BC7 radical during the cross-propagation. We also investigated the molecular conformations in the transition state during the cross-propagations and found that no steric interaction was observed during the reaction of the RMI radical to the BCms. This was consistent with the low $E_{act\text{-}21}$ values and the fast addition of the RMI radical to the BCms. During the reactions of the BCm radicals to the RMI monomer, the distances between the closest hydrogen atoms on the maleimide carbon-to-carbon double bond and the cyclic methylene moieties of the BCm radicals decreased according to the increased ring size. The enhanced steric repulsion during the transition state led to an increase in the E_{act} values with an increase in the m number.
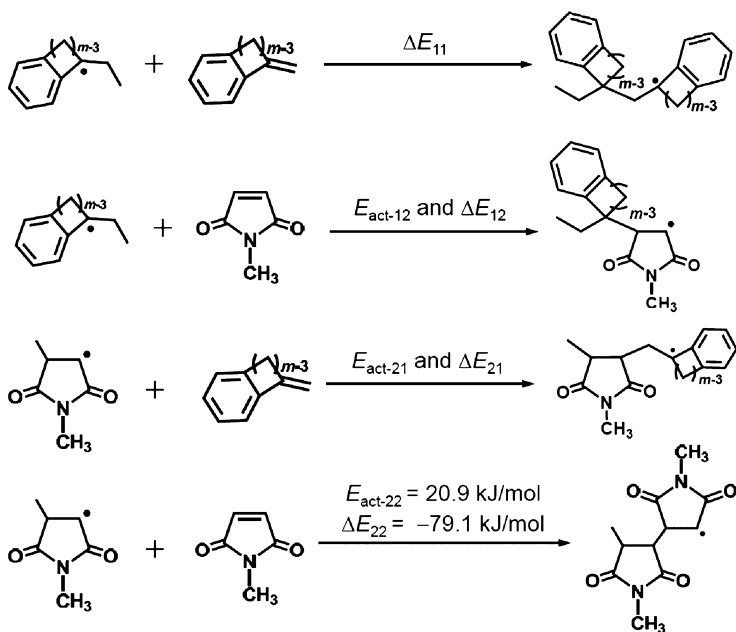
Scheme 2. Model reactions for homo- and cross-propagations observed during radical copolymerization of the RMIs with the BCms.

Table 3. Activation Energies (E_{act}) and Energy Differences in Reactant and Product (ΔE) for the Model Reactions of Propagations Observed during Copolymerization of MMI with BCms[a]

BCm	Cross-propagations (kJ/mol)				Homo-propagation (kJ/mol)
	E_{act-12}	ΔE_{12}	E_{act-21}	ΔE_{21}	ΔE_{11}
BC4	18.3	–61.3	9.2	–85.4	–60.9
BC5	29.4	–27.7	8.2	–97.9	–35.5
BC6	38.8	–14.4	7.1	–97.3	24.4
BC7	74.5	–2.5	33.4	–71.6	19.7

[a] Calculated by the DFT method at the B3LYP/6-31G*//B3LYP/6-31G* and B3LYP/6-311+G**//B3LYP/ 6-31G* levels of theory for the E_{act} and ΔE values, respectively, using the model reactions in Scheme 2. For the MMI homo-propagation, the E_{act-22} and ΔE_{22} values were calculated to be 20.9 and –79.1 kcal/mol, respectively.

Penultimate Unit Effect on Sequence-Controlled Copolymerization

The penultimate unit effects observed during the propagation include the electronic and steric interactions between the chain end unit of the propagating radical and the reacting monomer. The effects of the bulkiness and rigidity of the substituents of comonomers and the RMIs are significant, as shown in the copolymerization parameters in Table 2. For example, the greater penultimate effect was observed for the following cases; the BCMs with a larger ring size, O4 with a bulkier substituent than O3, and the combination of B2 with the RMIs containing large N-alkyl substituents. Similar effect was also observed for the monomer reactivity ratios of the olefins with saturated cyclohexyl and the unsaturated cyclohexenyl groups reported in literature (*35*). The cyclohexenyl substituent is expected to exhibit greater steric repulsion due to the fixed conformation. The propagation rate of a maleimide radical to an olefin (i.e., the k_{121} and k_{221} values) is reduced (Figure 3), while no greater effect by the steric bulkiness is expected for other propagations. As a result, the reduced k_{121} and k_{221} values led to an increase in the r_{12} and r_{22} value for the copolymerizations with the olefins including the cyclohexenyl moiety (See the results for CH2 and CH4 in Table 2).
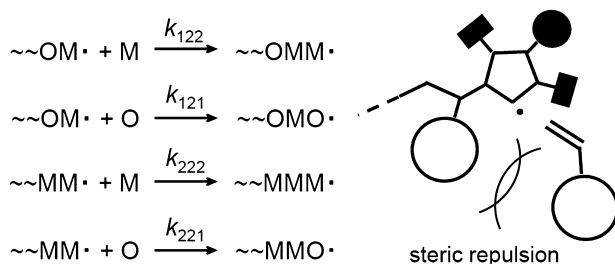
Figure 3. Elemental reactions for the copolymerization of the RMIs with olefins and steric repulsion between the bulky side groups of the olefin unit as the penultimate unit and the reacting monomer. M and O represent the RMI and olefin units, respectively.

The magnitude of the penultimate unit effect varied depending on the copolymerization solvent and temperature [Figure 1(c)], because the solvent-monomer and solvent polymer interactions during the copolymerization were determined by the Lewis acidity of the used solvent, i.e., the magnitude as the electron-pair acceptor toward the carbonyl moiety of the maleimide groups (*38*). The Lewis acid effect is closely related to a change in the monomer reactivity by both the polar and steric interactions. In general, the propagating rate constants of polar monomers, such as acrylates, methacrylates, and the RMIs, tend to increase by the introduction of an electron-withdrawing group in the side group and the use of a solvent with great Lewis acidity. Especially, the cross-propagation of the RMI radical to an olefin was accelerated by the use of the highly electron-pair accepting solvents, resulting in the decrease in the r_{12} and r_{22} values, as shown in

Table 2. Thus, the alternating tendency increased according to the increase in the Lewis acidity of the used solvent (*38*).

Optical and Mechanical Properties of the Copolymers

The RMI copolymers synthesized in this study were soluble in many organic solvents and transparent thin films were obtained by casting the solution and drying. The film strength, i.e., brittleness, was significantly dependent on the N-alkyl groups and the olefin substituents (*28–30*). For example, the flexibility of the poly(RMI-*alt*-BCm)s films increased in the order of MMI < EMI < BMI < EHMI, due to the increased free volume. In the UV-Vis spectra of the copolymer films (60–70 μm thickness), no absorption was observed and the transparency was greater than 90% in the visible light region. The thermal and optical properties of the RMI copolymers are summarized in Table 4. The all copolymers exhibited excellent thermal stability; T_{d5} > 330 °C and T_{max} > 370 °C. The T_g values were tunable depending on the structures of the olefins and the N-substituents, being valuable over the wide temperature range of –68 to 203 °C.

The refractive index values and the Abbe numbers (v_D) were 1.54–1.56 and 38–43, respectively, for the poly(RMI-*co*-BC5)s, and 1.50–1.51 and 46–52, respectively, for the poly(RMI-*alt*-olefin)s. These values were comparable to those for a commodity transparent polymer, e.g., n_D = 1.49–1.51 and v_D = 42–53 for poly(methyl methacrylate) [poly(MMA)] and other polymethacrylates (*41*). The larger the N-substituents of the RMIs and the substituents of the olefins, the lower the n_D values of the copolymers. Very recently, the optical property of methacrylate polymers including an MMI repeating unit was investigated (*42*). The positive orientational and photoelastic birefringence of poly(MMI), which is different from those for poly(MMA) and other polymethacrylates previously reported in the literature, is useful for the design of zero-zero-birefringence polymers for optical devices (*43*).

The viscoelastic properties of poly(RMI-*co*-B2)s were also investigated at the frequencies of 0.5–10 Hz in the range of –150 °C to a temperature over each T_g (*25*, *28–30*). The storage modulus (*E'*) values were determined to be 920, 500, 540, and 250 MPa at 30 °C for poly(BMI-*co*-B2), poly(EHMI-*co*-B2), poly-(BMI), and poly(EHMI), respectively. The flexural moduli of both copolymers were higher than those of the corresponding homopolymers, and the poly(BMI-*co*-B2) showed the highest *E'* value. The loss modulus (*E''*) values of the copolymers showed a peak at 155 and 103 °C for poly(BMI-*co*-B2) and poly(EHMI-*co*-B2), respectively. Similarly, the peak temperatures of tan δ were also determined as 180 and 143 °C, respectively. Based on the plots of the tan δ values as a function of the temperature determined by the flexural experiments at various frequencies, the apparent activation energies ($E_α$) were revealed to increase as the enlarged chain rigidity in the order of poly(EHMI-*co*-B2) < poly(EHMI) < poly(BMI-*co*-B2) and poly(BMI). This order agreed with the orders observed for the T_g values and viscoelastic data, such as *E''* and tan δ values. All the polymers exhibited broad and weak β-dispersions due to the side-chain dynamics over the temperature range of -100 to 0 °C, indicating that these high-T_g polymers have frozen main chain

surrounded by the dynamically moving side groups at room temperature. The coexistence of a rigid main-chain and the flexible side-groups is important for the design of the maleimide polymer materials with a high-T_g value and high toughness. On the other hand, the T_g values were –65 and –68 °C for poly(EMI-co-PIB22) and poly(EHMI-co-PIB22), respectively. These low-T_g copolymers including the PIB22 repeating units exhibited a characteristic fluidity. The flowing rate was significantly reduced by the introduction of the RMI repeating unit in the main chain, although both T_g values of the polyisobutene macromonomers and the poly(ERMI-co-PIB22)s as the grafted copolymers were much lower than room temperature. The poly(RMI-co-PIB22)s were frozen without any fluidity at room temperature, due to the highly branched structure and the intermolecular interaction of the polar RMI repeating units of the copolymers.

Table 4. Thermal and Optical Properties of Poly(RMI-*co*-BCm)s and Poly(RMI-*co*-olefin)s[a]

Polymer[a]	$M_w/10^4$	RMI mol%	T_{d5} (°C)	T_{max} (°C)	T_g (°C)	n_D	v_D
Poly(EMI-*alt*-BC5)	8.5	49.4	344	381	203	1.559	38
Poly(BMI-*alt*-BC5)	16.6	49.7	341	381	158	1.554	40
Poly(EHMI-*alt*-BC5)	21.7	50.7	330	377	109	1.543	43
Poly(BMI-*co*-O1)	8.0	60.3	371	425	105	1.514	48
Poly(BMI-*co*-O2)	14.4	67.9	357	420	108	1.510	48
Poly(BMI-*co*-O4)	20.2	71.6	345	420	123	1.511	46
Poly(BMI-*co*-B2)	18.9	64.4	377	422	148	1.503	48
Poly(EHMI-*co*-B2)	20.6	64.1	377	428	95	1.498	52
Poly(EHMI-*co*-B3)	6.1	68.8	361	427	62	–	–
Poly(EHMI-*co*-B4)	4.4	62.8	368	430	38	–	–
Poly(EHMI-*co*-B5)	4.1	64.5	376	426	–13	–	–
Poly(EHMI-*co*-PIB22)	33.3	61.3	312	404	–68	–	–
Poly(MMI-*alt*-isobutene)[b]	22.0	50.0	396		157	1.53	51
Poly(MMA)[b]			303		100	1.49	53
Polycarbonate[b]			454		140	1.58	29

[a] EMI: *N*-ethylmaleimide, BMI: *N-n*-butylmaleimide, EHMI: *N*-(2-ethylhexyl)male-imide, PhMI: *N*-phenylmaleimide, MMI: *N*-methylmaleimide, and MMA: methyl methacrylate. See Figure 2 for the structures of the olefins.　[b] Ref. (*24*).

Conclusions

The copolymers of the RMIs with the BCms and various olefins were synthesized by the radical copolymerization process. The yield and molecular

weight of the resulting copolymers decreased with an increase in the ring size of the BCm and the steric hindrance of the olefin substituents. We determined the monomer reactivity ratios for the copolymerization of the RMIs with the BCms and various olefins based on the propagation mechanism under the terminal and penultimate unit controls. The mechanism for highly 1:1 alternating and 2:1 sequence-controlled copolymer production depending on the steric bulkiness of the substituent of the comonomers was discussed. We also investigated the poly-mer properties, such as the thermal stability and transparency. We demonstrated the rational design of the thermally stable and transparent maleimide copoly-mers with tunable T_g values varying over the wide tempera-ture range. We concluded that the high-molecular-weight and high-T_g copoly-mers were produced during the copolymerization of MMI, EMI, and BMI with the BCms and various olefins containing an appropriate substituent and that the transparent and thermally stable films were readily obtained by casting the polymer solutions, while the copolymerization of EHMI with the isobutene oligomers and macromonomers produced low-T_g copolymers. The unique birefringence properties of the poly(RMI)s are expected to be powerful tool for the design of zero-zero-birefringence polymers for optical devices in the future. Thus, the sequence-controlled radical copolymerization of the RMIs with various olefins is valuable for the synthesis of high-performance transparent polymer materials. It is also noted that the radical copolymerization of the RMIs is useful not only as the method for high-performance polymer production, but also as the tool for the fundamental research of radical polymerizations, for example, mechanistic analysis of the penultimate unit effects on a radical polymerization process.

References

1. Lutz, J.-F. *Polym. Chem.* **2010**, *1*, 55–62.
2. Ouchi, M.; Badi, N.; Lutz, J.-F.; Sawamoto, M. *Nat. Chem.* **2011**, *3*, 917–924.
3. Merrifield, R. B. *Angew. Chem., Int. Ed. Engl.* **1985**, *24*, 799–809.
4. Langer, R.; Tirrell, D. A. *Nature* **2004**, *428*, 487–492.
5. Serizawa, T.; Hamada, K.; Akashi, M. *Nature* **2004**, *429*, 52–55.
6. Ida, S.; Ouchi, M.; Sawamoto, M. *J. Am. Chem. Soc.* **2010**, *132*, 14748–14750.
7. Matsumoto, A. *Top. Curr. Chem.* **2005**, *254*, 263–305.
8. Matsumoto, A.; Taketani, S. *J. Am. Chem. Soc.* **2006**, *128*, 4566–4567.
9. Kitamura, T.; Tanaka, N.; Mihashi, A.; Matsumoto, A. *Macromolecules* **2010**, *43*, 1800–1806.
10. Pfeifer, S.; Lutz, J.-F. *J. Am. Chem. Soc.* **2007**, *129*, 9542–9543.
11. Mizutani, M.; Satoh, K.; Kamigaito, M. *J. Am. Chem. Soc.* **2010**, *132*, 7498–7507.
12. Kakuchi, R.; Zamfir, M.; Lutz, J.-F.; Theato, P. *Macromol. Rapid Commun.* **2012**, *33*, 54–60.
13. Cubbon, R. C. P. *Polymer* **1965**, *6*, 419–426.
14. Otsu, T.; Matsumoto, A.; Kubota, T.; Mori, S. *Polym. Bull.* **1990**, *23*, 43–50.

15. Matsumoto, A.; Kubota, T.; Otsu, T. *Macromolecules* **1990**, *23*, 4508–4513.
16. Matsumoto, A.; Otsu, T. *Macromol. Symp.* **1995**, *98*, 139–152.
17. Matsumoto, A.; Kubota, T.; Otsu, T. *Polym. Bull.* **1990**, *24*, 459–466.
18. Matsumoto, A.; Umehara, S.; Watanabe, H.; Otsu, T. *J. Polym. Sci., Part B: Polym. Phys.* **1993**, *31*, 527–535.
19. Watanabe, H.; Matsumoto, A.; Otsu, T. *J. Polym. Sci., Part A: Polym. Chem.* **1994**, *32*, 2073–2083.
20. Otsu, T.; Watanabe, H.; Yang, J.-Z.; Yoshioka, M.; Matsumoto, A. *Makromol. Chem., Macromol. Symp.* **1992**, *63*, 87–104.
21. Barrales-Rienda, J. M.; Gonzalez de la Campa, J. I.; Ramos, G. I. *J. Macromol. Sci., Chem.* **1977**, *A11*, 267–286.
22. Otsu, T.; Matsumoto, A.; Kubota, T. *Polym. Inter.* **1991**, *25*, 179–184.
23. Doi, T.; Akimoto, A.; Matsumoto, A.; Otsu, T. *J. Polym. Sci., Part A: Polym. Chem.* **1996**, *34*, 367–373.
24. Doi, T.; Sugiura, Y.; Yukioka, S.; Akimoto, A. *J. Appl. Polym. Sci.* **1996**, *61*, 853–858.
25. Takeda, K.; Omayu, A.; Matsumoto, A. *Macromol. Chem. Phys.* **2013**, *214*, 2091–2098.
26. Omayu, A.; Ueno, T.; Matsumoto, A. *Macromol. Chem. Phys.* **2008**, *209*, 1503–1514.
27. Omayu, A.; Matsumoto, A. *Macromol. Chem. Phys.* **2008**, *209*, 2312–2319.
28. Hisano, M.; Takeda, K.; Takashima, T.; Jin, Z.; Shiibashi, A.; Matsumoto, A. *Macromolecules* **2013**, *46*, 3314–3323.
29. Hisano, M.; Takashima, T.; Jin, Z.; Shiibashi, A.; Matsumoto, A. *Macromol. Chem. Phys.* **2013**, *209*, 1612–1620.
30. Hisano, M.; Takeda, K.; Takashima, T.; Jin, Z.; Shiibashi, A.; Matsumoto, A. *Macromolecules* **2013**, *46*, 7733–7744.
31. *Alternating Copolymer*; Cowie, J. M. G., Ed.; Plenum: New York 1985.
32. Fukuda, T.; Kubo, K.; Ma, Y.-D. *Prog. Polym. Sci.* **1992**, *17*, 875–916.
33. Coote, M. L.; Davis, T. P. *Prog. Polym. Sci.* **1999**, *24*, 1217–1251.
34. Satoh, K.; Matsuda, M.; Nagai, K.; Kamigaito, M. *J. Am. Chem. Soc.* **2010**, *132*, 10003–10005.
35. Matsuda, M.; Satoh, K.; Kamigaito, M. *J. Polym. Sci., Part A: Polym. Chem.* **2013**, *51*, 1774–1785.
36. Matsuda, M.; Satoh, K.; Kamigaito, M. *Macromoleules* **2013**, *46*, 5473–5482.
37. Wang, Y.; Chen, Q.; Liang, H.; Lu, J. *Polym. Int.* **2007**, *56*, 1514–1520.
38. Yamamoto, D.; Matsumoto, A. *Macromol. Chem. Phys.* **2012**, *213*, 2479–2485.
39. Ueda, M.; Mano, M.; Mori, H.; Ito, H. *J. Polym. Sci., Part A: Polym. Chem.* **1991**, *29*, 1779–1787.
40. Chino, K.; Takata, T.; Endo, T. *Macromolecules* **1995**, *28*, 5947–5950.
41. Ozaki, A.; Sumita, K.; Goto, K.; Matsumoto, A. *Macromolecules* **2013**, *46*, 2941–2950.
42. Beppu, S.; Iwasaki, S.; Shafiee, H.; Tagaya, A.; Koike, Y. *J. Appl. Polym. Sci.* **2014**, *131*, 40423.
43. Tagaya, A.; Koike, Y. *Polym. J.* **2012**, *44*, 306–314.

Chapter 21

Dynamic Single Chain Polymeric Nanoparticles: From Structure to Function

Müge Artar, Elisa Huerta, E. W. Meijer, and Anja R. A. Palmans*

Institute for Complex Molecular Systems, Laboratory of Macromolecular and Organic Chemistry, Eindhoven University of Technology, P.O. Box 513, 5600 MB, Eindhoven, The Netherlands
***E-mail: a.palmans@tue.nl**

Achieving the perfection of Nature in forming ordered structures in three dimensions is one of the great challenges for supramolecular chemists. Recently, the merger of supramolecular and polymer chemistry resulted in the preparation of polymers with pendant supramolecular motifs that intramolecularly self-assemble in solution into structures of defined size and shape. This *review* summarizes the recent progress made in preparing and characterizing such compartmentalized structures in solution in which the internal structure arises from non-covalent bond formation, making the obtained particles dynamic and adaptable. In addition, the potential of these so-called dynamic single-chain polymeric nanoparticles (SCPNs) is explored. We highlight the potential of SCPNs for catalysis in water and sensing, functions that all arise as a result of the well-defined conformations that are attained by directional non-covalent interactions

Introduction

Polymer chemistry has made noteworthy steps towards the synthesis of polymers with a defined length. Controlled radical polymerizations nowadays allow to control the polymer molecular weight and the molar mass disperities while at the same time highly functionalized monomers are accepted during the polymerization procedure. However, synthetic polymers typically consist of a random sequence of monomers and form random coils in solution. In

contrast, an important feature of biomacromolecules is that they consist of an exact number of monomers that are positioned in a highly specific way along their backbone. Although the number of monomers that Nature uses is limited, biomacromolecules posses a much higher degree of complexity and functionality: secondary interactions confer a precisely defined three-dimensional (3D) structure in solution to biomacromolecules from which specific properties arise. For example, the compartmentalization present in enzymes is key for creating active sites in which substrates are readily and selectively activated and converted into products.

Several approaches have been followed to attain compartmentalized structures in synthetic macromolecules, and with those, some of the functionality proteins posses have become accessible (*1*). Star polymers and dendrimers afford containers of nanometer-sized dimensions in which embedded, site-isolated catalysts perform a variety of catalytic and cascade catalytic reactions (*2–6*). In addition, dendrimers have been actively explored for *i.a.* drug delivery applications (*7*). Alternatively, amphiphilic block copolymers self-assemble in water into compartmentalized structures and when catalysts are attached to the hydrophobic interior, catalysis in water becomes accessible for catalysts that are normally inactive in pure water (*8*). Finally, polymer chains have been trapped into forming particles of defined size with restricted conformations by internal crosslinking of pendant functional groups (*9, 10*). This crosslinking is typically done in ultradilute conditions to prevent intermolecular interactions.

In recent years, the potential of compartmentalized nanometer-sized particles by using pendant supramolecular motifs to fold polymers into single chain polymeric nanoparticles (SCPNs) has been explored by us and others. The advantage of reversible interactions to create SCPNs is that the system remains adaptive and and can respond to external triggers. Such systems mimic in many ways the functions of proteins. We here summarize recent progress made in the synthesis and characterization of these dynamic SCPNs, stabilized by non-covalent interactions. In addition, we outline our view on the future of this novel and exciting field.

Synthetic Access to Dynamic SCPNs

Control in polymer composition, size, and molecular mass distribution plays a crucial role in the formation of SCPNs. Ring-opening metathesis polymerization (ROMP) (*11*) and a number of controlled radical polymerization (CRP) (*12–15*) techniques have allowed polymerization of a large range of monomers with various functionalities to prepare well-defined polymers. These polymer chains possessing pendant groups can be triggered to induce an *intra*molecular collapse or folding of the polymer to form SCPNs.

SCPNs have been designed both in a non-dynamic and a dynamic fashion. In non-dynamic SCPNs, intramolecular crosslinks are formed by covalent bond formation while in dynamic SCPNs the crosslinks consist of non-covalent or dynamic covalent bonds. In non-dynamic SCPNs, many different types of covalent bond formation have been applied successfully for the intramolecular

crosslinking of the polymers (*16–23*). In dynamic SCPNs, reversible covalent bonds such as disulfides (*24*) or acyl hydrazones (*25*) have been utilized as well as non-covalent bonds such as diamides (*26*), 2-ureido-pyrimidinones (UPys) (*27*), benzene-1,3,5-tricarboxamides (BTAs) (*28*), a combination of BTAs and UPys (*29*), BTA-bipyridines (*30*), cucurbit[8]uril (*31*), thymine-diaminopyridine (*32*), six-point cyanuric acid-Hamilton wedge interactions (*33*) and a combination of the last two (*34*).

In our group, the first examples of SCPNs were prepared by direct polymerization of norbornenes functionalized with either a protected UPy or a dodecyl moiety, using ROMP with a second generation Grubbs catalyst (*27*). In a following approach, single-electron transfer living radical polymerization (SET-LRP) was utilized to synthesize alkyn-functionalized methacrylate-based polymers, followed by a post-modification to attach azide functionalized UPys to free alkynes on the methacrylate backbone via azide-alkyne 1,3-dipolar cycloaddition (*35*). In both cases, SCPNs were formed via incorporating pendant 2-ureidopyrimidinone units to polymer backbone and using their strong dimerization as a driving force for crosslinking or collapse of the single polymer chain. To control the dimerization by an external trigger, the 2-ureidopyrimidinone moieties on the polymers were functionalized with o-nitrobenzyl ether photolabile protecting groups (phUPy) at the terminal carbonyl of the UPy (*36*). The photolabile protecting groups were cleaved off by photoirradiation and the UPy moieties were allowed to dimerize in dilute solutions, resulting in the formation of polymeric nanoparticles (Figure 1). SCPN formation was demostrated by the change in apparent hydrodynamic volume, and thus the size difference between the free polymer and the collapsed nanoparticle via size exculsion chromatography (SEC). The size of the SCPNs could be tuned via varying the molecular weight of the polymer (*37*).
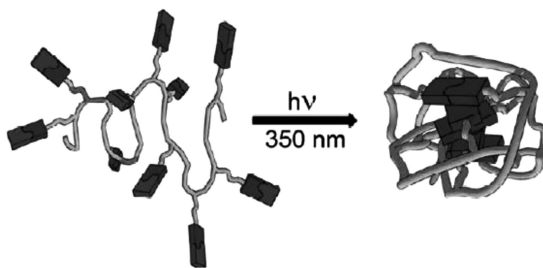
Figure 1. Folding and structure of UPy containing SCPN. (Reproduced with permission from reference (27). Copyright (2009) American Chemical Society.)

Foillowing these first experiments, Mes *et al.* showed that benzene-1,3,5-tricarboxamides (BTAs) can also be utilized as a supramolecular unit to form SCPNs (*28*). In this example, a prepolymer was synthesized via activators regenerated by electron transfer atom transfer radical polymerization (ARGET-ATRP), using isobornyl methacrylate and silyl-protected propargyl methacrylate as the monomers. The obtained prepolymers were functionalised

with azide substituted BTAs. The BTA moiety comprised one o-nitrobenzyl group protected amide in order to trigger the threefold hydrogen bonding into BTA aggregates via light. Later, both BTA and UPy moieties were utilized in one polymer chain by Hosono *et al.* by which orthogonal self-assembly was introduced into SCPNs (Figure 2) (*29*). An ABA triblock copolymer possessing different pendant functional groups in the A and B blocks was prepared via ATRP, to which a complementary BTA and phUPy moiety were ligated in a modular post-functionalization approach. The ABA block-copolymer formed both BTA-based helical aggregates and UPy dimers within one SCPN upon a two-step thermal/photoirradiation treatment under dilute conditions. The orthogonality of the BTA and UPy self-assembly was corroborated via variable-temperature NMR studies. The collapse of polymers after deprotection of the photolabile protecting groups of phUPys into SCPNs was indicated by significant reductions in the hydrodynamic volume by SEC and a decrease in the radius of gyration as evidenced by small-angle X-ray scattering (SAXS).
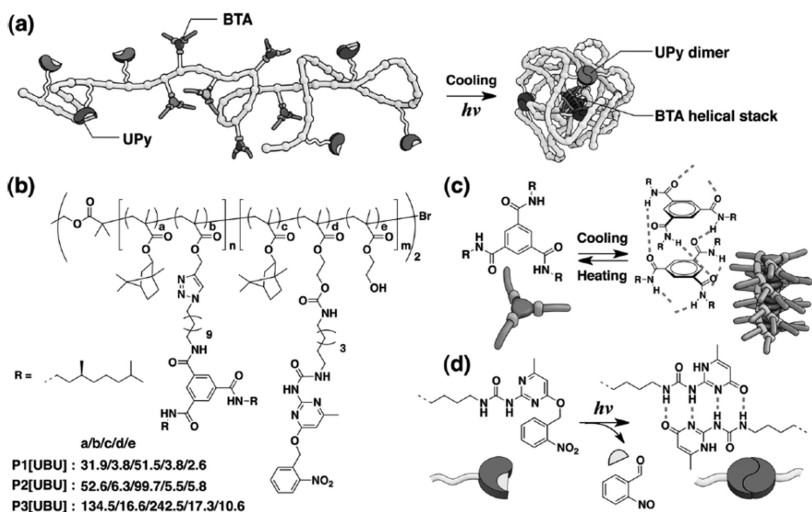
Figure 2. (a) Design of a triblock copolymer with BTA and UPy moieties that folds into a single chain polymeric nanoparticle cross-linked via orthogonal self-assembly. (b) Chemical structure of the triblock copolymers. (c) Helical self-assembly of chiral BTAs via threefold, symmetric hydrogen bonding. (d) Photoinduced dimerization of o-nitrobenzyl protected UPys via quadruple hydrogen bonding. (Reproduced with permission from reference (29). Copyright (2013) American Chemical Society.)

Water solubility was first introduced into BTA-based dynamic SCPNs by Terashima *et al.* (*38*). Ru-catalyzed living radical polymerization was used to prepare a segmented amphiphilic copolymer based on

oligo(ethyleneglycol)methacrylate (oEGMA) and a BTA-functional methacrylate (BTAMA). When the content of BTAMA was smaller than 20%, the copolymers were water-soluble. In addition, a combination of circular dichroism (CD) spectroscopy and scattering techniques showed that these copolymers fold into a single chain polymeric nanoparticles (SCPNs) as a result of the helical self-assembly of the pendant BTA units and/or hydrophilic-hydrophobic phase separation (*39*). Interestingly, their folding was reminiscent to the cooperative folding observed in proteins.

Recently, Sawamoto and coworkers reported on the single-chain folding of amphiphilic random copolymers prepared by the Ru-catalyzed living radical copolymerization of a pEG methacrylate (pEGMA) and an alkyl methacrylate (RMA) in water (*40*). In this system, folding of the single chains was achieved via hydrophilic/hydrophobic phase separation as being one of the simplest models in self-folding polymers without any additional non-covalent interaction and/or chemical linking. Detailed structural and chain-folding characterization on the resulting dynamic and reversible SCPNs disclosed the design rule for single chain folding as an alkyl methacrylate content between 20−40 mol% per chain. Notably, a sharp and reversible lower critical solution temperature (LCST) and phase separation in water was observed with these p(EGMA-co-RMA) random copolymers. Besides tunable hydrophobicity of the compartments depending on nature and content of the alkyl methacylate, a stimulus-responsive unfolding was observed via the addition of methanol.

Besides UPy and BTA motifs, the 3,3′-bis(acylamino)-2,2′-bipyridine substituted benzene-1,3,5-tricarboxamide (BiPy-BTA) unit was also utilized as a structure forming element in SCPN design by Gillissen *et al.* (*30*). Ring-opening metathesis polymerizations were applied to prepare polynorbornene based copolymers with pendant BiPy-BTA units using a third generation Grubbs catalyst. The polymers formed SCPNs in mixtures of tetrahydrofuran and methylcyclohexane via π−π interactions. In the self-assembled state, a strong fluorescence was observed due to the rigidification of the bipyridine moieties, which was utilized as a sensor by using metal binding affinity that enables quenching of the emission (see below).

Characterization of Dynamic SCPNs

As summarized above, the broad synthetic scope of polymer chemistry in combination with the molecular recognition that supramolecular chemistry affords, enables the design of various SCPNs. However, the verification of the single chain character and untangling the nature of the three dimensional architectures of the SCPNs has been less straightforward. In fact, we found that a combination of characterization techniques is required in order to exclude artifacts arising when those techniques are applied separately. Direct visualization using (cryogenic) transmission electron microscopy (TEM) is possible but low contrast and the small sizes of the parcticles typically hamper the elucidation

of the overall structure. Atomic force microscopy (AFM) images have also been frequently applied to visualize the size and shape of SCPNs. However, the method of sample preparation may yield unclear and even misleading images due to solvent evaporation effects. In addition, polymer-surface contacts have a significant impact on the conformation of the polymer chain (*41*). Size exclusion chromatography (SEC) is used to circumvent these issues allowing the determination of the hydrodynamic volume. However, SEC does not provide detailed information on the global conformations that the polymers adopt in solution. Spectroscopic techniques (nuclear magnetic resonance (NMR), fluorescence, ultraviolet (UV) and circular dichroism (CD) spectroscopy) all are usefull to provide evidence on the aggregation state of the supramolecular recognition motifs but they do not distinguish between *intra* and *inter* chain interactions. The most revealing method until now has been the combination of scattering techniques (dynamic light scattering (DLS), small angle X-ray scattering (SAXS) and small angle neutron scattering (SANS)) to analyze dynamic SCPNs. These techniques were recently added to our analysis repertoire as being the only label-free method to measure both the single chain character as well as give information on the global conformation that the SCPNs adopt in specific solvent conditions.

While the first studies on SCPNs relied strongly on the use of AFM and SEC to elucidate the single chain character of the particles obtained, Stals *et al.* monitored the polymer backbone collapse of UPy functionalized SCPNs using a combination of DLS, NMR, SEC and AFM (*42*). Hereto, a library of polymers with varying backbone structures, molecular weights and linking groups was prepared that contained between 5-10% of photoprotected pendant UPy groups. All characterizations were done in 3 different solvents, tetrahydrofuran, chloroform and dimethylformamide to assess the importance of solvent-polymer interactions in SCPN formation. After photodeprotection, UPy dimerization was observed by ^{1}H-NMR in tetrahydrofuran and chloroform, but not in dimethylformamide, a solvent that surpresses hydrogen bond formation. Moreover, changes in hydrodynamic radius were observed by DLS and SEC before and after deprotection, which were very sensitive to the solvent applied. AFM showed the formation of well defined particles. By combining the results of all techniques, the solvent emerged as the *only* decisive parameter for the formation of well-defined SCPNs. Later, complex polymeric architectures based on a block copolymer with a cylindrical brush block and a single-chain polymeric nanoparticle block with pendant UPy groups were investigated (*43*). The self-assembly of these constructs was studied with a similar combination of techniques but in this case, only high resolution AFM images provided clear evidence of SCPN formation.

For the systems in which folding is governed by BTA self-assembly, CD spectroscopy is a powerfull technique as shown by Mes *et al.* (*28*). When the BTAs are non-racemic, helical aggregates of one helicity are biased and this assembly process gives rise to a signature Cotton effect. Upon attaching BTAs to the polymer chains, the Cotton effect was found to be sensitive to the loading of BTAs per polymer chain and the length of the oligo(ethyleneglycol) side chain (*38*). In addition, the magnitude of the Cotton effect was only determined by the

local BTA concentration (*28*, *39*). However, the presence of a Cotton effect does not exclude interparticle interactions. Therefore, scattering techniques proved to be crucial to elucidate the single chain character in the BTA-based water-soluble systems. In recent studies, Gillissen *et al.* combined spectroscopy and small-angle neutron scattering to unravel the relation between interchain self-assembly and the polymer conformation (*39*, *44*). For the first time, SANS experiments revealed the asymmetric shape of these SCPNs with a constant cross section, R_{cs}, and variable length, L, with $L > R_{cs}$ (Figure 3). Detailed investigations corroborated the elongated and highly stretched structure at room temperature, which adopts a constant cross section regardless of the increase in the degree of polymerization.
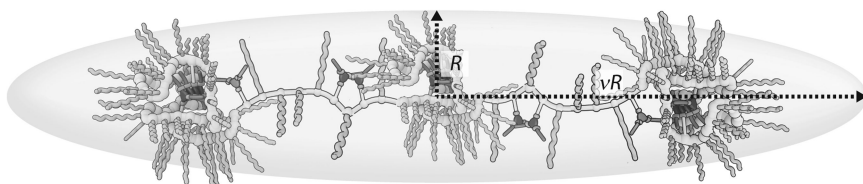
Figure 3. A tentative picture of a BTAMA/oEGMA based SCPN at 25 °C in H₂O. The drawn ellipsoid has the aspect ratio determined from the SANS profile under these conditions. (Reproduced with permission from reference (39). Copyright (2013) American Chemical Society.)

As mentioned in the previous section, a series of ABA-type triblock copolymers were synthesized and functionalized with phUPy and BTA groups (*29*). Following the significant reductions in the hydrodynamic volume in SEC and the decrease in the radius of gyration in small-angle X-ray scattering, AFM was performed to monitor the "partly" and "fully" folded states corresponding to before and after UV irradiation stages, respectively. The AFM images clearly showed a significant chain collapse after the UV irradiation due to UPy dimerization at both ends confirming the orthogonality achieved via design of the polymer chain (Figure 4). In a following investigation, the effect of the polymer topology on folding was studied via comparing ABA and BAB-type triblock copolymers as means of the differences in the degree of chain collapse (*45*). CD analysis results suggested that two different folded structures were adopted by ABA and BAB type polymers as a more tightly packed structure due to strong UPy association over the end blocks and a more loose packing structure since BTAs self-assemble separately in both end blocks, respectively. However, this could not be visualized by AFM images, highlighting our limits in elucidating the internal folded structure of SCPNs. Therefore, developing new methods, such as single-molecule force spectroscopy, to characterize the inherent structure of SCPNs may prove to be of crucial importance to gain further insights into the 3D structure of SCPNs.
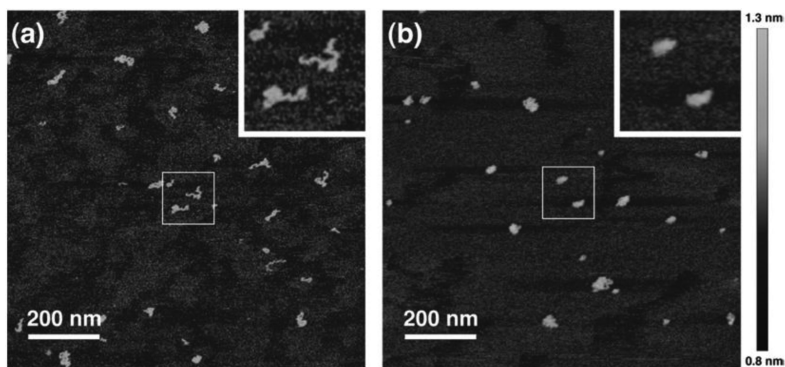
Figure 4. AFM height images of ABA copolymers capturinge two-steps of the molecular folding process (a) before and (b) after UV irradiation. The top-right insets show magnifications of the framed areas. (Reproduced with permission from reference (29). Copyright (2013) American Chemical Society.)

Functions of Dynamic SCPNs

To date, only a limited number of examples exist in which a function has been introduced into dynamic SCPNs. The type of supramolecular recognition motif is important to fold the polymer, while the nature of the side chain attached to the polymer determines in which medium the function can be exploited. Evidently, attaching water-soluble side chains are crucial to compatibilize SCPNs with water, which is imporant in view of future biomedical applications and catalysis in water.

The interest for catalysis in water intiated a number of examples of functional SCPNs. Terashima *et al.* prepared water-soluble segmented copolymers using the benzene-1,3,5-tricarboxamide motif as the supramolecular recognition unit and triphenylphosphine pendants for complexing Ru (*38*). While the BTA units folded the polymers in water into compact conformations, as evidenced by CD and SANS, complexation of the triphenylphosphine moieties with Ru afforded catalytically active SCPNs. Transfer hydrogenation reactions in water proceeded with turnover frequencies that were among the best reported for these types of Ru-based complexes in water. More detailed studies by Artar *et al.* revealed that the Ru metals crosslinked the middle segment of the polymers where the triphenylphosphine groups were located (Figure 5) (*46*). In fact, the combination of two orthogonal supramolecular interactions, hydrogen bonding between the BTA units and metal-ligand coordination between Ru and pendant triphenylphosphines, assisted in procuring active catalysts in water. Huerta *et al.* attached L-proline, a well-studied organocatalyst capable of catalyzing aldol reactions, to water-soluble BTA-based polymers (Figure 6) (*47*). The polymers folded into SCPNs up to high concentrations, as revelaed by dynamic light scattering. The obtained SCPNs were highly active in the aldol reaction of cyclohexanone and *p*-nitrobenzaldehyde in water. For a series of copolymers, the diastereomeric excess ranged from 0 to 90% and the enantiomeric excess from 40

to 70%. We concluded that the exact positioning of the catalyst inside the SCPN is crucial for improving the selectivity of the reactions.
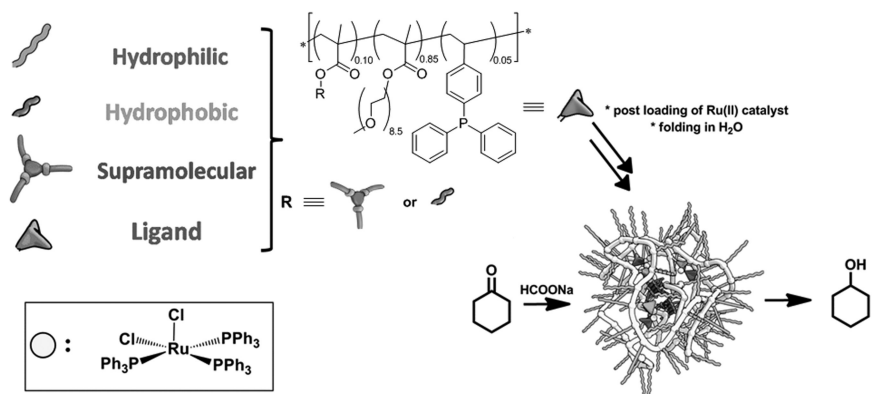
Figure 5. Design of catalytically active SCPNs for transfer hydrogenation of ketones in water.
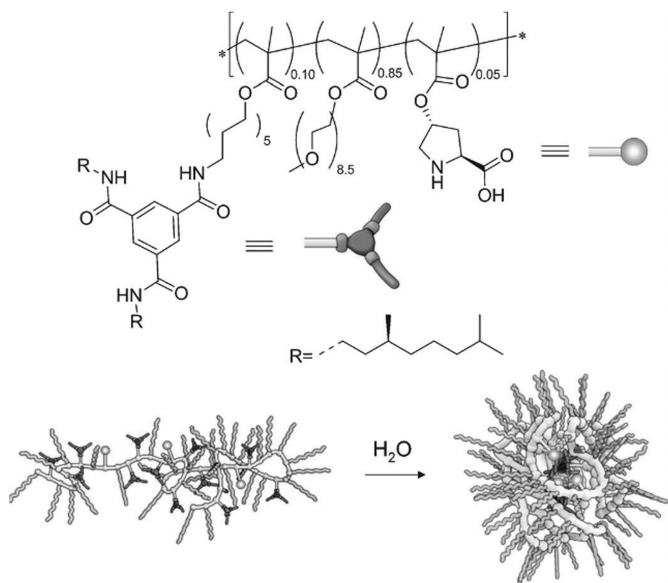
Figure 6. Chemical structure of L-proline-functionalized catalytic polymer (top) and schematic representation of the unfolded polymer and the formation of the compartmentalized catalytic structure in water (bottom).

Finally, preliminary explorations have been conducted to apply SCPNs as sensors (*30*). Bipyridine-based benzene-1,3,5-tricarboxamides show strong green fluorescence in the aggregated state, but are nonfluorescent when molecularly dissolved (*48*). Gillissen *et al.* showed that the attachment of a byridine-based BTA motif to a polymer backbone results in highly fluorescent SCPNs (*30*). The polymers were shown to fold intramolecularly via π-π interactions into fluorescent, compartmentalized particles in mixtures of tetrahydrofuran and methylcyclohexane. Light scattering analysis showed compact conformations of the folded polymers with hydrodynamic radii in the range of 10 nm. Due to the affinity of the 2,2′-bipyridine units to copper, the fluorescence was effectively quenched when Cu(II) was added to the SCPNs. As a result, the SCPNs obtained were effective sensors for this metal.

Conclusions and Future Perspectives

Folding polymer chains via pendant supramolecular recognition motifs into single chain polymeric nanoparticles is an emerging field of research, crossing the boundaries between polymer chemistry, supramolecular chemistry, catalysis and physical organic chemistry. It is clear that not only highly interesting, compartmentalized structures can be prepared, but also that these SCPNs are capable of a variety of interesting functions such as catalysis and sensing. Current challenges to be addressed are the lack of perfect control over the molar mass distributions and the necessity to develop methods that allow exact positioning of functional monomers along the polymer chain. These two issues are by no means trivial and especially the latter is one of the current "holy grails" in polymer chemistry (*49*). In addition, improving characterization techniques that allow visualization of the 3D structure of the SCPNs as well as give access to determining the internal structure of the functional particles are highly desirable.

We envisage that SCPNs will play an exciting role in the development of, for example, cascade catalytic reactions, possibly even in cellular environments. The site isolation of the catalysts in the interior of the SCPN in combination with high activity and selectivity are important prerequisites to obain this goal. We also foresee that novel applications, for example in the biomedical field, will soon be explored. In fact, the first examples applying non-dynamic SCPNs have already been presented (*50, 51*). The crucial step, however, is to combine different fields of research in order to take the next step. Evidently, our ability to fold synthetic macromolecules into defined, compartmentalized structures is still far from the perfection achieved in the folding of polypeptides into conformations that display selected functions. To mimic these natural systems, our current ability to form compartmentalized structures with an ordered interior is not enough. Precise location of self-assembling motifs within the polymer chain and enhanced control over polydispersities are of crucial importance to improve the scope of synthetic analogues. We believe that with these multidisciplinary studies, the frontiers in polymer and supramolecular synthesis, molecular analysis and three-dimensional architectures of polymers are pushed forward.

Acknowledgments

References

1. Meeuwissen, J.; Reek, J. N. H. *Nat. Chem.* **2010**, *2*, 615–621.
2. Bosman, A. W.; Vestberg, R.; Heumann, A.; Fréchet, J. M. J.; Hawker, C. J. *J. Am. Chem. Soc.* **2003**, *125*, 715–728.
3. Terashima, T.; Kamigaito, M.; Baek, K.-Y.; Ando, T.; Sawamoto, M. *J. Am. Chem. Soc.* **2003**, *125*, 5288–5289.
4. Helms, B.; Guillaudeu, S. J.; Xie, Y.; McMurdo, M.; Hawker, C. J.; Fréchet, J. M. J. *Angew. Chem., Int. Ed.* **2005**, *44*, 6384–6387.
5. Helms, B.; Fréchet, J. M. J. *Adv. Synth. Catal.* **2006**, *348*, 1125–1148.
6. Chi, Y.; Scroggins, S. T.; Fréchet, J. M. J. *J. Am. Chem. Soc.* **2008**, *130*, 6322–6323.
7. Grayson, S. M.; Fréchet, J. M. J. *Chem. Rev.* **2001**, *101*, 3819–3867.
8. Lu, A.; O'Reilly, R. K. *Curr. Opin. Biotechnol.* **2013**, *24*, 639–645.
9. Mecerreyes, D.; Lee, V.; Hawker, C. J.; Hedrick, J. L.; Wursch, A.; Volksen, W.; Magbitang, T.; Huang, E.; Miller, R. D. *Adv. Mater.* **2001**, *13*, 204–208.
10. Pyun, J.; Tang, C.; Kowalewski, T.; Fréchet, J. M. J.; Hawker, C. J. *Macromolecules* **2005**, *38*, 2674–2685.
11. Bielawski, C. W.; Grubbs, R. H. *Prog. Polym. Sci.* **2007**, *32*, 1–29.
12. Tsarevsky, N. V.; Matyjaszewski, K. *Chem. Rev.* **2007**, *107*, 2270–2299.
13. Ouchi, M.; Terashima, T.; Sawamoto, M. *Chem. Rev.* **2009**, *109*, 4963–5050.
14. Moad, G.; Rizzardo, E.; Thang, S. H. *Acc. Chem. Res.* **2008**, *41*, 1133–1142.
15. Rosen, B. M.; Perœc, V. *Chem. Rev.* **2009**, *109*, 5069–5119.
16. Beck, J. B.; Killops, K. L.; Kang, T.; Sivanandan, K.; Bayles, A.; Mackay, M. E.; Wooley, K. L.; Hawker, C. J. *Macromolecules* **2009**, *42*, 5629–5635.
17. Zhu, B.; Ma, J.; Li, Z.; Hou, J.; Cheng, X.; Qian, G.; Liu, P.; Hu, A. *J. Mater. Chem.* **2011**, *21*, 2679–2683.
18. Harth, E.; van Horn, B.; Lee, V. Y.; Germack, D. S.; Gonzales, C. P.; Miller, R. D.; Hawker, C. J. *J. Am. Chem. Soc.* **2002**, *124*, 8653–8660.
19. He, J.; Tremblay, L.; Lacelle, S.; Zhao, Y. *Soft Matter* **2011**, *7*, 2380–2386.
20. Croce, T. A.; Hamilton, S. K.; Chen, M. L.; Muchalski, H. l.; Harth, E. *Macromolecules* **2007**, *40*, 6028–6031.
21. Ruiz de Luzuriaga, A.; Ormategui, N.; Grande, H. J.; Odriozola, I.; Pomposo, J. A.; Loinaz, I. *Macromol. Rapid Commun.* **2008**, *29*, 1156–1160.
22. Sanchez-Sanchez, A.; Asenjo-Sanz, I.; Buruaga, L.; Pomposo, J. A. *Macromol. Rapid Commun.* **2012**, *33*, 1262–1267.
23. Cherian, A. E.; Sun, F. C.; Sheiko, S. S.; Coates, G. W. *J. Am. Chem. Soc.* **2007**, *129*, 11350–11351.
24. Tuten, B. T.; Chao, D.; Lyon, C. K.; Berda, E. B. *Polym. Chem.* **2012**, *3*, 3068–3071.

25. Murray, B. S.; Fulton, D. A. *Macromolecules* **2011**, *44*, 7242–7252.

26. Seo, M.; Beck, J. B.; Paulusse, J. M. J.; Hawker, C. J.; Kim, S. Y. *Macromolecules* **2008**, *41*, 6413–6418.

27. Foster, E. J.; Berda, E. B.; Meijer, E. W. *J. Am. Chem. Soc.* **2009**, *131*, 6964–6966.

28. Mes, T.; van der Weegen, R.; Palmans, A. R. A.; Meijer, E. W. *Angew. Chem., Int. Ed.* **2011**, *50*, 5085–5089.

29. Hosono, N.; Gillissen, M. A. J.; Li, Y. S.; Sheiko, S.; Palmans, A. R. A.; Meijer, E. W. *J. Am. Chem. Soc.* **2013**, *135*, 501–510.

30. Gillissen, M. A. J.; Voets, I. K.; Meijer, E. W.; Palmans, A. R. A. *Polym. Chem.* **2012**, *3*, 3166–3174.

31. Appel, E. A.; Dyson, J.; del Barrio, J.; Walsh, Z.; Scherman, O. A. *Angew. Chem., Int. Ed.* **2012**, *51*, 4185–4189.

32. Altintas, O.; Rudolph, T.; Barner-Kowollik, C. *J. Polym. Sci., Part A: Polym. Chem.* **2011**, *49*, 2566–2576.

33. Altintas, O.; Gerstel, P.; Dingenouts, N.; Barner-Kowollik, C. *Chem. Commun.* **2010**, *46*, 6291–6293.

34. Altintas, O.; Lejeune, E.; Gerstel, P.; Barner-Kowollik, C. *Polym. Chem.* **2012**, *3*, 640–651.

35. Berda, E. B.; Foster, E. J.; Meijer, E. W. *Macromolecules* **2010**, *43*, 1430–1437.

36. Folmer, B. J. B.; Cavini, E.; Sijbesma, R. P.; Meijer, E. W. *Chem. Commun.* **1998**, *17*, 1847–1848.

37. Foster, E. J.; Berda, E. B.; Meijer, E. W. *J. Polym. Sci., Part A: Polym. Chem.* **2011**, *49*, 118–126.

38. Terashima, T.; Mes, T.; de Greef, T. F. A.; Gillissen, M. A. J.; Besenius, P.; Palmans, A. R. A.; Meijer, E. W. *J. Am. Chem. Soc.* **2011**, *133*, 4742–4745.

39. Gillissen, M. A. J.; Terashima, T.; Meijer, E. W.; Palmans, A. R. A.; Voets, I. K. *Macromolecules* **2013**, *46*, 4120–4125.

40. Terashima, T.; Sugita, T.; Fukae, K.; Sawamoto, M. *Macromolecules* **2014**, *47*, 589–600.

41. van Roekel, H. W. H.; Stals, P. J. M.; Gillissen, M. A. J.; Hilbers, P. A. J.; Markvoort, A. J.; de Greef, T. F. A. *Chem. Commun.* **2013**, *49*, 3122–3124.

42. Stals, P. J. M.; Gillissen, M. A. J.; Nicolaÿ, R.; Palmans, A. R. A.; Meijer, E. W. *Polym. Chem.* **2013**, *4*, 2584–2597.

43. Stals, P. J. M.; Li, Y.; Burdyńska, J.; Nicolaÿ, R.; Palmans, A. R. A.; Meijer, E. W.; Matyjaszewski, K.; Sheiko, S. S. *J. Am. Chem. Soc.* **2013**, *135*, 11421–11424.

44. Stals, P. J. M.; Gillissen, M. A. J.; Paffen, T. F. E.; de Greef, T. F. A.; Lindner, P.; Voets, I. K.; Palmans, A. R. A.; Meijer, E. W. *Macromolecules* **2014**, *47*, 2947–2954.

45. Hosono, N.; Stals, P. J. M.; Palmans, A. R. A.; Meijer, E. W. *Chem. Asian J.* **2014**, *9*, 1099–1107.

46. Artar, M.; Terashima, T.; Sawamoto, M.; Meijer, E. W.; Palmans, A. R. A. *J. Polym. Sci., Part A: Polym. Chem.* **2014**, *52*, 12–20.

47. Huerta, E.; Stals, P. J. M.; Meijer, E. W.; Palmans, A. R. A. *Angew. Chem., Int. Ed.* **2013**, *52*, 2906–2910.

48. Brunsveld, L.; Zhang, H.; Glasbeek, M.; Vekemans, J. A. J. M.; Meijer, E. W. *J.Am. Chem. Soc.* **2000**, *122*, 6175–6182.
49. Lutz, J.-F. *Acc. Chem. Res.* **2013**, *46*, 2696–2705.
50. Perez-Baena, I.; Loinaz, I.; Padro, D.; Garcia, I.; Grande, H. J.; Odriozola, I. *J. Mater. Chem.* **2010**, *20*, 6916–6922.
51. Sanchez-Sanchez, A.; Akbari, S.; Moreno, A.J.; Lo Verso, F.; Arbe, A.; Colmenero, J.; Pomposo, J. A. *Macromol. Rapid Commun.* **2013**, *34*, 1681–1686.

Chapter 22

Sequence-Controlled Multi-Block Glycopolymers via Cu(0) Mediated Living Radical Polymerization

Qiang Zhang,[1] Jennifer Collins,[1] Athina Anastasaki,[1] Russell Wallis,[2] Daniel A. Mitchell,[3] C. Remzi Becer,[1] Paul Wilson,[1] and David M. Haddleton[1,*]

[1]Department of Chemistry, University of Warwick, CV4 7AL, Coventry, UK
[2]Department of Biochemistry, University of Leicester, LE1 9HN, Leicester, UK
[3]Clinical Sciences Research Institute, Warwick Medical School, University of Warwick, CV2 2DX, Coventry, UK
*E-mail: D.M.Haddleton@warwick.ac.uk

Synthetic glycopolymers with pendant saccharides bind to mammalian carbohydrate-recognition proteins with high affinity due to their multivalency and primary structure. However, glycoproteins function in nature via an exquisitely tuned "glycocode" and mimicking this code remains an interesting challenge in polymer chemistry. In order to address this we have synthesized glycomonomers via a [3+2] cycloaddition reaction between sugar-alkyne and azido-acrylates and these monomers were used to synthesize a series of sequence controlled glycopolymers (SCGP) using single electron transfer living radical polymerization (SET-LRP).

Introduction

Glycan-protein interactions are responsible for many physiological processes including cell-cell recognition, cell adhesion, cell signalling, pathogen identification and differentiation. These non-covalent interactions also play an

essential role in infectious disease processes such as pathogen-cell interactions and immune responses. This work was designed to utilize developments in SET-LRP (single electron transfer living radical polymerization), a Cu(0)-mediated controlled/living radical polymerization technique. This relatively new chemistry allows access to well-defined, high MW polymers at ambient and near ambient temperatures, SET-LRP gives polymers with outstanding PDI and end group fidelity. Typical PDI values are in the range of 1.05-1.10 up to very high monomer (>99%) conversion with little quantifiable bimolecular termination observed for a variety of acrylates. This advance allows sequence control of functionality within polymer chains.

Our targets were driven by dendritic cells (DC) recognition events, which are the most antigen presenting cells and form a major component of the human immune system. Dendritic cells act as messengers between the innate and adaptive immunity and their main function is to process antigen material and present it on the surface to other cells of the immune system such as T-cells. Dendritic cell-specific intercellular adhesion molecule-3-grabbing non-integrin (DC-SIGN; CD209) is a C-type lectin (carbohydrate-binding protein) present on both macrophages and dendritic cell subpopulations. DC-SIGN binds to microorganisms and host molecules by recognizing surface rich mannose containing glycans through multivalent glycan-protein interactions and notably serves a target molecule for several viruses such as human immunodeficiency virus (HIV) and hepatitis C virus (HCV) (*1–6*). Therefore, synthetic lectins are of interest with Davis *et. al.* reporting the discovery of a simple monocyclic host, which was prepared in five steps and 23% overall yield instead of 21 steps and 0.1% yield (*7*). Alternatively, non-carbohydrate inhibitors of mammalian lectins can be used to prevent the interaction between DC-SIGN and gp120 (*8–10*). The architectures of the multivalent ligands can have a large effect on carbohydrate binding to lectins and the use of linear polymers on effective lectin binding has been demonstrated by several research groups (*11–16*).

Carbohydrate sequence and conformation potentially supply a vast source of information and act to transfer biological information beyond the genetic code, namely "sugar code" or "glyco code", which has been proved to play a critical role during evolution (*17–19*). Sequence control in polymer synthesis had been largely ignored mainly due to the difficulty in precise control and characterization during monomer sequencing (*20–22*). Templated polymerization and step-growth polymerization could also result in sequence-specific polymers (*23–25*). Chain-growth copolymerization tends to be more promising for complex monomer sequence construction, including random, block, alternate and gradient microstructures (*25*).

Synthetic polymer chemistry has developed rapidly in the last few decades owing to much to the discovery of controlled/living radical polymerization and more recently the combination of this methodology with efficient click reactions (*26–30*). Currently, polymerization of functional monomers with desired chain length, architecture and composition is straightforward whereas sequence control structures (*24, 31*) and the and the control of folding of synthetic macromolecules remain important challenges in polymer chemistry (*32*). There are a few recent reports where sufficient control has been achieved in controlling the monomer

sequence along the polymer chain (*33–37*). Of note is a successful sequence controlled polymerization technique, single electron transfer living radical polymerization (SET-LRP) (*35, 38–40*), which allows for the facile synthesis of high-order multiblock copolymers *via* iterative monomer addition in an one-pot reaction featuring high yield, high chain end fidelity and requiring purification only at the last step (*35*).

The synthesis of glycopolymers featuring well-defined macromolecular architectures has been developed by using different polymerization techniques and click reactions (*41, 42*). However, direct transition metal-catalyzed polymerization of unprotected glyco monomers is still limited mainly due to the difficulty in synthesis of unprotected glyco monomers and optimization of polymerization conditions (*12, 37, 43–46*). This inspired us to introduce SET-LRP for the synthesis of sequence-controlled glycopolymers for a glycopolymer code. and the demonstration of their binding to the human lectin DC-SIGN (*47*).

Results and Discussion

Synthesis of Glycomonomers via CuAAC Click Reaction

In order to obtain some degree of control over the sugar sequence, different carbohydrate units can be inserted along the polymer backbone either through polymerization of different sugar monomers or via post-modification after polymerization. Based on the demand of carbohydrate diversity, direct polymerization of different functional glyco monomers is the first choice compared with multistep chemical modification following polymerization.

We decided to utilize a copper-catalyzed azide-alkyne cycloaddition (CuAAC), which provides a facile route for the synthesis of glycomonomers. The use of azide functionalized sugars and methacrylate type sugar monomers allows for novel 4-vinyl-1, 2, 3-triazole type sugar monomers to be synthesized *via* reaction with alkyne compounds in MeOH/H_2O or THF/H_2O with $CuSO_4$/sodium ascorbate catalysis (*12, 48*). In order to demonstrate an alternative approach, a one-pot Fischer type glycosylation reaction was first conducted to prepare alkyne-functionalised sugars, which were then reacted with an azide acrylate intermediate *via* a CuAAC reaction in MeOH/H_2O under the catalysis of $CuSO_4$/sodium ascorbate.

Three different stable solid acrylate glyco monomers were obtained through this protocol, Scheme 1. ^{1}H NMR clearly revealed the appearance of a triazole ring proton at ~7.9 ppm and vinyl peaks at 5.5-6.5 ppm after the click reaction, Figure 1. The ^{13}C NMR spectrum showed the existence of D-glucose C-1 peaks at 99.6 & 103.6 ppm, suggesting that the monomer is present as an anomeric mixture. The combination of this data with further ESI-MS and FT-IR analysis proved that targeted glyco monomer had been successfully synthesized. D-mannose and L-fucose acrylate monomers were also synthesized in same way.
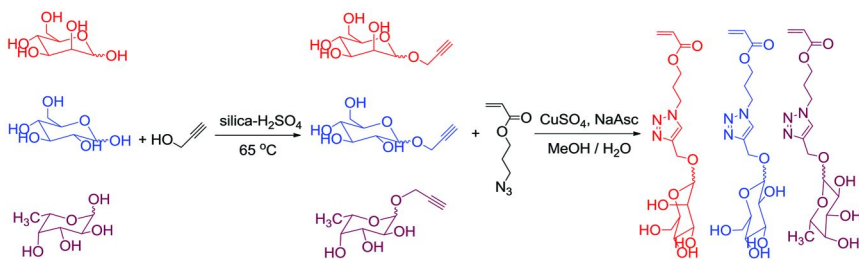
Scheme 1. Synthesis of glycomonomers via Fischer glycosylation & CuAAC.
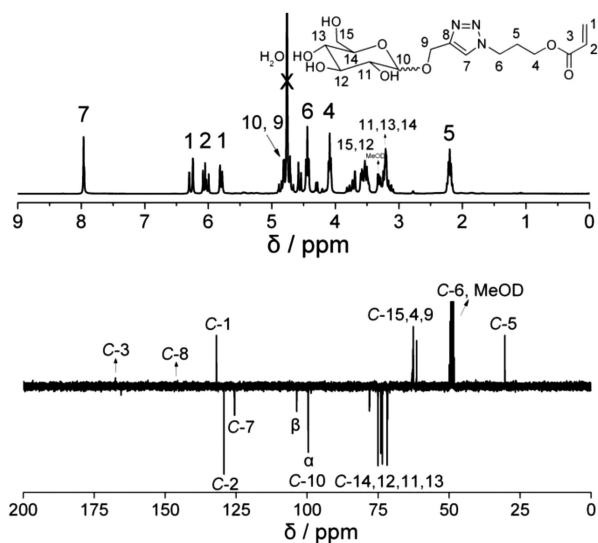
Figure 1. ^1H (top) and ^{13}C (bottom) NMR spectra of D-glucose acrylate monomer in MeOD.

Homopolymerization of Glycomonomers by SET-LRP in DMSO at Ambient Temperature

The glycomonomers had good solubility in DMSO and were polymerized at ambient temperature using the Cu(0)/Cu(II)/Me$_6$TREN system with EBiB as initiator and DMSO as solvent (Scheme 2). Monomer conversion reached 91% in 4 h and after 24 h full conversion was observed, Figure 2. The number average molecular weight (M_n) as measured by DMF SEC generally increased linearly with monomer conversion. However, the M_n by SEC is higher than the theoretical molecular weight mainly due to the different structure of glycopolymers with the PMMA calibration standards, which cause a significant difference of hydrodynamic volume of polymers in DMF. The molecular weight

distribution remained narrow ($M_w/M_n<1.10$) throughout the polymerization, even after full conversion; no significant bimolecular termination could be detected by SEC, which revealed high chain end fidelity. A linear agreement in the plot of Ln[M]$_0$/[M] versus time was observed, which indicates that the concentration of growing radicals remains fairly constant during propagation and termination is not significant.
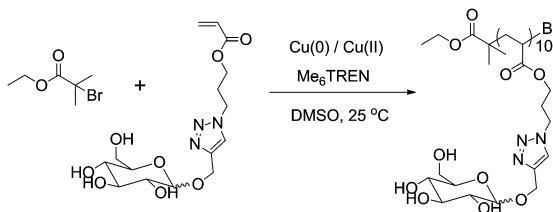
Scheme 2. Homo polymerization of D-glucose acrylate monomer with [EBiB]$_0$ = 33 mmol/L, [CuBr$_2$]$_0$ = 3.3 mmol/L, [Me$_6$TREN]$_0$ = 6 mmol/L in DMSO (3 mL), 25 °C. Reproduced with permission from reference (47). Copyright (2013) Wiley-VCH.

From the ^{1}H NMR spectrum, Figure 3, the resonance of the broad triazole ring protons at 8.1 ppm and D-glucose protons from 2.8 to 5.2 ppm indicated that glucose units have been attached to the polymer backbone. Furthermore, the ratio of integral for the triazole ring protons at 8.11 ppm with EBiB methyl groups at 1.04 to 1.12 is approximately 10: 9.4, which is in good agreement with the theoretical value (10: 9), suggesting the successful and efficient synthesis of D-glucose glycopolymers.

Synthesis of Multiblock Glycopolymers via an Iterative Monomer Addition Approach by SET-LRP

The synthesis of high-order multiblock glycopolymers with very short blocks (DP=2 for each block, (mannose)$_2$-(glucose)$_2$-(mannose)$_2$-(glucose)$_2$-(mannose)$_2$-(glucose)$_2$) was first explored by SET-LRP via iterative chain extension under similar reaction condition, Scheme 3. Long reaction times were required to ensure monomer conversion of each block was close to full conversion such that no purification procedure was necessary for subsequent steps of the reaction. The conversion of the first four blocks by NMR showed close to 100% as evidenced by disappearance of vinyl groups at 5.7-6.5 ppm. With the addition of monomer in DMSO for chain extension, the system became more diluted and traces of vinyl groups could be detected since 5th and 6th block (conversion is 99%, 97% in turn).
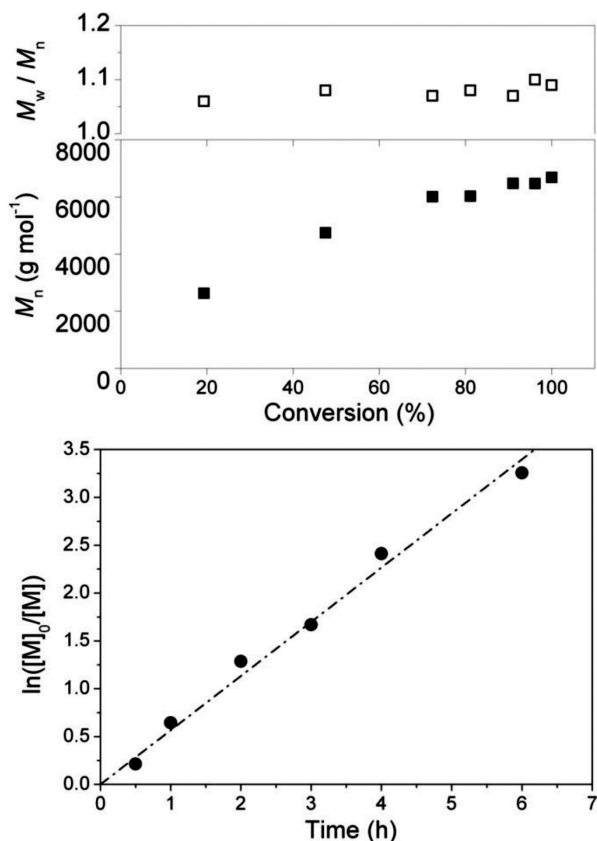
Figure 2. Dependence of M_n and M_w/M_n on conversion (top) and first order kinetic plots (bottom) for the polymerization of D-glucose glycomonomer via SET-LRP in DMSO. Reproduced with permission from reference (47). Copyright (2013) Wiley-VCH.

During the synthesis of the first five blocks, SEC traces (Figure 4) clearly shift after chain extension and M_w/M_n remained narrow (for the 5th block M_w/M_n = 1.15, even including the tailing peak), confirming that the polymerizations are well-controlled. A small tailing peak at low molecular weight which may be caused by termination reaction could be detected; however, when compared with the propagating polymer peak this ratio is small. After the 6th block the SEC trace became broader and the Mw/Mn increased to 1.21. Although no appreciable shoulder peaks at high MW were found, the SEC trace did not shift totally compared with the 5th block, suggesting partial termination. The addition of further blocks was, therefore, not attempted.
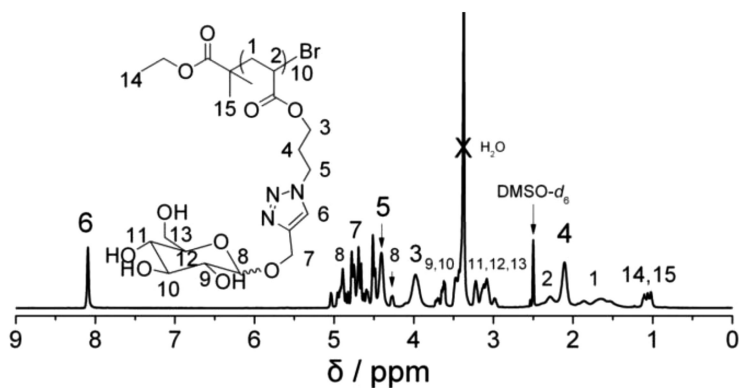
Figure 3. ¹H NMR spectrum of D-glucose glycopolymer in DMSO-d_6. Reproduced with permission from reference (47). Copyright (2013) Wiley-VCH.
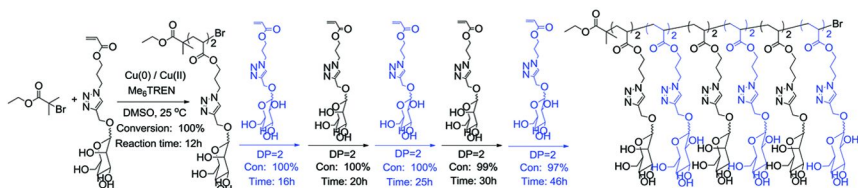
Scheme 3. Schematic representation for the synthesis of sequence-controlled multiblock glycopolymer by iterative addition of glycomonomers without intermediate purification (DP = 2 for each block). Reproduced with permission from reference (47). Copyright (2013) Wiley-VCH.

High resolution ESI-MS (Figure 5, Figure 6) and MALDI-ToF MS analysis (Figure 7) were performed to characterize the structure of glycopolymer during polymerization. High resolution ESI-MS spectra, Figure 5, show peaks belonging to the 1st block poly(mannose)$_2$, which reveal the exact structure of extremely low DP glycopolymer with only 1, 2, 3 and 4 mannose units initiated with EBiB and terminated with bromine. Typically, Figure 5, DP = 2 showed mass peaks at 943.3, 965.3 and 981.3 (*m/z*), which include H+, Na+ and K+ cations respectively. Peaks at 863.4, 885.4 and 901.4 (*m/z*) were attributed to dead polymer chains with a terminal hydrogen, which were mainly caused by disproportionation and a chain transfer side reaction that leads to the loss of the terminal bromine. However, the signals from these peaks were weaker than those of propagating polymer chains.
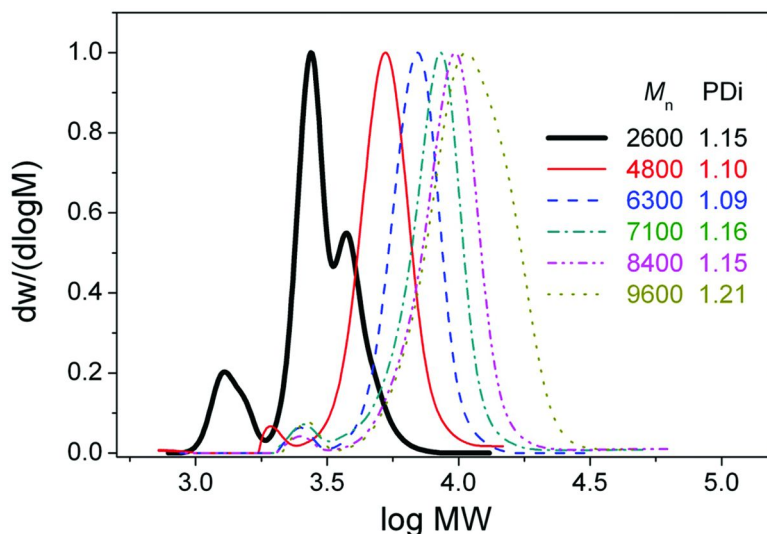
Figure 4. Molecular weight distributions (normalized to peak height) of multiblock glycopolymer obtained by SET-LRP via iterative chain extensions (DP = 2 for each block). Reproduced with permission from reference (47). Copyright (2013) Wiley-VCH.

Subsequent to the chain extension reaction, the main peaks (Figure 6) shifted to higher MW region by 2-3 units, which are in accord with theoretical values and SEC results.

As a comparison, MALDI-ToF MS was also used for the characterization of these glycopolymers, which showed similar results as in the ESI-MS analysis. Following the block copolymerization the polymer peaks have a significant shift to higher MW region, Figure 7, suggesting the success of block copolymerization. However, with the increase of MW and incorporation of more sugar units, the ionization of the glycopolymer tends to become more difficult. Thus, the resolution of the spectra decreased and it became impossible to define the exact structure after the 3rd block polymerization. After the 4th block polymerization no signal can be detected.

The ^{1}H NMR spectrum of the final polymer product also revealed peaks from mannose and glucose units, typically shown as peaks of C-1 protons at 4.8 and 4.9 ppm (Figure 8). Thus, the results showed the successful synthesis of a multiblock glycopolymer and that the microstructure is controlled.
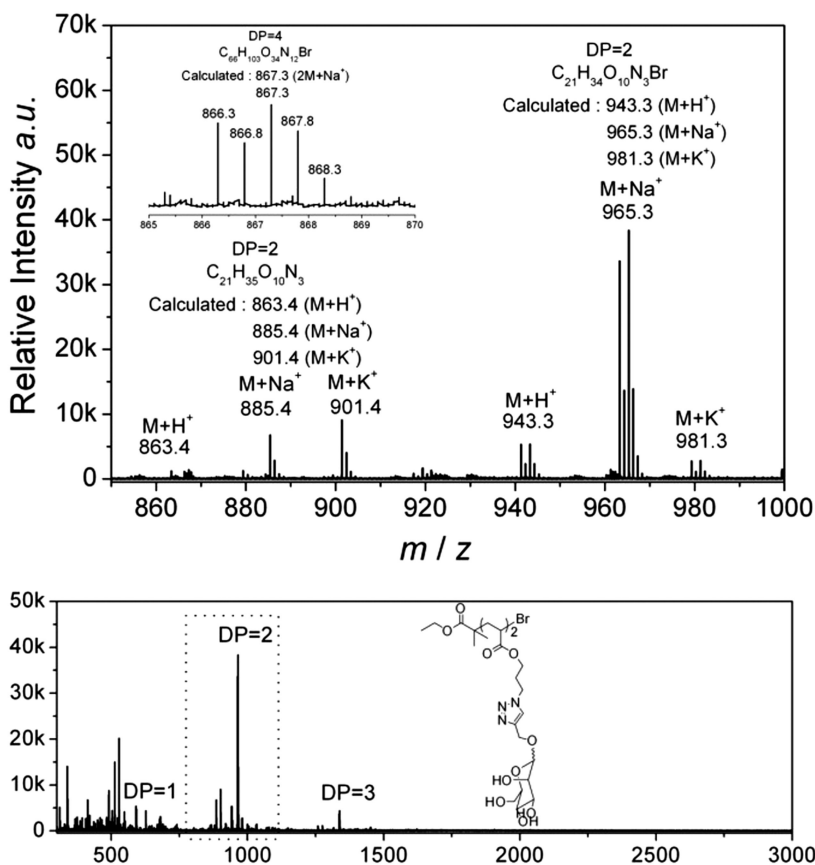
Figure 5. ESI-MS spectra of the 1st block poly(mannose)₂ by SET-LRP (top: whole spectra; bottom: zoom of 800-1000 region). Reproduced with permission from reference (47). Copyright (2013) Wiley-VCH.

The chain length of each block was then increased to DP = 4 with an overnight reaction carried out to ensure full conversion (the first three blocks) was achieved (Scheme 4).

The SEC traces shift totally after the 2nd block polymerization and no significant tailing or coupling peaks were found, Figure 9. However, after the 3rd monomer addition the PDI increased to 1.22 and tailing peaks at lower MW position were observed. After the 4th block with a conversion of 60% the PDI increased to 1.37 and double peaks were noticed, including the one overlapped with the 3rd peak due to termination and the shoulder peak at higher MW region due to on-going chain propagation.
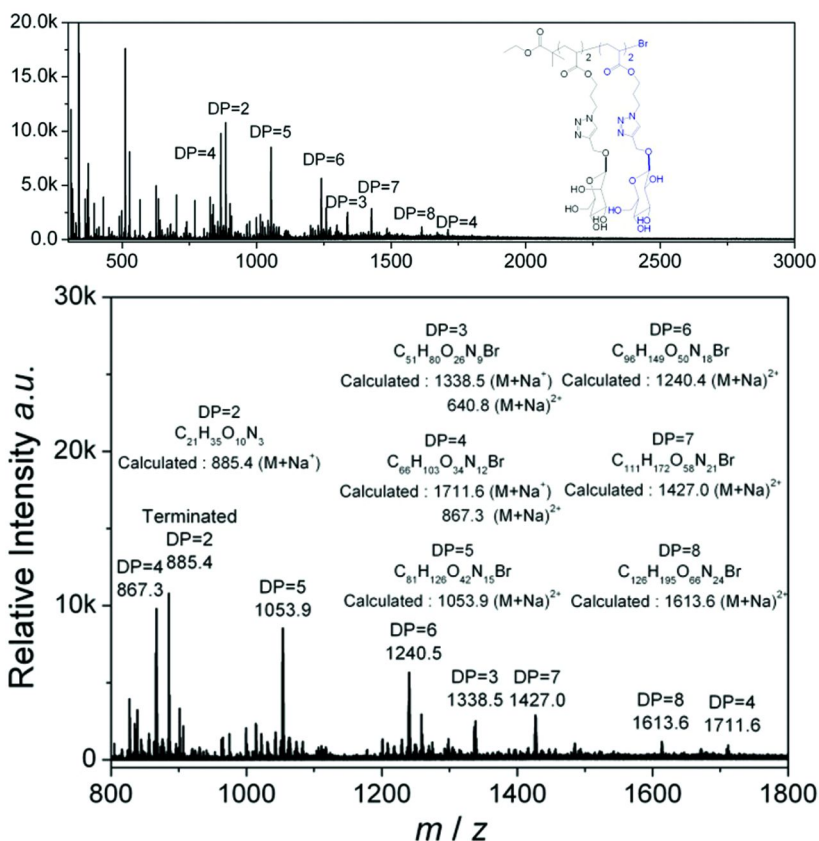
Figure 6. ESI-MS spectra of the 2nd block poly(mannose)$_2$-(glucose)$_2$ by SET-LRP(top: whole spectra; bottom: zoom of 800-1800 region). Reproduced with permission from reference (47). Copyright (2013) Wiley-VCH.

To summarize, these experiments demonstrated the successful synthesis of multiblock glycopolymers *via* a facile iterative monomer addition. However, after multiblock synthesis and full conversion polymerization termination was significant and chain propagation thus stopped. Further research especially on the reaction mechanism is necessary to develop a full understanding.
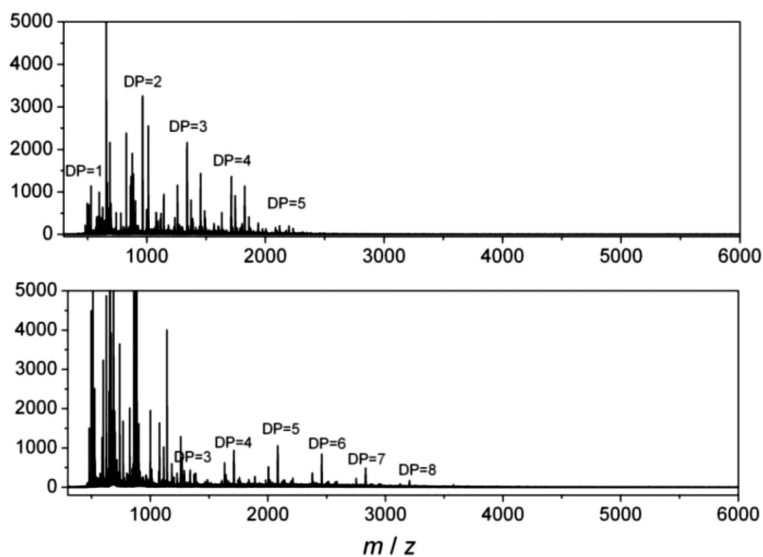
Figure 7. MALDI-ToF MS spectra of the 1st block poly(mannose)₂ (top) and 2nd block poly(mannose)₂-(glucose)₂ (bottom) glycopolymers obtained by SET-LRP. Reproduced with permission from reference (47). Copyright (2013) Wiley-VCH.
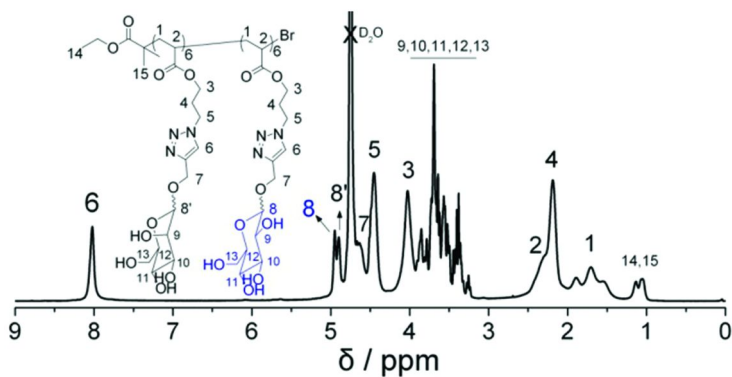
Figure 8. ¹H NMR spectrum of multiblock D-mannose/D-Glucose glycopolymer in D₂O. Reproduced with permission from reference (47). Copyright (2013) Wiley-VCH.
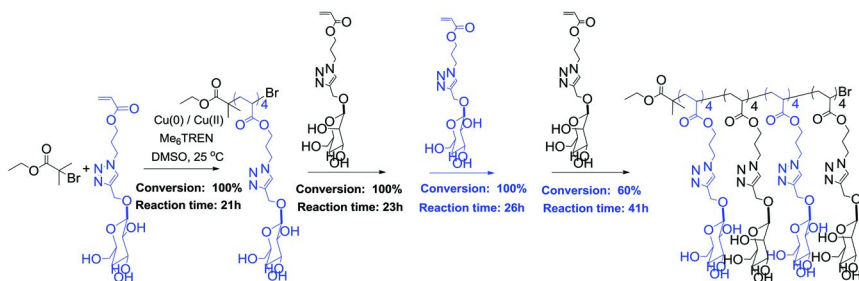
Scheme 4. Schematic representation for the synthesis of sequence-controlled multiblock glycopolymers by iterative addition of glyco monomers without intermediate purification (DP=4 for each block). Reproduced with permission from reference (47). Copyright (2013) Wiley-VCH.
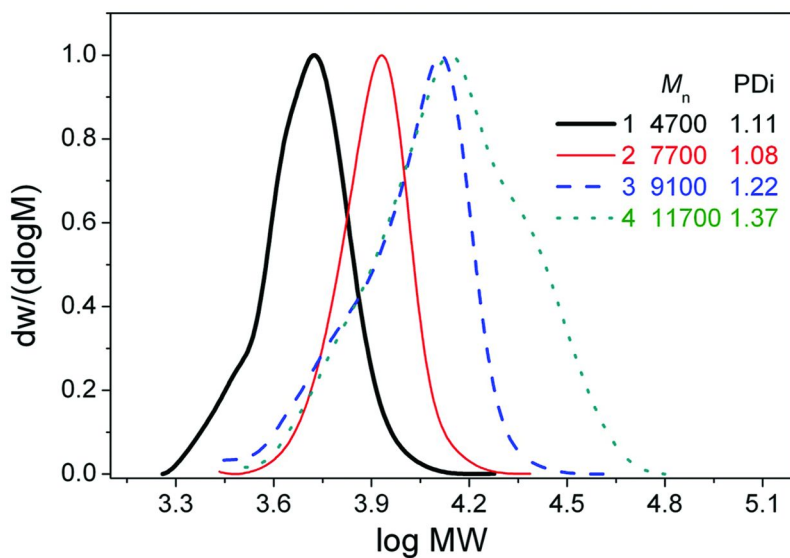
Figure 9. Molecular weight distributions (normalized to peak height) of multiblock glycopolymer obtained by SET-LRP via iterative chain extensions (DP=4 for each block). Reproduced with permission from reference (47). Copyright (2013) Wiley-VCH.

Control of Sugar Sequence in Glycopolymers via Iterative Monomer Addition before Full Conversion by SET-LRP

Cu(II) has been used as a deactivator to reduce the rate of SET-LRP in order to remove the period of slow reaction rate at the start of the reaction (*40, 49*). Cu(II) added initially has also been proved to play an important role in maintaining the chain end fidelity during one-pot multiblock copolymerization (*35, 50*) and preventing the star-star coupling in the synthesis of star copolymers (*51*). Livingness for a decablock copolymer could be kept up to more than 50% according to SEC, although tailing peaks caused by dead polymers in each block could be detected (*50*).

In previous experiments, radical coupling termination was not significant in the presence of Cu(II) added at the start of the reaction, however, termination by disproportionation and chain transfer still occurred during the polymerization. In order to reach full conversion, the reaction time was increased with the addition of new monomer which unavoidably diluted the reaction system. The total reaction time was more than one week, which is generally uncommon and possibly would lead to increased termination side reaction. However, due to the complexity of this reaction system the exact reason is still not perfectly understood.

In order to solve this problem it was thought better to add new monomer prior to full conversion. In order to test this strategy, new monomer was added after a period of around four hour in a one-pot polymerization, Scheme 5.
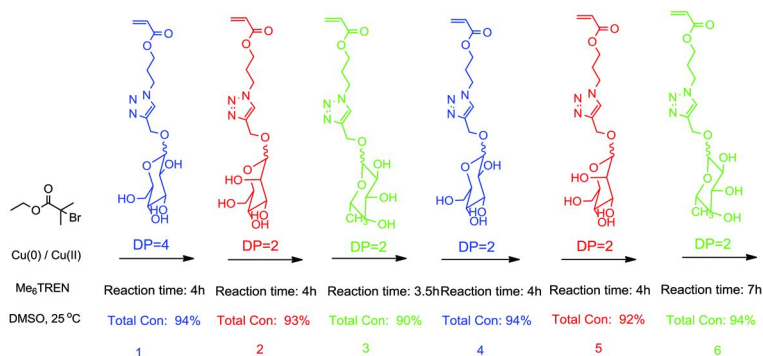
Scheme 5. Schematic representation for the synthesis of multiblock glycopolymers by iterative addition of glyco monomers at defined time period. Reproduced with permission from reference (47). Copyright (2013) Wiley-VCH.

The ^{1}H NMR showed that total conversion is around 90%-94% and after 5th block reaction time need to be prolonged to 7 h in order to reach a similar conversion. The high conversion means that the obtained glycopolymer is still highly sequence-controlled, although it is not strictly a multiblock copolymer. SEC analysis (Figure 10) revealed the total shift of elution traces after each monomer addition and final M_w/M_n is ≈ 1.13 and no significant tailing or coupling peaks were detected during the polymerization, indicating that the chain end fidelity is better than the long time scale full conversion reaction.
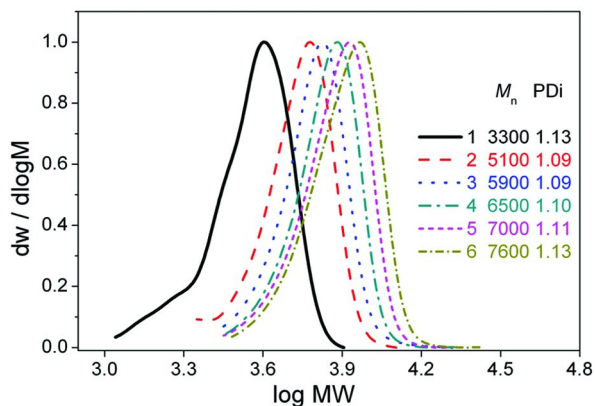
Figure 10. Molecular weight distributions (normalized to peak height) of multiblock glycopolymers obtained by SET-LRP via iterative addition of glyco monomers at defined time period. Reproduced with permission from reference (47). Copyright (2013) Wiley-VCH.

These results revealed that it is possible to control the glyco code during polymerization via controlled addition of different glyco monomers at high conversion. The "*cluster glycoside effect*" is defined as "*an affinity enhancement over and beyond what would be expected from the concentration increase of the determinant sugar in a multivalent ligand*" (*52*). Glycopolymers are a typical class of polyvalent glycosidic ligands can dramatically increase the affinity during the multivalent carbohydrate-protein interaction (*53*). The dense sugar units along the polymer backbone create a cluster glycoside effect and the binding ability of glycopolymers with lectins compared with monosaccharide was thus dramatically enhanced. It has been shown that the number of sugars, sugar density, ligand shape, size and linker spacing strongly contribute to the specific binding behaviour (*54–57*). In order to further understand the multivalent binding of polymeric ligands, it is of importance to control the density, distance and distribution of sugar units along the polymer chain.

Thus SET-LRP was utilized to synthesize a multiblock glycopolymer bearing sequential lectin-binding and lectin-non-binding segments. DEGEEA and mannose glycomonomer were used as monomers for the non-binding and binding blocks and the DP was controlled aT 6 and 3 Iin order to aid characterization, the reaction time was kept longer after each chain extension to gain a high conversion (total conversion was 93%-97% according to ^{1}H NMR) yet new monomer was added before full conversion in order to keep high chain end fidelity, Scheme 6.
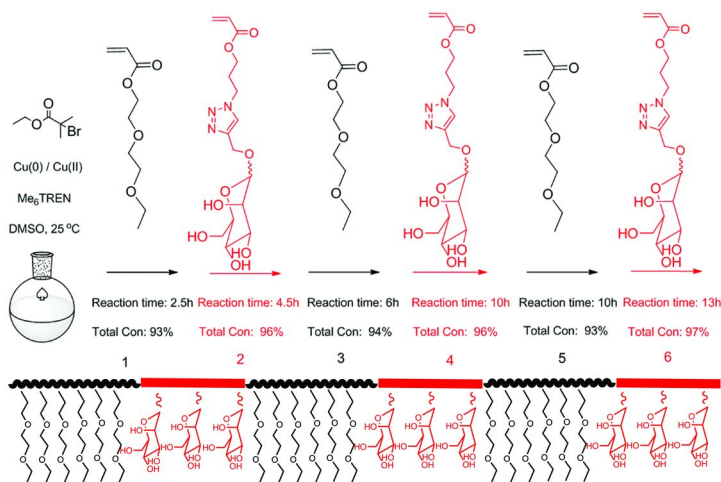
Scheme 6. Schematic representation for the synthesis of sequence-controlled multiblock glycopolymers by iterative addition of DEGEEA and mannose glycomonomer at defined time period. Reproduced with permission from reference (47). Copyright (2013) Wiley-VCH.

SEC analysis confirmed the MW increase after each chain extension, Figure 11. Although some tailing after chain extension (especially after the 4th block polymerization), causing a slight dispersity increase, the final dispersity was still relatively narrow (~1.2), indicating high chain end fidelity. The ^{1}H NMR spectrum (Figure 12) of the final product clearly showed resonances and correct ratio of mannose and DEGEEA units, such as 8.1 ppm (triazole ring proton) & 4.9 ppm (C-1 proton) for the mannose and 3.4 - 3.8 ppm (ethylene glycol protons) for the DEGEEA.
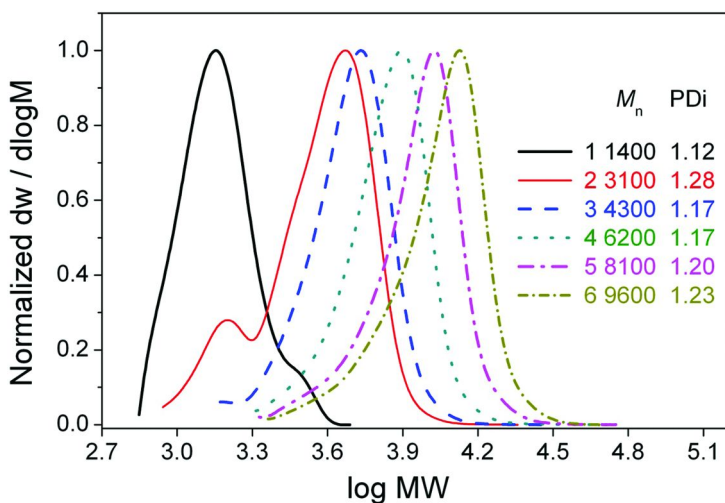
Figure 11. Molecular weight distributions of multiblock glycopolymer obtained by SET-LRP via iterative addition of DEGEEA and mannose glycomonomer at defined time period. Reproduced with permission from reference (47). Copyright (2013) Wiley-VCH.
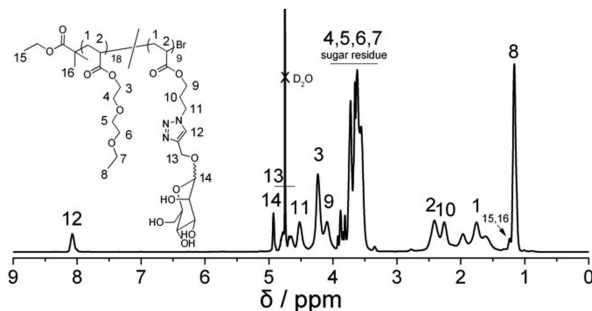
Figure 12. ^1H NMR spectrum of multiblock DEGEEA-mannose glycopolymer in D$_2$O. Reproduced with permission from reference (47). Copyright (2013) Wiley-VCH.

MALDI-ToF MS analysis supported a successful block structure and the MW increased after the chain extension, Figure 13. As previous characterization, resolution of the spectra decreased with incorporation of more sugar units. However, MADLI-ToF MS (linear mode) still revealed the appearance of polymer peaks at higher MW region although exact structure cannot be defined. In order to demonstrate the versatility of this synthetic protocol, the multiblock copolymerization of DEGEEA and D-glucose monomer was conducted in the same way and similar results were obtained (see experimental section). Homo mannose glycopolymer and random DEGEEA-Mannose glycopolymer with similar chains and DEGEEA to mannose ratio were also synthesised in order

to compare the different lectin-binding behaviour with sequence-controlled multiblock glycopolymer. These results show the successful synthesis of multiblock DEGEEA-Mannose glycopolymer, which means that sugar density and distribution along polymer chain can be adjusted by the control of monomer addition during SET-LRP.
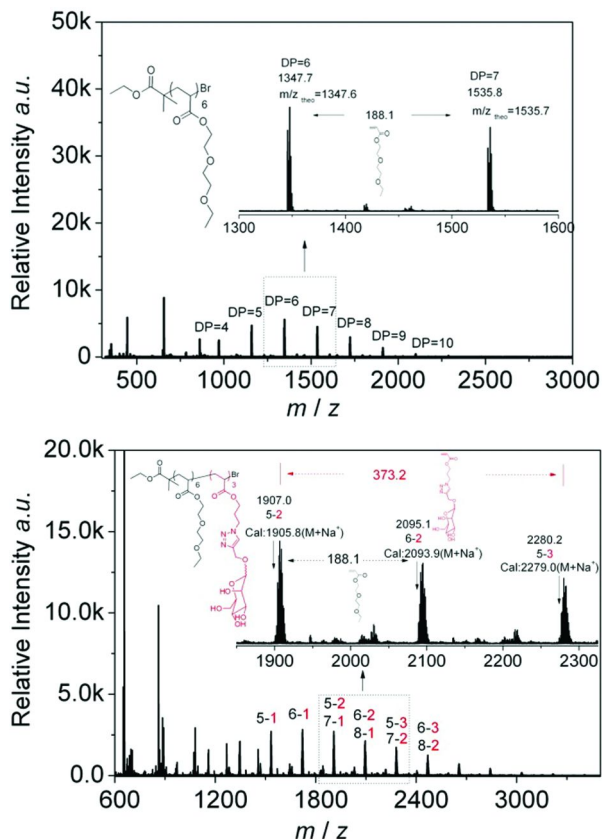
Figure 13. MALDI-ToF MS spectra of the 1st block poly(DEGEEA)₆ (top) and 2nd block poly(DEGEEA)₆-b-(mannose)₃ (bottom) glycopolymers obtained by SET-LRP. Reproduced with permission from reference (47). Copyright (2013) Wiley-VCH.

Chain End Group Functionalization of Multiblock Glycopolymer by CuAAC

High chain end fidelity was retained during SET-LRP and the functionality could be used for further modification (*35*). In order to obtain a terminal end functional glycopolymer for bio-conjugation, the bromine end group of a multiblock DEGEEA-Mannose glycopolymer was transformed into azido group and then used for CuAAC reaction with alkyne-functionalised dibromomaleimide, Scheme 7.
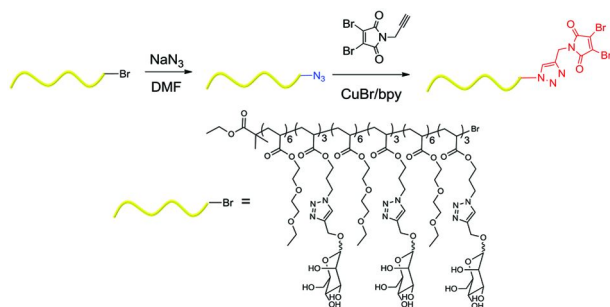
Scheme 7. Schematic representation for the azido and CuAAC modification of multiblock glycopolymer. Reproduced with permission from reference (47). Copyright (2013) Wiley-VCH.

FT-IR spectra (Figure 14) showed the appearance and disappearance of an azide absorbance at 2116 cm^{-1}, indicating the successful reaction with NaN$_3$ and a further CuAAC reaction. The dibromomaleimide modified polymer following the CuAAC reaction was characterized *via* DMF SEC equipped with RI and UV detectors (Figure 15). The elution traces by UV detector at $\lambda = 400$ nm showed a significant absorbance peak compared with azide-functionalised polymer, which is attributed to the clicked dibromomaleimide group according to previous research (*58*, *59*). The elution time of the peak in UV detector is the same as in RI detector indicating a maleimide-functionalised polymer.

These results show that the terminal bromine end groups have been successfully modified into dibromomaleimide groups *via* CuAAC reaction, which could be potentially used for conjugation with thiol-containing peptide and protein.
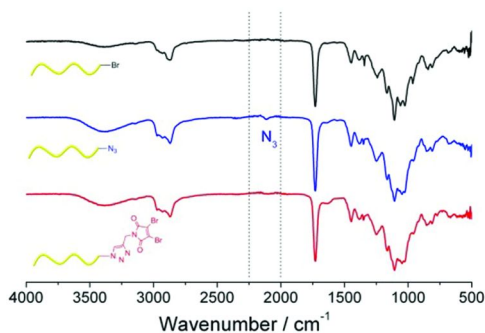
Figure 14. FT-IR spectra of azide and dibromomaleimide modified multiblock glycopolymer. Reproduced with permission from reference (47). Copyright (2013) Wiley-VCH.
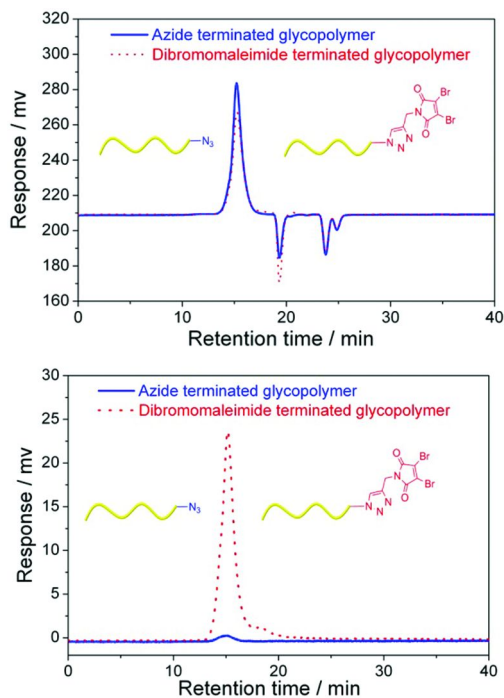
Figure 15. DMF SEC elution traces of the azide and dibromomaleimide modified glycopolymer via RI detector (left) & UV detector at 400 nm (right). Reproduced with permission from reference (47). Copyright (2013) Wiley-VCH.

Conclusion

In conclusion, we have prepared sequence controlled multi-block glycopolymers in various compositions by the polymerization of glycomonomers via SET-LRP. Glycomonomers containing mannose, glucose and fucose moieties were synthesized by the CuAAC click reaction of a sugar alkyne and azide acrylate, which were subsequently copolymerized in different sequences. Polymerizations were followed by ^{1}H NMR, SEC and HR ESI-MS or MALDI-ToF MS to obtain information on the products. This technique provides very precise control over the monomer sequence along the polymer chain. Moreover, the polymerization is performed in one pot by sequential addition of the subsequent monomers in a relatively a large scale, which is critical when compared with the preparation of synthetic glycans or lectins. The synthesized polymers reported here show distinct binding properties to DC-SIGN and an inhibition of the DC-SIGN binding to HIV gp120 using nano molar concentrations. We believe the approach presented here will help to open new avenues not only in polymer science but also in chemical biology and dendritic cell physiology.

References

1. Geijtenbeek, T. B. H.; Kwon, D. S.; Torensma, R.; van Vliet, S. J.; van Duijnhoven, G. C. F.; Middel, J.; Cornelissen, I. L. M. H. A.; Nottet, H. S. L. M.; KewalRamani, V. N.; Littman, D. R.; Figdor, C. G.; van Kooyk, Y. *Cell* **2000**, *100*, 587–597.

2. Marzi, A.; Gramberg, T.; Simmons, G.; Möller, P.; Rennekamp, A. J.; Krumbiegel, M.; Geier, M.; Eisemann, J.; Turza, N.; Saunier, B.; Steinkasserer, A.; Becker, S.; Bates, P.; Hofmann, H.; Pöhlmann, S. *J. Virol.* **2004**, *78*, 12090–12095.

3. Balzarini, J. *Antiviral Res.* **2006**, *71*, 237–247.

4. François, K. O.; Balzarini, J. *Med. Res. Rev.* **2012**, *32*, 349–387.

5. Toone, E. J. *Curr. Opin. Struct. Biol.* **1994**, *4*, 719–728.

6. Ambrosi, M.; Cameron, N. R.; Davis, B. G. *Org. Biomol. Chem.* **2005**, *3*, 1593–1608.

7. Ke, C.; Destecroix, H.; Crump, M. P.; Davis, A. P. *Nat. Chem.* **2012**, *4*, 718–723.

8. Borrok, M. J.; Kiessling, L. L. *J. Am. Chem. Soc.* **2007**, *129*, 12780–12785.

9. Mahalingam, A.; Geonnotti, A. R.; Balzarini, J.; Kiser, P. F. *Mol. Pharm.* **2011**, *8*, 2465–2475.

10. Doores, K. J.; Fulton, Z.; Hong, V.; Patel, M. K.; Scanlan, C. N.; Wormald, M. R.; Finn, M. G.; Burton, D. R.; Wilson, I. A.; Davis, B. G. *Proc. Natl. Acad. Sci. U.S.A.* **2010**, *107*, 17107–17112.

11. Gestwicki, J. E.; Cairo, C. W.; Strong, L. E.; Oetjen, K. A.; Kiessling, L. L. *J. Am. Chem. Soc.* **2002**, *124*, 14922–14933.

12. Geng, J.; Mantovani, G.; Tao, L.; Nicolas, J.; Chen, G.; Wallis, R.; Mitchell, D. A.; Johnson, B. R. G.; Evans, S. D.; Haddleton, D. M. *J. Am. Chem. Soc.* **2007**, *129*, 15156–15163.

13. Pieters, R. J. *Org. Biomol. Chem.* **2009**, *7*, 2013–2025.

14. Ponader, D.; Wojcik, F.; Beceren-Braun, F.; Dernedde, J.; Hartmann, L. *Biomacromolecules* **2012**, *13*, 1845–1852.

15. Miura, Y. *Polym. J.* **2012**, *44*, 679–689.

16. Becer, C. R. *Macromol. Rapid Commun.* **2012**, *33*, 742–752.

17. Feizi, T.; Chai, W. *Nat. Rev. Mol. Cell Biol.* **2004**, *5*, 582–588.

18. Gabius, H. J. *Naturwissenschaften* **2000**, *87*, 108–121.

19. Gabius, H.-J.; Siebert, H.-C.; André, S.; Jiménez-Barbero, J.; Rüdiger, H. *ChemBioChem* **2004**, *5*, 740–764.

20. Badi, N.; Lutz, J.-F. *Chem. Soc. Rev.* **2009**, *38*, 3383–3390.

21. Merrifield, R. B. *Angew. Chem., Int. Ed.* **1985**, *24*, 799–810.

22. Seeberger, P. H. *Chem. Soc. Rev.* **2008**, *37*, 19–28.

23. Połowiński, S. *Prog. Polym. Sci.* **2002**, *27*, 537–577.

24. Ida, S.; Terashima, T.; Ouchi, M.; Sawamoto, M. *J. Am. Chem. Soc.* **2009**, *131*, 10808–10809.

25. Lutz, J.-F. *Polym. Chem.* **2010**, *1*, 55–62.

26. Kolb, H. C.; Finn, M. G.; Sharpless, K. B. *Angew. Chem., Int. Ed.* **2001**, *40*, 2004–2021.

27. Becer, C. R.; Hoogenboom, R.; Schubert, U. S. *Angew. Chem., Int. Ed.* **2009**, *48*, 4900–4908.

28. Rosen, B. M.; Percec, V. *Chem. Rev.* **2009**, *109*, 5069–5119.

29. Ouchi, M.; Terashima, T.; Sawamoto, M. *Chem. Rev.* **2009**, *109*, 4963–5050.

30. Matyjaszewski, K.; Xia, J. *Chem. Rev.* **2001**, *101*, 2921–2990.

31. Hibi, Y.; Tokuoka, S.; Terashima, T.; Ouchi, M.; Sawamoto, M. *Polym. Chem.* **2011**, *2*, 341–347.

32. Schmidt, B. V. K. J.; Fechler, N.; Falkenhagen, J.; Lutz, J.-F. *Nat. Chem.* **2011**, *3*, 234–238.

33. Lutz, J.-F. *Nat. Chem.* **2010**, *2*, 84–85.

34. McHale, R.; Patterson, J. P.; Zetterlund, P. B.; O'Reilly, R. K. *Nat. Chem.* **2012**, *4*, 491–497.

35. Soeriyadi, A. H.; Boyer, C.; Nyström, F.; Zetterlund, P. B.; Whittaker, M. R. *J. Am. Chem. Soc.* **2011**, *133*, 11128–11131.

36. Nakatani, K.; Ogura, Y.; Koda, Y.; Terashima, T.; Sawamoto, M. *J. Am. Chem. Soc.* **2012**, *134*, 4373–4383.

37. León, O.; Bordegé, V.; Muñoz-Bonilla, A.; Sánchez-Chaves, M.; Fernández-García, M. *J. Polym. Sci. A: Polym. Chem.* **2010**, *48*, 3623–3631.

38. Percec, V.; Guliashvili, T.; Ladislaw, J. S.; Wistrand, A.; Stjerndahl, A.; Sienkowska, M. J.; Monteiro, M. J.; Sahoo, S. *J. Am. Chem. Soc.* **2006**, *128*, 14156–14165.

39. Nguyen, N. H.; Kulis, J.; Sun, H.-J.; Jia, Z.; van Beusekom, B.; Levere, M. E.; Wilson, D. A.; Monteiro, M. J.; Percec, V. *Polym. Chem.* **2013**, *4*, 144–155.

40. Levere, M. E.; Willoughby, I.; O'Donohue, S.; de Cuendias, A.; Grice, A. J.; Fidge, C.; Becer, C. R.; Haddleton, D. M. *Polym. Chem.* **2010**, *1*, 1086–1094.

41. Ting, S. R. S.; Chen, G.; Stenzel, M. H. *Polym. Chem.* **2010**, *1*, 1392–1412.

42. Slavin, S.; Burns, J.; Haddleton, D. M.; Becer, C. R. *Eur. Polym. J.* **2011**, *47*, 435–446.

43. Vázquez-Dorbatt, V.; Maynard, H. D. *Biomacromolecules* **2006**, *7*, 2297–2302.

44. Dai, X.-H.; Dong, C.-M. *J. Polym. Sci. A: Polym. Chem.* **2008**, *46*, 817–829.

45. Mateescu, A.; Ye, J.; Narain, R.; Vamvakaki, M. *Soft Matter* **2009**, *5*, 1621–1629.

46. Mizukami, K.; Takakura, H.; Matsunaga, T.; Kitano, H. *Colloids Surf., B* **2008**, *66*, 110–118.

47. Zhang, Q.; Collins, J.; Anastasaki, A.; Wallis, R.; Mitchell, D. A.; Becer, C. R.; Haddleton, D. M. *Angew. Chem., Int. Ed.* **2013**, *52*, 4435–4439.

48. Hetzer, M.; Chen, G.; Barner-Kowollik, C.; Stenzel, M. H. *Macromol. Biosci.* **2010**, *10*, 119–126.

49. Levere, M. E.; Willoughby, I.; O'Donohue, S.; Wright, P. M.; Grice, A. J.; Fidge, C.; Remzi Becer, C.; Haddleton, D. M. *J. Polym. Sci. A: Polym. Chem.* **2011**, *49*, 1753–1763.

50. Boyer, C.; Soeriyadi, A. H.; Zetterlund, P. B.; Whittaker, M. R. *Macromolecules* **2011**, *44*, 8028–8033.

51. Boyer, C.; Derveaux, A.; Zetterlund, P. B.; Whittaker, M. R. *Polym. Chem.* **2012**, *3*, 117–123.

52. Lee, Y. C.; Lee, R. T. *Acc. Chem. Res.* **1995**, *28*, 321–327.
53. Sigal, G. B.; Mammen, M.; Dahmann, G.; Whitesides, G. M. *J. Am. Chem. Soc.* **1996**, *118*, 3789–3800.
54. Kiessling, L. L.; Pohl, N. L. *Chem. Biol.* **1996**, *3*, 71–77.
55. Cairo, C. W.; Gestwicki, J. E.; Kanai, M.; Kiessling, L. L. *J. Am. Chem. Soc.* **2002**, *124*, 1615–1619.
56. Roy, R.; Page, D.; Perez, S. F.; Bencomo, V. V. *Glycoconjugate J.* **1998**, *15*, 251–263.
57. Richards, S.-J.; Jones, M. W.; Hunaban, M.; Haddleton, D. M.; Gibson, M. I. *Angew. Chem., Int. Ed.* **2012**, *51*, 7812–7816.
58. Jones, M. W.; Strickland, R. A.; Schumacher, F. F.; Caddick, S.; Baker, J. R.; Gibson, M. I.; Haddleton, D. M. *J. Am. Chem. Soc.* **2011**, *134*, 1847–1852.
59. Jones, M. W.; Strickland, R. A.; Schumacher, F. F.; Caddick, S.; Baker, J. R.; Gibson, M. I.; Haddleton, D. M. *Chem. Commun.* **2012**, *48*, 4064–4066.

Chapter 23

Sequence-Controlled Ring-Opening Polymerization: Synthesis of New Polyester Structures

Emilie Brulé,[1,2] Carine Robert,[1] and Christophe M. Thomas[1,*]

[1]PSL Research University, CNRS - Chimie ParisTech, Institut de Recherche de Chimie Paris, 75005 Paris, France
[2]Sorbonne Universités, UPMC Univ Paris 06, UFR926, F-75005, Paris, France
***E-mail: christophe.thomas@chimie-paristech.fr; Fax: +33(0)143260061; Tel: +33(0)144276721**

In order to obtain alternating/stereocontrolled polymers, coordination polymerization using well-defined metal complexes has played a leading role in the last two decades. We have described selected published efforts to achieve these research goals using discrete, structurally well-characterized metal complexes.

Keywords: Catalysis; Polyester; Ring-Opening Polymerization; Alternating

Introduction

Of the variety of biodegradable polymers known, linear aliphatic polyesters have a leading position and are commonly produced by ring-opening polymerization (ROP) of cyclic esters (*1*, *2*). In contrast to polyesterification, ROP of cyclic monomers proceeds under mild reaction conditions and avoids the formation of small molecule byproducts. Among the various ROP processes, including anionic, cationic, organocatalytic and coordination-insertion, the latter has gained increasing attention (*3*). It is now commonly accepted that the most efficient method for the production of well-controlled polyesters

in terms of molecular weight, composition and microstructure, is ROP with metal-coordination initiators (*4*). Therefore, a large number of investigations have been directed towards synthesizing efficient metal-based initiators and studying their reactivities. However, current aliphatic polyesters are far from being optimal and tailor-made structures are certainly needed. In the case of simple aliphatic polyesters, the available options for molecular optimization are relatively limited. Indeed, only a few macromolecular parameters can be varied, *e.g.* chain length, molecular weight distribution, chain-ends, architecture and microstructure. In particular, the control over chain microstructure (*i.e.* tacticity and monomer sequences) may lead to highly-optimized macromolecules with tailored properties (*5*). However, when polymers are made from more than one different type of monomer in a single pot process, it is difficult to control their primary structure to any significant extent.

Catalyst design is an efficient option for sequence/stereochemistry control. In this regard, the application of readily available stereopure monomers in association with stereocontrolled ROP has enabled the facile manipulation of the tacticity of the resultant polyesters, considerably affecting their properties. For instance it has been already demonstrated that tacticity may substantially influence the degradation rates of synthetic polyesters (*6*, *7*). In order to obtain alternating polymers, coordination polymerization using well-defined metal complexes has played a leading role in the last two decades. The goal of the proposed article is the description of catalysts that allow higher order sequence control of this latter type, and create alternating macromolecular structures with advanced properties. Herein, three practical examples will be discussed. It will first be shown that ROP techniques are interesting tools for preparing macromolecular architectures containing sequence-defined segments. For instance, heterotactic polylactides and alternating/syndiotactic polyhydroxyalkanoates prepared by ROP will be presented in this chapter. Also, comonomer sequences can be directly controlled in a ROP process. This aspect will be discussed in the second section of this chapter.

Synthesis of Heterotactic PLA from *rac*-Lactide

The earliest examples were reported by Coates with a class of β-diiminate zinc complexes (*8*).   These achiral derivatives featured high activities and selectivities, affording highly heterotactic polylactide (PLA) (P_r up to 0.94) from racemic lactide (*rac*-LA), by incorporating the (*R,R*)- and (*S,S*)-LA in an alternating fashion (Figure 1). Notably it was shown that the aryl groups' substituents on the β-diiminate ligand exert a significant influence upon the course of the polymerizations, affecting both the degree of stereoselectivity and the rate of polymerization. For instance, complex **1c** exhibited the highest activity and stereoselectivity of the zinc complexes studied for the polymerization of *rac*-lactide to PLA. However, changing the ligand substituents from isopropyl to *n*-propyl or ethyl groups resulted in a decrease in heterotacticity (Figure 2).
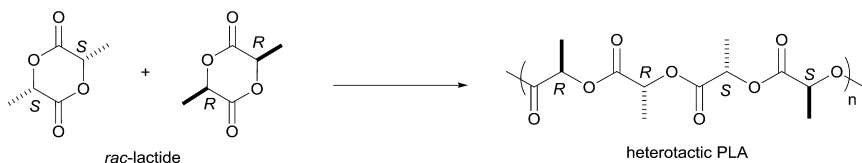
Figure 1. Synthesis of heterotactic PLA.

In 2004, Gibson and coworkers reported high levels of heterotacticity with aluminum initiators stabilized by tetradentate phenoxyamine (salan-type) ligands (*9*) (*e.g.* complexes **2c** and **2d**, Figure 2). The microstructures of the poly(lactide)s obtained were also found to be dependent upon the ancillary ligand substituents (P_r up to 0.96). In particular, it was shown that the size of the nitrogen substituents R^1 plays a crucial role on the tacticity of the polymer produced using these initiators. On the basis of the single-crystal X-ray analysis of complex **2d**, Gibson proposed that the alkylamino backbone substituents can closely approach the site of polymer chain growth and thereby influence monomer selectivity.

1a: R = Et
1b: R = *n*Pr
1c: R = *i*Pr

2a: R^1 = Me, R^2 = H
2b: R^1 = CH$_2$Ph, R^2 = H
2c: R^1 = CH$_2$Ph, R^2 = Cl
2d: R^1 = Me, R^2 = Me

3a: X = N(SiMe$_3$)$_2$
3b: X = OC$_6$H$_3$-2,6-*i*Pr$_2$
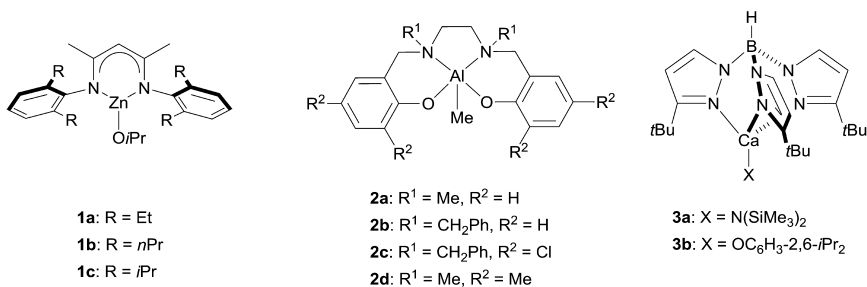
Figure 2. Stereoselective systems for the heterotactic ROP of rac-lactide.

Chisholm investigated a series of tris-pyrazolyl borate (Tp^R, R = *i*Pr, *t*Bu for instance) calcium complexes for lactide polymerization (Figure 2) (*10*). The monomeric amide or aryloxide complexes of the form (Tp^{tBu})CaX (**3a-b**) were shown to be highly active and stereoselective, leading to heterotactic PLA (P_r = 0.90). The use of bulky substituent as seen in the Tp^{tBu} ligand is necessary to confer single-site living polymerization behavior and stereoselectivity in the ring-opening event.

Moving towards a different metal-based system, Thomas and Davidson have recently reported the first examples of single-site germanium initiators for the ROP of LA (Figure 3) (*11*, *12*). Catalytic experiments showed that the C_3-symmetric Ge-based isopropoxide system **4** was active for the solvent-free ROP of *rac*-LA, to provide heterotactic-enriched PLA (up to 0.82). Having identified an active catalyst which displays promising selectivity, Davidson decided to investigate different germanium complexes with the aim of optimizing the selectivity and activity of germanium-based single-site initiators for ROP of LA. Unfortunately, the synthetic route used for **4** proved to be unsuitable for other Ge-O*i*Pr complexes.
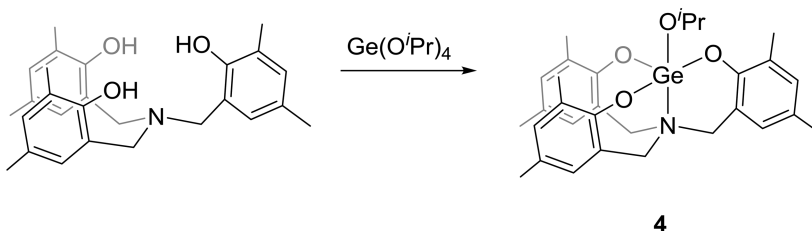
Figure 3. Synthesis of germanium-based complex 4.

In 2009 Hillmyer and Tolman prepared highly heterotactic PLA ($0.86 < P_r <$ 0.94 at 25°C, $P_r = 0.97$ at 0°C) from *rac*-LA using an easily accessible catalyst prepared *in situ* from indium trichloride, benzyl alcohol and triethylamine (*13*). The resulting robust system was found to operate under a variety of reaction conditions to yield heterotactic PLA with controlled molecular weight and a narrow molecular weight distribution.

As early as 2002, Coates described the catalytic behavior of a new heteroleptic yttrium alkoxide complex (*14*). Although this derivative revealed higher activity than the corresponding aluminum derivative, no stereoselectivity was observed for the polymerization of *rac*-LA. From this study, other research groups anticipated that rare-earth metal complexes supported by multidentate bis(phenoxide) ligands would be of interest in order to achieve effective ROP of *rac*-LA (*15*). For instance, Okuda reported the synthesis of several lanthanoid complexes such as **5** and **6** supported by 1,ω-dithiaalkanediyl-bridged bis(phenoxide) ligands (Figure 4) (*16*). Once again, the ancillary ligand proved to be crucial for polymerization selectivity. Among these bis(phenoxide) derivatives, scandium complexes **5a** and **6a** showed high heterotactic selectivity (P_r up to 0.95) which was attributed to a dynamic monomer-recognition process involving interconversion of the ligand configuration.

5a: Ln = Sc	**6a**: Ln = Sc
5b: Ln = Lu	**6b**: Ln = Lu
5c: Ln = Y	**6c**: Ln = Y
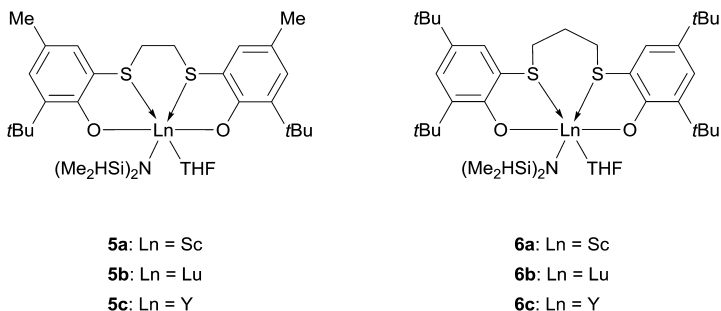
Figure 4. Lanthanide complexes supported by dichalcogen bridged bis(phenoxide) ligands.

The reactivity of yttrium, neodymium and lanthanum-based metal derivatives supported by amino-bis(phenoxide) ligands was also investigated (*17*). In

particular, the yttrium amido complexes **7a-d** (Figure 5) have demonstrated an interesting ability for mediating the heterotactic living polymerization of *rac*-LA (P_r up to 0.96) (*18*). It was demonstrated that the steric bulk of the *ortho*-phenoxide substituents plays a crucial role in achieving high selectivity for the chain-end controlled polymerization of *rac*-lactide. For instance, complex **7b**, which bears cumyl (α,α-dimethylbenzyl) groups in the *ortho* positions of the phenoxides, produced heterotactic-enriched polymer (P_r = 0.90), whereas complex **7a** gave lower selectivity (P_r = 0.80) for heterotactic PLA. By using bulkier groups as R^1 substituents, PLAs produced by **7c-d** were found to be substantially more heterotactic, with P_r values of respectively 0.95 and 0.96.
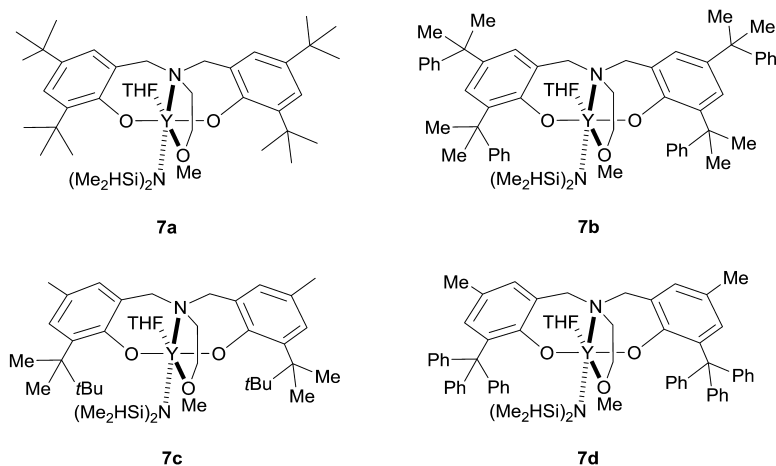
Figure 5. Stereoselective yttrium-based systems for the heterotactic ROP of rac-lactide.

Synthesis of Syndiotactic PHB from *rac*-BBL

Despite the increasing number of studies dealing with the ROP of *rac*-β-butyrolactone using metal complexes for the last decade, there is still a limited number of initiators capable of producing highly syndiotactic-enriched PHB (Figure 6) (*19, 20*).

Gross first showed that (*n*Bu)₃Sn(OMe) **8a** was able to polymerize *rac*-BBL with a moderate probability of racemic linkage between monomer P_r of 0.70 at 40°C (Figure 7) (*21*). When the temperature is increased, the selectivity decreased but the reactivity was improved with 70% yield of low molecular weight PHB after several days at 75°C. With less bulky (*n*Bu)₂Sn(OMe)₂ **8b** complex, a P_r value of 0.72 could be reached at 0°C (*22*). Kricheldorf further studied the influence of the number of butyl groups coordinated to the tin metal center and thus compared the reactivity of the least steric (*n*Bu)Sn(OMe)₃ **8c** (*23*). It was found that (*n*Bu)₂Sn(OMe)₂ **8b** exhibited the highest activity with molecular weight lower than 10 000 g.mol⁻¹, and that the stereoselectivity increased with the steric hindrance around the metal. Bis(tributyl) and bis(triaryl)

tin oxides **9a-b** (*22*) were also tested for the ROP of *rac*-BBL and induced similar syndiotacticity of 0.6-0.7 depending on temperature, suggesting a chain-end control of stereoselectivity rather than catalyst site. In the case of dialkyl tin oxide **10** as initiators, the nature of alkyl group is important since variation of reactivity and stereoselectivity was observed. Indeed while Me$_2$SnO **10a** was inactive, Et$_2$SnO **10b** and Bu$_2$SnO **10c** displayed highest reactivity with M_n up to 80 000 g.mol^{-1} and similar P_r of 0.72 at 100°C and 50°C respectively (*24*). It was the first example of selectivity occurring at high temperature. Surprisingly the bulkiest di(octyl)tin oxide **10d** led to poorer selectivity. More recently, the use of distannoxanes **11** as catalysts (*25*, *26*) was investigated but still moderate and similar syndiospecificity was obtained (P_r = 0.58-0.67) for the ROP of *rac*-BBL.

Since the reports using Sn(IV) complexes as catalysts for the preparation of syndiotactic enriched PHBs, almost all recent studies deal with the use of discrete metal complexes of group 3 and lanthanides except one using metals of group 4. Various bi- tri- and tetradentate ligands bearing nitrogen and/or oxygen atoms have been selected and initiators were either metal amides or alkoxides.
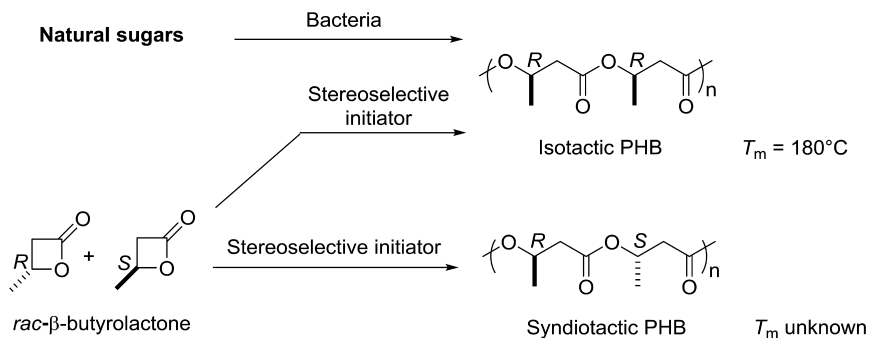
Figure 6. Synthesis of iso- or syndiotactic PHBs by the ROP of rac-BBL.
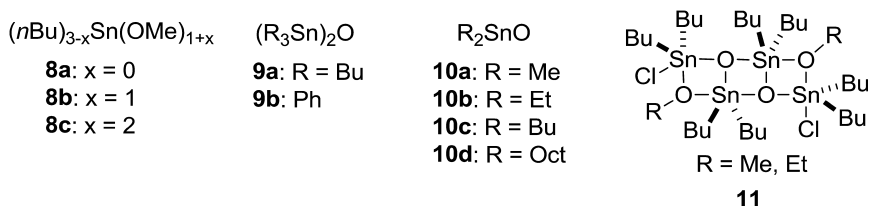
Figure 7. Sn(IV) complexes as initiators for the syndiotactic ROP of rac-BBL.

Bidentate pro-ligand guanidine was chosen by Carpentier and co-workers (*27*) who reported the synthesis new bis(guanidinate) isopropoxide complexes of yttrium **12a** and lutetium **12b** which display interesting syndioselectivity for the ROP of *rac*-BBL (Figure 8). P_r between 0.80 and 0.84 were obtained depending on the solvent of polymerization (THF or toluene) and a chain-end control mechanism was confirmed using ^{13}C NMR spectroscopy. Although the two complexes displayed similar selectivity, they differed regarding their reactivity. The yttrium complex **12a** was much more active than its lutetium counterpart **12b** with TOF of 50 h^{-1} and 2 h^{-1} respectively.

12a: Ln = Y
12b: Ln = Lu

13a: Ln = Y
13b: Ln = La
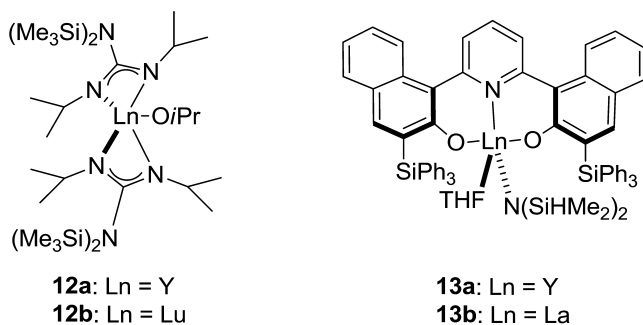
Figure 8. Rare earth metal complexes.

The same group also investigated the synthesis of rare earth metal (Sc, Y, La) complexes bearing sterically demanding *o*-substituted bis(naphthoxide)-pyridine and -thiophene tridentate ligands (*28*) (Figure 8). The complexes were characterized and shown to be mononuclear, 5-coordinate around the metal (coordination of amido group and THF) and *C*s-symmetrical. Among all of the complexes synthesized, bis(naphthoxide)-pyridine of yttrium **13a** and lanthanum **13b** were the only catalysts affording syndiotactic-enriched PHB with a high probability for racemic linkage of 0.87 and 0.86 respectively, in toluene. In order to reach a value of 0.87 using complex **13a**, 1 equivalent of isopropanol was added to generate *in situ* the isopropoxide complex and the reaction temperature was conducted at 50°C instead of 20°C to increase the reactivity (TOF of 200 h^{-1} *vs* 20 h^{-1} at 20°C without addition of isopropanol). While yttrium amido complex **13a** (without isopropanol addition) afforded a P_r lowered to 0.76, the lanthanum-amido complex **13b** displayed itself high syndioselectivity ($P_r = 0.86$) and was more productive than **13a** even at 20°C (TOF 720 h^{-1}).

Several examples of yttrium complexes bearing tetradentate ligands have also been reported as efficient initiators for the production of syndiotactic PHB. Thomas *et al.* (*29, 30*) investigated the activity and selectivity of amino-alkoxy-bis(phenoxide) complexes **14a-c** prepared *in situ* from the amido N(SiHMe$_3$)$_2$ counterparts (Figure 9). These complexes led to controlled polymerization of *rac*-BBL with polydispersity around 1.1 and experimental molecular weights close to theoretical ones. The authors showed that complex **10b** was able to convert 1740 equivalents and that **14b** and **14c** are very productive

with TOF up to 23500 h^{-1}. Moreover these complexes displayed the highest probability of racemic linkage to date (P_r = 0.94) at room temperature for **14c** and at -20°C for **14b**. Complex **14a** which contains *tert*-butyl groups in *ortho* positions was less syndioselective (P_r = 0.81). The authors further studied the influence of the nature of the *ortho* substituent situated on the phenoxide moieties on the resulting tacticity. Complexes substituted with chloro or $CMe_2(4-CF_3C_6H_4)$ groups were also synthesized and tested and the chloro complex led to atactic polymer while the CF_3-aryl analogue induce syndiotactic stereocontrol of 82% (*31*). DFT computations on model intermediates showed the importance of the presence of an *ortho*-aryl substituent for high syndiotacticity such as on **14b-c** since this aryl is involved in a stabilized CH···π interaction with the methylene group of opened BBL. Electronic properties are thus involved in the mechanism of polymerization as well as a chain-end control mechanism by acyl cleavage of BBL, confirmed by NMR studies. Thomas and coworkers also looked at the influence of the syndiotactic degree of the polymers on the thermal properties and it was demonstrated that the melting point (T_m) of the polymers increased linearly with the syndiotacticity. The highest T_m reached 183°C and corresponded to the 94% enriched syndiotactic PHB obtained with **14c**.
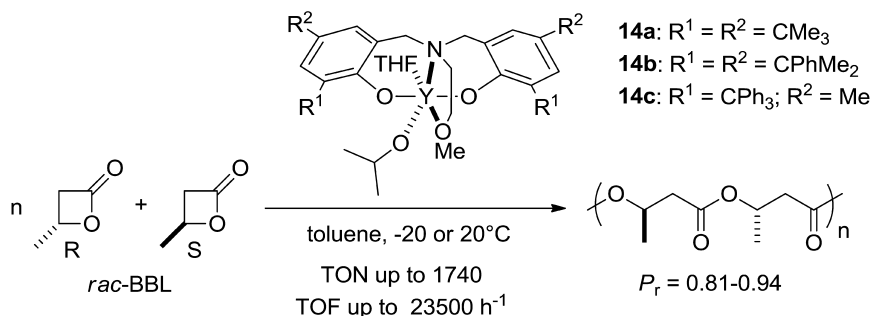
Figure 9. Amino-alkoxy-bis(phenolate) alkoxide-yttrium complexes for the synthesis of highly syndiotactic PHB.

More recently, Yao and co-workers utilized a similar amino-bis(phenol) pro-ligand to that of complex **14a** but the methoxide side chain was replaced by an amine group (Figure 10) (*32*). Moreover the rare earth metal (Y, Yb, Er, and Sm) complexes alkoxides were isolated and not prepared *in situ* as it was the case for **14a-c**. Three yttrium-alkoxide complexes **15a-c** were obtained by addition of 2,2,2-trifluoroethanol, benzyl alcohol and 2-propanol. In the case of ytterbium, erbium and samarium, only 2,2,2-trifluoroethoxide complexes **16a-c** were synthesized and the X-ray structure of all the complexes were obtained. For the polymerization of *rac*-BBL, it was shown that the polymerization was controlled with a narrow distribution of the PHB formed ($M_w/M_n < 1.26$) and that the activity of the complexes followed the trend of Yb>Er>Y>>Sm, which corresponds to an increase of ionic radii of the rare earth metals. The ytterbium complex **16a** displayed the highest productivity of these initiators with a TON of 1900 and a TOF of 12000 h^{-1} while a TOF of 45 h^{-1} was obtained with the samarium

analogue **16c**. No further characterization of the polymer was given. On the contrary, regarding the selectivity of the PHB formed, the metal did not have any influence as 82% syndiotactic-enriched polymers were obtained in all cases in toluene. There was no influence of the nature of the alkoxide neither since the three different yttrium complexes exhibited the same activity and selectivity. A ^{1}H NMR study of the polymer obtained using the benzyloxy yttrium complex **15b** and analysis of the chain-end groups revealed a coordination-insertion mechanism but some crotonate was also observed, typical of elimination side-reaction.

15a: R = *i*Pr
15b: R = CH₂Ph
15c: R = CH₂CF₃

16a: Ln = Yb
16b: Ln = Er
16c: Ln = Sm

Nu = N(SiHMe₂)₂
17a: R¹ = R² = CMe₂Ph
17b: R¹ = adamantyl, R² = Me
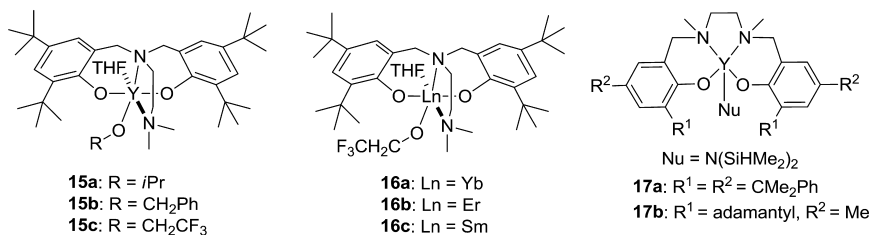
Figure 10. Amine-bridged amino-bis(phenoxide) alkoxy-rare earth metal and salan amido yttrium complexes.

Other tetradentate pro-ligands often used in catalysis are Schiff bases of salan- and salen-type. Pellechia *et al.* (*33*) reported the synthesis of amido-yttrium complexes of salan-type **17a-b** and binaphthyl-bridged salen-type for the ROP of *rac*-BBL (Figure 10). Complex **17a** was the most active although much less productive than the amino-bis(phenoxide) rare earth metal complexes described above (TOF of only 122 h^{-1} at 70°C). The syndioselectivity was also moderate as a probability of racemic linkage P_r of 0.81 was obtained with the best initiator **17a** at 20°C and 70°C. The salen-type complexes produced PHBs syndiotactic-enriched at 76% at 20°C. The less selective initiator was the bulky and rigid adamantyl-substituted salan complex **17b** (P_r = 0.64 at 20°C). Considering this latter result the author suggested that the selectivity originated from both the chirality of last inserted BBL unit (chain-end control mechanism) and the chirality of the ligand around the metal center (enantiomorphic site control).

Only one report deals with group 4 metal complexes for the production of syndiotactic-enriched PHB. Davidson *et al.* used amino-tris(phenol) pro-ligands **L¹H₃-L³H₃** bearing substituents with different steric and electronic properties (Figure 11) (*34*). Titanium(IV), zirconium(IV) and hafnium(IV) isopropoxide complexes **18a-c** were synthesized by addition of the appropriate precursor to the pro-ligands. In the solid state, dimer complexes were formed whereas in solution monomeric species are present, and the authors suggested that the initiator is predominantly monomeric in the presence of an excess of *rac*-BBL. Narrow distributions were obtained for the polymers in the presence of all complexes but the titanium initiators **18a** did not induce any selectivity and displayed only poor activity. The zirconium and hafnium analogs **18b-c** were more active although not very productive with similar TON and TOF of 300 and 40-50 h^{-1} respectively. Moreover syndiotactic-enriched PHB were obtained with both metal complexes

albeit moderate degrees of stereocontrol 64-76% were observed. The hafnium initiators were the most selective (P_r of 0.74-0.76) in the presence of ligands containing a *tert*-butyl group in *para* position (**L²**) of the third phenoxide group or without substitution (**L¹**) (Figure 12). The chloro-substituted Hf(IV) complex {Hf(**L³**)(O*i*Pr)}$_2$ led to a poorer selectivity of 68%. The MALDI-TOF analysis of the polymers indicated that the chain-end groups were isopropoxide and a proton on the other side.
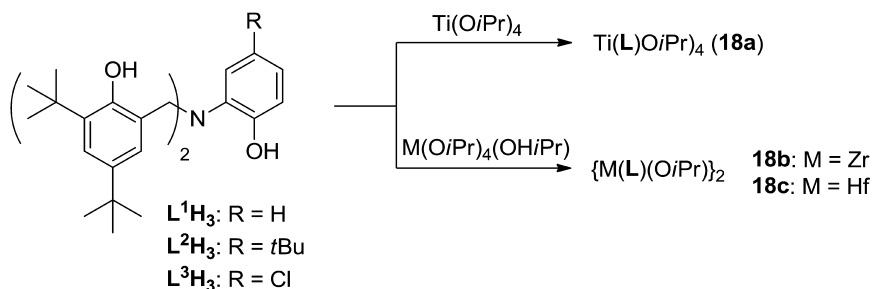
Figure 11. Tris(phenol) ligands coordinated to group 4 metals.
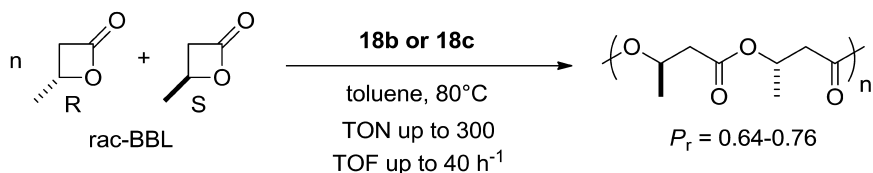
Figure 12. Tris(phenoxide) zirconium and hafnium(IV) complexes for the synthesis of PHB.

Other PHAs have also been prepared in a sequence-control approach using yttrium complexes. Thomas *et al.* (*35*) investigated the copolymerization of *rac*-BBL and *rac*-allyl-β-butyrolactone (*rac*-allylBBL) using the tetradentate amino-alkoxy-bis(phenoxide) yttrium-amido complex **7a** (Figure 13). Syndiotactic-enriched random copolymers were produced with a probability of racemic linkage between 0.80 and 0.84. Different ratios of both monomers were studied and in all cases 80% of *rac*-allylBBL was converted. A plot conversion vs time carried out for a 1:1 ratio of monomers showed that both monomers were consumed at the same time. The copolymers formed were determined to be monomodal and characterized by NMR spectroscopy. Moreover narrow distribution was observed as well as accordance of the experimental and theoretical molecular weights when up to 300 equivalents of monomers polymerized. Thermal analyses revealed that the copolymer is semi-crystalline but an increase of the amount of *rac*-allylBBL decreased the crystallinity of the copolymer (decrease of T_m and T_g). This result was predictable as the homopolymer poly(*rac*-allylBBL) is amorphous. The allyl side-chains of the copolymer were further functionalized by hydroxy groups and epoxides

without any change of distribution in the resulting polymer, and similar thermal properties to pristine copolymer were obtained. The encapsulation and release of *L*-leuprolide with some of these copolymers was also investigated (*36*).
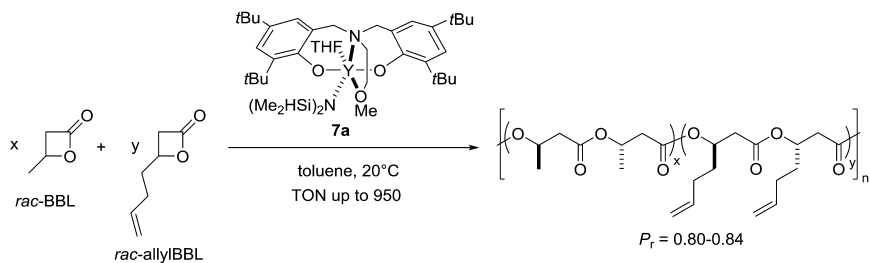
Figure 13. Synthesis of syndiotactic-enriched random copolymers.

Instead of polymerizing a mixture of racemic different monomers, Thomas and co-workers also decided to start from a mixture of enantiomerically pure BBL and β-lactone (different from BBL) of opposite absolute configuration to prepare alternating copolymers (Figure 14) (*37*). Regarding the catalyst, the addition of isopropanol to a salan yttrium-amido complex gave rise to a bimetallic salan yttrium-isopropoxide **19** which was the most efficient initiator compared to the amido complex. The rate of copolymerization was found to be similar for both monomers with different substitution although polymerization of each of them separately proceeded at different rate. Depending on the nature of the side chain of the β-lactone, alternations between 91 and 94% were obtained. Thomas *et al.* also reported the one-pot synthesis of this yttrium-isopropoxide dimer **19** along with the dimer $(salan)_2Y_2(\mu\text{-O}i\text{Pr})(\mu\text{-OH})$ by direct reaction of the salan pro-ligand and yttrium isopropoxide (*38*). The polymerization of *rac*-BBL with the mixture of these dimers was also investigated and highly syndiotactic PHB (P_r = 0.90) was formed. DFT calculations of the ROP of *rac*-BBL were undertaken with a salanY(O*i*Pr) in order to have a better understanding of the origin of the selectivity. It was first demonstrated that the initiation steps for (*R*)- or (*S*)-BBL were similar and that whatever enantiomer is inserted first, a syndiotactic polymer chain is preferred over an isotactic one.

Synthesis of Aliphatic Polyesters by Alternating Copolymerization

Although the ring-opening polymerization of cyclic esters takes place under mild reaction conditions without any byproducts, the low availability of structurally diverse monomers restricts the scope of the polymer architecture (Figure 15) (*39*, *40*). Alternatively, the ring-opening copolymerization of epoxides with cyclic anhydrides has the potential to produce a wide range of polymer backbone structures (*41*).
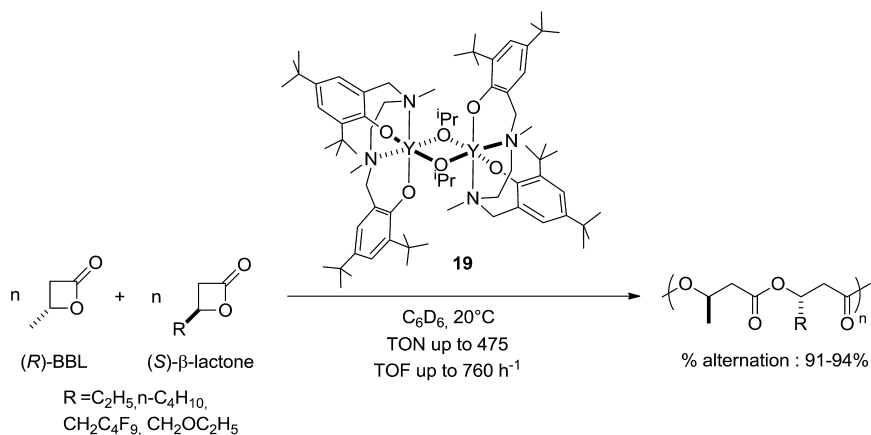
*Figure 14. ROP of a mixture of enantiopure β-lactones catalyzed by {salanY(OiPr)}₂ **19**.*
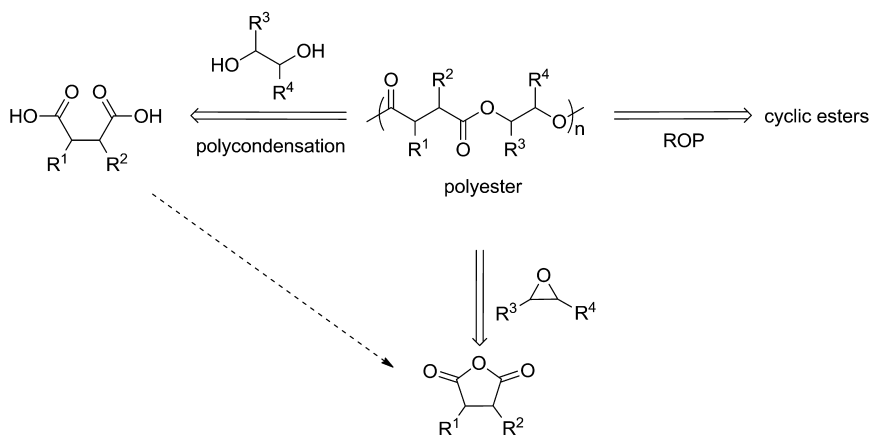
Figure 15. Synthetic approaches to aliphatic polyesters.

The coupling of epoxides with cyclic anhydrides to afford polyesters was first described by using tertiary amines (*42*) in the 1960s. Then Inoue reported a system of aluminum tetraphenylporphyrin (TPP)AlX **20a-c** with a covalently bound axial ligand and a quaternary ammonium or phosphonium salt, as an effective catalyst for the copolymerization of phtalic anhydride (PA) and propylene oxide (PO). These systems provided an alternating polyester with unusually narrow molecular weight distribution and without any side reactions such as chain transfer or termination (Figure 16) (*43*).

20a M = AlEt
20b M = AlCl
20c M = AlOCOCH$_3$
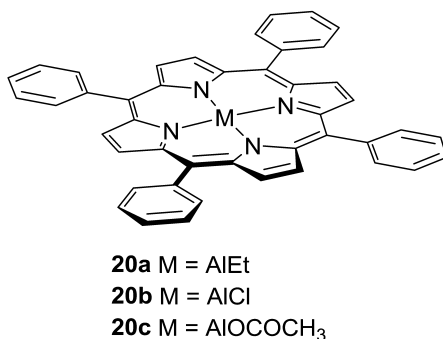
Figure 16. Metalloporphyrin complexes.

Taking into account how the diffusion of the residue of metallic compounds used as an initiator influences environment before and after biodegradation of the aliphatic copolymers, Maeda and Nishimura used common and nontoxic magnesium diethoxide to afford poly(ethylene succinate) and itaconic acid-based polymeric network respectively (*44*). However, catalysts reported for the ring-opening copolymerization of cyclic anhydrides with epoxides exhibit relatively long reaction times (days) and produce polyesters with low molecular weight values (<10 000 g.mol^{-1}).

One of the major improvements was the development of zinc-β-diiminate complexes **21** (*45*), which were previously reported as active catalysts for copolymerization of epoxides with CO_2(*46–51*), and ROP of cyclic esters (Figure 17) (*52*). Polyesters with molecular weights up to 55 000 g.mol^{-1} were achieved in a perfectly alternating microstructure by using complex **21** with R^1 = *i*Pr, R^2 = Et and R^3 = CN. Various anhydrides, such as diglycolic anhydride (DGA), succinic anhydride (SA) and maleic anhydride (MA), were thus used. However for the coupling of MA and PO, the Zn(BDI)OAc system displayed low activity and significant amounts of ether linkages in the polymer chain.

R^1= R^2= Et, ^{i}Pr
R^3= H, CN, Me

21
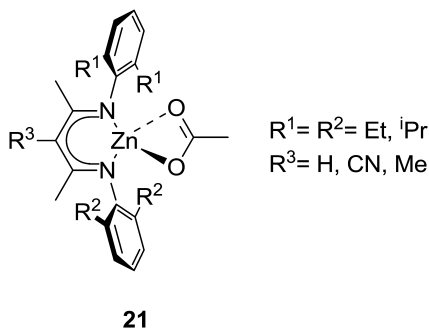
Figure 17. Zinc β-diiminate complexes.

Because chromium salen (III) complexes in the presence of onium salts have been very effective at coupling CO_2 and epoxides, it has been anticipated that

these complexes will be productive catalysts for the copolymerization of epoxides and cyclic anhydrides (*53*). Furthermore, whereas zinc-based catalysts such as β-diiminate system tend to form inactive hydroxides with water (*54*), chromium catalysts are presumed to form hydroxyl or *μ*-oxo species which remain active, opening the opportunity to produce polyesters without using drastically dried system. Thus chromium (III) salen complex **22** was recently reported by Coates as an efficient catalyst for copolymerization of various combinations of maleic anhydride and several epoxides without concomitant undesirable reaction of homopolymerization (Figure 18) (*55*). Moreover quantitative isomerization of the maleate form for all polymers afforded the fumarate analogues by using catalytic amount of diethylamine.

22 R = C$_4$H$_8$
23 R = C$_4$H$_4$

24
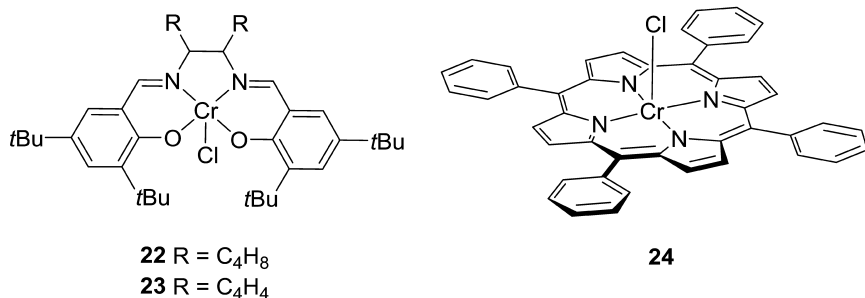
Figure 18. Various structures of chromium complexes.

Meanwhile Duchateau described the copolymerization of cyclohexene oxide (CHO) with various succinic-based anhydrides as cyclopropane-1,2-dicarboxylic acid anhydride (CPrA), cyclopentane-1,2-dicarboxylic acid anhydride (CPA) and PA by using chromium salophen **23** and (TPP)CrCl complex **24** in combination with a nucleophilic cocatalyst as 4-(*N,N*-dimethylamino)pyridine (DMAP) (*56*). Although the molecular weight shows a linear development with conversion, in all cases the observed molecular weights are far lower than the theoretical value for a living system (<1800 g.mol^{-1}), phenomena attributed by the authors to intramolecular transesterification and chain transfer reactions with water.

Investigations into the effect of catalyst structure on catalytic behavior involving variations in the salen-diimine backbone and the metal in the complexes revealed clearly that chromium catalysts performed best while the aluminum catalysts were the less active ones. Moreover for each metal, salophen complexes gave the highest activities, followed by the ethylene-bridged salen complexes (*57*). Various studies were also reported by using styrene oxide (SO), leading to polymers with higher T_g (*58*) and limonene oxide (LO) to perform a partially bio-based polyester (*59*).

Mainly oligoether formation was observed when metalloporphyrin or metallosalen were employed without cocatalyst (*43*, *56*, *57*). By contrast, with cocatalysts, the anhydride incorporation and the activity were dramatically improved. Of all cocatalysts tested (*i.e.*, *N*-heterocyclic nucleophiles, phosphines,

phosphoniums and [PPN]X (([PPN]$^+$ = bis(triphenylphosphoranylidene)-iminium)), [PPN]Cl exhibited the highest activity and in general only one equivalent was sufficient to reach the optimum activity. Whereas some of the bulk polymerizations afforded poly(ester-*co*-ether)s, solution polymerizations produced perfect alternating copolymers. Coates demonstrated that aliphatic hydrocarbons are also suitable solvents for MA/PO copolymerization and seem to have a positive effect on the selectivity of the catalyst **22** without the need of cocatalyst (*55*).

The first mechanism investigation proceeded by Inoue revealed that the copolymerization reaction carried out with (TPP)AlX **20** simultaneously takes place on both sides of the porphyrin plane. Infrared spectrum of equimolar mixture of (TPP)AlOCOCH$_3$ **20c** and Et$_4$NCH$_3$COO- indicated the formation equilibrium of a six-coordinated aluminum porphyrin featuring two carboxylate groups in the two axial positions (Figure 19). Taking advantage of the relatively stable nature of the reactive species, the growing copolymer was directly observed by spectroscopic investigation of the reaction mixture. Thus, the axial group of aluminum porphyrin as well as the anion of the quaternary organic salt are confirmed to be introduced at the terminal position of the copolymer.
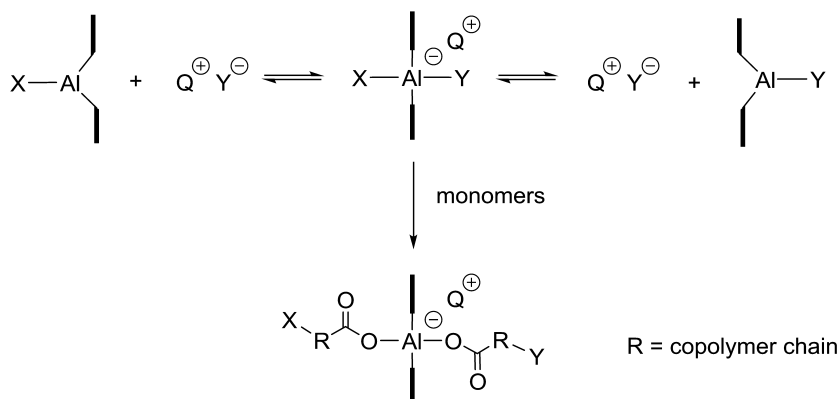
Figure 19. Mechanism using (TPP)AlX.

It is interesting to note that by using metalloporphyrin and metallosalen bimodal distribution of polymer chains are observed by size exclusion chromatograms and MALDI-TOF-MS spectra, in which two distributions differ by approximately a factor of 2 in molecular weight (*56*). However, a recent study of Darensbourg excluded the explanation of Inoue (*60*). The diacid formed by reaction of water and the anhydride acts as a bifunctional chain transfer agent responsible for the overall lower molecular weight. This hypothesis also explains the fact that low and high molecular weight chains are the results of mono- and bimetallic systems respectively.

The next major breakthrough came from Thomas, who reported a new strategy, based on tandem catalysis, to afford a large scope of polyesters structures from renewable resources by using commercially available chromium **22**,

aluminum **24**, cobalt (II) **25** and manganese **26** salen complexes in combination with [PPN]Cl (*41*, *61*). Interestingly, molecular weights observed are close to the theoretical ones with monomodal distributions and narrow polydispersity index. Surprisingly high catalytic activity is obtained by using aluminum complex **24** to afford polyesters from epoxides with low reactivity (such as limonene oxide and pinene oxide) and camphoric acid in mild conditions (Figure 20) (*41*).
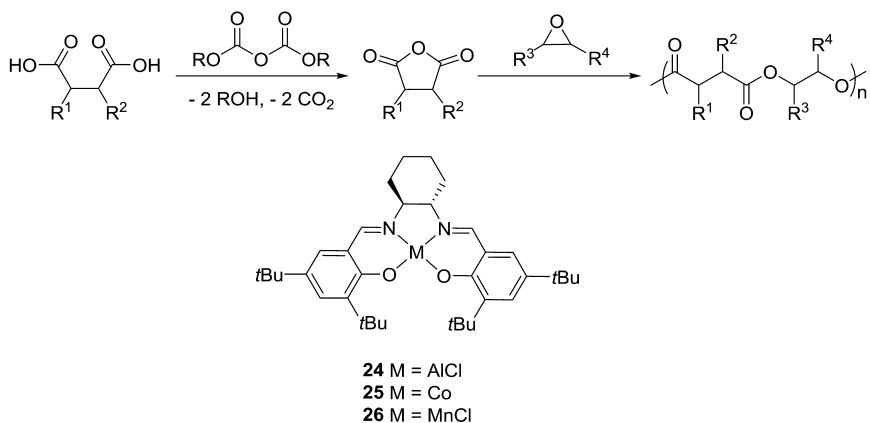
Figure 20. Tandem synthesis of polyesters from epoxides and dicarboxylic acids.

Bimetallic synergistic effect was frequently observed in the homopolymerization of epoxides (*62*) and the copolymerization with CO_2 (*63*) concerning coordination polymerization catalysts. According to the previous reports about chromium salan complexes, Lu's group developed mono- and bi-nuclear chromium salan complexes as catalysts for the copolymerization of MA and various epoxides as PO, CHO, epichlorohydrin (ClPO) and glycidyl phenyl ether (GO) (Figure 21) (*64*). As expected, the bi-nuclear complex **27** showed significantly higher activities than the mono-nuclear complex **28** (~7 times higher for the coupling of MA with GO). Notably, the binuclear catalyst exhibited excellent regioselectivity in the copolymerization of (*S*)-GO with MA, predominantly inducing the ring-opening at the methylene carbon of (*S*)-GO and retaining the stereochemistry at the methine carbon.
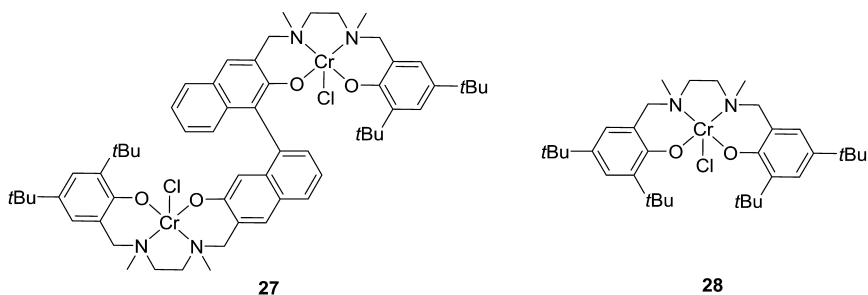
Figure 21. Bi- and mono-nuclear chromium salan complexes.

Corroles are known as trianionic tetradentate ligands which can stabilize various transition-metal centers (*65*). Very recently, manganese **29** and iron corrole complexes **30** in combination with [PPN]X (X= Cl, OAc, OBzF$_5$ or N$_3$) were found to be versatile catalysts active in the homopolymerization of epoxides, copolymerization of epoxides with CO$_2$, and copolymerization of epoxides with cyclic anhydrides affording a wide range of polymeric materials (Figure 22) (*66*). Although molecular weights close to the theoretical ones and narrow polydispersity index were obtained, a low productivity was reported.

29a M = Mn
29b M = MnCl
30a M = Fe(OEt$_2$)$_2$
30b M = FeCl

30c
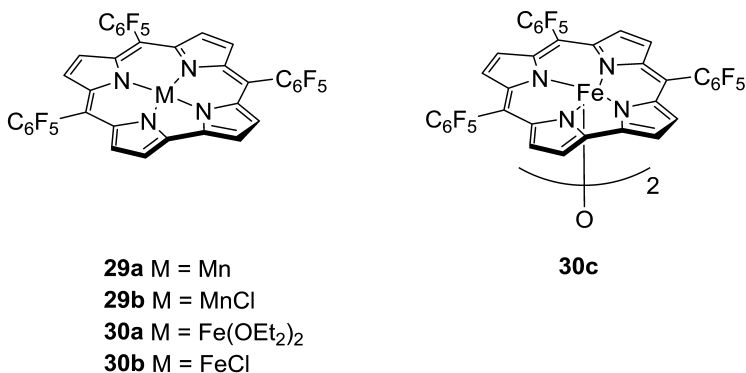
Figure 22. Corrole complexes.

Conclusion

In order to obtain alternating polymers, coordination polymerization using well-defined metal complexes has played a leading role in the last two decades. We have described selected published efforts to achieve these research goals using discrete, structurally well-characterized metal complexes. Different studies focused on the development of supporting ligands designed to control the structure of various heteroleptic complexes and their polymerization reactivity. In this aspect, coordination complexes with tuning of ligands play an important role not only in molecular weight and molecular weight distribution, but also in the production of stereoregular polyesters.

Acknowledgments

References

1. Dechy-Cabaret, O.; Martin-Vaca, B.; Bourissou, D. *Chem. Rev.* **2004**, *104*, 6147–6176.

2. Polyesters have also been produced by copolymerization of epoxides and anhydrides. See for instance: Jeske, R. C.; Rowley, J. M.; Coates, G. W. *Angew. Chem., Int. Ed.* **2008**, *47*, 6041–6044.

3. Duda, A.; Penczek, S. *Polymers from Renewable Resources: Biopolyesters and Biocatalysis*; Scholz, C., Gross, R. A. ACS Symposium Series 764; American Chemical Society: Washington, DC, 2000; p 160.

4. Nair, L. S.; Laurencin, C. T. *Prog. Polym. Sci.* **2007**, *32*, 762–798.

5. Badi, N.; Lutz, J.-F. *Chem. Soc. Rev.* **2009**, *38*, 3383–3390.

6. Thomas, C. M. *Chem. Soc. Rev.* **2010**, *39*, 165–173.

7. Stanford, M. J.; Dove, A. P. *Chem. Soc. Rev.* **2010**, *39*, 486–494.

8. Chamberlain, B. M.; Cheng, M.; Moore, D. R.; Ovitt, T. M.; Lobkovsky, E. B.; Coates, G. W. *J. Am. Chem. Soc.* **2001**, *123*, 3229–3238 and references therein.

9. The term salan was introduced by Atwood to refer to saturated salen ligands: Atwood, D. A. *Coord. Chem. Rev.* **1997**, *165*, 267–296.

10. Chisholm, M. H.; Gallucci, J. C.; Phomphrai, K. *Inorg. Chem.* **2004**, *43*, 6717–6725.

11. Chmura, A. J.; Chuck, C. J.; Davidson, M. G.; Jones, M. D.; Lunn, M. D.; Bull, S. D.; Mahon, M. F. *Angew. Chem., Int. Ed.* **2007**, *46*, 2280–2283.

12. Guo, J.; Haquette, P.; Martin, J.; Salim, K.; Thomas, C. M. *Angew. Chem., Int. Ed.* **2013**, *52*, 13584–13587.

13. Pietrangelo, A.; Hillmyer, M. A.; Tolman, W. B. *Chem. Commun.* **2009**, 2736–2737.

14. Ovitt, T. M.; Coates, G. W. *J. Am. Chem. Soc.* **2002**, *124*, 1316–1326.

15. Amgoune, A.; Thomas, C. M.; Carpentier, J.-F. *Pure Appl. Chem.* **2007**, *79*, 2013–2030.

16. Ma, H.; Spaniol, T. P.; Okuda, J. *Angew. Chem., Int. Ed.* **2006**, *118*, 7982–7985.

17. Amgoune, A.; Thomas, C. M.; Roisnel, T.; Carpentier, J.-F. *Chem. Eur. J.* **2006**, *12*, 169–179.

18. Bouyahyi, M.; Ajellal, N.; Kirillov, E.; Thomas, C. M.; Roisnel, T.; Carpentier, J.-F. *Chem. Eur. J.* **2011**, *17*, 1872–1883 and references therein.

19. Thomas, C. M. *Chem. Soc. Rev.* **2010**, *39*, 165–173.

20. Carpentier, J.-F. *Macromol. Rapid Commun.* **2010**, *31*, 1969–1705.

21. Kemnitzer, J. E.; McCarthy, S. P.; Gross, R. A. *Macromolecules* **1993**, *26*, 1221–1229.

22. Kemnitzer, J. E.; McCarthy, S. P.; Gross, R. A. *Macromolecules* **1993**, *26*, 6143–6150.

23. Kricheldorf, H. R.; Lee, S.-R.; Scharnagl, N. *Macromolecules* **1994**, *27*, 3129–3146.

24. Kricheldorf, H. R.; Eggerstedt, S. *Macromolecules* **1997**, *30*, 5693–5697.

25. Hori, Y.; Suzuki, M.; Yamaguchi, A.; Niehishita, T. *Macromolecules* **1993**, *26*, 5533–5534.

26. Arcana, M.; Giani-Beaune, O.; Schue, F.; Amass, W.; Amass, A. *Polym. Int.* **2000**, *49*, 1348–1355.

27. Ajellal, N.; Lyubov, D. M.; Sinenkov, M. A; Fukin, G. K.; Cherkasov, A. V.; Thomas, C. M.; Carpentier, J.-F.; Trifonov, A. A. *Chem. Eur. J.* **2008**, *14*, 5440–5448.

28. Grunova, E.; Kirillov, E.; Roisnel, T.; Carpentier, J.-F. *Dalton Trans.* **2010**, *39*, 6739–6752.

29. Amgoune, A.; Thomas, C. M.; Ilinca, S.; Roisnel, T.; Carpentier, J.-F. *Angew. Chem., Int. Ed.* **2006**, *45*, 2782–2784.

30. Ajellal, N.; Bouyahyi, M.; Amgoune, A.; Thomas, C. M.; Bondon, A.; Pillin, I.; Grohens, Y.; Carpentier, J.-F. *Macromolecules* **2009**, *42*, 987–993.

31. Bouyahyi, M.; Ajellal, N.; Kirillov, E.; Thomas, C. M.; Carpentier, J.-F. *Chem. Eur. J.* **2011**, *17*, 1872–1883.

32. Nie, K.; Fang, L.; Yao, Y.; Zhang, Y.; Shen, Q.; Wang, Y. *Inorg. Chem.* **2012**, *51*, 11133–11143.

33. Pappalardo, D.; Bruno, M.; Lamberti, M.; Pellecchia, C. *Macromol. Chem. Phys.* **2013**, *214*, 1965–1972.

34. Jeffery, B. J.; Whitelaw, E. L.; Garcia-Vivo, D.; Stewart, J. A.; Mahon, M. F.; Davidson, M. G.; Jones, M. D. *Chem. Commun.* **2011**, *14*, 12328–12330.

35. Ajellal, N.; Thomas, C. M.; Carpentier, J.-F. *J. Polym. Sci., Part A: Polym. Chem.* **2009**, *47*, 3177–3189.

36. Ajellal, N.; Thomas, C. M.; Aubry, T.; Grohens, Y.; Carpentier, J.-F. *New. J. Chem.* **2011**, *35*, 876–880.

37. Kramer, J. W.; Treitler, D. S.; Dunn, E. W.; Castro, P. M.; Roisnel, T.; Thomas, C. M.; Coates, G. W. *J. Am. Chem. Soc.* **2009**, *131*, 16042–16044.

38. Fang, J.; Tschan, M. J.-L.; Roisnel, T.; Trivelli, X.; Gauvin, R. M.; Thomas, C. M.; Maron, L. *Polym. Chem.* **2013**, *4*, 360–367.

39. Odian, G. *Principles of Polymerization*, 4th ed.; John Wiley and Sons: Hoboken, NJ, 2004.

40. Seppälä, J. V.; Korhonen, H.; Kylmä, J.; Tuominen, J. *Biopolymers*; Steinbüchel, A., Doi, Y., Eds.; Wiley-VCH: Weinheim, Germany, 2002; Vol. 3b, pp 327−369.

41. Robert, C.; de Montigny, F.; Thomas, C. *Nat. Commun.* **2011**, *2*, 586 doi: 10.1038 / ncomms1596.

42. Fischer, R. F. *J. Polym. Sci.* **1960**, *44*, 155–172.

43. Aida, T.; Inoue, S. *J. Am. Chem. Soc.* **1985**, *107*, 1358–1364.

44. Nakayama, A.; Kawasaki, N.; Hayashi, K.; Aiba, S.; Yamamoto, M.; Maeda, Y. *Polymer* **1997**, *38*, 4719–4725.

45. Jeske, R. C.; DiCiccio, A. M.; Coates, G. W. *J. Am. Chem. Soc.* **2007**, *129*, 11330–11331.

46. Cheng, M.; Lobkovsky, E. B.; Coates, G. W. *J. Am. Chem. Soc.* **1998**, *120*, 11018–11019.

47. Cheng, M.; Moore, D. R.; Reczek, J. J.; Chamberlain, B. M.; Lobkovsky, E. B.; Coates, G. W. *J. Am. Chem. Soc.* **2001**, *123*, 8738–8749.

48. Moore, D. R.; Cheng, M.; Lobkovsky, E. B.; Coates, G. W. *Angew. Chem., Int. Ed.* **2002**, *41*, 2599–2602.

49. Moore, D. R.; Cheng, M.; Lobkovsky, E. B.; Coates, G. W. *Angew. Chem., Int. Ed. Engl.* **2002**, *41*, 2599–2602.

50. Moore, D. R.; Cheng, M.; Lobkovsky, E. B.; Coates, G. W. *J. Am. Chem. Soc.* **2003**, *125*, 11911–11924.

51. Byrne, C. M.; Allen, S. D.; Lobkovsky, E. B.; Coates, G. W. *J. Am. Chem. Soc.* **2004**, *126*, 11404–11405.

52. Cheng, M.; Attygalle, A. B.; Lobkovsky, E. B.; Coates, G. W. *J. Am. Chem. Soc.* **1999**, *121*, 11583–11584.

53. Coates, G. W.; Moore, D. R. *Angew. Chem., Int. Ed.* **2004**, *43*, 6618–6639.

54. Cheng, M.; Moore, D. R.; Reczek, J. J.; Chamberlain, B. M.; Lobkovsky, E. B.; Coates, G. W. *J. Am. Chem. Soc.* **2011**, *123*, 8738–8749.

55. DiCiccio, A. M.; Coates, G. W. *J. Am. Chem. Soc.* **2011**, *133*, 10724–10727.

56. Huijser, S.; Nejad, E. H.; Sablong, R.; de Jong, C.; Koning, C. E.; Duchateau, R. *Macromolecules* **2011**, *44*, 1132–1139.

57. Nejad, E. H.; van Melis, C. G. W.; Vermeer, T. J.; Koning, C. E.; Duchateau, R. *Macromolecules* **2012**, *45*, 1770–1776.

58. Nejad, E. H.; Paoniasari, A.; Koning, C. E.; Duchateau, R. *Polym. Chem.* **2012**, *3*, 1308–1313.

59. Nejad, E. H.; Paoniasari, A.; van Melis, C. G. W.; Koning, C. E.; Duchateau, R. *Macromolecules* **2013**, *46*, 631–637.

60. Darensbourg, D. J.; Poland, R. R.; Escobedo, C. *Macromolecules* **2012**, *45*, 2242–2248.

61. Robert, C.; Thomas, C. M. *Chem. Soc. Rev.* **2013**, *42*, 9392–9402.

62. Widger, P. C. B.; Ahmed, S. M.; Coates, G. W. **2011**, *44*, 5666–5670.

63. Klaus, S.; Lehenmeier, M. W.; Anderson, C. E.; Rieger, B. *Coord. Chem. Rev.* **2011**, *255*, 1460–1479.

64. Liu, J.; Bao, Y.-Y.; Liu, Y.; Ren, W.-M.; Lu, X.-B. *Polym. Chem.* **2013**, *4*, 1439–1444.

65. Golubkov, G.; Bendix, J.; Gray, H. B.; Mahammed, A.; Goldberg, I.; DiBiblio, A. J.; Gross, Z. *Angew. Chem., Int. Ed.* **2011**, *40*, 2132–2134.

66. Robert, C.; Ohkawara, T.; Nozaki, K. *Chem. Eur. J.* **2014**, *20*, 4789–4795.

Chapter 24

Organic Synthesis of Periodic 2D Polymers

Junji Sakamoto*

Department of Applied Chemistry, Graduate School of Engineering, Osaka University, Yamadaoka 2-1, 565-0871 Suita, Osaka, Japan
***E-mail: sakamoto@chem.eng.osaka-u.ac.jp**

2D polymers are accessible by crosslinking polymerization of monomers in 2D confinement, whereas the synthesis of their periodic congeners is still underdeveloped. The presence of a periodic order is a seemingly small addition to the network structure but poses critical problems for its realization by organic synthesis. The present contribution provides a brief overview of general issues on the synthesis of periodic 2D polymers and describes how to overcome such problems by showing a concrete example based on a topochemical polymerization strategy.

2D network polymers are often simply called as 2D polymers (*1–8*). They are also sometimes referred to as sheet-like polymers because the 2D network structure forms an autonomous sheet shape (*9, 10*). The shape of 2D polymers should be reflected by their properties (*11, 12*). For example, the sheets can hardly entangle one another but will rather crumple up or stack, which must have a considerable impact on fundamental issues such as viscosity, elasticity and the like. This is contrasted with conventional linear polymers whose such properties are a consequence of their ability to entangle (*13*). 2D polymers have therefore attracted continuous attention for the last several decades as a new frontier of polymer science (*14–18*).

Chemical synthesis of a 2D polymer was reported already in 1935 which is based on crosslinking polymerization of an amphiphilic monomer forming a monolayer at the air/water interface (*19*). Since then, various ingenious approaches have been reported for the synthesis of 2D polymers at gas/liquid (*3, 20–24*), liquid/liquid (*25, 26*), liquid/solid interfaces (*27*), on solid surfaces

(*28–36*) or using other 2D templates such as clays (*37*), Langmuir-Blodget films (*1*), self-assembled monolayers (*4, 5*) and metal organic frameworks (*38*). Layered molecular assemblies such as lipid bilayers (*39–42*) and bulk liquid crystals (*2*) were also employed as 2D precursors to be transformed into 2D polymers.

2D polymers are regaining the spotlight since the recent isolation of grephene which unveiled supreme properties of graphene unique to its defined 2D structure (*43, 44*). Graphene, boron nitride and other inorganic "nanosheets" (*45*) represent 2D polymers with periodic internal orders. These periodic 2D polymers are exfoliated from their parent crystals that are available in bulk quantities. The synthesis appears to be straightforward, while the formation of the parent crystals relies on pyrolysis or calcination at high temperatures causing decomposion of organic species. This is contrasted with organic synthesis that is usually performed under mild conditions and thereby allows for the preparation of organic 2D polymers.

Organic synthesis can in principle provide attractive opportunities for the structure and property of 2D polymers to be tailored by design. However, most of the organic 2D polymers hitherto synthesized lack any internal order unlike graphene. This is associated with a long-standing problem in polymer chemistry as to "how to put order into polymer network" (*46*). The biggest hurdle lies in the fact that a periodic network is composed of uniform cyclic motifs so that the synthesis requires repetition of cyclizaions under a rigorous regio-chemical control by necessity. Many organic chemists stepped up to this challenge till now (*47–50*). Their approaches are classified into two main streams based on (i) iterative synthesis and (ii) polymerization (*51*). In iterative synthesis, a precursor compound is first synthesized and finally planarized by intramolecular multiple cyclizations. This approach affords a product with a defined 2D structure. Müllen's "nanographene" composed of 222 carbons represents a shining example here (Figure 1) (*52*). As a main drawback, however, the synthesis scheme comprises a number of reaction steps and the overall yield quickly fades away.
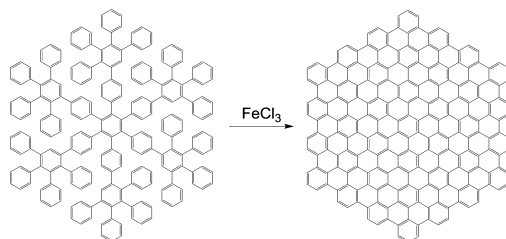
Figure 1. Chemical synthesis of a "nanographene" composed of 222 carbons

In contrast, polymerization is a one-step process which enables direct formation of a polymer whose structure is "infinitely" expanded. As trade-off, however, it usually gives rise to ill-defined network structures because the occurrence of errors in cyclization disorders the eventual network (*53*). In order to achieve a periodic 2D polymer, the polymerization therefore needs to proceed

without error or with automatic error correction. Two synthetic strategies based on topochemical polymerization (*54*) and equilibrium polymerization (*55*, *56*) were thus devised (*57*). The following part of the present contribution highlights a recent successful example of the synthesis of a periodic 2D polymer (*58*). The synthesis procedure comprises a preorganization of a photo-reactive monomer into a laminar single crystal, a photo-induced topochemical polymerization in each layer of the crystal and a solvent-induced delamination to isolate individual 2D polymer sheets (Figure 2) (*59*).
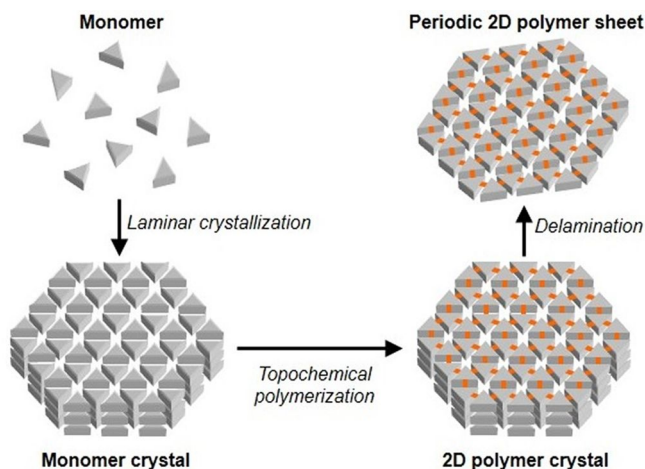
Figure 2. Synthesis of periodic 2D polymer sheets via topochemical polymerization

A cup-shaped monomer bearing three photo-reactive anthracene groups on the lateral faces was designed (Figure 3) (*60*, *61*). The "sticky" π faces of the anthracenes were laterally exposed in expectation of a laminar crystal formation of the monomer. The π–π interactions were also expected to be convertible to covalent bonds; the anthracenes in the crystal can undergo topochemcal cycloaddition (*62*, *63*). The actual reaction mode is determined by how monomers are packed in the crystal (see below). In fact, the monomer readily formed single crystals from e.g. a mixed solvent of 1,1,2,2,-tetrachloroethane (TCE)/tetrahydrofuran. The crystals grew into the shape of hexagonal columns. X-ray diffraction analysis proved a layered crystal structure as expected. In this structure, the monomers were adapted to be triangular prisms and hexagonally packed in each layer that was parallel to the hexagonal face of the crystal. The adjacent monomers in the layer oriented upside down, rendering an anthracene of one monomer in tight contact with an alkyne of its neighbor (4.4 and 3.6 Å). Such a crystal packing suggested the feasibility of the topochemical polymerization in each layer based on the anthracene/alkyne [4+2]-cycloaddition mechanism. Note that in this crystal structure, the photo-reactive groups formed sublayers that were sandwiched by non-reactive sublayers composed of terphenylene parts, whereby the layers could be protected from crosslinking across layers.
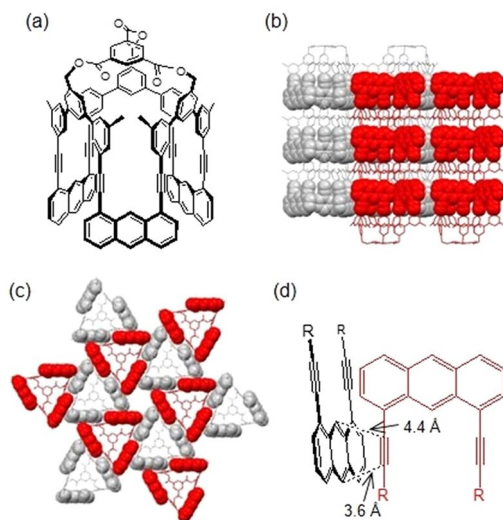
Figure 3. 2D preorganization in the monomer crystal. A rationally designed monomer (a) formed single crystals in a hexagonal columnar shape. X-ray diffraction analysis revealed a layered crystal structure. The monomers oriented up and down (shown in grey and black, respectively) (b) and packed hexagonally in the layer (c) so that 9,10 anthracene carbons of one monomer were opposed to alkynes of the adjacent monomers (d). Anthracenes and alkynes are displayed as space-filling and the others as stick models. (Reproduced with permission from reference (58). Copyright 2012 Nature Publishing Group.)

The monomer crystals were irradiated with a visible light (λ = 470 nm) to excite the anthracenes. This irradiation experiment was performed under exclusion of oxygen and in-situ monitoring of the anthracene fluorescence. A gradual disappearance of the fluorescence and a drastic change in solubility were caused by the irradiation. The crystals before irradiation readily dissolved in TCE at room temperature, whereas the irradiated crystals were insoluble in the same solvent even at 80 °C for one day. The crystals exhibited birefringence before and after the irradiation. These results strongly suggested that the irradiation induced topochemcal polymerization in the crystals. This was further supported by the exfoliation study and the transmission electron microscopy (TEM) analysis as follows.

When the irradiated crystals were kept in chloroform/pyridine, only bundles of layers were exfoliated. Full exfoliation down to individual monolayer sheets required more forcing conditions in *N*-methylpyrrolidone at 150 °C where the heterogeneous mixture turned to a homogeneous solution in 3 days. The exfoliated sheets dispersed in the solution were deposited on a mica surface and analyzed by atomic force microscopy (AFM). The monolayer sheets with a uniform thickness of 2.5 nm were thus observed (Figure 4). The sheets often had sharp edges and largely inherited the hexagonal macroscopic shape from the parent crystals.

Feasibility of the monolayer isolation proved that the polymerization proceeded without inter-layer crosslinking and covalently stabilized the monolayer to be free-standing.
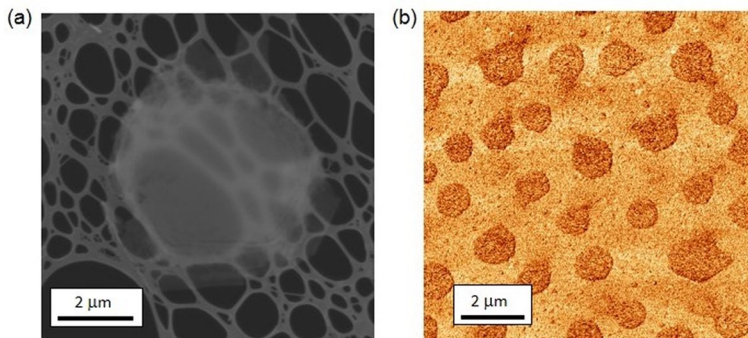
Figure 4. Exfoliation of periodic 2D polymer sheets. The irradiated crystals were delaminated in appropriate solvents: (a) a semi-exfoliated bundle of the sheets observed by scanning electron microscopy (SEM) on lacy carbon and (b) fully exfoliated monolayer sheets observed by AFM on mica. (Reproduced with permission from reference (58). Copyright 2012 Nature Publishing Group.)

The monolayer sheets were also deposited on a lacy carbon-coated copper grid. They could span over the micrometer-sized holes and stay intact during washing with chloroform and subsequent drying. This result also pointed to a high mechanical stability of the covalent monolayer sheets. In contrast, the monolayer sheets were found extremely sensitive to an electron beam, particularly when it was concentrated for their high-resolution imaging. Therefore, semi-exfoliated bundles composed of ~ 8 layers were alternatively used for TEM analysis; the bundles were found thick enough to withstand the electron beam but at the same time thin enough to allow for its transmission. The TEM imaging of the bundles visualized the internal structure of the sheets with a long-range periodic order as expected from the original crystal packing structure (Figure 5). The same periodic order was reproduced by electron microdiffraction analysis of the bundles under cryogenic conditions. These results proved that the polymerization proceeded retaining the original crystalline order.

Finally, Raman spectroscopic analysis of the crystals indicated that the irradiation vanished the anthracene signals at ~1380 and ~1560 cm^{-1} and at the same time decreased the intensity of the alkyne signal at ~2200 cm^{-1} by roughly half. As the monomer had three anthracenes and six alkynes in its structure, the Raman results provided a strong support to the topochemical [4+2] cycloaddition mechanism suggested by the crystal packing.
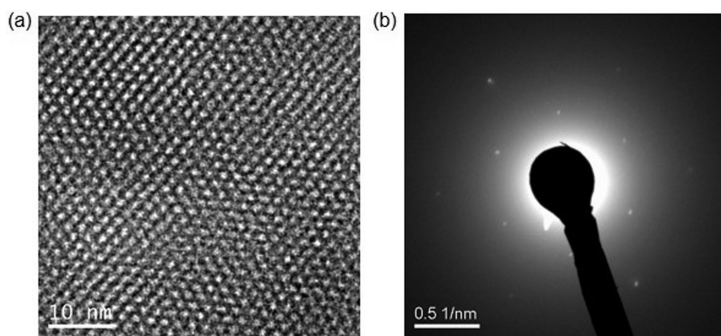
Figure 5. Visualization of a periodic internal structure of the sheets. High-resolution TEM imaging (a) and electron microdiffraction analysis of the semi-exfoliated bundles (b) revealed the internal order of the sheets inherited from the parent crystal. (Reproduced with permission from reference (58). Copyright 2012 Nature Publishing Group.)

To conclude, periodic 2D polymers represent a subclass of 2D polymers. 2D polymers have been synthesized for the last several decades, while periodic 2D polymers remained elucive. This is attributed to the highly demanding synthesis that requires a perfect regio-chemical control over the cyclization steps during polymerization. This synthetic hurdle was recently overcome by the approach exemplified above. The synthesis was based on topochemical polymerization with laminar single crystals of a rationally designed monomer. The solvent-induced delamination of the irradiated crystals afforded free-standing monolayer sheets of a periodic 2D polymer. This approach is free from any external template and relies on laminar crystallization of the monomer. As molecular crystals can be of respectable size and prepared in bulk quantities, this approach provides access to large sheets of periodic 2D polymers on a preparative scale (*8b*): the present 2D polymer sheet with an area over 1 μm^2 is more than 7 x 10^8 Da in molecular weight and composed of > 4 x 10^5 monomer units.

The synthesis also takes advantage of organic chemistry that offers plenty of room for the sheets to be designed in terms of structure and property. For example, the periodic 2D polymer has precise, small pores over the sheet. Such a 2D porous structure can be engineered for e.g. selective inclusion or filtration of small molecules. Moreover, a great variety of functional groups can be introduced on the sheet in a defined density and with precise spacing. This opens up a new possibility of controlled structural variation of 2D polymers. For example, each repeat unit of the present 2D polymer sheet carries three hydroxyl groups protected by a benzotriate cap. After removal of the cap by ester hydrolysis, the hydroxyl groups can be used for various chemical modifications. Today, many important progresses are being made in the field of 2D polymers. Not only the precision synthesis but also the large-scale production and structural variation of 2D polymers will be the key elements necessary to establish their structure-property correlations and demonstrate their full potential in applications that remain largely unexplored.

Acknowledgments

References

1. Asakusa, S.; Okada, H.; Kunitake, T. *J. Am. Chem. Soc.* **1991**, *113*, 1749–1755.
2. Stupp, S. I.; Son, S.; Lin, H. C.; Li, L. S. *Science* **1993**, *259*, 59–63.
3. Lefevre, D.; Porteu, F.; Balog, P.; Roulliay, M.; Zalczer, G.; Palacin, S. *Langmuir* **1993**, *9*, 150–161.
4. Stroock, A. D.; Kane, R. S.; Weck, M.; Metallo, S. J.; Whitesides, G. M. *Langmuir* **2003**, *19*, 2466–2472.
5. Edmondson, S.; Huck, W. T. S. *Adv. Mater.* **2004**, *16*, 1327–1331.
6. Baek, K.; Yun, G.; Kim, Y.; Kim, D.; Hota, R.; Hwang, I.; Xu, D.; Ko, Y. H.; Gu, G. H.; Suh, J. H.; Park, C. G.; Sung, B. J.; Kim, K. *J. Am. Chem. Soc.* **2013**, *135*, 6523–6528.
7. The term "2D polymer" is ambiguous. "2D polymer" literally means a polymer in 2D confinement regardless of the polymer topology. In fact, 2D linear polymers (i.e. linear polymers in 2D confinement) are also referred to as 2D polymers in literature. For references, see: (a) Sastri, V. R.; Schulman, R.; Roberts, D. C. *Macromolecules* **1982**, *15*, 939−947. (b) Tobochnik, J.; Webman, I.; Lebowitz, J. L.; Kalos, M. H. *Macromolecules* **1982**, *15*, 549−553. (c) Yethiraj, A. *Macromolecules* **2003**, *36*, 5854−5862. (d) Aoki, H.; Anryu, M.; Ito, S. *Polymer* **2005**, *46*, 5896−5902.
8. The scope of "2D polymers" was recently broadened to include bulk laminar crystals and thin bundles of layers. For references, see: (a) Berlanga, I.; Ruiz-González, M. L.; González-Calbet, J. M.; Fierro, J. L. G.; Mas-Ballesté, R.; Zamora, F. *Small* **2011**, *7*, 1207−1211. (b) Colson, J. W.; Dichtel, W. R. *Nat. Chem.* **2013**, *5*, 453−465.
9. Blumstein, A.; Herz, J.; Sinn, V.; Sadron, C. *C. R. Hebd. Seances Acad. Sci.* **1958**, *246*, 1856–1858.

10. Blumstein, A.; Ries, H. E., Jr. *J. Polym. Sci., Part B* **1965**, *3*, 927–931.

11. Blumstein, A. *Bull. Soc. Chim. Fr.* **1961**, 906–914.

12. Hill, T. L. *J. Polym. Sci.* **1961**, *54*, 58–59.

13. Jones, D. The last retort: Carpet polymers. *Chem. World* **2011**, *8*, Regular article; http://www.rsc.org/chemistryworld/restricted/2011/August/LastRetort.asp (accessed on April 16, 2014).

14. Blumstain, A. *Adv. Macromol. Chem.* **1970**, *2*, 123–146.

15. Rehage, H.; Veyssié, M. *Angew. Chem., Int. Ed. Engl.* **1990**, *29*, 439–448.

16. Abraham, F. F.; Nelson, D. R. *Science* **1990**, *249*, 393–397.

17. Diederich, F.; Rubin, Y. *Angew. Chem., Int. Ed. Engl.* **1992**, *31*, 1101–1123.

18. Perepichka, D. F.; Rosei, F. *Science* **2009**, *323*, 216–217.

19. Gee, G.; Rideal, E. K. *Proc. R. Soc. London, Ser. A* **1935**, *153*, 116–128.

20. Bresler, S.; Judin, M.; Talmud, D. *Acta Physicochim. URSS* **1941**, *XIV*, 71–84.

21. Beredjick, N.; Burlant, W. J. *J. Polym. Sci., Part A-1* **1970**, *8*, 2807–2818.

22. Dubault, A.; Veyssié, M.; Liebert, L.; Strzelecki, L. *Nat. Phys. Sci.* **1973**, *245*, 94–95.

23. Markowitz, M. A.; Bielski, R.; Regen, S. L. *J. Am. Chem. Soc.* **1988**, *110*, 7545–7546.

24. Michl, J.; Magnera, T. F. *Proc. Natl. Acad. Sci. U. S. A.* **2002**, *99*, 4788–4792.

25. Dubault, A.; Casagrande, C.; Veyssié, M. *J. Phys. Chem.* **1975**, *79*, 2254–2259.

26. Kambe, T.; Sakamoto, R.; Hoshiko, K.; Takada, K.; Miyachi, M.; Ryu, J.-H.; Sasaki, S.; Kim, J.; Nakazato, K.; Takata, M.; Nishihara, H. *J. Am. Chem. Soc.* **2013**, *135*, 2462–2465.

27. Tanoue, R.; Giguchi, R.; Enoki, N.; Miyasato, Y.; Uemura, S.; Kimizuka, N.; Stieg, A. Z.; Gimzewski, J. K.; Kunitake, M. *ACS Nano* **2011**, *5*, 3923–3929.

28. Takami, T.; Ozaki, H.; Kasuga, M.; Tsuchiya, T.; Ogawa, A.; Mazaki, Y.; Fukushi, D.; Uda, M.; Aono, M. *Angew. Chem., Int. Ed. Engl.* **1997**, *36*, 2755–2757.

29. Miura, A.; De Feyter, S.; Abdel-Mottaleb, M. M. S.; Gesquiere, A.; Grim, P. C. M.; Moessner, G.; Sieffert, M.; Klapper, M.; Müllen, K.; De Schryver, F. C. *Langmuir* **2003**, *19*, 6474–6482.

30. Grill, L.; Dyer, M.; Lafferentz, L.; Persson, M.; Peters, M. V.; Hecht, S. *Nat. Nanotechnol.* **2007**, *2*, 687–691.

31. Zwaneveld, N. A. A.; Pawlak, R.; Abel, M.; Catalin, D.; Gigmes, D.; Bertin, D.; Porte, L. *J. Am. Chem. Soc.* **2008**, *130*, 6678–6679.

32. Bieri, M.; Treier, M.; Cai, J.; Aït-Mansour, K.; Ruffieux, P.; Gröning, O.; Gröning, P.; Kastler, M.; Rieger, R.; Feng, X.; Müllen, K.; Fasel, R. *Chem. Commun.* **2009**, 6919–6921.

33. Abel, M.; Clair, S.; Ourdjini, O.; Mossoyan, M.; Porte, L. *J. Am. Chem. Soc.* **2011**, *133*, 1203–1205.

34. Küller, A.; Eck, W.; Stadler, V.; Geyer, W.; Gölzhäuser, A. *Appl. Phys. Lett.* **2003**, *82*, 3776–3778.

35. Schultz, M. J.; Zhang, X.; Unarunotai, S.; Khang, D.-Y.; Cao, Q.; Wang, C.; Lei, C.; MacLaren, S.; Soares, J. A. N. T.; Petrov, I.; Moore, J. S.; Rogers, J. A. *Proc. Natl. Acad. Sci. U. S. A.* **2008**, *105*, 7353–7358.

36. Weigelt, S.; Busse, C.; Bombis, C.; Knudsen, M. M.; Gothelf, K. V.; Lægsgaard, E.; Besenbacher, F.; Linderoth, T. R. *Angew. Chem., Int. Ed.* **2008**, *47*, 4406–4410.

37. Blumstein, A.; Blumstein, R. *J. Polym. Sci., Part B* **1967**, *5*, 691–696 and refs 9−11.

38. Yanai, N.; Uemura, T.; Ohba, M.; Kadowaki, Y.; Maesato, M.; Takenaka, M.; Nishitsuji, S.; Hasegawa, H.; Kitagawa, S. *Angew. Chem., Int. Ed.* **2008**, *47*, 9883–9886.

39. Hub, H.; Hupfer, B.; Koch, H.; Ringsdorf, H. *J. Macromol. Sci., Part A* **1981**, *15*, 701−715.

40. Kusumi, A.; Singh, M.; Tirrell, D. A.; Oehme, G.; Singh, A.; Samuel, N. K. P.; Hyde, J. S.; Regen, S. L. *J. Am. Chem. Soc.* **1983**, *105*, 2975–2980.

41. Ringsdorf, H.; Schlarb, B.; Tyminski, P. N.; O'Brien, D. F. *Macromolecules* **1988**, *21*, 671–677.

42. Liu, S.; Sisson, T. M.; O'Brien, D. F. *Macromolecules* **2001**, *34*, 465–473.

43. Morozov, S. V.; Novoselov, K. S.; Katsnelson, M. I.; Schedin, F.; Elias, D. C.; Jaszczak, J. A.; Geim, A. K. *Phys. Rev. Lett.* **2008**, *100*, 016602.

44. Lee, C.; Wei, X.; Kysar, J. W.; Hone, J. *Science* **2008**, *321*, 385–388.

45. Ma, R.; Sasaki, T. *Adv. Mater.* **2010**, *22*, 5082–5104.

46. Budd, P. M. *Science* **2007**, *316*, 210–211.

47. Diederich, F. *Nature* **1994**, *369*, 199–207.

48. Berresheim, A. J.; Müller, M.; Müllen, K. *Chem. Rev.* **1999**, *99*, 1747–1785.

49. Spitler, E. L; Johnson, C. A., II; Haley, M. M. *Chem. Rev.* **2006**, *106*, 5344–5386.

50. Diederich, F.; Kivala, M. *Adv. Mater.* **2010**, *22*, 803–812.

51. Sakamoto, J.; van Heijst, J.; Lukin, O.; Schlüter, A. D. *Angew. Chem., Int. Ed.* **2009**, *48*, 1030–1069.

52. Simpson, C. D.; Brand, J. D.; Berresheim, A. J.; Przybilla, L.; Räder, H. J.; Müllen, K. *Chem. Eur. J.* **2002**, *8*, 1424–1429.

53. There are several reports on periodic 2D polymers by on-surface polymerization. This is a potentially powerful method, while the accessible size of the products is so far limited. The method is also facing issues about how to scale-up the synthesis and separate the products from the surfaces. For references, see refs (*28–33*).

54. Wegner, G. *Z. Naturforschg.* **1969**, *24b*, 824–832.

55. Bauer, T.; Schlüter, A. D.; Sakamoto, J. *Synlett* **2010**, 877–880.

56. Bauer, T.; Zheng, Z.; Renn, A.; Enning, R.; Stemmer, A.; Sakamoto, J.; Schlüter, A. D. *Angew. Chem., Int. Ed.* **2011**, *50*, 7879–7884.

57. Sakamoto, J. Habilitation thesis, ETH Zurich, Switzerland, 2012.

58. Kissel, P.; Erni, R.; Schweizer, W. B.; Rossell, M. D.; King, B. T.; Bauer, T.; Götzinger, S.; Schlüter, A. D.; Sakamoto, J. *Nat. Chem.* **2012**, *4*, 287–291.

59. Topochemical polymerization was previously applied to on-surface synthesis of periodic 2D polymers. See refs (*28, 29*).

60. Kissel, P.; Schlüter, A. D.; Sakamoto, J. *Chem. Eur. J.* **2009**, *15*, 8955–8960.

61. Kissel, P.; van Heijst, J.; Enning, R.; Stemmer, A.; Schlüter, A. D.; Sakamoto, J. *Org. Lett.* **2010**, *12*, 2778–2781.
62. Bouas-Laurent, H.; Desvergne, J.-P.; Castellan, A.; Lapouyade, R. *Chem. Soc. Rev.* **2000**, *29*, 43–56.
63. Bouas-Laurent, H.; Desvergne, J.-P.; Castellan, A.; Lapouyade, R. *Chem. Soc. Rev.* **2001**, *30*, 248–263.

Sequence Matters: Determining the Sequence Effect of Electronic Structure Properties in π-Conjugated Polymers

Ilana Y. Kanal, Jonathon S. Bechtel, and Geoffrey R. Hutchison*

Department of Chemistry, University of Pittsburgh, 219 Parkman Avenue, Pittsburgh, Pennsylvania 15260
***E-mail: geoffh@pitt.edu**

Conjugated organic polymers offer a highly tailorable set of optical and electronic properties and show promise for a wide range of technological applications including light-emitting devices and solar cells. A key challenge is to tune the HOMO and LUMO energies and the HOMO-LUMO gap for particular applications. Sequence control of monomer order offers the ability to alter these optoelectronic properties, rather than synthesis of complex monomers. A set of over 4,000 sequenced hexamers is studied using stastical data mining of semiempirical quantum chemical calculations and compared to simple particle-in-a-box and Hückel models. The results suggest that conjugated polymers can be effectively tuned by sequence and block-length control in addition to monomer design.

Introduction

Organic π-conjugated oligomers and polymers have gained both scientific and technological interest for a wide range of potential applications (*1*, *2*). Notably, many properties of these molecules can be tailored to adjust optoelectronic properties, solid-state packing, solubility, and many others, allowing optimization for particular needs. For example, the first organic photovoltaic (OPV) was reported in 1986 by Tang (*3*), and device efficiencies have improved significantly by tuning orbital energies, optical band gap, and other properties, even though important challenges remain (*4–6*).

Current organic photovoltaic polymers employ the donor-acceptor approach in which electron-poor acceptor and electron-rich donor monomers are mixed to create copolymers with the desired optoelectronic properties (*7–11*). Much effort has been made on finding novel monomers or side-chains to tailor the properties of the resulting copolymers (*12*). To facilitate this effort, computational screening methods, including those from our group, have allowed rapid development of both sets of target monomers and new design principals (*13*, *14*).

Nature, on the other hand, creates biopolymers with a fairly limited set of monomers, but instead create complex function with sequence-controlled polymers for protein translation (*15*) and photosynthesis (*16*). Little effort has been made to target sequenced patterns in copolymers for OPV or other organic semiconductor applications (*7–9*). Typically, these materials involve random order (ADDADA), alternating order (ADADAD), or in simple blocks (AAADDD). Our motivation for this project is to determine whether a sequence effect exists which could allow fine-tuning of HOMO-LUMO band gap without creating complicated monomers. Recent experimental results, suggest that sequence is useful as a strategy to tailor properties of π-conjugated polymers (*17*). Using the sequence effect to tune the band gap of polymers for OPVs is an alternative to the standard methods such as modification of monomers (*18*).

In previous work, we sampled the sequence effect across over a thousand tetramers using density functional theory (DFT) calculations (*19*). In this work, we seek to understand the effects of sequence in larger oligomers, notably analyzing over four thousand hexamers. We will use the same set of initial monomers to allow comparisons of the sequence effect as a function of oligomer length with our previous work. We will compare sequence effects in hexamers to those found in tetramers, discuss how these changes can be considered as a function of the proportion or the block-length of the two constituent monomers, and use simplified models such as particle-in-a-box and Hückel theory to explain and predict the effects of monomer sequence on optoelectronic properties.

Computational Methods

Undoubtedly, large sequence effects can be found in specific cases with well-chosen monomers, but an important goal is to determine the average sequence effect expected in general. From a pool of 670 monomers, a group of 1,948 polymeric repeat units was generated since many of these fragments could potentially polymerize through multiple sites (See Figure S1 in Reference (*19*)). Twelve monomers were chosen at random from the homotetramers in the complete monomer set. To ensure sample diversity, the homotetramers were imagined to be in four quadrants (as demarcated with red lines in Figure 1) and three monomers were chosen from each section (Figure 2).
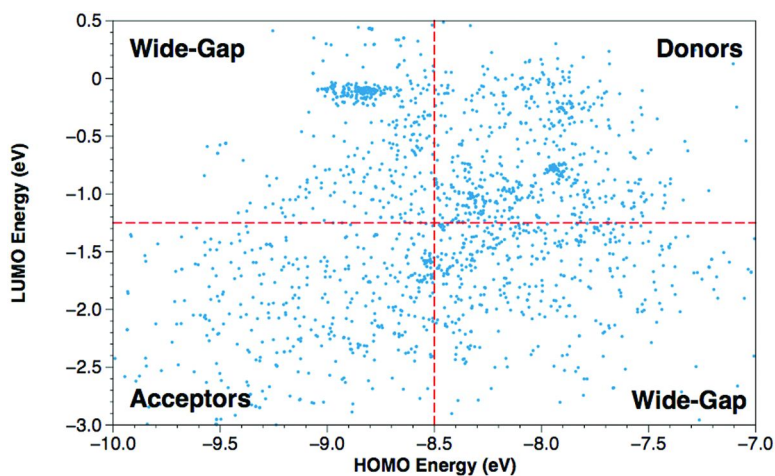
Figure 1. Diversity of monomers divided into four "quadrants" based on the computed HOMO and LUMO energies of the homotetramers. Three monomers were chosen, at random, from each of the quadrants (for a total of 12) to test the sequence effect. Reproduced with permission from reference (19). Copyright (2013) American Chemical Society.
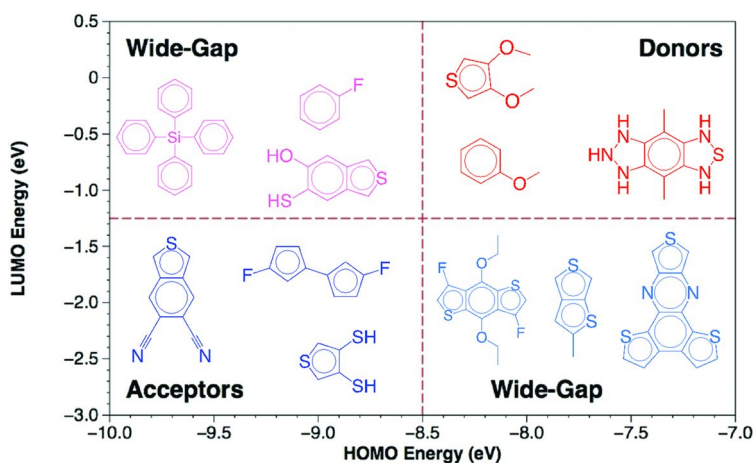
Figure 2. Chosen monomers and the energy quadrant from which they were chosen. Each monomer was combined with the 11 others to create 66 monomer pairs to create sequenced tetramers and hexamers. Reproduced with permission from reference (19). Copyright (2013) American Chemical Society.

Each of these twelve monomers was paired with every other monomer, resulting in 66 monomer pairs. A Python script created all permutations from the SMILES (*20*) string for each monomer. Each possible tetramer and hexamer sequence was formed, yielding 1,056 tetramer sequences and 4,244 hexamer sequences. From the resulting SMILES string for the co-oligomers, 3D structures were generated using a multistep process. An initial 3D structure was generated using Open Babel 2.3.2 (*21*) (accessed through its Python interface Pybel (*22*)) and minimized using the MMFF94 force field (*23–27*) (500 steps using steepest descent minimization, convergence at 1.0 kcal/mol). Next, a weighted-rotor search (MMFF94, 100 iterations, 20 geometry optimization steps) was carried out to find a low-energy conformer. This was then further optimized using MMFF94 (500 steps of conjugate gradient optimization, 1.0 kcal/mol convergence). Finally, Gaussian09 was used to optimize the structure using the PM6 (*28*) semi-empirical method. The Python library cclib (*29*) was used to extract the HOMO and LUMO eigenvalues. Statistical analysis was performed using RStudio (*30*, *31*). Although HOMO and LUMO eigenvalues are non-physical and do not directly correspond with the oxidation potential or electron affinity, they are common parameters for screening optoelectronic properties in conjugated oligomers (*13*, *32*).

In our previous study of the sequence effect, tetramer calculations were calculated using DFT (B3LYP functional) (*33*, *34*), but when progressing to the hexamers, the computational time and number of molecules increased drastically, so the semiempirical PM6 method was used for both tetramers and hexamers. The relative errors in the hexamer and tetramer calculations should be approximately equivalent for the comparisons examined.

After extracting the PM6-computed orbital eigenvalues, the data set was arranged with each sequence (AAAAAA, AADDAD, DDDDDD, etc.) in a vertical row, while horizontal rows represent a particular monomer combination. Each of these rows was averaged, and the analysis below discusses the average offsets — that is, the expected average effect of a particular sequence regardless of the monomer combination.

Results

Tetramers

In our previous work (*19*), trends were established regarding certain monomers effects on the associated tetramer HOMO-LUMO energy band gaps. Regardless of its coupling agent, a monomer with a five fused aromatic ring structure, trithieno[3,4-b:2′,3′- f:3″,2″-h]- quinoxaline (Scheme 1, left), consistently produced the lowest band gap across all sequence patterns, independent to which monomer it was coupled. Contrarily, coupled 4,4′-difluoro-[1,1′- bi(cyclopentane)]-1,1′,4,4′-tetraene (Scheme 1, right) tended to raise the band gap of its associated tetramers. This was an interesting finding, but demonstrated an already established idea: certain monomers make better photovoltaic devices than others (*12*, *35*).
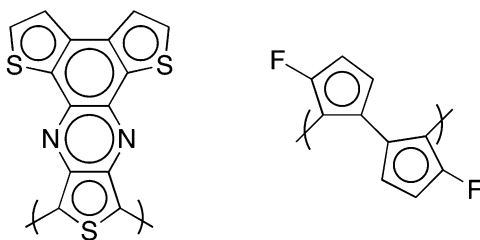
Scheme 1. (left) Trithieno[3,4-b:2',3'-f:3'',2''-h]quinoxaline, which was shown to have low energies and (right) 4,4'-Difluoro-[1,1'-bi(cyclopentane)]-1,1',4,4'-tetraene, which was shown to have high energies. Reproduced with permission from reference (19). Copyright (2013) American Chemical Society.

Beyond the effects of particular monomers on tetramer properties, sequence-dependent phenomena were also examined to identify patterns that can predict average energies of monomer sequences. Calculated HOMO, LUMO, and band gap values for each tetramer were averaged across the 66 monomer combinations. We then take the individual sequences (e.g., ADDA, DADD) and compute the normalized offsets compared to the average HOMO, LUMO, and band gap, expected from the particular monomer combinations. For example, we find that sequences with only single "A" monomers (i.e., a block length of one) have slightly higher normalized HOMO-LUMO gap energies than those with "AAA" blocks (Figure 3). We will use these normalized offsets as measures of the sequence effects below.
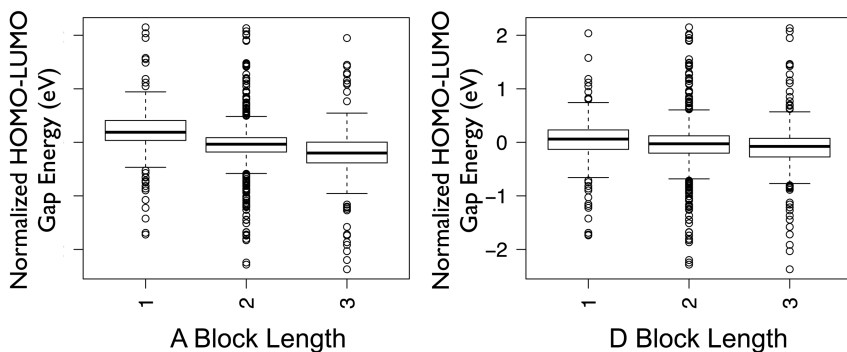
Figure 3. ANOVA plots for the A and D block lengths for HOMO-LUMO energy band gaps within hexamer sequences. The results show that while the length of the A block plays a role in the normalized energy, the length of the D block shows a much smaller effect.

Several clear patterns emerge from the normalized offsets. For example, LUMO and HOMO-LUMO band gap energies show, on average, a drastic jump between the ADDD and DAAA sequences. HOMO energies show the opposite trend with an energy decrease between the ADDD and DAAA sequences. DDDD

sequence values are consistently higher for the HOMO, LUMO, and band gap energy values. These observations support the hypothesis that sequence order affects the HOMO, LUMO, and band gap energies. To confirm our hypothesis, an analysis of variance (ANOVA) was performed for the sequenced averaged band gap energies, which showed a statistically significant difference in means among the sixteen sequence permutations (Tables 1-2).

Table 1. Range of HOMO, LUMO and HOMO-LUMO gaps as a function of all sequences and as a function of sequences containing 50% 'A' and 50% 'D', with standard deviations. Results show that there is a statistically significant difference between the tetramer and hexamer ranges for each group.

	Tetramer	Hexamer
Avg HOMO Energy Spread (eV)	0.11 ± 0.03	0.18 ± 0.06
Avg LUMO Energy Spread (eV)	0.30 ± 0.06	0.39 ± 0.07
Avg HOMO-LUMO Gap Energy Spread (eV)	0.40 ± 0.08	0.57 ± 0.09
50% 'A', 'D' HOMO Energy Spread (eV)	0.10 ± 0.02	0.16 ± 0.05
50% 'A', 'D' LUMO Energy Spread (eV)	0.28 ± 0.05	0.34 ± 0.06
50% 'A', 'D' HOMO-LUMO Gap Energy Spread (eV)	0.36 ± 0.06	0.49 ± 0.07

Since properties will depend on the fractions of A and D, the six sequenced tetramers with equal composition of A and D monomers (i.e., AADD, ADAD, ADDA, DAAD, DADA, and DDAA) were compared. An increase in HOMO energy of approximately 0.2 eV between the ADDA and DAAD sequences and an associated decrease in LUMO and band gap energy of approximately 0.2 eV between ADDA to DAAD is observed. Note that because not all of the monomers are symmetric, sequences such as AADD and DDAA are not necessarily geometrically equivalent. Additionally, the 'A' block length changes the HOMO, LUMO, and HOMO-LUMO gap energies, but the 'D' block length has little effect on the energies, as shown in Figure 3. With the tetramer set, however, it is not possible to separate between a block-length effect and a general position-dependent sequence effect.

Hexamers

Hexamers were produced using the same method as described for tetramers with the same twelve monomers to provide meaningful comparison. The number of sequence combinations in the analysis increases from 16 to 64, which in turn increases the number of calculations from 1,056 (tetramers) to 4,244 (hexamers). This provides more meaningful statistical results due to a significantly larger sample size.

Table 2. Statistical p-values for some of the patterns studied, to determine which factors change the HOMO, LUMO and HOMO-LUMO band gap values most significantly. The HOMO, LUMO and HOMO-LUMO band gap values for the hexamer sequences with 50% 'A' and 50% 'D' show significant differences in the sequences formed from different monomers.

	p-value	
Equal A/D Composition Data	*Tetramer*	*Hexamer*
HOMO	0.0064	1.4×10^{-7}
LUMO	3.0×10^{-6}	2.1×10^{-11}
HOMO-LUMO Gap	9.0×10^{-7}	1.9×10^{-14}
HOMO vs A Block Length	0.00026	7.9×10^{-13}
HOMO vs D Block Length	0.95	0.14
LUMO vs A Block Length	1.3×10^{-7}	$<2 \times 10^{-16}$
LUMO vs D Block Length	0.51	0.0015
HOMO-LUMO Gap vs A Block Length	3.4×10^{-8}	$<2 \times 10^{-16}$
HOMO-LUMO Gap vs D Block Length	0.62	0.0024
HOMO vs A+D Block Length	A: 2.5×10^{-4} D: 0.17	A: 7.2×10^{-13} D: 0.016
LUMO vs A+D Block Length	A: 1.3×10^{-7} D: 0.24	A: $<2 \times 10^{-16}$ D: 0.21
HOMO-LUMO Gap vs A+D Block Length	A: 3.2×10^{-8} D: 0.15	A: $<2 \times 10^{-16}$ D: 0.054

An important question is whether the observed effect was a sequence effect or a block length effect. As with the tetramer sequences, hexamer sequences with equal A and D composition were examined. As shown in Table 1, analysis of tetramers and hexamers with fifty percent composition suggest that the energy spreads of HOMO eigenvalues increase slightly from tetramers (0.10 ± 0.02 eV) to hexamers (0.16 ± 0.05 eV). LUMO eigenvalue ranges showed a similar trend (tetramer: 0.28 ± 0.05 eV; hexamer: 0.34 ± 0.06 eV). The HOMO-LUMO gap showed the greatest difference, with the tetramer spread 0.36 ± 0.06 eV increasing to 0.49 ± 0.07 eV for the hexamers. These results were found to be statistically significant (Table 2).

This shows that on average it should be possible to tune the hexamer band gap by about ~0.5 eV by varying the order in which the monomer units are combined in sequences, even with equal amounts of the two different monomers. The tetramers and hexamers with the highest band gaps are ADDA and ADDADA, respectively. The tetramers and hexamers with the lowest band gaps are DAAD and DDAAAD, respectively.

In order to determine if the observed variation in HOMO, LUMO and HOMO-LUMO band gap energies are derived from a sequence effect, rather

than a simple block-length effect, we studied the dependence of tetramer and hexamer energy on block length (A vs AA vs AAA, etc). This correlation was verified by examining block length for all species—AAAA, AAAD, AADA, AADD, etc.—and observing that, for all possible combinations of tetramers and hexamers, this relationship still exists. The analysis indicates that the length of the acceptor (A) chain is a statistically significant factor in HOMO, LUMO, and HOMO-LUMO band gap energy values.

It is not possible from the tetramer study alone to determine if there is a sequence effect independent of a block length effect, but the hexamers, with more combinations to consider, suggest that the block length *and* its placement within the hexamer (end, between alternating units, middle, etc.) both affect the energy. Surprisingly, the donor (D) block length is not correlated in a statistically significant manner to the HOMO, LUMO, or HOMO-LUMO energy values.

Discussion

In most cases, π-conjugated polymers and oligomers are considered excellent examples of the simple one-dimensional particle-in-a-box model, also known as the free-electron molecular orbital (FEMO), model with an infinite barrier height, and the potential inside the box is zero. Kuhn expanded on FEMO by introducing a one dimensional potential inside the box with a sine function as the potential energy, taking into account the difference in bond length between single and double bonds and explaining the affinity for electrons to not be equally distributed (*36*). The Kuhn model effectively captures the effective conjugation length, saturation of electronic properties and the finite band gap (*37*).

Rather than a sine potential, one can imagine conjugated sequenced oligomers as a particle in a box with the donor monomer represented by a positive potential and acceptor monomers by a negative potential (i.e., accepting electrons). Two piecewise functions, either step potentials or triangle potentials, were applied as $V(x)$ in the Schrödinger equation, and their shapes are depicted in Figure 4 for both tetramers and hexamers. With defined potential functions and boundary conditions (where the solution is zero on the boundaries), the eigenvalue value problem was solved for tetramers with equal A and D composition. When the two potential systems are compared, it is concluded that their results are consistent with one another, but with the triangle potentials showing slightly smaller effects, as shown in Figure 5. In these idealized PIB simulations, the sequences are exactly symmetric, even though as discussed earlier in PM6 calculations, sequences such as AADD and DDAA are not necessarily geometrically equivalent due to asymmetric monomers or conformational effects.

The PIB model shows that different perturbations of the first energy level are observed with varying A and D arrangements (Figure 5). Each of the different sequences shows a slightly different first energy level perturbation and the wave function shows greater perturbation at the ends than in the middle. The tetramers show that the sequence had an effect (Figure 5). The tetramer with the highest energy in the PIB model is ADDA. Interestingly, the hexamer with the highest energy is ADDADA, which has the same ADDA sequence as seen in the

tetramer in the terminal position of the sequence and exhibits no other AA or DD pairing. Other hexamer sequences that have the ADDA sequence are AADDAD and ADDAAD, in which there is either additional AA pairing, decreasing the energy, or the ADDA sequence is not in the terminal position and therefore exhibits lower energy. This result confirms the conclusion from the PM6 data that showed that the AA pairing is statistically influential to the energy of the sequence. In addition, the PM6 hexamer sequence that shows the highest energy is the ADDADA sequence, which further confirms the result since each of these methods is different, but estimate that the sequence which has the highest energy as the same sequence.
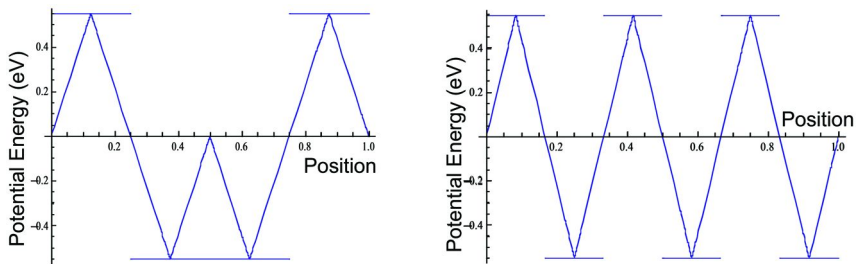
Figure 4. DAAD (left) and DADADA (right) step and triangle potential functions, overlaid. Step functions are represented by the horizontal lines. The y-axis is relative to V(x)=0.

Fundamental Solutions Energy Level Spacing Step vs Triangle Potentials
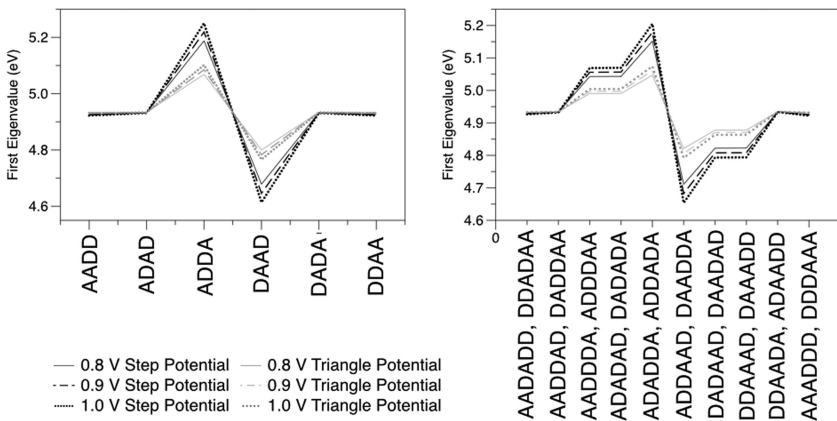
Figure 5. Comparison of energy levels for fundamental solutions between step (blue plots) and triangle (red plots) for V_o = 0.8, 0.9 and 1.0 V. Note that the step and triangle potentials have the same qualitative shape, but calculations show slightly different energy differences for each model.

The tetramer with the lowest energy in the PIB model is DAAD and the hexamer with the lowest energy is DAADDA. Similar to the hexamer highest energy case, the DAAD sequence is in the terminal position, but in contrast to the highest energy case, this hexamer contains a DD pair. The other sequences that contain the DAAD chain are DAADAD, with no additional pairing and thus has slightly higher energy, and DDAADA, which does not have the DAAD sequence in the terminal position and the energy is not the lowest. These relative sequence orderings from the particle-in-abox model do not match the lowest energy sequence from the PM6 calculations; the lowest energy sequence was DDAAAD. The PIB model trends do match the general trend from the PM6 data in that the D block length does not statistically affect energy values. This suggests that most of the trends between the PM6 calculated values and the PIB model values will show a weak correlation (i.e., an R^2 value of ~0.35 as in Figure 6). This led to creation of a Hückel model to better mimic the trends seen in the hexamer data.
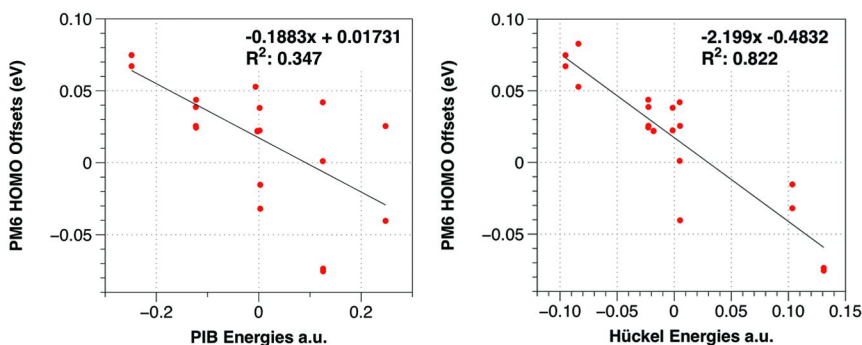
Figure 6. (left) Correlation between relative particle-in-a-box (PIB) model energies and relative PM6 HOMO energy offsets and (right) correlation between Hückel relative energies and PM6 HOMO energy offsets. In all cases, the relative offsets are changes to the orbital energies of particular sequences versus the average across all sequences for a particular donor-acceptor pair. Note that the slope of the correlation lines is negative.

Hückel Model

Beyond a simple PIB model, π-conjugated polymers are frequently treated using a π-electron Hückel model. Based on the poor correlation between the PIB treatment of the sequenced hexamers and the PM6 results, a similar Hückel treatment was used, with each site reflecting an "A" or "D" monomer. Since the Hückel model requires α (site energy) and β (electronic coupling) parameters, we extracted the average difference in HOMO energy between A and D monomers for all 66 combinations from the PM6 calculations (0.95 eV) and the coupling for homodimers AA or DD for all 12 monomers (0.25 eV). With these parameters, we find an outstanding correlation between the PM6-computed average HOMO offsets for each hexamer sequence and the Hückel predictions (Figure 6).

Since the Hückel model only requires solving a system of linear equations, we can use this computationally efficient method to explore the effects of sequence on longer oligomers. Scanning from tetramers to 24-mers, while the number of 50:50 sequences increases *exponentially* to over 2.6 million candidates, the range of HOMO energies increases only *logarithmically* (Figure 7). Thus, for optoelectronic properties, there is little reason to synthesize sequences beyond 6-8 monomer units, since the variations in HOMO energies will saturate.
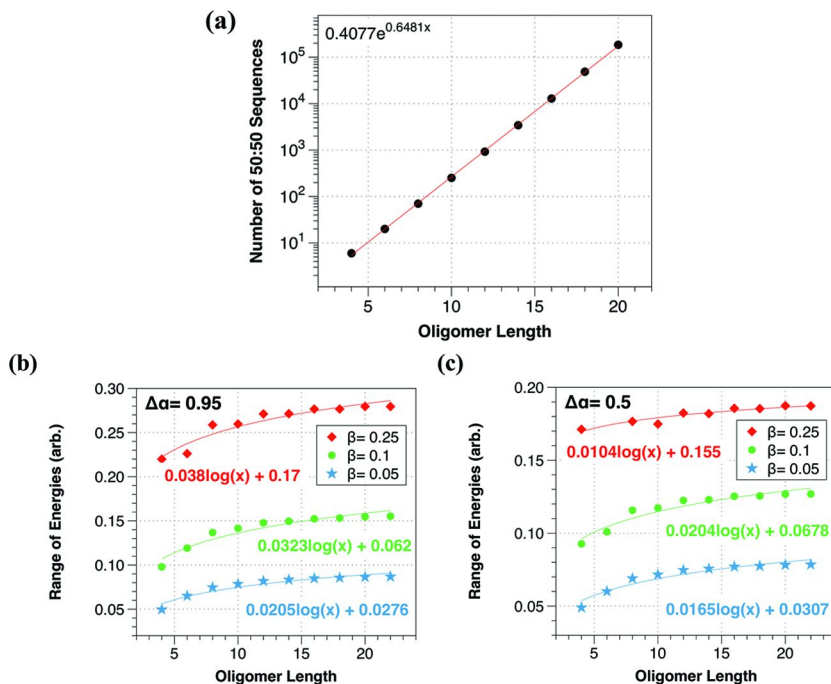
*Figure 7. (a) While the number of 50:50 sequences increases **exponentially** with oligomer length, Hückel calculations indicate that the spread of orbital energies only increases **logarithmically**. (b) Hückel calculations with a large difference (Δα) between A and D monomer site energies, indicate a high β delocalization effect yields the greatest sequence effect, while (c)) Hückel calculations with a smaller Δα indicate the sequence effect increases much faster for smaller β interactions.*

A pattern also emerges for the sequences with the most negative Hückel-computed HOMO energy (i.e., hardest to oxidize) and the least negative HOMO energy (i.e., easiest to oxidize) as compiled in Table 3. Remember that the slope of the PM6-Hückel correlation is negative, so the most stable, easiest to oxidize sequence would be the pattern $(DD)_x(AAAA)_{2x}(DD)_x$ where the subscripts sum to the total number of monomers (n). Since the most delocalized wavefunction in the PIB picture or Hückel model will have highest amplitude in the center of the π-conjugated oligomer, the "A" monomers will have the largest contribution

in the center of the wavefunction, and the "D" monomers will have the smallest perturbation on the edges. Indeed, the hexamer sequence DDAAAD is found to have one of the two highest averaged PM6-computed HOMO energies. The Hückel model, since it neglects atomistic detail is imperfect, and the highest PM6-computed HOMO energy is found instead for AAADDD (i.e., the ordering is reversed between PM6 and Hückel).

Table 3. Compilation of sequences with lowest and highest Hückel-computed eigenvalues, regardless of parameters.

Oligomer Size	Lowest Eigenvalue Sequence	Highest Eigenvalue Sequence
4	DAAD	ADDA
6	DDAAAD	ADDADA
8	DDAAAADD	ADADDADA
10	DDAAAAADDD	ADADADDADA
12	DDDAAAAAADDD	ADADADDADADA
14	DDDAAAAAAADDDD	ADADADADDADADA
16	DDDDAAAAAAAADDDD	ADADADADDADADADA

Conversely, the least stable, hardest to oxidize sequence would be the pattern $(ADAD)_x(DADA)_x$, again with the subscripts summing to the total number of monomers. The alternating pattern of A and D monomers introduces frequent barriers that disrupt the delocalized HOMO, and the sequence inverts, creating a kink exactly at the midpoint of the wavefunction. Indeed, the tetramer ADDA and hexamer ADADDA are found to be extrema from the averaged PM6-computed HOMO energies.

Finally, the Hückel model allows exploring different ranges of parameters. For example, the average ΔE for the PM6-computed monomer HOMO energies was 0.95 eV, which was used for the difference in β site energies in the Hückel results described above (with $\beta = 0.25$). This is clearly a large difference in orbital site energies, and in Figure 7, the range of orbital energies created by sequence variation decreases with decreasing β parameter. In other words, for a large energy difference between A and D monomers, a large β (i.e., highly delocalized) is needed to obtain significant variations in orbital energies from the sequence effect. On the other hand, for smaller differences in β (0.5 eV) between A and D sites, a smaller β (i.e., more localized) yields the largest variation in orbital energies (Figure 7).

This suggests two different regimes to obtain maximal variations of electronic structure from the sequence effect: for a large difference in monomer orbital energies (e.g., strong donor, strong acceptor) attempt to maximize the delocalization and electronic coupling between the monomers, but for

smaller variations in monomer orbital energies, attempt instead to maximize the localization between the monomers.

When the study was expanded to hexamers, a more complicated effect, which depends on block length and placement of that block or sequence within a hexamer emerged. Block length and placement impact the energy as shown through the general PIB model and the more detailed Hückel model and verified by the PM6 calculations. The result is encouraging since the PIB model does not take into account any details about the system. Two potential sequences of interest to study experimentally are ADDA and DAAD, which when arranged in the terminal or middle position would verify whether the changes in energy are seen in experiment. This would lead to new ways of exploring polymers in the hope of finding an ideal OPV material. In addition, these sequences can be applied to the screening project to further verify the results (with other monomers) and help with the mutation of polymers in the search for the ideal band gap for effective charge transfer.

Conclusions

The results from the tetramers suggested that the sequence in which the monomers are arranged on average has an effect on the energy. When expanded to hexamers, it is apparent that there is a more complicated effect that depends on block length and placement of that block or sequence within a hexamer. The fact that the block length and placement seem to have an impact on the energy as shown through the general PIB and Hückel models and verified by the PM6 calculations is encouraging since neither model takes into account the detailed molecular structure of the monomers or the conformational preferences in particular species.

For future applications of π-conjugated polymers, both monomer design and sequence control will yield the most significant control over electronic structure properties. Since sequence also controls polymer conformation and packing motifs, we believe further investigation is needed to predict and control charge transport and other related solid-state properties.

Acknowledgments

References

1. Wang, C.; Dong, H.; Hu, W.; Liu, Y.; Zhu, D. *Chem. Rev.* **2012**, *112*, 2208–2267.
2. Skabara, P. J. *Chem. Comm.* **2013**, *49*, 9242–9244.
3. Tang, C. W. *Appl. Phys. Lett.* **1986**, *48*, 183–185.

4. He, Z.; Zhong, C.; Su, S.; Xu, M.; Wu, H.; Cao, Y. *Nat. Photonics* **2012**, *6*, 593–597.

5. Liang, Y.; Yu, L. *Acc. Chem. Res.* **2010**, *43*, 1227–1236.

6. Janssen, R. A. J.; Nelson, J. *Adv. Mater.* **2012**, *25*, 1847–1858.

7. Facchetti, A. *Chem. Mater.* **2011**, *23*, 733–758.

8. Szarko, J. M.; Guo, J.; Rolczynski, B. S.; Chen, L. X. *J. Mater. Chem.* **2011**, *21*, 7849–7857.

9. Zhao, X.; Zhan, X. *Chem. Soc. Rev.* **2011**, *40*, 3728–3743.

10. Risko, C.; McGehee, M. D.; Brédas, J.-L. *Chem. Sci.* **2011**, *2*, 1200–1218.

11. Gong, X.; Tong, M.; Brunetti, F. G.; Seo, J.; Sun, Y.; Moses, D.; Wudl, F.; Heeger, A. J. *Adv. Mater.* **2011**, *23*, 2272–2277.

12. Mei, J.; Bao, Z. *Chem. Mater.* **2014**, *26*, 604–615.

13. O'Boyle, N. M.; Campbell, C. M.; Hutchison, G. R. *J. Phys. Chem. C* **2011**, *115*, 16200–16210.

14. Hachmann, J.; Olivares-Amaya, R.; Atahan-Evrenk, S.; Amador-Bedolla, C.; Sánchez-Carrera, R. S.; Gold-Parker, A.; Vogt, L.; Brockway, A. M.; Aspuru-Guzik, A. *J. Phys. Chem. Lett.* **2011**, *2*, 2241–2251.

15. Lutz, J. F.; Ouchi, M.; Liu, D. R.; Sawamoto, M. *Science* **2013**, *341*, 1238149–1238149.

16. Blankenship, R. E.; Tiede, D. M.; Barber, J.; Brudvig, G. W.; Fleming, G.; Ghirardi, M.; Gunner, M. R.; Junge, W.; Kramer, D. M.; Melis, A.; Moore, T. A.; Moser, C. C.; Nocera, D. G.; Nozik, A. J.; Ort, D. R.; Parson, W. W.; Prince, R. C.; Sayre, R. T. *Science* **2011**, *332*, 805–809.

17. Norris, B. N.; Zhang, S.; Campbell, C. M.; Auletta, J. T.; Calvo-Marzal, P.; Hutchison, G. R.; Meyer, T. Y. *Macromolecules* **2013**, *46*, 1384–1392.

18. Lutz, J.-F. *Polym. Chem.* **2010**, *1*, 55–62.

19. Kanal, I. Y.; Owens, S. G.; Bechtel, J. S.; Hutchison, G. R. *J. Phys. Chem. Lett.* **2013**, *4*, 1613–1623.

20. Weininger, D. *J. Chem. Inf. Comput. Sci.* **1988**, *28*, 31–36.

21. O'Boyle, N. M.; Banck, M.; James, C. A.; Morley, C.; Vandermeersch, T.; Hutchison, G. R. *J. Cheminformatics* **2011**, *3*, 33.

22. O'Boyle, N. M.; Morley, C.; Hutchison, G. R. *Chem. Central J.* **2008**, *2*, 5.

23. Halgren, T. A. *J. Comput. Chem.* **1996**, *17*, 490–519.

24. Halgren, T. A. *J. Comput. Chem.* **1996**, *17*, 520–552.

25. Halgren, T. A. *J. Comput. Chem.* **1996**, *17*, 553–586.

26. Halgren, T. A.; Nachbar, R. B. *J. Comput. Chem.* **1996**, *17*, 587–615.

27. Halgren, T. A. *J. Comput. Chem.* **2004**, *17*, 616–641.

28. Stewart, J. J. P. *J. Mol. Model* **2007**, *13*, 1173–1213.

29. O'Boyle, N. M.; Guha, R.; Willighagen, E. L.; Adams, S. E.; Alvarsson, J.; Bradley, J.-C.; Filippov, I. V.; Hanson, R. M.; Hanwell, M. D.; Hutchison, G. R.; James, C. A.; Jeliazkova, N.; Lang, A. S.; Langner, K. M.; Lonie, D. C.; Lowe, D. M.; Pansanel, J.; Pavlov, D.; Spjuth, O.; Steinbeck, C.; Tenderholt, A. L.; Theisen, K. J.; Murray-Rust, P. *J. Cheminformatics* **2011**, *3*, 37.

30. RStudio. *Integrated development environment for R*, Version 0.97.551 [Computer software]; Boston, MA, retrieved May, 2012.

31. Team, R. C. *R: A Language and Environment for Statistical Computing* (Version 0.97.551) [Computer software]; Boston, MA, 2012.

32. Savoie, B. M.; Jackson, N. E.; Marks, T. J.; Ratner, M. A. *Phys. Chem. Chem. Phys.* **2013**, *15*, 4538–4547.

33. Becke, A. D. *J. Chem. Phys.* **1993**, *98*, 5648.

34. Lee, C.; Yang, W.; Parr, R. G. *Phys. Rev., B: Condens. Matter* **1988**, *37*, 785–789.

35. Nelson, J. *Mater. Today* **2011**, *14*, 462–470.

36. Kuhn, H. *J. Chem. Phys.* **1949**, *17*, 1198–1212.

37. Torras, J.; Casanovas, J.; Alemán, C. *J. Phys. Chem. A* **2012**, *116*, 7571–7583.

Subject Index